Imperial College London

An Investigation of the Diagnostic Potential of Autofluorescence Lifetime Spectroscopy and Imaging for Label-Free Contrast of Disease

Dr Sergio Coda

Department of Medicine
Division of Experimental Medicine
Imperial College London

Thesis submitted for the award of Doctor of Philosophy (PhD)
Imperial College of Science, Technology and Medicine

Abstract

The work presented in this thesis aimed to study the application of fluorescence lifetime spectroscopy (FLS) and fluorescence lifetime imaging microscopy (FLIM) to investigate their potential for diagnostic contrast of diseased tissue with a particular emphasis on autofluorescence (AF) measurements of gastrointestinal (GI) disease.

Initially, an *ex vivo* study utilising confocal FLIM was undertaken with 420-nm-excitation to characterise the fluorescence lifetime (FL) images obtained from 71 GI samples from 35 patients. A significant decrease in FL was observed between normal colon and polyps (p = 0.024), and normal colon and inflammatory bowel disease (IBD) (p = 0.015). Confocal FLIM was also performed on 23 bladder samples. A longer, although not significant, FL for cancer was observed, in paired specimens (n = 5) instilled with a photosensitizer.

The first *in vivo* study was a clinical investigation of skin cancer using a fibre-optic FL spectrofluorometer and involved the interrogation of 27 lesions from 25 patients. A significant decrease in the FL of basal cell carcinomas compared to healthy tissue was observed (p = 0.002) with 445-nm-excitation.

A novel clinically viable FLS fibre-optic probe was then applied *ex vivo* to measure 60 samples collected from 23 patients. In a paired analysis of neoplastic polyps and normal colon obtained from the same region of the colon in the same patient (n = 12), a significant decrease in FL was observed (p = 0.021) with 435-nm-excitation. In contrast, with 375-nm-excitation, the mean FL of IBD specimens (n = 4) was found to be longer than that of normal tissue, although not statistically significant. Finally, the FLS system was applied *in vivo* in 17 patients, with initial data indicating that 435-nm-excitation results in AF lifetimes that are broadly consistent with *ex vivo* studies, although no diagnostically significant differences were observed in the signals obtained *in vivo.*

Acknowledgements

Firstly, I wish to thank my supervisors Chris Dunsby, Paul French, and Andrew Thillainayagam for giving me the opportunity to work on this PhD project and, most importantly, for all the immense support and guidance they provided over these intense four years. Chris requires specific mention for his unlimited generosity and seemingly endless multidisciplinary knowledge.

Within the Photonics group I would also like to extend my thanks to other post-docs and staff members with whom I have worked closely. In particular I should mention Gordon Kennedy, whose patience, support and expertise have been invaluable to master the use of the confocal microscope and understand the foundations of FLIM. I would also like to express my overwhelming gratitude and appreciation to Professor Gordon Stamp for his exceptionally knowledgeable advice on all aspects of clinical pathology. Additionally, I should acknowledge Alex Thompson, Kim Roche, Martin Lenz and Hugh Sparks for their continuous support when imaging/measuring samples often at unpredictable times. A special mention should also go to Dr Mona El-Bahrawy for providing useful insights into the histopathological correlation of the FLIM contrast observed and discussed in chapter 4. Special thanks go to Martin and Simon in the Optics workshop, without their expertise the development of the fluorescence lifetime spectroscopy system would not have been possible.

It is important that I thank all of my colleagues here at Imperial, both past and present. This includes (but is not necessarily limited to) Rakesh, Judith, Sanja, Tom, Dom, Romain, Sunil, Anca, Dan, Mark, Cliff, Ian, Doug, Sean, Sara, Yuri, Marcia, both Lionels, James, Hugh Mannings, Stephane, Joao, Hugo, Mirella, Alex, Vincent, and many others, all of whom provided useful advice and an opportunity to relax over a cup of coffee or tea.

I would also like to thank the patience of Dr Devinder Bansi, Dr Lakshmana Ayaru, Dr John Martin, Dr Geoff Smith, Sister Betty Arksey, Sister Catherine Bilbrough, Sister Rasheeda Hagger, Ms Sophia Hami, Ms Heena Asher, and all the nurses and administration staff in the Endoscopy Unit at the Charing Cross Hospital, who have supported me in providing welcome and regular sessions to collect the clinical data, despite its disruptive effect on tremendously busy endoscopy sessions, and to maintain and nurture my endoscopy skills. I should thank the Histopathology team and the Endoscope Re-processing Unit at the Imperial College Healthcare Trust for their continuous support of this project.

My most sincere thanks go to my clinical mentors, Paolo Trentino, Takuji Gotoda and Andrew Thillainayagam, who taught me the art of performing basic and advanced endoscopy, and enabled me to succeed and prosper as a specialist endoscopist.

Outside of the hospital and the laboratory I would like to thank Andrew and Suzan for their friendship and for making me and my family always feel welcome and cared for since we moved to London. Thanks also to Pippa, Danielle, Orli and Carol, who helped me organise meetings and made me always feel part of their team.

For their help and support I would also like to thank my parents, my in-laws, my brother and all of my friends. Most importantly, I would like to thank my wife and my daughter, for going through it all with me.

Finally, I would like to acknowledge the funding for my PhD, which was provided by the Engineering and Physical Sciences Research Council.

To Xhoana & Anja

Author declaration

All the work presented in this thesis is my own with the following exceptions:

The development of the spectrometer used in the skin cancer study presented in chapter 6. The time-resolved instrument was built at Imperial College London by Pieter De Beule.

Data collection for the skin cancer study discussed in chapter 6 was performed in collaboration with a number of researchers from both Imperial College London and Lund University (Sweden).

In the investigation of gastro-intestinal diseases presented in chapter 7 and 8, collection of data was performed in conjunction with Alex Thompson and Sister Kim Roche.

Selective histological sectioning and selective staining presented in chapter 4 was performed in collaboration with Dr Mona El-Bahrawy, Consultant Histopathologist at Hammersmith Hospital.

Work involving imaging of bladder tissue (with or without prior instillation with Hexvix) presented in chapter 5 was performed in collaboration with Dr. Erik Mayer, Dr. Daniel Cohen and Dr Ashok Kar.

Copyright Declaration

The copyright of this thesis rests with the author and is made available under a Creative Commons Attribution Non-Commercial No Derivatives license. Researchers are free to copy, distribute or transmit the thesis on the condition that they attribute it, that they do not use it for commercial purposes and that they do not alter, transform or build upon it. For any reuse or redistribution, researchers must make clear to others the license terms of this work.

Table of contents

Abstract 2
Acknowledgements 3
Author declaration 6
Copyright Declaration 7
Table of contents 8
List of figures 13
List of tables 23
List of Abbreviations 25
Chapter 1: Thesis outline 29
Chapter 2: Introduction to the gastrointestinal tract, conventional endoscopy and advanced endoscopic techniques 33
2.1 Anatomy of the gastrointestinal tract 33
2.1.1 Histology of the gastrointestinal tract 37
2.1.2 Pathology of the gastrointestinal tract 40
2.2 General indications for endoscopy 59
2.2.1 Upper GI endoscopy 59
2.2.2 Lower GI endoscopy 60
2.3 Introduction to endoscopy 62
2.3.1 Technical aspects 63
2.4 Advanced imaging and measurement of the gastrointestinal tract: novel techniques and future developments 68
2.4.1 Magnification and high definition endoscopy 70
2.4.2 Virtual chromoendoscopy 72
2.4.3 Fluorescence endoscopy 79
2.4.4 Confocal microscopy 83
2.4.5 Confocal laser endomicroscopy 84
2.5 Endoscope based Confocal Laser Endomicroscopy (eCLE) 87
2.6 Probe based Confocal Laser Endomicroscopy (pCLE) 89
2.6.1 Endocytoscopy (EC) 94
2.6.2 Two-photon and multi-photon microscopy 95
2.6.3 Second (SHG) and Third (THG) Harmonic Generation Imaging 96
2.6.4 Optical Coherence Tomography 97

2.6.5 Future potential clinical optical imaging modalities 98
2.6.6 Summary 103
2.7 Unmet clinical needs in GI endoscopy 105
Chapter 3: Introduction to fluorescence, fluorescence lifetime and autofluorescence spectroscopy and imaging 108
3.1 Introduction to fluorescence 108
3.1.1 Fluorescence Intensity and Quantum Yield 109
3.1.2 Fluorescence Spectra 110
3.1.3 Fluorescence Lifetime 110
3.1.4 Autofluorescence of biological tissue 114
3.1.5 Fluorescence lifetime imaging and spectroscopy 124
3.2 Development of endoscopic instrumentation to utilise autofluorescence lifetime for the study and diagnosis of gastrointestinal disease 129
3.2.1 Single point fluorescence lifetime spectroscopy (FLS) instrumentation 129
3.2.2 Single point fluorescence lifetime spectroscopy (FLS) instrumentation designed and built by the Photonics Group at Imperial College London 131
3.2.3 Fluorescence lifetime imaging (FLIM) instrumentation 131
3.2.4 Confocal FLIM endomicroscopy instrumentation designed and built by the Photonics Group at Imperial College London 132
3.2.5 Wide field FLIM endoscopy instrumentation designed and built by the Photonics Group at Imperial College London 134
3.3 Review of research and clinical experience with autofluorescence spectroscopy and imaging 136
3.4 Summary 145
Chapter 4: Fluorescence Lifetime Imaging (FLIM) of human gastrointestinal tissues: a pilot observational study conducted on ex vivo endoscopically resected specimens 148
4.1 Introduction 149
4.2 Materials and methods 152
4.2.1 Overview 152
4.2.2 Patient enrolment 154
4.2.3 Fluorescence lifetime imaging instrumentation 155
4.2.4 Sample preparation and protocol 156
4.2.5 Data processing, lifetime calculation and FLIM map generation 159
4.2.6 Statistical analysis of paired lifetime measurements 162
4.2.7 Criteria for interpretation of confocal images 163
4.3 Results 163
4.3.1 Colonic polyps 164

4.3.2 Colon cancer 176
4.3.3 Inflammatory bowel disease 180
4.3.4 Oesophageal disease 189
4.3.5 Summary 198
4.4 Discussion 199
4.4.1 Fluorescence lifetime changes with time following endoscopic excision 199
4.4.2 Characteristics of the GI mucosal tissue 200
4.4.3 Colonic polyps and cancer 201
4.4.4 Inflammatory bowel disease 202
4.4.5 Barrett's oesophagus and oesophageal disease 203
4.4.6 Known and unknown fluorophores in GI mucosal tissues 203
4.4.7 Fluorescence intensity 205
4.4.8 Future work 206
4.5 Conclusions 207
Chapter 5: Fluorescence Lifetime Imaging (FLIM) of bladder cancer: a pilot study conducted on human bladder specimens collected under Hexvix induced endoscopic fluorescence guidance 209
5.1 Introduction 209
5.1.1 FLIM of PDD agents in bladder cancer 211
5.1.2 FLIM of PDD in other tissues 212
5.1.3 Summary of previous work and aims 213
5.1.4 Normal bladder histology 214
5.1.5 Bladder cancer pathology 216
5.2 Materials and methods 218
5.2.1 Overview 218
5.2.2 Patient enrolment 218
5.2.3 Fluorescence lifetime imaging instrumentation 219
5.2.4 Sample preparation and protocol 219
5.2.5 Criteria for interpretation of confocal images 220
5.3 Results 221
5.3.1 Summary 228
5.3.2 Wide field FLIM imaging 229
5.4 Discussion 230
5.5 Conclusions 233
Chapter 6: *In vivo* time-resolved fluorescence lifetime spectroscopy of skin cancer 234
6.1 Introduction 234

6.1.1 Normal Skin 239
6.2 Materials and methods 240
6.2.1 Time-resolved fibre-optic probe fluorescence lifetime spectrometer 242
6.2.2 Experimental protocol 245
6.2.3 Fluorescence decay analysis 248
6.3 Results 250
6.3.1 Steady state spectral analysis 250
6.3.2 Time-resolved autofluorescence measurements 250
6.3.3 Paired analysis of normal tissue measurements 251
6.4 Discussion 254
6.5 Conclusions 256
Chapter 7: Fluorescence lifetime spectroscopy (FLS) of tissue autofluorescence in normal and diseased gastrointestinal tissue measured *ex vivo* using a fibre-optic probe 257
7.1 Introduction 257
7.2 Materials and methods 260
7.2.1 Patient enrolment 260
7.2.2 Fluorescence lifetime spectroscopy (FLS) instrumentation 260
7.2.3 Experimental procedure 268
7.3 Data analysis 271
7.3.1 Exponential fitting of fluorescence decays 271
7.3.2 Fluorescence data analysis 271
7.4 Results 272
7.5 Discussion 288
7.6 Conclusions 289
Chapter 8: Endoscopic fluorescence lifetime spectroscopy (FLS) of gastrointestinal disease: a translational investigation conducted *in vivo* during routine endoscopy 290
8.1 Introduction 290
8.2 Materials and methods 292
8.2.1 Patient enrolment 292
8.2.2 Fluorescence lifetime spectroscopy (FLS) instrumentation 293
8.2.3 Experimental procedure 294
8.3 Data analysis 297
8.4 Results 298
8.5 Discussion 304
8.6 Conclusions 307
Chapter 9: Conclusions and outlook 308

9.1 Summary of results 309
9.2 Investigation of fluorescence lifetime imaging for label free contrast of gastrointestinal disease 309
9.3 Investigation of fluorescence lifetime confocal microscopy of bladder cancer as an adjunct to PpIX fluorescence induced PDD 310
9.4 Investigation of time-resolved autofluorescence spectroscopy of skin cancer 311
9.5 Investigation of time-resolved autofluorescence spectroscopy of colonic polyps and inflammatory bowel disease *ex vivo* 311
9.6 *In vivo* measurements of endoscopic fluorescence lifetime spectroscopy of gastrointestinal disease 312
9.7 Challenges and prospects: what went wrong and how could future studies be improved 314
Chapter 4 314
Chapter 5 315
Chapter 6 315
Chapter 7 316
Chapter 8 316
9.8 Final remarks 316
References 318
Appendix 344
List of journal publications, book chapters and conference presentations related to the work in the thesis. 344
Peer Reviewed Articles 344
Book chapters 344
Conference proceedings and published abstracts 344
Seminars, invited talks and oral presentations 345
Honours and awards 347
List of all permission documents and emails seeking permission to republish all the third party copyrighted works in the thesis 348
Chapter 2 348
Chapter 3 383
Chapter 4 402
Chapter 5 410
Chapter 6 420
Chapter 7 422

List of figures

Figure 2-1: The gastrointestinal tract. Source: © 1998-2013 Mayo Foundation for Medical Education and Research [3]. 34

Figure 2-2: Schematic cross-section of the gut. The lumen is the inside space of the gut. The abdominal wall is external to the gut. The peritoneal cavity is a virtual space between the parietal and the visceral peritoneum. 37

Figure 2-3: Schematic illustration of colonic mucosal structure in sagittal (a) and transverse (b) section, showing the crypts, the basement membrane, and the lamina propria. The crypts consist mainly of columnar epithelial cells and goblet cells. Adapted and reproduced with permission from [7]. 38

Figure 2-4: Endoscopic image of the second portion of the duodenum, showing the typical valves of Kerckring. Source of acquisition: Drs Coda & Thillainayagam, Endoscopy Unit, Charing Cross Hospital, Imperial College Healthcare NHS Trust. 39

Figure 2-5: Endoscopic appearance of early gastric cancer: (a) 0-I, Protruded type; (b) 0-IIa, superficial elevated type; (c) 0-IIb, flat type; (d), 0-IIc, superficial depressed type; (e) 0-IIa+IIc, combined type (superficial elevation with depression); (f) 0-IIc+III, combined type (superficial depression with ulceration). Images provided courtesy of Dr Takuji Gotoda, Endoscopy Unit, National Cancer Center Hospital, Tokyo, Japan. 41

Figure 2-6: Controversies in diagnosing early gastric cancer: (a) a small depressed lesion is noticed on the posterior wall of the upper gastric body after contrast chromoscopy with indigo carmine dye solution; (b) lesion without invasive finding is noticed on the biopsy, which is classified as dysplasia (Vienna classification category 4.1.) by Western pathologists. In contrast, this lesion is classified as well differentiated adenocarcinoma (Vienna classification 4.2.) in Japan. (c) After the resection, submucosal invasive adenocarcinoma with lymphatic involvement (Vienna classification 5.2.) is found. Reproduced with permission from [13]. 42

Figure 2-7: Pathological classification of early GI cancers according to depth of invasion: m1, confined to the epithelium; m2, invasion to the lamina propria; m3, infiltration of the muscularis mucosa; sm1, up to the upper third of the submucosa; sm2, to the mid third; and sm3, to the lower third of the submucosa. 43

Figure 2-8: (a) early gastric cancer (0-IIa+IIc type, 15 mm) of the fundus, along the lesser curvature just below the cardia, after staining with indigo-carmine. (b) Residual ulcer after ESD. (c) En bloc excised lesion fixed orientated on a board for histopathological assessment. (d) Well differentiated (G1) intramucosal ADC of intestinal type, vertical margins free of tumour (H&E, 20x original magnification). Reproduced with permission from [26]. 44

Figure 2-9: (a) laterally spreading tumour (non-granular type, 40 mm) of the sigmoid colon. (b) ESD of the submucosal layer by It-knife. (c) Residual mucosal defect immediately after ESD. (d) Well differentiated (G1) ADC. The lesion is largely intramucosal, with focal infiltration of the muscularis mucosae (H&E, 10x original magnification). Reproduced with permission from [26]. 45

Figure 2-10: The Los Angeles classification for reflux oesophagitis. The diagram shows a sagittal section through the gastro-oesophageal region (oesophageal mucosa in pink, gastric mucosa in red). The mucosal breaks are shown in yellow. SCJ = squamocolumnar junction. Adapted and reproduced with permission from [29,30]. 46

Figure 2-11: (a) Conventional endoscopic view of BO with concomitant esophagitis. (b) Positive staining of Barrett's epithelium after absorption chromoscopy with methylene blue dye solution. (c) Villous cerebroid pits with finger-like projections seen with magnification endoscopy. (d) Histological section of (c) showing intestinal metaplasia with adjacent round and elongated glands, and numerous goblet cells. Adapted from [31]. 47

Figure 2-12: The Seattle biopsy protocol for detection of dysplasia in Barrett's oesophagus. Adapted and reproduced with permission from [32]. 48

Figure 2-13: Diagrammatic representation of endoscopic Barrett's oesophagus showing an area classified as C6M14. C = extension of circumferential metaplasia; M = maximal extent of the metaplasia; GOJ = gastro-oesophageal junction. Adapted from and reproduced with permission from [33]. 49

Figure 2-14: Retrograde endoscopic view of a gastric cancer involving the cardia and the gastric fundus. In retroflexion, the image is inverted and the endoscope appears at the top of the figures (white arrow in (a)). The luminal extension of the neoplastic infiltration is indicated by the green arrows in (a, b) and (c). Long, deep ulcerations in the context of the cancer are visible (purple arrows). Source of acquisition: Drs Coda & Thillainayagam, Endoscopy Unit, Charing Cross Hospital, Imperial College Healthcare NHS Trust. 51

Figure 2-15: Anterograde endoscopic view of a diffuse type gastric cancer infiltrating circumferentially the gastric body. The green arrows indicate the motionless thickening and stiffening of the gastric wall creating the so called leather bottle appearance, *linitis plastica*. Source of acquisition: Drs Coda & Thillainayagam, Endoscopy Unit, Charing Cross Hospital, Imperial College Healthcare NHS Trust. 51

Figure 2-16: Endoscopic image of ulcerative colitis. Source of acquisition: Drs Coda & Thillainayagam, Endoscopy Unit, Charing Cross Hospital, Imperial College Healthcare NHS Trust. 53

Figure 2-17: (a) the adenoma-carcinoma sequence in colorectal cancer. (b) The *de novo* colorectal cancer pathway. Adapted and reproduced with permission from [41,42]. 54

Figure 2-18: Endoscopic images of a sessile (a), pedunculated (b) and a flat (c) polyp. The true extension of the flat polyp (c) is revealed by chromoscopy with indigo carmine dye solution. Source of acquisition: Drs Coda & Thillainayagam, Endoscopy Unit, Charing Cross Hospital, Imperial College Healthcare NHS Trust. 56

Figure 2-19: Endoscopic views of a cancer of the transverse colon (a, b), and the sigmoid colon (c, d). In (a) and (b), the tumour involves almost ¾ of the luminal circumference from the distal margin, whereas in (c) and (d), the tumour involves approximately the entire circumference of the bowel. In (d), the transition zone between normal and neoplastic epithelium is clearly shown by inspection with Narrow Band Imaging (NBI). Source of acquisition: Drs Coda & Thillainayagam, Endoscopy Unit, Charing Cross Hospital, Imperial College Healthcare NHS Trust. 58

Figure 2-20: Image of a conventional video-endoscope (Olympus GIF Q160) with biopsy forceps inserted though the endoscope working channel. Adapted from [49]. 62

Figure 2-21: The endoscopy room 1 at Charing Cross Hospital, Imperial College Healthcare NHS Trust. 63

Figure 2-22: Image of a fibre-optic endoscope (Olympus) with biopsy forceps inserted though the endoscope working channel. The inset shows the dead space between the fibres seen through the eyepiece. Adapted from [53]. 64

Figure 2-23: Cross section of a typical fibre-optic gastrointestinal endoscope. Reproduced with permission from [54]. 65

Figure 2-24: Schematic diagram of the distal end of a typical video-endoscope. In the top diagram, the illumination light guides, the air/water nozzle for lens cleaning, the objective lens, and the suction/working channels are visible. In the bottom diagram, a cross-section of the tip of the endoscope is given to indicate the location of the CCD. 66

Figure 2-25: Cross-sectional view of a conventional video-endoscope (Olympus LUCERA 260 Series GI endoscope) showing the internal channels for suction/operation (red), air insufflation (green), and lens cleaning/irrigation (blue). Adapted from [55]. 66

Figure 2-26: (a) Conventional endoscopic view of Barrett's oesophagus with concomitant oesophagitis. (b) Positive staining of Barrett's epithelium after absorption chromoscopy with methylene blue dye solution (1%, 10 ml). (c) Villous cerebroid pits with finger-like projections seen with magnification endoscopy (pattern 5 according to Endo's classification [77]). (d) Histological section of (c) showing intestinal metaplasia with glands of different size and shape, and numerous goblet cells. Adapted from [31]. 70

Figure 2-27: Example images of areas of suspected early cancers of the gastric antrum (a, b) and cardia (c, d) imaged using standard WLE (a, c) and NBI (b, d) to demonstrate the contrast enhancement provided by NBI. Images provided courtesy of Professor Paolo Trentino (University of Rome "La Sapienza", Italy)..... 73

Figure 2-28: Schematic diagram showing the difference between a standard RGB filter (a) and the NBI filter (b). Compared to the full range of white light illumination, the filtered light penetrates the tissue less, highlighting the superficial details of the mucosa. Additionally, the filtered centered wavelengths fall within haemoglobin absorption bands (inset on right of (b)[71]), and this leads to a higher contrast for vascular structures. 74

Figure 2-29: The principle and flow chart of FICE imaging [109]. 77

Figure 2-30: Example images of a small hyperplastic polyp in WLE (a) and i-Scan (b) to demonstrate the contrast enhancement provided by i-Scan. Reproduced with permission from [110]. 78

Figure 2-31: Example images of a suspected early cancer of the gastric antrum imaged using standard WLE (a) and AFI (b), to demonstrate the contrast enhancement provided by AFI (Olympus, Japan). Images provided courtesy of Dr Chizu Yokoi (National Center for Global Health and Medicine, Tokyo, Japan). 83

Figure 2-32: Schematic diagram of confocal microscopy principles. The blue rays (pre- and post-objective and excitation filter) indicate the laser illumination delivered to the tissue sample. Only the fluorescence emitted from a tissue layer in focus (orange rays) will pass through the pinhole and will be detected. The light emitted from tissue layers out of focus (red and green rays) will be rejected. Illumination and collection therefore occur in the same focal plane (i.e. confocal). Adapted from [140]..... 84

Figure 2-33: Confocal endomicroscopy systems clinically approved and currently available on the market. (a) The probe based system (Mauna Kea Technology, France). (b) In the confocal laser endomicroscope (Pentax, Japan). Adapted and reproduced with permission from [144]..... 86

Figure 2-34: (a) eCLE and (b) corresponding histological images (30x original magnification) of normal colonic mucosa. (c) eCLE and (d) corresponding histological images (15x original magnification) of an adenomatous polyp. (e) eCLE and corresponding (f) histological images (20x original magnification) of a poorly differentiated adenocarcinoma; the red arrow and the red arrowhead indicate an area of neoangiogenesis and islands of malignant cells (dark cells) respectively. Adapted and reproduced with permission from [155]. 88

Figure 2-35: pCLE example images showing non-dysplastic BO (a) and BO with early oesophageal adenocarcinoma (b). Adapted and reproduced with permission from [159]. 90

Figure 3-1: Illustration of the decay of fluorescence from a sample over a period of picoseconds after removal of the excitation light. Adapted and reproduced with permission from [248,249]. 111

Figure 3-2: (a) Jablonski diagram showing electronic energy levels of ground (E_0) and excited (E_1) states and both radiative (Γ) and non-radiative (κ) decay pathways in a fluorescent molecule. (b) After a short pulse of light, fluorescence emitted from the sample decays away over a period of nanoseconds as excited molecules return to their ground state. FLIM produces images using the fluorescence lifetime determined at each pixel to provide image contrast, displayed through a false-colour scale, between tissues or different components within the tissue with different fluorescence decays. 112

Figure 3-3: Schematic diagram illustrating the interactions of light with biological tissue. Adapted and reproduced with permission from [277]. 116

Figure 3-4: Excitation and emission spectra of main endogenous tissue fluorophores. Adapted and reproduced with permission from [213]. 117

Figure 3-5: Cartoon showing the various layers making up the GI wall and the expected fluorophores contained in each layer. 122

Figure 3-6: The principle of time-gated detection for FLIM. The excitation light pulse is shown in purple with the fluorescence emission in green. Three detection time gates (t1, t2 and t3) are also shown. 125

Figure 3-7: Schematic diagram of the TCSPC acquisition procedure. 126

Figure 3-8: Phase shift and demodulation seen in frequency domain FLIM when exciting with sinusoidally modulated light. The phase shift, φ, is labelled as are the amplitudes of the excitation light, A_{ex} and emitted light A_{em} and the respective average intensities, I_{ex} and I_{em}. 127

Figure 3-9: Matched white light, fluorescence intensity and FLIM images of a fresh haemicolectomy specimen containing a moderately differentiated colonic adenocarcinoma. (a) white light image; (b) fluorescence integrated intensity image; (c) false colour FLIM map; (d) FLIM merge image showing clear visual contrast between areas of normal and malignant tissue. Adapted and reproduced with permission from [273]. 128

Figure 3-10: (a) Configuration of the modified TCSPC FLIM confocal endomicroscope. Adapted and reproduced with permission from [336]. (b) The FLIM confocal endomicroscope based on a commercially available confocal laser endomicroscope (Cellvizio GI, Mauna Kea Technologies, France). 133

Figure 3-11: (a) Schematic diagram illustrating the wide field FLIM endoscope set-up. Excitation light (dark grey) is directed onto the sample. Emitted fluorescent light (light grey) is collected by the endoscope and imaged onto the GOI. Adapted and reproduced with permission from [67]. (b) Photograph of the flexible ureteroscope (Flex X ureteroscope, Karl Storz GmbH, Germany) being adapted for wide field FLIM endoscopy. 134

Figure 3-12: The wide field FLIM portable handheld rigid arthroscope for arthroscopic/surgical applications. 135

Figure 4-1: (a, b) Experimental set up for *ex vivo* imaging using the inverted Leica SP5 confocal FLIM microscope. (c) Graphic of the estimated image section of a tissue sample (in light blue). Adapted and reproduced with permission from [405]. 156

Figure 4-2: (a) Endoscopic biopsy during endoscopy. (b) Sample placed in a plastic culture dish with a glass coverslip base for imaging. 157

Figure 4-3: (a) Transverse histological image (H&E, original magnification 40x) and corresponding en face confocal intensity (b) and FLIM (c) images obtained at different depths beneath the epithelial surface from a polyp of the sigmoid colon. Brightness, crypt size, tissue architecture, as well as the mean fluoresce lifetime, change as the depth of the focal plane increases from 0 to 40 μm beneath the epithelial surface. Note that no exact registration exists between histology and FLIM images; the figure serves solely to illustrate the relative geometric orientation of the histological section and the stack of FLIM images from the same sample. 158

Figure 4-4: (a) Screenshot from SPC-Image software fitting the fluorescence decay from images taken from a specimen of normal colonic mucosa (caecum) excited at an excitation wavelength of 420 nm excitation wavelength. (b) Inset showing the lifetime distribution histogram (top panel) and the multiexponential decay fitting parameters (lower panel). (c) Inset showing the decay graph for the pixel indicated by the blue crosshair. The double exponential fit to the data (blue points) can be seen (red line), with associated residuals in the bottom panel (black line). T1 = start of fit; T2 = end of fit; TMax = temporal bin corresponding to peak of decay; Bin = binning; Thld = threshold; Pos =

position of selected pixel; tm = weighted average lifetime of selected pixel; χ2r = reduced Chi-Square. 161

Figure 4-5: Matched intensity (a, c) and FLIM images (b, d) of a freshly resected adenomatous polyp (c, d) and contiguous normal colonic mucosa obtained from an adjacent region in the same patient (a, b). The inset in (b) shows the decay graph from the centre of the crypt lumen in the normal sample. (e) Mean lifetime distribution histogram calculated from the FLIM data. Subverted architecture with highly atypical crypts can be seen in the polyp (c, d) and a separation of the FLIM histograms is clear (e). (f) Spatially averaged fluorescence intensity emission spectra collected from the samples with a spectrometer. See text for description of arrows, arrowheads, and asterisks. ..167

Figure 4-6: (a) Emission spectra of main endogenous tissue fluorophores (adapted from [213]). (b) Graph showing the overlap (black dashed rectangle) of the intensity spectra from fresh biopsy specimens of rectal polyp and adjacent normal rectal mucosa (shown in figure 4-5) collected with a fibre-coupled spectrometer, and the emission spectra of flavins (FAD) in solution (2.5 μM) obtained using a spectrofluorometer [414] at room temperature (21 °C), λex = 420 nm, λem = 540 nm. 168

Figure 4-7: Matched intensity (a, c) and FLIM images (b, d) of a freshly resected adenomatous polyp (c, d) and contiguous normal colonic mucosa (a, b). Numerous merging crypts with distorted orifices can be seen in the polyp (c, d). (e) Mean lifetime distribution histogram calculated from the FLIM data. (f) Spatially averaged fluorescence intensity emission spectra collected from the samples with a spectrometer. 170

Figure 4-8: (a) Bar graphs showing the mean fluorescence lifetime observed in all polyps relative to a sample of healthy tissue from the same region of the colon. (b) Shift in the mean fluorescence lifetime of all polyp specimens included in the paired analysis. Lifetime shifts are calculated using a measurement of normal tissue obtained from the same or nearest region of colon. 171

Figure 4-9: Bar graph showing the ratio (polyp/normal) in the mean fluorescence intensity observed in all the polyp specimens relative to a specimen of healthy tissue from the same patient. The mean intensity for all the samples was obtained calculating the mean number of photons detected per pixel, across all the pixels of the intensity image. The error bars represent ± 1 standard deviation and were calculated via error propagation from the fluorescence intensity distribution in the normal and polyp images.....172

Figure 4-10: Haematoxylin and eosin (H&E) stain of a biopsy sample of normal colon (a) and adenomatous polyp from the same patient (autofluorescence intensity and FLIM images from this patient are shown in Figure 4-5). Numerous normal goblet cells can be seen in (a), while only a few goblet cells are visible in the tubular adenoma dysplastic epithelium (b). The epithelial membrane antigen (EMA) highlights epithelial cells and glands from stroma in the normal colon specimen (c, e) and in the polyp (d, f). Masson's Trichrome staining (MTS) highlights fibromuscular tissue in both the normal colon (g) and the polyp (h). Alcian Blue (AB) highlights intracellular mucins in goblet cells, and mucins discharged into the gland lumina, showing good contrast between normal colon mucosa (i, k) and adenoma (j, l). Collagen IV highlights the basal membrane, muscle and blood vessels in normal colon (m) and in the polyp (n). The distribution of mucosal collagen appears altered between the samples, with remarkably reduced stain uptake in the polyp, where only scant amounts of collagen IV can be seen in the basal membranes and around the adenomatous crypts. Vimentin shows fairly selective staining of stroma both in normal colon mucosa (o), and the polyp (p), confirming the presence of stromal distortion within the irregular and overwhelmed (squeezed) adenomatous glands. 175

Figure 4-11: Matched intensity and FLIM images of fresh biopsy specimens of normal rectal mucosa (a, b) and rectal cancer (c, d). (e) Mean lifetime distribution histograms calculated from the FLIM data. (f) Intensity spectra collected from the samples with a spectrometer. 178

Figure 4-12: (a) Bar graphs showing the mean fluorescence lifetime observed in all colon cancers relative to a sample of healthy tissue from the same region of the colon. (b) Shift in the mean fluorescence lifetime of all colon cancer specimens included in the paired analysis. Lifetime shifts are calculated using a measurement of normal tissue obtained from the same or nearest region of colon. 179

Figure 4-13: Bar graph showing the ratio (cancer/normal) in the mean fluorescence intensity observed in all the cancer specimens relative to a specimen of healthy tissue from the same patient. The mean intensity for all the samples was obtained calculating the mean number of photons detected per pixel, across all the pixels of the intensity image. The error bars represent ± 1 standard deviation and were calculated via error propagation from the fluorescence intensity distribution in the normal and cancerous images. 180

Figure 4-14: Matched intensity (a, c), and FLIM (b, d) images of fresh colon biopsy samples of normal mucosa (a, b) and ulcerative colitis (c, d). (e) Mean lifetime distribution histograms calculated from the FLIM data. 183

Figure 4-15: Matched intensity (a, c) and FLIM (b, d) images of fresh colon biopsy samples of normal mucosa (a, b) and ulcerative colitis (c, d). (e) Mean lifetime distribution histograms calculated from the FLIM data. 185

Figure 4-16: Matched intensity (a, c) and FLIM (b, d) images of fresh colon biopsy samples of normal mucosa (a, b) and Crohn disease (c, d). (e) Mean lifetime distribution histograms calculated from the FLIM data. (f) Spatially averaged intensity spectra collected from the samples with a spectrometer. 187

Figure 4-17: Bar graphs showing the mean fluorescence lifetime observed in all IBD specimens relative to a sample of healthy tissue from the same or nearest region of the colon. (b) Shift in the mean fluorescence lifetime of all IBD specimens included in the paired analysis. Lifetime shifts are calculated using a measurement of normal tissue obtained from the same or nearest region of colon. 188

Figure 4-18: Bar graph showing the ratio (IBD/normal) in the mean fluorescence intensity observed in all the IBD specimens relative to a specimen of healthy tissue from the same patient. The mean intensity for all the samples was obtained calculating the mean number of photons detected per pixel, across all the pixels of the intensity image. The error bars represent ± 1 standard deviation and were calculated via error propagation from the fluorescence intensity distribution in the normal and inflamed images. 189

Figure 4-19: Matched intensity and FLIM images of fresh oesophageal biopsy specimens of normal mucosa (a, b) and Barrett's oesophagus with low grade dysplasia (c, d). (e) Lifetime histograms calculated from the FLIM data. The upper and lower left insets provide magnified views (20x original magnification) of the H&E-stained histological sections of the normal and the BO specimen, respectively. Note that no exact registration exists between histology and FLIM images; the insets serve solely to illustrate the similarity of the confocal images with histology. 192

Figure 4-20: Bar graphs showing the mean fluorescence lifetime observed in all BO specimens relative to a sample of healthy oesophageal tissue. (b) Shift in the mean fluorescence lifetime of all BO specimens included in the paired analysis. 193

Figure 4-21: Bar graph showing the ratio (BO/normal) in the mean fluorescence intensity observed in all the Barrett's oesophagus specimens relative to a specimen of healthy tissue from the same patient. The mean intensity for all the samples was obtained calculating the mean number of photons detected per pixel, across all the pixels of the intensity image. The error bars represent ± 1 standard deviation and were calculated via error propagation from the fluorescence intensity distribution in the normal and Barrett's oesophagus images. 193

Figure 4-22: Matched intensity and FLIM images of fresh oesophageal biopsy specimens of normal mucosa (a, b) and reflux oesophagitis (c, d). (e) Lifetime histograms calculated from the FLIM data. (f) Intensity spectra collected from the samples with a spectrometer. 195

Figure 4-23: Intensity and FLIM images of fresh oesophageal biopsy specimens of normal oesophageal mucosa (a, b) and inflamed cardiac mucosa (c, d). (e) Lifetime histograms calculated from the FLIM data. 197

Figure 4-24: Model excitation-emission matrix (EEM) of lyophilised collagen powder from type I collagen from bovine Achilles tendon (C9879, Sigma-Aldrich). λ = wavelength. Reproduced with permission from [426]. 203

Figure 5-1: Light micrograph of the wall of the urinary bladder in transverse section. The mucosa appears corrugated in folds called *rugae* (dotted circle). Adapted and reproduced with permission from [462]. 215

Figure 5-2: Comparison of H&E and pCLE images of normal bladder mucosa with fluorescein staining. (A) Large, polygonal superficial cells consistent with umbrella cells. (B) Smaller, deeper urothelial cells consistent with intermediate cells. (C) Lamina propria containing blood vessels filled with erythrocytes. Reproduced with permission from [463]. 215

Figure 5-3: Comparison of *in vivo* confocal endomicroscopy images with fluorescein staining of low (a) and high grade urothelial carcinoma compared with corresponding H&E sections (c) and (d). (a, b) Crowding of uniform-appearing cells in low grade cancer cells. (c, d) Pleomorphic and distorted sheet of cells in high grade carcinoma. Adapted and reproduced with permission from [464]. 217

Figure 5-4: Matched intensity (a, c) and FLIM images (b, d) of tissue autofluorescence in freshly resected normal bladder (a, b) and bladder cancer (c, d) obtained from the same patient undergoing cystoscopy at St Mary's Hospital, London. The normal specimen (a, b) shows large umbrella cells (red arrows) organized in *rugae* (red dotted circles), and a smaller subtype of cells which may correspond to intermediate or basal cells (red arrowheads). The cancerous specimen (c, d) shows a villous pattern with small and uniform cells and no umbrella cells can be seen. (e) Mean lifetime distribution histogram calculated from the FLIM data. 222

Figure 5-5: Matched intensity (a, c) and FLIM images (b, d) of a freshly resected bladder cancer (c, d) and normal bladder tissue (a, b) obtained from an adjacent region in the same patient. (e) Mean lifetime distribution histogram calculated from the FLIM data. (f) Intensity spectra collected from the samples with a spectrometer. 225

Figure 5-6: (a) Emission spectra of main endogenous tissue fluorophores (Adapted from [213]). (b) Graph showing the overlap (black dashed rectangle) of the intensity spectra from a fresh biopsy specimen of bladder cancer (shown in figure 5-5) collected with a fibre-coupled spectrometer, and the emission spectra of PpIX in DMSO (25 μM) obtained using a spectrofluorometer [414] at room temperature (21 °C), λex = 405 nm, λem = 580-750 nm. 226

Figure 5-7: Matched intensity (a, c) and FLIM images (b, d) of a freshly resected bladder papilloma (c, d) and normal bladder tissue (a, b) obtained from an adjacent region in the same patient. (e) Mean lifetime distribution histogram calculated from the FLIM data. (f) Intensity spectra collected from the samples with a spectrometer. 227

Figure 5-8: (a) Bar graphs showing the mean fluorescence lifetime observed in all cancers relative to a sample of healthy tissue from an adjacent region of bladder. (b) Shift in the mean fluorescence lifetime of all cancers specimens included in the paired analysis (n = 5). 228

Figure 5-9: Bar graph showing the ratio (bladder cancer/normal) in the mean fluorescence intensity observed in all the cancer samples relative to a sample of healthy tissue from the same patient. The mean intensity for all the samples was obtained calculating the mean number of photons detected per pixel, across all the pixels of the intensity image. The error bars represent ± 1 standard deviation and were calculated via error propagation from the fluorescence intensity distribution in the normal and cancerous images. 229

Figure 5-10: Wide field FLIM images of normal bladder (a) and bladder cancer (b) obtained from the same patient. Fluorescence lifetime distribution histogram calculated from the FLIM data, fitting the mean lifetime to a double-exponential decay model. The field of view of the ureteroscope is 3.29 mm x 2.51 mm. 230

Figure 6-1: Annotated H&E stained section of the epidermis and dermis of normal skin. Adapted and reproduced with permission from [522]. 239

Figure 6-2: (a) Optical layout of the time-resolved fluorescence spectrometer. (b) An example of the raw data acquired with this system. The graph shows 16 spectrally resolved fluorescence decays obtained from human skin *in vivo* using an excitation wavelength of 355 nm. Reproduced with permission from [403]. 242

Figure 6-3: (a) Photograph illustrating the optical arrangement of the time-resolved spectrometer with the lid removed. (b) The custom built fibre probe (FiberTech Optica, Canada). 243

Figure 6-4: Illustration of the experimental measurements. Photograph reproduced with kind permission of patient and investigators. 246

Figure 6-5: The images show how the fluorescence measurements were planned (in the inset) and performed (main image) prior to the surgical excision. The small black solid circles indicate the sites of the single-point fluorescence lifetime measurements, and the large dotted white circles the sites of the wide-field steady state measurements. (a) Nodular BCC of the left shoulder (lesion 21, patient 20). (b) Actinic keratosis of the back (lesion 25, patient 24) 247

Figure 6-6: Graphs showing the steady state fluorescence emission spectra of healthy tissue (a) adjacent to a lesion, and lesional tissue (b) measurements acquired with the time-resolved spectrometer using 355 nm excitation from lesion numbers 11 and 18. 250

Figure 6-7: Graphs showing the mean fluorescence lifetime in all spectral channels for healthy (blue columns) and lesional tissue (red columns) for (a) 355 nm and (b) 445 nm excitation. The mean values were calculated over all BCC patients and the error bars represent the standard deviation of the measurements. 251

Figure 6-8: Lesion No. 6: Basal cell carcinoma (12 x 10 mm) located on the left shin. A total of 4 measurements (2 on the lesion, 2 on normal surrounding skin) were performed. 252

Figure 6-9: Graphs showing the lifetime shifts between the two measurements of the healthy tissue surrounding each lesion (i.e. $\Delta\tau = \tau_{normal}\,1 - \tau_{normal}\,2$) for (a) 355 nm and (b) 445 nm excitation. Figure adapted, with permission, from reference [403]. 253

Figure 6-10: Graphs showing the lifetime shifts for all BCC lesions (i.e. $\Delta\tau = \tau_{lesion} - \tau_{normal}$) with (a) UV and (b) blue excitation. Figure adapted and reproduced with permission from [403]. 254

Figure 7-1: (a) Optical configuration of the fibre-optic probe fluorescence lifetime spectroscopy system. Figure (b) shows the proximal end of the excitation branch; figures (c) and (d) respectively show side and face views of the common distal end; and figure (e) shows the proximal end of the fluorescence detection branch. Cores shown in green are fluorescence detection fibres; fibres coloured blue are used to deliver the laser excitation. The red and orange fibres are respectively the delivery and collection cores for the diffuse reflectance measurements; they were unused in this study. 261

Figure 7-2: (a) Annotated high angle photograph illustrating the optical arrangement of the time-resolved spectrometer with the lid removed. (b, c) The custom built fibre probe for use in GI endoscopy (Fibertech GmbH, Germany). 263

Figure 7-3: Photograph of the transportable trolley which houses the entire spectrometer, showing some important features of the system. 265

Figure 7-4: Screenshot of the user interface of the LabVIEW software used to control the spectrometer. 267

Figure 7-5: (a) Endoscopic biopsy forceps (Radial Jaw 3 LC forceps, Boston Scientific) and (b) polypectomy snares (Captivator single-use snares, Boston Scientific) in use at Charing Cross Hospital. Images adapted and reproduced with permission from [540]. 268

Figure 7-6: Diagram illustrating the different regions of the human colon. Source: American Society for Gastrointestinal Endoscopy (ASGE) Anatomical Images, Colon & Rectum [541]. 273

Figure 7-7: Summary of results from normal tissues grouped according to whether the patient was diagnosed with a polyp (n = 13) or IBD (n = 4). Figures (a) and (b) show the mean fluorescence emission spectra obtained with 375 and 435 nm excitation respectively. Figures (c) and (d) show the spectrally resolved fluorescence lifetimes for 375 and 435 nm excitation respectively. Figure (e) shows the spectrally averaged mean fluorescence lifetimes for both groups and for both excitation wavelengths. The error bars represent ± 1 standard deviation in all panels. 275

Figure 7-8: Summary of results from normal tissues grouped according to the location that the specimen was taken from. The number of specimens in each group was: rectum (n = 2), left (n = 8), transverse (n = 5), right (n = 3). Figures (a) and (b) show the mean fluorescence emission spectra obtained with 375 and 435 nm excitation respectively. Figure (c) shows the spectrally averaged mean fluorescence lifetimes for all four groups and for both excitation wavelengths. The error bars represent ± 1 standard deviation in all panels. 276

Figure 7-9: Summary of the measured absolute mean fluorescence emission wavelengths and spectrally averaged mean fluorescence lifetimes for all the normal samples divided according to their location in the colon for (a) 375 nm and (b) 435 nm excitation wavelengths 277

Figure 7-10: Comparison of normal tissue versus neoplastic and non-neoplastic polyp specimens: figures (a) and (b) show the mean fluorescence emission spectra obtained with 375 and 435 nm excitation respectively. Figures (c) and (d) show the spectrally resolved fluorescence lifetimes with 375 and 435 nm excitation respectively. Figure (e) shows the spectrally averaged mean fluorescence lifetimes for all three groups (normal tissues, neoplastic and non-neoplastic polyps) and for both excitation wavelengths. The error bars represent ± 1 standard deviation in all panels. 279

Figure 7-11: Shift in the spectrally averaged mean fluorescence lifetime for (a) 375 nm and (b) 435 nm excitation of neoplastic (red bars) and non-neoplastic (green bars) polyp specimens. Lifetime shifts are calculated using a measurement of normal tissue obtained from the same or nearest region of colon (paired analysis) 280

Figure 7-12: Correlation plot of the shift in mean emission wavelength ($\Delta\lambda$) vs. the shift in spectrally averaged mean lifetime averaged over all neoplastic polyp specimen pairs (polyp – normal), where the normal sample was taken from the same region of colon as the polyp, for 435 nm excitation wavelength. 281

Figure 7-13: Comparison of normal tissue and IBD specimens: figures (a) and (b) show the mean normalised fluorescence emission spectra obtained with 375 nm and 435 nm excitation respectively. Figures (c) and (d) show the spectrally resolved mean fluorescence lifetimes with 375 nm and 435 nm excitation, respectively. Figure (e) shows the mean fluorescence lifetime averaged over the emission spectral range 494-556 nm for both groups and for both excitation wavelengths. The error bars represent ± 1 standard deviation in all panels. 283

Figure 7-14: Bar graphs showing the shift in the spectrally averaged mean fluorescence lifetime observed in all IBD samples relative to a sample of healthy tissue from the same patient. (a, b) show lifetime shifts obtained with 375 nm and 435 nm excitation respectively. The lifetime shift for 375 nm excitation was obtained using the spectrally averaged mean lifetime calculated over the emission spectral range 494-556 nm. 284

Figure 7-15: Correlation plots of the shift in mean emission wavelength ($\Delta\lambda$) vs. the shift in spectrally averaged mean lifetime averaged over all IBD specimen pairs (IBD – normal) for 375 nm excitation wavelength. 285

Figure 7-16: Summary of all measured shifts in mean fluorescence emission wavelength and spectrally averaged mean fluorescence lifetime for (a) 375 nm and (b) 435 nm excitation wavelengths. The lifetime shift for 375 nm excitation was obtained using the spectrally averaged mean lifetime calculated over the emission spectral range 494-556 nm for all points 286

Figure 7-17: Summary of all measured absolute mean fluorescence emission wavelengths and spectrally averaged mean fluorescence lifetimes for (a) 375 nm and (b) 435 nm excitation wavelengths. 287

Figure 8-1: Photograph showing the FLS point probe system in the Endoscopy suite at Charing Cross Hospital. 293

Figure 8-2: Endoscopic images showing the fluorescence lifetime fibre probe spectrometer being deployed *in vivo* to measure normal (a-d) and inflamed (e-h) regions of tissue in the colon. Both measurements were made in the same patient. Each site is illuminated for 10 s with the 375 nm and the 435 nm laser source. During the data acquisition, the endoscope light source is temporarily switched off to avoid damaging to the fibre probe detector, and a semi-circular ring of blue light bleeding through from the outer edge of the fibre probe in contact with the tissue can be seen in figures (c) and (g). Each area of tissue examined with the probe (~0.9 mm^2) was removed by subsequent excisional biopsy (d, h). Source of acquisition: Drs Coda & Thillainayagam, Endoscopy Unit, Charing Cross Hospital, Imperial College Healthcare NHS Trust. 294

Figure 8-3: Endoscopic images showing the fluorescence lifetime fibre probe spectrometer being deployed *in vivo* to measure abnormal (a, b) and normal (c, d) regions of tissue in the gastric antrum (the distal section of the stomach). Both measurements were made in the same patient. Each areas of tissue examined with the probe (~0.9 mm^2) was removed by subsequent biopsy (d) for histological assessment. Source of acquisition: Drs Coda & Thillainayagam, Endoscopy Unit, Charing Cross Hospital, Imperial College Healthcare NHS Trust. 294

Figure 8-4: (a) Endoscopic image showing the florescence lifetime fibre probe spectrometer being deployed *in vivo* to measure a colon cancer (a) and a neighbouring normal area of mucosa (b, c, d). In (d), a red ring resulting from impression of the ferule on the mucosa is shown (laser switched off). Note that the acquisition time was the same of a normal measurement (~20 s) as shown by the time elapsed on the endoscopy monitor (left). Source of acquisition: Drs Coda & Thillainayagam, Endoscopy Unit, Charing Cross Hospital, Imperial College Healthcare NHS Trust. 295

Figure 8-5: Summary of results from normal tissues grouped according to the location that the measurement was performed. The number of specimens in each group was: rectum (n = 5), left (n = 5), right (n = 3). Figures (a) and (b) show the mean fluorescence emission spectra obtained with 375 and 435 nm excitation respectively. Figure (c) shows the spectrally averaged mean fluorescence lifetimes for both groups and for both excitation wavelengths. The error bars represent ± 1 standard deviation in all panels. 299

Figure 8-6: Comparison of normal colon versus neoplastic and non-neoplastic polyp measurements: Figures (a) and (b) show the mean fluorescence emission spectra obtained with 375 and 435 nm excitation respectively. Figures (c) and (d) show the spectrally resolved fluorescence lifetimes with 375 and 435 nm excitation respectively. Figure (e) shows the spectrally averaged mean fluorescence lifetimes for the three groups and for both excitation wavelengths. The error bars represent ± 1 standard deviation in all panels. 301

Figure 8-7: Shift in the spectrally averaged mean fluorescence lifetime for (a) 375 nm and (b) 435 nm excitation of neoplastic (red bars) and non-neoplastic (green bars) polyp specimens. Lifetime shifts are calculated using a measurement of normal tissue obtained from the same or nearest region of colon (paired analysis) 302

Figure 8-8: Summary of all measured absolute mean fluorescence emission wavelengths and spectrally averaged mean fluorescence lifetimes for (a) 375 nm and (b) 435 nm excitation wavelengths between *ex vivo* (squares) and *in vivo* (circles) normal colon (blue), and neoplastic (red) and non-neoplastic (green) polyps 303

List of tables

Table 2-1: The Paris endoscopic classification of superficial neoplastic lesions in the GI tract. 41

Table 2-2: The Vienna Classification of GI epithelial neoplasia. ESD = endoscopic submucosal dissection. 43

Table 2-3: General indications for upper GI endoscopy. 59

Table 2-4: General indications for lower GI endoscopy. FOBT = Faecal occult blood test; US = ultrasound; CT = computed tomography; IBD = inflammatory bowel disease. 61

Table 3-1: Spectral characteristics and absolute lifetime values of the main endogenous tissue fluorophores reported in literature [280-282]. 118

Table 4-1: Summary showing the histological diagnoses of all the *ex vivo* samples investigated with the confocal FLIM microscope. Note that the group "gastric disease" incorporates gastric cancer, gastritis and portal hypertensive gastropathy. "Oesophageal disease" incorporates Barrett's oesophagus and oesophagitis. LGD = low grade dysplasia; IBD = inflammatory bowel disease; BO = Barrett's oesophagus. 153

Table 4-2: Demographic details of patients. 163

Table 4-3: Summary of colonic polyp and normal specimens included in study. 164

Table 4-4: Summary of colon cancer specimens included in the study. 177

Table 4-5: Summary of IBD and normal specimens included in study. IBD = inflammatory bowel disease; UC = ulcerative colitis; CD = Crohn's disease. 181

Table 4-6: Summary of Barrett's and normal oesophagus specimens included in study. BO = Barrett's oesophagus. 190

Table 4-7: Mean fluorescence lifetime shift for all samples included in paired analysis. Tau = fluorescence lifetime; SD = standard deviation; IBD = inflammatory bowel disease, BO = Barrett's oesophagus. 198

Table 5-1: Summary showing the clinical diagnoses of all the *ex vivo* non diagnostic samples investigated with the confocal FLIM microscope. Note that the histological diagnoses correspond to the diagnostic samples collected during the bladder mapping. 220

Table 5-2: Mean fluorescence lifetime shift for all samples included in paired analysis (n = 5). τ (tau) = fluorescence lifetime, SD = standard deviation. 228

Table 6-1: Summary of the skin lesion characteristics with clinical and histological diagnoses. R = right, L = left, BCC = Basal Cell Carcinoma, SCC = Squamous Cell Carcinoma. 241

Table 6-2: Summary of the skin lesions studied with the FLS system, reporting the histological diagnoses. 247

Table 7-1: Summary showing the clinical diagnoses of all the *ex vivo* samples investigated with the endoscopic spectrometer. LGD, low grade dysplasia; IBD, inflammatory bowel disease; *Hp*+, *Helicobacter pylori* positive; BO, Barrett's oesophagus. 270

Table 7-2: Summary of colonic polyps included in study. 278

Table 7-3: Spectrally averaged fluorescence lifetime shift for neoplastic and non-neoplastic polyps. 280

Table 7-4: Summary of IBD (inflammatory bowel disease) specimens included in the study, divided by type of analysis performed. 281

Table 8-1: Table showing the clinical and histological diagnoses of all the *in vivo* measurement sites investigated with the endoscopic spectrometer. 297

Table 8-2: Summary of colonic polyps included in the *in vivo* study. 300

Table 8-3: Spectrally averaged fluorescence lifetime shift for neoplastic and non-neoplastic polyps...302

Table 8-4: Mean spectrally averaged fluorescence lifetimes observed in all the tissues investigated in this study. Data are presented for both the UV and blue laser and for both *ex vivo* and *in vivo* measurements. Uncertainties denote one standard deviation from the mean. Where no standard deviation is shown, only one measurement was made. SD = standard deviation; TRE = total relative error. 306

List of Abbreviations

5-ALA	5-aminolaevulinic acid
AF	Autofluorescence
AFI	Autofluorescence imaging
ALA	Aminolaevulinic acid
ATP	Adenosine triphosphate
AUC	Area under the curve
BCC	Basal cell carcinoma
BS	Beam splitter
CCD	Charge-coupled device
CFD	Constant fraction discriminator
CI	Confidence Interval
CW	Continuous wave
Δ	Delta (the symbol for difference)
DA	Discriminant analysis
DALM	dysplasia-associated lesional mass
DAPI	4', 6-diamidino-2-phenylindole
DASPI	2-(p-dimethylaminostyryl)-pyridylmethyl iodide
DMSO	Dimethyl sulphoxide (solvent)
EEM	Excitation emission matrix
ESS	Elastic scattering spectroscopy
F	Female
FAD	Flavin adenine dinucleotide
FAD/$FADH_2$	Oxidised/reduced form of flavin adenine dinucleotide
FLIM	Fluorescence lifetime imaging microscopy
FMN	Flavin mononucleotide
FOV	Field of view

FRET	Förster resonance energy transfer
FWHM	Full width at half maximum
GI	Gastro-intestinal
GOI	Gated optical intensifier
H&E	Haematoxylin and eosin stain
HDE	High definition endoscopy
HFUS	High frequency ultrasound
HP	Hydroxylysyl pyridinoline
IBD	Inflammatory bowel disease
IR	Infrared
IRF	Instrument response function
λ	Lambda (the symbol for wavelength)
LDA	Linear discriminant analysis
LED	Light emitting diode
M	Male
MCE	Magnifying chromoendoscopy
MHz	Megahertz
min	Minute
mm	Millimetres
MPE	Maximum permissible exposure
MPM	Multiphoton microscopy
MPT	Multiphoton tomography
mW	Milliwatts
MW	Molecular weight
NA	Numerical aperture
$NAD(P)^+$	Oxidised form of nicotinamide adenine dinucleotide
NAD(P)H	Reduced form of Nicotinamide adenine dinucleotide phosphate
NBI	Narrow band imaging

ND	Neutral density
NHS	National Health Service
NIR	Near infrared
nm	Nanometers
NMSC	Non-melanoma skin cancer
NREC	National Research Ethics Committee
ns	Nanosecond
μm	Microns
OCT	Optical coherence tomography
PCA	Principal component analysis
PD	Photodiode
PMT	Photomultiplier tube
PpIX	Protoporphyrin IX
ps	picosecond
PSF	Point spread function
REC	Research Ethics Committee
ROI	Region of interest
s	second
SCC	Squamous cell carcinoma
SD	Standard deviation
SHG	Second harmonic generation
SLM	Spatial light modulator
SMF	Single mode fibre
SNR	Signal-to-noise ratio
SPM	Self-phase modulation
SVD	Singular value decomposition
TAC	Time to amplitude converter
TAC	Time-to-amplitude converter

TCSPC	Time correlated single photon counting
TPE	Two photon excitation
UV	Ultraviolet
WLE	White light endoscopy
τ	Tau (the symbol for fluorescence lifetime)

Chapter 1: Thesis outline

Worldwide, gastrointestinal (GI) disease is a common cause of care-seeking and hospital admission, the a common cause of death, and the leading cause of cancer death [1]. It affects people of all ages, gender and ethnic backgrounds and the healthcare burden of GI and liver disease is enormous, with a progressive increase in the incidence and prevalence of most diseases such as colorectal and oesophageal cancers, Barrett's oesophagus, and inflammatory bowel disease. In the United Kingdom, the annual cost to the NHS of GI disease is at least £18.7 billion [2]. This burden will inevitably increase as the population ages and obesity becomes endemic. GI tract diseases comprise a wide spectrum of disorders including inflammation, ulcerations and pre-neoplastic and neoplastic lesions of the oesophagus, stomach, duodenum and colon. Possible causes include: damage due to either acute-life-threatening conditions or recurring injuries that are not immediately life threatening but severely impairing the quality of life; active or chronic immune response and accumulation of genetic mutations and interplay with environmental factors.

GI diseases are usually investigated by close inspection by means of standard white light endoscopy (WLE). However, it is possible that a diagnosis can be missed or delayed because a number of disorders, including early GI cancers, are frequently invisible or difficult to visualise under inspection with WLE. In addition, it is often difficult to distinguish between benign and early or pre-malignant lesions. There is therefore increasing interest in developing techniques to enhance the contrast of diseased tissue regions beyond what is possible with current state-of-the-art endoscopy equipment. This PhD primarily aimed to address this challenge by applying fluorescence lifetime imaging (FLIM) and spectroscopy (FLS) technologies to study diseased tissue with a view to developing new fluorescence lifetime-based tools for clinical endoscopy. Initially, single point FLS instruments could be used to guide biopsies or to undertake “optical biopsy” *in situ* and there is the future prospect of wide-field FLIM endoscopes that could enable rapid imaging of tissue with fields of view of several centimetres with the potential to be used as a label-free red-flag screening technique, alerting clinicians to regions requiring more detailed investigation, i.e. by conventional biopsy or resection.

This thesis begins with a discussion of the pathology of GI disease and describes the current status of GI endoscopy, reviewing recent technological advances in the field including autofluorescence imaging and spectroscopy, confocal laser endomicroscopy and other emerging approaches to minimally-invasive endoscopic detection of disease. It outlines the basic principles of fluorescence measurement and imaging, including of fluorescence lifetime and surveys the experimental work to date applying fluorescence lifetime spectroscopy and imaging

of some of the most common GI diseases. The description of the research undertaken for this thesis then begins with an experimental study of the fluorescence lifetime signatures of *ex vivo* human GI and bladder tissue using confocal FLIM microscopy. This is followed by a discussion of the development of three novel clinically-deployable multispectral fluorescence lifetime endoscopic instruments and their application to *ex vivo* and *in vivo* studies of GI disease.

Chapter 2 provides some background on the anatomy and histopathology of the GI tract for this interdisciplinary PhD thesis. The pathologies of inflammation, dysplasia and cancers of the GI tract are described with the causes of diseases and their effects. Early GI cancers are discussed in more detail, including a summary of the most controversial and divisive issues in endoscopic diagnosis and pathology. An overview of the current state-of-the-art of general endoscopy is then given, along with an introduction to the most recent advances in the field and a review of the pre-clinical and clinical experience with currently available "optical biopsy techniques" such as confocal endomicroscopy. The clinical utility and relevance to clinicians of these emerging techniques and a summary of the current unmet clinical needs in endoscopy are also discussed.

In **chapter 3**, the basic science underlying fluorescence, fluorescence lifetime and autofluorescence of biological tissue are introduced. Then, the optical instrumentation used for the experiments described in this thesis is introduced with a discussion of the challenges faced during this project. A FLIM confocal endoscope with subcellular resolution and a wide-field FLIM endoscopy system recently developed in the Photonics Group for clinical application are described with a discussion of initial results from proof of principle studies and the current limitations of these instruments. A review of published clinical and preclinical experience with autofluorescence spectroscopy and imaging is presented.

Chapter 4 presents the initial results from the first (to the best of the author's knowledge) *ex vivo* study of human GI tissue using confocal FLIM microscopy. This includes a survey of the typical morphological and lifetime characteristics in FL images of different GI tissue sites and states (normal, diseased), for which an *ex vivo* imaging protocol was designed to resect, transport and investigate the various tissue types. It was seen that the fluorescence lifetime of dysplastic or neoplastic samples could be either shorter or longer than that of normal tissue and that, within the same sample, epithelia and connective tissue presented different fluorescence lifetime distributions according to their structural composition. These fluorescence lifetime image data were compared to images from immunohistochemistry assays and selective stains on blocks of selected cases that enhanced the structural contrast of epithelia and connective tissue. Autofluorescence emission spectra were also measured and compared to spectra obtained from pure solutions of analytes using a spectrofluorometer to help determine the most prevalent fluorophores involved in the fluorescence decay signatures.

The confocal FLIM microscope was also applied to image "cold-cut" bladder tissue biopsy samples and these results are presented in **chapter 5**. For this study, imaging following treatment with a photosensitising agent (Hexvix®) instilled into the bladder prior to cystoscopy was undertaken. Fluorescence emission spectra from tissue samples were also compared with pure solutions of protoporphyrin IX. Based on this limited data set, it appears that the mean fluorescence lifetimes of suspected bladder cancer biopsies are consistently longer than those of the healthy biopsies for intra patient comparisons.

Chapter 6 describes the design, construction and clinical application of a compact, clinically deployable single point multispectral FLS fibre-probe system that was implemented for the autofluorescence lifetime measurements undertaken for this thesis. Using a first prototype of this system, a clinical investigation of skin cancer, with an emphasis on basal cell carcinoma (BCC), was conducted *in vivo* before surgical excision of the irradiated region, at Lund University Hospital in Sweden. A statistically significant decrease in the fluorescence lifetime of BCCs compared to neighbouring healthy tissue was observed that was in broad agreement with previous *ex vivo* studies.

In **chapter 7**, the application of a more compact, endoscopically deployable version of the fibre-optic FLS probe system to an *ex vivo* clinical investigation of GI diseases is presented with an emphasis on colonic polyps and inflammatory bowel disease. These measurements were undertaken in the Endoscopy Unit at Charing Cross Hospital where a total of 64 samples were collected from 24 patients undergoing endoscopy. FL measurements were initially performed *ex vivo* immediately following endoscopic biopsy or resection of the investigated lesion. Fluorescence lifetime was seen to provide contrast between normal and diseased tissue in both colonic polyps and inflammatory bowel disease. Furthermore, in the case of neoplastic polyps excited at 435 nm, this contrast was statistically significant. These results suggested that it may be possible to discriminate polyps from normal tissue and IBD using 435 nm excited fluorescence lifetime measurements and IBD from normal tissue and polyps using the fluorescence lifetime measured with 375 nm excitation but more extensive work is required to confirm their clinical utility.

Finally, **chapter 8** presents the application of this newly developed fibre-optic FLS instrument to an *in vivo* clinical trial undertaken in 17 patients undergoing GI endoscopy as part of their clinical investigations at Charing Cross hospital. Initial results found the fluorescence lifetimes of GI tissue measured *in vivo* to be in relatively good agreement with those measured *ex vivo.* Statistically significant differences were found for 375 nm excitation in the spectrally averaged mean fluorescence lifetimes from the three regions of normal colon investigated, with the greatest difference observed between right and left colon. The mean fluorescence lifetimes for

polyps were found to be shorter than those observed in normal tissue for 435 nm excitation - in agreement with the *ex vivo* results – but the lifetime differences between polyps and normal tissue were not significant for either excitation wavelength for this number of samples.

Chapter 9 summarises the key results and experiments from this thesis and presents an overview of the various themes addressed during this PhD. A discussion of the future potential clinical impact of this work is presented together with the plan to extend the *in vivo* measurements using the existing FLS fibre-optic point-probe system to validate the lifetime contrast observed and with a discussion of the prospects to develop a "red flag" FLIM endoscopic imaging modality.

The **appendix** includes a list of the journal publications, book chapters and conference presentations related to the work in the thesis.

Chapter 2: Introduction to the gastrointestinal tract, conventional endoscopy and advanced endoscopic techniques

New developments in endoscopic techniques may soon challenge histology as the diagnostic gold standard. The conceptual paradigm of a "red flag" technique, capable of examining tissue function and morphology in real time to replace conventional biopsies, is taking shape and starting to become a reality. These techniques offer the potential of increased detection rates of high-risk lesions, the ability to target biopsies and resections, reducing need for biopsy, and reducing costs and uncertainty for patients. However, whether they could be useful in clinical practice remains to be seen, and is still under investigation.

The first section of this chapter will introduce some background of essential anatomy and histopathology of the gastrointestinal tract to set the stage for the research conducted in this thesis. Indications for endoscopy and commonly encountered pathology are then briefly presented in the second section. The third section gives a brief general introduction to the standard technique of gastrointestinal endoscopy with a description of the equipment commonly used in the endoscopy suite. The fourth section of the chapter will introduce relevant clinical problems and the most recent advances in the field of endoscopy along with their fundamental principles, as well as their potential roles as tools for the endoscopist. The clinical and preclinical experience for each of these techniques is also briefly reviewed. Finally, a summary of the unmet clinical needs in endoscopy is discussed.

2.1 Anatomy of the gastrointestinal tract

The gastrointestinal tract (figure 2-1) extends from the mouth to the anal canal and most of its elements are housed in the abdomen (the lower third of the oesophagus, stomach, small and large bowel) and suspended by thin folds of elastic tissue (mesenteries) from the dorsal (posterior) abdominal wall and partly from the ventral (anterior) abdominal wall.

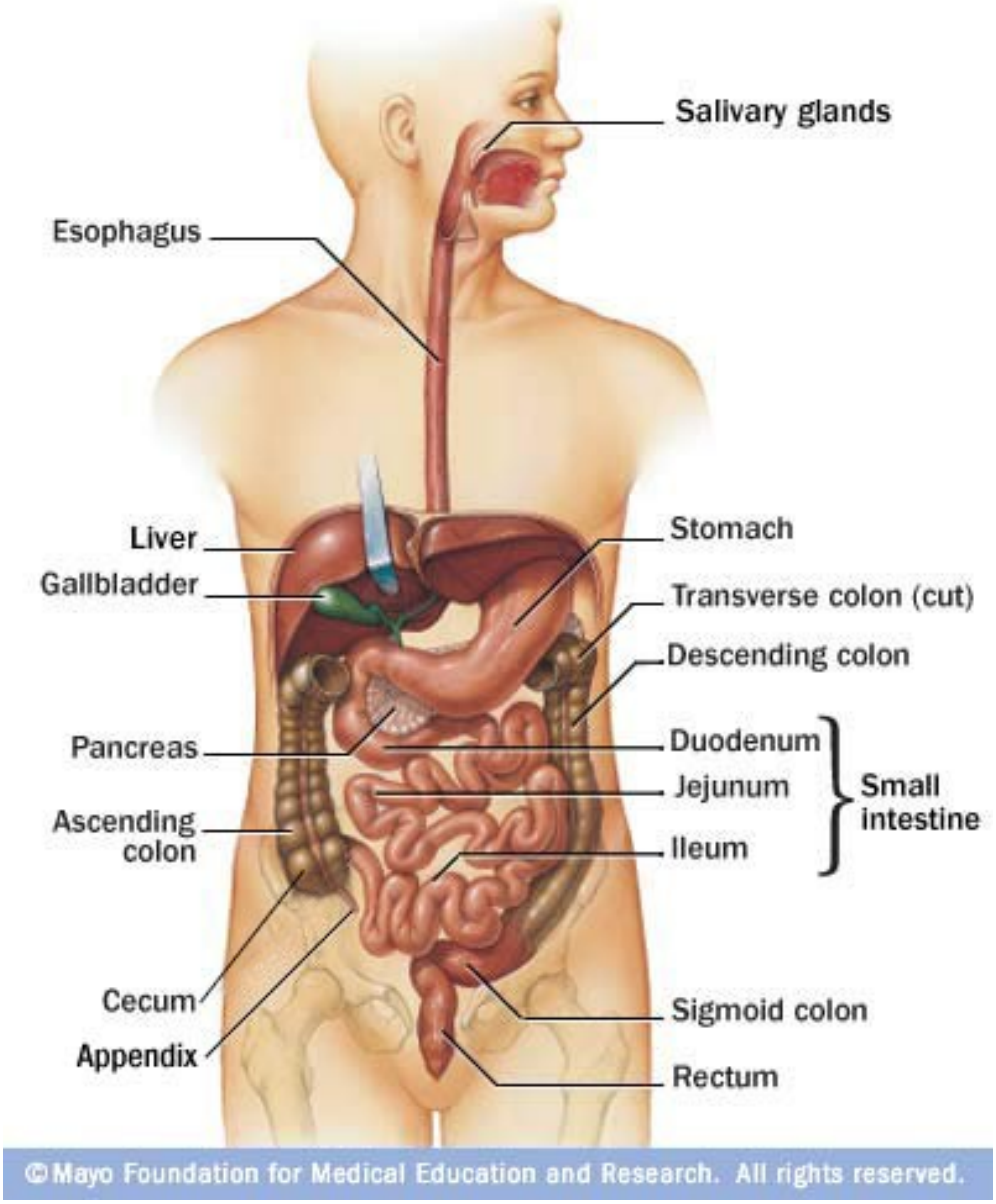


Figure 2-1: The gastrointestinal tract. Source: © 1998-2013 Mayo Foundation for Medical Education and Research [3].

The abdomen is separated from the thorax by the diaphragm, whose ligaments create openings (e.g. hiatus) for a number of structures, including the oesophagus, allowing them to pass through these two regions or posteriorly to them.

The whole GI tract is supplied by three major arteries: the coeliac trunk supplying the foregut, the superior mesenteric artery supplying the midgut, and the inferior mesenteric artery for the hindgut. The inferior vena cava is the major systemic vein draining all the abdominal viscera through the liver (sinusoids and hepatic veins), and returning all deoxygenated blood into the right atrium of the heart. Innervation of the GI tract is provided from the prevertebral plexus containing sympathetic, parasympathetic and visceral sensory fibres.

For more comprehensive and detailed information, the reader is referred to references [4] and [5,6].

Oesophagus

The oesophagus is a 40-cm-long tube (on average), extending from the pharynx to the abdomen, descending through the thorax mainly to the left of the midline and posteriorly to the trachea, and piercing the diaphragmatic hiatus at the level of the 10th thoracic vertebra, anteriorly to the vertebral column. Its upper and middle thirds are located in the mediastinum (thorax), whereas its lower third (about 3 cm) is normally housed in the abdomen. The abdominal oesophagus then becomes continuous with the stomach in a region referred to as the cardia.

Internally, the gastro-oesophageal junction (GOJ) is demarcated by a net transition from squamous oesophageal epithelium to gastric epithelium, called squamocolumnar junction (SCJ), but in some cases this transition may not exactly correspond to the same level of the anatomical junction, but can be found in the lower third of the oesophagus at a variable height above it.

Stomach

The stomach is a J-shaped saccular dilatation of the GI tract between the oesophagus and the duodenum. It is usually located in the left hypochondrium and epigastrium, but it may be variable in size and shape.

The stomach is divided into three regions: fundus, body and antrum. It has an anterior and posterior wall, and a lesser (right) and a greater (left) curvature.

The fundus is the most proximal region, typically located above the level of oesophageal orifice. The body is the widest region, extending from the fundus to the *incisura angularis* (angular notch) along the lesser curvature. The antrum is the distal end of the stomach, extending from the *incisura* to the pylorus (pyloric sphincter), which separates the stomach from the duodenum (small intestine).

The pyloric sphincter is a thickening of the gastric circular muscle layer and regulates the flow of chyme between the stomach and the duodenum.

Small intestine

The small intestine is the longest part of the GI tract (6-7 m) and extends from the pylorus to the ileocaecal valve. It consists of the duodenum, the jejunum, and the ileum.

Duodenum

It is the first part of the small intestine with a C-shaped structure open to the left, sheltering the head of the pancreas on its concave side. The duodenum is about 25 cm long and can be divided in four parts. The superior part, clinically referred as to bulb, is 5 cm long and extends from the

pyloric ring to the neck of the gallbladder. The second part is about 8 cm long and contains both the major duodenal papilla, which is the common outlet for bile and pancreatic juice, and the minor duodenal papilla, which is the orifice for the accessory pancreatic duct. The third part is the longest section (10 cm) and crosses anteriorly the posterior abdominal wall together with the inferior vena cava and the aorta, and posteriorly the superior mesenteric artery and vein. The fourth part (3 cm) turns upwards and ascends the up to the duodenojejunal flexure, where it terminates.

Only the pylorus and the duodenojejunal flexure are surrounded by a fold of peritoneum, the remainder of the duodenum is retroperitoneal and almost immobile. The peritoneal fold suspending the duodenojejunal flexure is often referred to as ligament of Treitz.

Jejunum

The jejunum represents the proximal 2-sixths of the small intestine, and is mostly located in the left quadrants of the abdomen, but parts may extend into the pelvis. Its inner mucosa is peculiarly lined by prominent circular folds (*plicae circulares*), which confer to this section a unique endoscopic appearance.

Ileum

The ileum comprises the distal three-sixths of the small intestine, and is mostly positioned in the right lower quadrant. Compared with the ileum, it has a thinner wall, and no or significantly less plicae circulares. The distal ileum (terminal ileum) opens to the large bowel through two lips protruding into the lumen of the caecum, and this flap constitutes what is commonly referred to as ileocaecal valve. The ileocaecal valve regulates the flux of contents from the small intestine to the colon and prevents reflux of colonic material to the ileum.

Colon

The large intestine is about 1-1.5 m long and extends from the ileocaecal valve to the anus. In a proximal to distal direction, it consists of the caecum (about 8 cm wide and 8 cm long) and appendix (about 8 cm long), ascending colon (15 cm long), transverse colon (about 50 cm long), descending colon (about 30 cm long), sigmoid colon (usually 40 cm long but its length and position are rather variable), rectum (about 18-20 cm long and inferiorly it widens to form the rectal ampulla) and anal canal (about 4 cm long).

The caecum and the appendix are located in the right iliac fossa, from where the large intestine continues upward as ascending colon up to the right flank and the right hypochondrium under the liver. Just below the liver, it bends to the left forming the hepatic flexure and crosses nearly horizontally the abdomen as the transverse colon to the left hypocondrium under the spleen. Just below the spleen, it bends sharply downward forming the splenic flexure, and continues

toward the left flank as the descending colon. Into the left groin, the descending colon enters the pelvic inlet as the sigmoid colon and continues medially on the posterior wall of the pelvis as the rectum. The anal canal is the most terminal part of the large intestine, and lies in the perineum between the anal verge and the rectum above. It turns posteriorly through the pelvic floor and opens at the anal orifice.

Compared to the small intestine, the colon has a large internal diameter. The main characteristics of the large bowel are: the *taeniae coli*, which is a longitudinal muscle organised into three narrow bands, though these are primarily present in the caecum and colon, and less in the rectum; and the *haustra coli*, which are responsible for its sacculated appearance.

The main function of the large bowel is the absorption of fluids and salts from the intestinal contents in order to form solid faeces.

From the caecum to the rectum there is a gradual significant decrease in the inner intestinal circumference. The sigmoid colon has the smallest diameter (2.5 cm when contracted) and therefore the highest intraluminal pressure of any other region of the large bowel. There is also an increase in thickness of the mucosa from the caecum (500 µm) to the rectum (1000 µm). Further on, we will investigate whether regional variations in thickness, diameter and perhaps changes in epithelial and connective tissue composition may have a role in the marked intra- and interpatient variability in autofluorescence and spectral properties of normal colonic tissue.

2.1.1 Histology of the gastrointestinal tract

The wall of the GI tract is composed of three layers: an interior mucous membrane, a muscular layer and an exterior serous layer (figure 2-2).

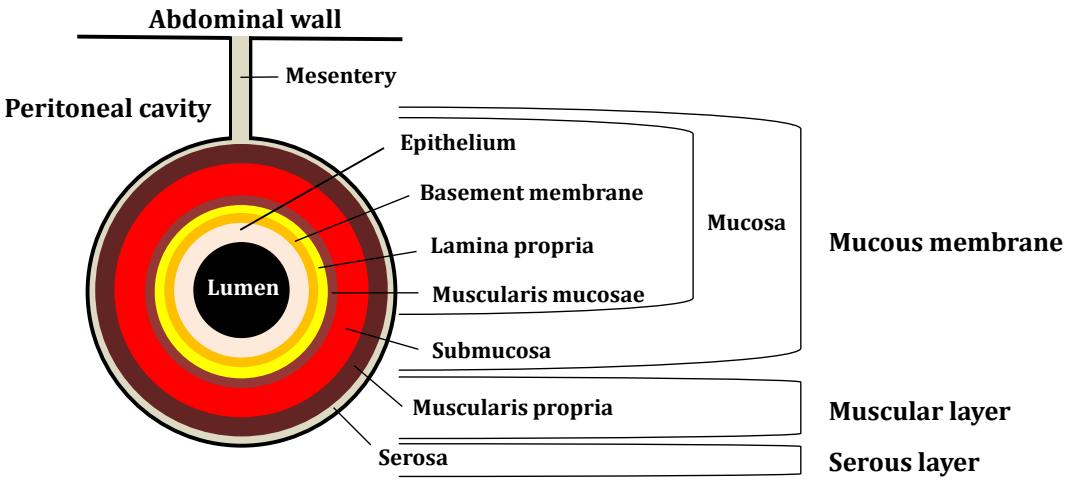


Figure 2-2: Schematic cross-section of the gut. The lumen is the inside space of the gut. The abdominal wall is external to the gut. The peritoneal cavity is a virtual space between the parietal and the visceral peritoneum.

The mucous membrane comprises the mucosa (inner) and the submucosa (outer), divided by the muscularis mucosae, a layer of smooth muscle. The mucosa is lined with columnar epithelium including goblet cells. The invagination of the mucosa creates glandular structures (*cryptae*) and, in the small intestine, finger-like projections (*villi*). The cells of the mucosa primarily produce mucus, digestive enzymes, and hormones.

The mucosa is therefore a mucous tissue lining various tubular structures consisting of epithelium, lamina propria, and a layer of smooth muscle (muscularis mucosae).

The basement membrane is a thin membrane upon which is posed a single layer of cells. The basement membrane is made up of proteins held together by type IV collagen.

The lamina propria is a thin highly vascular layer of connective tissue under the basement membrane lining a layer of epithelium.

A schematic illustration of the mucosal structure, for example in normal colon, in sagittal and transverse section, is shown in figure 2-3.

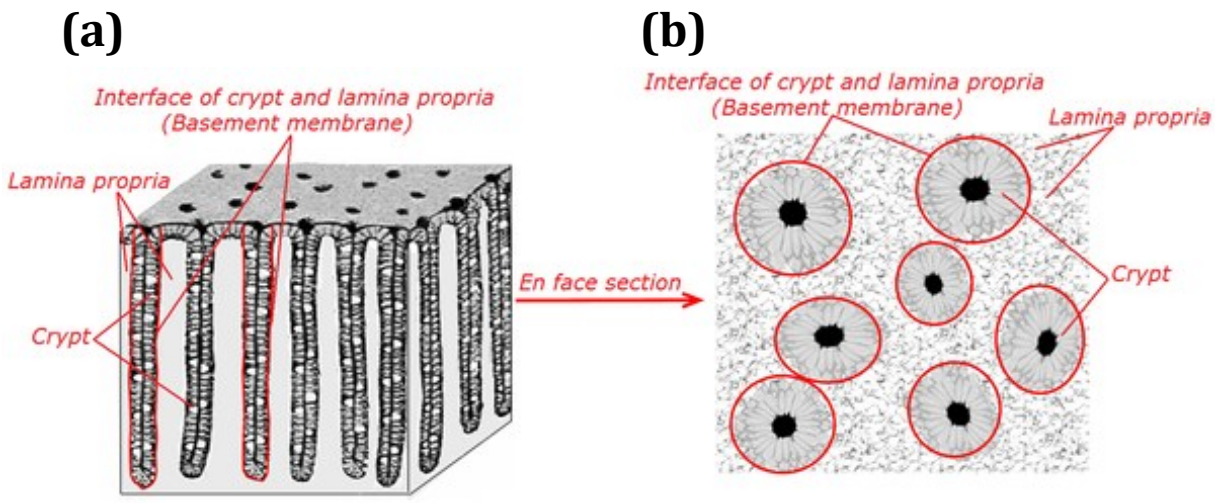


Figure 2-3: Schematic illustration of colonic mucosal structure in sagittal (a) and transverse (b) section, showing the crypts, the basement membrane, and the lamina propria. The crypts consist mainly of columnar epithelial cells and goblet cells. Adapted and reproduced with permission from [7].

The submucosa is a layer of loose connective tissue beneath the mucous membrane. The submucosa consists of loose tissue containing blood vessels and the submucosal nerve plexus.

The muscular layer consists of an inner circular and an outer longitudinal muscle sub-layers. It also contains the myenteric nerve plexus.

The serous coat (serosa) is composed of loose connective tissue lined by a simple flattened squamous epithelium (mesothelium), derived from mesoderm, the middle of the three primary germ layers of the embryo, lying between the ectoderm and endoderm.

Regional variations

The duodenum has large circular folds (valves of Kerckring) projecting into the lumen (figure 2-4).

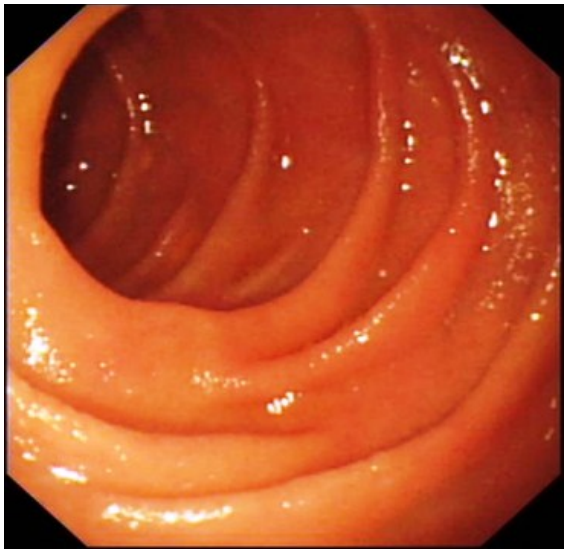


Figure 2-4: Endoscopic image of the second portion of the duodenum, showing the typical valves of Kerckring. Source of acquisition: Drs Coda & Thillainayagam, Endoscopy Unit, Charing Cross Hospital, Imperial College Healthcare NHS Trust.

Unlike the folds in the stomach, they are permanent, and they do not disappear when the lumen is distended.

In contrast with the haustral folds (*haustra coli*) of the large bowel, they are smaller and interspersed more seamlessly between each other, and involve the whole circumference of the bowel.

Also, the duodenum has the mucus Brunner's glands, which peculiarly extend up into the submucosa. Similar submucosal mucous glands are seen in the oesophagus, although in this organ, the ducts draining the mucus to the surface are frequently squamous-lined. Such glands and ducts are not present in any other region of the bowel.

The jejunum and ileum have *villi*, though those of the jejunum appear generally longer and more numerous than those of the ileum. Particularly, in the terminal ileum nodules of aggregated lymphatic tissue (Peyer's patches), can be recognized. Similarly, the mucosa and the submucosa of the appendix contain lymphoid follicles.

Unlike the small intestine, villi are not present in the large intestine. In general, intestinal glands extend from the muscularis mucosae and open to the luminal surface and contain numerous goblet cells. Goblet cells are columnar epithelial cells producing and secreting mucin.

2.1.2 Pathology of the gastrointestinal tract

Depending on the nature and characteristic of the injury, a wide variety of disorders can affect the GI tract. Herein, only some pathologies of relevance to the endoscopist, and more specifically those conditions that have been investigated in this study, are described. Extensive information on this subject can be found in references [8] and [9].

Early GI cancers

Early GI cancers are defined as being limited to the mucosa or submucosa but not invading the muscularis propria, regardless of the presence of lymph node metastases (except oesophagus). The overall incidence of lymph node metastasis in early cancers of the GI tract is extremely low (0-5%)[10,11]. This allows for less invasive endoscopic treatments, thereby improving the quality of life when compared to surgery [12].

Early detection of these cancers is the critical goal for diagnostic endoscopy since it allows endoscopic intervention with disease localised without lymph node involvement and greatly improves patient survival, particularly as new local endoscopic treatment options are available [13,14].

The endoscopic classification of these lesions was first established by the Japanese Gastric Cancer Association (JCGA) [15]. It was then ratified in 2002 at an international consensus meeting in Paris [16] and has now been accepted worldwide (see table 2-1) [17]. The lesions are divided into three main groups: protruding, flat (non-protruding and non-excavated), and excavated.

The lesion height is measured in comparison with the height of the closed jaws of the biopsy forceps (2.5 mm) above the surrounding mucosa. Lesions protruding > 2.5 mm above the level of the closed jaws of the biopsy forceps (i.e. 3 mm) are classified as protruding, whereas those protruding below this level (i.e. 2 mm or lower) are classified as flat. Lesion morphology assists with evaluating the risk of invasive disease and guides the approach to the type of resection required (e.g. endoscopic or surgical) [18].

Classification	Grade
Protruding	
• Pedunculated	0-Ip
• Sessile	0-Is
Non-protruding and non-excavated	
• Slightly elevated	0-IIa
• Completely flat	0-IIb
• Slightly depressed	0-IIc
• Elevated and depressed types	0-IIc + IIa
Excavated	
• Ulcer	0-III
• Excavated and depressed types	0-IIc + III or 0-III + IIc

Table 2-1: The Paris endoscopic classification of superficial neoplastic lesions in the GI tract.

In figure 2-5, the diverse endoscopic appearance of early gastric cancer is classified according to the Paris endoscopic classification.

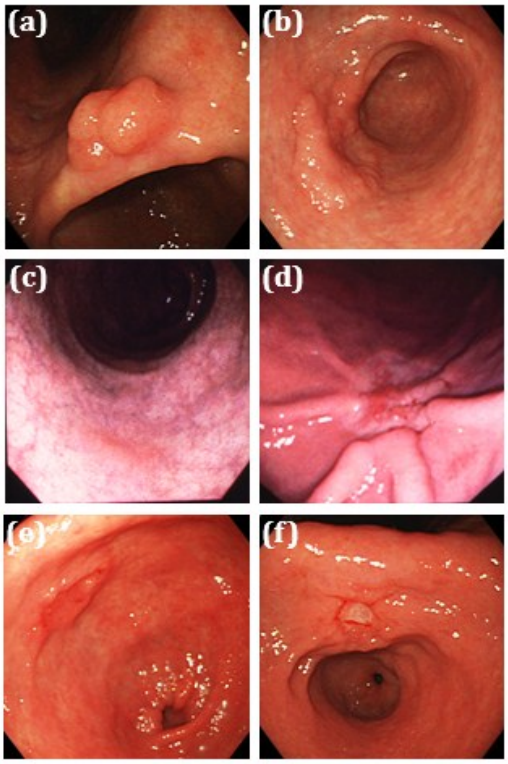


Figure 2-5: Endoscopic appearance of early gastric cancer: (a) 0-I, Protruded type; (b) 0-IIa, superficial elevated type; (c) 0-IIb, flat type; (d), 0-IIc, superficial depressed type; (e) 0-IIa+IIc, combined type (superficial elevation with depression); (f) 0-IIc+III, combined type (superficial depression with ulceration). Images provided courtesy of Dr Takuji Gotoda, Endoscopy Unit, National Cancer Center Hospital, Tokyo, Japan.

Usually, early cancers are detected as 0-I and 0-III types in most of the world, but widespread use of newer imaging methods have enabled identification of superficial lesions such as faint mucosal irregularity or discoloration, which had been previously overlooked. Over 50% of cancers diagnosed in Japan are early cancers while its frequency is only 10% in the West [19].

Apart from the diagnostic difficulty of biopsy as a reason for the low incidence of early GI cancer in the West, different histological criteria between the West and Japan would be another reason. For example, in the context of early gastric cancer, most mucosal cancer of intestinal type in Japan is not diagnosed as cancer in the West, but classified as dysplasia (figure 2-6) [13].

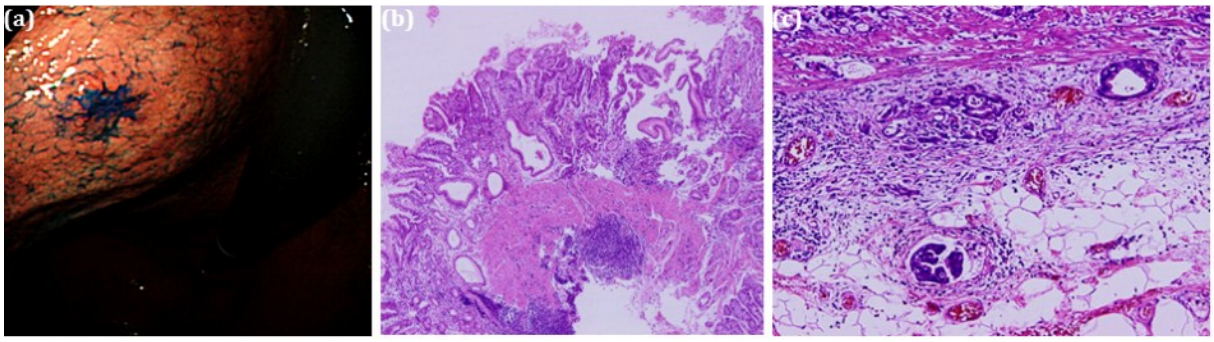


Figure 2-6: Controversies in diagnosing early gastric cancer: (a) a small depressed lesion is noticed on the posterior wall of the upper gastric body after contrast chromoscopy with indigo carmine dye solution; (b) lesion without invasive finding is noticed on the biopsy, which is classified as dysplasia (Vienna classification category 4.1.) by Western pathologists. In contrast, this lesion is classified as well differentiated adenocarcinoma (Vienna classification 4.2.) in Japan. (c) After the resection, submucosal invasive adenocarcinoma with lymphatic involvement (Vienna classification 5.2.) is found. Reproduced with permission from [13].

There are large discrepancies in the diagnostic criterion between the Western and Japanese pathologist. These differences have caused considerable problems in the interpretation of Japanese cancer research by Western clinicians and researchers.

Carcinoma is defined as invasion into the submucosal layer, muscularis mucosa, or at least lamina propria in the West. However, in Japan, cellular atypia and structural atypia is also considered as GI neoplasia regardless of invasive findings.

The Vienna classification (table 2-2) has been introduced in 1998 to develop common worldwide terminology for GI epithelial neoplasia and resolve these discrepancies [20,21].

The lesions are divided into five categories. Non-invasive neoplasia includes low and high-grade dysplasia (LGD and HGD) in which the basement membrane is not infiltrated. Invasive lesions include intramucosal neoplasia infiltrating the submucosa.

Category	Treatment
1. Negative for neoplasia/dysplasia	No treatment
2. Indefinite for neoplasia/dysplasia	Follow-up
3. Non-invasive low grade neoplasia (low grade adenoma/dysplasia)	Follow-up
4. Non-invasive high grade neoplasia	Endoscopic resection, surgery
4.1 High grade adenoma	
4.2 Non-invasive carcinoma (carcinoma in situ)	
4.3 Suspicion of invasive carcinoma	
5. Invasive neoplasia	Surgery (recently ESD)
5.1 Intramucosal carcinoma	
5.2 Submucosal carcinoma or beyond	

Table 2-2: The Vienna Classification of GI epithelial neoplasia. ESD = endoscopic submucosal dissection.

However, the practical application of this classification has been problematic because the judgment of invasion beyond the basement membrane is often difficult to define. Modified criteria based on objective molecular analysis, such as DNA aneuploidy, have been proposed [22].

To quantify the risk of lymph node metastases, mucosal (m) and submucosal (sm) layers have each been divided into three sections: m1 (epithelium), m2 (lamina propria), and m3 (muscularis mucosae) and sm1, sm2, and sm3. In addition, sm1 is subclassified into a, b, and c according to the degree of horizontal extension (figure 2-7).

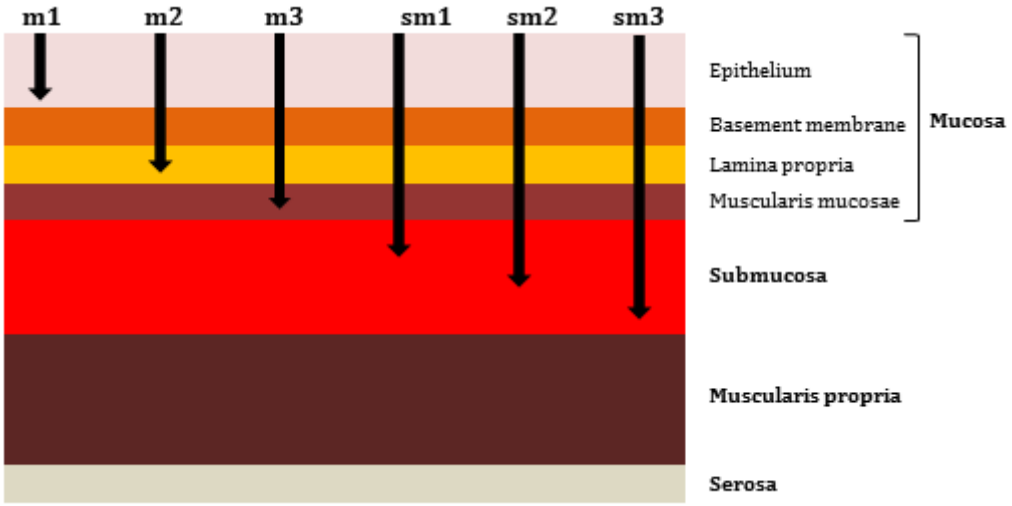


Figure 2-7: Pathological classification of early GI cancers according to depth of invasion: m1, confined to the epithelium; m2, invasion to the lamina propria; m3, infiltration of the muscularis mucosa; sm1, up to the upper third of the submucosa; sm2, to the mid third; and sm3, to the lower third of the submucosa.

It is the depth that mainly determines the necessity of intervention. The depth of invasion is measured microscopically from histology sections and the risk of lymph node metastasis is known to be related with a defined micrometric cut-off.

In squamous cell carcinoma (SCC) of the oesophagus, when infiltration is less than 200 µm, the risk of nodal metastases is low [23]. For early oesophageal adenocarcinoma and early gastric cancer (EGC), a submucosal infiltration micrometric cut-off of 500 µm has been proposed [24]. In the colon, the risk of lymph node metastasis is negligible when the tumour invasion is less than 1000 µm [25].

Endoscopic mucosal resection is now accepted worldwide as a first line treatment modality for early cancers of the GI tract [13]. Endoscopic Submucosal Dissection (ESD) is a new and more radical treatment for EGICs providing high rates of en bloc resection and low rate of recurrence compared with conventional endoscopic mucosal resection (EMR) [26]. This method facilitates one piece resection even in patients with large or ulcerative lesions.

The key steps of the ESD procedure for stomach and colon are shown in figure 2-8, figure 2-9, and [27].

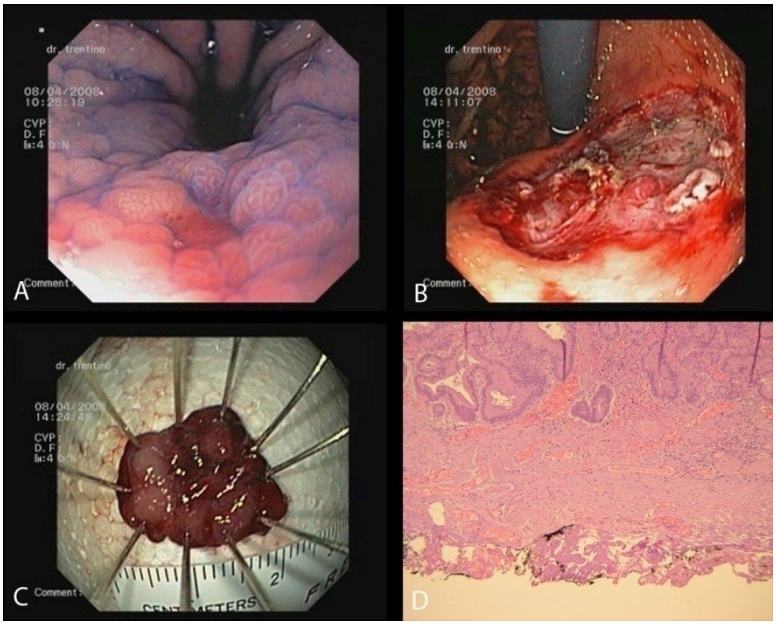


Figure 2-8: (a) early gastric cancer (0-IIa+IIc type, 15 mm) of the fundus, along the lesser curvature just below the cardia, after staining with indigo-carmine. (b) Residual ulcer after ESD. (c) En bloc excised lesion fixed orientated on a board for histopathological assessment. (d) Well differentiated (G1) intramucosal ADC of intestinal type, vertical margins free of tumour (H&E, 20x original magnification). Reproduced with permission from [26].

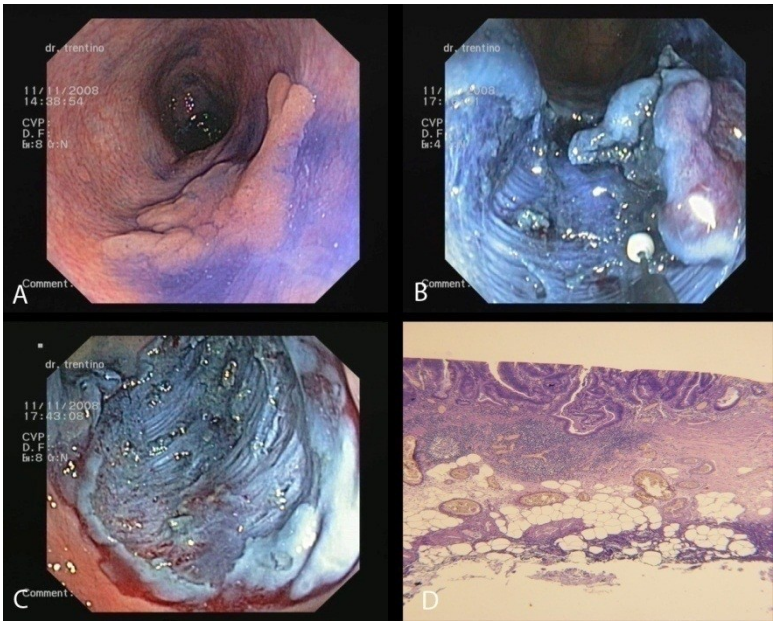


Figure 2-9: (a) laterally spreading tumour (non-granular type, 40 mm) of the sigmoid colon. (b) ESD of the submucosal layer by It-knife. (c) Residual mucosal defect immediately after ESD. (d) Well differentiated (G1) ADC. The lesion is largely intramucosal, with focal infiltration of the muscularis mucosae (H&E, 10x original magnification). Reproduced with permission from [26].

Reflux oesophagitis

The oesophagus is lined by a stratified squamous epithelium, whose function is essentially to make it resistant to a variety of irritants, including acids and alkalis. Secretion of mucin and bicarbonate by submucosal glands also concurs to protect its mucosal lining. A high pressure area at the distal end, referred to as lower oesophageal sphincter, prevents reflux of gastric content into the oesophageal lumen. Conditions that alter these defence mechanisms, can predispose to and cause gastro-oesophageal reflux disease (GORD) and reflux oesophagitis.

Endoscopic features of GORD are erythema, friability, longitudinal erosions and ulceration, usually located on the top of the oesophageal folds.

The Los Angeles classification, the most commonly used endoscopic classification of the reflux oesophagitis is illustrated in figure 2-10 [28,29].

The term mucosal break is introduced to encompass the old terms erosion and ulceration.

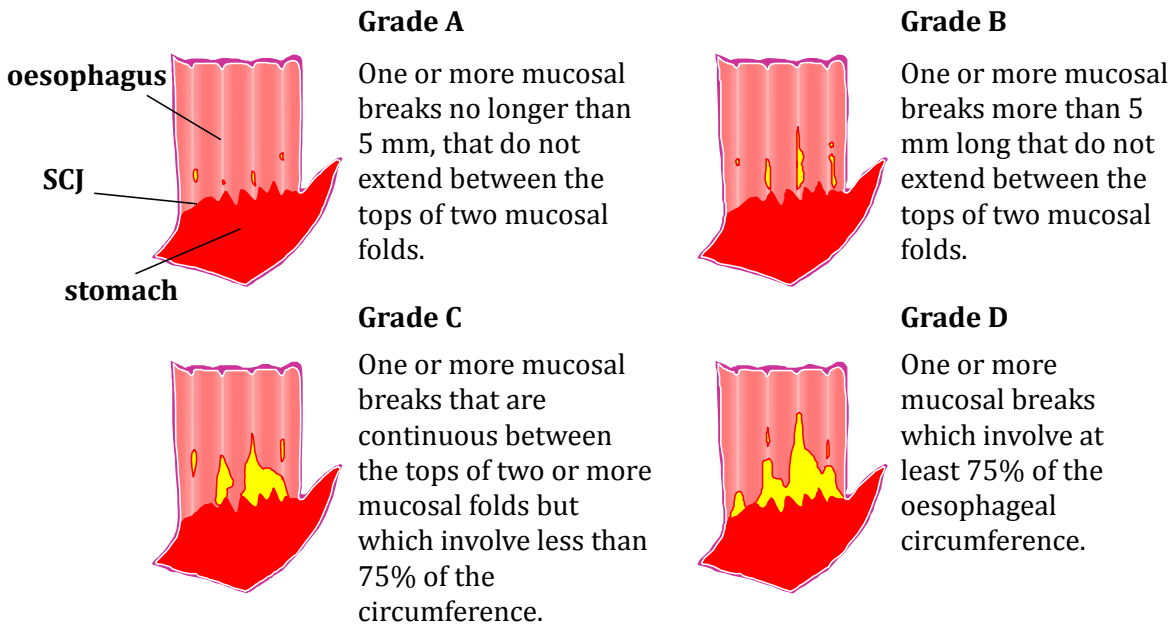


Figure 2-10: The Los Angeles classification for reflux oesophagitis. The diagram shows a sagittal section through the gastro-oesophageal region (oesophageal mucosa in pink, gastric mucosa in red). The mucosal breaks are shown in yellow. SCJ = squamocolumnar junction. Adapted and reproduced with permission from [29,30].

Hyperaemia, intraepithelial infiltrates of eosinophils and neutrophils, and basal layer hyperplasia, are common findings. Complications of reflux oesophagitis include ulceration, strictures and Barrett oesophagus.

Barrett's oesophagus

Barrett's oesophagus (BO) is a condition in which squamous mucosa is replaced by columnar epithelium as a result of chronic gastric (and probably duodenal) content reflux. This replacement is referred to as intestinal metaplasia, histologically defined as the presence of "goblet cells".

The conventional endoscopic view, before and after the spray of an absorptive dye (methylene blue), followed by optical magnification with a zoom endoscope (110 to 150x, Olympus GIFQ160Z), and the histological characteristics of BO are shown in figure 2-11.

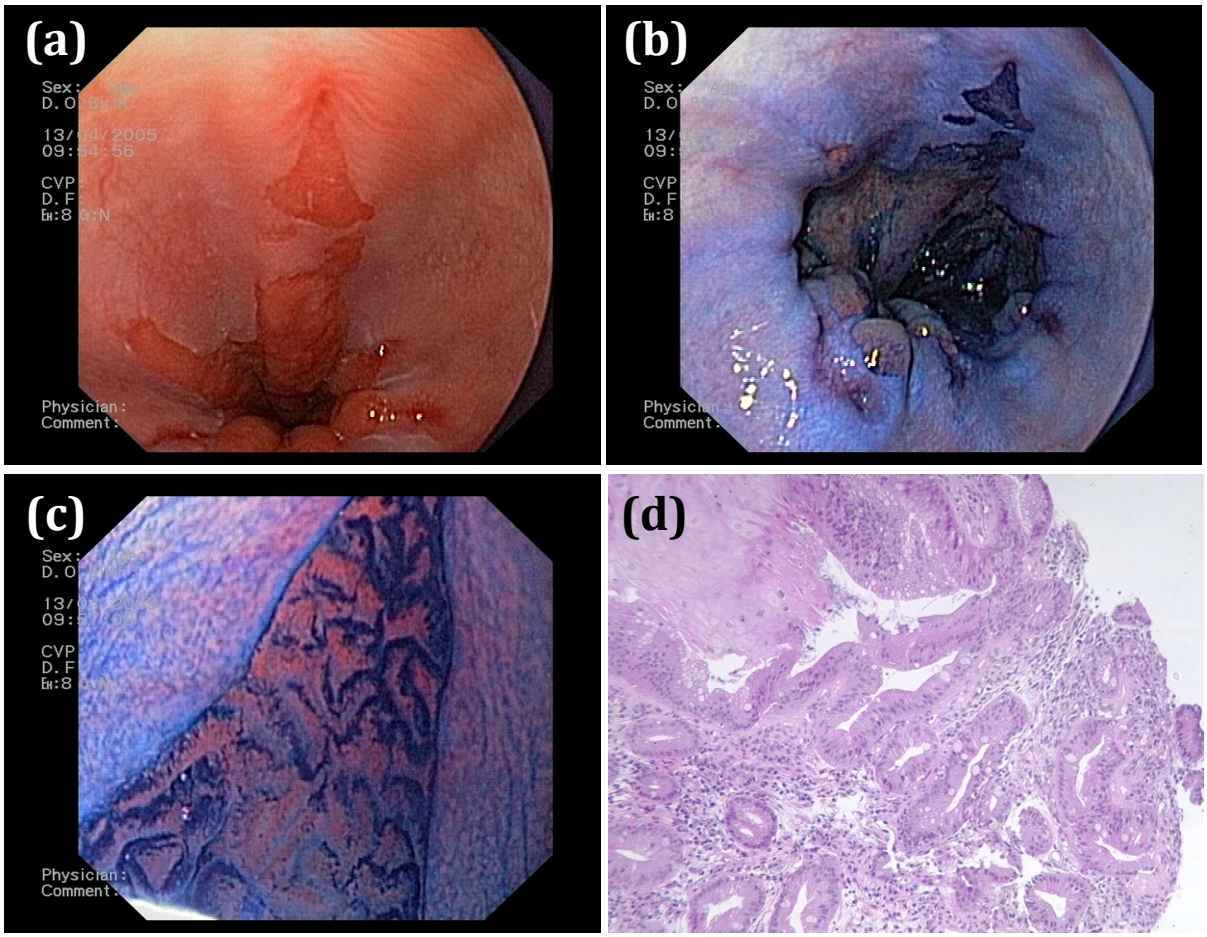


Figure 2-11: (a) Conventional endoscopic view of BO with concomitant esophagitis. (b) Positive staining of Barrett's epithelium after absorption chromoscopy with methylene blue dye solution. (c) Villous cerebroid pits with finger-like projections seen with magnification endoscopy. (d) Histological section of (c) showing intestinal metaplasia with adjacent round and elongated glands, and numerous goblet cells. Adapted from [31].

Barrett's oesophagus is associated with an increased risk of oesophageal adenocarcinoma, particularly when dysplasia arises within its epithelium. To date, dysplasia can be detected only histologically. Therefore, when BO is identified, a protocol consisting of 4 quadrant biopsies every 1 to 2 cm (figure 2-12) with biopsies of mucosal abnormalities are taken above the level of the lower oesophageal sphincter. Although it has never been validated, this protocol is currently the standard method for detecting dysplasia in patients with BO.

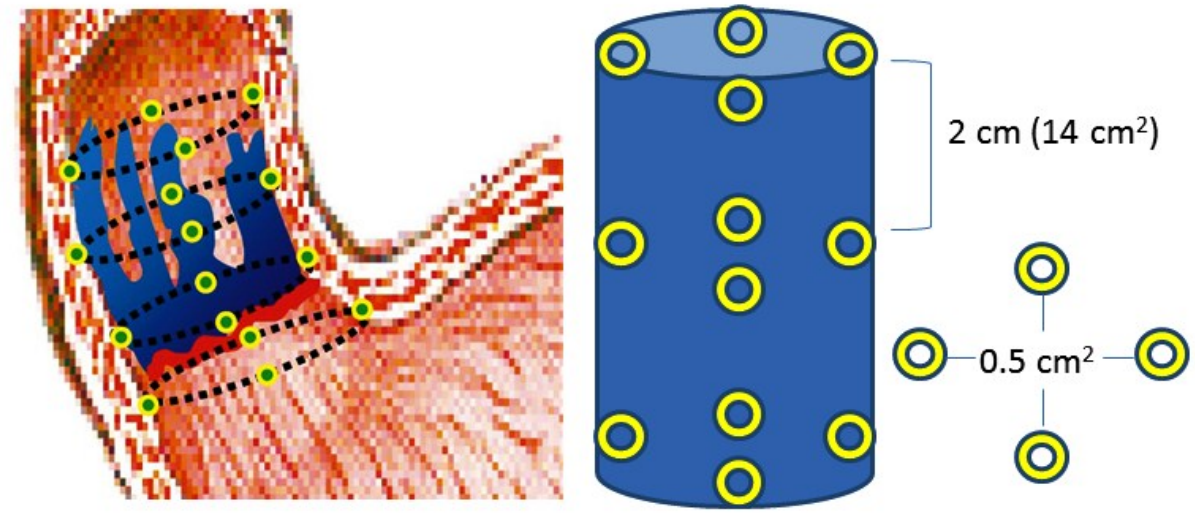


Figure 2-12: The Seattle biopsy protocol for detection of dysplasia in Barrett's oesophagus. Adapted and reproduced with permission from [32].

However, since each 2 cm segment has an average mucosal area of 14 cm^2, and the total mucosal surface obtained by 4 biopsies is no more than 0.5 cm^2, it is clear that only a small fraction of the Barrett's segment (less than 3.5% of the total surface of a 2-cm-long segment) is sampled, therefore dysplasia can easily go undetected [32]. *A fortiori*, many patients with BO without dysplasia (low risk of progression to ADC) clearly undergo unnecessary biopsies.

Standard videoendoscopy identifies BO and visible mucosal abnormalities (e.g. nodules, depressed areas) but cannot distinguish intestinal metaplasia from dysplasia. This underscores the need for novel imaging techniques that may help target areas of dysplasia, thus assisting in the early diagnosis of dysplasia and cancer and allow for their timely treatment.

BO can be circumferential or appear in the form of one or multiple tongues or patches or isles of red velvet coloured mucosa extending from the gastro-oesophageal junction. Depending on the length of the columnar segment involved (< or >3 cm) it is subdivided into short or long BO.

The endoscopic classification of Barrett's oesophagus is illustrated in figure 2-13. This classification was named the "Prague C & M classification" because it was first presented at an open meeting at the Prague September 2004 United European Gastroenterology Week.

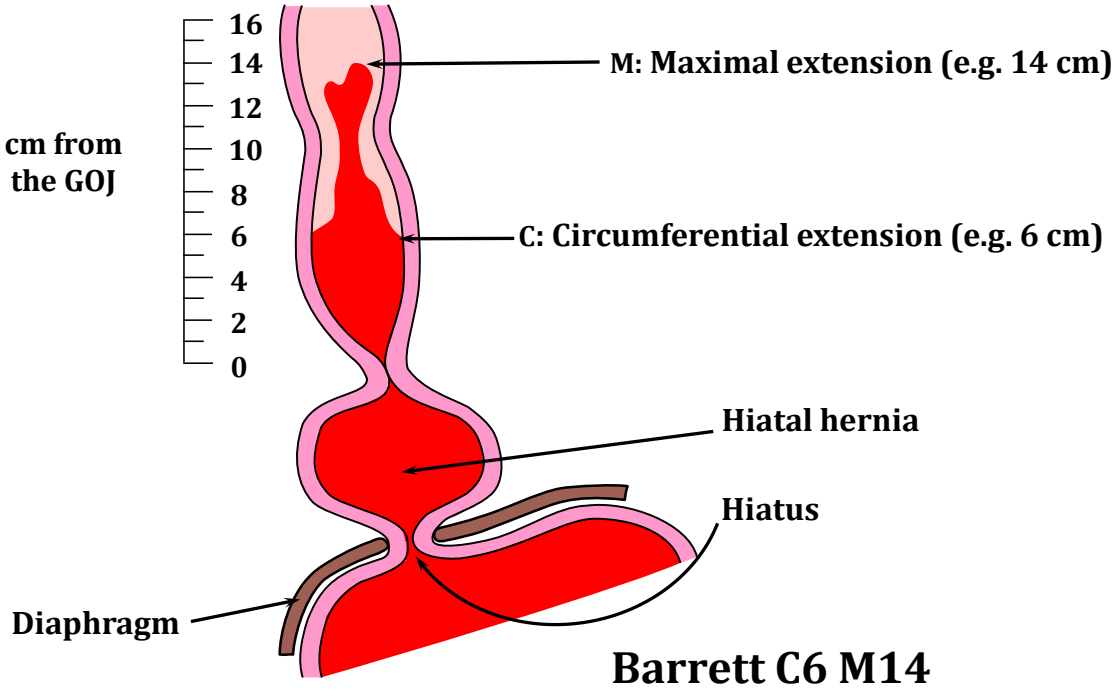


Figure 2-13: Diagrammatic representation of endoscopic Barrett's oesophagus showing an area classified as C6M14. C = extension of circumferential metaplasia; M = maximal extent of the metaplasia; GOJ = gastro-oesophageal junction. Adapted from and reproduced with permission from [33].

Goblet cells are essential for the diagnosis of BO. Their distinct mucus vacuoles confer to these cells the characteristic appearance of wine goblets. Foveolar mucus cells are insufficient for the diagnosis.

Increased epithelial proliferation, atypical mitoses, and hyperchromatic nuclei, irregular distribution of chromatin, high nucleus-cytoplasm ratio can be observed in both low (LGD) and high grade dysplasia (HGD). Gland architecture is subverted, showing irregular gland shapes, abnormal cellular and nuclear orientation and crowed clusters of cells (e.g. gland-within-gland). In HGD, both cytological and morphological changes appear more severe. Intramucosal carcinoma is defined by the invasion of neoplastic cells into the lamina propria but still within the muscularis mucosae.

Oesophageal cancers

Cancers of the oesophagus, despite the recent advances in diagnosis and treatment, remain a highly lethal malignancy that increased dramatically in incidence during the last 3 decades, and this is particularly true for the adenocarcinoma [34].

Two main types of oesophageal cancer exist: adenocarcinoma and squamous cell carcinoma.

Adenocarcinoma of the oesophagus

Adenocarcinoma typically originates within a segment of Barrett's oesophagus, through progression to dysplasia, and is often associated with long-standing GORD. It usually involves the lower third of the oesophagus and may extend to the gastric cardia and fundus.

Initially, it may appear as a small nodule or a flat or raised or depressed dyschromic area in the context of intact columnar epithelium. Exophytic masses up to 5 cm can then develop over the years, or alternatively infiltrate diffusely the oesophageal wall or assume the appearance of a large ulceration. BO is frequently present in and around the tumour.

Intestinal type morphology is commonly seen, with crowded back-to-back glands producing abundant mucin.

Squamous cell carcinoma of the oesophagus

Squamous cell carcinomas (SCC) usually affect the middle third of the oesophagus, and originate from small areas of squamous dysplasia. Early lesions appear as grey-whitish plaques or thickenings. Advanced forms of SCC may appear as polypoid or either infiltrative or ulcerated lesions, often causing strictures of the lumen and invading external surrounding organs (e.g. trachea, mediastinum, etc.).

Histologically, nests of malignant cells reproduce the architecture of a squamous epithelium.

Adenocarcinoma of the stomach

Gastric adenocarcinoma can be classified in two variants, intestinal and diffuse. Cancers of intestinal type tend to present as bulky exophytic masses composed of irregular glands (figure 2-14), while the diffuse type usually shows an infiltrative tendency, with typical signet-ring cells and scant glandular structure.

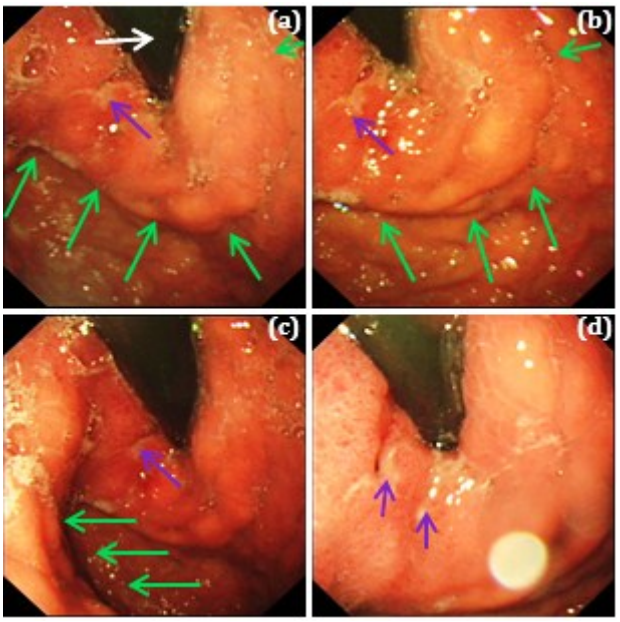


Figure 2-14: Retrograde endoscopic view of a gastric cancer involving the cardia and the gastric fundus. In retroflexion, the image is inverted and the endoscope appears at the top of the figures (white arrow in (a)). The luminal extension of the neoplastic infiltration is indicated by the green arrows in (a, b) and (c). Long, deep ulcerations in the context of the cancer are visible (purple arrows). Source of acquisition: Drs Coda & Thillainayagam, Endoscopy Unit, Charing Cross Hospital, Imperial College Healthcare NHS Trust.

Most gastric cancers arise from the gastric antrum, along the lesser curvature. Neoplastic cells in the intestinal type have mucin filled vacuoles, and abundant mucin is present in gland lumina. On contrary, diffuse type neoplastic cells tend to infiltrate the mucosa either individually or in scattered clusters, do not form glands and have large mucin vacuoles pushing the nuclei to the base, giving the appearance of signet ring cells.

Diffuse type gastric cancer may elicit a strong desmoplastic reaction that thickens and stiffens the wall creating leather bottle morphology, referred to as *linitis plastica* (figure 2-15).

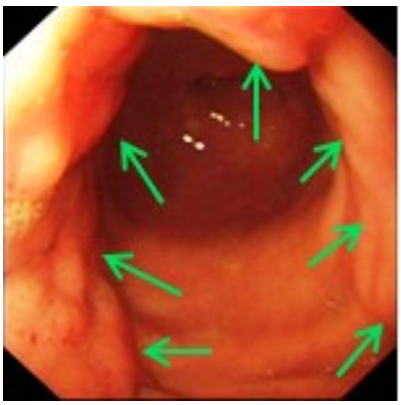


Figure 2-15: Anterograde endoscopic view of a diffuse type gastric cancer infiltrating circumferentially the gastric body. The green arrows indicate the motionless thickening and stiffening of the gastric wall creating the so called leather bottle appearance, *linitis plastica*. Source of acquisition: Drs Coda & Thillainayagam, Endoscopy Unit, Charing Cross Hospital, Imperial College Healthcare NHS Trust.

Inflammatory bowel disease

Inflammatory bowel disease (IBD) is an idiopathic condition characterised by chronic or recurring immune response and inflammation of the GI tract. IBD comprises Crohn's disease (CD) and ulcerative colitis (UC), which can be distinguished on the basis of disease morphology and distribution of the regions usually involved. CD can affect any part of the GI tract from the mouth to the anal canal, whereas UC usually affects only the colon, and in most cases only the rectum is involved, extending up to the splenic flexure at the most. In addition, the inflammation in CD may extend into the full thickness of the wall of the segment affected, while in UC it only involves the mucosa and the submucosa.

Dysplasia and malignant transformation represent the most important complication of these diseases and the risk begins to rise at 8-10 years after onset. The risk of cancer is influenced by the duration and extent of disease and is also linked to the endoscopic appearance at colonoscopy [35-37]. At present, annual endoscopic surveillance is recommended after 8-10 years of disease.

In patients with UC, if no lesions are observed, four biopsy specimens are taken randomly at every 10 cm between the rectum and the caecum for a total of 40-50 biopsies per colonoscopy [38].

However, even this massive sampling examines less than 1% of the total colonic mucosa surface. Thus, there is a strong interest in developing novel techniques that may be able to guide targeted biopsies and assist in discriminating between normal and dysplastic areas.

Collagenous colitis and lymphocytic colitis are two other types of bowel inflammation that affect the colon. Collagenous colitis and lymphocytic colitis are also collectively called microscopic colitis and are not related to CD or UC. In microscopic colitis there is no sign of inflammation on the surface of the colon visible during the endoscopic examination, therefore a biopsy is necessary to make a diagnosis. Microscopic colitis does not increase the risk of colon cancer.

Crohn's disease

The most common regions of the GI tract affected by Crohn's disease are the terminal ileum (40% of cases), the ileocaecal valve and the caecum. The presence of aphthous ulcers, which may progress and become serpiginous, and skip lesions (clear-cut delineated areas of disease) is characteristic of CD. Strictures can occur as a result of transmural inflammation. Linear ulcers may develop and extend deeply to become fistulae.

Crypts are damaged by intense infiltration of neutrophils (crypt abscesses). Crypt architecture appears distorted as a consequence of relapsing destruction and regeneration attempts to

restore the damaged glands. Changes such as pseudo-pyloric metaplasia, Paneth cell metaplasia, and non-caseating granulomas are frequently observed in CD.

Ulcerative colitis

Ulcerative colitis almost always begins in the rectum and extends proximally into the colon in a contiguous manner (figure 2-16). Based on the amount of colorectal involved, three types of disease distribution are recognized; (1) ulcerative proctitis; (2) left-sided colitis; (3) pancolitis.

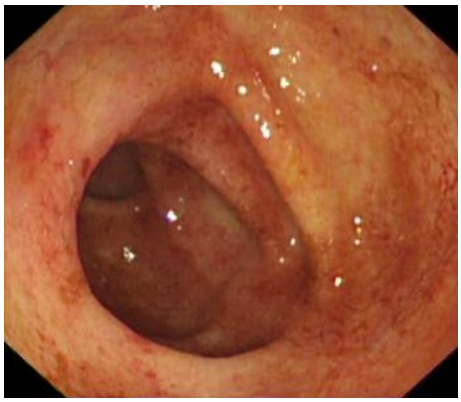


Figure 2-16: Endoscopic image of ulcerative colitis. Source of acquisition: Drs Coda & Thillainayagam, Endoscopy Unit, Charing Cross Hospital, Imperial College Healthcare NHS Trust.

The affected mucosa appears erythematous, friable, and granular, with broad-based superficial ulcers that can merge into larger ulcerations. Regenerating mucosa can protrude into the lumen forming mucosal elevations such as pseudopolyps or mucosal bridges.

As with CD, neutrophil infiltration, crypt abscesses, architectural distortion, and epithelial metaplasia are frequently observed in UC, though the inflammation generally tends to be more uniform, diffuse and limited to the mucosa.

Polyps

The entire GI tract can be affected by polyps but they are most common in the colon. Polyps are overgrown areas of mucosal epithelium that carry a risk of becoming malignant.

Polyps may take various sizes and shapes (sessile, pedunculated, and flat) and are normally classified into 2 groups: neoplastic (consisting of adenomas with low grade or high grade dysplasia, and carcinomas) and non-neoplastic (hyperplastic, inflammatory pseudopolyps, hamartomas). Neoplastic polyps are of greatest clinical significance because of their established role in the stepwise process that results in colorectal cancer (adenoma-carcinoma sequence) [39]. However, macroscopic discrimination between neoplastic and non-neoplastic polyps during endoscopy is extremely difficult; thus, they are all removed when detected.

It is ascertained that the majority of colorectal carcinomas pass through a premalignant adenoma phase, termed adenoma-carcinoma sequence (figure 2-17(a)) [39,40].

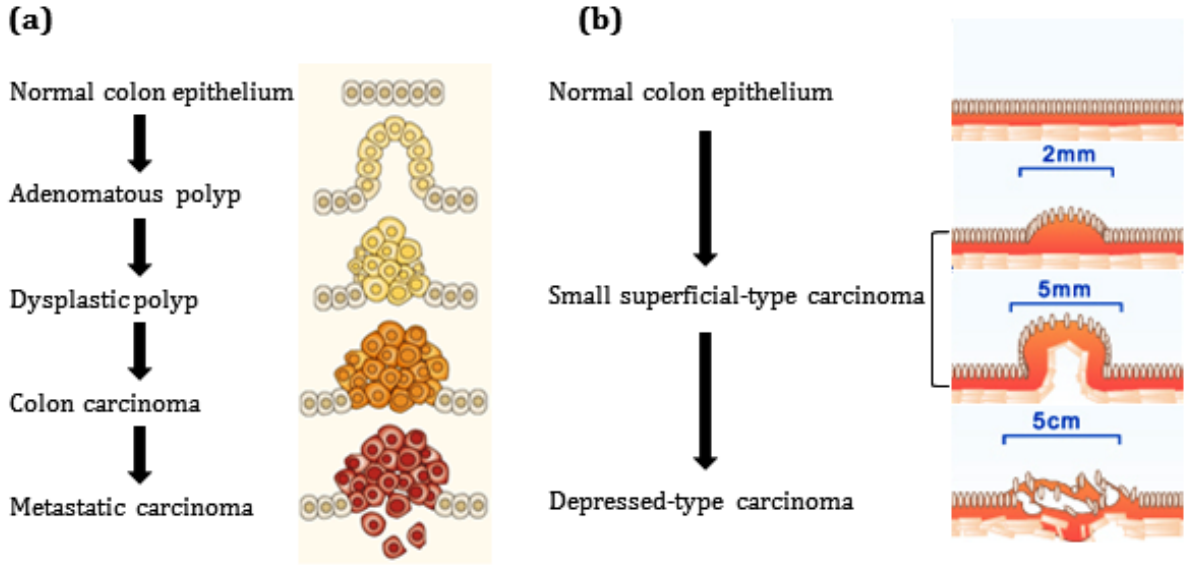


Figure 2-17: (a) the adenoma-carcinoma sequence in colorectal cancer. (b) The *de novo* colorectal cancer pathway. Adapted and reproduced with permission from [41,42].

Adenomas originate as diminutive polyps; as they grow and increase in size they can then assume either the form of a sessile or pedunculated polyp and a tubular or villous microscopic architecture. Adenomatous change is referred to as LGD. Low-grade dysplastic adenomas that progress toward cancer develop high-grade dysplasia.

However, only two thirds of colorectal cancer seems to develop through the stage of adenoma, the other third may develop *de novo* from normal epithelium (figure 2-17(b))[43,44]. The different clinico-pathological features of flat polyps, compared to sessile and pedunculated polyps, may explain the proportion of *de novo* carcinomas.

Flat polyps are prevalently located in the right colon and their prevalence increases with age. Early recognition of these polyps is important due to the greater incidence of high grade dysplasia and carcinoma compared to sessile and pedunculated polyps (8-61% in Japan, 12-4% in Western Countries) [45].

Flat and depressed lesions larger than 10 mm in diameter, are almost twice as likely as protruded lesions, of similar size, to contains areas of severe dysplasia or foci of invasive carcinoma [46]. Similarly, the incidence of flat type early cancer increases with age, has a higher frequency in right colon, has smaller size than polypoid type early cancer and has lower frequency of adenomatous component [45].

Inflammatory polyps

Inflammatory polyps may form as a result of recurrent abrasion and ulceration followed by intervening healing periods.

Hyperplasia of the epithelium and of the lamina propria, mixed inflammatory infiltrates, and erosion are the most distinctive histological features.

Hamartomatous polyps

Hamartomatous polyps usually occur in the context of the following diseases: Juvenile polyposis; Peutz-Jeghers syndrome; Cowden and Ruvalcaba-Ryley syndromes; and Cronkhite-Canada syndrome.

Juvenile polyps are typically red and pedunculated, with cystic dilatation of glands.

The hamartomatous polyps of Peutz-Jeghers syndrome are large and pedunculated with a lobulated structure. Arborizing network of connective tissue is a histological hallmark of these polyps.

Hyperplastic polyps

Hyperplastic polyps are common epithelial protrusions found most frequently in the rectum and left colon, and are typically small in diameter (about 5 mm).

They are essentially made of piled up goblet cells creating a serrated surface architecture- when seen in cross-section- that is characteristic of these polyps.

It is appreciated that these lesions have no malignant potential, but it is important to distinguish them from sessile serrated adenomas, which conversely can carry a risk of becoming malignant.

Adenomatous polyps

Colonic adenomas are characterised by the presence of epithelial dysplasia. These polyps are precursors to colorectal cancer. They range from about 3 mm to 15 cm and can be sessile, pedunculated, and flat (figure 2-18).

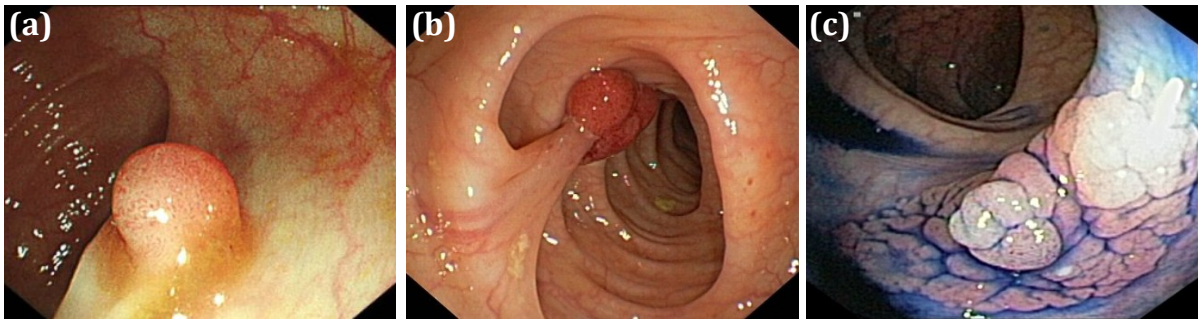


Figure 2-18: Endoscopic images of a sessile (a), pedunculated (b) and a flat (c) polyp. The true extension of the flat polyp (c) is revealed by chromoscopy with indigo carmine dye solution. Source of acquisition: Drs Coda & Thillainayagam, Endoscopy Unit, Charing Cross Hospital, Imperial College Healthcare NHS Trust.

The histological hallmark of dysplasia is the presence of hyperchromatic, elongated and stratified nuclei. These changes can be best seen at the head of the polyps (intraluminal protruded portion). Notably, a reduction of the number of goblet cells is observed. Pedunculated polyps have a fibromuscular stalk, which contain blood vessels originating from the submucosal layer, and are usually free from dysplastic epithelium.

Based on their architecture, adenomatous polyps can be classified as tubular, tubulovillous, or villous. In general, small, rounded or tubular glands are seen in tubular adenomas, while villous adenomas are covered by soft *villi*. Tubulovillous adenomas combine both tubular and villous features.

Sessile serrated adenomas do not display the typical cytological features of dysplasia that are commonly seen in other adenomas. Serrated architecture often overlaps histologically with that seen in hyperplastic polyps. Therefore, diagnosis of these polyps can be challenging. Differential diagnosis is often based on clinicopathological correlation, as these polyps are most commonly found in the right colon, and the presence of serrated architecture seen throughout the full length of the glands, including the crypt base. In contrast, hyperplastic polyps are more common in the rectum, left colon, and their serrated appearance is typically confined to the surface of the glands.

Intramucosal carcinoma is defined by the breach of the basement membrane (towards the lamina propria and the muscularis mucosae) by dysplastic cells. Invasion beyond the muscularis mucosa, and into the submucosa, including the submucosal stalk of a pedunculated polyp, constitutes invasive carcinoma.

Adenocarcinoma of the colon

Colorectal cancer develops within pre-existing foci of adenomatous tissue. This occurs usually, but not always, in a polypoid lesion.

At least two genetic pathways have been identified involving both a stepwise accumulation of multiple mutations (genetic abnormalities) and epigenetic events, such as gene silencing, which enhance progression once mutations have occurred. These are: 1) the classic adenoma-carcinoma sequence (figure 2-17a), whose pathognomonic molecular defects involve the adenomatous polyposis coli gene (APC); 2) the microsatellite instability, which is associated with defects in DNA mismatch repair systems.

Right-sided colon cancers often present as polypoid, exophytic masses and rarely cause obstruction due to the large diameter of these regions of colon. In contrast, left-sided colon cancers grow circumferentially as annular lesions causing narrowing of the lumen and obstruction.

Histologically, colorectal carcinoma is composed of irregularly infiltrating malignant glands. The cells are columnar and have elongated ("cigar-shaped"), tall nuclei. Cells have irregular size and shape, increased nuclear-to-cytoplasmic ratio, and high mitotic index, indicating rapid growth of the cancer.

The invasive tumour is usually surrounded by a desmoplastic response and focal necrosis is common.

Based on the degree of differentiation (from well to poorly differentiated), gland formation can be jeopardised. Missing crypts, total loss of goblet cells, and indistinguishable intercellular space are common findings.

The endoscopic views of advanced colon carcinomas are shown in figure 2-19.

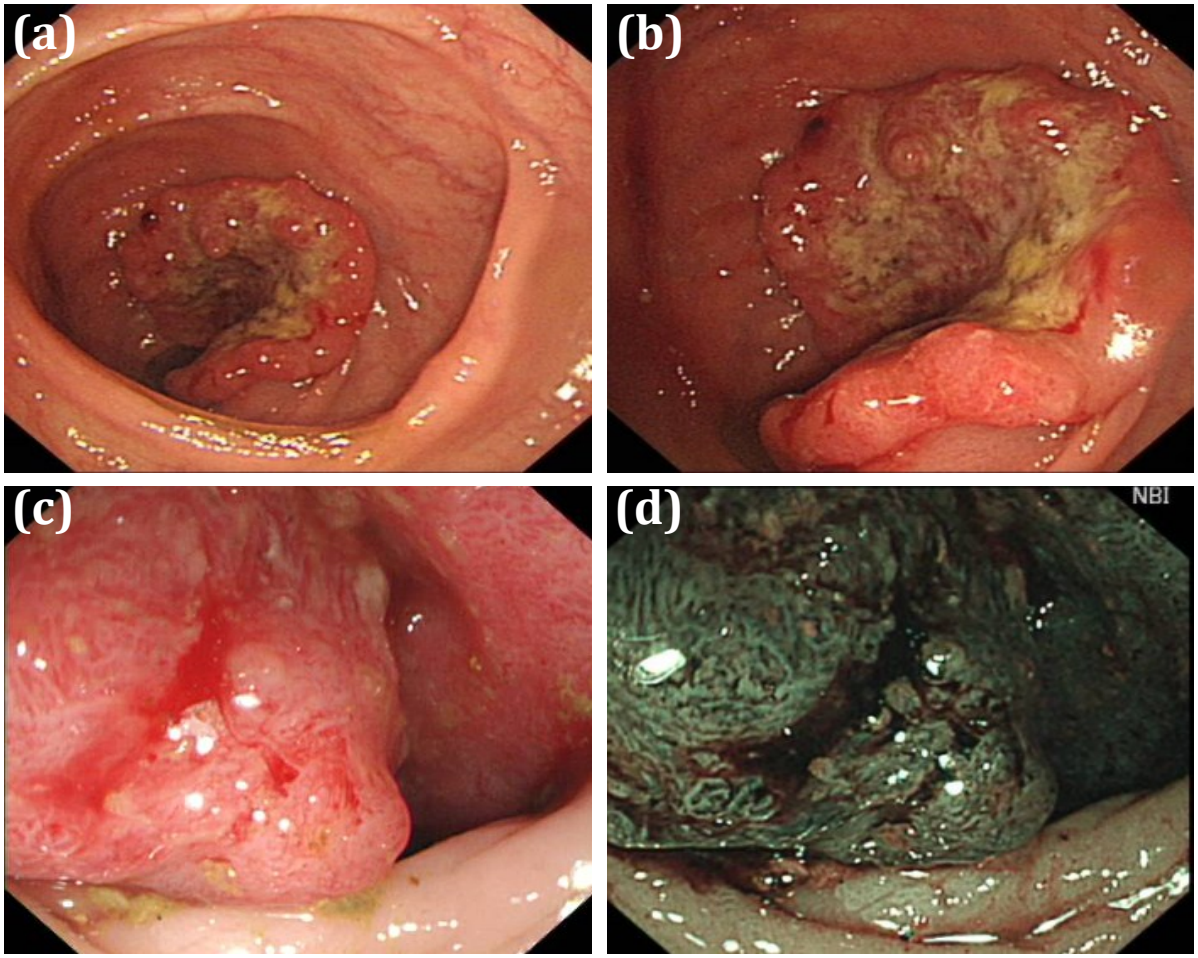


Figure 2-19: **Endoscopic views of a cancer of the transverse colon (a, b), and the sigmoid colon (c, d). In (a) and (b), the tumour involves almost ¾ of the luminal circumference from the distal margin, whereas in (c) and (d), the tumour involves approximately the entire circumference of the bowel. In (d), the transition zone between normal and neoplastic epithelium is clearly shown by inspection with Narrow Band Imaging (NBI). Source of acquisition: Drs Coda & Thillainayagam, Endoscopy Unit, Charing Cross Hospital, Imperial College Healthcare NHS Trust.**

2.2 General indications for endoscopy

Depending on the patient's symptoms, objective signs and clinical history, the indications for endoscopy can be classified as indications for upper and lower GI endoscopy, and each group is further divided in diagnostic and therapeutic according to the aim of the procedure [38,47].

2.2.1 Upper GI endoscopy

Table 2-3 shows the most widely accepted indications worldwide for upper GI endoscopy.

Diagnostic	Therapeutic
Dyspepsia	Bleeding
Dysphagia	Feeding tube placement
Weight loss & Malabsorption	Dilatation of strictures
Diarrhoea	Stenting of strictures
Anaemia	Tumour debulking
Nausea & vomiting	
Screening	

Table 2-3: General indications for upper GI endoscopy.

Patient preparation & sedation

Preparation consists in giving nil by mouth for 6 hours before the procedure. Following consent, the patients are accompanied to the endoscopy room and positioned on a bed, on their left lateral position.

Prior to gastroscopy, a local anaesthetic spray (xylocaine) is usually administered with or without a light sedative - typically 2-2.5 mg midazolam IV. Patients are then asked to insert a mouth guard when they feel ready for the procedure to commence.

Common pathology

Pathologies frequently encountered during upper GI endoscopy are:

- Hiatus hernia
- Oesophagitis
- Vascular lesion
- Ulcer
- Cancer

All of them have been described in more detail in section 2.1.2.

2.2.2 Lower GI endoscopy

Specific indications for colonoscopy are summarised in table 2-4. Indications for lower GI endoscopy can be further classified according to the risk that the procedure may carry (bleeding, perforation), and the potential diagnostic yield provided. For example, bleeding consistently has the highest yield for cancer and large polyps, while surveillance for ulcerative colitis and after polypectomy typically provides the lowest cancer yields [48].

High-risk indications include:

- Polypectomy of large polyps
- Stricture dilation
- Stent placement
- Acute colonic pseudo-obstruction

Pre-existing conditions associated with high-risk colonoscopy are:

- Sigmoid volvulus
- Caecal volvulus
- Prior radiation therapy
- Chronic steroid use
- Colonic strictures
- Severe diverticular disease
- Severe colitis
- Pelvic adhesions
- Severe collagenous colitis

Diagnostic	Therapeutic
Bleeding	Bleeding
FOBT-positive stools	Polypectomy
Anaemia (malabsorption syndrome excluded)	Dilatation of strictures
Change in bowel habit	Stenting of strictures
Abdominal pain and constipation	Tumour debulking
Chronic diarrhoea	
Abnormal imaging (x-ray, US, CT)	
Surveillance (polyps, IBD, cancer resection)	
IBD assessment	
Screening	

Table 2-4: General indications for lower GI endoscopy. FOBT = Faecal occult blood test; US = ultrasound; CT = computed tomography; IBD = inflammatory bowel disease.

Patient preparation & sedation

Preparation consists in a low residue diet 3-5 days before the procedure and the administration of stimulants and bowel cleansers typically 12-24 hours before the procedure. Following consent, the patients are accompanied to the endoscopy room and positioned on a bed, on their left lateral position. A combination of pain killers and sedatives is generally given intravenously, along with antispasmodics if required.

Common Pathology

Common pathologies detected at colonoscopy include:

- Haemorrhoids
- Polyps
- Colitis
- Cancer
- Diverticula
- Ulcer
- Vascular lesions

Most of the above listed diseases have been described in more detail in section 2.1.2.

2.3 Introduction to endoscopy

Diagnosis of GI illnesses is usually made on the basis of the patient's clinical history and objective physical examination. In addition, visual inspection and assessment of the inner surfaces of the organ of concern is often necessary, and this procedure, commonly referred to as endoscopy, is typically performed by inserting a flexible plastic tube (endoscope) through which light can be delivered at distance (figure 2-20).

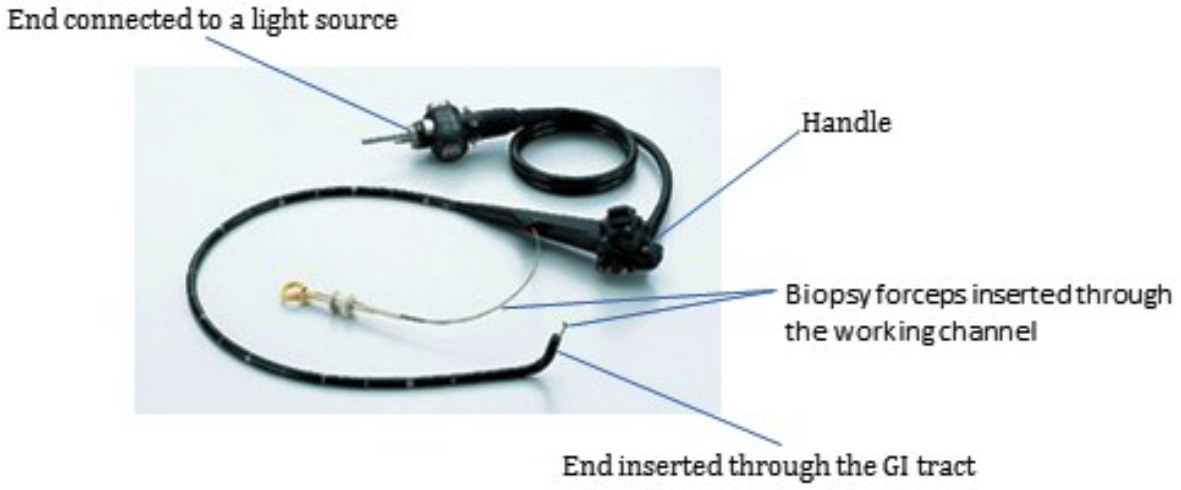


Figure 2-20: Image of a conventional video-endoscope (Olympus GIF Q160) with biopsy forceps inserted though the endoscope working channel. Adapted from [49].

For the assessment of the upper GI tract (i.e. oesophagus, stomach, duodenum), the endoscope is swallowed by the patient typically after topical anaesthesia of the pharynx with or without light sedation. Assessment of the lower GI tract (colon and terminal ileum) is performed through the anus. In essence, there are three main components of the GI tract that can be assessed through an endoscopic investigation: the lumen; the wall and lesions intrinsic to the bowel; and masses external to the bowel, which may compress *ab extrinseco* and erode into the lumen. In many cases, a biopsy, followed by histopathological assessment of the tissue removed, is often required for confirmation. To this end, various devices can be inserted through the endoscope to take biopsy samples (figure 2-20) or perform minimally invasive endoluminal surgery (e.g. polypectomy, endoscopic mucosal resection, etc.).

This section briefly describes some basic concepts and terminology in GI endoscopy, along with an introduction to both flexible fibre-optic endoscopes and modern video-endoscopy systems employed for diagnosis and therapy. More comprehensive information can be found in references [50-52].

2.3.1 Technical aspects

A number of considerations are necessary to give a full panorama of what is endoscopy and how it is performed safely and effectively.

Appropriately trained endoscopists and assistants, a purpose-built endoscopy suite (figure 2-21), state of art equipment and facilities, including a dedicated area for endoscope disinfection, and recovery bays, are clearly indispensable. It is essential to have mobile equipment on trolleys that can be transferred to the bedside at all times. Adequate resources and storage for the multiple endoscopic procedures are also essential. It is critical that all electric devices such as electrocautery units are checked periodically. This also includes devices employed for research only.



Figure 2-21: The endoscopy room 1 at Charing Cross Hospital, Imperial College Healthcare NHS Trust.

Fibre-optic endoscopes

The main part of a flexible fibre-optic endoscope (figure 2-22) is the fibre-bundle, which transmits the image through thousands of ultrathin (6-12 μm) glass fibres.

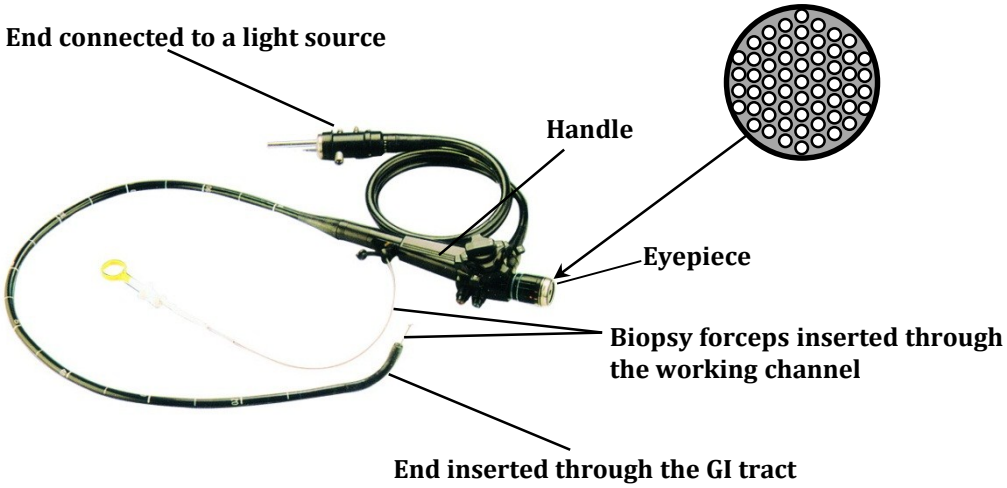


Figure 2-22: Image of a fibre-optic endoscope (Olympus) with biopsy forceps inserted though the endoscope working channel. The inset shows the dead space between the fibres seen through the eyepiece. Adapted from [53].

Each fibre has an inner core of glass surrounded by an outer layer typically made of a lower refractive index glass. Light enters and propagates along each individual fibre undergoing total internal reflection.

The fibres are arranged coherently into a bundle, allowing an image to be transmitted with the number of image pixels being defined by the number of fibres within the bundle. The dead space between the fibres is responsible for the fine mesh visible through the eyepiece (inset in figure 2-22).

Excessive bending or torqueing may break the individual fibres, and a broken fibre usually appears as a black spot in the visualised image. An eye-piece typically magnifies the image at the endoscopist's end of the bundle by a factor of 15 to 30x.

Other components include the objective lens system, which focuses objects at the distal tip onto the bundle; the light source; a nozzle for air insufflation; a nozzle for water flushing to clean the objective lens; and a suction channel, which removes gas and fluids and allows passage of a variety of accessories through the endoscope into the intestinal lumen (figure 2-23).

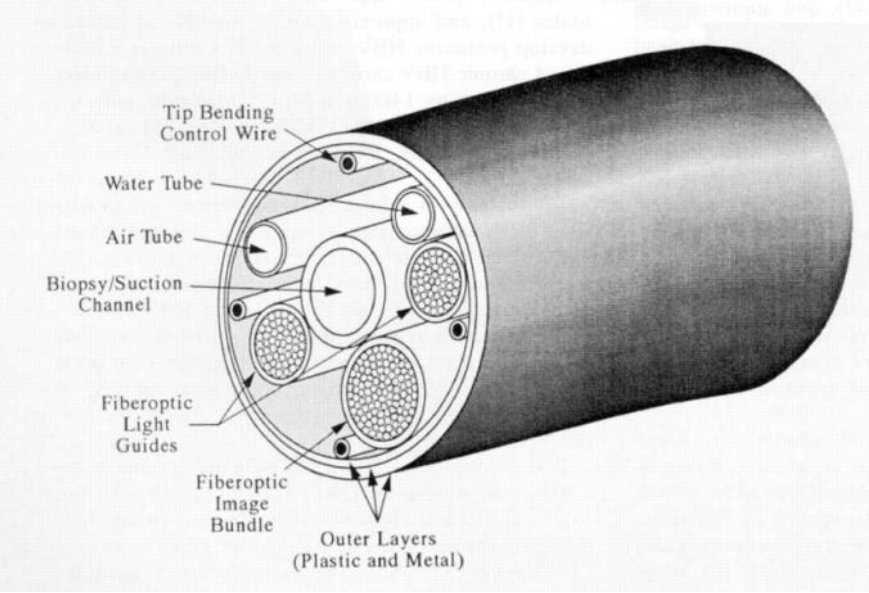


Figure 2-23: Cross section of a typical fibre-optic gastrointestinal endoscope. Reproduced with permission from [54].

The handle has valves for suction, air insufflation and suction, and control knobs (up-down and right-left) to orientate the tip of the endoscope in the four cardinal directions. A small mark at 12 o'clock in the field of view facilitates orientation for photography and indicates the "up" deflection of the tip.

Conventional fibre-optic endoscopes have a field of view of 110-120 degrees and a depth of focus of 3 to 100 mm away from the tip.

Video-endoscopes

Electronic video-endoscopes are now used worldwide. The image is generated by a charge-couple device (CCD) located at the distal end of the endoscope. A CCD is essentially an array of hundred thousand individual photo cells (pixels) receiving photons reflected from the illuminated tissue, and producing electrons in response according to the amount of light collected. Modern high resolution endoscopes are able to discriminate mucosal details up to 10 μm in diameter, which is over 10 times higher than the resolution capability of the average naked human eye.

Figure 2-24 illustrates a schematic diagram of the distal end of a typical video-endoscope.

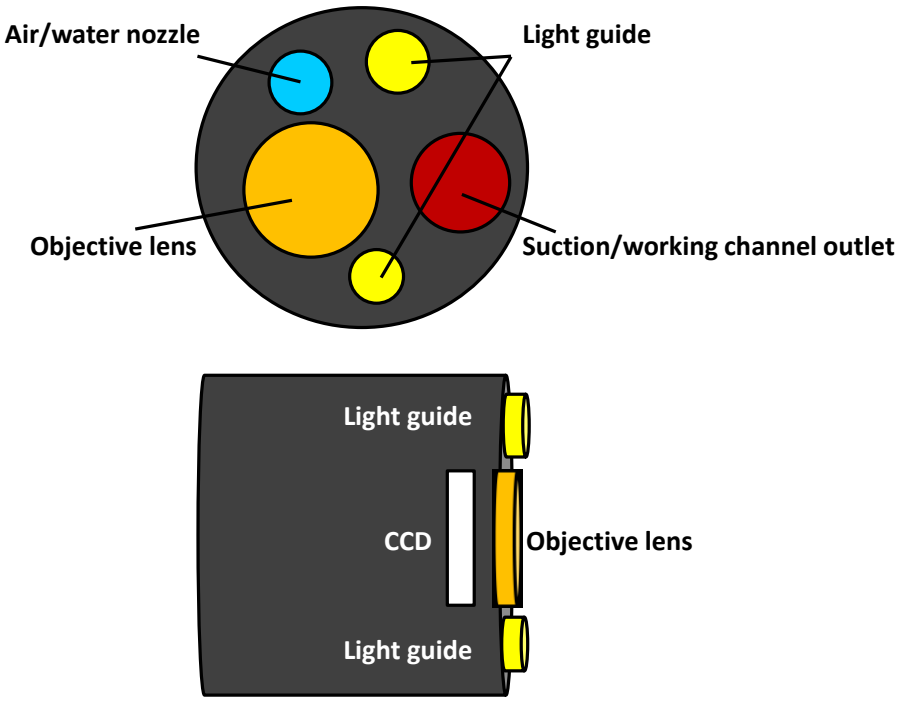


Figure 2-24: Schematic diagram of the distal end of a typical video-endoscope. In the top diagram, the illumination light guides, the air/water nozzle for lens cleaning, the objective lens, and the suction/working channels are visible. In the bottom diagram, a cross-section of the tip of the endoscope is given to indicate the location of the CCD.

As with fibre-optic endoscopes, video-endoscopes are equipped with controls for air, water, suction to remove air or liquids and to feed down the endoscope a variety of accessories, and wheels for up-down and right-left bending of the distal tip (figure 2-25).

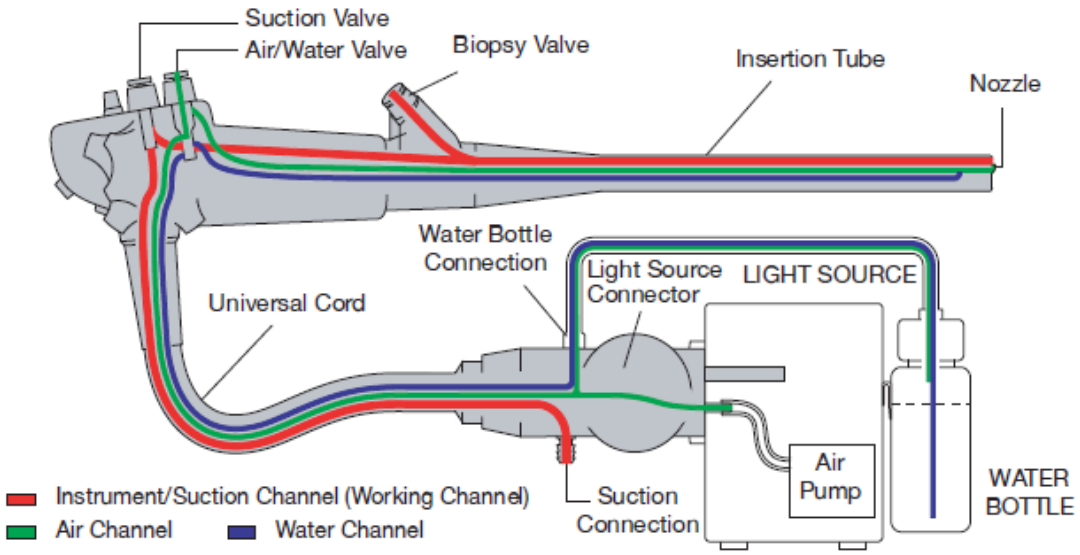


Figure 2-25: Cross-sectional view of a conventional video-endoscope (Olympus LUCERA 260 Series GI endoscope) showing the internal channels for suction/operation (red), air insufflation (green), and lens cleaning/irrigation (blue). Adapted from [55].

The accessory channel of a standard video-endoscope has a diameter of 2.8 mm. Therapeutic endoscopes have a larger channel (6 mm) for removal of blood clots and debris. On the handle control, buttons have been designed to switch between white light imaging and other auxiliary imaging functions (e.g. NBI, AFI, i-Scan, etc.), activate video-recording, freezing the image and taking pictures.

Inherent advantages of video-endoscopes are the distance of the control unit from the endoscopist's face, and the possibility for everyone in the endoscopy suite to watch the monitor and take an active part in the procedure, therefore allowing more accurate assistance.

Image documentation and storage for subsequent analysis and interpretation, follow-up, teaching and research, are also of great value.

Video-endoscopes are also typically more robust and less sensitive to bending and torqueing than fibre-optic bundles.

Accessories

The endoscopic examination is performed under direct vision, and a variety of accessories can be fed through the working channel of the endoscope to increase the information and accuracy of the procedures beyond the visual appearance and the subjective interpretation of the operator. These includes biopsy forceps, cytology brushes, needles for injection, snares and knifes for cold or diathermic therapy, ultrasound probes, and pH and impedance probes.

Biopsy forceps are the most commonly used accessory in endoscopy. They vary in diameter (2.3 to 7 mm) and are for single use only. After obtaining the specimen, the tissue is removed from the cup and put in a pre-filled formalin pot for histological assessment.

2.4 Advanced imaging and measurement of the gastrointestinal tract: novel techniques and future developments

Traditionally, endoscopy has depended upon using white light to evaluate the mucosal surface of the GI tract. It is only recently that this frontier was breached with the advent of novel imaging technologies. One such example is autofluorescence imaging, which is based on the principle that excitation of tissue with specific wavelengths (e.g. in the blue) can lead to emission at longer wavelengths. The emitted light can report on subtle changes in the concentration of specific chemicals in tissue that have the ability to fluoresce when excited.

In recent years, a range of innovative techniques have been developed and adapted for clinical endoscopy with the aim of providing a "red flag" technique, and perhaps ultimately revealing lesions that are still invisible under conventional white light endoscopy. Some of these methods enhance and optimize the inherent contrast available in fresh tissue, and offer the possibility of assessing both tissue structure and function in real-time.

Optical biopsy techniques, which interrogate the mucosal surface of the GI tract with light without the need to physically remove the tissue, are highly desirable as they could facilitate clinical decision making in ambiguous situations. This would bring more accurate and reliable information directly at the point of service, circumventing the cost and time required for histology, and improving the overall quality of care for patients. In theory, these novel techniques offer the yearned possibility of increased detection rates of high-risk lesions, the ability to target biopsies and resections, reducing need for biopsy, and reducing costs and uncertainty for both patients and clinicians.

Whether these techniques could be useful in clinical practice is still under investigation. Further validation studies are urgently awaited, and several groups worldwide are currently working toward this milestone.

Commercially available techniques include high-definition endoscopy (HDE) [56-58], narrow band imaging (NBI) [59], magnifying chromoendoscopy (MCE) [60], autofluorescence imaging (AFI) [61] and confocal laser endomicroscopy (CLE), whether by integrated technology or through-the-scope probe-based confocal endomicroscopy (pCLE) [62,63]. Amongst these techniques, endoscopic confocal microscopy has gained prominence since 2004, when the first *in vivo* study appeared on the clinical scene [62]. Probe-based confocal laser endomicroscopy (pCLE), an evolution and miniaturization of confocal laser endomicroscopy (CLE), was subsequently launched in 2007 [63,64] for clinical applications in gastroenterology, and highly promising results have been recently reported since then. Many other potential applications are yet to be validated and research to make CLE label-free is currently in progress.

However, to-date, none of these techniques have become widespread in clinical practice or been able to demonstrate sufficiently specific contrast for easy and rapid detection of dysplasia. As such, there is still a need to develop diagnostic endoscopic imaging technologies to interrogate tissue and identify lesions that cannot be detected using existing techniques.

The advent of biophotonics in endoscopy has opened new horizons and created important new opportunities for enhanced disease identification and histochemical characterisation. One such example is fluorescence lifetime imaging microscopy, often referred to as FLIM of autofluorescence, which offers the potential to improve the overall diagnostic accuracy by proving label-free quantitative contrast [65-68].

A number of other translational label-free optical techniques are currently being investigated owing to their potential to acquire non-invasive biochemical information and to image with subcellular resolution beyond what is possible with currently available techniques but the published experience is limited.

Optical coherence tomography (OCT) allows imaging at greater depths within tissue compared to CLE but does not normally supply functional information. Raman spectroscopy and coherent anti-Stokes Raman scattering (CARS) microscopy can be used to obtain highly detailed spectroscopic information but usually require long data acquisition times and could not be used for wide-field imaging [69].

Point spectroscopy using probes inserted through the working channel of conventional endoscopes has been able to differentiate non-neoplastic from neoplastic tissues and to probe the biochemical environment of diseased tissue [70]. The altered autofluorescence spectra reflect changes in the molecular composition and biochemical environment of diseased tissue. Some examples of studies in GI disease using diffuse reflectance spectroscopy (DRS), which detects changes in the physical properties of cells, include *in vivo* detection of dysplasia in colon polyps [71] and Barrett's oesophagus [70,72], and, recently, near-infrared diffuse reflectance imaging has also been applied to *ex vivo* surgical specimens of colon cancer [73].

An alternative to intrinsic optical signals is the use of exogenous labels such as labelled monoclonal antibodies against the carcinoembryonic antigen (CEA), or the epidermal growth factor receptor (EGFR), or photosensitizers administered topically. These markers can then be imaged using a range of instruments such as confocal endomicroscopy or prototype fluorescence endoscopes [74-76]. These techniques are generally referred as to molecular imaging. However, most of these diagnostic applications are still in early stage development.

The following sections review the fundamental principles of the most recent advanced techniques in endoscopy, with a particular emphasis on autofluorescence imaging and spectroscopy, and confocal laser endomicroscopy.

2.4.1 Magnification and high definition endoscopy

As in modern television technology, high definition videoendoscopes utilize CCDs with over a million pixels compared to older CCDs with an average of 300,000.

Magnifying endoscopes (zoom endoscopes) have a lens system built into the distal tip of the instrument. This zoom can be used to magnify areas of GI mucosa from x6 to x150. The main difficulty when using this endoscope is to keep the instrument still, and maintain the interface between tissue and tip of the instrument constant for accurate focusing. Particularly in upper GI endoscopy, breathing and peristalsis require continuous adjustments.

Magnification is often combined with the use of vital dyes (chromoscopy) to enhance the contrast in the surface (figure 2-26).

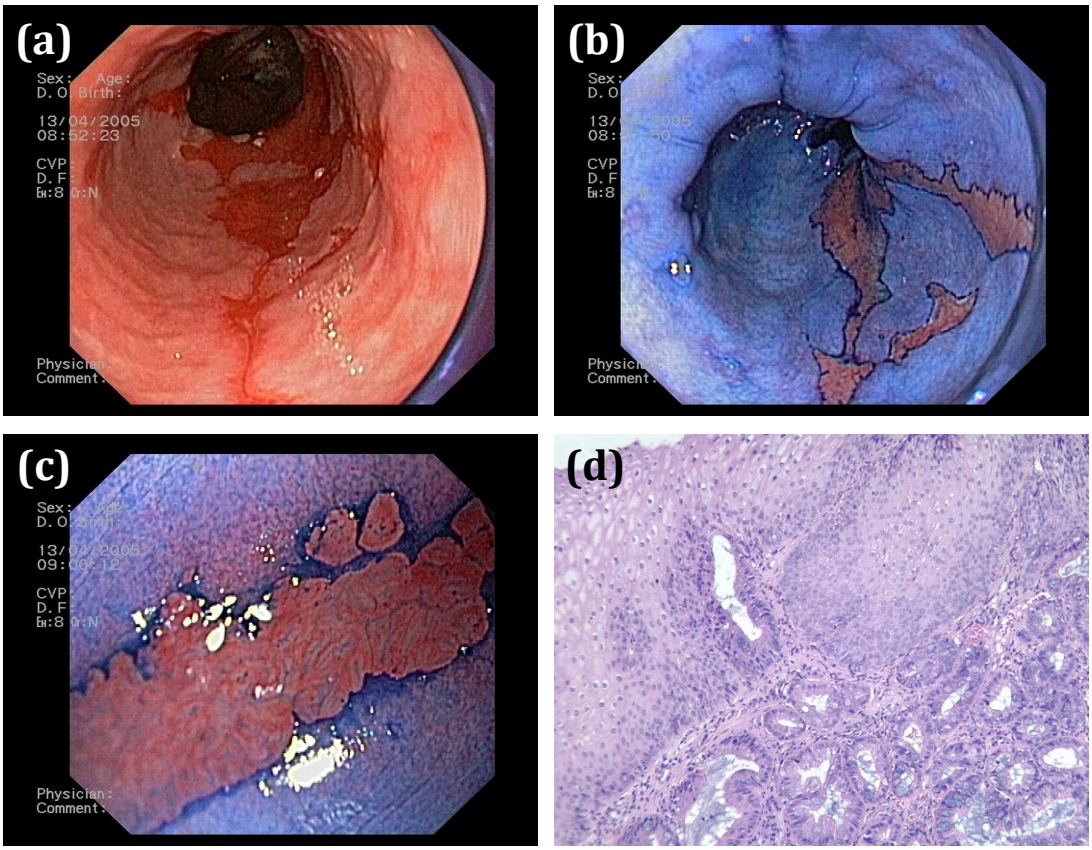


Figure 2-26: (a) Conventional endoscopic view of Barrett's oesophagus with concomitant oesophagitis. (b) Positive staining of Barrett's epithelium after absorption chromoscopy with methylene blue dye solution (1%, 10 ml). (c) Villous cerebroid pits with finger-like projections seen with magnification endoscopy (pattern 5 according to Endo's classification [77]). (d) Histological section of (c) showing intestinal metaplasia with glands of different size and shape, and numerous goblet cells. Adapted from [31].

Clinical experience

Upper GI tract

Lugol's vital staining is the most commonly used method to enhance the detection of oesophageal squamous dysplasia and early squamous cell carcinoma in high risk populations, and variable sensitivity (91%-100%) and specificity (40% to 95%) have been reported [78-80].

In Barrett's oesophagus, methylene blue is undoubtedly the preferred dye to enhance the detection of dysplasia and early cancer, although its value is still controversial due to the reported wide range of sensitivities (32%-98%) and specificities (23%-100%)[81], high level of interobserver variability [82], and inconsistent rates of increased detection [83-87].

Using magnifying endoscopy and methylene blue, Endo *et al.* proposed a classification of five oesophageal pit patterns to distinguish metaplastic epithelium from gastric phenotypes. Based on correlation with histology and mucin phenotypes, types 4 and 5 were found to be highly related to the presence of intestinal metaplasia [77].

The clinical experience with other staining methods in Barrett's oesophagus remains limited and their role has not yet been established. Among others, use of indigo carmine in combination with enhanced magnification endoscopy has been found useful in distinguishing non-dysplastic from dysplastic pit patterns [88].

Four different mucosal pit patterns were identified using magnifying endoscopy with acetic acid in patients with short-segment Barrett's oesophagus without dysplasia. In this study, types 3 and 4 were shown to contain intestinal metaplasia in respectively 87% and 100% of biopsy specimens [89].

In my personal experience in the upper GI tract, magnification with both methylene blue or acetic acid coloration of the mucosal surface in Barrett's oesophagus showed a very high correlation with histology in detecting specialized intestinal metaplasia [31].

Methylene blue staining with magnifying endoscopy has also been applied to detect gastric intestinal metaplasia and dysplasia with 84% and 83% accuracy, respectively. In this study, specific mucosal patterns were identified and classified in three groups: non-metaplastic, non-dysplastic mucosa; metaplastic mucosa; and dysplastic mucosa [90]. However, in some cases it is practically difficult to achieve reliable and clear pattern identification (and inter-observer agreement) due to uneven spreading of the dye and heterogeneous staining of the gastric mucosa.

Lower GI tract

By using magnifying endoscopes and indigo-carmine dye spraying, Kudo *et al.* [60] have proposed a classification of five different polyp pit patterns associated with a percentage of correlation with the histology. This classification was meant to predict an increasing risk of neoplastic changes and assist clinicians in their therapeutic strategy planning. Kato *et al.* [91], in one of the largest studies comparing these pit patterns with histology (3438 lesions) found an accuracy of 75% for non-neoplastic lesions, 94% for adenomas and 85% for carcinomas.

Magnifying endoscopy is gaining more importance as some of the colon cancers may not develop via the classical sequence adenoma-cancer but have only the transient phase of a small flat adenoma (*de novo* sequence)[44].

In a multicentre trial with 1000 colonoscopies, the number of adenomas detected was almost 40% higher with the combination of magnification and chromoendoscopy compared with standard colonoscopy [92].

In contrast, in another large study including 203 patients, high resolution endoscopy yielded a higher adenoma detection rate, and a higher number of flat adenomas <5 mm, than pan-colonic chromoendoscopy with indigo carmine [93].

High definition endoscopy combined with dye staining is expected to become the standard of care for selected patients who need surveillance (e.g. colorectal cancer, ulcerative colitis, Barrett's oesophagus). However, many aspects of this technique still need to be standardized e.g. the amount of dye to spray, the use of a spraying catheter, the power to be applied when spraying which in turn determines the more or less homogeneous coloration of the target area. Nonetheless, although the effectiveness of chromoendoscopy has been shown [94,95], staining of the entire colon remains a time-consuming procedure.

2.4.2 Virtual chromoendoscopy

Narrow Band Imaging (NBI)

NBI (Olympus Corporation, Japan) is a digital filter technique that improves the visibility of capillaries, veins and other subtle tissue structures, by optimising the absorbance and scattering of light without the use of contrast or absorptive dyes. Example images of NBI in comparison with conventional white light endoscopy (WLE) are shown in figure 2-27.

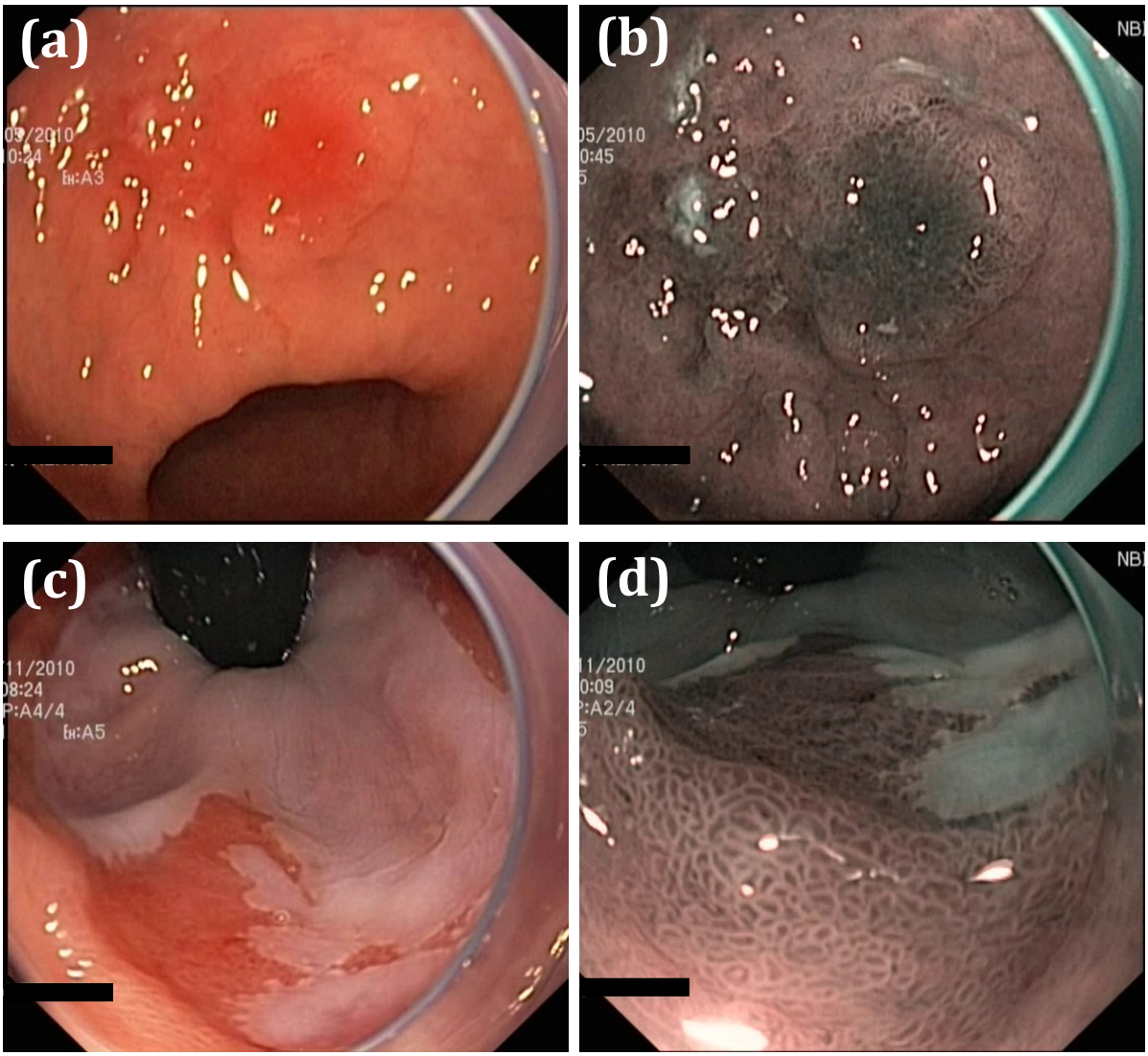


Figure 2-27: Example images of areas of suspected early cancers of the gastric antrum (a, b) and cardia (c, d) imaged using standard WLE (a, c) and NBI (b, d) to demonstrate the contrast enhancement provided by NBI. Images provided courtesy of Professor Paolo Trentino (University of Rome "La Sapienza", Italy).

This system adapts the conventional additive RGB (red, green and blue) colour model of a conventional electronic endoscope with an ordinary light source and through the application of narrow band filters to enhance the tissue microvascular architecture (figure 2-28).

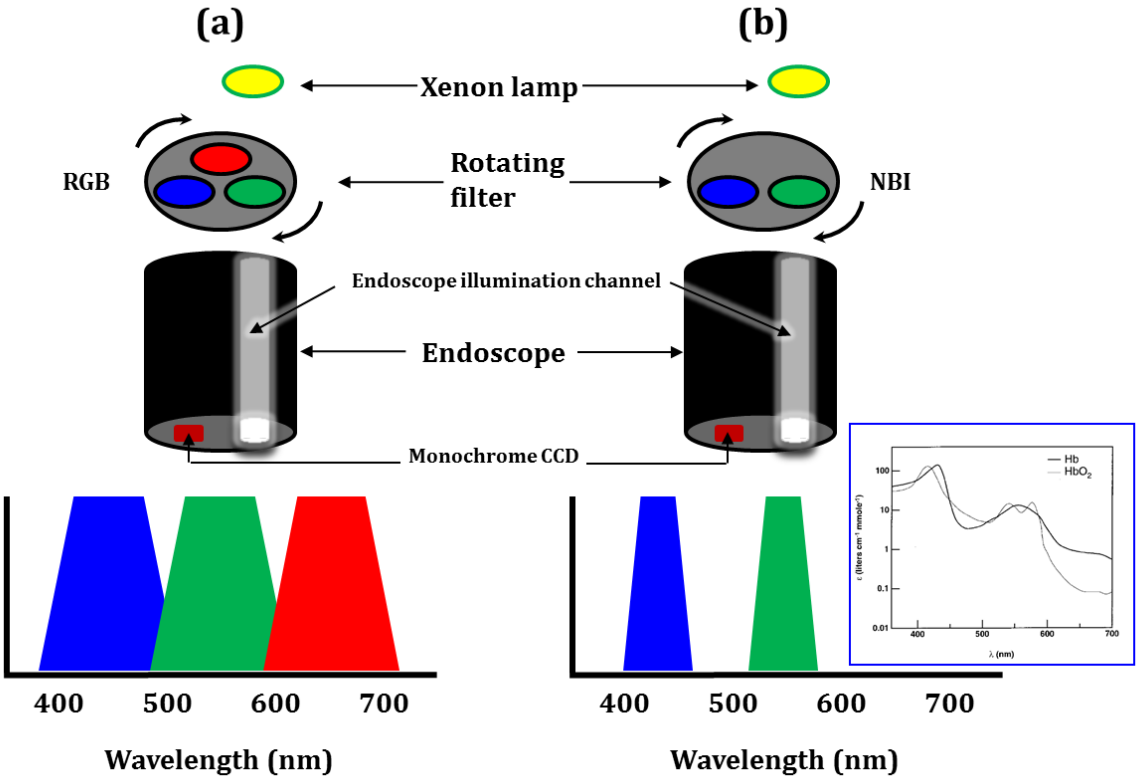


Figure 2-28: Schematic diagram showing the difference between a standard RGB filter (a) and the NBI filter (b). Compared to the full range of white light illumination, the filtered light penetrates the tissue less, highlighting the superficial details of the mucosa. Additionally, the filtered centered wavelengths fall within haemoglobin absorption bands (inset on right of (b)[71]), and this leads to a higher contrast for vascular structures.

NBI uses two bands of light, at 415 nm (blue) and at 540 nm (green). Narrow band blue light preferably displays superficial capillary networks, while green light selectively displays deeper subepithelial vessels, and when combined, they offer an extremely high contrast image of the tissue surface. Commercial NBI systems apply image processing so as to display capillaries on the surface in brown and veins in the subsurface in cyan.

NBI is based upon the phenomenon that incident light with longer wavelength undergoes less scattering and thus penetrates further into the tissue. Blue light penetrates only superficially, whereas red light penetrates into deeper layers. The choice of the two bands of light at 415 nm and 540 nm is determined by the peaks of absorption of haemoglobin (maxima at 415, 542 and 577 nm for oxyhaemoglobin, and at 430 nm and 555 nm for deoxyhaemoglobin [71] (see inset on right of figure 2-28(b)), thus the centered wavelengths resulting from the narrowband filtering lead to a higher contrast for vascular structures.

The first prototype of NBI-system was developed by Gono *et al.* in Japan [59,96]. White light from a Xenon lamp is conveyed through a rotary RGB filter that separates the white light into the colours red, green, and blue, which are used to sequentially illuminate the mucosa via the illumination channel of the endoscope (figure 2-28). The red, green, and blue reflected light is detected sequentially by a monochromatic charged coupled device (CCD) placed at the tip of the endoscope, and the three images are integrated into a single colour image by the video processor. In addition to the conventional RGB filters for white light endoscopy, the narrow band imaging system has filters of which the band-pass ranges have been narrowed and the relative contribution of blue light has been increased.

Compared with chromoendoscopy, NBI offers the advantage of providing contrast without the use of dyes but the general endoscopists' confidence with this system is still under debate. One aspect of NBI is that images are less bright than those of WLE; therefore it is often difficult to observe large areas from a distant view as the image quality significantly degrades with distance. This makes it more suited to detailed mucosal inspection rather than screening.

Clinical experience

Various studies have reported on the usefulness of NBI for enhanced detection of dysplasia and neoplasia both in the upper and in the lower GI tract. The results are inconsistent and suggest that the clinical utility of NBI in day-to-day practice is limited.

NBI as an adjunct technique to high-resolution endoscopy, showed a comparable performance to chromoendoscopy when applied in a randomised cross-over study of 28 patients with BO, and did not improve the overall sensitivity for identifying patients with high grade dysplasia or early cancer [97]. In a study with 56 patients with BO undergoing endoscopic surveillance for previously detected dysplasia, NBI detected significantly more dysplasia, and with recourse to fewer targeted biopsies, compared to WLE alone [98].

In a recent study by Sharma *et al.* [99] in 123 patients with BO with mean circumferential and maximal extents of 1.8 and 3.6 cm, respectively, NBI revealed more areas of dysplasia in patients with fewer biopsies when compared to high definition WLE plus four quadrant biopsies (Seattle protocol, see section 2.1.2).

The vascular pattern intensity (VPI), a measure of microvascular density, was proposed by *East et al.* [100,101] as a new classification parameter to discriminate neoplastic from non-neoplastic polyps with NBI.

In a study of 62 patients with hereditary non-polyposis colorectal cancer, the adenoma detection rate was almost doubled when a second inspection with NBI was performed compared to standard colonoscopy alone [102].

Using microvascular networks as a marker of neoplasia in a variety of organs including colon, oesophagus, and lungs, a meta-analysis of 11 studies comparing NBI-based diagnoses of neoplasia with histopathology revealed a high diagnostic precision for detection of neoplasia, with an overall sensitivity and specificity of 94% and 83% respectively [103]. In contrast, other studies have failed to demonstrate an improved detection of neoplastic polyps [56,104,105] and dysplasia in patients with longstanding ulcerative colitis [106].

FICE and i-Scan

Along with NBI, the most recent development in virtual chromoendoscopy is the computed post-processing spectral estimation technology invented by Professor Miyake [107,108] and introduced by Fujinon with the Fuji intelligent chromoendoscopy (FICE) system (Fujinon Corporation, Japan). A similar system has been released in April 2007 by the Pentax Corporation, the so called i-Scan technology (Pentax, Japan).

In contrast to NBI, where the illumination light is filtered to achieve contrast, in FICE and i-Scan the contrast is obtained after the illumination has reached the tissue by processing the spectral reflectance captured by the CCD.

The FICE system is based on computed spectral estimation of photons reflected from an ordinary white light image. In this way, white light images are sent to a Spectral Estimation Matrix processing circuit and reconstructed in three distinct virtual single-wavelength images: red; green; and blue. By combining these three single wavelength images, a resultant FICE enhanced colour image is then obtained as shown in figure 2-29.

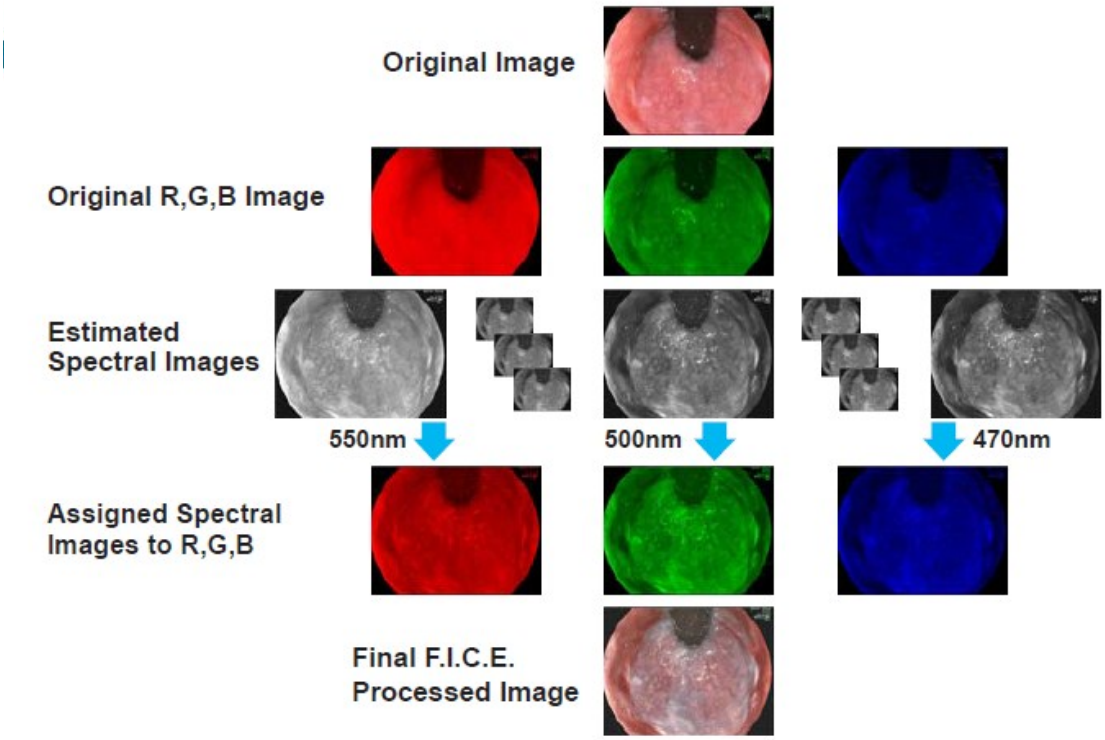


Figure 2-29: The principle and flow chart of FICE imaging [109].

i-Scan technology is based on digital filter enhancement and software manipulation of colour tone, sharpness and contrast of high-definition images (1.25 million pixels). i-Scan can be used in three modes depending on the level of enhancement desired: (1) Surface Enhancement (SE), for easier demarcation of edges and flat lesions by enhancing light-to-dark contrast; (2) Contrast Enhancement (CE) for better identification of depressed lesions by enhancing areas of low intensity; and (3) Tone Enhancement (TE) for improved mucosal structure assessment by increasing the illumination and emphasis on vascular features.

Example images of i-Scan in comparison with conventional WLE are shown in figure 2-30.

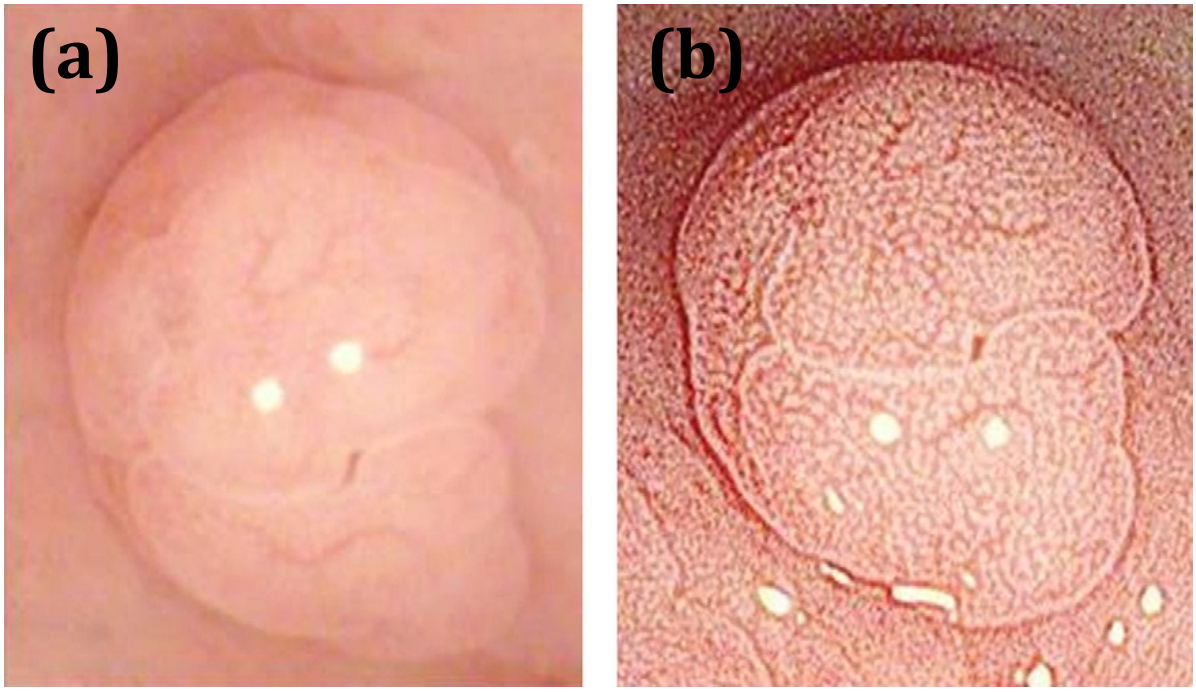


Figure 2-30: Example images of a small hyperplastic polyp in WLE (a) and i-Scan (b) to demonstrate the contrast enhancement provided by i-Scan. Reproduced with permission from [110].

Clinical experience

In patients with BO complicated by suspected HGD or early cancer, FICE showed similar sensitivity to acetic acid chromoendoscopy (87% for both techniques on a "per lesion" basis, and 92% vs. 83% on a "per patient" analysis for FICE and chromoendoscopy respectively) [111]. An increase in sensitivity was observed by combining targeted biopsies plus standard 4 quadrant random biopsies (88% and 96% in the "per patient" analysis for FICE and chromoendoscopy respectively).

When compared to WLE, transnasal FICE provided clearer delineation of the oesophagogastric junction by identifying the palisade vessels, a reliable, but often invisible to WLE, anatomical marker of oesophageal origin for measuring the extension of Barrett mucosa with accuracy [112]. However, detection of dysplasia was not attempted due to the limited FOV of the endoscopes used.

In a study by Neumann *et al.* [113], double-balloon enteroscopy-assisted FICE failed to improve the detection or delineation of ulcers and erosions in 3 patients with Crohn's disease but was found to be useful for the characterization of adenomatous polyps and angiodysplasias of the small bowel.

Hoffman *et al.* [110] reported a significantly increased detection rate of small (≤5 mm) adenomas for i-Scan when compared to WLE alone (11 vs. 5 respectively). The inspection was conducted in the last 30 cm of colon during the withdrawal phase of colonoscopy. Interestingly,

the same detection rate was found for both conventional chromoendoscopy with methylene blue and i-Scan, although chromoendoscopy was considerably more time consuming than i-Scan (13 vs. 5 minutes). They also showed that i-Scan is a useful adjunct technique to vital staining with Lugol's solution for identifying mucosal breaks in patients with non-erosive reflux disease (NERD) [114].

2.4.3 Fluorescence endoscopy

Fluorescence provides a powerful means of achieving optical contrast in microscopy and endoscopy based on specific molecular characteristics of the tissue. It will be introduced in more detail in chapter 3.

Fluorescence endoscopy can use endogenous (autofluorescence imaging) or exogenous fluorophores (i.e. fluorescein) to achieve contrast and distinguish between normal and diseased tissue.

Particularly, autofluorescence is generated by intra- and extracellular endogenous fluorophores such as collagen, elastin and pyridine nucleotides, and the distribution of these fluorophores can be different in normal and diseased tissue.

However, intensity-based autofluorescence contrast is often not sufficiently specific because it is difficult to make quantitative intensity measurements.

Photodynamic Diagnosis (PDD)

One of the major issues in measuring tissue autofluorescence is that the fluorescent signal is often weak. Exogenous sensitizers aim to provide highly specific contrast, but must be certified for human use, which of course requires assessments for safety and pharmacokinetics, etc.

PDD uses photo-sensitising chemicals to enable abnormal tissues to be more easily identified compared to conventional diagnostic techniques. While PDD is a widely used technique in urology and dermatology employing 5-aminolaevulinic acid sensitisation, its development and use in gastroenterology has not been so rapid, despite initial promising results [115-117]. Disadvantages of this technique include the high concentrations of 5-ALA often required, the inherent risk of photosensitivity and the long procedural time.

A number of different aromatic compounds have been used in PDD, most of which were previously employed in photodynamic therapy. These include various derivatives of haematoporphyrin, chlorins, and phtalocyanines. However, 5-aminolevulinic acid (5-ALA) emerged quite early among all other compounds due to its lower potential phototoxicity [118] and high tumour selectivity [119]. 5-ALA is a precursor in the biosynthesis of haem, whose exogenous administration can interfere with the synthesis of ALA feedback mechanism and

induce accumulation of the fluorescent precursor protoporphyrin IX (PpIX). PpIX is preferentially up taken by malignant tissues, and its tumour selectivity has been demonstrated for a variety of neoplasms, including cancers of the GI tract [120-123].

The recent introduction of a more selective and less phototoxic esterified derivative of 5-ALA, hexaminolevulinate (Hexvix, PhotoCure ASA, Norway), coupled to the development of a prototype fluorescence videoendoscope (13902 PIKS, Karl Storz, Germany) adjusted to the optimal emission wavelength of this sensitizer (375–400 nm), has prompted new enthusiasm in exogenous induced fluorescence.

The PDD videoendoscope prototype is equipped with a 300 W xenon lamp (D-light C, Karl Storz, Germany) and a 380-430 nm band pass filter that can be operated by pressing a switch on the handle. A 450 nm long pass filter is integrated in the CCD at the distal end of the endoscope.

Clinical experience

PDD with photosensitizers administered either intravenously or topically has also been applied to detection of dysplasia and early cancer in Barrett's oesophagus [117,124-126], ulcerative colitis [127,128], adenomatous and hyperplastic polyps [129,130], and in the biliary tree [131].

The recent introduction of a more selective and less phototoxic esterified derivative of 5-ALA, hexaminolevulinate (Hexvix, PhotoCure ASA, Norway), coupled to the development of a prototype fluorescence videoendoscope (13902 PIKS, Karl Storz, Germany) adjusted to the optimal emission wavelength of this sensitizer (375–400 nm), has prompted new enthusiasm in exogenous fluorescence contrast agents.

The PDD videoendoscope prototype is equipped with a 300 W xenon lamp (D-light C, Karl Storz, Germany) and a 380-430 nm band pass filter that can be operated by pressing a switch on the handle. A 450 nm long pass filter is integrated in the CCD at the distal end of the endoscope.

Enlicher *et al.* [132] observed selective Hexvix fluorescence of neoplastic polyps (with intraepithelial dysplasia) in contrast with invasive cancers, which only showed a weak fluorescence, and hyperplastic polyps, which did not fluoresce at all. It was suggested that hexaminolevulinate-based fluorescence endoscopy may be thereby useful for enhanced detection of premalignant lesions.

Mayinger *et al.* [75] reported a higher adenoma detection rate (38% more polyps) and overall accuracy superior to white light-endoscopy (81% vs. 69% respectively) using Hexvix administered topically as an enema. PDD was shown to be particularly sensitive to detection of flat polyps, which were almost completely missed by standard white-light inspection (13/16 vs. 3/16).

In a study by Ortner *et al*. [133] conducted in 53 patients with BO, delayed observation of 5-ALA fluorescence induced spectra helped discriminate LGD from non from non-dysplastic Barrett epithelium with a sensitivity of 76% and a specificity of 63%. An aqueous solution of 5-ALA was sprayed on the oesophageal mucosa during follow up gastroscopy, 8 weeks after initial screening endoscopy using the Seattle protocol. A second gastroscopy was performed after 1-2 hours, using an optical fibre inserted through the working channel of a therapeutic gastroscope. Fluorescence measurements were made in a circumferential pattern on the Barrett's segments and biopsies were taken from areas exhibiting high fluorescence intensity of PpIX in delayed fluorescence spectra to correlate spectra results with histology. The optical fibre used allowed fluorescence to be collected from an area of 1 mm^2. Immediate and delayed fluorescence spectra were then recorded from all biopsies *ex vivo* and as a 27% sampling error was found, they compared only the *ex vivo* spectra with histology. All samples included in the analysis were examined by three pathologists. Protein expression immunohistochemistry of p53 was also performed in all the samples examined by the third pathologist. Importantly, despite taking fewer specimens (median 7 vs. 28 with fluorescence spectroscopy and standard screening endoscopy, respectively), dysplasia was detected in 14 of 53 patients (four of which with HGD, six with short segments) compared to only five patients (all with long segments) previously diagnosed by standard screening endoscopy. In addition, three early cancers were detected for the first time. In a similar crossover study by the same group [134] conducted on 42 patients with longstanding ulcerative colitis, dysplastic mucosa was discriminated from non-dysplastic mucosa with a sensitivity and specificity of 73% and 81%, respectively. Interestingly, flat dysplasia was detected by fluorescence guided spectroscopy in 10 patients, only three of which were previously diagnosed by standard colonoscopy with four quadrant biopsies.

Autofluorescence Imaging (AFI)

AFI is a technique based on the principle that excitation of tissue with specific wavelength (e.g. in the blue) leads to emission of a longer wavelength of light. In the GI tract, AFI detects subtle changes in the concentration of specific chemicals in tissue that have the ability to fluoresce when excited (endogenous fluorophores). Malignant transformation is associated with emission of relatively longer wavelength of light (shift from green toward the red end of the spectrum).

Currently, the only commercially available AFI devices are RGB–based videoendoscopes with trimodal (WLE + NBI + AFI) capability (EVIS LUCERA SPECTRUM, Olympus Medical Systems Co, Japan). Two separate monochromatic CCDs are located at the tip of these endoscopes. One CCD is for high definition WLE and NBI, and the other CCD is specific for AFI.

In AFI mode, blue light (390-470 nm) and green light (540-560 nm) is sequentially generated by a xenon lamp and conveyed through a rotating colour filter wheel. An interference filter situated proximally to the AFI CCD blocks the blue light excitation but allows tissue autofluorescence (500-630 nm) and reflected green light to filter through [135].

The autofluorescence and green reflectance images are captured and integrated by the video processor into a single pseudocolour image where normal mucosa typically appears green, and dysplastic or neoplastic tissue purple (figure 2-31).

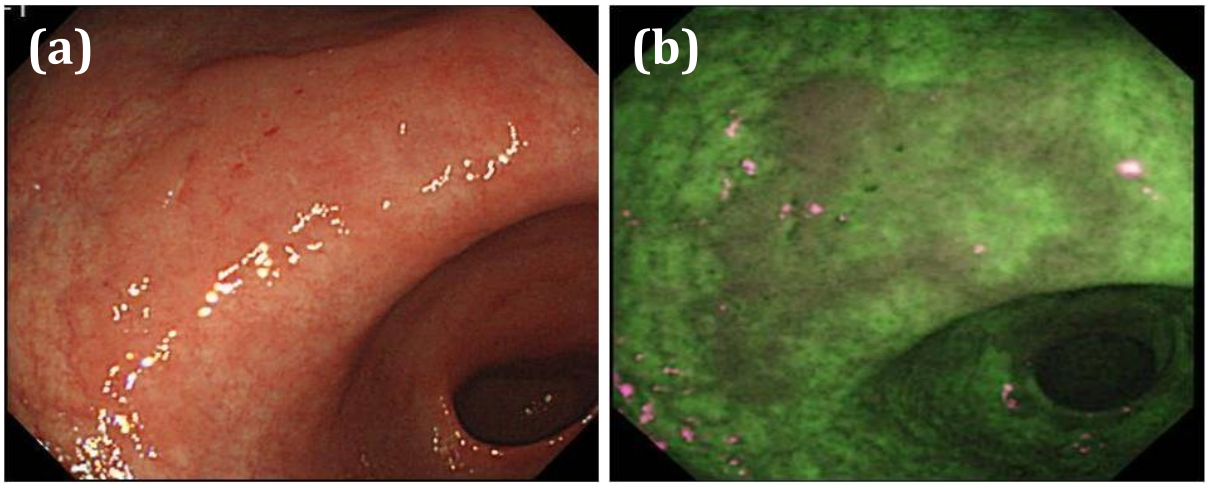


Figure 2-31: Example images of a suspected early cancer of the gastric antrum imaged using standard WLE (a) and AFI (b), to demonstrate the contrast enhancement provided by AFI (Olympus, Japan). Images provided courtesy of Dr Chizu Yokoi (National Center for Global Health and Medicine, Tokyo, Japan).

However, the reason for the difference in fluorescence between normal and diseased tissue observed in current commercial AFI systems is still unclear and intensity-based contrast is often not sufficiently specific [135-137].

The clinical experience with AFI will be discussed in chapter 3 together with research and preclinical studies of autofluorescence imaging and spectroscopy.

2.4.4 Confocal microscopy

Confocal microscopy was invented by Minsky in the 1950s [138,139]. Since its conception and development, confocal microscopy has been extensively used in biology and medicine for imaging living intact tissues without having to physically cut up and prepare thin sections as in histology.

In confocal microscopy, the light source, the sample plane, and the detector are all confocal, i.e. in conjugate image planes (figure 2-32). The illumination light is focused to a point in the sample and all the fluorescence collected by the objective lens from that point is forced to pass through a pinhole to reach the detector. Although other parts of the sample are also illuminated, light from out of focus planes in the sample is blocked by the pinhole and does not reach the detector.

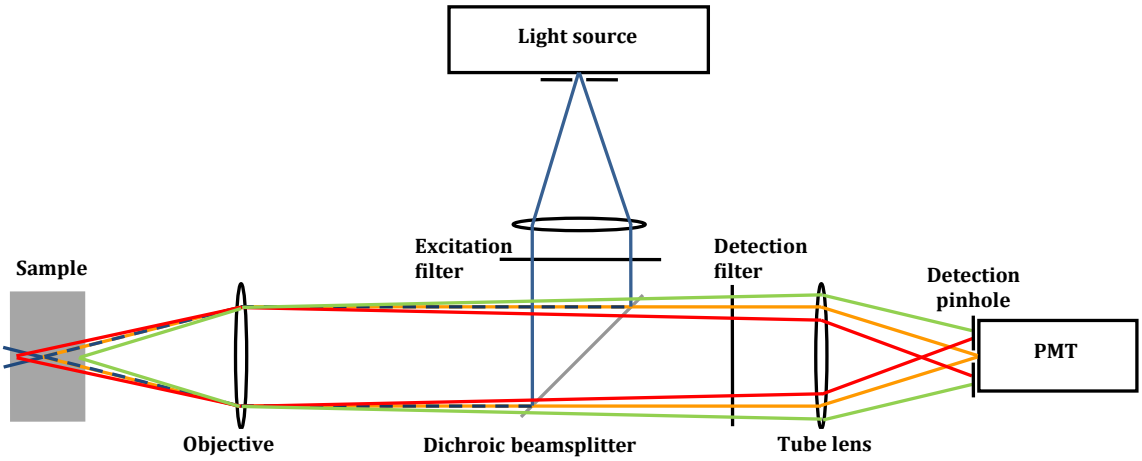


Figure 2-32: Schematic diagram of confocal microscopy principles. The blue rays (pre- and post-objective and excitation filter) indicate the laser illumination delivered to the tissue sample. Only the fluorescence emitted from a tissue layer in focus (orange rays) will pass through the pinhole and will be detected. The light emitted from tissue layers out of focus (red and green rays) will be rejected. Illumination and collection therefore occur in the same focal plane (i.e. confocal). Adapted from [140]

Thus, the main advantage of a confocal microscope is its optical sectioning ability, giving insight into the three-dimensional tissue structure and providing a virtual real-time histological diagnosis.

2.4.5 Confocal laser endomicroscopy

Confocal laser endomicroscopy (CLE) is one of the newest advancements in diagnostic endoscopy and is a highly promising technique for investigating the mucosal surface together with its immediate sub-surface areas. Cell structures and tissue morphological characteristics can be visualized to a maximum depth of 250 µm.

Two types of confocal endomicroscope have been developed: a confocal laser endomicroscope (CLE, Pentax, Japan), in which a miniaturized confocal scanner has been integrated into the distal tip of a conventional endoscope, and a probe based system (pCLE, Cellvizio, Mauna Kea Technology, France), which can be passed through the working channel of standard endoscopes and has an external laser scanning unit.

Endoscope based Confocal Laser Endomicroscopy (eCLE)

The confocal laser endomicroscope is based on micro-electro-mechanical system (MEMS) scanning mirror technology. The MEMS scanning mirror oscillates to provide a scan pattern to the beam of light.

A single mode (Gaussian beam profile) fibre, acting as both the illumination point source and the detection pinhole, and a miniature objective lens at the distal end of a conventional video

endoscope (EG3870K, EC-3870CILK, Pentax, Japan) enable confocal microscopy in addition to standard videoendoscopy.

A blue laser integrated into the endoscope light source is coupled into a single mode fibre that delivers an excitation wavelength of 488 nm to the sample, and fluorescence emitted by the sample is detected at wavelengths above 505 nm. Viewing of a specific tissue depth is enabled by scanning successive points within the tissue in a grid of pixels along the x and y axes (parallel to the tissue surface) to produce sections of 475 x 475 μm (FOV) at variable imaging depth (range 0-250 μm). The lateral resolution is 0.7 μm and the axial resolution is 7 μm. eCLE can produce conventional white light endoscopic images and confocal images at the same time with a pixel density of 1024 x 512 pixels at an acquisition rate of 1.6 frames per second or 1024 x 1024 pixels at 0.8 frames/second [141,142].

The distal tip of the endoscope contains an air and water jet nozzle, 2 light guides, an auxiliary water jet channel (used for topical application of the contrast agent, and a 2.8-mm working channel. Actuation of imaging plane depth is controlled using two remote control buttons on the handle [62].

Probe based Confocal Laser Endomicroscopy (pCLE)

pCLE consists of a coherent single mode fibre bundle, a miniature microscope objective and two scanning mirrors at the proximal end of the bundle. The bundle has an outer diameter of 2 mm and can be introduced through the working channel of most endoscopes. In pCLE, a laser is sequentially focused onto single fibres at the proximal end of the bundle. The light exiting the fibre at the distal end is focused to a point in the sample using a miniature objective. Confocal fluorescence is focused by the objective onto the same fibre in the bundle. The light is detected on a detector, and the beam is eventually scanned over all fibres in the fibre bundle to build up an image. The lateral and axial resolution range from 2.5 to 5 and 15 to 20 μm respectively [143]. pCLE has a fixed image plane depth varying between 55 μm and 130 μm depending on the probe used [142].

Comparison of eCLE and pCLE

The main advantage of eCLE over pCLE is that the imaging plane depth is user tunable because the laser scanner is integrated into the endoscope (figure 2-33(b)) and allows optical sectioning of the tissue at higher axial resolution (lateral resolution 0.7 μm, axial resolution 7 μm vs. 2.5 μm and 15 μm respectively), whereas in pCLE the imaging plane depth is fixed and cannot be adjusted (figure 2-33(a)) [141,143,144].

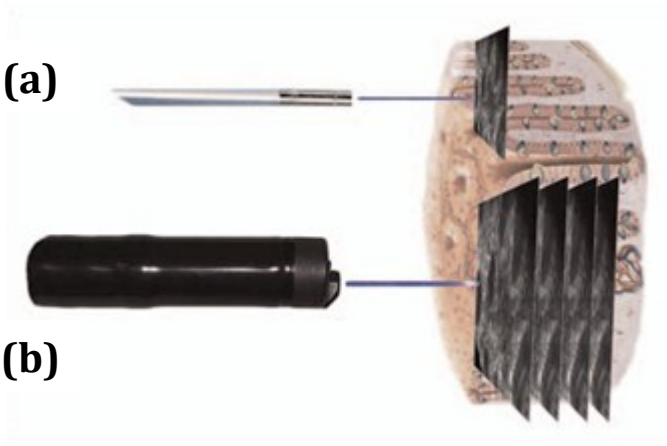


Figure 2-33: Confocal endomicroscopy systems clinically approved and currently available on the market. (a) The probe based system (Mauna Kea Technology, France). (b) In the confocal laser endomicroscope (Pentax, Japan). Adapted and reproduced with permission from [144].

In pCLE, the resolution is limited by the number of fibres (30,000) but the image acquisition is faster than that of eCLE (12 vs. 0.8-1.6 frames per second). One disadvantage of eCLE is the insertion tube diameter of the distal tip (12.8 mm) compared to the standard outer diameters of conventional endoscopes (9-11.1 mm). In contrast, pCLE, due to the small diameter of the bundle, permits the imaging of narrowed lumina such as the biliary and pancreatic ducts, ureters and neoplastic or inflammatory strictures. Disadvantages of pCLE include limited lifespan (20 procedures), higher maintenance cost [141], and occupation of the endoscope working channel.

Problems with current CLE systems

A general drawback of this technique is that intravenous, e.g. fluorescein sodium, and topical fluorescence agents, e.g. acriflavine, are used to achieve contrast. The avoidance of contrast agents would reduce both procedural time and any potential for associated adverse effects.

Fluorescein diffuses through the extracellular matrix of the epithelium and the lamina propria but does not stain cell nuclei [145]. Acriflavine is a carcinogenic dye [146], and this clearly limits its clinical utility [141].

Another drawback is the duration of the procedure, which can be almost twice as long as conventional endoscopy. In a study of contrast dynamics in porcine models, it has been reported that the best contrast and image quality can be achieved within the first 8 min after intravenous injection of 1% fluorescein with highest signal-to-noise ratio (SNR) after 5 min. The SNR decreased significantly after 8 minutes [147]. Furthermore, confocal endomicroscopy does not yet provide functional information about the tissue, and is an examiner-dependent technique. Interobserver and intraobserver variability has not been adequately studied [148], and the interpretation of the intensity images is often somewhat challenging among users, who may

require substantial supplementary training in histology or the presence of the pathologist in the endoscopy room to achieve acceptable diagnostic accuracy [149,150].

2.5 Endoscope based Confocal Laser Endomicroscopy (eCLE)

In 2004, Kiesslich *et al.* [62] showed that colonic dysplasia was detected using eCLE with a sensitivity of 97.4% and a specificity of 99.4%. Other potential applications are detection of dysplasia in Barrett's oesophagus and differentiation of benign and malignant biliary strictures. Kiesslich *et al.* proved that the overall accuracy for eCLE in predicting Barrett's oesophagus and associated neoplasia is 96.8% and 97.4% respectively [151]. Detection by eCLE of dysplasia in Peutz–Jeghers syndrome, and *in vivo* diagnosis and characterization of *Helicobacter pylori* gastritis and Whipple's disease has also been reported [152-154].

The potential of eCLE to differentiate colorectal lesions was recently demonstrated by Sanduleanu *et al.* [155]. In this study, low grade dysplasia was distinguished from high-grade dysplasia with high accuracy (96.7%), and eCLE predicted the final histology for all cases with 95.7% accuracy (figure 2-34).

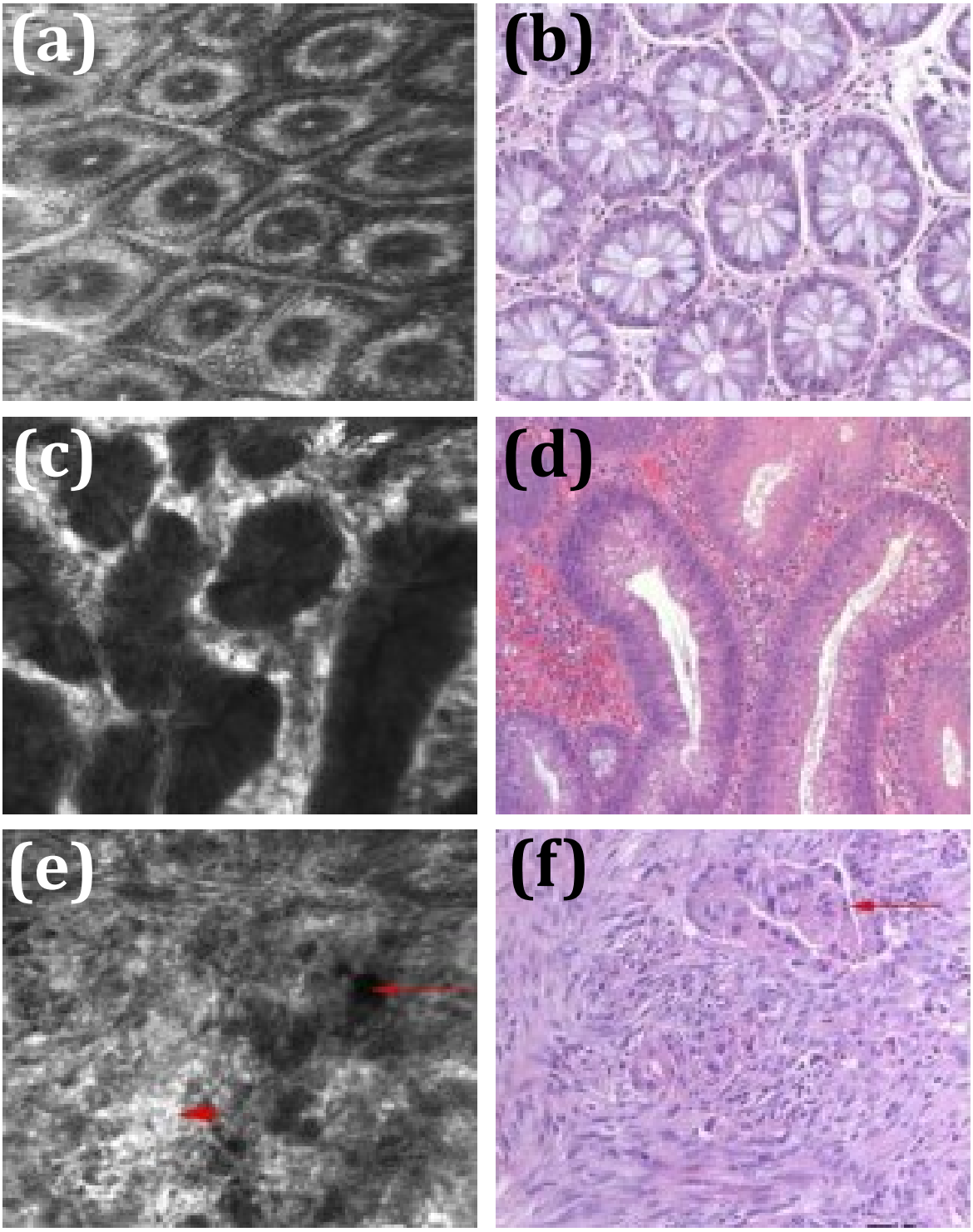


Figure 2-34: **(a) eCLE and (b) corresponding histological images (30x original magnification) of normal colonic mucosa. (c) eCLE and (d) corresponding histological images (15x original magnification) of an adenomatous polyp. (e) eCLE and corresponding (f) histological images (20x original magnification) of a poorly differentiated adenocarcinoma; the red arrow and the red arrowhead indicate an area of neoangiogenesis and islands of malignant cells (dark cells) respectively. Adapted and reproduced with permission from [155].**

Spectrally encoded confocal microscopy (SECM), a variant of CLE that facilitates the incorporation of confocal microscopy into small, portable catheters or endoscopes, was applied on 50 gastro-oesophageal biopsy samples from 36 patients and revealed subcellular details of various mucosal types and associated clinical conditions, including fundic gland polyps, eosinophilic oesophagitis and dysplasia in BO, all of which were confirmed and correlated with histopathology [156]. However, in SECM, contrast is due to reflected or simply back scattered light and not fluorescence.

In a pilot study conducted on 43 *ex vivo* endoscopic biopsy specimens using SECM, Yoo *et al.* [157] were able to identify and count individual eosinophils with 100% sensitivity and specificity for diagnosing eosinophilic oesophagitis when a cut-off threshold of 15 eosinophils per field was used. A high degree of correlation with histology and intra- and interobserver agreement was also observed. Other key histopathological features of this disease, including basal cells hyperplasia and eosinophil abscess and degranulation, were also accurately identified.

2.6 Probe based Confocal Laser Endomicroscopy (pCLE)

Oesophagus

Barrett's oesophagus

In a prospective, double blind review of 20 pCLE images of 40 sites of BO tissue by using matching biopsies as the reference standard, the preliminary evaluation accuracy and inter-observer agreement of pCLE was assessed among eleven experts in BO imaging from 4 different endoscopy centres from the United States and Europe [158]. Although the study was limited by the small sample size, high preliminary accuracy in diagnosis of BO dysplasia and neoplasia was achieved with both inexperienced (90%) and experienced observers (95%). The main strength of the present study relative to other published data is the inclusion of a large group of endoscopists, only four of whom had previous experience with pCLE. Their high performance demonstrated that rapid training in image interpretation is feasible.

The first international multicentre, randomized, controlled trial using pCLE in 101 patients with Barrett's oesophagus (BO) was published in September 2011. The sensitivity and specificity of pCLE in addition to high definition white light endoscopy (HD-WLE) was compared with HD-WLE alone for the detection of high grade dysplasia and adenocarcinoma [159]. Use of pCLE with HD-WLE showed increased "per-location" sensitivity for the detection of HGD and AC compared to HD-WLE alone (68.3% vs. 34.2%). Instead, "per-location" specificity was slightly reduced (87.8% vs. 92.7%). Nevertheless, no statistically significant differences in "per-patient" sensitivity were observed between HD-WLE, NBI or pCLE. However, a high negative predictive

value was collectively observed, and authors speculated that pCLE might facilitate early rule-out of dysplasia with high degree of confidence, allowing better informed decisions to be made for the management and subsequent treatment of patients with BO (figure 2-35).

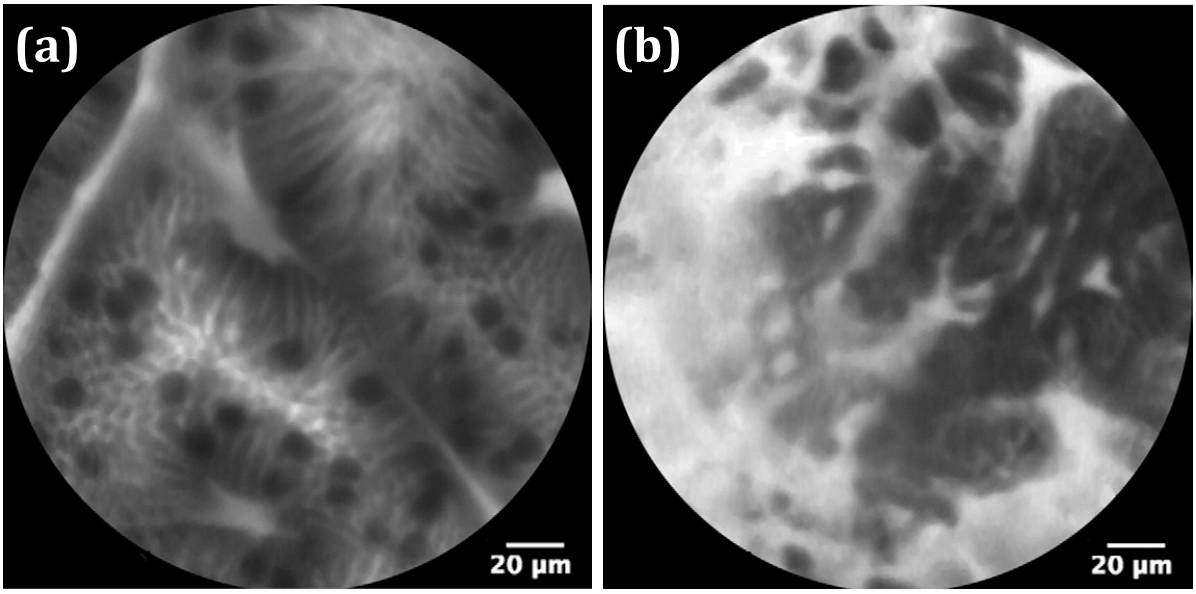


Figure 2-35: pCLE example images showing non-dysplastic BO (a) and BO with early oesophageal adenocarcinoma (b). Adapted and reproduced with permission from [159].

In a study by *Bajbouj et al.* [160], optical biopsy with pCLE was compared to standard endoscopic biopsy in the endoscopic evaluation of 68 patients (670 pairs of biopsies) with Barrett's oesophagus. Confocal images were interpreted live during examination as well as in a blinded controlled manner 3 months post endoscopy, and findings compared with histology. pCLE was found to be comparable to endoscopic biopsy in excluding neoplasia, but due to low its low PPV and sensitivity, authors concluded that pCLE may currently not replace the standard practice for the diagnosis of BO associated neoplasia.

Eosinophilic oesophagitis

A description of EO using pCLE, which was confirmed by corresponding histopathological analysis, was recently reported by Neumann *et al.* [161]. pCLE revealed small cells such as eosinophils within dilated intercellular spaces, capillary ectasia and mild mucosal oedema.

Biliary and pancreatic ducts

Current techniques to detect malignant biliary and pancreatic strictures are of low sensitivity. The delay in tissue confirmation of malignancy can place a patient at risk for progression of disease precluding surgical resection. On the other hand, the inability to confirm whether a stricture is benign or malignant could lead to unnecessary surgery.

The first international multicentre experience with pCLE to diagnose indeterminate pancreatobiliary strictures has been published in November 2011 [162]. A total of 102 patients undergoing endoscopic retrograde cholangiopancreatography (ERCP) for diagnosis of their clinical conditions were recruited in five academic centres. pCLE outperformed tissue sampling in sensitivity (98% vs. 45%), negative predictive value (97% vs. 69%), and overall accuracy (81% vs. 75%). However, pathology was unbeatable in specificity and positive predictive value. Delivery of the confocal miniprobe through a cholangioscope or via a catheter did not lead to significant differences in sensitivity and specificity. The authors suggested that pCLE may potentially increase diagnostic accuracy of ERCP in discerning benign from malignant strictures.

Loeser *et al.* [163] used pCLE in 14 patients with indeterminate biliary strictures together with standard biopsies and brushings. In parallel, they also examined rat bile ducts *ex vivo* using multiphoton microscopy to better understand the nature of the human bile duct structures visualized during confocal endomicroscopy. Of the 14 patients, 6 patients had a diagnosis of cancer. None of the criteria used to evaluate possible malignancy in the confocal images was found to be sufficiently specific for malignancy. An abnormal reticular network, which may reflect changes in lymphatic vessels, was never seen in benign strictures and the authors proposed that in the absence of markers of potential malignancy, if a normal reticular pattern is visible then the diagnosis of malignancy is unlikely. The reticular pattern seen in normal tissue was believed to be a network of lymphatic vessels as shown in multiphoton reconstructions of intact rat bile ducts and confirmed by special stains.

In 2008, Meining *et al.* [164] used pCLE to examine the biliary tract of 14 patients with biliary strictures at the liver hilus or the common bile duct. Patterns indicative of neoplasia were identified and pCLE predicted neoplasia with an overall accuracy of 86%, surprisingly outperforming preoperative tissue sampling (79%). After surgery, histopathology revealed invasive adenocarcinoma in 2 patients in which preoperative biopsy specimens were negative for neoplasia, whereas pCLE indicated the presence of malignancy. Also the median signal-to-noise ratio derived from a region of interest in both normal and neoplastic epithelium was significantly different (lower in neoplasia) accounting for less broad intrinsic fluorescence intensity distribution in neoplastic tissue, which reflects different concentration of fluorophores following structural neoplastic rearrangement. A dark grey background with poor mucosal structure and large white streaks (vessels) was mainly seen in neoplastic strictures. On the contrary, a reticular pattern of different grey scales and villous structure without white streaks was seen in patients without neoplasia.

Peroral pancreaticoscopy and pCLE has also been reported by the same group in a case of intraductal papillary mucinous neoplasm (IPMN) [165]. IPMN often goes unrecognized in

patients with chronic pancreatitis and its diagnosis is rather challenging. Based on the findings obtained with these two imaging methods, the diagnosis of IPMN was formed and was then confirmed by histology.

Colon

Inflammatory Bowel Disease

Normal-appearing mucosa in the terminal ileum (TI) of 27 patients with IBD and normal mucosa from 30 controls were imaged using Cellvizio Ultra-High Definition coloflex miniprobes (Mauna Kea Technologies, France) and then sampled for histologic confirmation [166]. By manual segmentation they were able to quantify epithelial cells and gaps introducing a novel endomicroscopic parameter called "gap density", defined as the number of gaps per 1000 epithelial cells. They found that the epithelial gap density of the TI in patients with IBD is 3 times higher than that of normal patients. The hypothesis is that higher gap density reflects increased cytokine-induced epithelial cell shedding and this parameter could be used to predict better response to conventional IBD therapy. There was no positive correlation of gap density with disease activity. On the contrary, severe clinical activity was associated with lower gap densities, suggesting that this parameter may play a role more as an indicator of the underlying disease mechanism rather than of the degree of disease activity. Though patients with Crohn's disease displayed different distributions from those with ulcerative colitis, gap density could not differentiate between the 2 disease populations due to the limited sample size.

In another study from the same group [167], pCLE of the TI was performed in 8 patients with Crohn's disease and 6 controls. In parallel, optical sections were obtained from the small intestines of IL-10-deficient knockout and normal mice using a rigid FIVE 1 confocal probe (Optiscan Pty. Ltd., Australia). In patients with Crohn's disease, the mean gap density, identified by the absence of acriflavine-stained nuclei, was found to be 6 times higher than that of control patients (117 vs. 17.7 gaps per 1000 cells). Consistently, the mean gap density in IBD induced mice was 1.7 times higher than that of normal mice.

Confocal imaging of dysplasia-associated lesional mass (DALM) in a patient with chronic ulcerative colitis, was also reported [168]. Morphological characterization with pCLE was performed both over the lesion and adjacent inflamed mucosa, showing features suggestive of dysplasia and inflammation respectively. The main aspect of inflamed mucosa consisted of dilation of crypt openings, irregular arrangement of crypts, crypt destruction and fusion, and crypt abscess. Dark mucin-depleted goblet cells and villiform epithelial digitations were recognized as dysplastic features in agreement with the Mainz classification for prediction of intraepithelial neoplasia [62].

A prospective pilot study on 22 patients under surveillance for ulcerative colitis was conducted by van den Broek *et al.* [169] using NBI plus HDE followed by pCLE before taking targeted and random biopsies. Reasonable diagnostic accuracy was achieved though movement artefacts significantly impaired significantly the video quality.

Colorectal neoplasia and dysplasia

Considering histology as gold standard, Buchner *et al.* demonstrated that pCLE can accurately discriminate between hyperplastic and adenomatous polyps, and detect residual adenomatous tissue after endoscopic mucosal resection (EMR) [170]. They then compared pCLE to NBI and FICE, collectively named as virtual chromoendoscopy, in 119 polyps (81 neoplastic, 38 hyperplastic) from 75 patients [171]. The pCLE had higher sensitivity compared to virtual chromoendoscopy (91% vs. 77%) for classification of colorectal polyps using histopathology as gold standard. In this study, high-definition WLE was used as the primary inspective technique. Prior to pCLE imaging, either FICE or NBI, depending on availability, were used after detection of a suspicious lesion.

They have also examined the learning curve faced by clinicians in correctly identifying benign and neoplastic colorectal lesions by using pCLE [172]. Accuracy of image interpretation and acquisition increased with the number of images observed (up to 86% beyond 60 lesions).

Considering histology as a gold standard, Buchner *et al.* demonstrated that pCLE can accurately discriminate between hyperplastic and adenomatous polyps, and has higher sensitivity than virtual chromoendoscopy (99% vs. 77%) [171].

In a recent prospective multicentre study, 92 patients who had their lesion removed by EMR in a previous colonoscopy were referred for follow-up colonoscopy within one year and inspection of EMR scars (n = 129) with NBI or FICE and pCLE to detect residual neoplasia. Accuracy of pCLE alone and in combination with NBI or FICE against histopathology as the gold standard, was of 81% and 90% respectively, whereas the cumulative accuracy of virtual chromoendoscopy (NBI + FICE) alone was 77% [173].

In vivo characterization of 32 superficial colorectal neoplastic lesions with pCLE was performed by De Palma *et al.* in 20 consecutive patients [174]. Probe-based CLE presumptive diagnoses were compared with histopathology of resected lesions or targeted biopsies. The sensitivity and specificity of p-CLE to differentiate neoplastic from hyperplastic lesions were 100% and 84.6% respectively.

The use of molecular biomarkers in combination with confocal endomicroscopy was first investigated by Hsiung *et al.* [175] to develop a fluorescent probe for detecting colon cancer. They identified a specific heptapeptide sequence, VRPMPLQ, which was conjugated with

fluorescein and tested in patients undergoing colonoscopy. The fluorescein-conjugated peptide was administered topically and was found to bind more strongly to dysplastic cells than to adjacent normal cells with 81% sensitivity and 82% specificity.

Wang *et al.* [63] conducted a pioneering observational study using pCLE in 54 patients undergoing bowel cancer screening colonoscopy with the aim to track the uptake and distribution of fluorescein from the crypts to the lamina propria after topical administration. This contributed to further understanding of the functional anatomy of the colonic glands in normal, hyperplastic and adenomatous tissue *in vivo*. As with histology, the typical shape and size of glands for each tissue type were clearly discriminated and there was correlation between tissue morphology and time of transit, with significantly longer time of passage through adenomatous mucosa (> 5 s) compared to hyperplastic or normal tissue. High diagnostic accuracy was achieved using the speed of absorption of fluorescein (contrast ratio) as a discriminant function to distinguish normal from diseased mucosa (89%), hyperplasia from adenoma (96%), and even tubular from villous adenoma (93%).

Focal high-grade dysplasia was identified using pCLE in a patient with longstanding ulcerative colitis presenting with colorectal squamous metaplasia, which had been incidentally found with random rectal biopsies (10 cm from the anal verge) at surveillance colonoscopy. Histology of pCLE targeted biopsies confirmed the presence of squamous dysplasia. pCLE showed disorganized vascularity with abnormal capillary loops as well as crowded and intensely dense nuclei in the squamous tissue.

Moderate to good interobserver agreement among three international experts and 76% accuracy in diagnosis of neoplasia was achieved using pCLE in a study on 53 patients with 75 colorectal lesions, 50 of which were neoplastic [176]. The authors concluded that current accuracy and interobserver agreement do not yet support routine clinical use in screening or surveillance colonoscopy.

2.6.1 Endocytoscopy (EC)

Endocytoscopy (EC, Olympus Corporation, Japan) is a novel imaging technique, enabling microscopic imaging of the GI mucosal surface with a magnification up to 1400x.

EC is based on a contact light microscope which enables real-time visualization of cellular structures of the superficial epithelial layer in a plane parallel to the mucosal surface. Cytological and architectural features, such as the size and shape of cells, nuclei and the nucleus:cytoplasm ratio, can be assessed.

This technique uses a fixed focus, high power objective lens that projects highly magnified images onto a CCD at a rate of 30 frames per second [177].

As for CLE, two types of endocytoscopy systems are currently available on the market. A probe based handheld miniprobe (pEC), providing magnification up to 570x and 1400x, which can be passed through the working channel of a conventional endoscope, and a system integrated into the distal tip of an endoscope (iEC) providing magnification up to 580x.

FOVs are 300 x 300 μm, 120 x 120 μm, and 400 x 400 μm for 570x pEC, 1400x pEC, and 580x iEC respectively. The axial resolution varies from 0 to 50 μm and the lateral resolution from 1.7 to 4 μm.

Using both systems, contact with the tissue surface is necessary for imaging. Endocytoscopy requires preparation of the mucosal layer with absorptive contrast agents like methylene blue or toluidine blue [178]. Prior to imaging and tissue staining the mucosal surface must be treated with a mucolytic to remove excess mucous. Repeat staining is often needed after ~ 5 minutes of imaging.

Clinical experience

Promising initial results, primarily in identifying and discriminating neoplastic from non-neoplastic tissue, have been shown in a few prospective studies [177,179-181]. Notably, EC was able to detect dysplasia in aberrant crypt foci of normal colon mucosa surrounding cancer [180], and discriminate invasive colon cancers from adenomatous polyps [179]. In contrast, only a limited role was found in detecting and predicting early oesophageal squamous cell carcinoma [182]. The potential of EC for the *in vivo* characterization of duodenal mucosa in celiac disease has also been reported [183].

Nevertheless, there is currently a paucity of interest and research on EC, possibly due to the requirement of topical staining, the relative lack of axial discrimination and the low resolution images compared to other microscopy techniques such as CLE.

2.6.2 Two-photon and multi-photon microscopy

Biological tissues are of course inherently three dimensional (3D) and typically have a high degree of scattering due to discontinuities in refractive index and the heterogeneity of their constituents, which makes high resolution 3D imaging challenging.

Optically sectioned fluorescence imaging can be realized with single-photon confocal (visible light) or multiphoton excitation. In multiphoton microscopy (MPM), the excitation occurs through the absorption of multiple photons of lower energy (typically halved in two photon microscopy). No pinhole is required to prevent out-of-focus fluorescence from reaching the

detector as excitation only occurs at the excitation spot. However, high incident power is required for multiphoton absorption to take place.

A major advantage of MPM is the longer wavelength light necessary to induce fluorescence (generally near-infrared, 700-1000 nm). Tissue absorption and scattering are limited in near infrared (NIR) allowing for deep-penetration imaging.

A number of groups have developed miniaturized MPM endoscopes [184-187]. However, there is no commercially available multiphoton endoscope system to date.

Recently, Rivera *et al.* [188] demonstrated a compact flexible raster scanning microendoscope capable of MPM and SHG by imaging *ex vivo* mouse tissue at 800 nm excitation. Images were acquired at 4.1 frames/s with a FOV of 110 μm × 110 μm using a double clad fibre and a mode-locked Ti:Sapphire as the excitation source. The distal end of the fibre was mounted onto a resonant/non-resonant scanner, which moved the fibre tip in a raster pattern across the back aperture of a miniaturized gradient-index lens assembly, enabling 2D lateral scanning.

2.6.3 Second (SHG) and Third (THG) Harmonic Generation Imaging

Similarly to MPM, SHG and THG also depend on respectively two or three photons interacting simultaneously with the tissue under investigation. A long excitation wavelength, typically in the 700-1000 nm range, is required for these phenomena to take place [189]. However, unlike MPM, in which two photons are absorbed to produce a single fluorescent photon, with SHG and THG photons are scattered and not absorbed by the tissue, to produce a new photon with twice (SHG) or thrice (THG) the energy of the incident photons. With these techniques, due to the absence of absorption, heating and damage of the sample are less likely to occur. Another advantage is their capability for three-dimensional imaging.

SHG techniques allow the imaging of “non-centrosymmetric” structures such as collagen, with reported tissue penetration depths between 100–300 μm with laser excitation in the NIR range. Therefore, they have been increasingly applied to characterize the structural changes occurring in the extracellular matrix during disease. One such example is the desmoplastic reaction that typically accompanies the progression of many cancers.

An important potential application of SHG microscopy in gastroenterology is imaging fibrosis in chronic liver disease. Fibrosis is characterized by an increased density of collagen resulting from an inflammatory response associated with a number of conditions (e.g., viral hepatitis, steatosis and liver cancer) and is often associated with organ dysfunction and, ultimately, failure. Sun *et al.* [190] characterized the changes in the distribution and quantity of collagen in a rat model of induced liver fibrosis using SHG microscopy. An automated segmentation

approach to quantify large collagen colonies with high connectivity (aggregated collagen) was compared with conventional histological stains, such as Masson's trichrome, showing good correlation with pathology.

2.6.4 Optical Coherence Tomography

Optical coherence tomography (OCT) is a high speed (~4 frames per second [191]) vertical plane imaging modality combining confocal scanning capability with low coherence interferometry, resulting in excellent rejection of scattered light and deep tissue penetration. The use of near-infrared light (from about 800 nm to 2500 nm) allows it to penetrate into scattering media more deeply (up to 4 mm, depending on tissue type) than confocal microscopy, with typical lateral and axial resolution of 15 μm and 10 μm respectively, although research systems have demonstrated axial resolutions on the order of 1 μm [191,192].

OCT is the optical equivalent of ultrasound imaging where ultrasound waves are replace by light [193]. As with endoscopic ultrasound (EUS), two main OCT imaging are available, linear and radial.

The basic components of an OCT system are a low-coherent light source and a beam splitter, which splits the light into two identical beams, one directed to the tissue and the other to a mirror. The signals coming back from the tissue and the mirror are combined using an interferometer, which, following signal processing steps allows cross-sectional images to be obtained. Contrast in OCT is essentially due to reflected or simply back scattered light from refractive index mismatches within tissue.

Clinical experience

Optical discrimination of the GI tissue layers was first described in a landmark paper by Tearney *et al.* [194] in normal and diseased tissues collected *post-mortem* and imaged using OCT.

Zuccaro *et al.* [195] showed that OCT was able to discriminate normal oesophageal mucosa from cancer. However, this novel technique has the intrinsic potential to reach the muscularis mucosae and thus discriminate non-invasive from invasive neoplasia. In a comparative study in normal tissue, Das *et al.* [196] have shown that OCT has a higher resolution than high-frequency (20-30 MHz) EUS for imaging this layer with accuracy. Accurate delineation of this layer would in fact assist clinicians in determining whether endoscopic therapy rather than surgery should be indicated.

In vivo endoscopic OCT was also used to assess the efficacy of radiofrequency ablation (RFA) in treating persistent rectal bleeding from radiation proctitis unresponsive to conventional therapy [197].

A form of OCT, termed comprehensive volumetric microscopy, has been proposed that acquires a 3D microscopic image of the full thickness distal oesophagus [198,199]. In a preliminary study by Suter *et al.* [200], volumetric microscopy of the distal oesophagus was performed in 66 patients referred for Barrett's oesophagus screening using a custom balloon catheter (2.5 cm diameter) that enabled spiral cross-sectional optical frequency domain imaging (OFDI), a high speed 2nd generation embodiment of OCT. Using histopathology as the gold standard, OFDI showed increased sensitivity for detection of specialized intestinal metaplasia compared to standard endoscopy.

Columnar and squamous epithelium in a region of heterotopic gastric mucosa (cervical inlet patch) in the upper oesophagus were clearly distinguished using a through-the-scope 3D OCT prototype probe. En face images were acquired up to 400 μm depth underneath the tissue surface and were compared with histology. Biopsies taken from the imaged lesion confirmed the endoscopic finding [201].

2.6.5 Future potential clinical optical imaging modalities

Raman spectroscopy

The Raman effect was first described in 1928 [202]. Since then, Raman spectroscopy has been used to probe the biochemical signatures of a multitude of biological molecules. The Raman effect results from energy exchange between incident light and scattering molecules within the tissue. It is also referred to as inelastic scattering as Stokes Raman scattered light has less energy than the incident light. Compared to Stokes Raman scattering, in anti-Stokes Raman scattering, the scattered photon has a higher energy than the absorbed photon.

Raman signals have typical narrow peaks generally associated with the vibration of a particular chemical bond in a molecule. As the bond stretches and shrinks, a shift in frequency, which is characteristic of a particular molecule, is indicated in the spectrum.

Therefore, Raman spectroscopy can provide highly specific molecular fingerprint information, which is chemically sensitive and label-free. Raman spectroscopy can be integrated with confocal microscopy for high spatial resolution. However, Raman signals are usually weak (cross-section typically 1000 times lower than fluorescence) and images require high laser power (typically >10 mW), ultrasensitive detectors and long acquisition times (>30 min), which are unsuitable for *in vivo* clinical use.

Clinical experience

The feasibility of *in vivo* Raman spectroscopy for *in vivo* use in GI endoscopy was first demonstrated in 2000 [203]. Raman spectra were obtained from various GI tract organs, including oesophagus and colon, during endoscopy using a custom built fibre-optic near-infrared Raman spectroscopic system at 785 nm excitation, but due to the limited set of data, only subtle differences were observed between normal and pathological states. Later on, distinctive *in vivo* Raman spectra were shown by the same group between 10 adenomas and 9 hyperplastic colon polyps with 95% accuracy [204]. Principal component and linear discriminant analyses were used to develop a diagnostic prediction model for classifying colon polyps based on their spectral emission. Raman spectra were also analysed from 20 hyperplastic and 34 adenomatous polyps, showing similar accuracy (93%) to the *in vivo* measurements.

Microscopy based Raman spectroscopy at 830 nm excitation, was used to classify and discriminate between normal and pathological states, with a particular focus on early epithelial malignancies, in a variety of organs, including larynx, oesophagus, and bladder [205]. Tissues were obtained during endoscopic or surgical procedures and immediately snap frozen. Histological assessment preceded the spectral measurements so that only samples with clearly defined pathologies and blind unanimous agreement from three expert histopathologists were measured. In the oesophagus study, Raman spectra were measured from 50 samples classified in eight different tissue states: normal squamous epithelium, cardiac BO, fundic BO, intestinal metaplasia, HGD, adenocarcinoma, squamous dysplasia, and SCC. No agreement was achieved on samples with LGD so this group was excluded from the analysis. Multivariate linear discriminant analysis was performed on the 8 groups, and by combining the spectra into three clinically significant groups: normal; BO; and BO neoplasia. 93.2% and 88.6% of cases were correctly predicted by the three and eight-group models, respectively. The development of a custom built confocal Raman fibre optic probe for endoscopic use was then presented by the same group [206]. Raman spectra were obtained from 58 oesophageal biopsy specimens and the probe performance was compared to a conventional spectrometer at both 2 and 10 s acquisition times. Subsequent *ex vivo* work using this probe at 830 nm excitation in 72 oesophageal samples from 35 patients, with acquisition periods of 10 and 2 s, reported a 73% overall correct classification in spectrally separating histological diagnoses into three clinically significant groups: normal, low risk (BO) and high risk (dysplasia and cancer) [207]. Recent *ex vivo* work using the probe in 298 fresh and 39 snap frozen oesophageal specimens collected during surgery or endoscopy from 28 patients, confirmed the ability of this system to discriminate BO and neoplasia with high levels of sensitivity and specificity (88% and 87% respectively [208].

Using a fibre-optic Raman endoscopy system under trimodal imaging guidance (WLE+NBI+AFI), an *in vivo* pilot study was recently conducted in 27 patients with suspected oesophageal cancer [209]. A non-negativity constrained least squares minimization (NNCLSM) biomolecular modelling and linear discriminant analysis were used to develop a diagnostic algorithm for separating normal oesophageal mucosa from cancer with 97% sensitivity and 95% a specificity.

Impressively, the full promising potential of moving the Raman spectroscopy into real-time during routine endoscopy, has been recently realized in the context of a national gastric cancer screening programme in Singapore, where a large number of Raman spectra (2465 normal and 283 gastric cancer) were acquired at 785 nm excitation from 305 patients [210]. The algorithm analysis developed had modest overall diagnostic accuracy but, most importantly, the study showed that real time acquisition per measurement (< 0.5 s) with a reasonably low power (1.5 W/cm^2) can be achieved, which is critical for *in vivo* clinical applications. Previous *in vivo* work published by the same group, combining NIR AF (Near-infrared autofluorescence) and Raman spectroscopy, revealed significant differences in both the spectral intensities and Raman peaks of different colonic tissues, including normal colon, hyperplastic and adenomatous polyps [211]. Intensities of adenomatous polyps were significantly lower than hyperplastic polyps, and normal tissue (p = < 0.001). The spectral shapes from different types of colonic tissues showed different decreasing trends from 810 to 1050 nm. Based on previous experience [212], they assumed porphyrins to be the major endogenous fluorophores responsible for NIR AF emission in tissue, particularly in proliferative lesions [213]. Increased contents of porphyrins for the adenomatous polyps as compared to hyperplastic polyps and normal colonic tissue were found using the NNCLSM biochemical modelling.

As anticipated in pioneering studies [204,214], with further development this technique has the ambitious potential to distinguish adenomas from hyperplastic or inflammatory colonic polyps, and low grade from high grade dysplasia within Barrett's oesophagus, which still remain the major controversial issues in GI pathology.

Coherent anti-Stokes Raman scattering (CARS) microscopy

Based on contrast derived from molecular vibration, CARS has the potential to provide fast imaging on a molecular level label-free and with 3D sectioning capability.

Unlike Stokes Raman spectroscopy, CARS employs multiple photons to probe the molecular vibrations, and produces a signal in which the emitted waves are coherent with one another. As a result, the CARS signal is orders of magnitude stronger than spontaneous Raman emission and, hence, can provide much faster imaging.

A detailed comparison of Raman imaging and CARS microscopy was carried out by Krafft *et al.* [69] on *ex vivo* colon tissue sections, offering the intriguing prospects of a combined complimentary method for label-free live-cell imaging at video-rate speed, which is ideal for most clinical applications.

Although prototype endoscopes capable to collect CARS signals have been developed [215,216], progress toward delivering *in vivo* CARS imaging in GI endoscopy is still awaited.

Diffuse reflectance spectroscopy

Diffuse reflectance spectroscopy – also known as elastic scattering spectroscopy (ESS) – is used to study the diffuse component of the reflected light that has been scattered multiple times within the tissue sample to be investigated.

A white light source, rather than a laser, is typically used to illuminate the sample and the reflected light is collected and transmitted by optical fibres to the analysing spectrometer. Delivery and collection fibres are usually separated by a set distance in order to allow the spectrometer to preferentially detect diffuse (rather than specular) reflections. The resulting data then consist of the diffuse reflectance of the sample as a function of wavelength.

As the propagation of light through a biological specimen depends on its intrinsic absorptive and scattering properties, the light elastically scattered can report on architectural changes at both cellular and subcellular level associated with disease, such as cellular and nuclear enlargement and crowding, and increased nucleus-to-cytoplasm ratio [217,218].

Diffuse reflectance spectroscopy has been widely used in clinical studies of skin cancer [219-221], cervix [222,223], and bladder [224,225]. A number of clinical studies have also been performed in the GI tract, demonstrating that diffuse reflectance spectra contain diagnostically useful information.

Clinical experience

Pioneering work with ESS was conducted by Mourant *et al*. in 1996 [226]. Reflectance spectra were taken *in vivo* from the colon of 15 patients and the stomach of 17 patients. The ratio of the area under the reflectance curve between 540 and 580 nm to that under that between 400 and 420 nm was used to discriminate neoplastic from non-neoplastic colon tissue. The slope of the spectrum in the 435 to 440 nm range was used to reasonably separate active colitis from quiescent colitis and normal colon mucosa. Gastric dysplasia was found in only one case, and this was separated from normal and inflamed gastric epithelia using the ratio between 355 and 360 nm to that between 630 to 635 nm.

Using multiple linear regression for spectral classification, adenomatous polyps were distinguished from hyperplastic polyps with sensitivity and specificity of 89 and 75%, respectively [227].

Zonios *et al.* [71] collected diffuse reflectance spectra *in vivo* on adenomatous polyps and adjacent normal colon in 13 patients undergoing colonoscopy. Significant spectral differences were observed, especially around 420 nm (Hb absorption valley), and these were attributed to the increased Hb concentration (6 times higher) of polyps relative to normal colon. In contrast, oxygen saturation was found to be similar in both normal and adenomatous tissue.

Wallace *et al.* measured diffuse reflectance spectra in 13 patients with a diagnosis of Barrett's oesophagus or suspected oesophageal cancer. The sites measured were subsequently excised and submitted for pathological assessment. The data were analysed by a model in which a site was classified as dysplastic if more than 30% of the nuclei were enlarged, with 'enlarged' defined as greater than 10 μm in diameter. Based on this model, the samples were correctly classified with high sensitivity and specificity (90 and 90%, respectively) for detecting either the presence of high grade or low grade dysplasia.

In a study by Lovat *et al.* [72], ESS measurements were collected *in vivo* from 81 patients with HGD or early cancer within Barrett oesophagus, and matched with histological specimens taken from identical sites within the segment of BO. All biopsies were reviewed by three GI pathologists and classified as low risk (non-dysplastic or low grade dysplasia) or high risk (high grade dysplasia or cancer). ESS detected high risk sites with a high sensitivity 92% but the specificity was only 60%. The specificity increased to 79% when ESS was used to discriminate high risk sites from areas of inflammation. A concurrent study from the same group, conducted on 45 patients undergoing colonoscopy, showed that ESS was able to discriminate with 84% sensitivity and 84% specificity between adenomatous and hyperplastic polyps, 80% sensitivity and 75% specificity between cancers and adenomas, 77% sensitivity and 82% specificity between IBD and normal colon, and 85% sensitivity and 88% specificity between dysplastic polyps and IBD [228].

Low-coherence enhanced backscattering (LEBS) spectroscopy, a variant of ESS, was recently proposed as an endoscopic pre-screening method for colorectal cancer (CRC) screening. Based on the concept of field carcinogenesis, micro-scale spectral changes were measured in biopsies of endoscopically normal rectum obtained from 219 patients undergoing colonoscopy to predict whether their colon harboured cancer or advanced adenomas elsewhere [229]. LEBS-detectable alterations in endoscopically normal rectum were seen to mirror neoplasia progression from patients with no neoplasia, to 5 to 9 mm adenoma and to advanced adenomas. For advanced adenomas, the LEBS signals had a sensitivity of 100% and a specificity of 80%. Further studies

with an endoscopically compatible fibre-optic probe are under way for validation of these results *in vivo*.

Angle-resolved low coherence interferometry

Changes in density and size of cell nuclei are considered characteristic biomarkers of dysplasia. By analyzing the angular distribution of the backscattered light from a sample at different depths, this technique enables the measurement of cellular and nuclear morphology and offers the potential to assess cellular structure and organization *in vivo*.

Pyhtila *et al.* [230] developed a probe-based frequency-domain angle resolved low-coherence interferometry (fa/LCI) system with sub-second acquisition time to make depth-resolved (up to 150 μm) quantitative measurements of changes in the size and texture of cell nuclei in tissue samples. Three oesophageal specimens from 3 patients, who underwent oesophagectomy for Barrett's neoplasia, were measured to examine the average nuclear size and density in healthy and dysplastic tissue, and findings were in complete concordance with histology.

Fluorescence Spectroscopy

Optical spectroscopy involves the study of the interactions of photons with biological tissue. The technique can be used either as point spectroscopy or as spectroscopic imaging. In point spectroscopy, a fibre probe is brought into contact with the tissue. Point by point measurements typically take 1-5 seconds for their execution and make it possible to take many more samples than can be currently achieved by conventional biopsies for histology, providing real time results. With point spectroscopy it is also possible to combine different optical techniques e.g. diffuse reflectance, time-resolved autofluorescence and light scattering spectroscopy, in one optical biopsy.

Fluorescence spectroscopy is an attractive technique for clinical use as it can be developed into a real-time adjunct for endoscopic examinations. Although prospective comparative studies of this technique and white light endoscopy have not yet been reported, it may well be envisaged that it may help in picking up early changes invisible to standard visualization by WLE.

Studies of autofluorescence spectroscopy and imaging, which provided useful guidance and reference material for the investigations conducted in this thesis, will be presented in chapter 3.

2.6.6 Summary

The aim of this section was to introduce the latest technologies that have the potential to change the way GI diseases are currently detected and characterised at endoscopy. They offer improved image resolution, contrast, and tissue penetration, and may report on biochemical and molecular changes beyond the discrimination of existing endoscopic methods.

Virtual chromoendoscopy and fluorescence endoscopy may be used in combination with magnification and high definition endoscopy for enhanced visualization of mucosal structures. Confocal endomicroscopy and endocytoscopy may allow for *in situ* disease characterization at cellular and sub-cellular level. Moreover, detailed morphological and molecular information may be achieved with light-scattering, autofluorescence and Raman spectroscopy. Furthermore, OCT may offer the visualization beyond the mucosa extending the view of the endoscopist to the deeper layer of the GI wall.

However, the adoption of any of these techniques in clinical practice still requires further extensive evaluation.

2.7 Unmet clinical needs in GI endoscopy

The diagnostic accuracy of both conventional and advanced endoscopy is still not satisfactory [160,169,231-233]. Despite all the recently achieved technological advances described in this chapter, easy and accurate detection of dysplasia, early detection of malignancies and accurate discrimination of inflammatory disease from neoplasia remain the main challenges in GI endoscopy. There are at least five main domains where the clinical needs are still not met, which are:

1. Polyps
2. Early stage neoplastic lesions
3. Flat and elevated dysplasia in inflammatory bowel disease (IBD)
4. Dysplasia in Barrett's oesophagus (BO)
5. Inflammatory conditions characterised by macroscopically inconspicuous mucosa such as eosinophilic oesophagitis and microscopic colitis.

In these conditions, the ability to detect and discriminate dysplasia or neoplasia from regenerative, inflammatory or hyperplastic changes would be of great interest to the endoscopist and benefit to the patient.

Ideally, endoscopists should be able to detect, characterise and confirm the nature of a lesion at the bedside, minimising uncertainties and targeting biopsies and resections only where necessary. However, under conventional WLE inspection, at present the sole established technique available to most of humanity, premalignant conditions and early cancers with minimal or absent mucosal abnormalities can frequently escape detection.

For colonic polyps, miss rates of up to 25% during colonoscopy have been reported [234-236]. Interval cancers have also been found in patients with a history of adenomatous (premalignant) polyps, despite regular colonoscopy surveillance [237,238]. As discussed in section 2.1.2, adenomas usually originate as diminutive polyps. However, only two thirds of colorectal cancer seems to develop through the stage of adenoma, the other third growing *de novo* from normal epithelium [43]. Aberrant crypt foci, defined as colonic crypts with a larger diameter and a thicker epithelium than normal mucosa, have been proposed as one of the earliest stages of malignant transformation. However, these changes are too subtle to be visualised with a standard endoscope [239]. Similarly, detection of flat polyps, which are characterised by a high malignant potential compared to sessile and pedunculated polyps [45,46], can be extremely difficult because of the less well-defined subtle findings.

Detection of early stage neoplastic lesions of the GI tract is still a grey area in clinical endoscopy due to the minute changes such as faint mucosal irregularities or discoloration, which can be

easily overlooked. For instance, apart from Japan, only 10% of gastric cancers are detected at an early stage in most of the world [19]. Although chromoendoscopy is increasingly employed, the identification of early cancer remains poor unless an obvious abnormality such as an ulcer or mass is found.

Dysplasia and malignant transformation represent the most important complication in patients with IBD. At present, annual endoscopic surveillance is recommended after 8-10 years of disease. In patients with UC, if no lesions are observed, four biopsy specimens are taken randomly at every 10 cm between the rectum and the caecum for a total of 40-50 biopsies per colonoscopy [38]. However, even this massive sampling regimen examines less than 1% of the total colonic mucosa surface. In addition, the natural history of dysplasia in the context of IBD is poorly understood. Dysplasia in IBD can be flat (endoscopically invisible) or elevated (endoscopically detectable)[240]. Elevated lesions are referred to as dysplasia-associated lesions or masses (DALMs), and are broadly separated into adenoma-like and non-adenoma-like depending on whether they resemble or not endoscopically to sporadic adenomas unrelated to IBD. It is still unclear if all elevated dysplastic lesions begin as flat endoscopically invisible dysplasia, and it is extremely difficult if not impossible to discriminate dysplasia from regenerative or inflammatory changes both in presence or absence of a visible lesion (i.e. pseudopolyps, DALM, raised or depressed areas of mucosa). One of the major problems faced by clinicians during endoscopic surveillance for cancer in patients with IBD is the histological finding of dysplasia detected in random (non-targeted) biopsies of diffusely inflamed mucosa as well as of macroscopically normal mucosa, and not in those targeted to a visible lesion.

In Barrett's oesophagus, up to 40% of high grade dysplasia was found to be associated with inconspicuous synchronous occult foci of adenocarcinoma after oesophagectomy [241,242]. Standard videoendoscopy identifies BO and obvious mucosal abnormalities (e.g. nodules, raised and depressed areas) but cannot distinguish intestinal metaplasia from dysplasia or other types of metaplasia (cardiac, oxyntic) not at risk of malignancy. Moreover, the current standard method for detecting dysplasia in patients with BO is a random 4 quadrant biopsies protocol, but dysplasia can easily be missed as only a small fraction of the Barrett's segment (less than 3.5% of the total surface of a 2-cm-long segment) is sampled [32].

Finally, in frequently encountered benign conditions like eosinophilic oesophagitis and microscopic colitis, whose incidence has rapidly increased over the last few decades, there is no sign of inflammation on the mucosal surface during the endoscopic examination, and therefore multiple random biopsies are necessary for the diagnosis. However, the diagnostic yield of random biopsies is often low and incurs a high cost [243,244].

Beside these considerations, another important emerging need is the increasing demand for endoscopy arising from screening and symptomatic work in an era of increasingly finite resources. This poses the difficult question of how to maintain and advance achievements in research and education, whilst meeting the rising demand on endoscopy services and constrained capacity.

Chapter 3: Introduction to fluorescence, fluorescence lifetime and autofluorescence spectroscopy and imaging

This chapter provides an introduction to the principles, techniques and prior knowledge that directly relate to the experiments described in this thesis. The first section will introduce the principles and properties of fluorescence and fluorescence lifetime, and the methods used for their measurement will be discussed. Relevant definitions and examples will be provided to clarify the terminology used throughout this thesis. It will also review the current knowledge relating to the interaction of light with biological tissue and the origins of tissue autofluorescence. Autofluorescence is a complex phenomenon that has been studied widely, but its origins are still not entirely known for many tissue types. The known endogenous fluorophores of biological tissue are then described in detail, followed by a discussion on the expected and possible fluorophores within the different structures of the gastrointestinal wall.

The second section will give an overview of the state of the art of endoscopic instrumentation for fluorescence lifetime spectroscopy (FLS) and imaging (FLIM), with an emphasis on the systems in current development at Imperial College.

In the third section, a comprehensive literature review of autofluorescence spectroscopy and imaging in the gastrointestinal tract, focusing on studies of premalignant and malignant conditions. Finally, a summary with the motivation for the work presented in this thesis is discussed.

3.1 Introduction to fluorescence

Fluorescence is defined as the emission of light by a medium (e.g. tissue) that has absorbed light of a different wavelength. In most cases, the emitted light has a longer wavelength, and therefore lower energy, than the absorbed radiation. Stokes coined the term “fluorescence” to describe this phenomenon in 1852 [245].

Fluorophores are molecules within tissue that spontaneously emit light when illuminated by light at appropriate wavelengths. When these molecules are illuminated they can absorb energy from the incident photons and an electron within the molecule may enter an excited state. The absorption spectrum is characteristic of the absorbing species. An electronically excited molecule may remain in an excited state for a period of picoseconds to nanoseconds before subsequently returning to its ground state by the spontaneous emission of a photon.

Because this process is not 100% energy efficient, the emitted photon will necessarily have less energy, and therefore a longer wavelength, than the absorbed photon. Thus fluorescence will

have a longer wavelength than the excitation light; this phenomenon is known as Stokes' shift. A fluorophore in the excited electronic state may also return to the ground state by a number of non-radiative processes (i.e. without the emission of fluorescence). The likelihood that radiative or non-radiative decay occurs depends on the fluorophores' physicochemical environment and may be sensitive to factors such as local pH or viscosity.

It should be noted that while the excitation of a fluorophore molecule is usually by a single photon, it is possible for it to be excited by absorbing 2 lower energy photons at virtually the same time. The 2 photons will each have half the energy (and therefore double the wavelength) that a single exciting photon would have and so together provide the necessary total energy to promote an electron from the ground state to an excited electronic state. This two-photon excitation forms the basis of multiphoton microscopy [246].

When investigating fluorescence, one may consider the intensity, the wavelength of both the excitation light and the emitted fluorescent light, and the lifetime of the emitted fluorescent light. These values will be different for different fluorophores. Thus, a fluorophore may be characterised by its quantum yield, its excitation and emission spectra and its fluorescence lifetime [247].

3.1.1 Fluorescence Intensity and Quantum Yield

The intensity of the fluorescence emitted by a fluorophore is a function of its concentration and its quantum yield. When a fluorophore absorbs photons, not all of the excited molecules will fluoresce as some may return to the ground state by non-radiative means.

The quantum yield (Φ) of the fluorophore may be defined as the number of molecules that emit fluorescence divided by the total number of molecules excited (equation 3-1).

$$\Phi = \frac{number\ of\ photons\ emitted}{number\ of\ photons\ absorbed} \qquad \textbf{Equation 3-1}$$

It may also be expressed in terms of the radiative (Γ) and non-radiative (k) decay rates of the excited fluorophore (equation 3-2).

$$\Phi = \frac{\Gamma}{(\Gamma+\kappa)} \qquad \textbf{Equation 3-2}$$

Absolute values of quantum yield for a fluorophore are very difficult to determine as they require knowledge of both the absorbed and emitted radiation fluxes and the fluorophore

concentration. This is particularly difficult in biological tissues, where a number of light-matter interactions such as scattering and absorption complicate the measurement.

3.1.2 Fluorescence Spectra

For each fluorophore there is a range of vibrational energy levels in the excited electronic state into which the fluorophore can be excited from the ground state by absorbing a photon. Consequently, photons of different amounts of energy (i.e. light of different wavelengths) may excite a fluorophore and generate fluorescence. The range of wavelengths of light that can excite a fluorophore is referred to as the fluorophore's excitation spectrum. Similarly, a fluorophore in the excited state can undergo radiative electronic transition to a range of vibrational energy levels in the ground state. Thus the emitted photons from a fluorophore will have varying amounts of energy and so the emitted fluorescent light will be of a range of different wavelengths. The range of wavelengths of light that can be emitted following excitation of a fluorophore is known as the fluorophore's emission spectrum. Because of the Stokes' shift the emission spectrum of a fluorophore will always be red-shifted with respect to the excitation spectrum. As different fluorophores have different fluorescence spectra, the spectral resolution of fluorescence from a heterogeneous sample may help discriminate between different fluorophores.

3.1.3 Fluorescence Lifetime

Following light absorption, a fluorophore will remain in an excited electronic energy state for a very short period of time before returning to their ground state via emission of fluorescent light, in a manner somewhat similar to the radioactive decay of an unstable atom.

Thus, fluorescent light from a sample does not instantaneously cease the moment that the excitation light is extinguished; rather, it decays away over a period of nanoseconds as excited fluorophore molecules in the sample return to their ground state (figure 3-1).

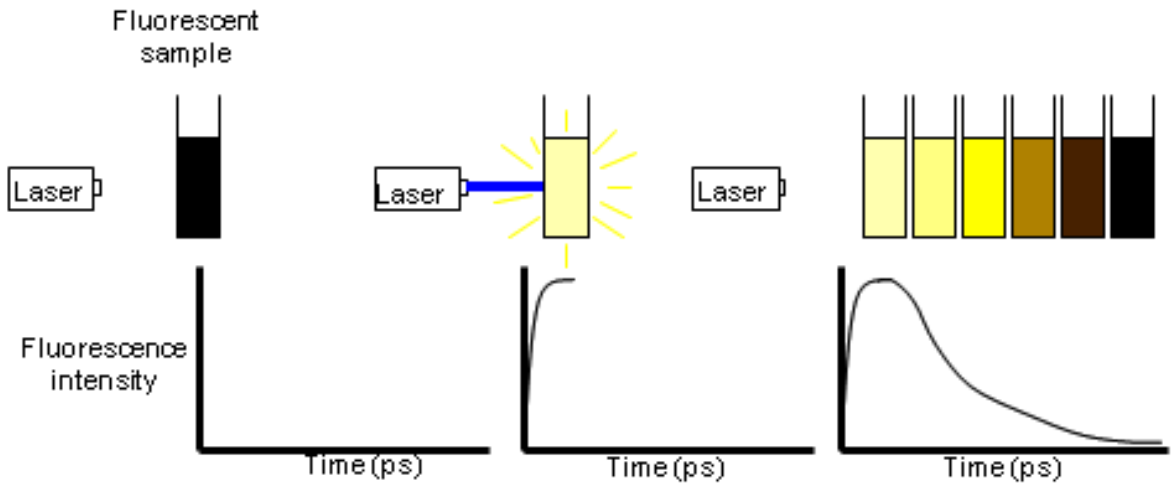


Figure 3-1: Illustration of the decay of fluorescence from a sample over a period of picoseconds after removal of the excitation light. Adapted and reproduced with permission from [248,249].

This period is referred as to fluorescence lifetime (FL) and the energy transfer is schematically illustrated with the classical Jablonski diagram (figure 3-2 (a)).

Thus, fluorescence lifetime is the average time a fluorophore takes to radiatively decay after having been excited from its ground energy level, and, like the quantum yield, is also a function of the radiative and non-radiative decay rates and so can provide quantitative fluorescence based molecular contrast. The key point is that different fluorophores decay at different rates, and this parameter can be mapped at every pixel in an image in order to produce a fluorescence lifetime image (figure 3-2 (b)).

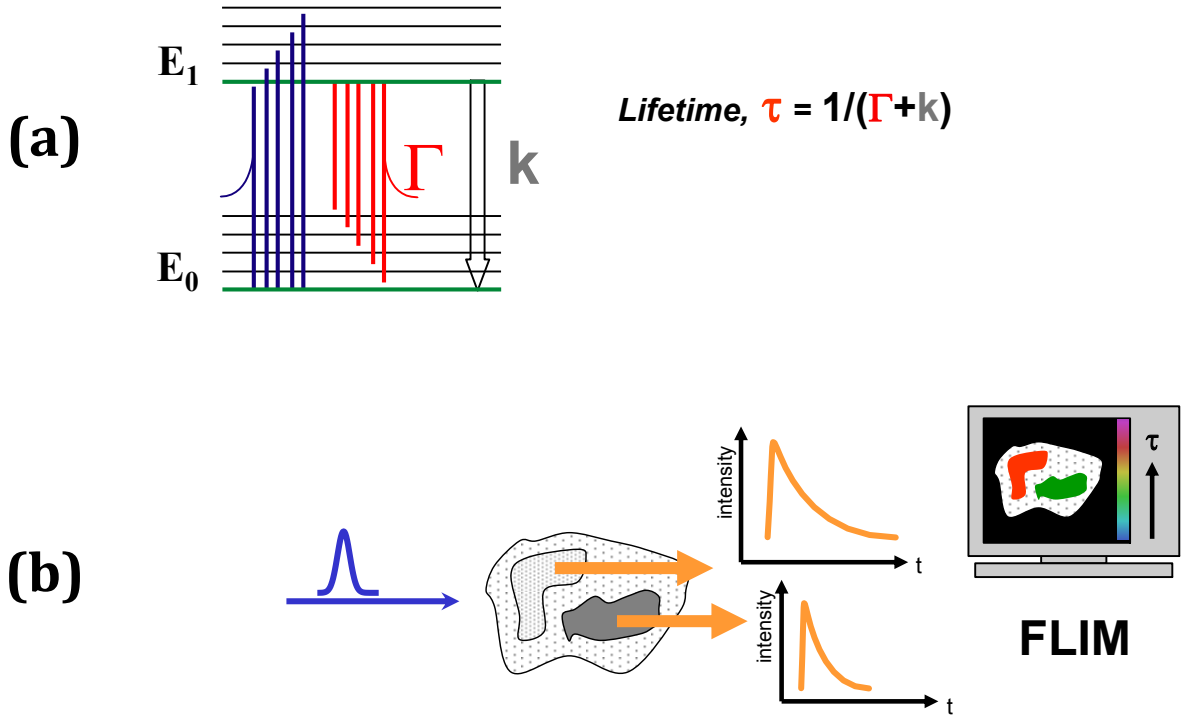


Figure 3-2: **(a) Jablonski diagram showing electronic energy levels of ground (E_0) and excited (E_1) states and both radiative (Γ) and non-radiative (κ) decay pathways in a fluorescent molecule. (b) After a short pulse of light, fluorescence emitted from the sample decays away over a period of nanoseconds as excited molecules return to their ground state. FLIM produces images using the fluorescence lifetime determined at each pixel to provide image contrast, displayed through a false-colour scale, between tissues or different components within the tissue with different fluorescence decays.**

The rate of this decay is dependent on the fluorescence lifetime (τ) of the sample, which is defined as the average time that a fluorophore molecule remains in the excited state before returning to the ground state. Typical fluorescence lifetimes are of the order of picoseconds (10^{-12} s) to nanoseconds (10^{-9} s). The fluorescence decay is approximately exponential for a single fluorescent species. A mathematical description of this single exponential decay in fluorescence intensity from such a fluorophore following cessation of the excitation light is shown in equation 3-3:

$$I_t = I_0 e^{-\frac{t}{\tau}} \qquad \textbf{Equation 3-3}$$

where I_t is the fluorescence intensity from the sample at time t after the excitation light has ceased, I_0 is the fluorescence intensity at time 0 (i.e. at the instant the excitation light is removed) and e is the exponential constant (e = 2.718281…). Thus, unlike quantum efficiency, fluorescence lifetimes can be determined from *relative* intensity measurements without the

requirement for knowledge of fluorophore concentrations and radiation fluxes. Just as fluorophores have characteristic fluorescence spectra, they also have different fluorescence lifetimes. The temporal resolution of fluorescence adds an extra dimension of contrast to distinguish and contrast between different fluorophores in a heterogeneous medium.

The lifetime of a fluorophore depends on the rate of decay from the excited electronic state back to the ground state by both radiative (Γ) and non-radiative (κ) means (equation 3-4):

$$\tau = \frac{1}{\Gamma + \kappa} \qquad \textbf{Equation 3-4}$$

The radiative decay rate (Γ) is essentially a function of the fluorophore and is relatively unaffected by its surrounding environment. Conversely, the non-radiative decay rate (κ) depends on the fluorophores' local physicochemical environment. It may be sensitive to a number of different parameters such as viscosity, temperature, pH and oxygen concentration as all these factors may impact on the intermolecular events that account for the non-radiative transition of an excited fluorophore to its ground state. Therefore, fluorescence lifetime can be influenced by, and so can be used as an indicator of, a certain fluorophore's local environment. Thus, the measurement of temporally resolved fluorescence affords the possibility of obtaining functional as well as structural information.

A single exponential decay model provides an accurate description of fluorescence decay only if a single fluorescent species is present in the sample being excited. If more than one fluorophore or fluorescent species is present the various fluorophores will each contribute to the sample's fluorescent decay. In heterogeneous samples such as tissue a mixture of fluorescent components in a variety of environments would be expected resulting in a very large number of separate decays. For example, a protein may contain a large number of residues of the fluorescent amino acid tryptophan; the different positions of the tryptophan moieties within the protein and the different conformations of the protein will all affect the fluorescence lifetimes [250]. A multiexponential decay rather than a single exponential may then be more appropriate model, where the intensity profile of a fluorescent sample with *n* exponential decay components is expressed by the following equation [251,252]:

$$I(t) = \sum_{i=1}^{n} \alpha_i e^{-t/\tau_i} \qquad \textbf{Equation 3-5}$$

where τ_i represent the decay constants and α_i the pre-exponential factors.

Having recorded the fluorescence decay and extracted the decay constants τ_i and pre-exponential factors α_i, the sample under investigation can therefore be parameterised using a single value obtained calculating the intensity weighted mean fluorescence lifetime according to equation 3-6:

$$\tau_{mean} = \frac{\sum_{i=1}^{n} \alpha_i \tau_i^2}{\sum_{i=1}^{n} \alpha_i \tau_i} \qquad \textbf{Equation 3-6}$$

An alternative way to parameterise the sample is to calculate the amplitude weighted mean fluorescence lifetime and this can be achieved according to equation 3-7:

$$\tau_{mean} = \frac{a_1 \tau_1 + a_2 \tau_2}{a_1 + a_2} \qquad \textbf{Equation 3-7}$$

An important characteristic of the fluorescence lifetime is that it is an inherently ratiometric quantity as it depends on the intensity decay as a function of time and not on the absolute intensity [252]. As such, unlike measurements with the intensity signal alone, measurements of the fluorescence lifetime do not suffer from uncertainties due to variations in fluorophore concentration or excitation power [253,254]. For this reason, considerable research efforts have been directed towards the development of instruments for time-resolved fluorescence spectroscopy and imaging [255-259]. Additionally, the fluorescence lifetime has been shown to be sensitive to the local environment of a fluorophore, reporting on factors such as pH [260], ionic concentration [261], viscosity [262] and temperature [263,264]. Most importantly from the perspective of this thesis, the fluorescence lifetime has been shown to help discriminate between healthy and diseased tissue [265-273].

3.1.4 Autofluorescence of biological tissue

When studying autofluorescence of biological tissue, the molecular composition is often unknown and so tissue autofluorescence can present a complex signal resulting from an unknown number of endogenous fluorophores with unknown relative concentrations. Interpretation of autofluorescence data is therefore highly challenging, typically requiring *a priori* knowledge of tissue structure and physiological function to yield quantitative information. Nevertheless, the potential for label-free contrast as a diagnostic tool is compelling and empirical autofluorescence contrast is finding its way into clinical practice while an increasing number of *ex vivo* and *in vivo* studies, including this thesis, are directed at understanding the molecular origins of tissue autofluorescence and the contrast available.

In biological tissue, autofluorescence can provide a source of label-free optical contrast, offering the potential to discriminate between healthy and diseased tissue. The prospect of detecting molecular changes associated with the early manifestations of diseases such as cancer is particularly exciting. For example, accurate and early detection of cancer allows earlier treatment and significantly improves prognosis [274].

The autofluorescence signal excited in biological tissue will depend on the concentration and the distribution of the fluorophores present, on the presence of chromophores (principally haemoglobin) that absorb excitation and fluorescence light, and on the degree of light scattering that occurs within the tissue [275]. Autofluorescence therefore reflects the biochemical and structural composition of the tissue, and consequently is altered when tissue composition is changed by disease states such as inflammation or cancer. In order to exploit autofluorescence for clinical applications, it is first necessary to investigate the autofluorescence "signatures" of normal and diseased tissue states.

The interactions of light with biological tissue

Biological tissue is a complex optically turbid medium and only a small fraction of incident light is returned as fluorescence. When incident light reaches the surface of a tissue it may be directly reflected or it may enter the tissue. Light is scattered within the tissue due to small differences in the refractive index caused by cell nuclei and cell organelles [276]. It may then exit the tissue surface as diffusely reflected light or be absorbed by molecules within the tissue. If the light is absorbed by a fluorophore it may be converted to fluorescence. This fluorescence light is again scattered within the tissue and may be reabsorbed by another molecule or may exit the tissue (figure 3-3). Thus the measurement of tissue fluorescence is complicated by the tissue scattering and absorption of both the excitation and the fluorescence emission light. It follows that the fluorescence intensity and excitation and emission spectra of the tissue may be altered.

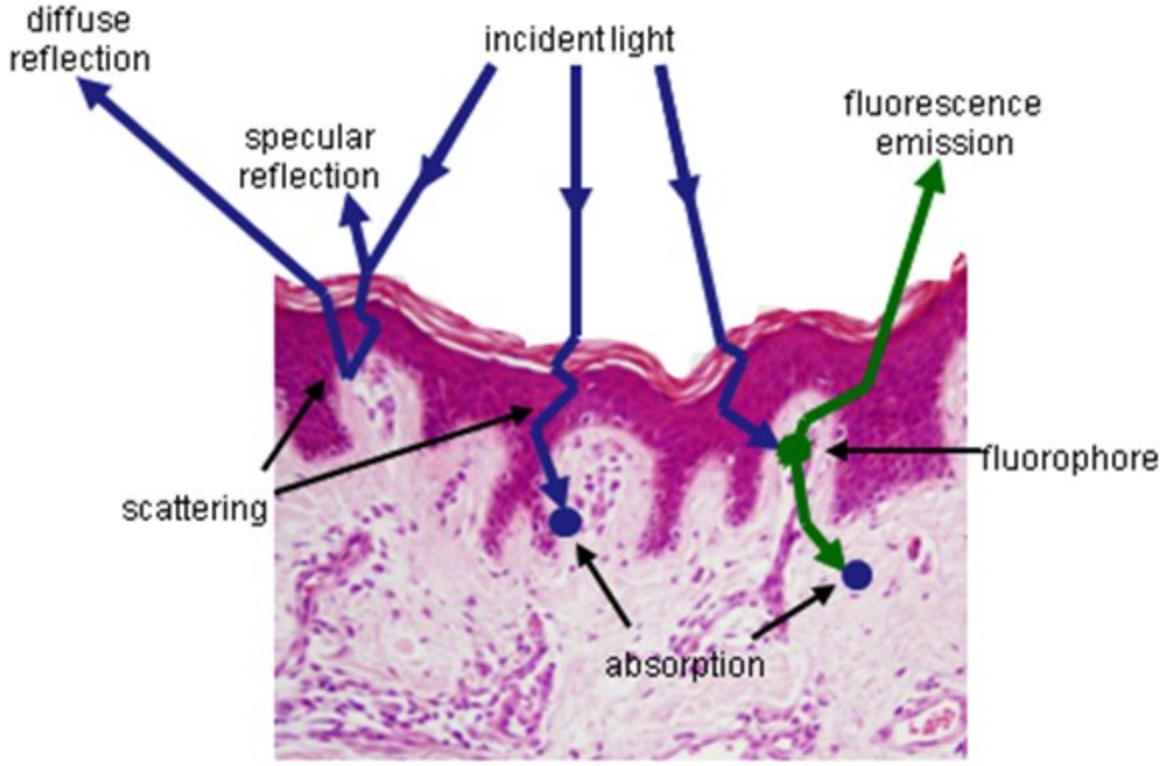


Figure 3-3: Schematic diagram illustrating the interactions of light with biological tissue. Adapted and reproduced with permission from [277].

Fluorescence lifetime values are less affected by the effects of absorption and scattering in tissue [278]. The principal absorber of excitation and emission light in the UV and visible wavelengths in biological tissue is haemoglobin [279]. Its absorption is wavelength dependent and generally decreases with increasing wavelength, with maximal absorption at around 420 nm. As a result, the penetration depth of light into biological tissue ranges from a few hundred micrometres for UV light to several centimetres for near-infrared as light absorption by haemoglobin decreases [280]. Only those fluorophores contained in the tissue layers to which the excitation light penetrates and from which emitted light can reach the tissue surface will contribute to the tissue fluorescence measured at the surface.

The origins of tissue autofluorescence

Biological tissue contains a number of fluorophore molecules. These endogenous fluorophores account for the autofluorescence observed from biological tissue on illumination with an appropriate wavelength of excitation light. Analysis of tissue autofluorescence provides insights into the structure, composition and metabolic status of tissue.

The main tissue fluorophores include collagen and elastin (crosslinks), reduced nicotinamide adenine dinucleotide (NADH), oxidized flavins (FAD and FMN), and porphyrins. As shown in figure 3-4, these fluorophores have their excitation maxima in the UVA or the blue (325-450 nm) spectral region and emit fluorescence in the near-UV to the visible (390-700 nm) region of the spectrum.

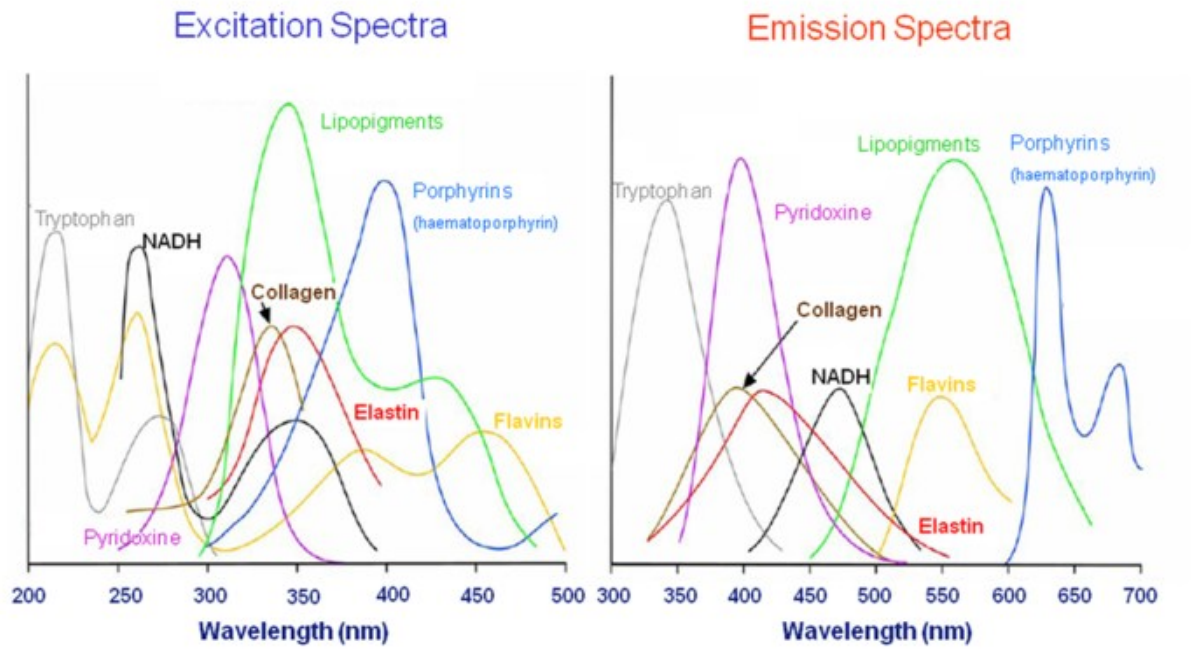


Figure 3-4: Excitation and emission spectra of main endogenous tissue fluorophores. Adapted and reproduced with permission from [213].

The excitation and emission spectra of the main tissue fluorophores are reported in table 3-1.

Unfortunately, many of the endogenous fluorophores found in biological tissue have similar or overlapping emission spectra (e.g. collagen, elastin and NADH). This necessarily limits the contrast that can be achieved by imaging spectrally-resolved fluorescence at a single excitation

wavelength. Investigators using point measurement techniques of spectrally-resolved fluorescence usually compare the emission spectra at two or three excitation wavelengths to help differentiate between the different fluorophores present. Fluorescence lifetimes can help differentiate between the different biological fluorophores.

The main endogenous fluorophores fall into three categories: the aromatic amino acids (tryptophan, tyrosine and phenylalanine); molecules involved in tissue metabolism (NADH and flavins); structural matrix proteins (elastin and collagen). In addition, other fluorophores that, depending on their concentrations, may contribute to tissue autofluorescence are porphyrins, vitamin A, vitamin B6 and lipoproteins.

Fluorophore	**Optimal Excitation (nm)**	**Emission Spectra (nm)**	**Lifetime (ns)**
Tyrosine	250-290	300	2.5
Phenylalanine	240-270	280	7.5
Tryptophan	250-310	350	3.03
NAD(P)H free	300-380	450-500	0.3
NAD(P)H protein bound	300-380	450-500	2.0-2.3
FAD	290-520	520-570	2.91
FAD protein bound	420-500	520-570	<0.01-1
FMN	420-500	520-570	4.27-4.67
Riboflavin (Vitamin B2)	420-500	520-570	4.12
Elastin	300-370	420-460	≤ 2.3
Collagen	280-350	370-440	≤ 5.3
Melanin	300-800	440, 520, 575	0.1/1.9/8
Keratin	290	525	1.4
Protoporphyrin IX	400-450	635-710	up to 15
Lipofuscin	340-395	430-460, 540	1.34

Table 3-1: Spectral characteristics and absolute lifetime values of the main endogenous tissue fluorophores reported in literature [280-282].

Aromatic amino acids

The aromatic amino acids tryptophan, tyrosine and phenylalanine are all fluorescent [275] and proteins containing these amino acids are found throughout all biological tissues. However, they require UV-B or UV-C light for excitation as the excitation maxima of all 3 amino acids are below 300 nm [275]; UV-B and UV-C light are both potentially harmful to living tissue and have extremely poor tissue penetration. It is unlikely that aromatic amino acid fluorescence accounts for any of the tissue fluorescence measured in the experiments reported in this thesis.

Pyridine nucleotides and flavins

The pyridine nucleotides and the flavoproteins are intracellular molecules found predominantly within mitochondria. They play an important role as electron carrier co-enzymes in the electron transport chain of aerobic cellular metabolism for ATP production [283].

NADH derives from the nicotinamic acid and was discovered from deproteinised yeast extracts by Harden and Young in 1904 [284].

NADH and NAD(P)H are the reduced forms of the two nucleotides Nicotinamide adenine dinucleotide (NAD+) and nicotinamide adenine dinucleotide phosphate (NADP+). The difference between NADH and NAD(P)H in terms of their structure is a single phosphate group.

The oxidised form NAD^+ normally prevails over the one reduced. In contrast to NADH, the reduced form NAD(P)H predominates. However, NADH is found in greater concentrations than NAD(P)H within the cell and the fluorescence of NADH prevails over that of NAD(P)H [285].

Flavins are co-enzymes derived from riboflavin and were first isolated from egg white by Kuhn and Karrer in 1935 [286]. The most common forms of flavins are flavin mononucleotide (FMN) and flavin adenine dinucleotide (FAD). An isoalloxazine ring is responsible for the fluorescence emitted from their oxidised forms.

Nicotinamide adenine dinucleotide is fluorescent in its reduced form (NADH) but only minimally so in its oxidised form (NAD^+) [287]. The opposite is true for flavin adenine dinucleotide (FAD) and flavin mononucleotide (FMN); their reduced form does not fluoresce whereas their oxidised forms are fluorescent [287]. Because of this difference, measuring the fluorescence from tissue NADH and flavins can report on the ratio of oxidised and reduced electron carriers ("redox ratio") and hence yield information on the tissue metabolic activity [287,288]. NADH fluorescence is maximal at excitation wavelengths of around 340 nm and little fluorescence occurs with excitation at wavelengths longer than 400 nm; the peak of its emission spectrum is at 460 nm [287]. Most intracellular NADH is found in the mitochondria, where it is usually bound to enzymes [289]. Protein binding increases the fluorescence quantum yield of NADH, affects its emission maximum and lengthens its fluorescence lifetime from 0.4 ns to 1.0-

4.0 ns [290,291]. Skala *et al.* [292] recently demonstrated a decrease in protein-bound NADH lifetimes measured *in vivo* from severe dysplasia in the hamster cheek pouch model of oral carcinogenesis.

FMN fluorescence quantum yield is roughly 10 times greater than that of FAD [293]. The flavins have excitation maxima of around 450 nm and emission maxima of 515-530 nm. The flavins have a broad absorption spectrum between 200 and 500 nm with an emission peak at 525 nm [293,294]. The fluorescence lifetime of FAD is around 4.7 ns; that of FMN is around 5 ns but becomes much shorter with protein binding [275,293,295,296].

Structural extracellular proteins

Collagens are one of the most important contributors to tissue autofluorescence. They are found in extracellular matrix throughout the body [297]; tissues such as connective tissue, cartilage and bone are particularly rich in collagen. A large fraction of collagen autofluorescence is attributable to the cross-linkages that form between collagen molecules [298], although there is also some contribution from aromatic amino acids and from other fluorescent residues within collagen monomers [299].

At least 6 different types of fluorescent collagen cross-linkages have been described [298,300] and excitation and emission spectra have been measured for each of these crosslinks. These spectra, together with the spectra of the aromatic amino acids found within the collagen molecules, contribute to the excitation and emission spectra of the different collagen proteins.

Collagen type IV (the principal component of basement membranes) has emission peaks at 344 nm, 365 nm, 392 nm and 430 nm, with corresponding optimal excitation wavelengths of 280-310 nm, 310-350 nm, 340-350 nm, and 320-380 nm [301]. In general, most collagens have excitation maxima of around 320-330 nm and emission maxima of around 400 nm. The fluorescence decays of collagen are similarly complex due to the contributions of different crosslinks and other fluorescent components [302].

Elastin is another insoluble polymeric structural protein found particularly in elastic tissue such as arterial wall, lung parenchyma and skin. Like collagen, elastin autofluorescence is believed to be partly due to its cross-linkages. As elastin autofluorescence is due to several fluorophores, its fluorescence decay profile is complex, with a mean lifetime of around 2.2 ns [302,303].

Porphyrins

The porphyrins consist of a family of proteins derived from the tetrapyrrole molecule-porphyrin. They are found as intermediate metabolic products during the synthesis of haem. Protoporphyrin IX is the more studied type of porphyrin. Normally the concentration of these

molecules is low, and once haem is bound to iron in haemoglobin, their fluorescence is quenched and cannot be detected.

The absorption spectrum of porphyrins consists of 4 peaks, the Soret absorption maximum at ~405 nm and four smaller Q-bands ranging from 500-630 nm. Their fluorescence emission spectra peak between 624-633 nm, depending on the porphyrin. When excited at this wavelength, protoporphyrin IX was found to have a fluorescence peak at 633 nm [304]. Porphyrins are known to exhibit long fluorescence lifetimes up to 17 ns [305] [280-282].

Lipofuscin

Lipofuscin is an intracellular pigment that has been found in a number of tissues, including the skin, brain, heart, liver and retina [282] [306]. In the colon, the presence of lipofuscin has been associated with *melanosis coli* and the use of anthraquinone laxatives [307,308]. It is found in histiocytes or macrophages and is considered to represent a cellular degradation product from cells undergoing apoptosis. It consists of aggregates of granules arising from the phagocytosis of degraded lipid from organelles of apoptotic cells. Lipofuscin accumulation is documented to be reversible if intake of the offending agent is suspended. Within the colon, the pigment is only found in the lamina propria sparing the crypts.

Lipofuscin has an excitation spectrum between 440-470 nm, with an emission spectrum between 510-700 nm [309]. This falls within the excitation wavelength range used for the experiments of this thesis. However, its contribution to GI tissue autofluorescence is considered to be minimal [310] and has not been widely investigated.

Schweitzer et al. [309] reported a fluorescence lifetime of 190 ps for the pigmented retinal epithelium, which is rich in lipofuscin, in a healthy volunteer using 468 nm excitation and 510-700 nm emission.

Origin of the intrinsic autofluorescence contrast in the GI tract

The GI tract wall is composed by a complex combination of known and unknown fluorophores that occur in different concentrations, states (e.g. free/bound, oxidised/reduced) and at different depths. Each layer has a distinct fluorophore composition, so that even though each fluorophore has distinct fluorescence properties (e.g. lifetime), the fluorescence measured at the tissue surface results from the contributions of the fluorophores in each layer.

Figure 3-5 shows a schematic diagram of the GI structure wall and the fluorophores expected to be contained in each layer based on *a priori* anatomical knowledge of the GI tissue composition.

Epithelium

As discussed above, aromatic amino acids are ubiquitous constituents of biological tissue and are all fluorescent. However, their excitation maxima fall outside the wavelengths typically employed for autofluorescence studies.

The more studied intracellular fluorophores are NADH, FAD and FMN. Stringari *et al.* [311] have recently postulated a free/bound NADH gradient along the epithelial cells associated with cellular proliferation and differentiation along the axis of small intestine crypt-*villi*. According to their study, proliferative cells at the base of the crypt are characterized by a glycolytic metabolic phenotype, thus they exhibit predominantly free NADH, while differentiated cells at the surface of the crypts have an oxidative phosphorylation phenotype and exhibit primarily protein bound NADH.

Although not as widely investigated as NADH and flavins, mucins, which are found predominantly in the goblet cells, could also represent another possible source of intracellular fluorescence [312].

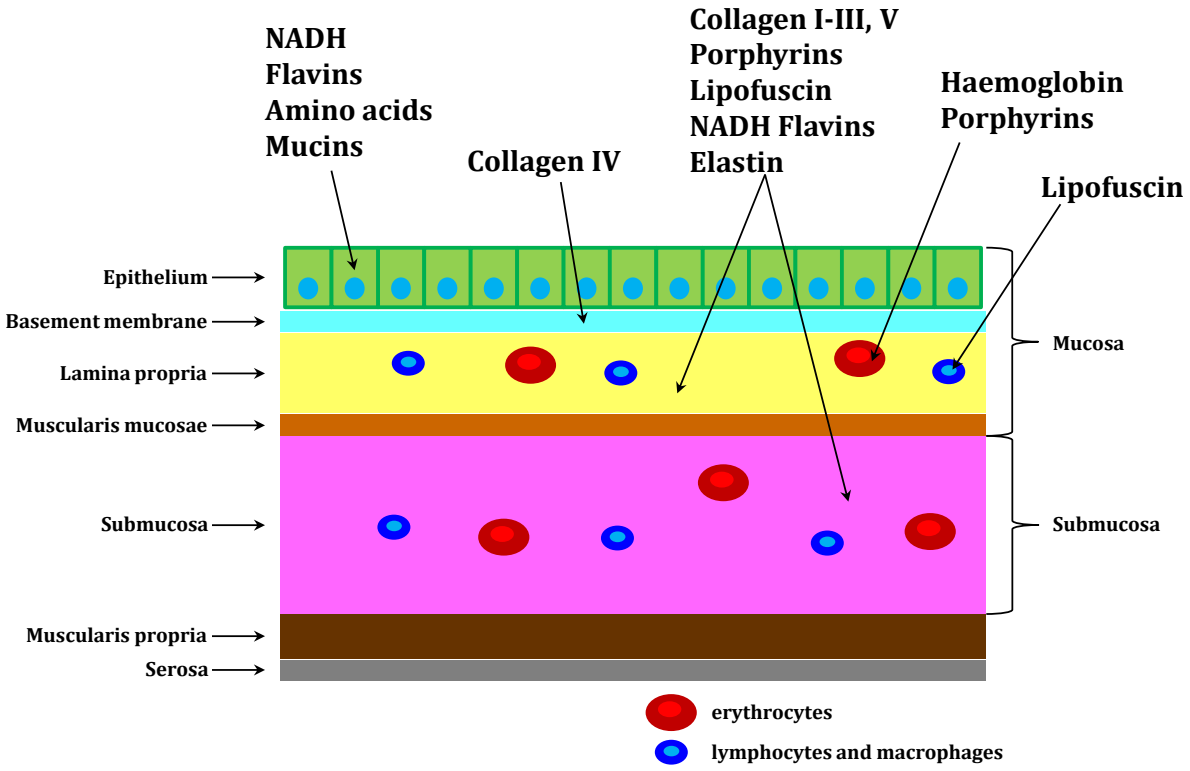


Figure 3-5: Cartoon showing the various layers making up the GI wall and the expected fluorophores contained in each layer.

Basement membrane

Collagen type IV is primarily found in the basement membrane (linings surrounding the crypts – see figure 2.3) and it is considered to be the source of autofluorescence emitted from this layer [301].

Lamina propria

The predominant fluorophores found in the stroma of the lamina propria are collagen types I-III and V [7,313]. In normal colon, collagen type I was found to be the major collagen type in normal intestine (68%), followed by types III (20%) and V (12%) [314].

Contributions from porphyrins within erythrocytes have been recently suggested by Stringari *et al.* [311], although this was based on fluorescence lifetime values and no spectral evidence of porphyrins identification was provided. Normally, the concentration of porphyrins within erythrocytes is low (< 50-100 μg/dL [315,316]), and haemoglobin predominates [317] (free erythrocyte porphyrins/haemoglobin ratio = 1.69 μg ± 0.67 μg per gram of haemoglobin [318]). Haemoglobin fluorescence has also been reported in measurements of normal blood cells at 457.9 nm [319] and of human lyophilized ferrous haemoglobin powder using two-photon microscopy [320]. However, it is still not clear the extent to which these molecules contribute to the fluorescence of this layer and further research is needed.

Contributions from lipofuscin within lymphocytes and macrophages may also be expected [321-323], although it does not generally contribute greatly to GI tissues fluorescence emission [310], especially in normal (non melanotic) mucosa. Interestingly, lipopigments are reportedly absent in both neoplastic and hyperplastic colonic polyps [324].

Contributions from NADH and flavins within myofibroblasts, lymphocytes and macrophages are also possible.

The lamina propria contains a vascular network of blood vessels which drain into larger vessels in the submucosal layer. The walls of small arteries have multiple layers of smooth muscle cells and as they penetrate within the lamina propria become thinner and composed of less collagen and elastin. Veins are known to have smooth muscle only and no elastic fibres.

Banerjee *et al.* [301] used excitation wavelengths between 280 and 350 nm to characterize the autofluorescence signatures of normal, dysplastic and neoplastic colon tissue *ex vivo.* Elastin did not appear to contribute to any of the autofluorescence peaks observed.

Muscularis mucosae

This thin layer consists of smooth muscle fibres and myofibroblasts. Contribution from myofibroblasts intracellular fluorophores may be possible.

Submucosa

As for the lamina propria, contributions from collagen I-III and V are expected to be prominent. Type V collagen is produced in relatively large amounts by smooth muscle cells and was found to increase in Crohn's disease [314]. Other contributions may arise from erythrocyte porphyrins, intracellular NADH and flavins within myofibroblasts and lymphocytes, and lipofuscin in macrophages. Arterioles may also contain a small amount of elastin.

Muscularis propria

The intrinsic fluorescence from the muscularis propria is weak as this layer is essentially composed of muscle fibres, although minor contributions from myofibroblasts intracellular fluorophores might still be possible. However, the muscularis propria is a deep layer (~1000 μm in normal colon [325]), often beyond the depths reachable by UV and blue light excitation wavelengths.

Serosa

Serosa is the deepest layer, consisting of simple squamous epithelium (mesothelium) and a small amount of underlying loose connective tissue composed of mainly collagen type I. The oesophagus is not lined by a serosa.

3.1.5 Fluorescence lifetime imaging and spectroscopy

As discussed in section 3.1.1, fluorescence lifetime (FL), is defined as the average time a fluorophore takes to decay after having been excited from its ground energy level. Different fluorophores decay at different rates, and this parameter can be mapped at every pixel in an image in order to produce a fluorescence lifetime image (figure 3-2(b)).

Fluorescence Lifetime Imaging Microscopy (FLIM) is a powerful means to map the decay rate of fluorescence emitted from tissue samples, providing quantitative contrast. It can be achieved for a variety of fluorescence imaging instruments including wide field imaging, confocal microscopy, and two-photon microscopy.

Optical fibre probe-based fluorescence lifetime spectroscopy (FLS), can resolve the fluorescence emission spectrum and fluorescence decay rate to provide a wealth of label-free information from biological tissue.

The measurement of fluorescence lifetimes

As mentioned in section 3.1, fluorescence lifetime can report on fluorophore type and its local refractive index as well as its chemical environment, and can therefore be a useful contrast parameter. There are two main ways of performing FLIM: time domain, and frequency domain.

Time-Domain FLIM

The measurement of fluorescence lifetime in the time domain is performed by recording the intensity decay of fluorescence after excitation with a very short pulse of light, and can be done either by time-gating, as is used in wide-field microscopes, or by time-correlated single photon counting (TCSPC) as is used in confocal microscopes and spectroscopy systems. Time-domain measurements are the most intuitive as they involve directly measuring the decay of fluorescence intensity over time.

Time-Gating

Time-gated FLIM is a technology most widely used in wide-field microscopes, and involves acquiring a number of images with very short exposure times at a number of delay times after the arrival of an excitation light pulse, as shown in figure 3-6. By comparing the relative intensities in the different time "gates" a profile of the decay can be built up to which a decay can then be fitted.

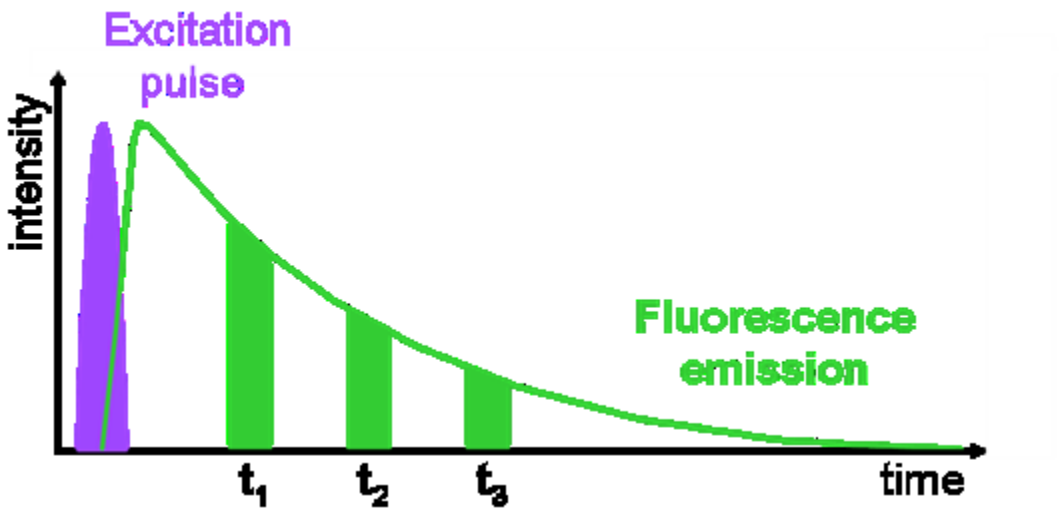


Figure 3-6: The principle of time-gated detection for FLIM. The excitation light pulse is shown in purple with the fluorescence emission in green. Three detection time gates (t1, t2 and t3) are also shown.

Time-Correlated Single-Photon Counting

TCSPC is the gold-standard of fluorescence lifetime detection. In this method the arrival time of each detected photon relative to the excitation light pulse is measured, therefore giving an accurate picture of the decay profile.

When a fluorescence photon is detected, typically by a "photomultiplier tube (PMT)", an electronic signal is sent to a "time to amplitude converter (TAC)", which starts to linearly charge a capacitor that is subsequently stopped when the laser next emits a light pulse. The charge on the capacitor is then fed into an "analogue to digital converter (ADC)" and the time recorded in memory. Repetition of this process for many detected photons allows a histogram of photon

arrival times to be built up, and decay models can then be fitted to these data. A summary of the recording steps is given in figure 3-7. As TCSPC relies on point detectors it is used mainly in confocal, multiphoton and point spectroscopic systems [326]. TCSPC has the advantage of light efficiency as all detected photons are recorded, and accuracy, as the time-precision of the system can be very fine.

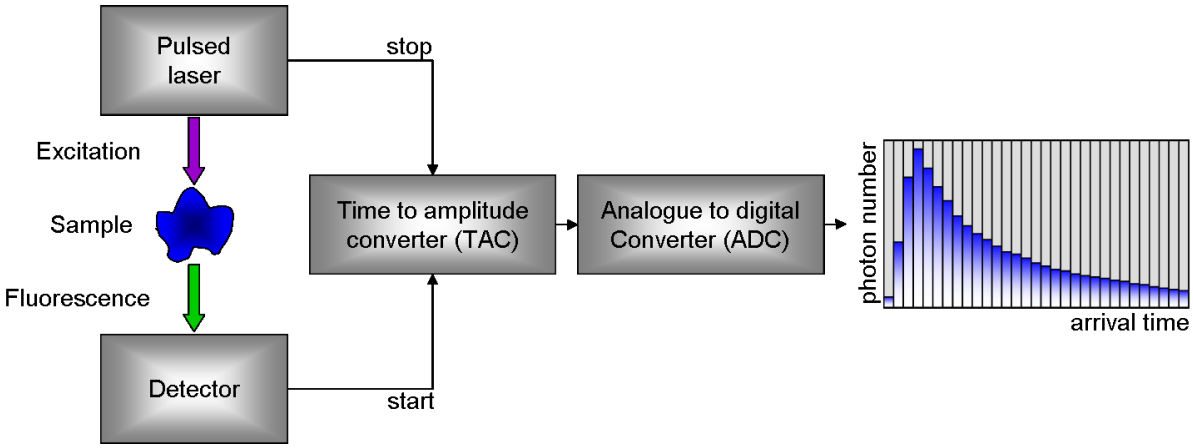


Figure 3-7: Schematic diagram of the TCSPC acquisition procedure.

Frequency Domain FLIM

Frequency domain FLIM uses sinusoidally varying (or otherwise modulated) excitation light. The resultant fluorescence is then also sinusoidally modulated but with a reduction in the modulation depth (and average intensity) and a shift in phase, as shown in figure 3-8.

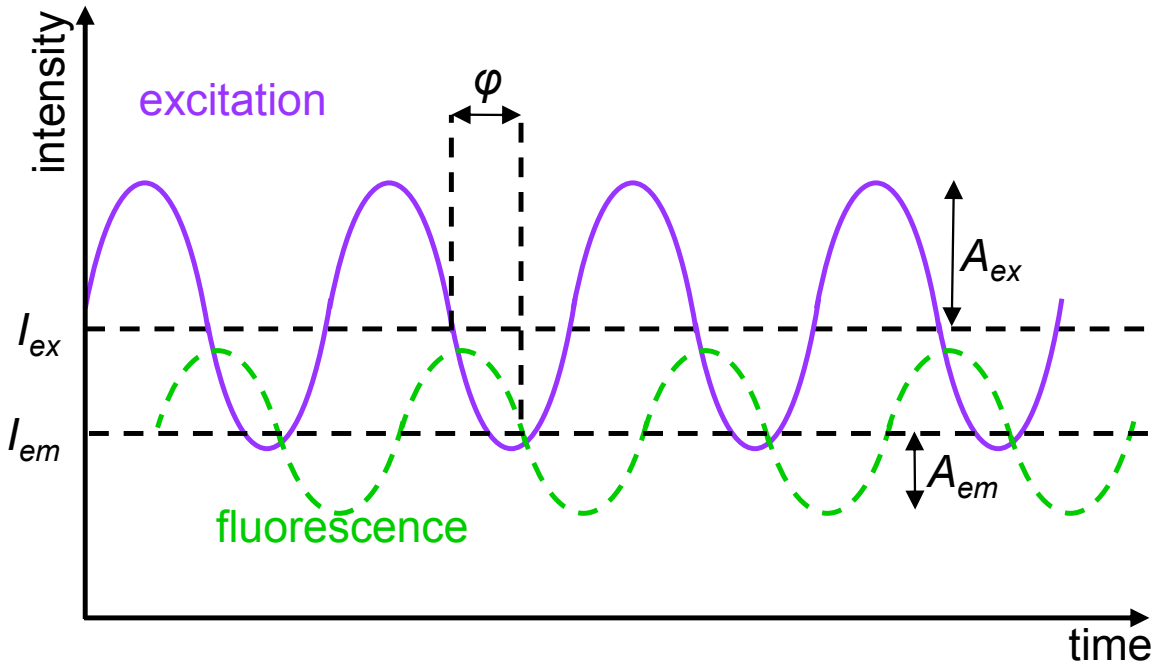


Figure 3-8: Phase shift and demodulation seen in frequency domain FLIM when exciting with sinusoidally modulated light. The phase shift, φ, is labelled as are the amplitudes of the excitation light, A_{ex} and emitted light A_{em} and the respective average intensities, I_{ex} and I_{em}.

Instrument Response Function

When a fluorescence decay measurement is performed, it should be noted that the signal received depends not only on the sample being analysed, but also on the response of the measuring system. No fluorescence lifetime measurement apparatus is perfect and as such there is a finite temporal extent of both the excitation light pulse and a limited resolution of the detection system. These factors combine to form an instrument response function (IRF) that must be taken into account when fitting fluorescence decays. The method used to obtain the IRF depends on the system being used, but usually involves measuring the time response of a fluorophore with a short lifetime (e.g. erythrosin B, daspi) or a scatterer (e.g. Ludox).

Displaying FLIM Images

Once a decay model has been fitted to every pixel within an image, it is then necessary to display those data in an accessible and informative manner. The most straightforward way to do this is to make a false-colour image, in this manner an 8-bit colour image is formed where typically blue represents shorter lifetimes and red is for longer lifetimes, corresponding to a lifetime scale specified by the user. This display strategy takes no account of intensity though and therefore some important structural information may be lost; this may be remedied by merging the FLIM map with the integrated intensity image. In this way the structural information is maintained and pixels with low signals which may have less accurate lifetime fits are given less

emphasis. Images are merged in LabVIEW (National Instruments, USA). An example of FLIM map, intensity image and merge are shown in figure 3-9.

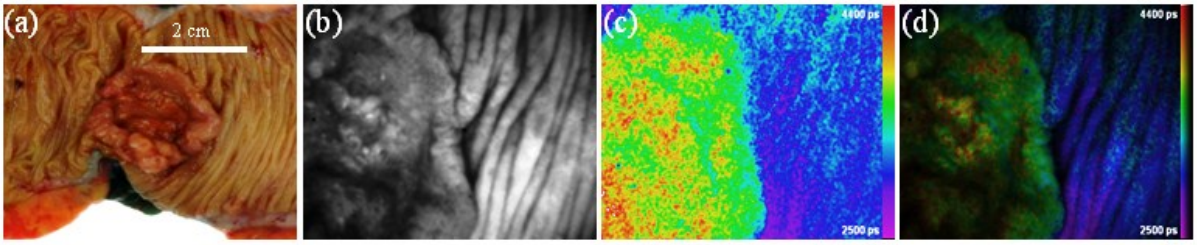


Figure 3-9: Matched white light, fluorescence intensity and FLIM images of a fresh haemicolectomy specimen containing a moderately differentiated colonic adenocarcinoma. (a) white light image; (b) fluorescence integrated intensity image; (c) false colour FLIM map; (d) FLIM merge image showing clear visual contrast between areas of normal and malignant tissue. Adapted and reproduced with permission from [273].

3.2 Development of endoscopic instrumentation to utilise autofluorescence lifetime for the study and diagnosis of gastrointestinal disease

Fluorescence lifetime technology can be used to detect changes in tissue state caused by diseases such as cancer [273], atheroma [327] and osteoarticular arthritis [328,329]. This is due to changes in the environment or changes in the relative concentration, both of which may affect the fluorescence lifetime of endogenous fluorophores such as collagen, elastin, reduced nicotinamide adenine dinucleotide (NADH), oxidized flavin adenine dinucleotide (FAD) and flavin mononucleotide (FMN), and porphyrins. It is also possible to use exogenous probes to distinguish disease states, which holds promise for minimally invasive tissue analysis. Whilst there have previously been a few demonstrations of fluorescence lifetime applied to endoscopy, which are discussed in detail below, there is still a significant amount of technological development and clinical study required before it can become a clinically viable method.

The development and implementation of fluorescence lifetime measurement capability in endoscopic instruments for clinical use has provided the fundamental motivation for the studies described in this thesis.

During this PhD, three endoscopic instruments consisting of a single point fibre-probe FLS system, a FLIM confocal endomicroscope and a wide-field FLIM fibre-optic endoscope have been developed for *ex vivo* and *in vivo* studies of fluorescence lifetime of tissue autofluorescence as a result of multidisciplinary team working. A novel compact FLS fibre-optic probe system was constructed *ex novo* and a full characterisation is presented in chapter 7. The contrivance of this instrument is demonstrated through its application to both *ex vivo* and *in vivo* measurements. The FLIM confocal endomicroscope and the wide-field fibre optic FLIM endoscope were not used in the studies presented in this thesis as further refinements and developments of these instruments are still ongoing.

3.2.1 Single point fluorescence lifetime spectroscopy (FLS) instrumentation

Single point spectroscopic measurements for studying tissue autofluorescence are typically obtained using a spectrofluorometer and a fibre-optic based probe to deliver the excitation light and collect the resulting fluorescence from a sample, often combined with a spectrograph to capture fluorescence emission spectra and also reflected light spectra [330]. With broadband illumination, reflected light spectra can provide information concerning the elastic scattering properties of tissue samples and this has been used to identify diseased tissue [225].

Fluorescence spectral measurements have been combined with fluorescence lifetime measurements in spectrofluorometers and fibre-optic probe instruments [255,256,266,303]. Multispectral fluorescence lifetime measurements are often realized using dichroic filters with multiple time-resolved detection channels or using a scanning spectrometer with a single time-resolved detector [303] and spectrographs have been used with array detectors, including gated intensified CCDs [256], streak cameras [255] and time-correlated single photon counting (TCSPC) [331], e.g. [332].

Fluorescence lifetime spectroscopy (FLS) in the GI tract was pioneered by Mycek *et al.*, whose *in vivo* study [265] on 24 polyps (13 adenomas, 11 non-adenomas) from 17 patients, using an excitation wavelength of 337 nm and detection in the range 530-570 nm, demonstrated shorter average lifetimes for adenomas compared to non-neoplastic polyps (9300 ± 400 ps vs. 10500 ± 700 ps). They deployed a portable spectrometer specifically designed for use during endoscopy utilizing a nitrogen laser as excitation source to provide UV radiation with pulse durations of 4 ns at 20 Hz repetition rate. The laser pulses were attenuated by neutral density (ND) filters and coupled by a lens into a 600 μm diameter optical fibre. Tissue exposure was less than 0.5 μJ of excitation energy per pulse. The same fibre was used to collect AF emission from the tissue and directed through a bandpass filter with a centre wavelength of 550 nm. An avalanche photodiode was used to detect the decay signal, which was then recorded by a digitizing oscilloscope and finally transferred to a computer running LabVIEW software.

FLS was further developed to measure fluorescence spectra and lifetime decays simultaneously, using a spectrograph-coupled intensified charge coupled device (ICCD) to collect the fluorescence emission in a single-shot with data acquisition times less than 1 s. The system was housed in a compact, portable three-shelf cart for clinical use and applied to the study of several human tissues *in vivo* including normal skin [256] and Barrett's oesophagus [266].

FLS systems have then been implemented using a scanning monochromator with single channel lifetime measurement, two pulsed lasers providing excitation at 337 nm and 391 nm, and a sterilizable custom-made bifurcated probe [303], and applied to studies of *ex vivo* human glioblastoma [333] and *in vivo* atherosclerotic plaque disruption in animal model [334].

A streak camera-based FLS system was used by Glanzmann *et al.* [255] to acquire *in vivo* time-resolved spectra of diseased and surrounding normal bladder, bronchi, and oesophagus, from 9 patients during endoscopy. They also investigated the fluorescence decay of photosensitizers Hexyl-ALA and mTHPC in patients undergoing PDT for early cancers of the bladder and the oesophagus, respectively. This instrument utilized a nitrogen laser providing 337 nm excitation pulses at a repetition rate between 1 and 50 Hz, a high speed streak camera in "analog mode" that allowed short acquisition times (15 s total measurement time per location) with

subnoanosecond resolution, and a 4 m long fibre probe (core diameter 550 μm, outer diameter 630 μm, NA = 0.22) specifically designed to be inserted into the biopsy channel of a conventional endoscope. The nitrogen laser was enclosed in a Faraday cage and the whole system mounted on a mobile trolley.

3.2.2 Single point fluorescence lifetime spectroscopy (FLS) instrumentation designed and built by the Photonics Group at Imperial College London

In 2007, De Beule *et al.* [258] developed a fibre probe-based fluorimeter capable of simultaneously measuring spectrally and time resolved fluorescence with dual excitation wavelength, 355 and 440 nm, designed to excite both NADH and flavoproteins. This instrument employed two compact pulsed laser sources operating at 37.1-40 MHz together with a multichannel time-correlated single photon counting (TCSPC) detection system to provide parallel fluorescence lifetime measurement in 16 spectrally resolved channels. This laser radiation was coupled into the excitation channel of a custom built fibre-optic probe that housed seven optical fibres, each with a diameter of 200 μm and a numerical aperture of 0.22, six of which served to collect fluorescence and one to deliver the excitation. This system was used to excite 23 freshly excised skin specimens with an average output power up to 200 mW for the 355-nm-laser diode and up to 1 mW for the 445 nm laser source, respectively. The whole instrument was mounted on a 60 x 60 cm^2 breadboard to facilitate transportation, and was fully enclosed for safe use in clinical settings. The laser beams were combined using a dichroic mirror and subsequently coupled into a 200 μm diameter multimode fibre using a 10x microscope objective. Data acquisition was controlled using the Becker-Hickl "SPCM" software package. Later on, the initial blue laser diode was replaced by a high power laser diode providing 3.7 mW average output power at 445 nm excitation and the acquisition was controlled by a custom-written LabVIEW program. Further development of this system has led to the FLS instrument that has been used for the experiments described in chapter 6, chapter 7 and 8 of this thesis.

3.2.3 Fluorescence lifetime imaging (FLIM) instrumentation

Wide-field FLIM is usually implemented with gated imaging detectors that sample the fluorescence signal. Crucial to the translation of fluorescence lifetime technology to endoscopy is the development of compact and real time systems that are suitable for *in vivo* clinical applications. Since the end of the '90s, several FLIM endoscope designs have been proposed [66-68,335-338], and current efforts are directed to implement and validate this technology for modern endoscopy.

In 2005, Munro *et al.* [68] reported the first flexible FLIM fibre-optic endoscope design, based on a wide field time gated FLIM for real time FLIM endoscopy. Excitation was provided by a frequency tripled Nd:YVO4 laser producing 10 ps pulses at a repetition rate of 80 MHz and a wavelength of 355 nm with up to 350 mW average power, was used as excitation source. The excitation light was coupled into a multimode fibre and introduced through the working channel of the endoscope. Proof of principle was shown on fresh human stomach and lamb's kidney tissue.

A multispectral FLIM flexible side-view endoscope, which was built around a flexible imaging fibre bundle, was then presented by Elson *et al.* [335]. The excitation source was a nitrogen laser providing 700 ps pulses at 20 Hz and a wavelength of 337 nm. The illumination was delivered using a separate adjacent multimode fibre. This set up was used *in vivo* in a hamster cheek pouch oral pre-cancer model, and in three patients undergoing surgery for glioblastoma multiforme [339,340].

Recently, Cheng *et al.* [338] presented the design of a small diameter flexible wide field FLIM endoscope capable of simultaneous multispectral FLIM imaging, which was built around an imaging fibre bundle. A frequency-tripled Nd:YAG laser was used as the excitation source (355 nm). Wide-field time-gated FLIM was implemented using an intensified charge-coupled device (ICCD) camera. The system was validated on a hamster cheeck pouch model of oral cancer.

3.2.4 Confocal FLIM endomicroscopy instrumentation designed and built by the Photonics Group at Imperial College London

The FLIM confocal endomicroscope (figure 3-10) is based on a commercially available probe based confocal laser endomicroscope (pCLE, Cellvizio GI, Mauna Kea Technologies, France), which is licensed for clinical use in the GI tract and for bronchoscopy [341]. This instrument is a laser scanning single-photon fluorescence fibre bundle endomicroscope that is capable of recording optically sectioned images with a variety of fibre probes using an excitation wavelength of 488 nm. The system has been adapted to also incorporate a Mai Tai Ti:Sapphire pulsed laser (Newport Spectra-Physics Ltd, United Kingdom) to generate shorter wavelength pulsed excitation light for FLIM acquisitions.

The infrared output is frequency doubled to produce ~100 fs pulses of 355-495 nm light at a repetition rate of 80 MHz. The probe has a lateral resolution of ~1.4 μm, a working distance of 60 μm and a field of view of 240 μm. The diameter of the distal tip is 2.6 mm, which is compatible with any endoscope/laparoscope having a working channel of 2.8 mm diameter or greater. The set-up was configured to change between FLIM and the standard fluorescence

intensity imaging [336]. Fluorescence from the sample is collected by the fibre probe and descanned by the laser scanning unit. The whole system is portable and is mounted on a breadboard fixed on a robust trolley specifically designed and built by the Photonics Group.

This is the first microconfocal FLIM endoscope employing a fibre bundle probe and time correlated single photon counting in a clinically viable instrument.

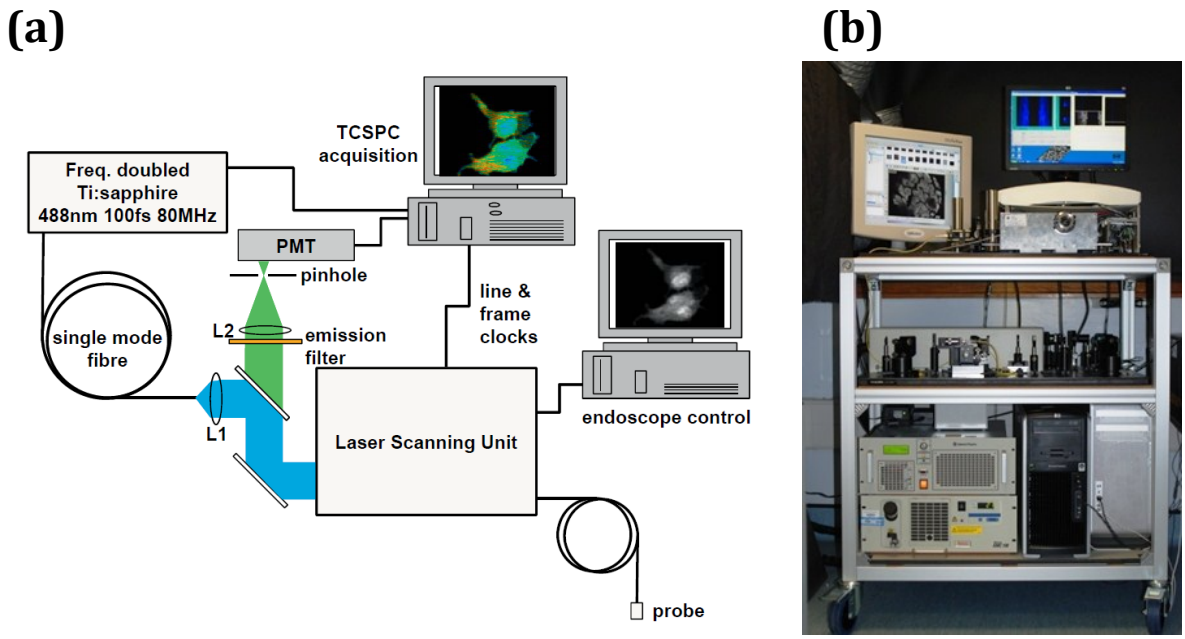


Figure 3-10: (a) Configuration of the modified TCSPC FLIM confocal endomicroscope. Adapted and reproduced with permission from [336]. (b) The FLIM confocal endomicroscope based on a commercially available confocal laser endomicroscope (Cellvizio GI, Mauna Kea Technologies, France).

The greatest technological barrier to overcome is the background fluorescence from the fibre probes. At wavelengths typically used for autofluorescence studies (310 and 420 nm) [275,280], the fluorescence from the fibres occurs over the whole 3 m length, is very strong and completely masks the fluorescence arising from the few µm thick sample section to investigate. This limit fixed at 420 nm the shortest excitation wavelength currently exploitable with this implementation. One possible way to overcome this limitation is the construction of lower background fluorescence fibres prototypes.

This limitation prompted the design of experiments using a bench confocal FLIM microscope to explore the potential for contrast available at 420 nm excitation in freshly excised GI tissue from patients undergoing endoscopic procedures. This work will be presented in chapter 4.

However, it should be noted that when applied to Forster resonance energy transfer (FRET) imaging of live COS-7 cells in culture transfected with fluorescent proteins (EGFP and EGFP–mCherry tandem FRET construct) this system showed a clear decrease in the lifetime of the EGFP donor expected for FRET in the tandem construct. The optically sectioned FLIM images

were acquired in 2 s, which approaches the acquisition time required for investigating *in vivo* spatiotemporal dynamics of cell-signalling processes in animal models [342].

3.2.5 Wide field FLIM endoscopy instrumentation designed and built by the Photonics Group at Imperial College London

The wide field FLIM system (figure 3-11(a)) has been used previously for wide field imaging of large pieces of biological tissue [270,273]. A Vanguard frequency-tripled Nd:YVO4 laser (Newport Spectra-Physics Ltd, United Kingdom) is used to generate excitation light. This is a compact laser with a relatively small footprint. Its combination of high laser powers (up to 350 mW) and relative portability make it useful for future *in vivo* FLIM endoscopy applications. It provides picosecond pulsed 355 nm ultraviolet excitation at an 80 MHz repetition rate. This wide-field FLIM setup is currently being adapted for endoscopy e.g. using a flexible ureteroscope (Flex X ureteroscope, Karl Storz GmbH, Germany) as shown in figure 3-11(b). This instrument has the exciting potential to rapidly screen fields of view of several square centimetres and plus provide a "red-flag" screening tool, at the expense of optical sectioning capacity. Ultimately, this system could be used to guide the subsequent use of probe-based optical techniques such as FLS to provide complementary spectral and lifetime measurements, with the ultimate goal of reducing or eliminating the need for tissue removal, processing and evaluation.

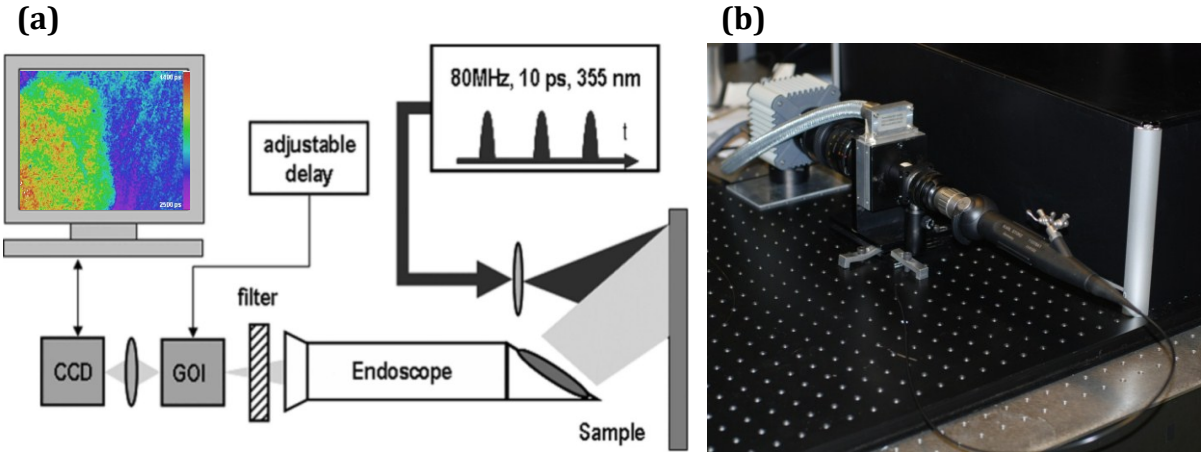


Figure 3-11: (a) Schematic diagram illustrating the wide field FLIM endoscope set-up. Excitation light (dark grey) is directed onto the sample. Emitted fluorescent light (light grey) is collected by the endoscope and imaged onto the GOI. Adapted and reproduced with permission from [67]. (b) Photograph of the flexible ureteroscope (Flex X ureteroscope, Karl Storz GmbH, Germany) being adapted for wide field FLIM endoscopy.

Aside from this flexible endoscopy setup, a handheld wide filed imaging rigid arthroscope is also currently under development for arthroscopic/surgical applications. This system implements

rapid wide field time-gated imaging (6 gates per 0.2 s, 1.2 s total acquisition time) using a fibre-taper coupled CCD and gated optical image intensifiers from Kentech Instruments Ltd (figure 3-12).

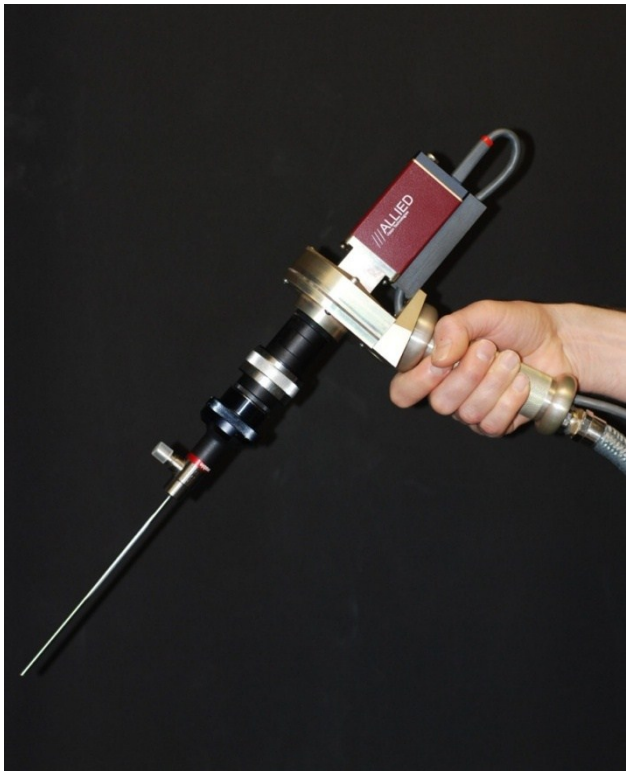


Figure 3-12: The wide field FLIM portable handheld rigid arthroscope for arthroscopic/surgical applications.

3.3 Review of research and clinical experience with autofluorescence spectroscopy and imaging

One of the first reports on the use of quantitative fluorescence diagnostic techniques to discriminate between normal and diseased tissue appeared in 1965 [343]. The authors found that the fluorescence intensities of *ex vivo* cancerous tissue from oesophagus, stomach, breast and thyroid were less than that of normal tissue using excitation at 330 nm. Since then, there have been a large number of studies regarding the utility of fluorescence diagnostic techniques in the detection of disease and several comprehensive reviews have been published on the progress in this field [213,275,280,282,330]. The majority of these studies claim the potential of fluorescence techniques to detect early neoplastic changes, particularly in epithelial surfaces.

Nowadays, there is an increasing interest in exploiting spectroscopic readouts of tissue autofluorescence and a number of groups have shown that GI disorders, including cancer, exhibit different autofluorescent signals from those of normal tissue. Results are reviewed here by organ site.

Oral cavity

Evaluation of oral cavity, pharynx and larynx using AF imaging systems has become an essential tool for the screening of head and neck squamous cell cancers as a result of pioneering *ex vivo* studies [344,345]. Fluorescence spectroscopy and imaging of oral mucosa have been evaluated by several groups with the aim to detect malignant or premalignant conditions using excitation wavelengths in the UV [280,346] and for a wide range of UV and visible wavelengths (250-500 nm) [345].

Uppal and Gupta [347] carried out enzymic measurements of NAD(P)H concentration on samples from nine patients with oral squamous cell carcinoma. All measurements were carried out on malignant tissue and normal appearing mucosa adjacent to the lesion from the same patient. They showed that the concentrations of NAD(P)H in malignant sites of oral cavity tissue were significantly lower than in the healthy mucosa.

Oesophagus

A number of important papers published in the 1990s presented AF emission spectra that were collected *in vivo* from Barrett's oesophagus, malignant and normal tissue at 410 nm excitation [348-351]. These results showed that fluorescence of normal oesophageal mucosa and non-dysplastic Barrett's epithelium could be distinguished from that of dysplasia and cancer in patients with Barrett's oesophagus.

Mayinger *et al.* [352] used an innovative optical system delivering either white or violet-blue light for excitation of tissue AF during routine endoscopy. Nine patients displayed a

spinocellular carcinoma and 4 had an adenocarcinoma of the oesophagus. As a result, both types of cancer exhibited different emission spectra compared to those of normal oesophagus.

The combined use of three different spectroscopic techniques (reflectance, fluorescence and light-scattering spectroscopy) has been shown to provide useful complementary information in patients with dysplastic Barrett's oesophagus [70]. At 337 and 397 nm excitation, the progression from non-dysplastic, to low-grade, to high-grade dysplasia was accompanied by a broadening of the spectral lineshape together with a shift toward longer wavelengths (600–750 nm). In a subsequent study from the same group, the fluorescence spectra of NADH and collagen in dysplastic tissue appeared considerably different from non-dysplastic mucosa [353]; dysplastic epithelium was characterized by low collagen and high NADH fluorescence intensity compared to normal oesophagus. This study advanced the concept of tissue fluorophores as quantitative biochemical markers of dysplastic change.

Pfefer *et al*. [266] used excitation wavelengths of 337 and 400 nm and compared the measurement of fluorescence emission spectra to fluorescence decay profiles acquired at 550 nm *in vivo* in 37 patients undergoing routine endoscopic surveillance for BO. In this study time-resolved fluorescence was unable to achieve sensitivity and specificity values above 60% for discriminating high risk (carcinoma, high grade dysplasia) from low risk (low grade dysplasia, non-dysplastic or indefinite for dysplasia) tissue, whereas moderate overall accuracy was achieved using steady-state fluorescence only.

Further work to investigate the differences in the metabolic pathway between normal tissue and cancer was made using FLIM to measure intracellular oxygen concentration with a ruthenium based fluorescent probe (RTDP) in cultured normal and adenocarcinoma cells (from Barrett's epithelium) of human oesophagus [354]. Higher intracellular levels of oxygen and NADH fluorescence intensity were sensed in the adenocarcinoma cells, while there was no significant variation in NADH lifetime between normal and neoplastic cell lines.

The clinical diagnosis of adenocarcinoma in patients with short-segment Barrett's oesophagus (which is defined as intestinal metaplasia occurring in columnar epithelium <3 cm in length) is often challenging and controversial. Niepsuj *et al.* [355] used an adapted laser-induced fluorescence endoscopy device (LIFE, Xillix Technologies Corp., Canada) with blue light excitation (425-455 nm) in 34 patients with documented short-segment Barrett's oesophagus. In this study, a red-shift (to longer wavelengths) of the fluorescence emission was observed in metaplastic Barrett's mucosa compared to normal oesophagus, and autofluorescence endoscopy increased the detection rate of high-grade dysplasia when compared with WLE.

Lin *et al.* [356] studied *ex vivo* biopsy specimens from 30 patients with Barrett's oesophagus using high resolution AFI under 266 nm, 355 nm, and 408 nm excitation along with an image acquired using the same set-up under white light illumination. Distinct cellular organization and morphology related to disease progression could be identified and the pathological evaluation was confirmed by expert pathologists.

More recently, AFI with blue light excitation has been combined with high-definition white light endoscopy and NBI in a single endoscope with two charge-coupled devices. This technology is referred as to as "trimodal imaging" and has been applied to identify inconspicuous Barrett's neoplasia [357] and assist endoscopic mucosal resection (EMR) of early neoplasia in Barrett's oesophagus [358]. In an international multicentre study involving 84 patients with Barrett's oesophagus, the addition of AFI to high-resolution endoscopy increased the detection rate of early neoplasia within the Barrett segment, and additional viewing with NBI increased the overall specificity [357]. However, as with AFI alone, the increased detection of dysplasia was only marginal (11%), and did not translate into a real benefit for the patients. Moreover, AFI alone was associated with a high false positive rate (81%); therefore, the authors used NBI with optical magnification to further characterize areas detected by AFI, reducing the false positive rate to 26% (at the expense of misclassifying two lesions as falsely negative).

Another large multicentre randomized trial with patients affected by Barrett's oesophagus compared the diagnostic accuracy of surveillance with AFI-targeted biopsies plus 4-quadrant biopsies in comparison with the conventional Seattle protocol only. The investigators suggested that the AFI-guided biopsies improved the diagnostic accuracy for neoplasia in comparison with the conventional approach when using four quadrant biopsies. However, because of decreased sensitivity, they concluded that AFI alone was not suitable for replacing the standard Seattle protocol [359].

Endoscopic molecular imaging using fluorescently labelled targeted peptides is being increasingly investigated for detection of inconspicuous dysplasia in BO. For example, glycans have been shown to be altered in GI cancers [175,360-362]. They have the potential to be used as a molecular target for fluorescence endoscopic imaging of GI mucosa. Glycan changes can be detected using lectins, which have specific affinity for particular glycans. AFI and a fluorescently labelled lectin, *Tritiicum vulgare* agglutinin (WGA), have been used to detect changes in glycan expression on the epithelial cell surface associated with the transition from BO through dysplasia to ADC [363]. In particular, AFI was used to image WGA in four oesophagectomy specimens obtained immediately after surgery. The specimens were intubated from the proximal end and both baseline WL and AFI images were acquired. Fluorescein-labelled WGA was sprayed over the oesophageal mucosa and imaged with 395-475 nm excitation. Specimens

were then opened along their vertical axis and imaged using an IVIS camera (Caliper Life Sciences), to enable quantification of fluorescence and registration with histology. A highly significant statistical correlation between WGA fluorescence and the degree of dysplasia was found ($p = 0.0002$), with areas of HGD and cancer showing lower fluorescence intensity and WGA binding relative to areas of non-dysplastic BO and normal oesophageal mucosa.

Stomach

Chwirot *et al.* [364] reported the first study on AF imaging of gastric cancers *ex vivo*. In particular, they imaged 21 surgically resected specimens using excitation at 325 nm and 442 nm, and measured the fluorescence emission in six regions of the visible spectrum. In all the spectral channels, the AF intensity of neoplastic tissue was found to be lower than that of areas of normal stomach in the same specimen.

Immediately after surgery, Abe *et al.* [365] applied laser-induced fluorescence endoscopy (LIFE), which employs endoscopic AF imaging with excitation at 442 nm and emission detected in two bands around 520 nm and > 630 nm, to 61 gastric cancers resected from 50 patients. Comparison of these data with the histopathological diagnosis showed that depth of infiltration and mucosal thickening were correlated with differentiated cancers but not with undifferentiated cancers, which displayed a scattered pattern of tumour infiltration without altering the mucosal thickness.

Silveira *et al.* [366] used fluorescence spectroscopy with excitation at 488 nm to detect benign and malignant lesions of *ex vivo* human gastric mucosa. Biopsies with endoscopic diagnosis of gastritis and gastric cancer of the antrum were collected from 35 patients during the endoscopic examination. On each biopsy fragment the AF spectrum was collected at 2 random points via a fibre-optic catheter coupled to the excitation laser. Analysis of fluorescence spectra was able to identify the normal tissue from neoplastic lesions with 100% of sensitivity and specificity.

Ohkawa *et al.* [367] found that LIFE applied to 79 patients with gastric cancer, provided high sensitivity but poor specificity with limited clinical utility. Also, only a small degree of correlation was observed between histopathology and AF findings.

Ito *et al.* [368] stained and imaged biopsy specimens of freshly resected gastric cancers from three patients with gastric cancer using an antibody anti-carcinoembryonic antigen (CEA) and tagged with a novel fluorescent label (ICG-sulpho-OSu), and an infrared fluorescence endoscope. They found that there was a good correlation between the intensity of the infrared fluorescent signal and the cancerous sites, suggesting that this technique can spot cancer cells and generate a relatively strong fluorescent signal to detect small cancers.

Xiao *et al.* [369] acquired AF images of gastric cancer *ex vivo* using a laser scanning confocal microscope with two detection channels in the green (505-530 nm) and red (> 580 nm). The two spectrally resolved image channels were then merged and presented to the clinician. Sixteen gastric cancer specimens and corresponding normal gastric tissue were imaged using both 488 and 543 nm excitation wavelengths. Normal stomach appeared green whereas a red-brown image was found to be characteristic of all neoplastic specimens. Subsequently, the same group used a helium–cadmium laser system (Liconix 4240) at 442 nm excitation to acquire spectra *in vivo* from 38 patients with various gastric diseases, including cancer [370]. Interestingly, all spectra showed one major peak at 510 nm and three minor peaks at 590, 670 and 710 nm. The intensity and shape of the spectra at 510 nm were found to be significantly different between cancer and normal gastric mucosa, and dysplasia and normal mucosa, but not between cancer and dysplasia.

Mayinger *et al.* [371] used light-induced AF spectroscopy for *in vivo* diagnosis of gastric cancer studying normal and cancerous gastric mucosa in 15 patients with adenocarcinoma and 16 patients with signet-ring cell gastric carcinoma. A system capable of exciting tissue AF alternately with white or violet-blue light was used. Endogenous fluorescence spectra emitted by the tissue were collected with a fibre-optic probe and analysed with a spectrograph. Both types of cancers emitted a less intense signal compared to normal tissue (2300 vs. 3700 a.u. approximately), with a lower total intensity between 480 and 570 nm. A higher red-to-green ratio was also observed in cancers compared to normal gastric mucosa. The sensitivity of fluorescence spectroscopy for the diagnosis of carcinoma decreased by 30% with the presence of signet-ring cells, which may be explained by the scattered and frequently submucosal infiltration of this subtype of adenocarcinoma (diffuse type according to the Lauren classification [372]).

Kim *et al.* [373] performed preoperative AFI in 20 patients with early gastric cancers and then compared the endoscopic characteristics with histology after endoscopic submucosal dissection (ESD). Categorization of AFI images of gastric cancers into four patterns proved to be useful to delineate the dissection margins in the majority of cases.

Liver and Pancreas

Izuishi *et al.* [131] published the first pilot study using AF endoscopy in cancer of the biliary tract. They performed percutaneous transhepatic AF cholangioscopy in 9 patients with bile duct cancer using LIFE. Normal mucosa appeared as light blue whereas cancerous legions displayed a dark red fluorescence and also a white fluorescence in the majority of cases suggesting an additional contrast parameter for the diagnosis of bile duct cancer by AF endoscopy.

Chandra *et al.* [374] observed significant differences between the fluorescence and reflectance properties of normal, pancreatitis, and adenocarcinoma tissues. Measurements were associated with a larger collagen content detected in adenocarcinoma and pancreatitis than in normal tissue. Reflectance data indicated that adenocarcinoma had higher reflectance in the 430 to 500 nm range compared to normal and only inflamed tissues. Subsequently [375], they used a fibre optic probe-based spectroscope to assess the diagnostic accuracy in 50 freshly-resected specimens of pancreatic adenocarcinoma and chronic pancreatitis. They developed a classification algorithm - the spectral areas and ratios classifier (SpARC) - which they showed could discriminate between healthy and diseased tissue and identify cancer with reasonable sensitivity and specificity (85% and 89% respectively).

Liang *et al.* [376] evaluated the ability of two-photon microscopy (TPM) to detect the number of hepatitis C virus (HCV) infected cells in frozen sections of liver biopsy specimens from 9 patients with chronic HCV-related hepatitis. TPM was able to determine the number of infected hepatocytes with considerably higher sensitivity than that achieved by biochemical detection of HCV proteins or viral RNA.

Preliminary data from our group have shown AF lifetime contrast between cancerous and healthy tissue in one specimen of unfixed *ex vivo* liver containing metastatic colorectal carcinoma and in one unfixed pancreas containing an area of pancreatic adenocarcinoma. This was achieved using wide-field FLIM and the lifetime of neoplastic tissue AF induced by 355 nm excitation was shorter than AF from surrounding non-neoplastic tissue [273].

In a recent study conducted on freshly-excised GI tissue from 10 normal and 5 transgenic mice, excitation spectral signatures of epithelium, lamina propria, collagen, and lymphatic tissue were determined using hyperspectral two-photon microscopy with 740 nm excitation and three emission channels (350–505 nm, 505–560 nm, and 560–650 nm). Based on the 3D sectioned two photon images acquired, the morphology of these four main components was clearly visualized and compared to cross-sectional histology with a high degree of concordance [323].

Colon

A large body of literature exists on the use of AF spectroscopy to investigate colonic polyps and adenocarcinomas. Typically, colonic neoplasms have shown decreased AF intensity compared to that of normal colon. This can be attributed to the decrease with neoplasia of mucosal collagen, which is the dominant fluorophore, as a consequence of the enlargement of crypts that progressively displace the lamina propria. In addition, the submucosal contribution to the fluorescence in adenomatous tissue is reduced compared to that in normal colon due to the

increased thickness of the polyp and absorption by haemoglobin, as a result of increased intra-tumoural microvessel density.

The fluorescent architecture of normal colon, colonic adenoma and adenocarcinoma was studied by fluorescence microscopy in frozen tissue sections excited in the range 351 to 364 nm [377-379]. Collagen, present in all the layers of the GI wall, was responsible for the blue fluorescence emitted from normal tissues and adenomas, whereas the yellow-amber fluorescence was mainly attributed to the lamina propria. Interestingly, adenomas displayed cytoplasmic blue-green fluorescence increasing with the degree of epithelial dysplasia. This cytoplasmic fluorescence was not emitted from normal mucosal cells. The lamina propria of adenomas exhibited less fluorescence from collagen and was richer in blue-green fluorescent eosinophilic granules than that of normal colon [377]. Dysplastic adenomas displayed higher fluorescence intensity than normal tissue and lower fluorescence intensity than adenocarcinomas [379]. Conversely, Fiarman *et al.* [380], using confocal microscopy in frozen tissue sections with 488 nm excitation, claimed that the fluorescence from normal colonic mucosa arises primarily from the lamina propria, whereas the epithelium is the main source of fluorescence in adenomas and hyperplastic polyps. In normal tissue, the epithelium/lamina propria fluorescence intensity ratio was significantly lower than that of adenomas and hyperplastic polyps, and no statistically significant difference was seen between the ratios of both types of polyps.

Izuishi *et al.* [381] did not observe any significant differences between the fluorescence intensities of frozen sections of normal, adenomatous and cancerous tissue obtained using 400 to 440 nm excitation and 520 nm emission. Likewise, the concentration of flavins measured by high-performance liquid chromatography was not significantly different between normal and diseased tissue. Interestingly, the invasion of the submucosal layer was associated with a decreased fluorescence emission, in agreement with the hypothesis that collagen is the main source of colon AF. The screening effect of mucosal thickening and replacement of submucosa by cancer cells was proposed as a reason for the decreased fluorescence observed in cancerous tissue.

Bottiroli *et al.* [322] identified different patterns of fluorescence intensity and spectra of AF emission between neoplastic and non-neoplastic tissue using a micro-spectrofluorometer with 366 nm excitation. The different patterns were related to distinct layers of the GI wall, and in the 480-580 nm band in particular, the spectra of neoplastic epithelia displayed higher intensity than those of normal colon epithelia, suggesting the role of different arrangements in the neoplastic stromal compartment as a possible explanation for the differences observed.

Using 370 nm excitation, Manoharan *et al.* [382] showed spectral differences between adenomas and normal mucosa, and proposed a model to extract quantitative contributions from different tissue structures like mucosal collagen, submucosa and dysplastic cells.

Kapadia *et al.* [383] obtained fluorescence emission spectra from 35 normal specimens and 35 adenomatous polyps of the colon at 325 nm excitation. They used multivariate linear regression analysis of the spectra and a binary classification scheme to develop and optimize an algorithm that differentiates adenomatous polyps from normal mucosa and hyperplastic polyps, retrospectively. The algorithm prospectively discriminated 16 adenomatous polyps from 16 hyperplastic polyps and 34 normal tissues, with a sensitivity of 100% and specificity of 98%.

A similar study was conducted *in vivo* by Cothren *et al.* [384] at 370 nm excitation from 31 adenomas, 4 hyperplastic polyps and 32 normal sites of the colon. Following the sequence normal to hyperplasia to adenoma, they identified a characteristic decrease in the maximum fluorescence intensity at 460 nm and a relative increase in the fluorescence intensity at 680 nm. Using these spectral features, each tissue state was differentiated with high sensitivity and specificity. Later on, they also used an algorithm that was able to detect dysplasia *in vivo* during endoscopy with 90% sensitivity and 95% specificity [385].

Richards-Kortum *et al.* [386] measured fluorescence emission spectra from normal colon tissues and adenomatous colonic polyps, *in vitro* at a range of excitation wavelengths, spanning the ultraviolet and visible spectrum. They found that the spectral differences between normal and adenomatous colon tissues were greatest at 330, 370 and 430 nm excitation. Furthermore, at an excitation wavelength of 370 nm, fluorescence intensities at 404, 480 and 680 nm were found to be most useful for differentiating adenomas from normal colon tissues.

In two consecutive studies by Schomacker *et al.* [387,388], emission spectra from normal sites (n = 86), hyperplastic (n = 35), adenomatous polyps (n = 49), and adenocarcinomas (n = 7) were collected both *in vivo* and *ex vivo* at 337 nm excitation. The spectra of neoplastic and non-neoplastic tissue were differentiated with a diagnostic accuracy of 87%, which is about the same as that of routine clinical pathology. Interestingly, the spectra emitted from *ex vivo* and *in vivo* tissues were also different and this change was attributed primarily to NADH, whose fluorescence was shown to decay with a half-life of approximately 100 minutes after resection.

Yang *et al.* [389] excited fresh biopsies of normal (n = 39) and malignant colonic tissue (n = 35) using a range of excitation (290 to 340 nm) and emission (360-450 nm) wavelengths. They then evaluated the ratio of the fluorescence emission intensities at 360 nm to 380 nm for excitation at 325 nm, and the ratio of the fluorescence emission intensities measured at 450 nm with excitation at 290 nm to 340 nm. An algorithm based on the ratio of these fluorescence

intensities separated adenocarcinomas from normal tissues with 94% sensitivity and 92% specificity.

Chwirot *et al.* [390] observed that the intensity of AF emission at 325 nm excitation from 50 surgically-resected specimens of neoplastic and premalignant conditions was lower than that of contiguous normal colon. The spectral bands centred at around 440 nm and 475 nm seemed to be most promising in terms of possible future clinical applications.

Distinctive fluorescence emission spectra have also been shown *in vivo* from 32 adenomas and 114 hyperplastic polyps at 337 nm excitation [129].

Mycek *et al.* [265] performed time-resolved AF spectroscopy *in vivo* on 24 polyps (13 adenomas, 11 non-adenomas) from 17 patients. This was the first study in the colon that demonstrated differences in fluorescence lifetime decay between normal and dysplastic tissue. Adenomas showed faster average decays than those of non-adenomas (9.3 ± 0.4 ns vs. 10.5 ± 0.7 ns).

Statistically significant AF lifetime contrast was observed between cancerous and healthy colon tissue in a series of 16 unstained *ex vivo* colonic tumours surgically resected, using wide-field FLIM. In this study, the lifetime of neoplastic tissue AF induced by 355 nm UV excitation was longer than AF from surrounding non-neoplastic tissue [273].

In a randomized trial on 100 patients undergoing screening colonoscopy, AFI was not able to significantly improve the diagnostic accuracy, with adenoma miss-rates similar to WLE [391].

In a multicentre prospective randomized controlled study, the use of trimodal imaging did not improve the detection rate for adenomas compared with standard endoscopy. NBI and AFI showed very little accuracy and specificity in differentiating adenomas from non-adenomas (63%, 75%, and 37%, 62% respectively) [233]. Also, differentiation of adenomas from hyperplastic polyps by using trimodal imaging in patients with patients with hyperplastic polyposis was unsatisfactory [392].

Another study from Japan showed that the fluorescence intensity of images aquired using an AFI system is inversely proportional to the degree of dysplasia in colonic adenomas [393]. This study suggested that the dysplastic changes, including an increased number and density of cells and crypts, and the enlargement of nuclei and crypts, might somehow alter the tissue permeabilty and thus jeopardise the way back to the surface of the emitted fluorescence.

Since the assessment of AFI images is strictly dependant on colour presented to the clinician by the image processing system usedintensity, quantifying the intensity of the colour “magenta” by calculating a fluorescence index, has been proposed as a method to discriminate lymphomas

from reactive lymphoid hyperplasia [394], and to evaluate the degree of dysplasia in colonic neoplasms [393].

The ratio between AF signal intensities in colonic adenomas and normal specimens, obtained at 365 and 405 nm excitation wavelength, has also been used to discriminate adenomas from normal colon mucosa, and neoplastic from non-neoplastic polyps [395]. The excitation wavelengths were targeted to detect NADH fluorescence. Reflected ligth images at 550 and 610 nm excitation were also acquired to evaluate the haemoglobin concentration of the samples, which was shown not to influence on the overall fluorescence intensity detected.

3.4 Summary

Recent advances in GI endoscopy constitute an unprecedented leap forward in basic and clinical research for both patients and clinicians.

High-definition and magnifying endoscopy have contributed to higher detection rates compared to standard white light endoscopy alone and are expected to prospectively replace conventional equipment in daily practice. Contrast enhancement techniques, whether dye-based or computed, have been combined with conventional WLE to further improve its accuracy during routine endoscopy, especially in detecting early cancers, but histology is still required to clarify the diagnosis.

New developments have brought the optical resolution down to a few micrometres enabling for the first time *in vivo* tissue microscopy during endoscopy. However, although of invaluable assistance for tissue characterisation, techniques such as CLE and EC have not yet made transition between research and clinical use. In addition, these techniques can only infer structural aspects but they do not provide functional information about the tissue.

None of the currently available techniques has been able to provide a red flag technique for easy and rapid detection of early changes of disease. In this respect, autofluorescence spectroscopy and imaging, either incorporated into an endoscope or to be used via the endoscope working channel, seem promising and further research is awaited.

There appear to be two separate research communities, one working with sophisticated endoscopic technology and the other with disease biomarkers, who seemingly tend to work independently. It would seem sensible to integrate these two approaches to identify risk predictors and determine which modality is best for different patient populations.

It is still unknown which technique or combination of techniques offers the best potential. The optimal method will probably entail the ability to survey wide areas of tissue in concert with the

ability to obtain the degree of detailed information provided by point measurements. This would be possible by coupling a wide field modality to a mode of single point measurement.

Raman spectroscopy offers the exciting prospect of revealing highly specific biochemical changes before morphological differences between normal and diseased tissue become detectable. However, it cannot be readily extended to provide a wide-field screening tool that can image fields of view of several centimetres.

One optical technology potentially capable of this is FLIM. Nevertheless, to date FLIM has only been investigated in the GI tract *ex vivo* on a relatively small number of samples and further studies are required to establish these initial findings. Systematic studies of the fluorescence lifetime signatures in normal and diseased tissue *in vivo* are crucial for a complete understanding of the origin of the autofluorescence contrast observed, and for assessing the ability of fluorescence lifetime technology for accurate clinical diagnosis.

Amongst the unmet clinical needs discussed in section 2.7, enhanced detection and discrimination of neoplastic polyps together with assisting with the implementation of novel time-resolved endoscopic instruments for in *vivo* clinical use provided the motivation for the studies described in this thesis.

Polyps are undoubtedly of greatest interest to the endoscopist because of their high prevalence in the general population, and, if neoplastic, for their established role in the stepwise process that results in colorectal cancer. Clearly, endoscopists spend a lot of time and emotional energy searching for polyps, and worry about the potential impact of cancer on their patients. Optical biopsy techniques, which interrogate the mucosal surface with light without the need to physically remove tissue, would be highly desirable as they could facilitate clinical decision making in ambiguous situations reducing time to diagnosis. This would bring accurate and reliable information directly at the point of service, circumventing the cost and time required for histology, reducing uncertainty for patients and the attendant psychological morbidity, and therefore improving the overall quality of care.

The overarching hypothesis for all the experiments described in this thesis was that fluorescence lifetime imaging/metrology is able to generate contrast between different types and states of human tissue (GI, skin, bladder), including between normal and neoplastic tissue.

The general aims of this work were:

- To explore the origin of the fluorescence signals and characterize the potential origins of fluorescence lifetime contrast associated with normal and diseased tissue using the excitation and emission wavelengths compatible with the FLIM/FLS endoscopes developed during the project.
- To translate fluorescence lifetime technologies from the optical bench to the bedside and from *ex vivo* to *in vivo* applications.
- To try and determine whether *in vivo* FLIM/FLS is possible, practicable and clinically useful and what can add to the existing techniques.

Chapter 4: Fluorescence Lifetime Imaging (FLIM) of human gastrointestinal tissues: a pilot observational study conducted on ex vivo endoscopically resected specimens.

This chapter describes the results obtained by imaging a number of fresh, unfixed, unstained tissues collected from patients undergoing GI endoscopy as part of their clinical investigations, with a confocal FLIM microscope. These initial observational experiments were performed on a spectrum of tissue types containing a wide range of structures and potential fluorophores in order to try and determine the potential origins of the contrast generated by FLIM and the relative contributions to tissue autofluorescence from the different areas and structures within the tissue. This observational study is a another step towards testing the hypothesis that fluorescence lifetime imaging/metrology is able to generate contrast between different types and states of human GI tissue and is a necessary step towards exploring the potential applications of FLIM both for *ex vivo* tissue FLIM analysis and *in vivo* tissue imaging.

The FLIM confocal microscope represents a convenient platform for initial systematic observations due to its inherent capacity for optical sectioning, relative ease of use and a fast and clinician-friendly interface for image acquisition and processing. Although this microscope offers great versatility in terms of excitation and emission wavelengths, the excitation wavelength of 420 nm was chosen because of its compatibility with the clinically deployable confocal FLIM endomicroscope that has been developed by the Photonics Group. The system and the experimental protocol are described here as well as the experiments with synthetic fluorophores in solution, and the immunohistochemistry assays and selective stains that have been performed on selected cases to enable histopathological correlation of the fluorescence lifetime contrast observed.

The work presented in this chapter shows that confocal fluorescence lifetime imaging has the potential to provide useful diagnostic information in a range of GI tissue types and states of disease. Particularly, this was seen to be the case in colonic polyps and inflammatory bowel disease, where a statistically significant decrease in fluorescence lifetime was found between lesional and normal specimens (p = 0.024 and 0.015 for polyps and IBD, respectively).

As discussed in chapter 3, data on the diagnostic potential of fluorescence lifetime measurements have already been observed in previous studies [265-268,270,271,273,396,397] and it is opportune to investigate the application of FLIM to other tissue types and diseases,

including pre-neoplastic conditions. However, it is important to draw a distinction between wide field FLIM, where the entire sample is illuminated and, depending on sample scattering and absorption, fluorescence emission is indistinctly collected from all layers, and confocal FLIM, where the sample is illuminated with a focussed beam of light, and although other parts of the sample are also illuminated, the fluorescence detected comes only from the tissue layer in focus.

4.1 Introduction

The medical conditions relevant to this chapter have been introduced in chapter 2. Some summary of the most relevant parts of this chapter are provided here together with further relevant work in this area.

Prevention in endoscopy is based on early detection of potentially curable cancers or precursor conditions that have a significant risk of progression to malignancy. Thus, early diagnosis is the critical goal since it allows endoscopic or surgical intervention on a localised disease without lymph node involvement, which greatly improves patient survival.

Traditionally, white light endoscopy (WLE) has been used to evaluate the mucosal surface of the GI tract but inflammatory disorders, dysplasia and early stage cancers are frequently invisible or difficult to visualise. Diagnosis of early and premalignant lesions is indeed difficult even for experienced endoscopists because they appear similar to benign lesions and normal mucosa.

Although several novel imaging techniques that can be operated in conjunction with standard WLE have recently become available in the clinical arena – such as narrow-band imaging (NBI) [59], autofluorescence imaging (AFI) [61] and more recently confocal endomicroscopy (CLE) [62,398] – there is still no "red flag" technique for detection of GI pre-malignant lesions that can progress into cancer. Furthermore, there is currently no reliable technology that can indicate when it is safe and appropriate not to biopsy. Thus, the current clinical best practice in GI endoscopy is for tissue abnormalities to be biopsied and sent for histological assessment and interpretation, which confers a significant burden on healthcare systems [2,399].

In most cases, multiple random biopsies are still required to confirm or reject the endoscopic diagnosis. For example, diagnosis of benign conditions like eosinophilic esophagitis and microscopic colitis is only possible by random biopsy as on endoscopy the mucosa typically looks normal or shows only very subtle signs of disease. However, the diagnostic yield of random biopsies is often low and incurs a high cost [243,244].

Another point to consider is that although histopathological assessment is quoted as a "gold standard", it is not. For instance, the accuracy of routine clinical pathology in colonic polyp differentiation is only approximately 87% [265]. It is also accepted that histopathology suffers

from subjectivity on grading low and high grade dysplasia in Barrett's oesophagus [400]. In fact, the differences between inflammatory regenerative changes, low-grade and high-grade dysplasia and cancers are difficult to classify because of overlapping morphological features. There is a need for more objective assessment as the histopathologist is disadvantaged by reviewing material out of context and with demonstrable levels of poor to moderate inter-observer agreement at best about what constitutes "dysplasia".

Sampling error combined with the delay in obtaining histological confirmation of disease can place a patient at risk of progression of the disease that precludes endoscopic/surgical resection, and often causes psychological distress. In addition, the inability to confirm whether a tissue is benign or malignant at the time of endoscopic examination leads to unnecessary biopsies, repeat endoscopies and imaging and treatments. There is therefore a need to develop diagnostic endoscopic imaging technologies to interrogate tissue and identify lesions that cannot be detected using existing techniques.

A non-invasive method of diagnosis would remove the need for a physical biopsy and could provide improvements in diagnostic accuracy for a number of conditions.

The advent of novel imaging technologies is creating important new opportunities for contrast. One such example is fluorescence imaging, which can be implemented in endoscopes and can use endogenous (AFI) or exogenous fluorophores (PDD) to achieve contrast.

However, the reason for the difference in fluorescence between normal and diseased tissue observed with AFI is still unclear and intensity-based contrast is often not sufficiently specific [135-137]. Only a few clinical studies have been performed, showing mixed results [391,401] a high false positive rate [357] or an overall sensitivity inferior to standard WLE [233,359,392,402].

The development of endoscopic Fluorescence Lifetime Imaging (FLIM) offers the opportunity to add an additional contrast parameter to the clinical environment. As the FLIM signal is generated by endogenous fluorescent molecules it can provide both histological and biochemical information. It has therefore the potential to provide an *in vivo* label-free "optical biopsy" avoiding multiple unnecessary and/or random biopsies.

Wide-field FLIM has been shown to provide intrinsic contrast between benign and neoplastic GI tissue *ex vivo* [273] and single point fluorescence lifetime measurements have been successfully applied *in vivo* to colonic polyps [265] and skin cancer [403], and *ex vivo* to skin [258,270] and GI endoscopic biopsy samples [404].

A number of other translational label-free optical techniques are currently being investigated owing to their potential to acquire non-invasive biochemical information and to image with sub-cellular resolution but the published experience is limited.

Near-infrared diffuse reflectance imaging offers another potential source of optical contrast, and has been applied to detecting colon cancer [73] but further miniaturization of the imaging system is still required for clinical application. Optical coherence tomography (OCT) allows imaging at greater depths within tissue but typically does not supply functional information. Raman spectroscopy and coherent anti-Stokes Raman scattering (CARS) microscopy can be used to obtain highly detailed spectroscopic information [69] but usually require long data acquisition times and cannot be readily extended to wide-field imaging modalities. Point spectroscopy with probes inserted through the working channel of conventional endoscopes has been able to differentiate non-neoplastic from neoplastic tissues [70].

In this chapter, preliminary observational work performed using excitation at 420 nm with detection by a time-resolved fluorescence lifetime imaging confocal microscope to investigate FLIM contrast in GI tissue that has been freshly biopsied/resected from patients undergoing endoscopy is described.

The aim of this study was to image a relatively large number of GI endoscopic specimens in order to explore the origin of the fluorescence signals and characterize the potential origins of fluorescence lifetime contrast associated with normal and diseased tissue morphology using confocal FLIM at 420 nm excitation. This excitation wavelength was chosen to be compatible with FLIM confocal endoscopes that are expected to utilise excitation in the blue spectral region (~405-445 nm) where there is an optimal balance between excited tissue autofluorescence and unwanted background fluorescence, e.g. from glass fibre bundles.

4.2 Materials and methods

4.2.1 Overview

Between May 2010 and December 2011, a total of 71 endoscopic samples from different GI sites were collected from 35 patients undergoing either upper or lower GI endoscopy at Charing Cross Hospital, Imperial College Healthcare NHS Trust. All samples were imaged using a confocal FLIM microscope with 420 nm excitation. Fluorescence was detected using time correlated single photon counting (TCSPC) over the range 450-680 nm.

A total of 481 confocal images were acquired (mean 6 images per sample; minimum = 1, maximum = 19). FLIM image processing was performed using commercially available software SPC-Image 3.1 (Becker & Hickl GmbH, Germany). This was done manually and in many steps, becoming often a laborious and time-consuming process which is prone to error. Therefore, given the large number of images acquired, it was necessary to introduce a selection strategy based on objective criteria in order to reduce the workload to a reasonable level.

Criteria for image selection were:

1. Number of photons per pixel above 1000, as a number below this threshold would prevent accurate determination of the fluorescence lifetime using a double exponential decay fitting model.
2. Presence of recognisable histological structures based on resemblance to corresponding histological and representative confocal microscopy images.
3. Easy orientation of mucosal side.
4. Plane of the mucosa imaged at a depth of 100 ± 30 μm, in order to simulate the fixed imaging plane depth of the probe based confocal laser endomicroscope.

This selection considerably reduced the number of images to manually process. Finally, only two images (1 normal, 1 disease) per patient data set were selected according to the highest fidelity to histological structures, best image quality and resolution, and the highest number of photons per pixel.

Data from each diseased sample were compared to data from normal sample taken from an endoscopically normal area near the lesion, fitting the fluorescence decay to a double-exponential decay model and analysing the resulting mean fluorescence lifetime. Only paired samples were included in the analysis. All samples were submitted for histopathology following the imaging and measurements. Normal tissue and some of the most common GI diseases - including colonic polyps and cancer, inflammatory bowel disease (IBD) and Barrett's oesophagus (BO) - were investigated (table 4-1).

Tissue group	Histological diagnosis	No. of samples
Colonic polyps	11 adenomas with LGD 2 mixed hyperplastic adenomatous polyp with LGD 1 hyperplastic polyp 1 nonspecific reactive changes	15
IBD	5 active chronic ulcerative colitis 1 severe chronic ulcerative colitis with multifocal LGD 1 ischaemic colitis 1 active chronic Crohn's disease	8
Colon cancer	4 adenocarcinoma	4
Gastric disease	2 chronic gastritis 1 adenocarcinoma	3
Oesophageal disease	2 BO with LGD	7
	3 BO	
	2 reflux oesophagitis	
Other (polypectomy scar)	1 stromal fibrosis	1
Normal colon tissue	20 normal colonic mucosa 1 lymphocytic colitis 1 severe chronic ulcerative colitis	22
Normal stomach tissue	1 normal gastric mucosa 1 intestinal metaplasia and mild dysplasia	2
Normal oesophageal tissue	6 normal oesophageal mucosa 1 papillary hyperplasia 1 parakeratotic achantotic squamous epithelium	8
Normal duodenal tissue	1 normal duodenal mucosa	1
Total number of normal tissue specimens	33	
Total number of diseased tissue specimens	38	
Total number of specimens	71	

Table 4-1: Summary showing the histological diagnoses of all the *ex vivo* samples investigated with the confocal FLIM microscope. Note that the group "gastric disease" incorporates gastric cancer, gastritis and portal hypertensive gastropathy. "Oesophageal disease" incorporates Barrett's oesophagus and oesophagitis. LGD = low grade dysplasia; IBD = inflammatory bowel disease; BO = Barrett's oesophagus.

4.2.2 Patient enrolment

Patients were recruited from those attending the Endoscopy Unit at Imperial College Healthcare NHS Trust's Charing Cross Hospital Site.

Patients who participated in the research were recruited by the clinical team and gave their informed written consent to participate. The study was carried out with the approval of the National Research Ethics Service (REC reference number 09/H0706/28).

The use of human tissue in this research complied with the requirements of the Human Tissue Act (2004). Patients agreed to the collection of an additional normal biopsy and the use of tissue samples not needed for histopathology for research.

Inclusion Criteria

Patients were recruited if clinically diagnosed with one of the following conditions and if they required biopsy or endoscopic resection: Barrett's oesophagus; atrophic gastritis and intestinal metaplasia; gastric cancer; biliary reflux disease or portal gastropathy; small intestinal enteropathies; duodenal ampullary disease and pancreatobiliary benign and malignant strictures; inflammatory bowel diseases; colorectal cancers and polyps.

Exclusion Criteria

The following exclusion criteria were used:

- Unable to give informed consent
- Under 18 years old
- Prisoner
- Having a blood borne infection e.g. Hepatitis, HIV.

Pseudo-anonymisation

All recorded data was tagged using a linked anonymised identifier for each patient. Data analysis and correlation with histology was also anonymous. The clinical researchers (SC, KLR & AVT) held the link but did not disclose this to the research group and maintained patient confidentiality as part of their normal medical duty. This link was electronically stored on an encrypted standalone electronic storage medium that is stored on College property and its access is also restricted physically by storage in locked cupboard in a room with restricted access. These data will be kept for 10 years as per the Imperial College policy.

Minimum Data Set

A minimum data set was collected from each participant as follows:

- Patient data (potentially relevant data was collected from the patient/medical records including patient demographics).

- Lesional data (clinical diagnosis, site of lesion, size).
- FLIM data (duration of imaging, imaging parameters).
- Histological data (histological diagnosis, images of histology slides).

4.2.3 Fluorescence lifetime imaging instrumentation

The bench-top FLIM system used for this study was an inverted Leica SP5 confocal microscope (Figure 4-1). At least one FLIM image was acquired using a 40x 0.75 NA objective from all specimens. An additional image or images were acquired over a larger field of view (FOV) in some cases using a 20x 0.75 NA objective. The confocal pinhole was set at 1 Airy unit for all imaging.

The size of the scanned image was chosen according to the structures observed in the sample and therefore a digital zoom of 1, corresponding to a FOV of 387.5 x 387.5 μm, was selected. This ensured that the same area of tissue was sampled in all cases in a consistent way with a field of view large enough to allow for averaging over many crypts.

All samples were excited at 420 nm excitation. This wavelength was chosen because of its compatibility with the FLIM endomicroscopes that are being developed by our group for potential *in vivo* clinical applications. This wavelength falls within the excitation spectra of a number of important tissue fluorophores, such as flavins, porphyrins, collagen and elastin. Typical excitation wavelengths used by other investigators for studying the autofluorescence characteristics of different types of tissue lie between 310 and 420 nm [275,280]. Fluorescence was detected over the range 450-680 nm.

Excitation light was generated using a Mai Tai Ti:Sapphire laser (Newport Spectra-Physics). The infrared output was tuned to 840 nm and frequency doubled to produce ~100 fs pulses of 420 nm light at a repetition rate of 80 MHz. Fluorescence lifetimes were measured using TCSPC (SPC830 card, Becker and Hickl GmbH, Germany).

As discussed in section 3.1.5, in TCSPC, high gain photomultiplier tubes are used to measure the arrival times of single fluorescence photons. The excitation light is set to be sufficiently weak so that less than one fluorescence photon is detected per excitation pulse. Therefore, after many thousands of excitation pulses a histogram of photon arrival times can be built up. The distribution of the arrival times of emitted photons relative to the excitation pulse reflects the fluorescence decay from the point being measured. The excitation beam is scanned across the sample to produce a photon arrival histogram for each pixel in the image.

For TCSPC, image acquisition and data processing is performed using the commercially available software SPCM and SPC-Image respectively (Becker & Hickl GmbH, Germany).

The optical average power was restricted to a maximum of 1 mW in the sample plane. Typically used excitation powers were 0.5 mW.

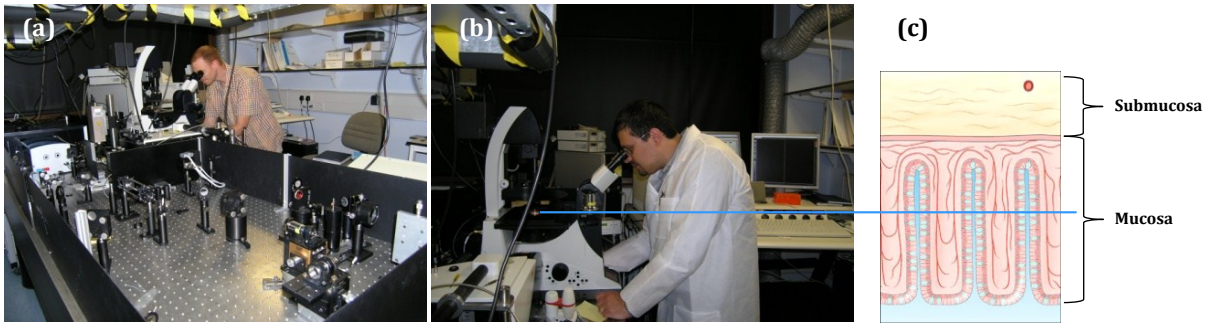


Figure 4-1: (a, b) Experimental set up for *ex vivo* imaging using the inverted Leica SP5 confocal FLIM microscope. (c) Graphic of the estimated image section of a tissue sample (in light blue). Adapted and reproduced with permission from [405].

Additionally, fluorescence from the sample could be directed into a fibre-coupled spectrometer (HR4000, Ocean Optics Inc., B.V., The Netherlands) allowing the emission spectrum averaged over the whole scan field to be measured.

Lifetime calibration

For each imaging session an instrumental response function for the system was taken using fluorescence from a drop of erythrosin B solution (10-40 μM), which has a single exponential decay with a lifetime of 89 ps [406].

4.2.4 Sample preparation and protocol

During routine endoscopy, pinch biopsy samples were taken by endoscopic "jumbo" biopsy forceps (Radial Jaw 3 LC forceps, Boston Scientific) or superficial lesions removed with cold or hot snare (Captivator single-use snares, Boston Scientific) according to standard patient care (Figure 4-2a). Care was taken to avoid contamination of the accessory devices (e.g. forceps, snares, etc.) with formalin. Samples were 5-15 mm in diameter. Where clinically possible, at least one biopsy of healthy tissue was also taken from each patient with a suspicious region. The healthy biopsy was taken as close as possible to the suspicious region.

The freshly-excised samples were placed in a pot with chilled tissue culture medium (phenol red-free DMEM, Invitrogen-Gibco, USA) and packaged for transport to the Physics FLIM laboratory (Blackett laboratories 623-628) immediately after excision. All tissues were confined using tertiary containment and taken to the Physics department by taxi.

Prior to imaging, the samples were removed from the container and rinsed with fresh buffer solution (HBBS, Invitrogen-Gibco, USA) to remove DMEM, blood and excess mucus.

The samples were then placed in a plastic culture dish with a glass coverslip base (Figure 4-2b). For larger specimens (polyps), the tissue was kept moist by placing it onto gauze, soaked in the buffer solution, which had been previously cut with a hole in the middle to allow imaging and tailored to accommodate the sample.

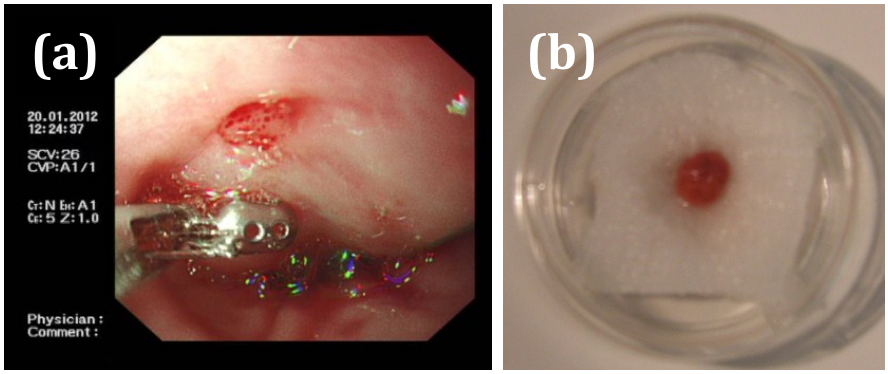


Figure 4-2: (a) Endoscopic biopsy during endoscopy. (b) Sample placed in a plastic culture dish with a glass coverslip base for imaging.

The samples were first examined with either a 10x or a 20x objective in transillumination mode to determine the correct orientation so that they could be imaged with the epithelial surfaces facing down the microscope objective. Polyps, in contrast, could be easily orientated with visual inspection only. Subsequently, the 40x objective was selected and focused onto the surface of the specimen, which was assigned as a nominal depth of 0 µm. Finally, the acquisition of a fluorescence intensity image using a 10 s exposure allowed the presence of a clear fluorescence signal to be collected.

The acquisition time for each FLIM image was set at 120 seconds. Images were acquired at increasing epithelial depths from the surface until tissue details were no longer resolvable, typically every 7-10 µm (figure 4-3).

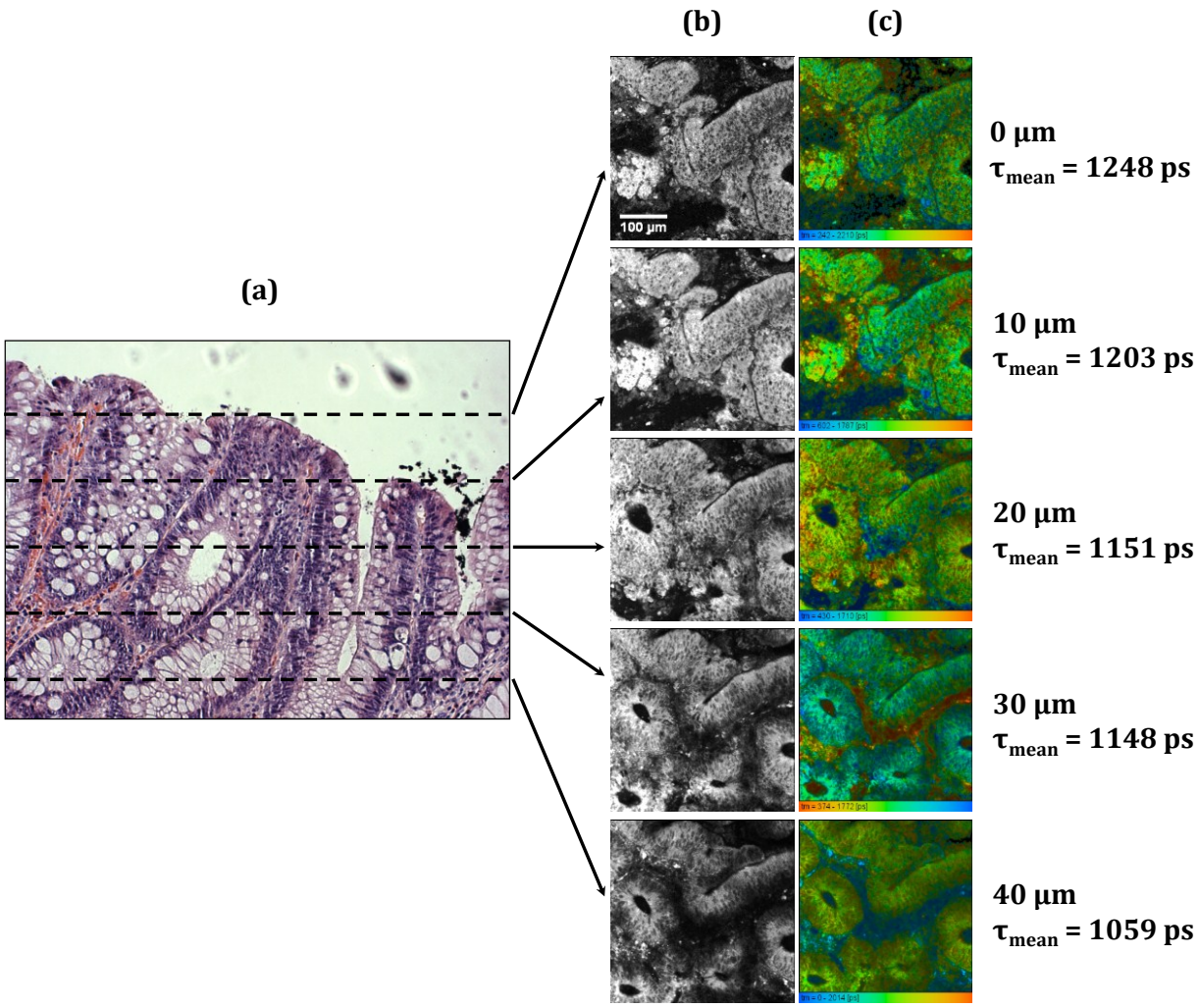


Figure 4-3: (a) Transverse histological image (H&E, original magnification 40x) and corresponding en face confocal intensity (b) and FLIM (c) images obtained at different depths beneath the epithelial surface from a polyp of the sigmoid colon. Brightness, crypt size, tissue architecture, as well as the mean fluoresce lifetime, change as the depth of the focal plane increases from 0 to 40 µm beneath the epithelial surface. Note that no exact registration exists between histology and FLIM images; the figure serves solely to illustrate the relative geometric orientation of the histological section and the stack of FLIM images from the same sample.

To prevent deterioration, samples were kept moist during imaging and handled minimally. There were no visible changes in the texture, thickness or appearance of the samples over the duration of the measurements. All samples were imaged in the FLIM laboratory within 60-120 minutes of resection. Following imaging, the tissue was removed from the dish and transferred to a hospital prefilled container with 10% formaldehyde solution. The samples were then sent to the hospital histopathology laboratory at Charing Cross Hospital for diagnostic assessment.

The tissue slices were then subjected to histopathological examination after paraffin embedding as per current clinical practice. All samples were sectioned at 4-µm-thickness and stained with

haematoxylin and eosin (H&E). The histopathological classification of mucosal lesions was made according to the World Health Organization classification.

Correlation with histopathological analysis

After histological assessment, the H&E-stained tissue sections were requested and reviewed by two experienced histopathologists (GWS & MAEl-B) to correlate the histological findings with the FLIM images. Specific staining and immunohistochemistry were also performed in selected cases to help correlate and evaluate the structures observed.

Tissue crush and diathermy artefacts

Images presenting tissue curling or crush artefacts caused by the biopsy forceps were not processed.

Thermal artefact after diathermy snare excision is a common artefact encountered in surgical histopathology. Polyps less than 10 mm in size are usually resected by cold snaring whereas for polyps greater than 10 mm or those that are stalked, diathermy polypectomy is generally preferable. Sometimes the presence of diathermy is such to render the histological diagnosis impossible, and the heating of tissue during diathermy would be expected to alter the fluorescence properties. However, all of the tissue specimens removed using hot snaring were sufficiently large that the area imaged using the optical system (the head of the polyp) was unaffected by any specimen heating.

4.2.5 Data processing, lifetime calculation and FLIM map generation

Time-Correlated Single-Photon Counting (TCSPC) is currently the gold-standard of fluorescence decay measurement.

Data processing was performed using commercially available software SPC-Image 3.1 (Becker & Hickl GmbH, Germany).

The fluorescence decay profiles were analysed using an instrumental response function obtained by imaging a single drop of erythrosin B solution (10-40 μM) prior to or following the experiments. During the data processing, if the IRF determined at the time of the experiments was found to be inaccurate (long decay, contamination, etc.) the option “auto IRF” was used to calculate an automatic IRF from the data trace with an estimation method provided by the SPC-Image software. The recourse to this method was necessary in only a few cases.

Fluorescence decay fitting model

The autofluorescence of biological tissue tends to show a complex exponential decay profile due to the multiplicity of fluorophores present and their different states e.g. oxidised/reduced and

free/protein bound. It can be described using a multi-exponential model i.e. the sum of a number of single exponential decays as expressed in equation 3.5.

As the number of lifetime decay components to be fitted increases, so must the fluorescence intensity emitted from the tissue, for the model to fit accurately. A double-exponential decay model is commonly used when imaging biological tissue, and often expressed as a weighted mean of the two lifetime components.

Thus, given the nature of the samples investigated in this study, a double exponential decay analysis in each individual pixel of the image was routinely performed and the mean lifetime was calculated using equation 3.7.

Data processing with Becker & Hickl SPC-Image 3.1 software

Once the data was imported, an intensity image was displayed in the top left quadrant of the software package's window (see figure 4-4). This image is calculated from the integrated number of counts for each pixel and is autoscaled by default. The IRF was then loaded as "instrumental response" and appeared in the decay box at the bottom of the screen.

In the decay graph (Figure 4-4(c)), the blue points show the measured photon decay data trace for a particular pixel in the image, the red line is the fit to the data, and the IRF is shown by the green line. Deviations between photon data and fit are shown at the bottom as weighted residuals. The two vertical black cursor lines (T1 and T2) indicate the time channels defining the range of data used for the fit process [407].

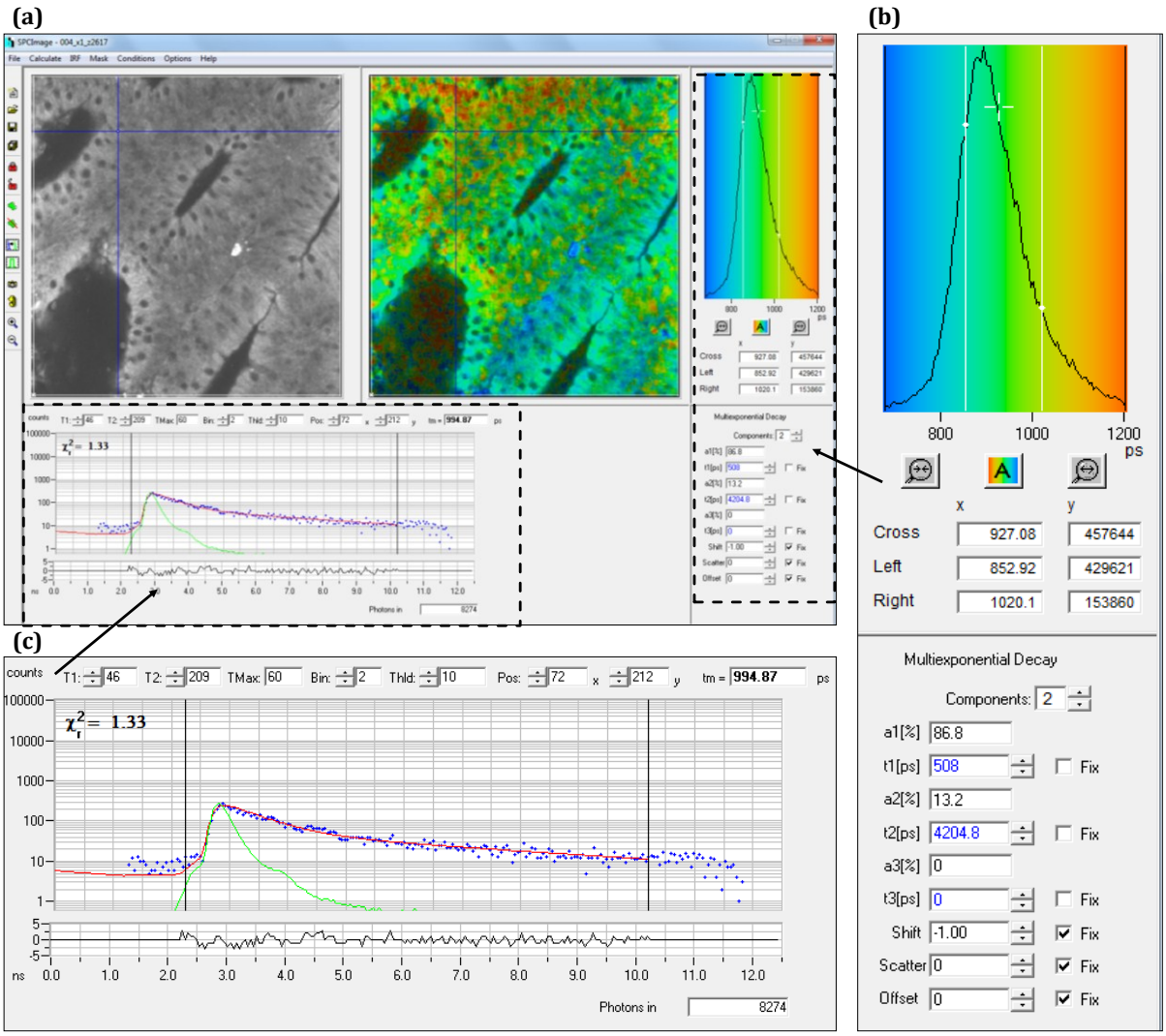


Figure 4-4: (a) Screenshot from SPC-Image software fitting the fluorescence decay from images taken from a specimen of normal colonic mucosa (caecum) excited at an excitation wavelength of 420 nm excitation wavelength. (b) Inset showing the lifetime distribution histogram (top panel) and the multiexponential decay fitting parameters (lower panel). (c) Inset showing the decay graph for the pixel indicated by the blue crosshair. The double exponential fit to the data (blue points) can be seen (red line), with associated residuals in the bottom panel (black line). T1 = start of fit; T2 = end of fit; TMax = temporal bin corresponding to peak of decay; Bin = binning; Thld = threshold; Pos = position of selected pixel; tm = weighted average lifetime of selected pixel; χ2r = reduced Chi-Square.

The fit model "incomplete multiexponential" option, with a maximum number of 20 iterations, was applied to account for incomplete decays and prevent distortions in the lifetime values that are caused by fluorescence photons generated by the previous excitation pulse.

The binning value indicates the number of surrounding pixels which are summed into each decay trace. Therefore, increasing the binning value will increase the number of photons in each decay trace, though at the cost of loss in spatial resolution in the resulting FLIM map.

We chose to fit a double exponential decay model, and therefore binning factor 2 in the SPC-Image software (equivalent to 5 x 5 pixel smoothing) was used for the analysis of all images.

The threshold value allows the user to select the minimum number of photons in the peak of a fluorescence curve required in a pixel in order for the decay to be fitted. The value of this threshold was set by eye depending on the brightness of the sample to reject dark featureless regions.

The shift parameter determines how the instrumental response function is located relative to the peak of the fluorescent signal. The scatter parameter allows directly scattered excitation light to be included in the fit model and this was fixed to zero for all fits.

The software also allows a vertical offset to be included to compensate for background fluorescence or detector dark noise. As both of these were low compared to the fluorescence signal from the sample, this offset was fixed to zero for all fits.

For the paired samples (normal and diseased) within the same patient, the temporal shift of the IRF was fixed to the same value for both samples according to the best χ^2_r (reduced Chi-Square) obtained in the normal sample. The χ^2_r measures the goodness of the fit, and a low χ^2_r (approaching to 1) generally indicates that the fitting model is appropriate.

For the final calculation of the fluorescence lifetime histogram, intensity weighting was used. This means that bright pixels with greater lifetime accuracy were given greater weight than dim pixels with poor lifetime accuracy. This also served to minimise the effect of the manually determined threshold chosen on the resulting lifetime values.

At the end of the fitting, the lifetime and the distribution histogram were displayed next to the intensity image (see right hand side of figure 4-4(a) and inset (b)). The final FLIM map is a composite of the fluorescence intensity (encoded image brightness) and lifetime (encoded using colour).

The software calculates the average value of the lifetime ("Cross value") within the image and the range of the standard deviation ("Left" and "Right" cursors), which includes 66% of all values found within the region of interest (33% on each side of the mean value).

4.2.6 Statistical analysis of paired lifetime measurements

Since the data presented here is not normally distributed, a nonparametric test was selected to statistically test the significance of the differences observed.

The Wilcoxon signed-rank test was used to confirm the hypothesis that when comparing two matched samples, healthy and diseased, their median fluorescence lifetime ranks differed. This was calculated using the MATLAB function "signrank" (MATLAB Statistical toolbox, MathWorks,

USA), which performs a two-sided signed rank test of the null hypothesis that data comes from a continuous, symmetric distribution with zero median, against the alternative that the distribution does not have zero median.

4.2.7 Criteria for interpretation of confocal images

The criteria applied to interpret endoscopic microscope images were based on histological characteristics of tissue. These include well-established features and structures seen on microscopy of standard histological sections [8,9,408] and recently published criteria for confocal laser endomicroscopy [62,151,409-411]. These criteria were used to identify the tissue types and describe the morphological alterations.

Equally, the terminology used to describe the structures observed is based on both standard histopathological nomenclature and the confocal endomicroscopy criteria for classification of e-CLE and pCLE patterns of normal, regenerative, and neoplastic tissue based on evaluation of crypts and vascular architecture, named, respectively, the Mainz [62] and Miami [412] criteria.

A comprehensive online video library of pCLE images with training and testing sections – Cellvizio.net, Mauna Kea Technologies [413], and attendance to national and international training workshops, have also provided invaluable reference and assistance for the understanding and interpretation of the images acquired.

For each image, analysis and interpretation was supported by two experienced GI pathologists (GWS & MAEl-B).

4.3 Results

All analysis was performed based on the histological diagnosis for each sample. Samples were excluded if microscopic analysis revealed normal large bowel mucosa in abnormal samples or histological abnormalities in normal specimens. The laser used for fluorescence excitation caused no tissue damage that could be detected at the microscopic level.

Table 4-2 summarises the demographic details of patients undergoing GI endoscopy whose tissue has been imaged.

No. of patients	Male	Female	Age range
35	23	12	22-95

Table 4-2: Demographic details of patients.

TCSPC FLIM data was acquired over a FOV of 387.5 x 387.5 μm. Paired representative images from normal and diseased tissues are shown in each of the following specific result sub-sections. A paired analysis approach was used when calculating the shift in the mean

fluorescence lifetime (i.e. relative to the normal tissue obtained from the same patient) and when performing tests on statistical significance. This approach was motivated by the high inter-patient variability observed in normal specimens from different patients (see figure 4-8(a)).

Although excluded from the paired analysis, unpaired samples, for which it was not clinically possible to obtain an associated normal or diseased specimen, were also processed and characterized.

The diagnostic groups are shown in table 4-1. The following gallery of images summarizes the findings seen in some of the different types of tissue examined.

4.3.1 Colonic polyps

As discussed in section 2.1.2, polyps are normally classified into 2 groups: neoplastic (consisting of adenomas with low grade or high grade dysplasia, and carcinomas) and non-neoplastic (hyperplastic, inflammatory pseudopolyps, hamartomas). Neoplastic polyps are of greatest clinical significance because of their established role in the process that results in colorectal cancer. However, macroscopic discrimination between neoplastic and non-neoplastic polyps during endoscopy is extremely difficult.

Of the total of 23 specimens measured (13 polyps and 10 normal) from 10 patients, 4 specimens were excluded from the analysis: 1 polyp and 1 normal sample from 1 patient as the normal specimen was found to be abnormal by histopathology (lymphocytic colitis); 1 polyp and 1 normal from the same patient as the clinically identified polyp was not confirmed at the histopathological assessment. The polyp specimens included in the analysis are summarised in table 4-3-3.

No. of patients	8
No. of polyps	11
• **Neoplastic**	10
• **Non-neoplastic**	1
No. of normal specimens	8
Total number of specimens	19

Table 4-3: Summary of colonic polyp and normal specimens included in study.

Paired representative images from normal and pre-neoplastic (adenoma) tissues are illustrated in figure 4-5 and figure 4-7, and obvious morphological differences are apparent with neoplastic progression. The normal colon sample shows a symmetric arrangement of regular and uniform

crypts. The crypts are almost equidistant and present circular openings in a symmetric arrangement. One representative crypt opening is shown with an asterisk in each fluorescence intensity figure. Goblet cells are known to surround the crypts and are orientated with their long axis perpendicular to the inner ring of the crypt. In the figures, cellular structures are apparent with large dark inclusions, which are therefore identified as goblet cells. At this excitation wavelength, the main intracellular fluorophore is expected to be due to flavins (see section 3.1.4), and mucin filled vacuoles would be expected to exclude intracellular flavins and so appear darker. Examples of identified goblet cells are shown in the figures by red arrows.

In contrast, a solid structure with aberrant crypts with almost no openings and no apparent gland formation is observed in the polyp specimen. The crypts appear condensed and displaced by large dense branching bands of interstitial space mostly free of cells. Crypts are distorted and elongated (asterisk), and significantly fewer goblet cells can be observed, which are now replaced by crowded elongated cells with large dark regions, which are assumed to be the nuclei, pointing toward the exterior rim of the crypts (red arrowheads). This change in cell orientation is consistent with that observed in histopathology of adenomatous polyps.

The polyp sample shows a net decrease of the average lifetime values compared to normal mucosa. In addition, within each sample, irrespective of healthy or diseased status, crypts and surrounding stroma (lamina propria) exhibit a fluorescence lifetime separation: longer fluorescence lifetime values (red in the colour scale) are found at the edge and, in the case of the normal sample, in the centre (luminal openings) of the crypts (see inset in figure 4-5(b)), while the stroma surrounding the crypts is instead characterised by a shorter lifetime (blue). It is worth noting that, in the centre of the crypt lumen, which would be expected to be empty, fluorescence is observed, with mean fluorescence lifetime longer than that of the surrounding structures (see inset of figure 4-5(b)). Goblet cells are known to produce mucous that passes into the crypt lumen and eventually flows into the colon lumen to facilitate the movement of the faecal mass along the colon. This fluorescence was therefore attributed to the presence of mucous residues within the crypts lumen.

The FLIM images therefore seem to provide some functional information in addition to the morphological features seen in the fluorescence intensity images.

The lifetime shift observed may be attributed to the different tissue fluorophore composition of these structures, which was shown schematically in figure 2-3. Crypts are lined by an epithelium consisting of a single layer of goblet and columnar cells that sit on the basement membrane. Underneath this structure, the lamina propria is a thin vascular layer of connective tissue. The basement membrane is made of proteins held together by type IV collagen, and the lamina

propria is mainly composed of loose connective tissue containing mainly collagens I-III, lymphocytes, myofibroblasts and a network of capillaries and lymphatics.

Intracellular fluorophores such as flavins (NAD(P)H fluorescence is unlikely given the excitation wavelength used) and mucins may be responsible of the longer mean fluorescence lifetimes observed at the edge and in the lumina of the crypts. In contrast, collagen type I-III and collagen type IV may be responsible of the shorter lifetimes in the pixels corresponding areas such the lamina propria and the external rim of the crypts (basement membrane).

Mucin depletion can be seen in the polyp specimen, where only a few goblet cells can be distinguished and the crypts openings appear void. Interestingly, this finding is accompanied by a shortening of the lifetime at the edge of the crypts, and particularly, in the lumina. Differences in mucins content has been further confirmed for this pair of samples using a mucin-specific staining (see section Colonic polyps – selective staining and figure 4-10(i-l)).

In the polyp, the mean fluorescence intensity, averaged across all the pixels of the intensity images, was higher than that of the normal specimen (879 ± 390 vs. 421 ± 158 mean detected photons per pixel), measured using identical image acquisition parameters for both normal and polyp specimen and similar image depths.

The spatially averaged fluorescence emission spectra acquired using the spectrometer show similar spectra for the normal and polyp specimens, see figure 4-5(f), with a peak at approximately 520 nm. This is in reasonable agreement with the emission maxima of flavins (515-530 nm).

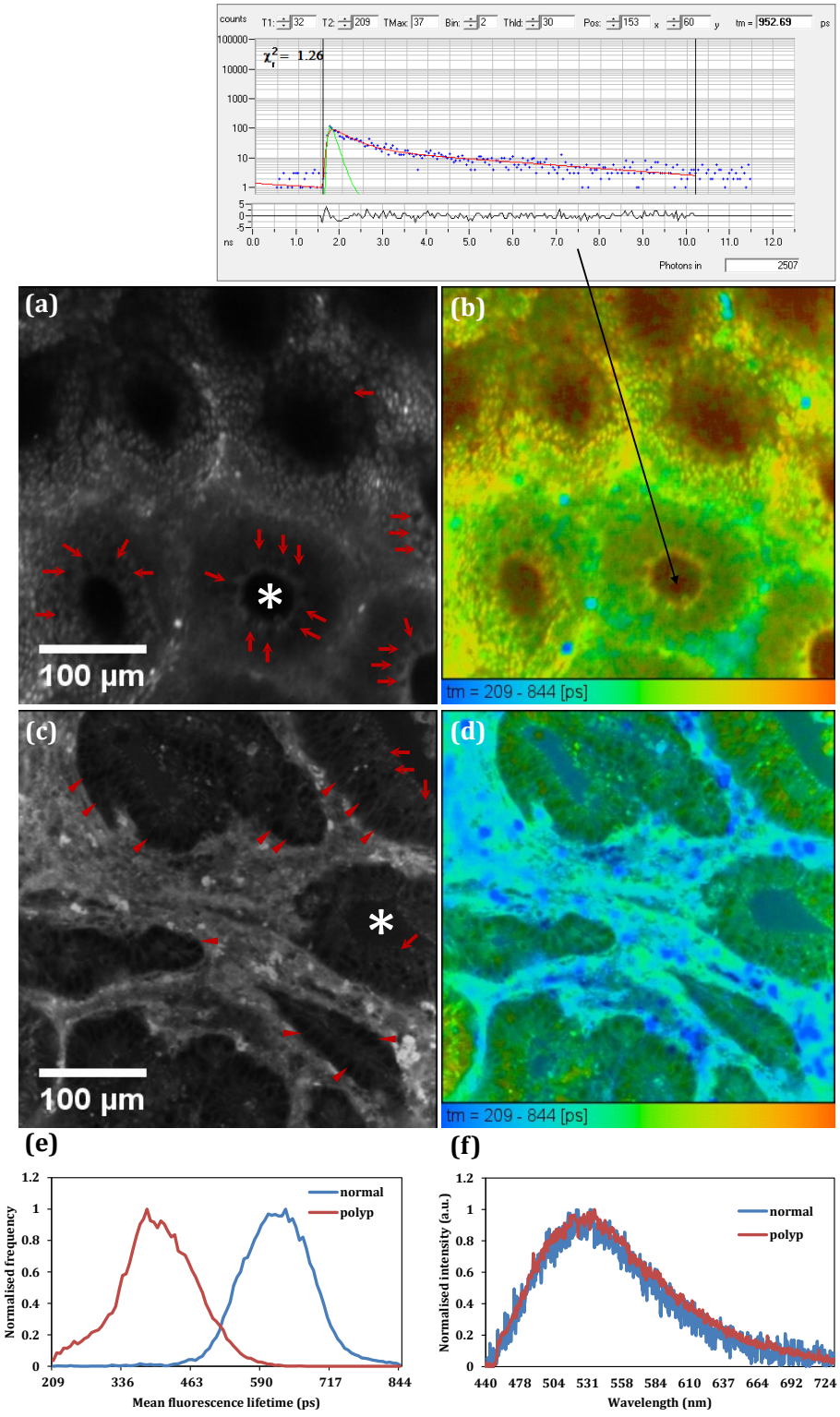


Figure 4-5: **Matched intensity (a, c) and FLIM images (b, d) of a freshly resected adenomatous polyp (c, d) and contiguous normal colonic mucosa obtained from an adjacent region in the same patient (a, b). The inset in (b) shows the decay graph from the centre of the crypt lumen in the normal sample. (e) Mean lifetime distribution histogram calculated from the FLIM data. Subverted architecture with highly atypical crypts can be seen in the polyp (c, d) and a separation of the FLIM histograms is clear (e). (f) Spatially averaged fluorescence intensity emission spectra collected from the samples with a spectrometer. See text for description of arrows, arrowheads, and asterisks.**

The emission spectra were compared to spectra of purified flavins in solution (Flavin adenine dinucleotide disodium salt hydrate, Sigma-Aldrich, USA) obtained using a spectrofluorometer at 420 nm excitation and 540 nm emission wavelength (figure 4-6). A 2.5 µM solution of FAD dissolved in MilliQ water was made up immediately prior to the measurement. The spectra were acquired at room temperature (21 °C) from 440 nm to 730 nm (10 nm steps) at 40 s acquisition per wavelength (Figure 4-6 (b)). The black dashed rectangle in figure 4-6(b) shows the overlap between the emission spectra of the polyp and normal specimen, collected with a fibre-coupled spectrometer, and the emission spectra of purified flavins in solution. As expected, the peak and the line shape of the emission spectra appeared to be similar to that observed for flavins, with a minor contribution from another fluorophore, e.g. NADH or collagen, sub-optimally excited at 420 nm excitation. Contribution from lipopigments is usually not expected in normal (non melanotic) mucosa and colonic polyps [324], and elastin does not significantly contribute to colon tissue autofluorescence [301].

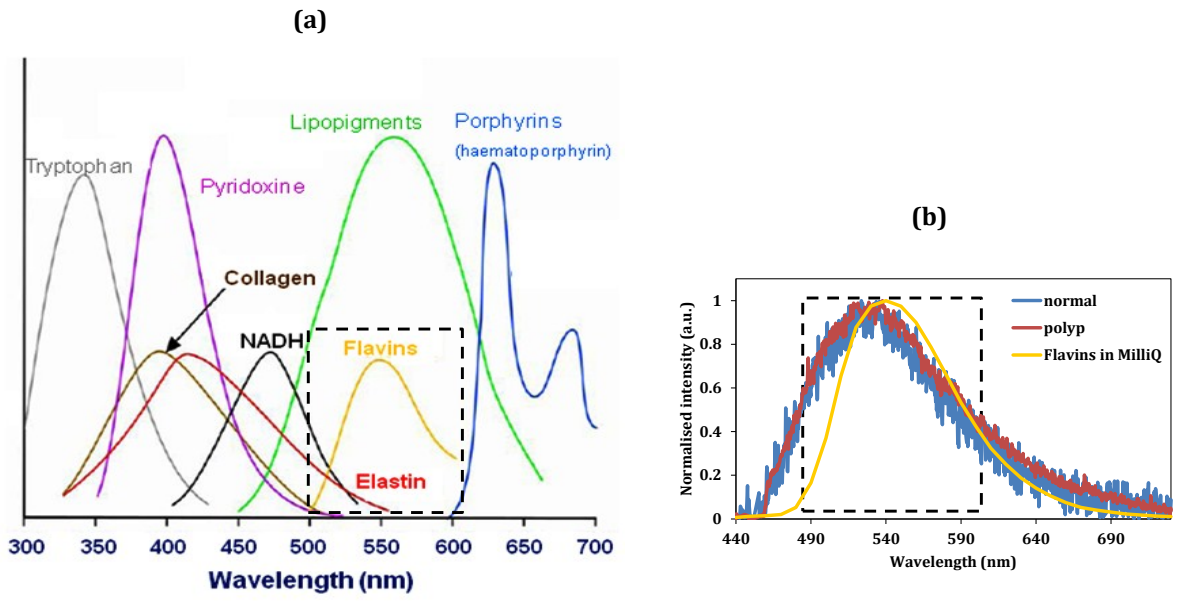


Figure 4-6: (a) Emission spectra of main endogenous tissue fluorophores (adapted from [213]). (b) Graph showing the overlap (black dashed rectangle) of the intensity spectra from fresh biopsy specimens of rectal polyp and adjacent normal rectal mucosa (shown in figure 4-5) collected with a fibre-coupled spectrometer, and the emission spectra of flavins (FAD) in solution (2.5 µM) obtained using a spectrofluorometer [414] at room temperature (21 °C), λex = 420 nm, λem = 540 nm.

In figure 4-7(a, b), the normal specimen shows a regular crypt architecture, and again, the interior rim of the crypts and the lumina (asterisks) exhibit longer lifetime values compared to the surrounding stroma. In contrast, the adenoma shows crowded tubulovillous crypts with openings almost entirely obliterated, which exhibit longer lifetime values at the edge but shorter in the centre of the crypt and in the surrounding stroma. Elongated cigar-shaped cells with small bright structures and dark vacuoles (red arrowheads) line the crypt openings.

It should be noted that in this case the quality of the image for the normal sample was poorer than that seen in Figure 4-5(a) and this may be due to a greater imaging depth.

Overall, the polyp shows a brighter surface in contrast to that more opaque of the normal mucosa. The polyp again emitted a slightly higher intensity spectrum compared to the normal sample (figure 4-7(f)), with peaks similar to the previous samples (approximately 520-530 nm). Accordingly, the mean fluorescence intensity for the polyp specimen, averaged across all the pixel of the intensity images, was also found to be higher than that of the normal specimen (133 ± 50 vs. 55 ± 32 mean detected photons per pixel).

The mean fluorescence emission wavelength was also slightly longer for the polyp compared to that of the normal specimen (566 nm vs. 562 nm). The mean fluorescence lifetime values observed seem again in line with the range of lifetimes reported for protein-bound flavins (see section 4.3.1).

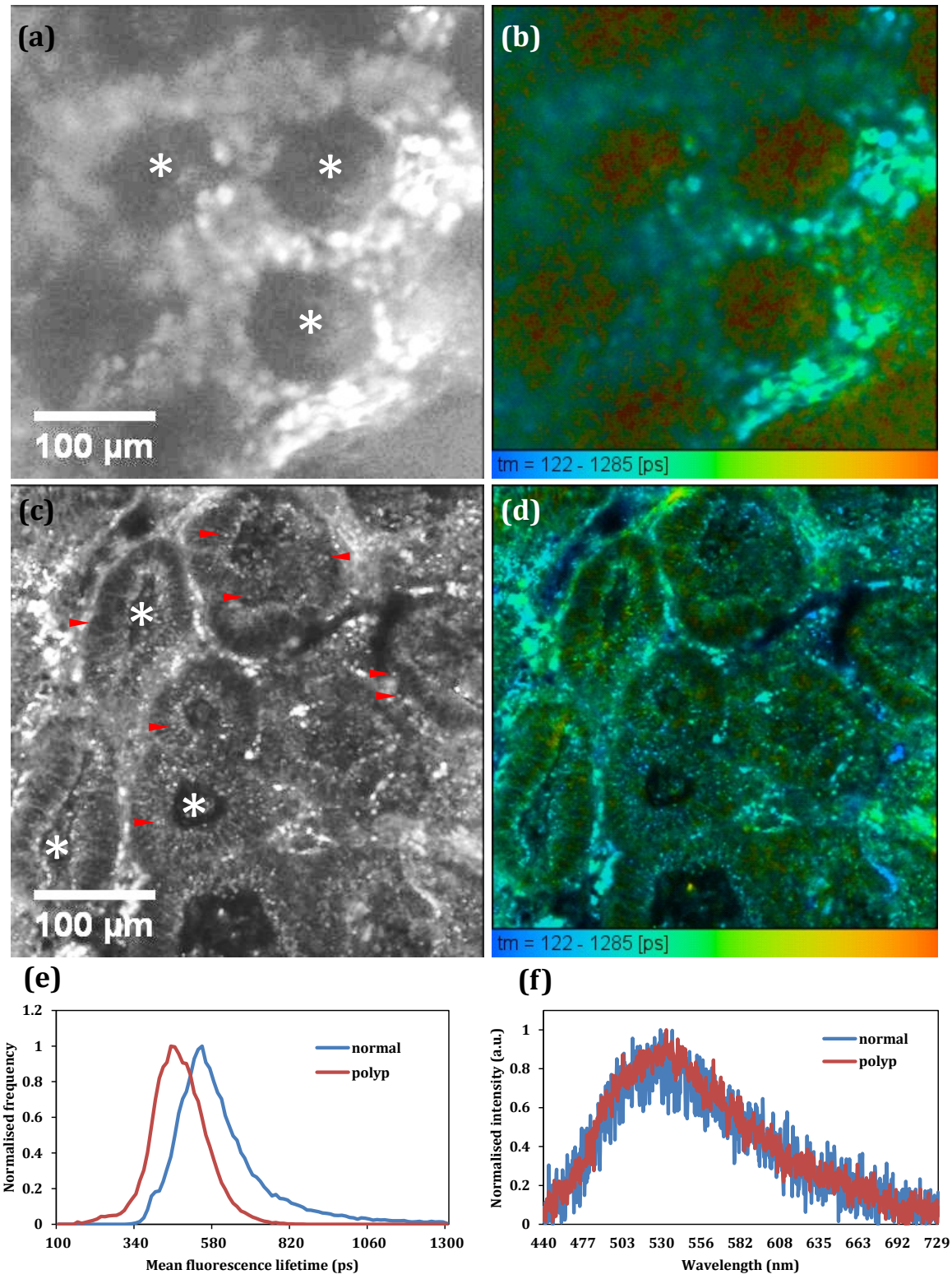
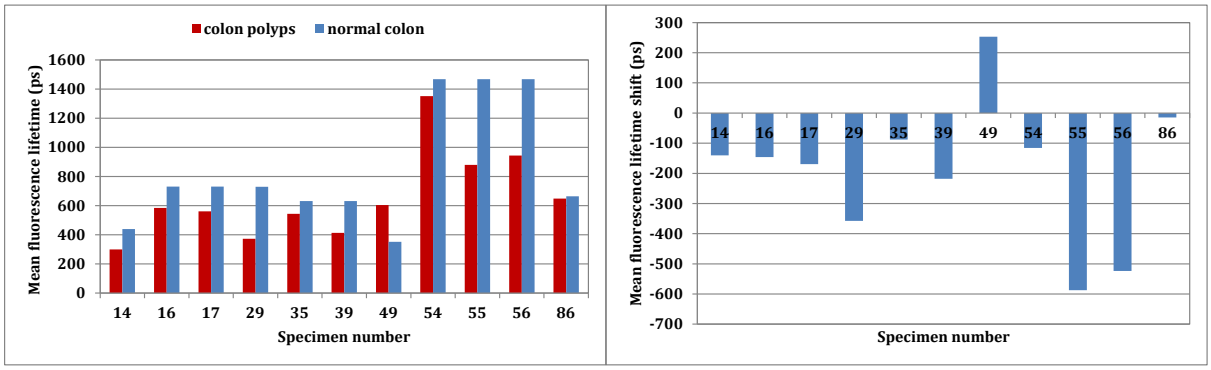


Figure 4-7: **Matched intensity (a, c) and FLIM images (b, d) of a freshly resected adenomatous polyp (c, d) and contiguous normal colonic mucosa (a, b). Numerous merging crypts with distorted orifices can be seen in the polyp (c, d). (e) Mean lifetime distribution histogram calculated from the FLIM data. (f) Spatially averaged fluorescence intensity emission spectra collected from the samples with a spectrometer.**

Figure 4-8(a) shows a summary of results for all the polyp specimens included in the paired analysis. It is evident from this chart that there is considerable inter-patient variation in the measured lifetimes of the normal specimens. The analysis of paired lifetime shifts within individual patients should circumvent any potential problems that this variation could cause. Figure 4-8(b) shows the shift in the intensity-weighted mean fluorescence lifetime ($\Delta\tau$) for each normal-polyp pair. The mean fluorescence lifetimes for polyps were shorter than those observed in normal tissue and this trend was observed in all polyps but one (sample 49, a recurrent adenoma with LGD). It should be noted that sample 29 was a hyperplastic polyp, sample 86 was a mixed adenomatous-hyperplastic polyp, and all the remainders were adenomatous polyps.



(a) **(b)**

Figure 4-8: (a) Bar graphs showing the mean fluorescence lifetime observed in all polyps relative to a sample of healthy tissue from the same region of the colon. (b) Shift in the mean fluorescence lifetime of all polyp specimens included in the paired analysis. Lifetime shifts are calculated using a measurement of normal tissue obtained from the same or nearest region of colon.

The ratio of mean fluorescence intensity, averaged across all the pixels of the intensity images to the corresponding value for the polyp specimen, was found to be greater than 1 for all polyps (n = 11) indicating that the fluorescence intensity from the polyp specimens was always greater than the paired normal specimen. Figure 4-9 shows the paired ratio (polyp/normal) of the fluorescence intensity for all the polyps relative to a specimen of healthy colon from the same patient.

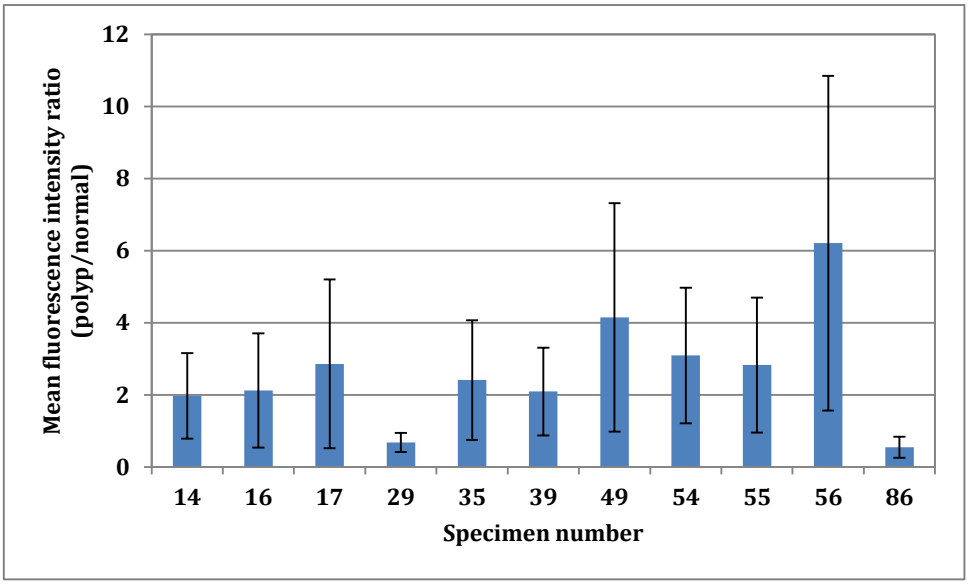


Figure 4-9: Bar graph showing the ratio (polyp/normal) in the mean fluorescence intensity observed in all the polyp specimens relative to a specimen of healthy tissue from the same patient. The mean intensity for all the samples was obtained calculating the mean number of photons detected per pixel, across all the pixels of the intensity image. The error bars represent ± 1 standard deviation and were calculated via error propagation from the fluorescence intensity distribution in the normal and polyp images.

Colonic polyps - selective staining

In addition to the standard Haematoxylin and eosin (H&E) stain for conventional histopathological assessment, a number of immunochemistry assays and selective stains have been performed on selected cases in order to enhance the different structural contrast derived from epithelia and connective tissue, and compare this with the fluorescence lifetime contrast obtained using the confocal FLIM microscope.

This correlation was performed in an attempt to aid our understanding of the fluorophores that are prevalent in structures, such crypts and connective tissue.

The following types of staining methods were used: epithelial membrane antigen (EMA); Masson trichrome; Alcian Blue (AB); Collagen IV; Vimentin. Each of them has a specific molecular target to highlight different components of the intestinal wall.

EMA highlights epithelium for thickness and crypt architecture, and separates clearly epithelial cells and glands from stroma. EMA stains normal and neoplastic epithelium including adenocarcinomas from a range of sites. Strong staining of the apical portion of duct lining cells in glandular epithelia is seen. Staining with this antibody was chosen to identify any correlation with fluorescence of intracellular origin.

In Masson trichrome staining (MTS), three dyes are employed to highlight selectively collagen fibres, muscle, fibrin, and erythrocytes. As a result, the collagen fibres are stained blue, the

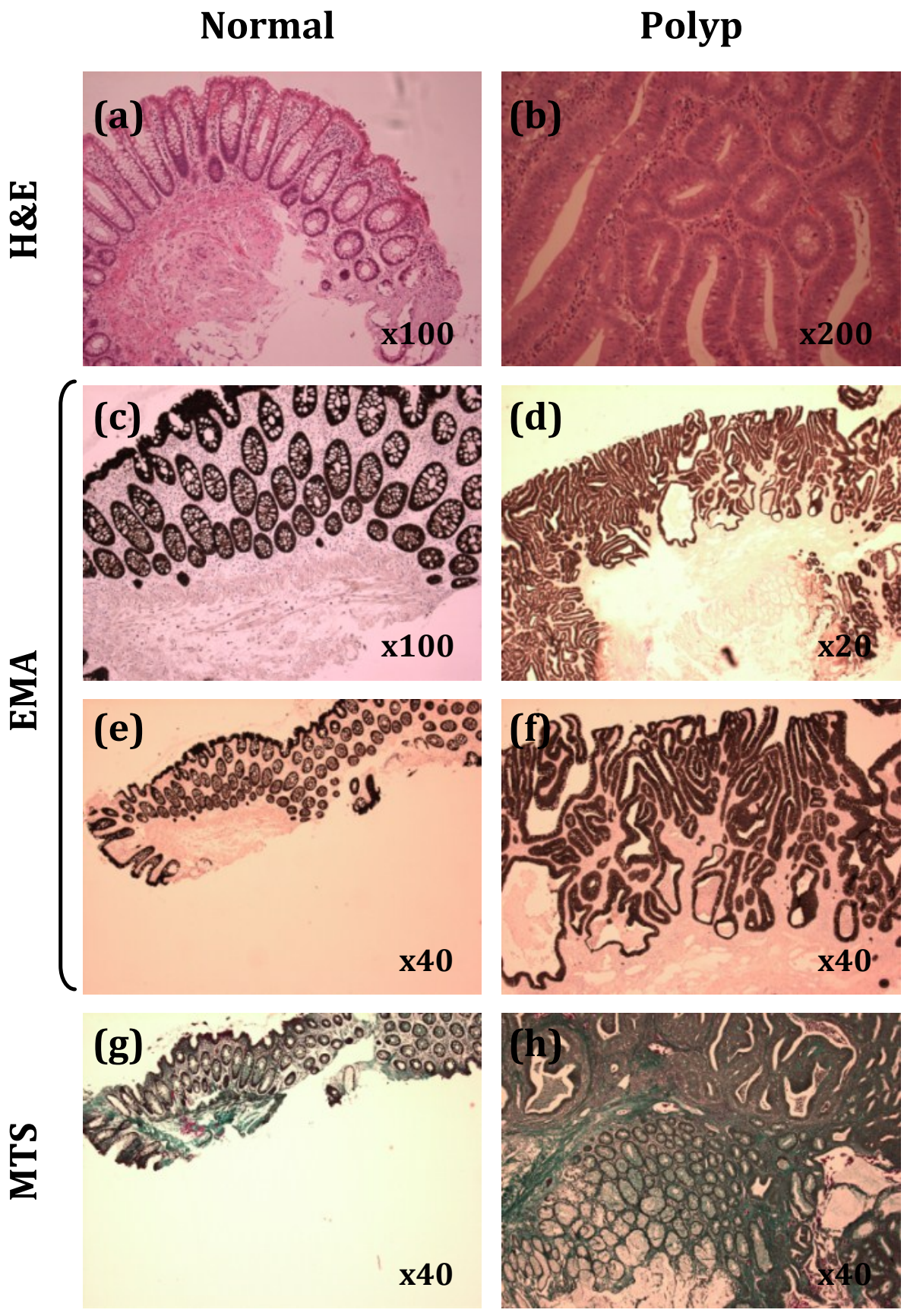
nuclei will be stained black, cytoplasm, muscle and erythrocytes red, and fibrin pink. Masson's Trichrome is most useful to differentiate collagen from other fibres, particularly smooth muscle and elastin, and to identify an increase in collagen.

AB is a specific stain for acid mucins of epithelial origin (sulphomucins and sialomucins), which are found in the goblet cells located in the intestine. AB does not stain neutral mucins, which are found primarily in the surface epithelia of stomach and duodenum. AB provides good contrast between normal and diseased samples. For example, mucin and numerous goblet cells are commonly seen in normal samples, while they are almost invariably lacking in polyps or cancers.

Collagen IV staining highlights basal membranes, muscle and vessels. This antibody reacts selectively with collagen type IV, which is the major constituent of the basement membranes. Adenomas have less type IV collagen in their basement membranes, leading to sparser, trabecular staining in neoplasms versus a more rigid meshwork pattern in normal glands.

Vimentin staining highlights primarily collagen type I, and therefore selectively stains stroma.

Figure 4-10 shows a gallery of images obtained using these stains to differentiate the tissue structure of the same specimens of figure 4-5 (freshly resected adenomatous polyp and adjacent normal colonic mucosa), with the aim to establish a correlation between the fluorescence lifetime contrast observed and the different tissue components selectively highlighted.


Normal
Polyp
H&E
EMA
MTS
(a)
x100
(b)
x200
(c)
x100
(d)
x20
(e)
x40
(f)
x40
(g)
x40
(h)
x40

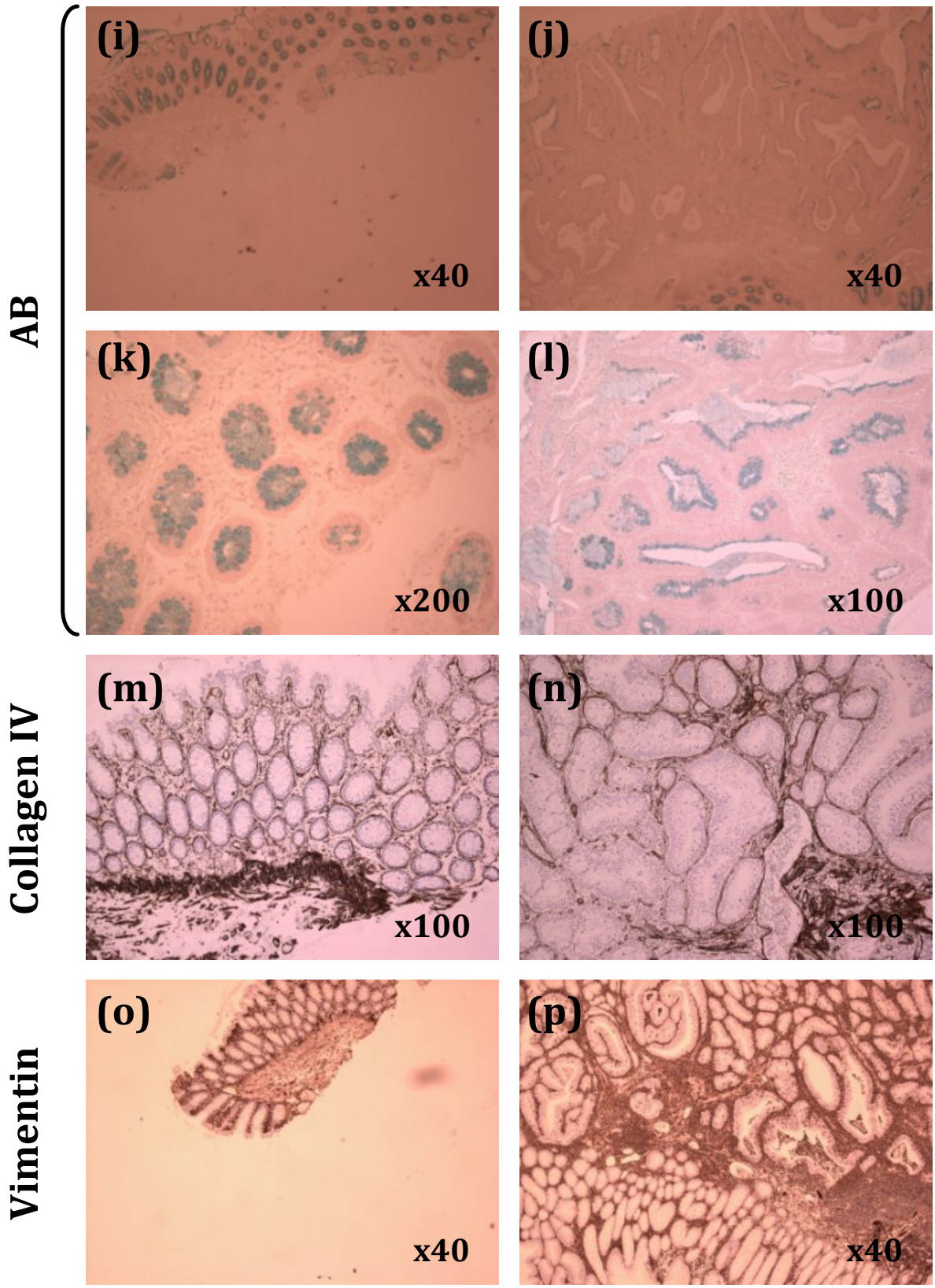


Figure 4-10: Haematoxylin and eosin (H&E) stain of a biopsy sample of normal colon (a) and adenomatous polyp from the same patient (autofluorescence intensity and FLIM images from this patient are shown in Figure 4-5). Numerous normal goblet cells can be seen in (a), while only a few goblet cells are visible in the tubular adenoma dysplastic epithelium (b). The epithelial membrane antigen (EMA) highlights

epithelial cells and glands from stroma in the normal colon specimen (c, e) and in the polyp (d, f). Masson's Trichrome staining (MTS) highlights fibromuscular tissue in both the normal colon (g) and the polyp (h). Alcian Blue (AB) highlights intracellular mucins in goblet cells, and mucins discharged into the gland lumina, showing good contrast between normal colon mucosa (i, k) and adenoma (j, l). Collagen IV highlights the basal membrane, muscle and blood vessels in normal colon (m) and in the polyp (n). The distribution of mucosal collagen appears altered between the samples, with remarkably reduced stain uptake in the polyp, where only scant amounts of collagen IV can be seen in the basal membranes and around the adenomatous crypts. Vimentin shows fairly selective staining of stroma both in normal colon mucosa (o), and the polyp (p), confirming the presence of stromal distortion within the irregular and overwhelmed (squeezed) adenomatous glands.

These staining methods have been able to differentially stain epithelial crypts from connective tissue and intracellular mucins, confirming the structures recognized in the FLIM images.

Interestingly, mucins are well represented in normal colon, while they are hardly seen in dysplastic or neoplastic tissue (see figure 4-10(i-l)). Mucins could therefore represent another possible cause for the AF contrast observed, although they have not been as widely investigated as the more common fluorophores such as NADH, flavins and collagen.

Another important finding is that collagen is found in large amounts in the mucosal layer (see figure 4-10(g-h, m-p). This seems in contrast with the general assumption that collagen is predominantly located in the submucosal layer. For 420 nm excitation we expect the dominant tissue fluorophores within the mucosa to be intracellular flavins, and collagen types I-IV. Collagen type IV is primarily found in the linings surrounding the colonic crypts (basal membranes, see figure 4-10(m-n)), whereas collagen types I-III are predominant in the stroma of the lamina propria figure 4-10(g-h, o-p).

4.3.2 Colon cancer

Colorectal cancer develops within pre-existing foci of adenomatous tissue. This occurs usually, but not always, in a polypoid lesion. Colorectal carcinoma is composed of irregularly infiltrating malignant glands. The cells are columnar and have elongated “cigar-shaped” nuclei with coarsely granular chromatin pattern. The invasive tumour is usually surrounded by a desmoplastic response and focal necrosis is common.

All of the 8 specimens measured (4 cancer and 4 normal) from 4 patients, were included in the paired analysis (table 4-4). Interestingly, at the histopathological assessment, 1 cancer specimen was found to be not a primary colon cancer but the secondary localisation of a metastatic undifferentiated non-small cell lung adenocarcinoma.

No. of patients	4
No. of cancer	4
No. of normal specimens	4
Total number of specimens	8

Table 4-4: Summary of colon cancer specimens included in the study.

Paired representative images from normal and neoplastic colon tissues are illustrated in figure 4-11. Figure 4-11 shows the fluorescence intensity and FLIM images of 2 biopsy samples (1 normal, 1 diseased) from the same patient diagnosed with stenosing rectal adenocarcinoma.

The normal sample (figure 4-11(a, c)) shows a honeycomb arrangement of crypts of uniform shape and size, and each crypt has a central circular opening. Goblet cells can be identified (red arrows) due to the presence of dark vacuoles containing mucin, and the crypts are separated by an interstitial tissue exhibiting a higher fluorescence intensity and shorter fluorescence lifetime than the epithelium.

The cancerous specimen (figure 4-11(b, d)) shows an irregular cribriform structure without significant gland formation and back-to-back arrangement of crowded cells with very little intervening stroma. The crypts visible in normal colon are missing and there are no goblet cells, but crowded and highly disorganized nests of fusing cells with large and dark regions, which are assumed to be the nuclei, are present (red arrows). In these dark regions, surrounded by smaller and brighter white dots (indicated by red arrowheads) a granular pattern can be seen. This feature is consistent with the coarse granular chromatin pattern observed in histopathology ("salt-and-pepper" or stippled chromatin pattern), typically associated with neoplastic diagnosis. At this excitation wavelength, the main intracellular fluorophores are expected to be flavins, which are found predominantly within mitochondria. In malignant cells, mitochondria show variable shape and volume, and large mitochondria can be sometimes observed. Degenerative changes also lead to the formation of cytoplasmic inclusions, such as apoptotic bodies and lipofuscin granules. These intracellular changes might be causing the small and bright dots with higher fluorescence intensity than the surrounding structures.

The lifetime histogram (figure 4-11(e)) shows a net lifetime shift between normal and cancerous tissue, with an increased average lifetime value for the cancer sample.

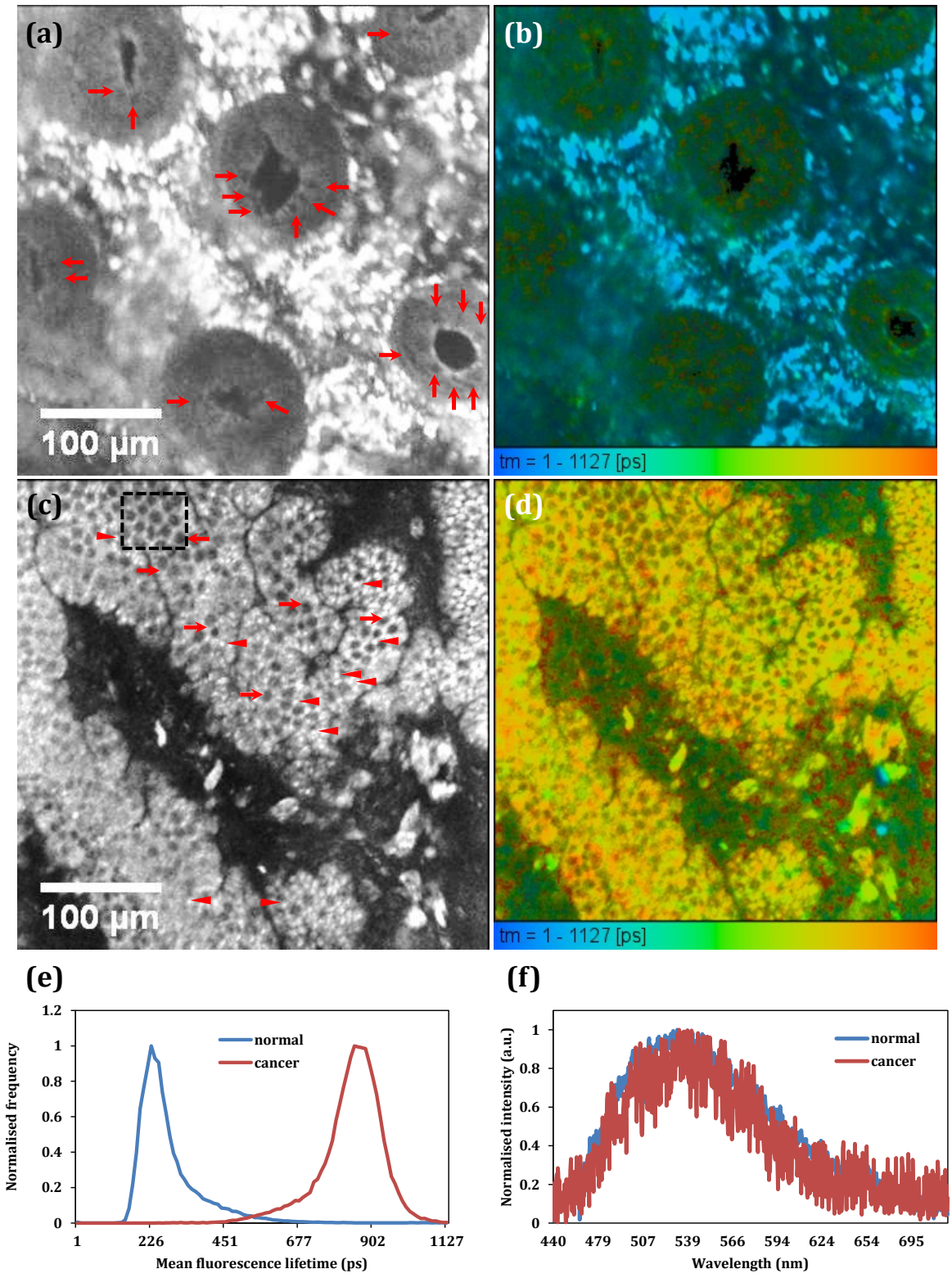


Figure 4-11: Matched intensity and FLIM images of fresh biopsy specimens of normal rectal mucosa (a, b) and rectal cancer (c, d). (e) Mean lifetime distribution histograms calculated from the FLIM data. (f) Intensity spectra collected from the samples with a spectrometer.

In addition to comparing morphological differences, the emission spectra from normal and neoplastic tissue were also analysed. The mean fluorescence intensity from the cancer specimen

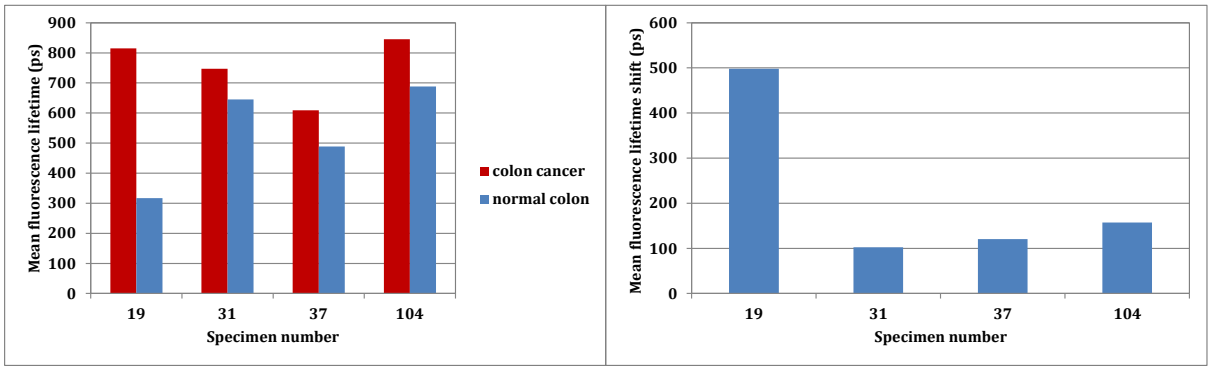
was lower than that of normal rectum (104 ± 43 vs. 114 ± 84 mean detected photons per pixel). It should be noted that the cancer emitted a lower intensity spectrum compared to the normal sample, which is contrast with what seen in polyps (figure 4-7). In the discussion, it is speculated that the reason for this difference may be possibly due to the different amount and distribution of interstitial space and connective tissue between these two different tissue states.

However, interestingly, the shapes of the two spectra were similar (figure 4-11(f)). In addition, the peak and the line shape of the emission spectra, again appeared to be similar to that observed for flavins by us (figure 4-6) and other investigators [213,287,415].

The mean fluorescence emission wavelength was longer for the cancer compared to that of the normal specimen (585 nm vs. 566 nm).

Figure 4-12(a) shows a summary of results for all the colon cancer specimens included in the paired analysis. Figure 4-12(b) shows the shift in the intensity-weighted mean fluorescence lifetime ($\Delta\tau$) for each normal colon-cancer pair. All of these cancers were shown to be invasive adenocarcinomas at the histological assessment. The mean fluorescence lifetimes for cancer were all longer than those observed in the corresponding normal tissue.

No difference in lifetime trend was observed between the metastatic (sample 104) and the primary cancer specimens (the remainder three).



(a) **(b)**

Figure 4-12: (a) Bar graphs showing the mean fluorescence lifetime observed in all colon cancers relative to a sample of healthy tissue from the same region of the colon. (b) Shift in the mean fluorescence lifetime of all colon cancer specimens included in the paired analysis. Lifetime shifts are calculated using a measurement of normal tissue obtained from the same or nearest region of colon.

Figure 4-13 shows the paired ratio (cancer/normal) of the fluorescence intensity for all the cancer specimens relative to a specimen of healthy colon from the same patient.

The ratio of mean fluorescence intensity, averaged across all the pixels of the intensity images to the corresponding value for the cancer specimen, was found to be less than 1 in three out of four

cases, indicating that the fluorescence intensity from the cancer specimen was lower than the paired normal specimen in 3 patients and higher in 1 patient (sample 37).

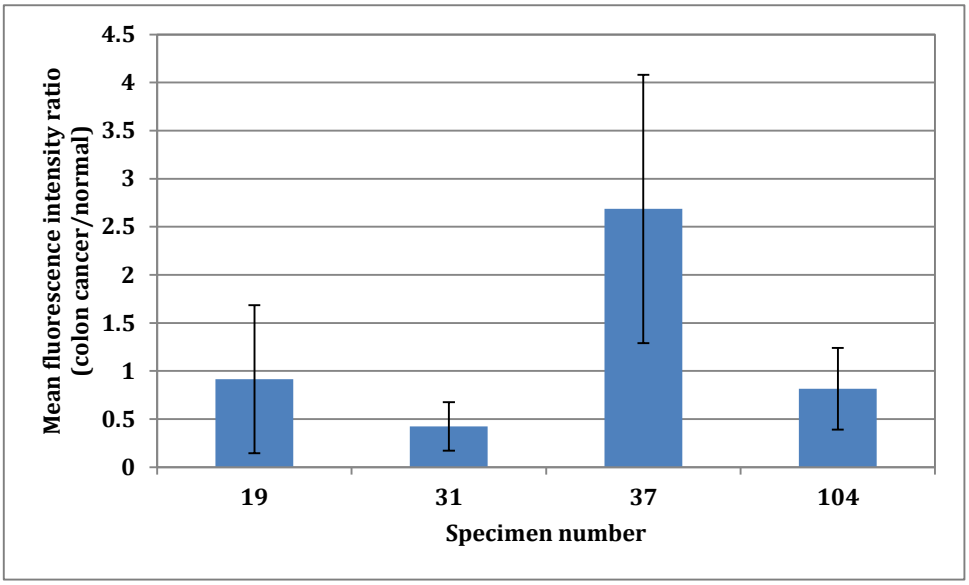


Figure 4-13: Bar graph showing the ratio (cancer/normal) in the mean fluorescence intensity observed in all the cancer specimens relative to a specimen of healthy tissue from the same patient. The mean intensity for all the samples was obtained calculating the mean number of photons detected per pixel, across all the pixels of the intensity image. The error bars represent ± 1 standard deviation and were calculated via error propagation from the fluorescence intensity distribution in the normal and cancerous images.

4.3.3 Inflammatory bowel disease

Clinical conditions characterised by chronic or recurring immune response and inflammation of the gastrointestinal tract are typically referred to as inflammatory bowel diseases (IBD). The two most common IBDs are ulcerative colitis and Crohn's disease. Surveillance for colorectal cancer is necessary for patients with IBD as they have an increased risk of developing dysplasia and cancer. The risk of cancer is influenced by the duration and extent of disease and is also linked to the endoscopic appearance at colonoscopy [35-37].

Of the total of 16 specimens measured (8 inflamed samples and 8 normal) in 8 patients, 2 specimens (1 normal, 1 diseased) from 1 patient were excluded from the analysis as the normal specimen was found to be histologically abnormal (severe chronic ulcerative colitis with mild to moderate activity). The IBD specimens included in the analysis are summarised in table 4-5.

No. of patients	7
No. of IBD specimens	7
• **UC**	6
• **CD**	1
No. of normal specimens	7
Total number of specimens	14

Table 4-5: Summary of IBD and normal specimens included in study. IBD = inflammatory bowel disease; UC = ulcerative colitis; CD = Crohn's disease.

Paired representative images from normal and IBD specimens are illustrated in figure 4-14 and figure 4-15 for ulcerative colitis, and figure 4-16 for Crohn's disease.

Ulcerative colitis

Ulcerative colitis (UC) is an idiopathic IBD that almost always begins in the rectum and extends proximally into the colon in a contiguous manner. Based on the amount of colon involved, three types of disease distribution are recognized; (1) ulcerative proctitis; (2) left-sided colitis; (3) pancolitis.

Dysplasia and malignant transformation represent the most important complication of this disease and the risk begins to rise at 8-10 years after onset. At present, annual endoscopic surveillance is recommended after 8-10 years of illness. If no lesions are observed, four biopsy specimens are taken randomly at every 10 cm between the rectum and the caecum for a total of 40-50 biopsies per colonoscopy. However, even this massive sampling examines less than 1% of the total colonic mucosa surface. Thus, there is a strong interest in developing techniques that may be able to guide targeted biopsies and assist in discriminating between normal and dysplastic areas.

Figure 4-14 and figure 4-15 show the fluorescence intensity and FLIM images of biopsy specimens (normal, diseased) taken from two patients affected by chronic active distal UC.

Regular crypt architecture can be seen in the uninflamed mucosa (figure 4-14(a, b)) showing numerous mucin rich goblet cells assorted around the inner rim of the crypt openings (arrows). In contrast, both intensity and FLIM images of the inflamed tissue (figure 4-14(c, d)) show distanced crypts surrounded by an interstitial matrix fully infiltrated by small circular bright cells (arrowheads) containing dark dots in their centres (nuclei). This morphology is reflected histologically, where a loosening of the interstitial space is observed, and the mucosa is chronically infiltrated by inflammatory cells (neutrophils, lymphocytes and plasma cells).

Erythrocytes extravasated from capillaries of the lamina propria may also be present [411,416]. Goblet cell depletion and small crypt openings are also visible (asterisk), as a consequence of severe crypt destruction. This would be expected to increase the contribution of mucosal collagen fluorescence in the diseased sample.

A decrease in lifetime is observed for the inflamed sample with a bimodal distribution of the average lifetime values compared to the normal counterpart, suggesting that at least two predominant fluorophores are involved in this sample figure 4-14(e).

The mean fluorescence intensity was lower for the inflamed specimen compared to that of normal colon (706 ± 261 vs. 1021 ± 316 mean detected photons per pixel).

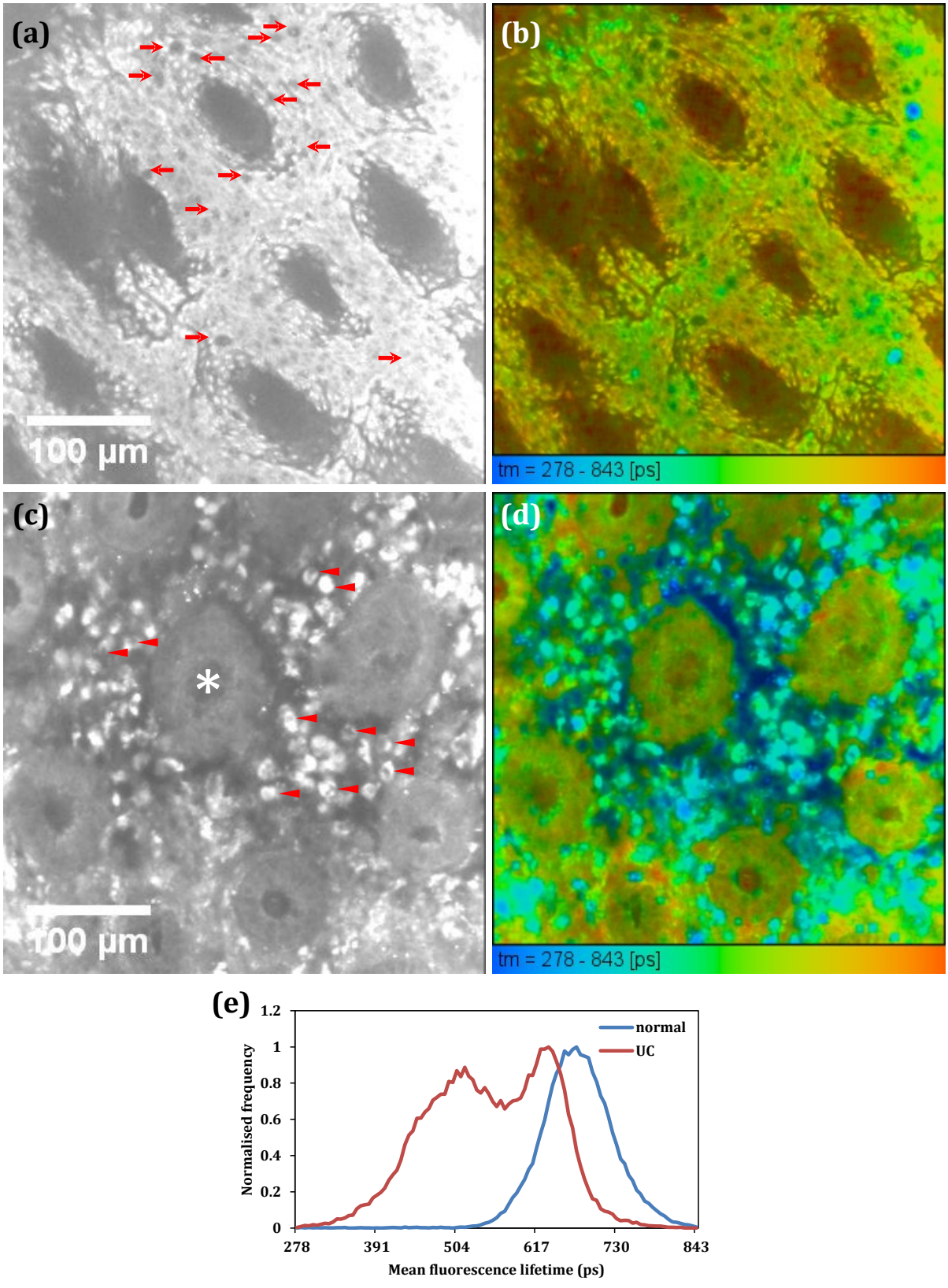


Figure 4-14: **Matched intensity (a, c), and FLIM (b, d) images of fresh colon biopsy samples of normal mucosa (a, b) and ulcerative colitis (c, d). (e) Mean lifetime distribution histograms calculated from the FLIM data.**

In figure 4-15(c, d), a nearly sagittal view of the inflamed sample was obtained, showing almost the full length of a crypt duct replete with extravasated mucous and cellular infiltration, possibly representing a crypt abscess (asterisk). According to the exhibited mean lifetime values in the FLIM images, cells with very short fluorescence lifetime values (blue on false colour scale) can be seen (white arrowheads) and regions of longer fluorescence lifetime (red on false colour scale) can also be seen (white arrows), which may be due to accumulation of mucin.

In comparison with figure 4-14(e), a more clear separation in the mean lifetime histograms is shown in Figure 4-15(e), and the trend towards shorter lifetimes is repeated for the inflamed tissue. The mean fluorescence intensity was again lower for the inflamed specimen compared to that of normal colon (762 ± 190 vs. 778 ± 175 mean detected photons per pixel).

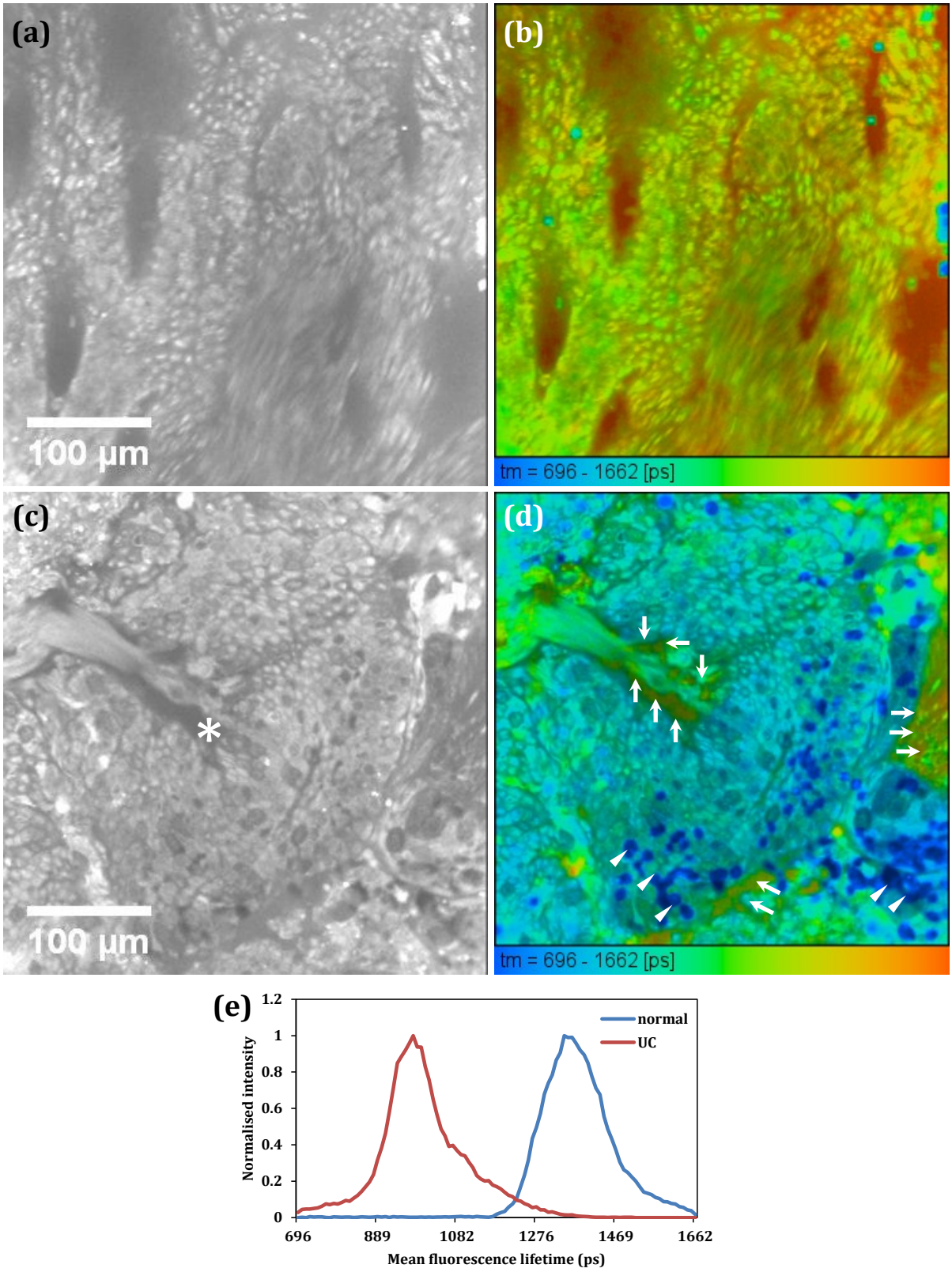


Figure 4-15: **Matched intensity (a, c) and FLIM (b, d) images of fresh colon biopsy samples of normal mucosa (a, b) and ulcerative colitis (c, d). (e) Mean lifetime distribution histograms calculated from the FLIM data.**

Crohn's disease

Crohn's disease (CD) is a chronic idiopathic disorder characterized by a typically transmural inflammation that can affect any part of the GI tract.

Figure 4-16 shows the fluorescence intensity and FLIM images of two biopsy specimens (1 normal, 1 diseased) taken from the same patient affected by CD.

The normal specimen (figure 4-16(a, b)) shows a regular crypt architecture and numerous cellular structures with large dark inclusions, which are therefore identified as goblet cells.

The intensity and FLIM images of the inflamed tissue figure 4-16(c, d) show irregular crypt architecture, with aggregates of small circular bright cells containing dark dots in their centres (nuclei), indicated by red and white dotted circles in figure 4-16(c) and figure 4-16(d), respectively). This morphology is reflected histologically by the presence of nodules consisting of inflammatory cells (neutrophils, lymphocytes and plasma cells) as well as extracellular matrix, and lymphoid aggregates. These nodules are referred to as "non-caseating granulomata" and are characteristic of CD. According to the exhibited mean lifetime values in the FLIM images, these aggregates are composed of a mixture of cells with very short (blue on false colour scale) and relatively longer (green on false colour scale) fluorescence lifetime values.

A decrease in mean fluorescence lifetime is observed for the inflamed sample compared to the normal colon (figure 4-16(e)).

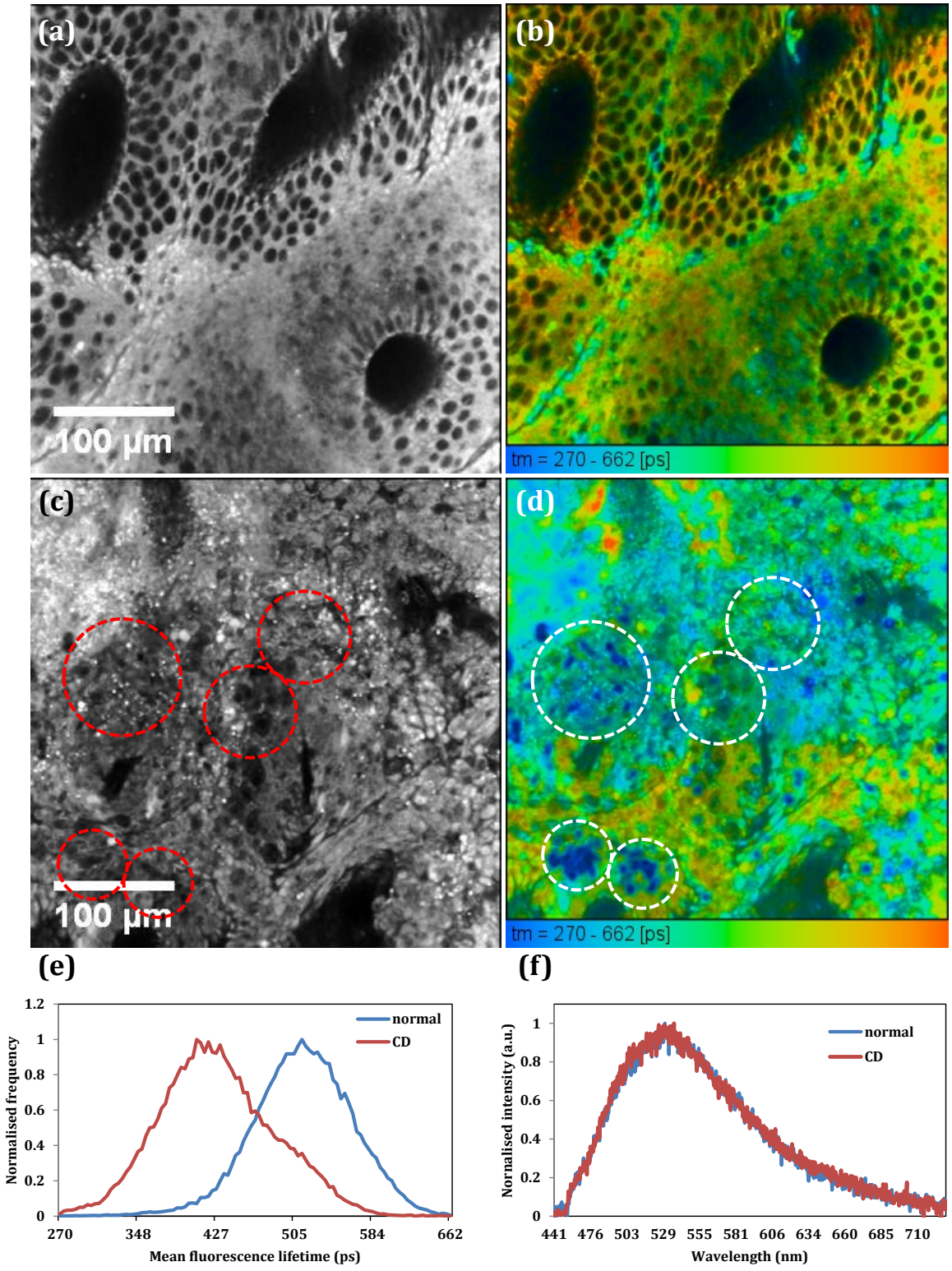


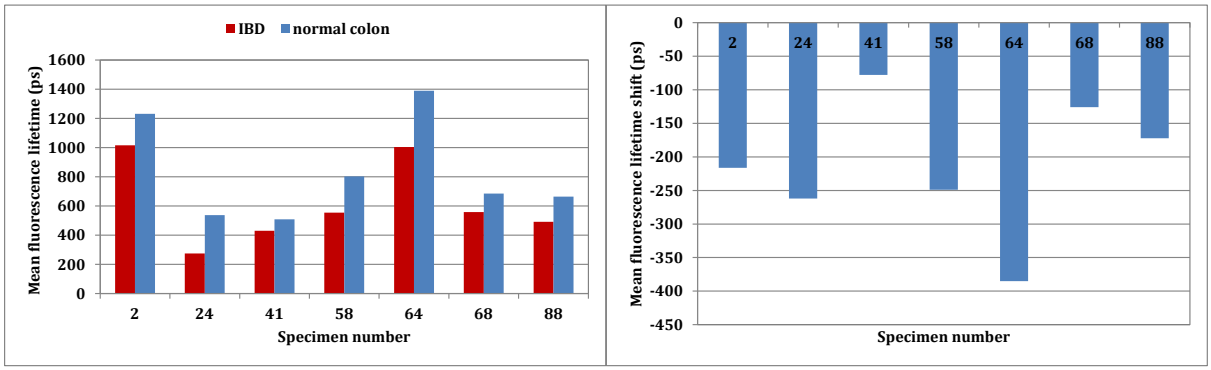
Figure 4-16: Matched intensity (a, c) and FLIM (b, d) images of fresh colon biopsy samples of normal mucosa (a, b) and Crohn disease (c, d). (e) Mean lifetime distribution histograms calculated from the FLIM data. (f) Spatially averaged intensity spectra collected from the samples with a spectrometer.

It is worth noting that although no difference can be seen in the emission spectra from the two samples, the mean fluorescence intensity for the inflamed sample was higher than that of the

normal colon (877 ± 273 vs. 596 ± 257 mean detected photons per pixel), and, once again, the peak and the line shape of the emission spectra appeared to be similar to that observed for flavins.

Figure 4-17(a) shows a summary of results for all the IBD specimens included in the paired analysis. Figure 4-17(b) shows the shift in the intensity-weighted mean fluorescence lifetime ($\Delta\tau$) for each normal colon-IBD pair. Despite the considerable inter-patient variation for both normal and diseased specimens, the mean fluorescence lifetimes for IBD were all found to be shorter than those observed in normal colon.

No difference in lifetime trend was observed between Crohn's disease (sample 41) and ulcerative colitis (all the remainders).



(a) **(b)**

Figure 4-17: Bar graphs showing the mean fluorescence lifetime observed in all IBD specimens relative to a sample of healthy tissue from the same or nearest region of the colon. (b) Shift in the mean fluorescence lifetime of all IBD specimens included in the paired analysis. Lifetime shifts are calculated using a measurement of normal tissue obtained from the same or nearest region of colon.

Figure 4-18 shows the paired ratio (IBD/normal) of the fluorescence intensity for all the IBD specimens relative to a specimen of healthy colon from the same patient.

The ratio of mean fluorescence intensity, averaged across all the pixels of the intensity images to the corresponding value for the inflamed specimen, was found to be less than 1 in four out of seven cases, indicating that the fluorescence intensity from the inflamed specimen was lower than the paired normal specimen in four cases and higher in three cases.

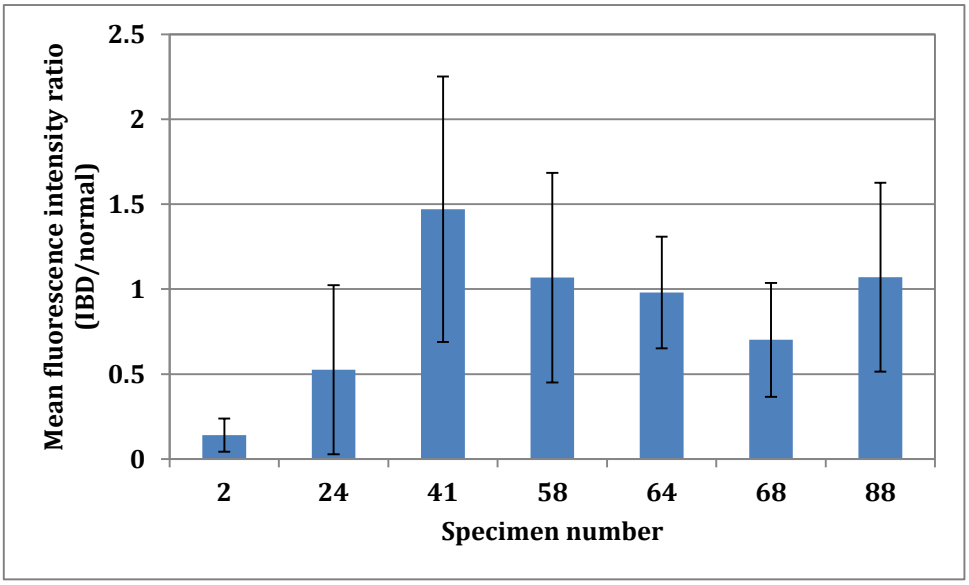


Figure 4-18: Bar graph showing the ratio (IBD/normal) in the mean fluorescence intensity observed in all the IBD specimens relative to a specimen of healthy tissue from the same patient. The mean intensity for all the samples was obtained calculating the mean number of photons detected per pixel, across all the pixels of the intensity image. The error bars represent ± 1 standard deviation and were calculated via error propagation from the fluorescence intensity distribution in the normal and inflamed images.

4.3.4 Oesophageal disease

Barrett's oesophagus

Barrett's oesophagus (BO) is a condition in which squamous mucosa is replaced by columnar epithelium as a result of gastric (and probably duodenal) content reflux. This replacement is referred to as intestinal metaplasia, histologically defined as the presence of goblet cells.

Goblet cells are essential for the diagnosis of BO. Their distinct mucus vacuoles confer to these cells the characteristic appearance of wine goblets. Foveolar mucus cells are insufficient for the diagnosis.

Increased epithelial proliferation, atypical mitoses, hyperchromatic nuclei, irregular distribution of chromatin, and high nucleus-cytoplasm ratio can be observed in both low (LGD) and high grade dysplasia (HGD). Gland architecture is subverted, showing irregular gland shapes, abnormal cellular and nuclear orientation and crowded clusters of cells (e.g. gland-within-gland).

Barrett's oesophagus is associated with an increased risk of oesophageal adenocarcinoma, particularly when dysplasia arises within its epithelium. To date, dysplasia can be detected only histologically. Therefore, when BO is identified, a protocol consisting of 4 quadrant biopsies every 1 to 2 cm with biopsies of mucosal abnormalities (Seattle protocol) should be taken above the level of the lower oesophageal sphincter. Although it has never been validated, this protocol

is currently the standard method for detecting dysplasia in patients with BO. Standard videoendoscopy identifies BO but cannot distinguish intestinal metaplasia from dysplasia. This underscores the need for novel imaging techniques that may help target areas of dysplasia, thus assisting in the early diagnosis of dysplasia and cancer and allow for their timely treatment.

All of the measured specimens (5 diseased and 5 normal) in patients with BO were included in the analysis and are summarised in table 4-6.

No. of patients	5
BO	5
No. of normal specimens	5
Total number of specimens	10

Table 4-6: Summary of Barrett's and normal oesophagus specimens included in study. BO = Barrett's oesophagus.

Paired representative images from normal and Barrett's oesophagus are illustrated in figure 4-19. Figure 4-19 shows the fluorescence intensity and FLIM images of two biopsy specimens (1 normal, 1 diseased) taken from the same patient affected by Barrett's oesophagus complicated by focal LGD. In normal oesophagus, the outlets of the submucosal mucous glands, which drain to the surface via ducts that are frequently squamous-lined, can be recognized (red asterisks). In pathology, these glands provide evidence that the location of the biopsy is the oesophagus, because such ducts are not present in the stomach. Normal squamous oesophageal epithelium (a, b) appears as flattened "scale-like" [417] tiles (red dotted rectangle), whereas a "villous-like" (intestinal) tissue architecture can be seen in the columnar-lined mucosa (c, d) with distorted and elongated appearance of glands and numerous dark goblet cells (red solid rectangle). An increase in the number of dark cells with an irregular border along the epithelium has been reported in Barrett's-associated dysplasia using confocal endomicroscopy. Furthermore, the loss of the regular basement membrane integrity and the disruption of the villous epithelial structure are strongly suggestive of high-grade dysplasia and/or early carcinoma [149]. The H&E-stained histological sections (20x original magnification) of the normal and the BO specimens for this patient are shown in the upper and lower left insets respectively. Although they do not correspond precisely to the tissue slices observed, there is similarity of the confocal images with histology. For example, flat, thin "scale-like" squamous cells and the outlets of the submucosal mucous glands can be seen in the normal specimen (figure 4-19(a) and upper left inset), as opposed to the columnar epithelium with numerous goblet cells lining the ducts of the metaplastic mucosal glands (similar to the intestinal glands) in the BO specimen (figure 4-19(c) and lower left inset).

The mean lifetime histograms (e) show a narrower distribution of lifetimes for the Barrett's epithelium and a tendency to shorter lifetime values compared to the normal mucosa.

The mean fluorescence intensity was lower for the metaplastic epithelium compared to that of normal oesophagus (172 ± 47 vs. 133 ± 55 mean detected photons per pixel).

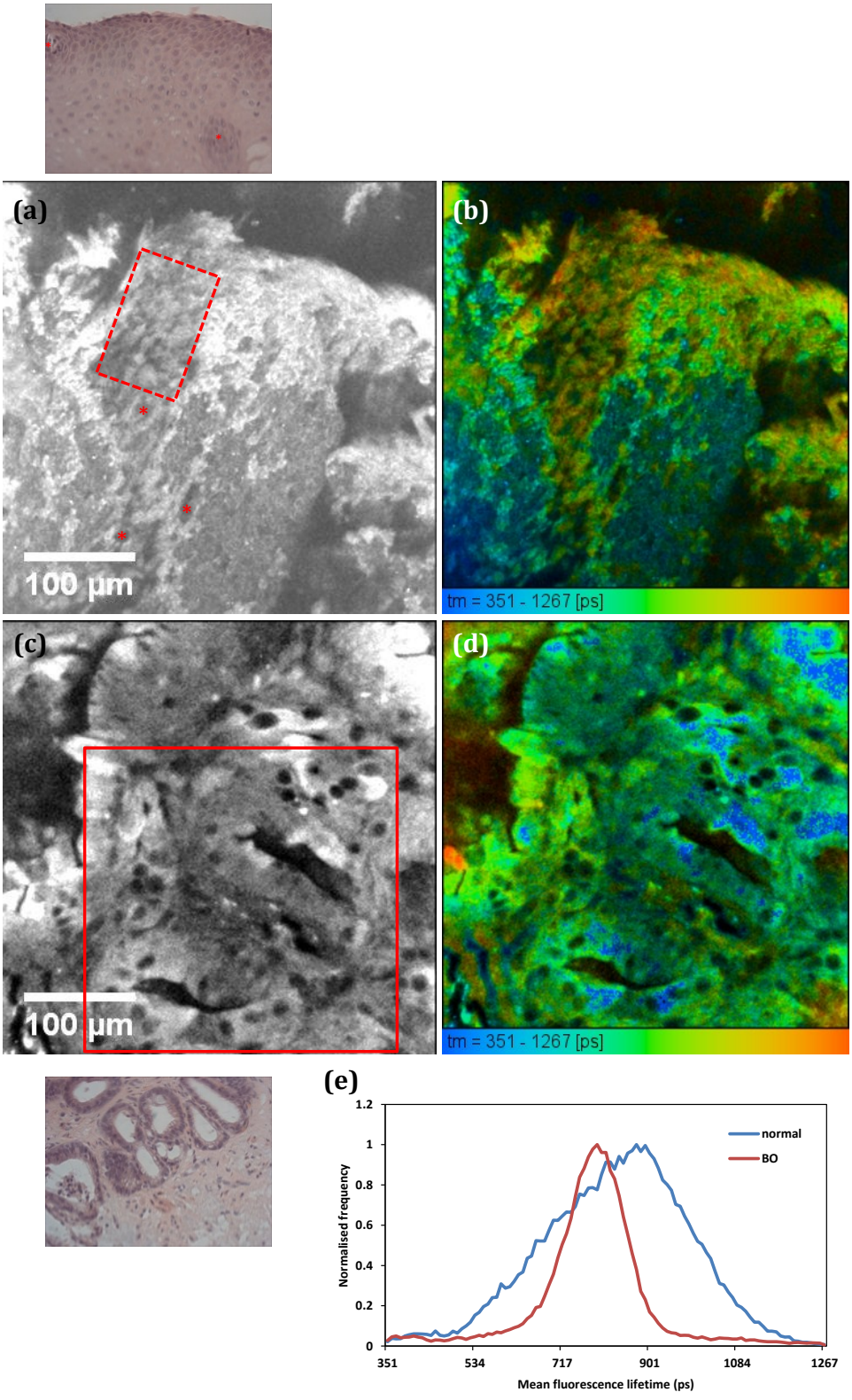
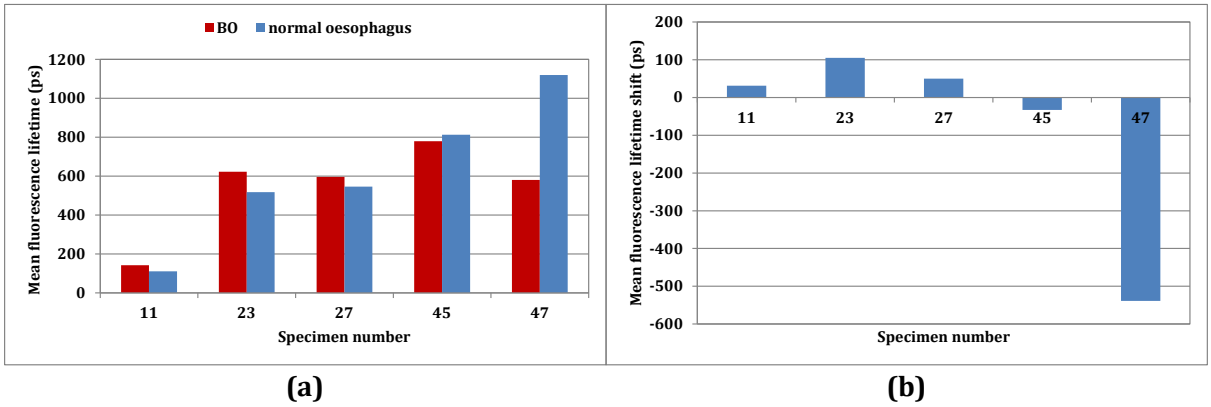


Figure 4-19: **Matched intensity and FLIM images of fresh oesophageal biopsy specimens of normal mucosa (a, b) and Barrett's oesophagus with low grade dysplasia (c, d). (e) Lifetime histograms calculated from the FLIM data. The upper and lower left insets provide magnified views (20x original magnification) of the H&E-stained histological sections of the normal and the BO specimen, respectively. Note that no exact registration exists between histology and FLIM images; the insets serve solely to illustrate the similarity of the confocal images with histology.**

Figure 4-20(a) shows a summary of results for all the BO specimens included in the paired analysis. Figure 4-20(b) shows the shift in the intensity-weighted mean fluorescence lifetime ($\Delta\tau$) for each normal oesophagus-BO pair. The mean fluorescence lifetimes for BO were longer than those observed in normal tissue in three of five specimens.



(a) **(b)**

Figure 4-20: Bar graphs showing the mean fluorescence lifetime observed in all BO specimens relative to a sample of healthy oesophageal tissue. (b) Shift in the mean fluorescence lifetime of all BO specimens included in the paired analysis.

Figure 4-21 shows the paired ratio (BO/normal) of the fluorescence intensity for all the BO specimens relative to a specimen of healthy oesophagus from the same patient. The fluorescence intensity from the BO specimens was higher than that of the correspondent normal specimen in all cases (n = 5).

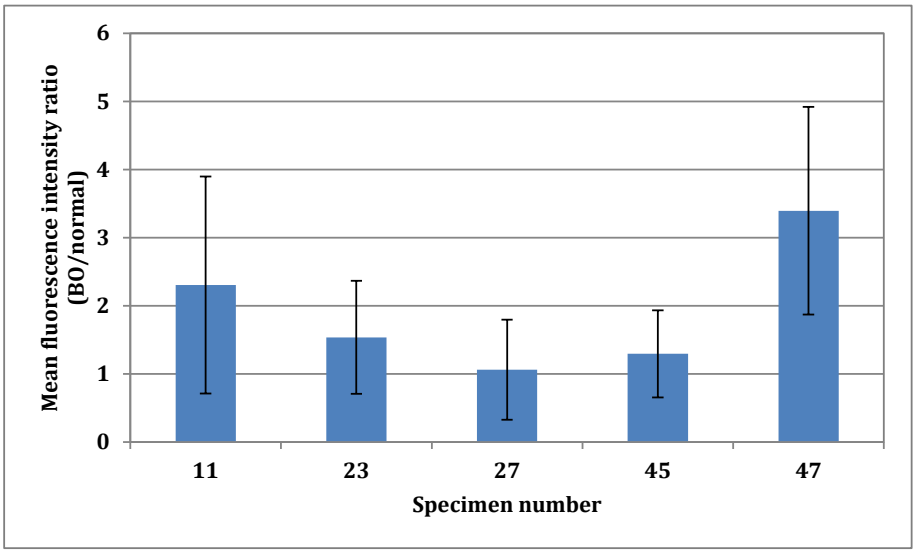


Figure 4-21: Bar graph showing the ratio (BO/normal) in the mean fluorescence intensity observed in all the Barrett's oesophagus specimens relative to a specimen of healthy tissue from the same patient. The mean intensity for all the samples was obtained calculating the mean number of photons detected per pixel, across all the pixels of the intensity image. The error bars represent ± 1 standard deviation and were calculated via error propagation from the fluorescence intensity distribution in the normal and Barrett's oesophagus images.

Reflux oesophagitis

Gastro-oesophageal reflux disease (GORD) is a common disorder of the GI tract, affecting up to 20% of the population in Western countries [418].

Endoscopic changes in reflux disease may present as non-erosive abnormalities such as erythema, friability and granularity of the mucosa, or, most commonly, as erosive oesophagitis, with the presence of erosions or ulcerations as described in section 2.1.2.

Histologically, erosive esophagitis is characterized by epithelial injury and active inflammation. Epithelial injury is represented by oedema, which appears as a widening of the intercellular spaces, loss of cell cohesion, necrosis and sloughing [3]. Regenerative changes may occur in the epithelium adjacent to the eroded area. The presence of neutrophil infiltrate in both the epithelium and lamina propria is the hallmark of active inflammation. Occasionally eosinophils may predominate. The intensity of cellular infiltrate usually correlates with the degree of epithelial injury.

Figure 4-22 shows the fluorescence intensity and FLIM images of two biopsy specimens (1 normal, 1 diseased) taken from the same patient affected by grade D erosive oesophagitis – according to the Los Angeles endoscopic classification of GORD (see section 2.1.2)- which has caused a severe narrowing (stricture) of the lower oesophagus.

As seen above in the normal oesophageal epithelium, a uniform pattern of flat and scale-like polygonal cells can be observed (red dotted rectangle in figure 4-22(a)). In contrast, the mucosal damage in the inflamed sample (figure 4-22 (c, d)) is testified by a dense cellular infiltration into the squamous epithelium (arrowheads in the intensity images, small “blue cells” in the FLIM images as opposed to normal “green-yellow” squamous cells in the upper right region of figure 4-22(d)) and numerous fibrous bands of connective tissue (arrows) which confer to the tissue a finely granular appearance (red solid rectangle in figure 4-22(c)).

The histograms show a net lifetime shift between normal and inflamed tissue. In particular, decreased average lifetime values can be observed for the inflamed sample. It is interesting to note that the distribution of at least two components of the mean fluorescence lifetime vary asymmetrically across the 2 samples, possibly reflecting changes in the proportion of fluorophores involved in the emitted fluorescence. A shift in binding partners of flavins or changes in the ratio of free:protein-bound flavin fluorescence in the “blue cells” (assumed to be inflammatory cells) might be responsible of their shorter lifetime values.

The mean fluorescence emission wavelength was longer for the inflamed specimen compared to that of normal oesophagus (555 nm vs. 401 nm). The mean fluorescence intensity for the

inflamed sample was higher than that of normal oesophagus (450 ± 171 vs. 285 ± 115 mean detected photons per pixel).

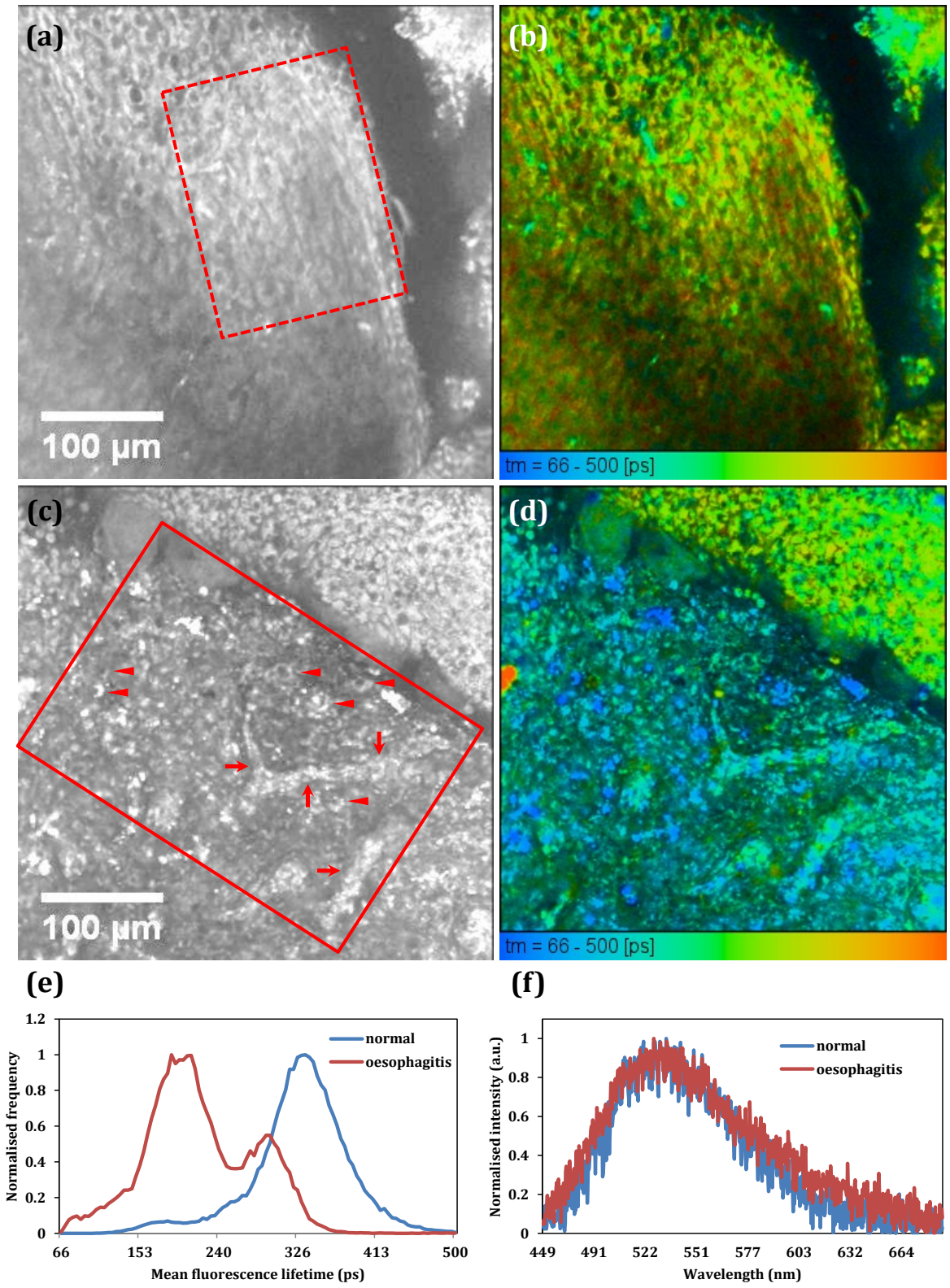


Figure 4-22: Matched intensity and FLIM images of fresh oesophageal biopsy specimens of normal mucosa (a, b) and reflux oesophagitis (c, d). (e) Lifetime histograms calculated from the FLIM data. (f) Intensity spectra collected from the samples with a spectrometer.

Carditis

The term cardia refers to the point where the oesophagus becomes the stomach. It is unclear whether the cardia is present from birth or rather arises as a metaplastic mucosa in the distal oesophagus as a consequence of gastro-oesophageal reflux disease [419]. When sampling at or just below the squamocolumnar junction (SCJ), cardiac mucosa often occurs in biopsy specimens taken.

Figure 4-23 shows the fluorescence intensity and FLIM images of two biopsy specimens (1 normal, 1 diseased) taken from the same patient affected by grade D erosive oesophagitis – according to the Los Angeles endoscopic classification of GORD - which has caused a severe narrowing (stricture) of the lower oesophagus. In this case, the diseased sample was taken at the level of the gastro-oesophageal junction, where the disease appeared to be more severe.

The pattern of flat and scale-like polygonal cells can be observed in figure 4-23(a) and figure 4-23(b). Uniform and homogeneous squamous cells with scattered outlets of submucosal mucous glands (asterisks) can be discerned, confirming the evidence that the location of the biopsy is the oesophagus.

In the sample from cardia, "fundic-like" tissue architecture can be seen (figure 4-23 (c, d)) with tortuous foveolar pits and numerous dark goblet cells (red arrows). The presence of intraepithelial inflammation is identified by small bright round cells (red arrowheads in the intensity images, cells with a short fluorescence lifetime (blue on false colour scale) in the FLIM images) which are haphazardly distributed in the epithelium and may represent inflammatory cells, as seen by other investigators [410,420].

The mean lifetime histograms (figure 4-23(e)) show a narrower distribution of lifetimes for the inflamed epithelium and a tendency to shorter lifetime values compared to the normal mucosa. As an aside, it is interesting to note that longer lifetime values can be observed in proximity and at the mouth of the mucous glands (asterisks) in the normal oesophagus specimen, where mucin-rich cells are usually located.

The mean fluorescence intensity was remarkably higher for the inflamed epithelium compared to that of normal oesophagus (237 ± 150 vs. 64 ± 20 mean detected photons per pixel).

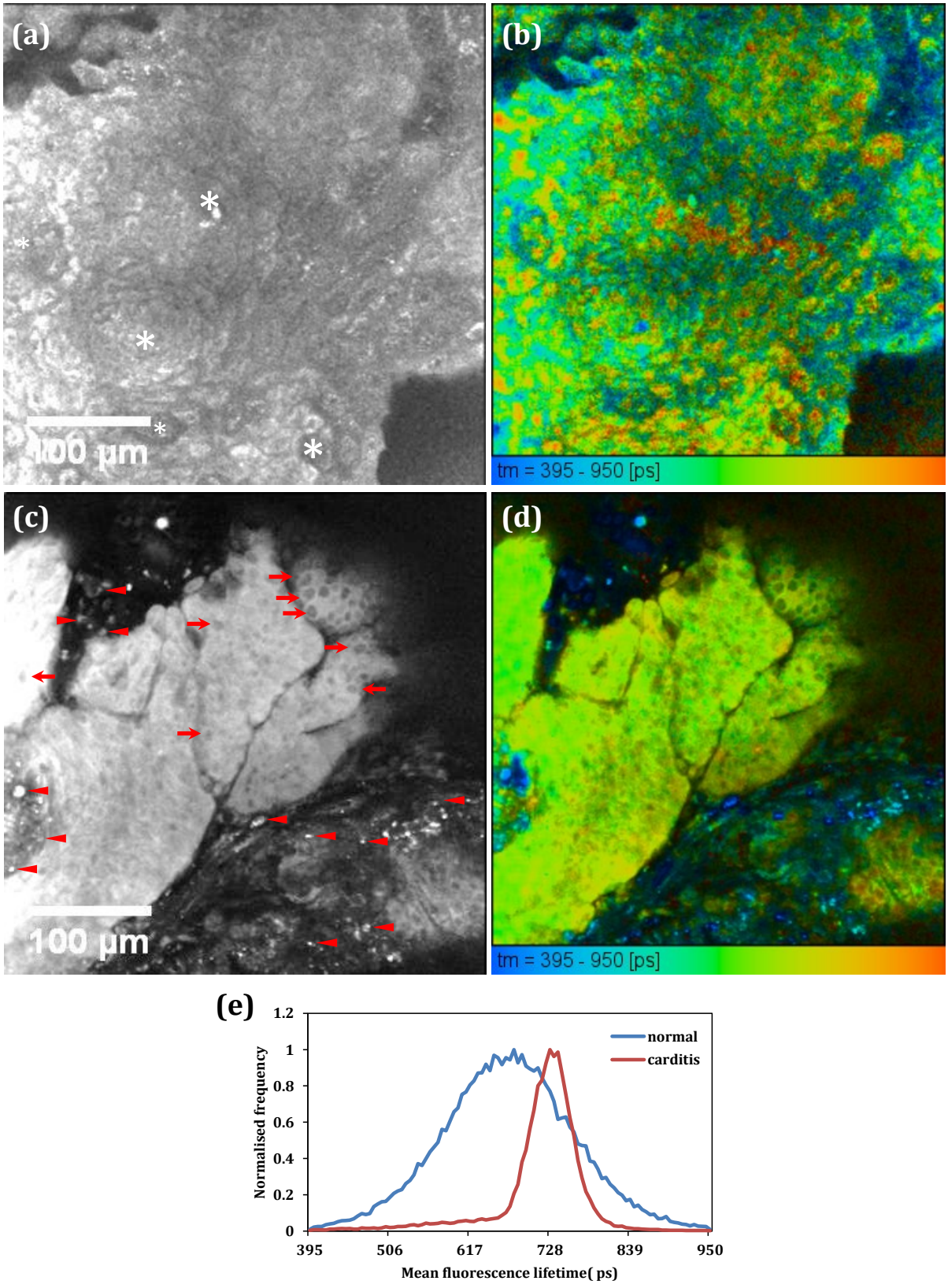


Figure 4-23: **Intensity and FLIM images of fresh oesophageal biopsy specimens of normal oesophageal mucosa (a, b) and inflamed cardiac mucosa (c, d). (e) Lifetime histograms calculated from the FLIM data.**

4.3.5 Summary

Our preliminary data is summarised in table 4-7 and reveals that the mean fluorescence lifetime of dysplastic or neoplastic samples may be either shorter or longer than that of normal tissue depending on the disease considered. The quoted errors are the standard deviation of the values across all specimens for each tissue group.

Diagnostic group	Mean τ disease ± SD (ps)	Mean τ normal ± SD (ps)	Δτ (lesion - normal) ± SD (ps)	P value
Colon polyps (n=11)	655 ± 302	706 ± 336	-191 ± 234	0.024
Colon cancer (n=4)	754 ± 105	534 ± 168	220 ± 187	0.125
IBD (n=7)	619 ± 284	832 ± 345	-213 ± 101	0.015
BO (n=5)	544 ± 238	622 ± 375	-77 ± 262	1

Table 4-7: Mean fluorescence lifetime shift for all samples included in paired analysis. Tau = fluorescence lifetime; SD = standard deviation; IBD = inflammatory bowel disease, BO = Barrett's oesophagus.

There is a statistically significant contrast between the lesion and normal tissue for polyps (p = 0.024) and IBD (p = 0.015), with the general trend being that the lesions present a decrease in fluorescence lifetime. In contrast, the mean fluorescence lifetime of colon cancer was longer than that of normal tissue with a mean delta tau shift of 220 ± 187 ps, but this shift was not found to be statistically significant using the Wilcoxon signed rank test (p = 0.125) possibly due to the small number of specimens collected for this disease type. The lack of statistical significance for the Barrett's oesophagus group is due to the small number of specimens imaged, the relatively large standard deviations on the lifetime shifts, and the small mean shift in fluorescence lifetime observed.

Given the excitation wavelength used, we have attributed FLIM contrast primarily to contributions from intracellular fluorescence from flavins (FAD, FMN) in the epithelium, and to a lesser extent to mucosal collagen, which are also supported by histopathology studies.

Although the limited number of samples, together these results suggest that label-free single photon FLIM imaging is feasible and effective to discern normal from pre-cancer, cancer, and inflammatory disease by providing both biochemical and structural details label-free in fresh, unfixed, unstained specimens. However, clearly more samples are required to confirm and quantify this result.

4.4 Discussion

In this observational study, autofluorescence from a number of GI tissue specimens was excited using a confocal FLIM microscope at 420 nm.

As discussed in section 3.1.5, FLIM is a potential new clinical imaging technique. UV and blue light generate measurable AF but have very limited tissue penetration, measured to be typically <1 mm in skin [421]. Consequently, excitation at these wavelengths would be unable to induce fluorescence from within solid organs by external illumination.

Single photon-excited FLIM is therefore best suited to imaging tissues from endoscopically accessible surfaces such as the luminal lining of the GI tract, the bladder, and the skin, or during surgery where the tissue surface of an organ is exposed.

FLIM images are normally presented by merging the false-colour FLIM maps with the corresponding fluorescence intensity images. These intensity-weighted FLIM maps combine the biochemical information provided with FLIM with the structural information provided by the fluorescence intensity images.

This preliminary work presents the experimental observation that the fluorescence lifetime of diseased tissue autofluorescence induced by 420 nm visible excitation may be either shorter (e.g. polyps, IBD and BO) or longer (colon cancer) than AF from adjacent normal tissue.

In a paired analysis using the Wilcoxon signed rank test, a statistically significant lifetime contrast between normal and lesional tissue was found for polyps and IBD. In contrast, the shift in fluorescence lifetime was found not significant in colon cancer and BO. Further measurements would be needed to establish if the trends observed for these disease types are significant.

4.4.1 Fluorescence lifetime changes with time following endoscopic excision

All the specimens were imaged within 60-120 minutes of biopsy/resection. Although the AF of fresh tissue *ex vivo* shows similar intensity and spectral line shapes to that of *in vivo* tissue [422], some physical and metabolic changes may inevitably occur. For instance, AF from intracellular fluorophores such as NAD(P)H has been reported to decay *ex vivo* over a time scale of 118 minutes due to tissue deoxygenation, while the fluorescence from collagen and flavins remained relatively constant [388]. The haemoglobin content may also change, altering the absorption properties of the tissue.

All the samples were kept in chilled tissue culture medium to minimize this degradation and to preserve tissue viability for as long as possible. However, it is likely that any change to *ex vivo* tissue fluorescence would affect all areas of a sample without distinction and so would be

unlikely to alter the lifetime contrast between normal and neoplastic tissue [273]. Interestingly, in a recent study from our group using multiphoton excitation conducted on four repeatedly imaged samples of freshly excised normal skin at the same field of view over a three hour period, which is the same timescale of hours pertinent to our study, the decrease in mean fluorescence lifetime was shown to be only marginal (less than 5% from the initial value averaged over four spectral channels) [423].

4.4.2 Characteristics of the GI mucosal tissue

Tissue biopsy samples from GI tract are essentially composed of epithelia. This is because it is unlikely (but not impossible) to reach the submucosal layer of the GI wall with biopsy forceps. As discussed in chapter 2, the GI tract from the cardia to the rectum is lined by a simple columnar epithelium. The cells forming a simple columnar epithelium are tall. The nuclei of cells within the epithelium are usually located at the same height within the cells, close to the base. In contrast, the oesophagus is lined by a stratified squamous epithelium consisting of many cell layers. Basal cells often form a well-defined layer at the interface of the epithelium with the underlying connective tissue.

The connective tissue and the epithelium are separated by a basement membrane. As mentioned above, though an endoscopic biopsy is unlikely to reach the submucosal layer, it is sometimes possible to find a component of submucosa in samples resected by cold snaring (polyps) or when biopsy is taken from atrophic areas or ulcerated lesion. The submucosa is the layer of connective tissue that supports the mucosa and contains blood vessels, lymphatic vessels, and nerves.

Another important point to consider is the average thickness of the mucosal layer in the GI tract, which is about 500 μm in normal mucosa and almost the double in cancer [325], and the average thickness of an endoscopic biopsy sample, which may vary from 2 to 10 mm. However, in confocal microscopy, the thickness of the optical section (i.e. the thickness of sample slice from which emitted light is collected by the detector) is determined by the numerical aperture of the objective, wavelength used and size of the confocal pinhole aperture and not by the sample thickness. Therefore, in contrast to wide field microscopy or single point spectroscopy of biopsy samples, here the samples have theoretically the same optical section thickness, regardless of their original thickness. However, in thicker samples such as large polyps or cancers, deeper focal planes may show reduced signal intensity due to absorption and scatter. In our experiments, an imaging depth of 200 μm was reached.

4.4.3 Colonic polyps and cancer

Previous work in our group using wide field FLIM with excitation at 355 nm has shown statistically significant contrast between cancerous and healthy colon tissue in a series of 18 unfixed colonic samples following surgical resection, with 16 colonic adenocarcinomas showing longer lifetime values compared to surrounding normal tissue, and 2 serrated adenoma showing a decrease in fluorescence lifetime [273]. Shorter AF lifetime values have been reported in colonic adenomas using time-resolved spectroscopy at an excitation wavelength of 337 nm [265]. The findings with 420 nm excitation reported in this chapter seem in accordance with these studies, though undoubtedly more samples are required to build a more statistically significant sample size.

In cancer-associated changes there are a number of factors that would be expected to alter the tissue AF and fluorescence lifetime. These include changes in: a) the metabolic state of cells (e.g. intracellular NADH and flavin concentrations, and protein binding state [278,424,425]); b) tissue architecture and morphology (e.g. mucosal expansion displacing submucosal type I collagen away from the tissue surface; epithelial destruction and regeneration; tumour degradation of extracellular matrix or new matrix formation; inflammatory infiltrate) [426]; c) tissue oxygenation and pH.

It has been previously ascertained that dysplasia and cancers favour a metabolic pathway different from normal tissue. One of the biochemical hallmarks of carcinogenesis is the shift from oxidative phosphorylation to glycolysis. This observation is known as the Warburg effect [427]. It is also widely accepted that there is an increase in metabolic activity in cancer cells, which finds its basis in altered tumour vascularisation and imbalance between oxygen demand and supply [428]. Based on these assumptions, changes in the redox ratio NADH/FAD with cancer development have been investigated in *ex vivo* human fresh bladder [272], cervix [429], colon [430] and in the animal model of oral carcinogenesis *in vivo* [292,431].

Using multiphoton microscopy at 800 nm excitation, a quantitative analysis of the redox ratio NADH/FAD was performed by Zhuo *et al.* [430] to quantitatively monitor colonic cancer progression. The redox ratio was shown to increase with progression from dysplasia to cancer.

Skala *et al.* [292] demonstrated a decrease in protein-bound NAD(P)H and flavins lifetimes measured *in vivo* from severe dysplasia in the hamster cheek pouch model of oral carcinogenesis. Our measurements show that dysplastic adenomas and cancer display opposite lifetime trends, which may be due to differences between the concentration and distribution of the most prevalent GI tissue fluorophores involved (e.g. flavins, collagen).

It is widely accepted that morphological changes in dysplasia include mucosal thickening, crypt enlargement, "back to back" aspect of dysplastic cells, and lamina propria displacement. In cancer, a highly disorganised architecture, abundant and unregulated epithelial proliferation, and contraction of epithelial interstitial space are common findings. The progressive enlargement and obliteration of the crypts may be responsible for displacing the underlying lamina propria, thus decreasing the total amount of mucosal collagen fluorescence [353,432]. It is reasonable to assume that the fluorescence emitted from cancer and neoplastic polyps, at the wavelength used in this study, may be due more to contributions of flavins, rather than from collagen and elastin, which is reinforced by the measurements of fluorescence emission spectrum presented.

However, in addition to the enlargement of the crypts, in neoplastic polyps we also observed large bands of interstitial matrix, with only sparse cellular infiltrate, and this, together with the observations made using immunochemistry assays and selective stains, may support the assumption that collagen, although here sub-optimally excited, may be another principal contributor to the changes in AF lifetime observed.

In normal colon specimens excited at 735 nm using MPM, peak fluorescence emission intensity in the 410-490 nm wavelength range has been reported [433]. It was suggested that this fluorescence at relatively longer wavelengths could be attributed to flavins and possibly lipofuscin, which are respectively found in cells within the interstitial space and leukocytes within the lamina propria. Also, lipopigments have emission spectra similar to flavins [213].

4.4.4 Inflammatory bowel disease

The picture is less clear in inflammatory conditions, whose metabolic pathway is still not completely understood due to differences in in disease states (acute, chronic, active, quiescent) and the wide variation of both metabolic and structural factors involved such as cytokines secretion, epithelia destruction and regeneration, inflammatory cells infiltrates, autophagy, etc.

In contrast to normal cervix and cervical intraepithelial neoplasia (CIN) at different grades, reduced epithelial redox ratios have been shown in inflammatory cervical epithelial tissues. However, both inflammatory and dysplastic tissues displayed a large decrease in stromal quantity, indicating a marked loss of collagen [429].

Possible explanations include cytokine-induced inflammatory response and apoptosis, resulting in reduced proliferation rate of epithelial cells. Collagen fibres are replaced by the infiltrating lymphocytes, which promote further degradation of collagen [280,434]

These observations may support the significant difference in the mean fluorescence lifetime values observed between inflammatory and polyp specimens.

4.4.5 Barrett's oesophagus and oesophageal disease

Barrett's oesophagus represents a highly heterogeneous clinical entity, whose histochemical characteristics vary considerably among biopsies and patients. This may also partly explain the mixed results obtained in this particular disease group.

Interestingly, in the cases of reflux oesophagitis and carditis, presumed inflammatory cell infiltrates showed shorter fluorescence lifetime than normal epithelium. It is speculated that a shift in binding partners of flavins or changes in the ratio of free:protein-bound flavin fluorescence might explain this finding.

4.4.6 Known and unknown fluorophores in GI mucosal tissues

For 420 nm excitation we expect the dominant fluorescence signal to be due to intracellular flavins within the mucosa with perhaps some additional signal from mucosal collagen in the lamina propria, which can be excited at this wavelength [309]. Data from a previous study in our laboratory also showed that fluorescence from lyophilised collagen powders from various anatomical sources could be excited at 420 nm (Figure 4-24)[435].

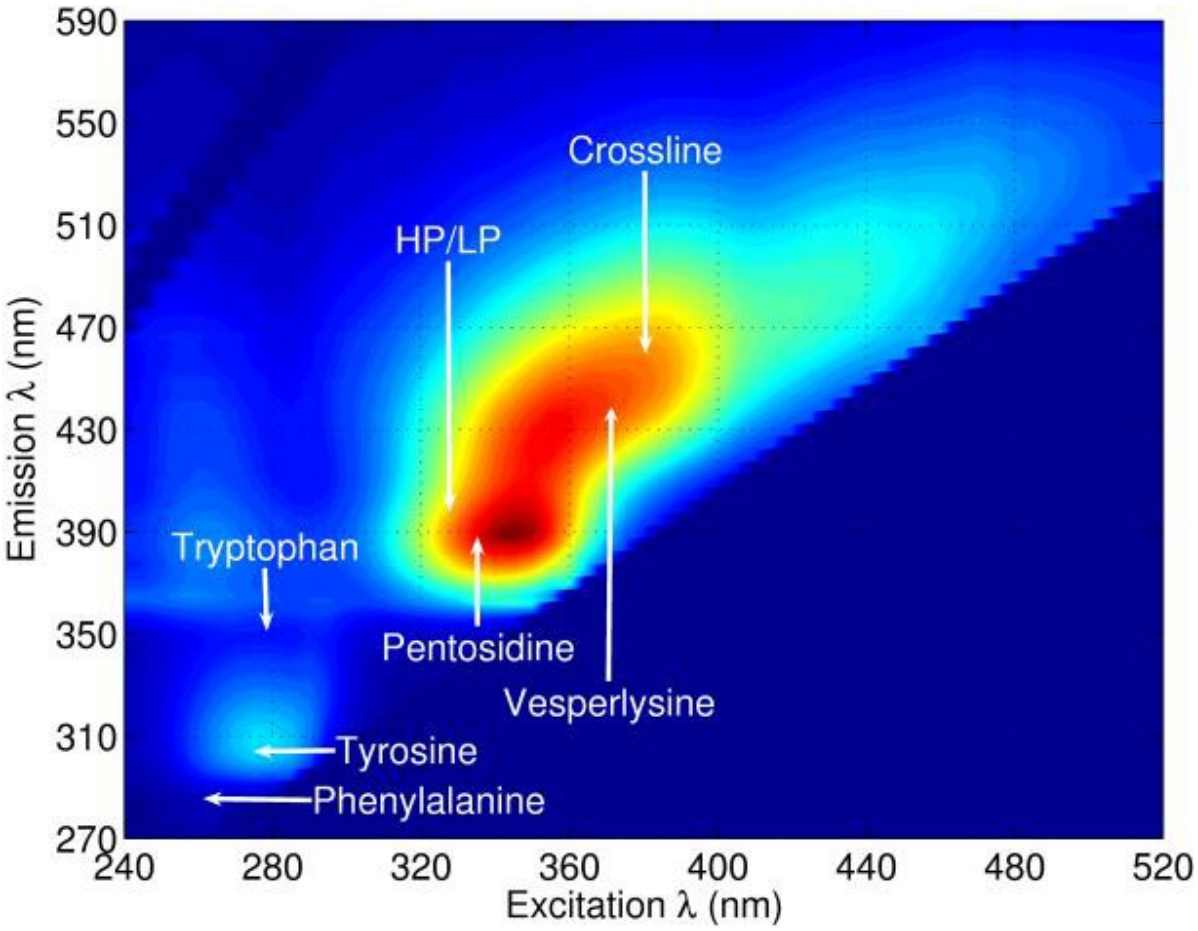


Figure 4-24: Model excitation-emission matrix (EEM) of lyophilised collagen powder from type I collagen from bovine Achilles tendon (C9879, Sigma-Aldrich). λ = wavelength. Reproduced with permission from [426].

Contributions from lipopigments might also be expected [321,322], although they do not generally contribute greatly to tissues fluorescence emission [310], especially in non melanotic mucosa, and are reportedly absent in both neoplastic and hyperplastic colonic polyps [324].

The fluorescence emission spectra peak measured in the paired specimens of colon polyp (figure 4-7(f)) and cancer (figure 4-11(f)) at ~530 nm is broadly consistent with the emission spectra of flavins [436] and collagen [309].

Flavins have a mean fluorescence lifetime of around 4.7 ns for FAD and 5 ns for FMN, and shorter decay components typically in the range ~0.01-1 ns when protein bound [275].

Collagen type IV is primarily found in the linings surrounding the colonic crypts (basal membranes), whereas collagen types I-III are predominant in the stroma of the lamina propria [7,313]. In our samples, large amounts of mucosal collagen were indeed highlighted by the selective stains presented. Collagen fluorescence is particularly complex and a range of values are reported in the literature, e.g. 1.05-5.3 ns [302,437].

The fluorescence lifetime measured in this study in the range 0.1-1.4 ns is also broadly consistent with a combination of the longer decay components found for collagen and those of free and protein-bound flavins.

In our study, it is speculated that there are at least three central players responsible of the changes in AF intensity and lifetime observed: flavins, collagen, and mucins.

Fluorescence emission spectra were measured from 5 pairs of specimens in an attempt to identify by observing the resultant peak and line shape the most prevalent fluorophores involved in producing the fluorescence decay signatures.

Each pair included one normal and one diseased specimen excised from 3 different locations of the GI tract (oesophagus, colon and rectum) and representative of the three main disease categories investigated (inflammation, pre-cancer, cancer). In all cases, especially for the normal samples, the peak and the line shape of the emission spectra, appeared to be similar to that observed for flavins [213,287,415]. The emission spectra were also compared to spectra of synthetic flavins in solution obtained using a spectrofluorometer at 420 nm excitation to reinforce this assumption.

Mucins are a family of glycosylated proteins produced by epithelial tissues and discharged through a duct opening on an internal or external surface. They form secretions which serve to lubricate, enhance or inhibit cell signaling, and offer a chemical barrier to microbes and toxics.

To date, we have found no previous studies that investigated mucin fluorescence and its relative contribution to changes in normal and disease autofluorescence. As mucin often takes an

inhibitory role, from a clinical perspective, it is often perceived as an extraneous and confounding constituent of glandular tissues, something that needs to be discarded to unmask more relevant information beneath.

However, it must be noted that the role of mucin secretion in Barrett's oesophagus is well known in histochemistry, where the relative proportions of different types of mucins (neutral, sialomucins, or sulfomucins) are often invoked to discriminate between intestinal metaplasia from other types of epithelium such as columnar non metaplastic oesophageal epithelium and gastric metaplasia (fundic epithelium)[438,439].

In one study by Adur *et al.* [312], higher fluorescence lifetime values in mucinous ovarian epithelium were found in cells with abundant mucin content. Also in our study, where mucin can be reliably located - essentially in the crypts openings lumina - longer lifetime values can be observed in the corresponding pixels in contrast with mucin-devoid areas such the stroma or the external rim of the crypts.

In our images, mucin depletion has been observed in polyps and cancer compared to their paired normal specimens. Differences in mucins content have been further confirmed using mucin-specific staining such as AB, showing good contrast between the normal and diseased samples.

As mentioned in section 4.2.4, prior to imaging, samples were thoroughly rinsed with fresh buffer solution. Nevertheless, although unlikely, the presence of small sources of contamination (e.g. residues of the tissue culture medium used to transport the specimens between the campuses, blood, excess mucus, and for the colon specimens, any residues of bowel cleansing preparation) cannot be excluded. Thus, when interpreting the findings, this aspect should also be considered but it is unlikely to be the cause of contrast seen between normal and diseased samples as they were all treated in the same way.

4.4.7 Fluorescence intensity

In general, *in vivo* studies of tissue AF describe reduced fluorescence measured at the tissue surface from cancerous and dysplastic areas compared to normal tissue [275,280,381].

In this study, a decrease in mean fluorescence intensity was seen in the cancer and the IBD specimens compared to adjacent samples of healthy mucosa, whereas the contrary was seen for polyps and IBD. However, unlike fluorescence lifetime, fluorescence intensity measurements are affected by sample scattering and absorption, which increase with imaging depth, making quantitative measurements more difficult.

Izuishi *et al.* [381] hypothesized that under blue light excitation the main source of tissue fluorescence is submucosal collagen and that the reason for the decreased fluorescence in colon cancer is a decrease in collagen fluorescence as a consequence of a screening effect of the thickened mucosa overlying the submucosal layer or replacement of the submucosa by cancer cell infiltration. Also, the increased blood volume in neoplastic tissues migth explain a decrease in fluorescence intensity due to haemoglobin absorption.

4.4.8 Future work

The results of this chapter show that confocal FLIM with excitation at 420 nm can be used to characterize the main tissue components and compartments, and help discriminate normal from inflammatory, dysplastic and neoplastic tissue in fresh human GI biopsy specimens, without the addition of exogenous contrast agents.

It is envisaged that in the future, confocal FLIM may have an important role in the study of GI disease since it is able to provide evidence of non-endoscopically evident mucosal damage, which could only be confirmed by histopathology. For instance, in this study, changes in mean fluorescence lifetime were observed in specimens endoscopically classified as "normal", which eventually showed abnormalities on histological examination.

The difference in mean lifetimes as measured by delta tau is encouraging, particularly when applied to colonic polyps. Proven colon cancers display a negative lifetime shift, but clearly many more samples need to be studied to confirm and quantify these initial findings.

Based on this experience, the following improvements for future research work have been proposed:

- Increase the sample size.
- Reduce the excision/imaging interval. This could be achieved by moving the confocal FLIM microscope to the hospital. The images were acquired within 60-120 minutes after removal of samples by forceps biopsy or polypectomy snare. How lifetime changes over this time period is unknown. However, imaging time for normal/diseased pairs in this study was always reasonably well-matched.
- Better registration between confocal and histological images.
- Simultaneous image acquisition and data processing, and simultaneous processing of entire data sets (batch fitting). This would significantly reduce the time required to complete the analysis of a high number of images. In this study, only two images (1 normal, 1 disease) per patient data set were selected. Data processing was performed manually for each individual image selected, a laborious and time-consuming process which is prone to error.

- Sample orientation; there is no ideal method to ensure that the epithelial surfaces are correctly positioned facing the objective lens. Nevertheless, the method developed in this study enabled to clearly distinguish mucosal from submucosal side in most cases.
- Inherent contrast available; use of contrast dyes may help to enhance nuclear contrast (acetic acid to contrast nuclei, glucose to energise cells).

We are encouraged by other reports that have shown some of the features that we have observed [156,323,440]. Similarly, Professor Hillman's group have presented hyperspectral two-photon microscopy (TPM) paired images and emission spectra from normal and transgenic mouse GI tissue [323]. However, their study involved freshly excised small intestine and colon from 15 (10 normal and 5 transgenic APC *Min/*+) mice, and was mainly carried out to determine the TPM excitation spectral properties of the four layers of the normal GI tract wall.

To the best of our knowledge, our study represents the most comprehensive survey of fluorescence lifetime images in normal and diseased human gastrointestinal mucosal tissues and the only study to use confocal FLIM at 420 nm excitation to image autofluorescence from freshly-resected specimens from patients undergoing endoscopic procedures.

Further work is warranted to identify the optimum fluorescence imaging parameters for contrasting a given disease and tissue type, including the optimization of the excitation and emission wavelengths.

4.5 Conclusions

We have presented an observational study of time-resolved confocal FLIM of gastrointestinal samples collected from patients undergoing endoscopy as part of their clinical investigations. Utilizing a FLIM confocal microscope, we have studied the autofluorescence signatures of fresh endoscopically resected GI tissue. We found that FLIM imaging allows the visualization of tissue details in some of the most common GI diseases.

FLIM contrast can be generated within and between biological tissues. Of particular interest, is the preliminary data that suggest FLIM is able to contrast between normal and dysplastic tissue.

In fresh tissue, and by analogy *in vivo*, this contrast may be primarily attributed to the different fluorescence lifetimes of flavins and collagen [435] at the excitation wavelength used. The ability to generate this contrast suggests potential clinical applications for confocal FLIM including the *in vivo* detection and characterisation of dysplasia and early GI cancers, and the discrimination with inflammatory diseases. Currently, the application of the confocal FLIM endomicroscope in *ex vivo* and *in vivo* studies of tissue autofluorescence is still limited by the background fluorescence from the fibre probes. However, further refinement of this endoscope

is ongoing and in the future, the construction of lower background fluorescence fibres prototypes may overcome this barrier.

Future work is more likely to involve the collection of a larger, more significant data set to allow confirmation of the observations made in the results section of this chapter.

Firstly, this will allow us to build a bank of *ex vivo* data to permit detailed investigation of the optical signatures of other GI disease types meaning that the worth of confocal FLIM can be assessed over a wider range of GI conditions, including liver, biliary and pancreatic disorders.

Secondly, an increased database of information would also facilitate the development and implementation of FLIM in endoscopic instruments for clinical use. Once the observed changes have been confirmed to a higher degree of significance and the best opportunities for contrast between healthy and diseased tissue have been assessed, the development of imaging instrumentation could be accelerated.

Chapter 5: Fluorescence Lifetime Imaging (FLIM) of bladder cancer: a pilot study conducted on human bladder specimens collected under Hexvix induced endoscopic fluorescence guidance

The work reported in this chapter used the FLIM confocal microscope described in the previous chapter to analyse the autofluorescence from *ex vivo* "cold-cut" tissue samples of human bladder. The specimens were excised from patients undergoing cystoscopy as part of their clinical investigations.

In this series, autofluorescence imaging, with or without instillation of a photosensitising agent into the bladder prior to cystoscopy, was performed and a consistently longer overall lifetime for biopsies of bladder cancer was observed. Fluorescence emission spectra were also compared with pure solutions of protoporphyrin IX (PpIX) in an attempt to detect the fluorescence signature of this important fluorophore, which accumulates preferentially in malignant tissue.

The aim of the work described in this chapter was to assess whether the fluorescence patterns seen could report on the disease state of the tissue. These observations were directed at understanding the fluorescence contrast available, especially when associated with the artificial enhancement of the fluorescent signal resulting from abnormal accumulation of PpIX.

As for the GI specimens, the FLIM confocal microscope served as a very convenient platform for systematic observations due to its inherent optical sectioning capability, wide wavelength tunability, relative ease of use, and a fast and clinician-friendly interface both for image acquisition and processing.

5.1 Introduction

Bladder cancer (BC) is the fourth commonest cancer affecting men. Cancer research UK has recently reported that 10,090 people were diagnosed with bladder cancer in 2007 in the UK [441]. With over 150,000 people dying worldwide from this illness, BC has the highest lifetime treatment costs per patient of all cancers. The high recurrence rates and continuous invasive surveillance required are the key contributors to the economical and human toll of the disease.

The majority of bladder cancers arises from the transitional layer and are called transitional cell carcinoma (TTC). The most common type of TCC is the papillary form. On cystoscopy, it is often obvious and appears as an anemone-like series of fronds, or digitations, frequently on a stalk,

protruding in the lumen of the bladder. However, the sessile type and the carcinoma *in situ* (CIS) are flat and almost invisible cancers, which are usually found only on biopsy.

As for the GI tract, early detection and subsequent immediate treatment in patients with superficial tumours confers an overall 90% survival rate [441], whereas once the muscularis propria is invaded, there is a 30% mortality rate at 5 years after diagnosis [442].

Current endoscopic techniques rely on the clinician taking biopsies using white light cystoscopy (WLC) from areas of abnormal tissue for histological diagnosis of suspected bladder cancer, enabling further treatment and management. Urinary cytology and conventional white light cystoscopy with bladder mapping have therefore represented the gold standard diagnostic tool for many years but these are not without their limitations. While WLC can easily detect macroscopic lesions, flat and early cancers such as CIS and dysplasia with minimal/absent or nonspecific urothelial abnormalities can escape detection [443]. Significantly, WLC light cystoscopy can miss lesions not visible to the naked eye, and has poor overall sensitivity (56-68%) [444,445]. Furthermore, given that up to 83% of patients with CIS can develop invasive cancer, achieving the optimal inspection of the bladder wall remains a principle obstacle in the early detection and precise staging of bladder cancer [446].

The advent of novel imaging technologies is creating important new opportunities for the progression in tumour identification and characteristics. One such example is fluorescence cystoscopy; often referred to as blue light photodynamic diagnosis (PDD). This offers the opportunity to improve the quality of the endoscopic diagnosis and treatment of bladder cancers by enhancing the visual contrast between benign and malignant tissue by inducing a photodynamic process, resulting in selective emission of fluorescence from cancer cells.

PDD (see section 2.4.3) relies on the administration of a photosensitising agent (typically 5-Aminolevulinic Acid (5-ALA), to induce the accumulation of protoporphyrin IX (PpIX), a fluorescent by-product involved in the haem cycle, which has been shown to build up in rapidly proliferating and therefore neoplastic cells [447].

ALA-induced PpIX fluorescence for detection of bladder cancer was first described by Baumgartner *et al.* in 1993 [448]. ALA was instilled intravescically in 56 patients and after a period of 2-4 hours, a strong red fluorescence was exclusively emitted by the epithelial tumours.

In a cohort of 104 patients with suspected primary or recurrent bladder cancer, Kriegmair *et al.* [119] reported a higher sensitivity for blue light cystoscopy compared to WLC (97% vs. 73%) in detecting dysplasia and early bladder cancers.

Work by Jichlinski *et al.* [449] using topically administered PpIX in 34 patients with known bladder cancer reported a good correlation between the PpIX fluorescence and the

histopathological diagnosis. In addition, PpIX permitted the detection of 47 unsuspected lesions that were overlooked by WLC in 18 patients, 40% of which were early cancers.

A study by Lange *et al.* [450] showed that topical application of an ester form of ALA resulted in a twofold increase of PpIX fluorescence intensity at a considerably lower concentration compared to ALA.

Intravenous injection of photosensitizers (Photofrin) has also shown promise as a way to differentiate malignant lesions from normal bladder mucosa when applied in 21 patients at 337 and 405 nm excitation [451].

A blue light PDD system has been recently introduced by Karl Storz (D-LIGHT C system, Karl Storz GmbH & Co. KG, Germany) for endoscopic tissue characterization during cystoscopy in combination with hexaminolevulinate hydrochloride, an ester of 5-ALA (Hexvix, PhotoCure, Norway) administered via intravescical instillation. Following administration of the fluorescence marker, in the fluorescence mode (blue light), malignant tissue can be differentiated from benign tissue as tumorous areas fluoresce in red, while normal tissue exhibits a blue colour. The false colours are generated by the image display software, with blue representing low and red representing a high fluorescence intensity.

PDD of bladder cancer has recently been shown in large case series to improve detection of small papillary tumours, CIS and satellite lesions from previously resected tumours [452]. Evidence that PDD outperforms the gold standard white light in diagnosis of bladder cancer has been provided [119,449,453]. However, PDD appears to be not enough sensitive at differentiating between inflamed and cancerous tissue, offering low specificity (41.4-98.5%) and giving a high false positive rate, limiting its clinical uptake [454]. Thus, the development of PDD aims at increasing the specificity by discriminating neoplasms from inflammatory lesions.

Hence, the integration of PDD with an emerging technology that has the potential to provide more specific contrast on the basis of the tissue fluorophore composition would be highly desirable. As described in section 3.1.5, fluorescent lifetime imaging microscopy (FLIM) is a novel technique that measures the characteristic decay of molecules (fluorophores) rather than solely the fluorescent intensity [273].

5.1.1 FLIM of PDD agents in bladder cancer

There are relatively few reports in the literature on FLIM of bladder cancer [65,272,273,455].

Mizeret *et al.* [65,456] presented the development of instrumentation for time-resolved fluorescence imaging in 1997. Results obtained on a single freshly resected human bladder were contextually presented to illustrate the potential of the technique. At 417 nm excitation, an area

corresponding to erythematous urothelium exhibited a shorter mean fluorescence lifetime than the surrounding normal mucosa (1.65 ± 0.4 ns vs. 2.6 ± 0.2 ns).

Cicchi *et al.* [272,455] used a combination of 4 different systems - two photon intrinsic fluorescence (TPE), second harmonic generation microscopy (SHG), fluorescence lifetime imaging microscopy (FLIM), and multispectral two photon emission detection (MTPE) - to investigate different states of *ex vivo* fresh biopsies of bladder. They focused on normal mucosa and carcinoma in situ (CIS), reporting significant morphological and spectroscopic differences, and both in spectral emission and fluorescence lifetime distribution. In particular, using two-photon excitation at 740 nm and 890 nm, and emission filters centered at 460 nm and 510 nm to selectively detect NADH and FAD fluorescence respectively, they found differences in the fluorescence lifetime components ratio of NADH and FAD with a higher concentration of protein-bound NADH and of free FAD in CIS compared to normal bladder.

Previous work in our group using wide-field time-gated FLIM at 355 nm excitation showed a decreased fluorescence lifetime in bladder exhibiting squamous cell carcinoma relative to surrounding healthy transitional mucosa (one surgical specimen) [273].

In terms of time-resolved measurements of ALA induced PpIX fluorescence, pioneering work has been done by Konig *et al.* [305]. Decay times of 230 ps (weak component) and 17 ns (main component) were obtained in mice with subcutaneous grafts of human bladder cancer 3 hours after intravenous administration of 5-ALA. Control measurements of PpIX in dimethylsulfoxide confirmed the experimental findings showing decay times of approximately 17 ns for the main component, whereas the weak component exhibited a decay time of around 3 ns. The authors did not explain the difference between the two weak components.

In a study by Glanzmann *et al.* [255], the *in vivo* fluorescence lifetime of PpIX excited at 418 nm in three patients with bladder cancer was found to be 1590 ± 120 ps. The photosensitizing agent Hexyl-ALA was instilled into the patient's bladder during 4 hours prior to the measurements. This value was close to the value found *in vitro* for PpIX in organic solution (1700 ± 600 ps) and higher than that found for PpIX in ethanol (1250 ± 500 ps). They also reported a longer AF mean lifetime at 337 nm excitation in bladder cancer (invasive papillary carcinoma) compared to surrounding normal tissue (4250 ± 55 ps vs. 5410 ± 150 ps), in a patient undergoing cystoscopy.

5.1.2 FLIM of PDD in other tissues

Cubeddu *et al.* [457] reported a long lifetime for PpIX of 1500-1800 ps using FLIM with a gated (two gates) intensified camera at 405 nm excitation in five patients with basal cell carcinomas or squamous cell carcinomas of the skin (total of 6 lesions). Delta-aminolevulinic acid was

topically administered to the patients 1 hour before the measurement, and all tumours were localised on the basis of the longer decay time detected in neoplastic tissues due to the stronger emission of PpIX. Furthermore, two fluorescence methods, fluorescence lifetime imaging at 405 nm and multicolour imaging at 390 nm, were used by Andersson-Engels *et al.* [458] to identify and separate basal cell carcinomas from normal surrounding skin from two patients, 2 hours after topical application of 20% ALA ointment. High ratios of mean lifetime and amplitude between tumour and surrounding healthy tissue were observed in all of the 5 lesions, as a result of the longer lifetime decay of the exogenous neoplastic fluorescence compared to the natural endogenous fluorescence of normal skin.

Kantelhardt *et al.* [459] used FLIM *in vivo* at 750 nm excitation in mice with intracranial grafts of human glioma cell lines in mouse after intraperitoneal administration of 5-ALA. They found significantly longer mean fluorescence lifetimes of 5-ALA induced PpIX fluorescence in the tumour areas compared to contralateral normal brain (3240 ps vs. 1810 ps, respectively) [460].

In vivo time resolved spectral measurements at excitation-emission range specific for PpIX detection (410 nm-633 nm), were applied by Chang *et al.* [461] to discriminate normal oral mucosa from premalignant oral lesions such as leukoplakia and erythroleukoplakia and squamous cell carcinoma. Significantly longer lifetime values were reported in oral premalignant and malignant lesions relative to normal oral mucosa (10000 ps vs. 3500 ps). It was assumed that the wide lifetime shift was caused by abnormal accumulation of PpIX in cancerous tissue. Similarly, Chen *et al*. [268] using a 2-component decay model, found that the average lifetime for dysplastic samples was longer than that for normal mucosa, and the longer lifetime (component 2) was recognized to be from PpIX.

5.1.3 Summary of previous work and aims

It is therefore proposed in this study that there are differences in the fluorescence lifetime signatures between various bladder tissue states. Showing that FLIM can differentiate between normal, inflamed and cancerous *ex vivo* human bladder tissue samples and validating the molecules contributing to differences in the fluorescence lifetime would aid in developing a novel endoscopic system to give a real-time optical tissue diagnosis during cystoscopy.

The hypothesis of the experiments described in this chapter was that FLIM is able to detect the lifetime signature of PpIX, which is used in PDD of bladder cancer after the application of hexaminolevulinate (Hexvix).

The aim was to assess whether confocal FLIM at 405 nm excitation is able to contrast normal from neoplastic bladder in virtue of the differences in both natural and PpIX induced

fluorescence, which are expected to lengthen the measured fluorescence lifetime in cancer compared to normal tissue.

5.1.4 Normal bladder histology

The wall of the bladder consists of three layers (mucosa, muscularis propria, and adventitia). The mucosa is composed of urothelium and lamina propria and has either no or often only a discontinuous muscularis mucosae. Therefore, the lamina propria and the submucosa tend to merge and a well delineated submucosa is not identifiable. The urothelium (inner layer) is lined by the so called transitional cells (i.e. between nonkeratinizing squamous and pseudostratified columnar epithelium), which represent the most common source of bladder cancer.

The urothelium is composed of three layers: superficial, intermediate, and basal.

- The superficial layer is a single layer of "umbrella cells", which are large and elliptical with abundant eosinophilic cytoplasm and often binucleated. One umbrella cell covers several underlying cells.
- The intermediate layer contains small cuboidal cells with well-defined borders and cytoplasm rich in glycogen.
- In the basal layer, cells are more cylindrical and lie on the basal membrane.

The lamina propria is located between the basal membrane and the muscularis propria, and contains dense connective tissue, blood vessels lymphatics, and adipose tissue.

The muscularis propria consists of a trabecolature of circular and longitudinal muscle bundles.

The adventitia (outer layer) separates the bladder from other organs.

A transverse section through the urinary bladder wall is shown in figure 5-1. When the bladder empties, the mucosa folds in ridges called *rugae* (dotted circle). Vice versa, the *rugae* are effaced when the bladder fills. The transitional epithelium allows the bladder to expand as it fills [6].

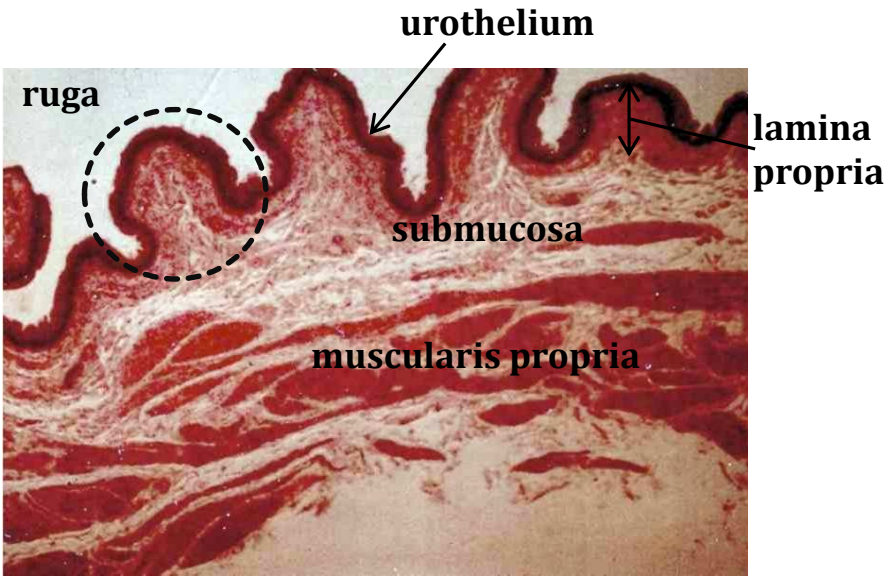


Figure 5-1: **Light micrograph of the wall of the urinary bladder in transverse section. The mucosa appears corrugated in folds called *rugae* (dotted circle). Adapted and reproduced with permission from [462].**

Recently, Sonn *et al.* [463] reported the first *in vivo* microscopic evaluation of human bladder urothelium using a confocal laser endomicroscope (Cellvizio, Mauna Kea Technologies, France). A comparison of H&E and confocal endomicroscopy (pCLE) images of normal bladder mucosa is illustrated in figure 5-2.

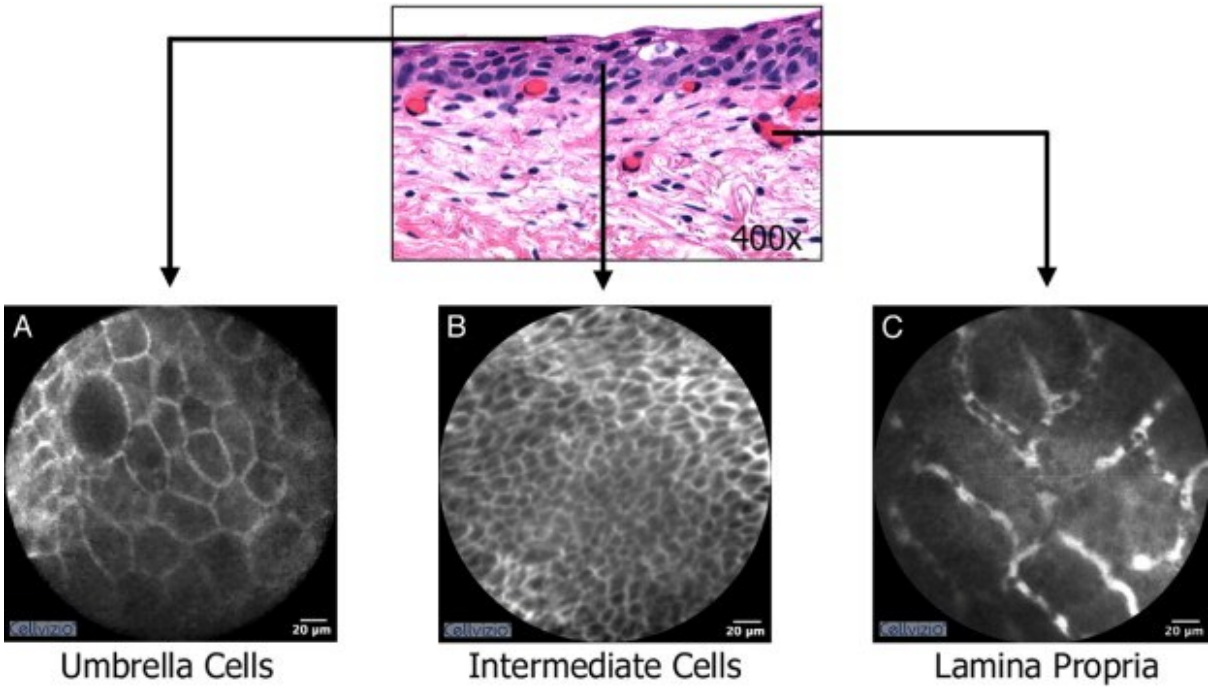


Figure 5-2: **Comparison of H&E and pCLE images of normal bladder mucosa with fluorescein staining. (A) Large, polygonal superficial cells consistent with umbrella cells. (B) Smaller, deeper urothelial cells consistent with intermediate cells. (C) Lamina propria containing blood vessels filled with erythrocytes. Reproduced with permission from [463].**

5.1.5 Bladder cancer pathology

The transitional cells represent the most common source of bladder cancer. Other bladder cancers, such as sarcomas, adenocarcinomas and squamous and small cell carcinomas are relatively rare.

The histological patterns of bladder cancer vary from papillary, to nodular, or completely flat (CIS). Endoscopically, papillary cancers usually appear as red raised excrescences with variable size from 1 to 5 cm. Early or flat types appear as areas of reddening, granularity, and thickened lining. Low grade papillary cancers show an overall orderly architecture and only cytological features (e.g. atypical and hyperchromatic nuclei, mitotic figures, variation in nuclear size and shape, loss of polarity) can help to make a precise diagnosis. High grade forms are characterised by increased thickness of the urothelium, lack of cohesiveness (i.e. presence of loosely jointed, dyscohesive cells), increased cells shedding, infiltration of the deeper layers, and "pagetoid" spread of malignant cells.

Comparison of H&E and confocal endomicroscopy (pCLE) images of bladder cancer mucosa is given in figure 5-3. In low grade papillary tumours (figure 5-3(a, b)), densely arranged small and uniformly shaped cells (homogeneous and monomorphic) were observed. High grade carcinoma (figure 5-3(c, d)) showed a more pleomorphic population of cells with irregular shape and presence of fibrovascular stalks (due to neoangiogenesis) [464].

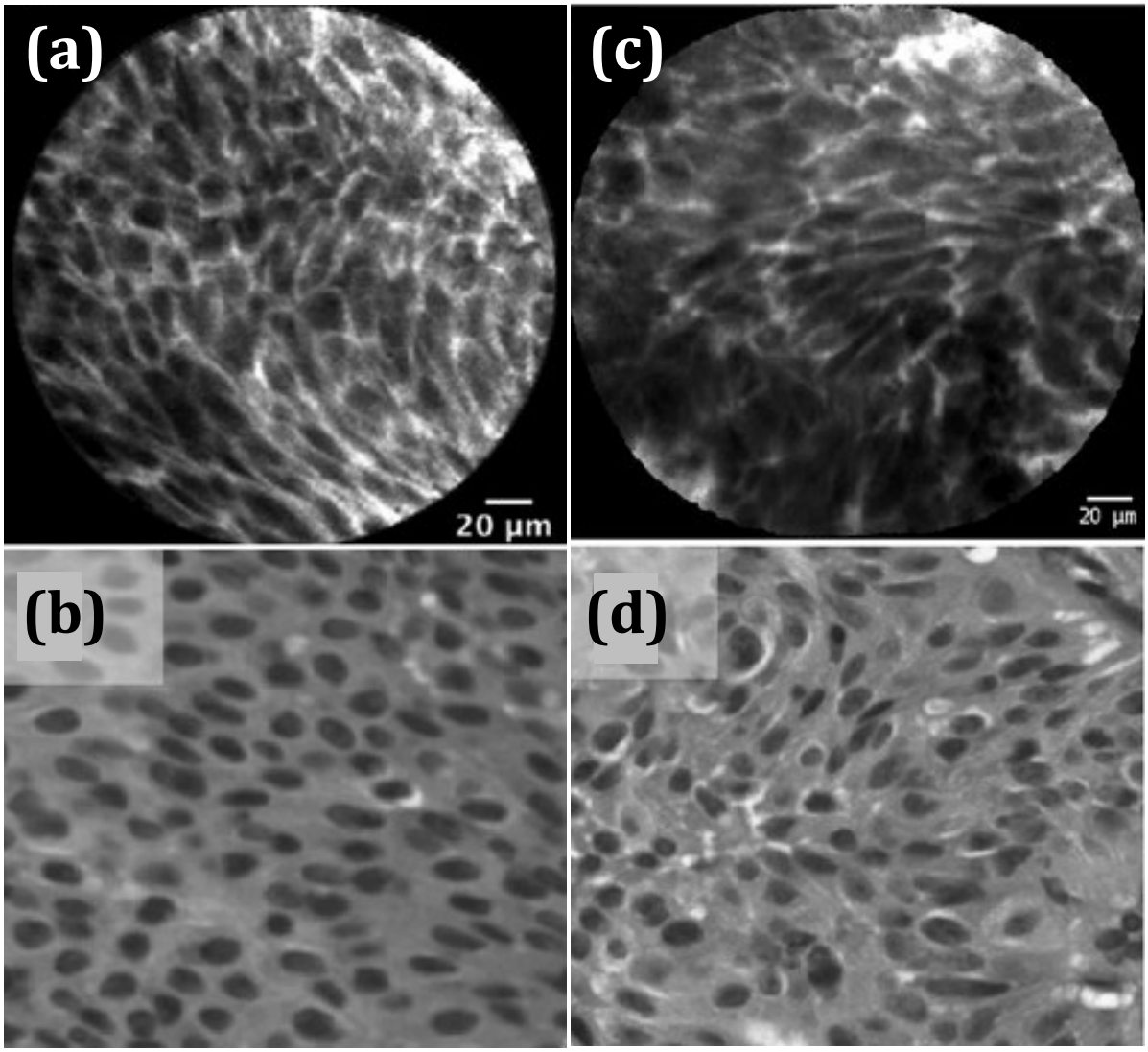


Figure 5-3: Comparison of *in vivo* confocal endomicroscopy images with fluorescein staining of low (a) and high grade urothelial carcinoma compared with corresponding H&E sections (c) and (d). (a, b) Crowding of uniform-appearing cells in low grade cancer cells. (c, d) Pleomorphic and distorted sheet of cells in high grade carcinoma. Adapted and reproduced with permission from [464].

5.2 Materials and methods

5.2.1 Overview

Between August 2010 and February 2012, a total of 23 non diagnostic (not submitted for histopathological examination) bladder samples were obtained as "tru-cut" biopsies from 13 patients undergoing rigid cystoscopy at St Mary's Hospital for suspected cancer.

Adjacent tissue was biopsied from normal and lesional areas, and submitted for histopathological evaluation during a process called bladder mapping, where multiple biopsies are taken from several different locations in the bladder to better determine the extent of cancer or dysplasia.

The true histological diagnoses of the tru-cut specimens studied were later confirmed on the basis of the diagnostic samples collected during the bladder mapping.

All samples were imaged using a confocal FLIM microscope (Leica SP5 confocal microscope, Leica Microsystems) - see section 4.2.3 - with 405 nm excitation provided by a frequency-doubled Ti:Sapphire laser oscillator (BB Mai Tai, Newport Spectra-Physics). Fluorescence was detected over the range 432-750 nm using time-correlated single photon counting (TCSPC).

A total of 120 confocal images were acquired (mean 5 images per sample; minimum = 1, maximum = 27), 36 of which were selected and manually processed using the Becker & Hickl SPC-Image 3.1 software (see section 4.2.5).

Data processing and image selection was performed as described in section 4.2.1. Each diseased sample was compared to a normal sample taken from an endoscopically normal area near the lesion, fitting the fluorescence decay to a double-exponential decay model and analysing the resulting mean fluorescence lifetime. Only paired samples were included in the analysis.

5.2.2 Patient enrolment

Patients were consented for the use of excess tissue in medical research. All cold-cut bladder tissue biopsies in these experiments were obtained in accordance with Outer West London Research Ethics Committee approval number 08/H0719/37. The use of human tissue in this study complied with the requirements of the Human Tissue Act (2004).

Patients agreed to the collection of an additional normal biopsy and the use of tissue samples not needed for histopathology for research.

Inclusion Criteria

Patients were recruited if clinically diagnosed with bladder cancer and if they required biopsy or cystoscopic resection.

Exclusion Criteria

The following exclusion criteria were used:

- Unable to give informed consent
- Under 18 years old
- Prisoner
- Having a blood borne infection e.g. Hepatitis, HIV.

Pseudo-anonymisation

All recorded data was tagged using a linked anonymised identifier for each patient. Data analysis and subsequent correlation with histology was also anonymous.

The clinical care team (DC, AK & EM) held the link but did not disclose this to the research group and maintained patient confidentiality as part of their normal medical duty at all times.

5.2.3 Fluorescence lifetime imaging instrumentation

The FLIM confocal microscope has been described in section 4.2.3. All samples were excited at 405 nm because porphyrins have their Soret absorption maximum at this wavelength. Their fluorescence emission spectra peak between 624-633 nm, depending on the porphyrin. When excited at this wavelength, protoporphyrin IX was found to have a fluorescence peak at 633 nm [304].

When relatively larger bladder cancer specimens were obtained (dates 15/12/2010, 24/05/11), fluorescence lifetimes were further measured either using time-gated wide field imaging or confocal endomicroscopy to contribute towards the development of a wide field FLIM flexible ureteroscope prototype (Karl Storz GmbH, Germany) and a FLIM confocal endomicroscope respectively, for future *in vivo* clinical application – see section 3.2.

Lifetime calibration

As for the GI specimens, the instrumental response functions were obtained by imaging a drop of Erythrosin B solution (10-40 μM), which has a single exponential decay with a lifetime of 89 ps [406].

5.2.4 Sample preparation and protocol

In patients undergoing cystoscopy that were suitable candidates for *in vivo* Hexvix instillation and surveillance using blue light cystoscopy, Hexvix (50 ml at concentration of 8 mmol/l) was instilled into bladder tissue *in vivo* for an hour, before being washed out prior to blue light cystoscopy. This "incubation" period is known to induce the accumulation of PpIX in rapidly proliferating cells. PpIX is a fluorescent by-product involved in the haem cycle and therefore requires respiration in order to accumulate *in vivo* before the fluorescent properties of the

tissue are measured. Samples were extracted with the guidance of the Storz D-light system, and then brought to the Photonics Group laboratory for spectral and fluorescence lifetime analysis.

A summary of the clinical and histological diagnoses of all the *ex vivo* samples investigated is given in Table 5-1.

Tissue type		
Cystoscopic diagnosis	**Histological diagnosis**	**Number of samples**
Bladder neoplasia	10 TCC 1 papilloma	11
Normal bladder tissue	12 normal bladder	12
Total number of normal tissue specimens	12	
Total number of diseased tissue specimens	11	
Total number of specimens instilled with Hexvix	10	
Total number of specimens not instilled	13	
Total number of specimens	23	

Table 5-1: Summary showing the clinical diagnoses of all the *ex vivo* non diagnostic samples investigated with the confocal FLIM microscope. Note that the histological diagnoses correspond to the diagnostic samples collected during the bladder mapping.

Each sample was excised by transurethral endoscopic resection. Following excision, the specimens instilled *in vivo* were kept in physiological Hartmann's solution warmed to 37 °C and transported immediately after resection to the Photonics Group FLIM laboratory.

Sample preparation and imaging was then performed as described in the section 4.2. Particular care was taken to image the mucosal side of the biopsies as we expected the majority of relevant fluorescence (especially PpIX) to originate from there.

Fluorescence emission spectra for bladder tissue samples were also measured (QE65000, Ocean Optics Inc., B.V., The Netherlands) to validate the molecules involved in producing the fluorescence decay signatures, and compared to spectra obtained from pure solutions of flavins and PpIX.

5.2.5 Criteria for interpretation of confocal images

The criteria applied to interpret endoscopic microscope images were based on histological characteristics of tissue. These include well-established features and structures seen on microscopy of standard histological sections [8,9,408,465-467] and recently published criteria for confocal laser endomicroscopy of the urinary tract [463,464,468,469].

5.3 Results

All analysis was performed based on the histological correlation achieved for all samples with the adjacent diagnostic specimens collected during the bladder mapping. Samples were excluded if histological analysis of their diagnostic pair revealed normal tissue in clinically abnormal samples or histological abnormalities in clinically normal specimens.

Before presenting the images and the results for the bladder specimens instilled with Hexvix included in the analysis, it is considered necessary to illustrate the fluorescence intensity and FLIM images of two biopsy specimens (1 normal, 1 diseased) taken from a patient affected by bladder cancer, who did not receive Hexvix instillation. In this way, the autofluorescence contrast arising from the two tissue states (in this pair of specimens) is presented, along with a description of the morphological differences observed.

In figure 5-4(a, b), a layer of cells (red arrows) can be seen. The cellular fluorescence intensity is higher in some regions (red dotted circles), which may align with the *rugae*. Most cells have a well-defined nucleus, as seen from the absence of cellular autofluorescence in the centre of the cell, which is consistent with flavin (or possibly NAD(P)H) fluorescence. Some cells appear much smaller (red arrowheads), which may be deeper intermediate or basal cells (see figure 5-2), with the majority of larger cells likely corresponding to umbrella cells (also see figure 5-2). This seems consistent with the known size difference between umbrella and the deeper intermediate or basal cells on histology, and with the observations made by several investigators [463,464,468]. The ridges and slopes within the tissue, coupled with the increased brightness of the (assumed) umbrella cells, may also be responsible for the presence of areas of different brightness in the images.

In contrast, in figure 5-4(c, d), an almost flat and uniform villous pattern (red solid square) of smaller and densely packed urothelial cells is seen in the cancerous sample. This is also in accordance with both histological [8,9,408,465-467] and confocal endomicroscopy features [463,464,468,469].

In the cancer specimen, the mean fluorescence intensity was higher than in the normal bladder (54 ± 19 vs. 46 ± 20 mean detected photons per pixel).

The lifetime histograms (figure 5-4(e)) show a slightly broader distribution of lifetimes for the normal tissue, but otherwise the histograms are similar.

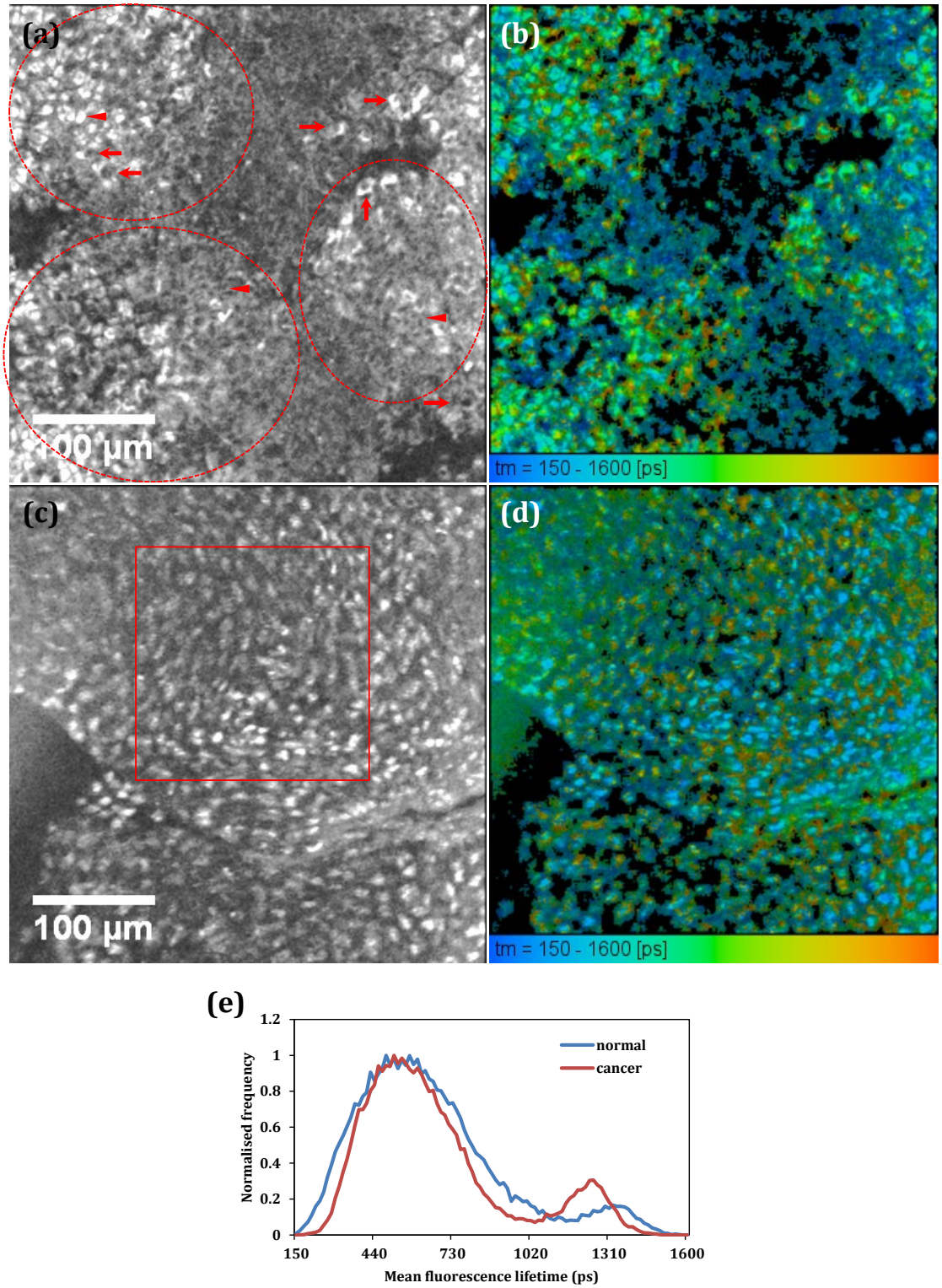


Figure 5-4: **Matched intensity (a, c) and FLIM images (b, d) of tissue autofluorescence in freshly resected normal bladder (a, b) and bladder cancer (c, d) obtained from the same patient undergoing cystoscopy at St Mary's Hospital, London. The normal specimen (a, b) shows large umbrella cells (red arrows) organized in *rugae* (red dotted circles), and a smaller subtype of cells which may correspond to intermediate or basal cells (red arrowheads). The cancerous specimen (c, d) shows a villous pattern with small and uniform cells and no umbrella cells can be seen. (e) Mean lifetime distribution histogram calculated from the FLIM data.**

Of the total of 23 specimens imaged (11 cancers and 12 normal) from 13 patients, 13 specimens were excluded from the paired analysis because it was not possible to obtain a normal or a cancerous specimen (7), because Hexvix was not administered (2), and because a good image of the mucosal side could not be obtained despite repeated attempts (4). Therefore, 10 specimens (5 cancers, 5 normal) from 5 patients, who received intravescical instillation of Hexvix prior to cystoscopy, are included in the paired analysis presented in this section.

Figure 5-5 shows two paired representative images from normal and diseased tissues instilled intravescically prior to cystoscopy, resection and imaging. Figure 5-5(e) shows the histograms of the intensity-weighted mean fluorescence lifetimes (τ mean) for a normal-cancer pair. Figure 5-5(f) shows the fluorescence emission spectra collected over the entire fields of view.

In figure 5-5(c), a compact layer of small densely packed monomorphic cells can be seen, which is different from the architecture of normal urothelium shown in Figure 5-5(a) and previously described for Figure 5-4(a). The cancer sample exhibited a broader and longer distribution of fluorescence lifetime values compared to the normal sample (Figure 5-5(e)).

Again, compared to the bladder cancer specimen, in normal bladder there appear to be considerably more cell size heterogeneity, with a prominent population of cells exhibiting shorter fluorescence lifetime values (blue on false colour scale). This seems consistent with the known size difference between umbrella and the deeper intermediate or basal cells on histology for the normal bladder.

The rather homogeneous appearance of small and uniform cells seen in the bladder cancer specimen is also consistent with histology. The change in fluorescence lifetime between the two populations of cells in normal and neoplastic tissue could be attributed to the different ratio of NAD(P)H/flavins, and to their different distribution of free/protein bound states as it is known that neoplastic metabolism is associated with changes in the relative concentrations of NADH and FAD [278,470]. In the cancer cells, an increase in protein bound NAD(P)H and free flavins might be responsible of their longer lifetime distribution

It is interesting to note that the cancer specimen emitted a higher mean fluorescence intensity than the normal bladder (160 ± 38 vs. 125 ± 41 mean detected photons per pixel) with a peak fluorescence emission wavelength of approximately 500 nm that is consistent with the emission maxima of flavins and NAD(P)H (Figure 5-5(f)) [213,287,415]. Normally, as seen with *in vivo* blue light cystoscopy, higher fluorescence intensity in the cancer specimen would be expected because of the preferential accumulation of PpIX in neoplastic tissue. In addition to the emission peak at 500 nm, the characteristic double-peaked emission spectrum of PpIX at 630 and 700 nm was also seen in both specimens (Figure 5-6(a, b)).

PpIX was also shown in separate solution phase experiments (Figure 5-6(c)) to have a peak emission spectrum at ~630 nm when measuring purified PpIX in solution with a spectrofluorometer [414]. A 25 μM solution of synthetic PpIX (Protoporphyrin IX, Sigma-Aldrich, USA) in dimethylsulfoxide (DMSO, Molecular probes, Life Technologies, USA) was made up immediately prior to the measurement. The spectra were acquired at room temperature (21 °C) from 580 nm to 750 nm using 405 nm excitation.

The longer fluorescence lifetime in the cancerous specimen is consistent with a greater concentration of PpIX in this specimen compared to normal tissue and with the longer fluorescence lifetime of PpIX compared to tissue autofluorescence, c.f. figure 5-4.

Emission spectra showed a peak at ~500 nm and at ~630 nm, both consistent with the fluorescence peak of flavins and PpIX respectively.

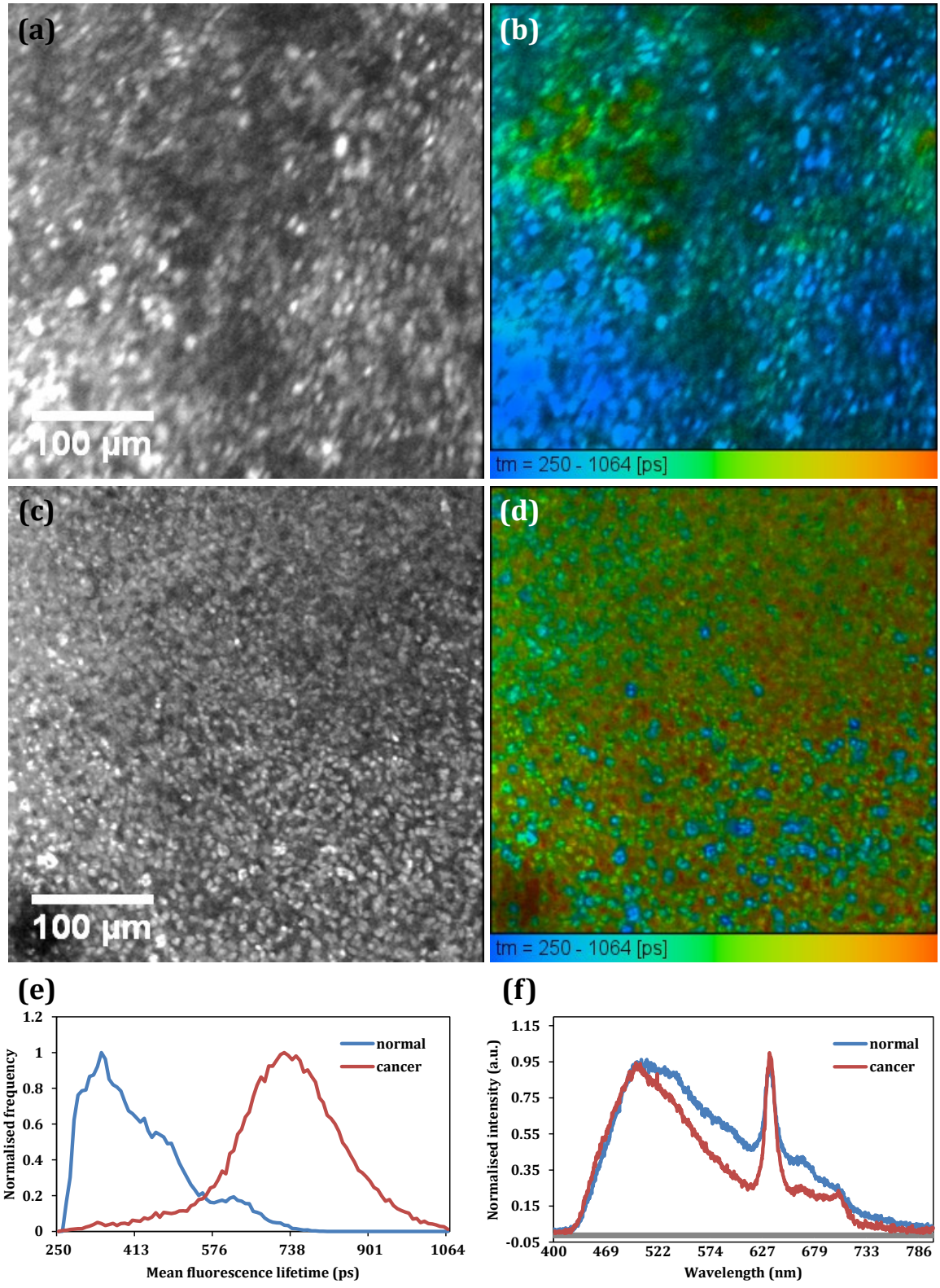


Figure 5-5: **Matched intensity (a, c) and FLIM images (b, d) of a freshly resected bladder cancer (c, d) and normal bladder tissue (a, b) obtained from an adjacent region in the same patient. (e) Mean lifetime distribution histogram calculated from the FLIM data. (f) Intensity spectra collected from the samples with a spectrometer.**

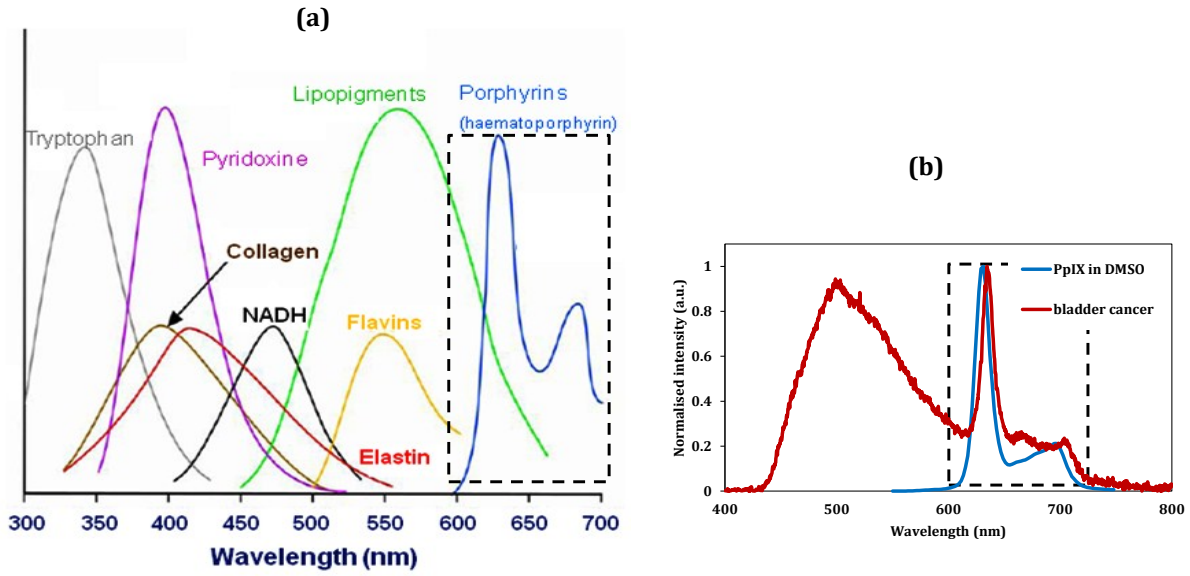


Figure 5-6: (a) Emission spectra of main endogenous tissue fluorophores (Adapted from [213]). (b) Graph showing the overlap (black dashed rectangle) of the intensity spectra from a fresh biopsy specimen of bladder cancer (shown in figure 5-5) collected with a fibre-coupled spectrometer, and the emission spectra of PpIX in DMSO (25 μM) obtained using a spectrofluorometer [414] at room temperature (21 °C), λex = 405 nm, λem = 580-750 nm.

Figure 5-7 shows the fluorescence intensity and FLIM images of two biopsy specimens (1 normal, 1 diseased) taken from the same patient affected by a bladder papilloma. Papilloma is a rare form of bladder tumour and is usually found in younger patients. It appears as a delicate anemone-like exophytic structure with a stalk and multiple finger-like digitations on the top. The typical papillary fronds [442], or cloves, lined by normal appearing urothelium (red dotted ovals) can be seen almost in cross section in the papilloma specimen (figure 5-7(c, d)), in contrast with the structure of the normal specimen (figure 5-7(a, b)). As for the other tumours in this study, the papilloma showed a longer mean fluorescence lifetime compared to normal bladder (figure 5-7(e)); however its mean fluorescence lifetime decay was by far the longest amongst all diseased specimens.

Substantially similar emission spectra (figure 5-7(f)) and mean fluorescence intensities were displayed by both papilloma and normal bladder (14 ± 3 vs. 13 ± 3 mean detected photons per pixel). It is worth noting, however, that the peak and the line shape of the emission spectra appeared once again to be similar to those observed for flavins (at 520 nm) and porphyrins (double peak at 630 and 700 nm).

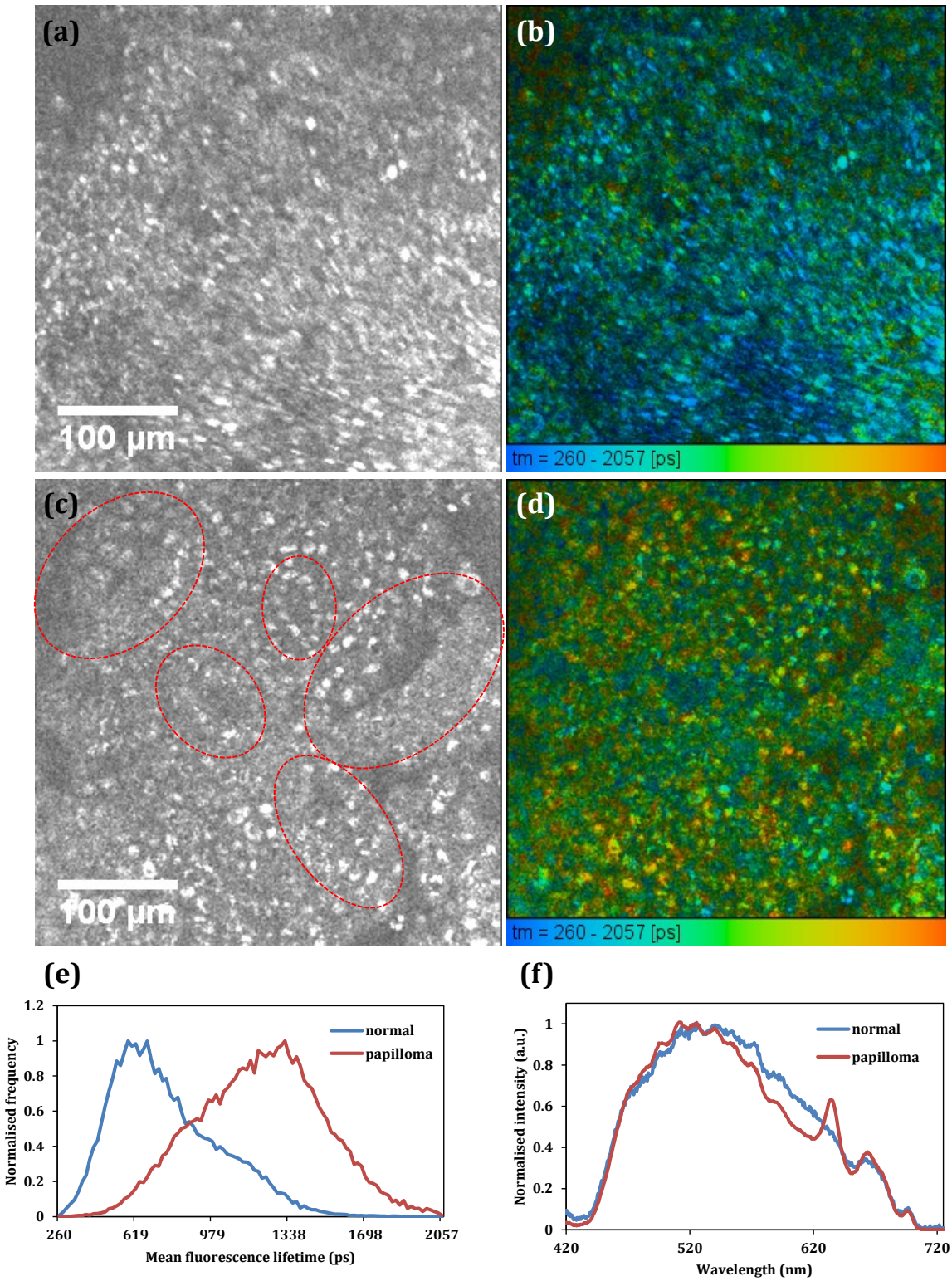


Figure 5-7: **Matched intensity (a, c) and FLIM images (b, d) of a freshly resected bladder papilloma (c, d) and normal bladder tissue (a, b) obtained from an adjacent region in the same patient. (e) Mean lifetime distribution histogram calculated from the FLIM data. (f) Intensity spectra collected from the samples with a spectrometer.**

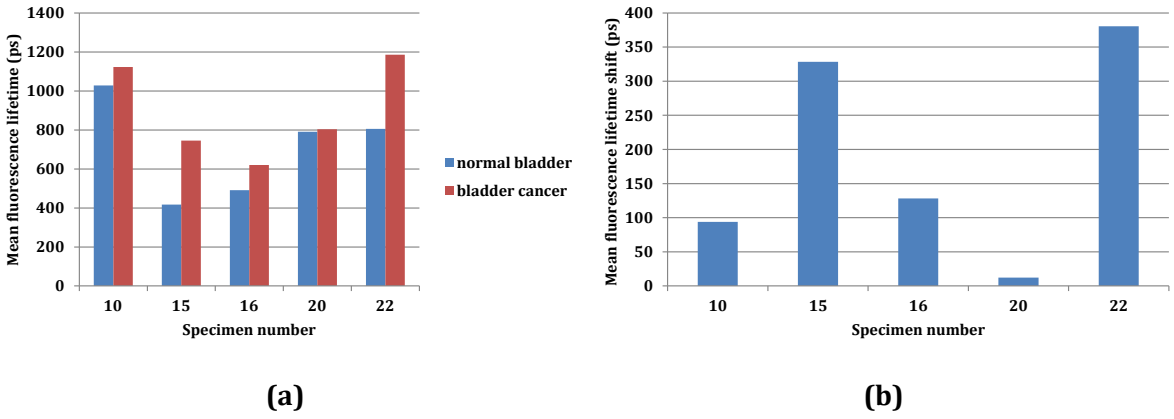
5.3.1 Summary

The data for all samples included in the paired analysis is summarised in Table 5-2.

Mean τ disease ± SD (ps)	Mean τ normal ± SD (ps)	Δτ (disease - normal) ± SD (ps)	*P* value
895 ± 246	707 ± 250	189 ± 158	0.0625

Table 5-2: Mean fluorescence lifetime shift for all samples included in paired analysis (*n* = 5). τ (tau) = fluorescence lifetime, SD = standard deviation.

Figure 5-8 (a) shows a summary of results for all the cancer specimens included in the paired analysis. Figure 5-8(b) shows the shift in the intensity-weighted mean fluorescence lifetime ($\Delta\tau$) for each normal-cancer pair. The mean fluorescence lifetime for the cancer specimen was longer than that observed in normal tissue and this trend was observed in all cases. However, this difference was not found to be statistically significant (p = 0.06). It is interesting to note that the longest mean lifetime value was observed in the papilloma sample, (sample No. 22), which has low malignant potential compared to TCC (Figure 5-7).



(a) **(b)**

Figure 5-8: (a) Bar graphs showing the mean fluorescence lifetime observed in all cancers relative to a sample of healthy tissue from an adjacent region of bladder. (b) Shift in the mean fluorescence lifetime of all cancers specimens included in the paired analysis (*n* = 5).

Figure 5-9 shows the paired ratio (disease/normal) of the fluorescence intensity for all the cancer specimens (n = 5) relative to a sample of healthy bladder tissue from the same patient.

The ratio of mean fluorescence intensity, averaged across all the pixels of the intensity images to the corresponding value for the cancer specimen, was found to be greater than 1 in three out of five cases, indicating that the fluorescence intensity from the cancer specimen was higher than the paired normal specimen in 3 patients and lower in 2 patients (samples 10 and 16).

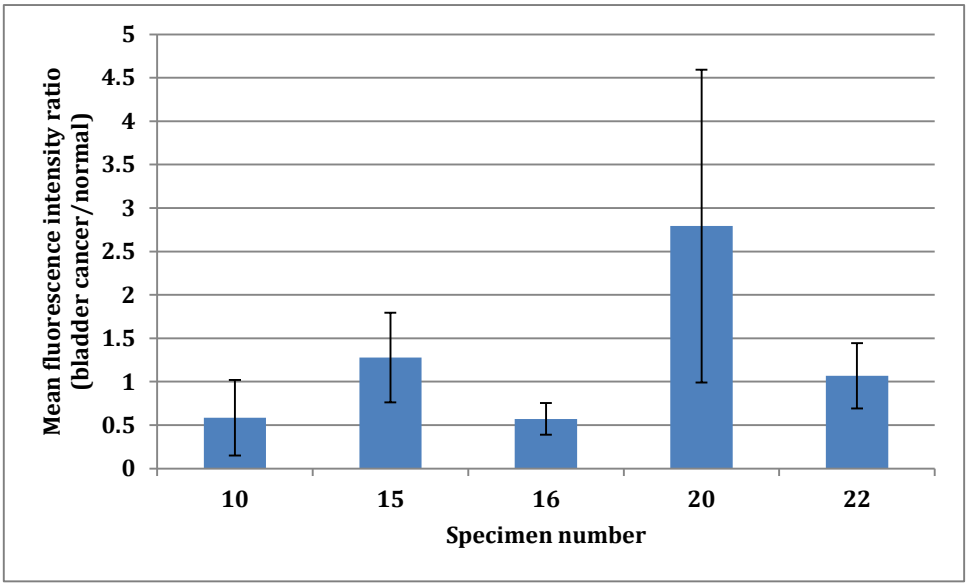


Figure 5-9: Bar graph showing the ratio (bladder cancer/normal) in the mean fluorescence intensity observed in all the cancer samples relative to a sample of healthy tissue from the same patient. The mean intensity for all the samples was obtained calculating the mean number of photons detected per pixel, across all the pixels of the intensity image. The error bars represent ± 1 standard deviation and were calculated via error propagation from the fluorescence intensity distribution in the normal and cancerous images.

5.3.2 Wide field FLIM imaging

As mentioned above, when relatively larger bladder cancer specimens were obtained, fluorescence lifetimes were further measured using time-gated wide field imaging to contribute towards the development of a wide field FLIM flexible ureteroscope prototype (Flex X ureteroscope, Karl Storz GmbH, Germany), for future *in vivo* clinical application. The wide field FLIM endoscope setup is described in section 3.2.5.

In these experiments, the specimens were excited at 405 nm using a separate multimode fibre and the resulting fluorescence collected through the endoscope coupled to a GOI. In the future, following further development of this FLIM endoscopy system, the excitation light will be delivered using an additional fibre that is integrated into the same endoscope.

Figure 5-10 shows the wide field FLIM images of two biopsy specimens (1 cancer, 1 normal) taken from a patient affected by bladder cancer, who did not receive Hexvix instillation. Macroscopically, the cancerous sample had a red papillary growth rising from the mucosal layer, consisting of finger-like epithelial projections and *villi*.

Neoplastic tissue had visibly less intense fluorescence than the normal specimen, and exhibited a shorter mean fluorescence lifetime compared to normal bladder.

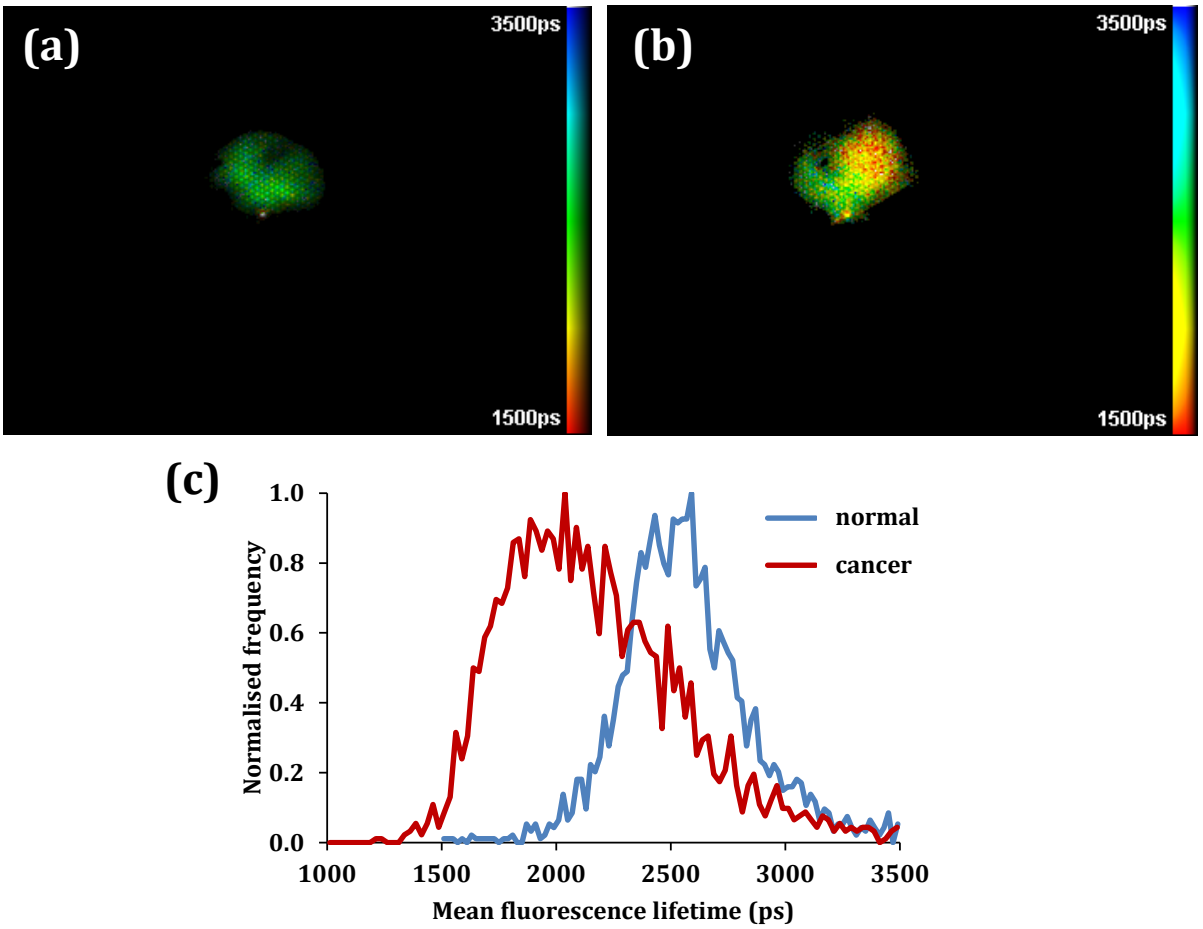


Figure 5-10: Wide field FLIM images of normal bladder (a) and bladder cancer (b) obtained from the same patient. Fluorescence lifetime distribution histogram calculated from the FLIM data, fitting the mean lifetime to a double-exponential decay model. The field of view of the ureteroscope is 3.29 mm x 2.51 mm.

5.4 Discussion

The objective of this study was to investigate the potential for FLIM when applied to induced PpIX fluorescence in the bladder. These observations might help develop a FLIM endoscope that may be used to detect the lifetime signature of PpIX *in vivo* during cystoscopy, and increase the detection rates and the specificity over standard fluorescence intensity imaging alone, e.g. with the Storz blue light system.

PpIX is a fluorescent by-product involved in the haem cycle, which is used in PDD of bladder cancer after the instillation of products such as Hexaminolevulinate (Hexvix). Previous studies suggested that the combination of natural and PpIX induced fluorescence lengthens the measured lifetime, and makes it possible to differentiate between normal, inflamed and cancerous tissues [457,458,471].

These results suggest that the combination of autofluorescence and PpIX induced fluorescence, which were both measured by the broad detection band employed, lengthens the fluorescence lifetime in cancer compared to normal.

Based on this limited set of data it appears that the mean fluorescence lifetime of bladder cancer biopsies are consistently longer than the healthy biopsies for intra patient comparisons, although this difference was not found to be statistically significant ($p = 0.06$).

The increase in the mean fluorescence lifetime for the cancerous specimens could be due to there being a larger proportion of PpIX in neoplastic tissue when compared with normal tissue as it is well known that PpIX has a long mean lifetime (up to 15 ns) [280-282].

In our study, we have not observed very long values of fluorescence lifetime as it would be normally expected in presence of PpIX accumulation. However, previous studies have shown that PpIX fluorescence lifetime goes through significant changes when bound to intracellular partners. For example, the fluorescence lifetimes of photosensitizers such as Photofrin, 5-ALA, and mTHPC were all shortened compared to those in solution [472,473].

In addition, the spectral analysis of each cancer biopsy revealed spectral peaks that are consistent with published values for the emission spectrum of flavins and PpIX fluorescence [213,255,287,415]. This result is also in good agreement with those obtained from Glanzmann *et al.* [255], where a strong emission band between 510 and 560 nm, corresponding to the tissue autofluorescence only, was distinguished both spectrally and temporally at 418 nm excitation from the 5-ALA induced PpIX fluorescence with its characteristic emission peak at 633 nm. A longer AF mean lifetime was also reported at 337 nm excitation for bladder cancer compared to surrounding normal tissue (4250 ± 55 ps vs. 5410 ± 150 ps).

Notwithstanding the obvious differences, longer fluorescence lifetimes induced by exogenous administration of PpIX relative to adjacent healthy tissue have also been reported in skin cancer [457,458], oral dysplasia and cancer [268,461], and in a number of tumour-bearing animal model studies [459,460,474], including chick chorioallantoic membrane [475], rat prostate adenocarcinoma cells in organic solution [476], and rat epithelial cells incubated with 5-ALA [477].

This chapter also reports preliminary work using wide field FLIM to study bladder autofluorescence. Shorter mean fluorescence lifetime for cancer relative to adjacent normal bladder was found in two paired specimens. This contrast is similar to that observed in previous work from our group using wide field time domain FLIM instrumentation at 355 nm excitation [273], showing a decreased fluorescence lifetime in a freshly resected bladder containing a moderately differentiated squamous cell carcinoma. This result is also in agreement with an

earlier study employing frequency-domain FLIM at 363 nm excitation, showing a decreased fluorescence lifetime in bladder exhibiting an erythematous urothelium [65]. Further work is required to investigate this more thoroughly.

In this study, an increase in mean fluorescence intensity (mean ratio bladder cancer/normal = 1.26) was seen in the cancer specimens compared to adjacent samples of healthy mucosa. However, unlike fluorescence lifetime, fluorescence intensity measurements are known to be affected by a number of factors, including the relative difference in the focal plane for each individual sample measured, the different depth of penetration reached by the excitation light, and scattering of emitted fluorescence as it propagates back through the sample.

The detection bandwidth used in our study enabled to measure both AF and PpIX intensity together. It is therefore difficult to separate their relative contributions to the resulting fluorescence intensity detected. For example, it is possible that PpIX fluorescence increased for cancer relative to autofluorescence and this masked the lower fluorescence intensity compared to the normal specimen. The observation here in two sample pairs that AF intensity decreases in cancer is consistent with earlier reports of autofluorescence studies [478,479]. Koenig *et al.* [478] studied 53 patients with bladder cancer undergoing cystoscopy with mucosal biopsies or transurethral resection of a bladder tumour. Tissue was excited at 337 nm using a fibre-optic probe inserted through the working channel of the cystoscope. Cancer exhibited lower fluorescence intensity compared to healthy bladder mucosa. Importantly, in non-malignant tissue, including normal and inflamed mucosa, a peak at 385 nm was consistently seen, which instead was not observed in malignant lesions. Based on this observation, they developed an algorithm to distinguish malignant from non-malignant tissue, with 97% sensitivity and 98% specificity.

A decrease in autofluorescence intensity for bladder cancer, independent of grade and stage of tumour, was also observed by Anidjar *et al.* [479] at different excitation wavelengths (308, 337 and 480 nm).

In our study, other than in fluorescence lifetime and intensity, morphological differences were also observed between the two tissue states although these differences were not quantified. The patterns provided by confocal FLIM in freshly excised bladder specimens were found to be similar to those characterised by pCLE [463,464], and to those of conventional H&E histopathology. The tissue morphology observed in our images was also similar to that shown by Cicchi *et al.* [272] using a combination of two-photon excitation fluorescence, second harmonic generation (SHG) and FLIM microscopy at 740 nm and 840 nm excitation.

The fluorescence spectrum and lifetime trends observed (greater 630 nm emission peak and longer fluorescence lifetime) support the idea that Hexvix induced PpIX in the bladder preferentially accumulates in cancerous tissue and also demonstrates the potential for FLIM to differentiate normal and diseased tissue based on Hexvix induced lifetime contrast in the bladder. Intensity measurements were confusing due to the wide spectral detection band employed detecting both AF and PpIX fluorescence. Future work is more likely to involve the spectral separation of AF and PpIX contributions using narrower detection bands. However, a larger data set is required to confirm this promising result.

5.5 Conclusions

Our data, although based on only a small number of *ex vivo* specimens, suggests that FLIM is able to differentiate between normal and neoplastic tissue, confirmed on histological diagnosis, with a consistently longer overall lifetime for biopsies of bladder cancer compared to paired normal specimens. Our AF emission spectra suggest that this may be due to the different lifetimes of flavins in combination with PpIX when bladder tissue is excited at 405 nm. Further study to characterize bladder biopsies obtained during PDD using blue light cystoscopy using FLIM *ex vivo* is necessary before a novel endoscopic system can be used for *in vivo* optical biopsy. Our work suggests that FLIM may become a useful adjunct to blue light PDD, and can possibly offer a novel technological solution to the challenge of accurate diagnosis of bladder cancer.

Chapter 6: *In vivo* time-resolved fluorescence lifetime spectroscopy of skin cancer

This chapter presents results from an *in vivo* a clinical investigation conducted at Lund University Hospital using a novel, compact, multidimensional, clinically deployable fluorescence lifetime spectrometer. A cohort of 25 patients with suspected skin cancer was studied immediately before surgical excision of their lesions.

Particular emphasis was given to basal cell carcinoma (BCC), which was the most prevalent lesion type in the group of patients recruited in the study.

In the first part of this chapter, a brief introduction to skin cancer, novel optical techniques applied to the diagnosis of skin cancer, and to the anatomy of normal human skin is provided. The design, construction and application of the spectrometer are then described along with the experimental protocol, the clinical procedure and the main results. A statistically significant decrease in the fluorescence lifetime of BCCs compared to neighbouring healthy tissue was observed.

This was the first *in vivo* study of autofluorescence lifetime using an instrument developed by the Photonics Group and was published in the Journal of Biophotonics, Vol. 5, February 2012 [403]. The article was also highlighted as the Editor's Choice and publicised by the journal in a press release.

This study served not only to illustrate the clinical applicability of optical spectroscopy for the diagnosis of skin cancer but, more importantly, preceded and pioneered the application of the same technology and instrumentation for use in the gastrointestinal tract.

6.1 Introduction

Malignant tumours of the skin include cutaneous melanoma, basal cell carcinoma (BCC) and squamous cell carcinoma (SCC). Melanoma is the type of skin cancer that develops from melanocytes (nevi), whereas BCC and SCC develop from basal cells and keratinocytes respectively.

BCC and SCC, collectively known as non-melanoma skin cancer (NMSC), account for 90% of all skin malignancies and represent a significant health problem worldwide. Despite the extended survival prognosis of these diseases compared to malignant melanoma, their incidence appears to be increasing. In the UK and the USA respectively, there are approximately 100,000 and 1,000,000 new cases reported every year [480,481].

For instance, amongst white populations in Europe, the USA, Canada and Australia the average increase in NMSC has been between 3 and 8% per year since the 1960s [482,483].

Basal cells are found in the deepest layer of the epidermis and around the hair follicles. BCCs are predominantly found on areas of skin exposed to the sun (i.e. face, nose, forehead, cheeks, back, and legs), and are often diagnosed in middle or old age. Lesions start typically as a small lump with shiny edges and a depressed or sunken centre. They then tend to grow upwards and become crusty and ulcerated, infiltrating the epidermis, the dermis and other neighbouring types of tissue such as cartilage or bone, although, unlike melanomas, they rarely metastasise to other parts of the body. A synchronous or metachronous development of a BCC is possible, and once affected, the risk of being re-affected by another BCC increases in turn.

Squamous cell skin cancers are responsible for about 20% of all skin cancers. They arise in areas of direct exposure to the sun, or can also develop in scarred, burnt or ulcerated areas of skin.

SCCs affect predominantly older people and present as shallow ulcers, often with a scaly crust and elevated and hardened edges, which tend to infiltrate to the deeper layers of the skin if left untreated. The spreading of SCCs to regional lymph nodes and metastases is uncommon.

Diagnosis of skin cancer is currently based on a patient's anamnesis and on visual inspection of the suspected lesion. However, in many cases the diagnosis still remains unclear and a biopsy, followed by histopathological assessment of the excised tissue, is often required for confirmation. Nonetheless, non-melanoma skin cancers are occasionally difficult to classify because of overlapping morphological features or ambiguous differentiation. In these circumstances pathologists have to recourse to immunohistochemistry.

Taking a skin biopsy is quite an invasive procedure, which is not devoid of risks and complications (pain, bleeding, scarring). This method often leads to unnecessary excision of benign lesions [484,485] and, additionally, the delineation of the margins of the lesion can be extremely difficult so, a significant section of surrounding healthy tissue is usually resected to ensure that no cancerous tissue remains. Another point to consider is that the histopathological analysis is an expensive and time consuming process that ideally should be left only for selected cases. Clearly, a non-invasive method of assessing skin lesions, capable of avoiding unnecessary biopsies and reducing uncertainties for patients and clinicians would be desirable.

Skin offers the advantage of being the largest and most easily accessible organ of the body, which makes it particularly attractive for optical diagnostic methods.

A number of non-invasive technologies based on autofluorescence imaging and spectroscopy have been investigated for the detection and delineation of skin diseases over the last decades.

These include diffuse reflectance measurements [219,225,397], polarisation-resolved reflectance spectroscopy and imaging [486-488], steady state fluorescence spectroscopy [489], time-resolved fluorescence spectroscopy [490,491] and imaging [270,423,492], confocal reflectance microscopy [493-495], optical coherence tomography (OCT) [496,497], Raman spectroscopy [498], and multiphoton microscopy (MPM) [490,499-501].

Rajaram *et al.* studied non-melanoma skin cancer *in vivo* using a combination of diffuse reflectance and fluorescence spectroscopy [397] at 337 nm excitation, while Blackwell *et al*. used an instrument recording fluorescence decays in four spectral channels to compare the fluorescence signature of human skin from diabetic and non-diabetic subjects *in vivo* [491].

Using a single-point spectroscopy probe, Brancaleon *et al.* [489] measured the emission spectra collected *in vivo* and from fresh frozen samples of both BCC and SCC excited at four different wavelengths (350, 360, 390 and 420 nm). Interestingly, a loss of autofluorescence from a region surrounding the malignant tissue was reported, and this area corresponded to a visible loss of collagen and elastin at the histological assessment.

The spectroscopic data suggest that NAD(P)H, flavins, keratin, collagen and elastin [298,490,502] constitute the principal contributors of skin autofluorescence, and the spectral and temporal properties of the emission from these fluorophores reflect changes in tissue metabolism and environment due to the presence of disease. There is therefore a compelling need to develop instruments that can probe these subtle changes measuring the autofluorescence properties of skin (and other organs) for early and enhanced diagnosis of early stage cancers [397,485,503-507]. A number of instruments have been presented that are capable of monitoring both the fluorescence lifetime and emission spectrum of a sample [255,256,258,508], and significant differences between the fluorescence lifetimes of healthy and diseased tissue in NMSC have been shown in both *ex vivo* [258,270] and *in vivo* studies [397,491].

The recent emergence of a clinically licensed and commercially available two photon microscope [509], has prompted the application of multiphoton microscopy to studies of skin disease [499-501].

Using step-wise two-photon microscopy (TPM) at 810 nm excitation, Eichhorn *et al.* [500] measured the spectra from fresh skin (n = 150) and formalin fixed, unstained sections (n = 27) of melanocytic lesions. They observed a single spectral emission peak at 490 nm in benign nevi and at 600 nm in nodular melanomas, with both peaks appearing in dysplastic nevi.

Two photon microscopy has also been used to study the morphological features of skin malignancies and been reported to show good correlation with histology. *Ex vivo* studies of non-

melanoma skin cancer samples excited at 780 nm [499] showed irregularly distributed keratinocytes with dilated intercellular gaps. Higher cytoplasmic fluorescence intensity was found in pleomorphic cells and dyskeratotic cells compared to the surrounding cells. Nests of BCC cells were found in a third of the BCC specimens.

Although most researchers have focused on skin cancers, investigations have also been extended to non-cancer applications such as skin aging [510], inflammatory conditions such as atopic dermatitis [511] and hypertrophic scars [512]. The application of fluorescent precursors as exogenous source of contrast (induced fluorescence) to skin imaging, such as protoporphyrin IX, is also being increasingly investigated [513].

Most recently, due to the improvement of FLIM instrumentation, fluorescence lifetime contrast of skin lesions has also been reported. Previous work from our group [270], using a wide field FLIM system to excite freshly-resected specimens of BCC at 355 nm, revealed a significant lifetime difference between cancers and normal perilesional skin (1.40 ns vs. 1.55 ns respectively).

Conversely, using TPM with excitation at 740 nm, another group has reported longer lifetime values for BCC compared to normal tissue [492].

Recent *ex* and *in vivo* work in our group [423] using multispectral multiphoton FLIM to differentiate BCC cells from normal keratinocytes showed statistically significant increases in the fluorescence lifetimes of neoplastic cells. In addition to differences in fluorescence and morphology, the new parameter of "merging cells" was proposed, which together with existing criteria [514] provided a good sensitivity (79%) and specificity (93%) for identifying BCCs from FLIM images using a visual architectural analysis. It is important to consider this work in the context of current and past work on MPM and FLIM of autofluorescence of human skin. Seidenari *et al.* [514] combining multiphoton intensity imaging and FLIM for the diagnosis of BCC, cells with a longer fluorescence lifetime were always observed for BCCs and this morphological descriptor provided the highest sensitivity (100%) and specificity (70%) of all of the descriptors identified. An overall sensitivity for the diagnosis of BCC from other lesions and normal skin of 97% was obtained when two or more descriptors were considered and a specificity of 100% with five descriptors or more. A number of studies have also described criteria for diagnosis of BCC, using reflectance confocal laser scanning microscopy showing high sensitivity (91.6-100%) and specificity (88.5-97%). These morphological descriptors included: polarised elongated nuclei; linear telangiectasia-like horizontal vessels; basaloid cord and nodules; nests of cells tightly packed in palisading structures; and peritumoural clefting [515-519]. In a recent *in vivo* study comparing reflectance confocal microscopy and a multiphoton tomography for BCC diagnosis, elongated cells and palisading structures were recognised, and

the nucleus of elongated BCC cells was found to be significantly longer than other measured normal skin cells, whereas no significant discrimination was possible using the cell density and nucleus/cytoplasm ratio of BCC as morphological descriptors [520].

Melanomas have also been studied both *ex vivo* and *in vivo* with excitation at 760 nm [501,521], and, when fitted to a double exponential decay model, keratinocytes and melanocytes could be differentiated according to their fluorescence lifetimes, although no difference was observed between benign and malignant tissue.

The work presented here is a clinical investigation of autofluorescence lifetime of non-melanoma skin cancer performed using a fibre probe based time-resolved spectrometer utilising single photon dual fluorescence excitation at 355 and 445 nm.

The hypothesis was that measurements of fluorescence lifetime and diffuse reflectance spectra permitted normal and diseased skin to be distinguished, particularly when applied to basal cell carcinomas and surrounding health skin prior to surgical excision. The aim was to apply for the first time *in vivo* a fluorescence lifetime spectrometer developed by the Photonics Group and demonstrate its potential for clinical diagnosis.

6.1.1 Normal Skin

The skin is composed of three main layers: the epidermis; dermis; and subcutaneous tissue.

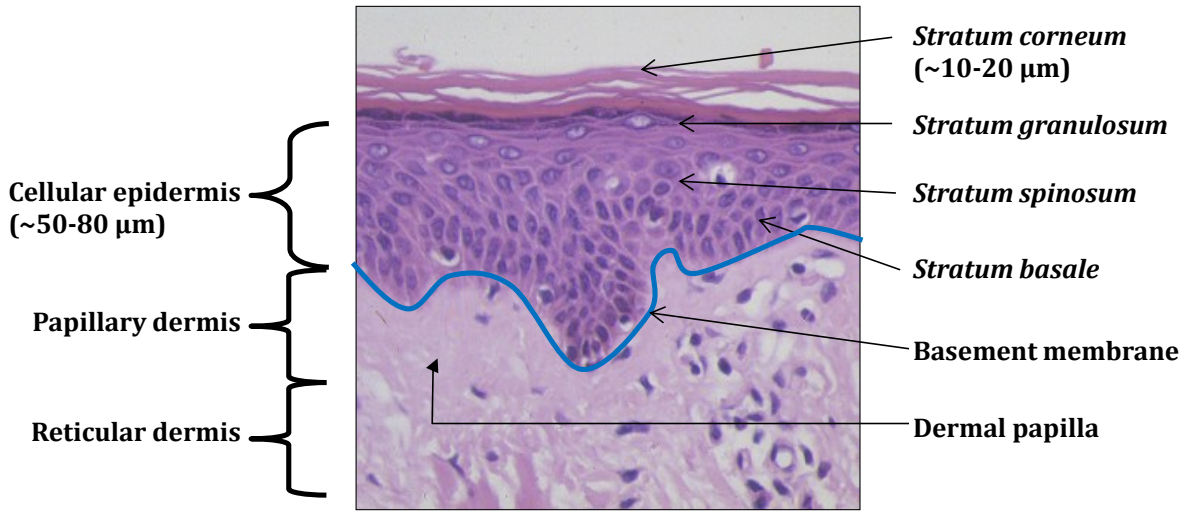


Figure 6-1: Annotated H&E stained section of the epidermis and dermis of normal skin. Adapted and reproduced with permission from [522].

The epidermis is the most superficial layer of the skin and is organised into four distinct layers defined by their histological appearance as *stratum corneum*, *stratum granulosum*, *stratum spinosum*, and *stratum basale* (see figure 6-1). Keratinocytes constitute 90% of the cells found in this layer, and undergo changes in cellular morphology (terminal differentiation) as they progress from the *stratum basale* to the *stratum corneum*. The epidermis is separated from the dermis by the basement membrane (blue line in figure 6-1) and varies in thickness depending on age and region of the body (typically 60-100 µm [523]). The basement membrane is mainly composed of collagen type IV, and adheres to the *stratum basale* by means of large glycoprotein molecules called laminins.

Melanocytes are usually found in the lower part of the epidermis and in the papillary dermis. Their primary role is to produce and distribute melanin to the surrounding keratinocytes to protect their nuclei from UV photodamage. Langerhans dendritic cells are found in the *stratum spinosum* of the epidermis and have immune surveillance function. Merkel cells are involved in sensory perception and are located in the basal layer near associated sensory nerve endings.

The dermis lies underneath the basement membrane, providing physical support and nutrition for the epidermis above. The dermis is divided into two layers: a superficial layer adjacent to the epidermis, called the papillary dermis; and a deep layer, the reticular dermis, which can be distinguished by a change in the orientation of the collagen fibres. The papillary dermis forms protrusions, called dermal papillae, which interdigitate with the epidermal ridges (see figure 6-1). Various structures are located within the dermis, including the pilosebaceous unit (hair

and sebaceous gland), nerves, sweat glands, sensory receptors and blood vessels. The dermis is composed of a matrix of proteoglycan macromolecules, type I and III collagen and elastin.

The subcutaneous tissue lies under the dermis and contains loose connective tissue and approximately 80% of all body fat [524]. Regional variation can be found in normal skin depending on body site e.g. thicker on the palms and soles.

6.2 Materials and methods

This study was carried out in collaboration with researchers from the departments of Oncology, Dermatology and Atomic Physics at Lund University, Sweden, as part of a European research network (Photonics4Life). The study involved the use of two spectrometers, one of which was a time-resolved spectrometer built at Imperial College London [258], and the other was a steady state spectrometer developed at Lund University [525].

The Imperial instrument is a time-resolved fluorescence spectrometer utilising a fibre-optic probe to deliver excitation and collect autofluorescence decay profiles in multiple spectral channels [403]. The Lund system is a compact steady state spectrometer, which combines measurements of spectrally resolved fluorescence for four excitation wavelengths, and measurements of diffuse reflectance obtained using a white LED source.

It should be noted that the description of the steady state spectrometer developed by the Lund investigators is beyond the scope of this thesis, but more detailed information on this instrument can be found in references [328,403,525].

The time-resolved fluorescence spectrofluorometer was transported in a van from London to Lund by the Imperial investigators, including myself, taking a ferry across the North Sea from Harwich (UK) to Esbjerg (Denmark). The compact steady-state spectrometer developed by the Swedish team was available on site.

Both spectrometers were set up in a room in the dermatology clinic at Lund University Hospital, where all measurements took place.

A total of 27 lesions on 25 patients at Lund University Hospital were investigated *in vivo* before surgical excision of the irradiated region. Patients were all of skin phototypes I-III according to the Fitzpatrick scale [413].

The experiments were performed by a multidisciplinary team of both clinicians and non-clinical researchers from the University of Lund and Imperial College London.

Patients were assessed and recruited from the local team of physicians during dermatology outpatient clinics. The study was conducted with the approval of the local Ethics Committee and in accordance with the ethical principles of the Declaration of Helsinki.

The lesion characteristics with clinical (pre-excision) and histological diagnoses are summarised in table 6-1.

Lesion	Patient	Location	Size (mm)	Clinical diagnosis	Histological diagnosis
1	1	R cheek	10x10	BCC	BCC
2	2	Back	6	Lentigo melanoma	Benign pigmented naevus
3	3	R cheek	9	Ulcerated BCC	BCC
4	4	L abdomen	12	BCC or melanoma	Melanoma (superficial spreading)
5	5	L forearm	10x14	Morbus of Bowen	SCC in situ
6	6	L leg	10x12	BCC	BCC
7	7	R arm	18x15	BCC	Melanoma (naevoid type)
8	8	Head	25	SCC	Highly diff. SCC
9	9	Head	10x10	Actinic Keratosis	Actinic Keratosis
10	9	R chest	30	Nodular BCC	Nodular BCC
11	10	Back	50x40	Invasive BCC	Invasive BCC, focal spinocellular diff.
12	11	R foot	40x60	Kaposi's sarcoma	Kaposi's sarcoma
13	12	L back	12x7	Melanoma	Melanoma (superficial spreading)
14	13	R thigh	10x10	Unknown	Keratoacanthoma
15	14	R cheek	15x15	Unknown	Highly diff SCC
16	15	R ear	10x10	Unknown	SCC
17	16	R thigh	7x7	Dysplastic naevus	Pigmented naevus with dysplasia
18	17	Back	15x30	BCC	BCC
19	18	L cheek	6x7	Nodular BCC	Nodular BCC
20	19	L shin	12x12	BCC	BCC
21	20	L shoulder	7x8	Unknown	Nodular BCC
22	21	R shoulder	3x3	Dysplastic naevus	Blue naevus
23	22	R index finger	15x15	Pyogenic granuloma	Pyogenic granuloma
24	23	R elbow	12x10	Arsenic keratosis	SCC in situ
25	24	Back	3x4	Actinic keratosis	Actinic keratosis
26	25	upper back	10x8	Actinic keratosis	Actinic keratosis
27	25	lower back	6x6	BCC	BCC

Table 6-1: Summary of the skin lesion characteristics with clinical and histological diagnoses. R = right, L = left, BCC = Basal Cell Carcinoma, SCC = Squamous Cell Carcinoma.

6.2.1 Time-resolved fibre-optic probe fluorescence lifetime spectrometer

The time-resolved fluorescence spectrometer was configured as shown in figure 6-2(a).

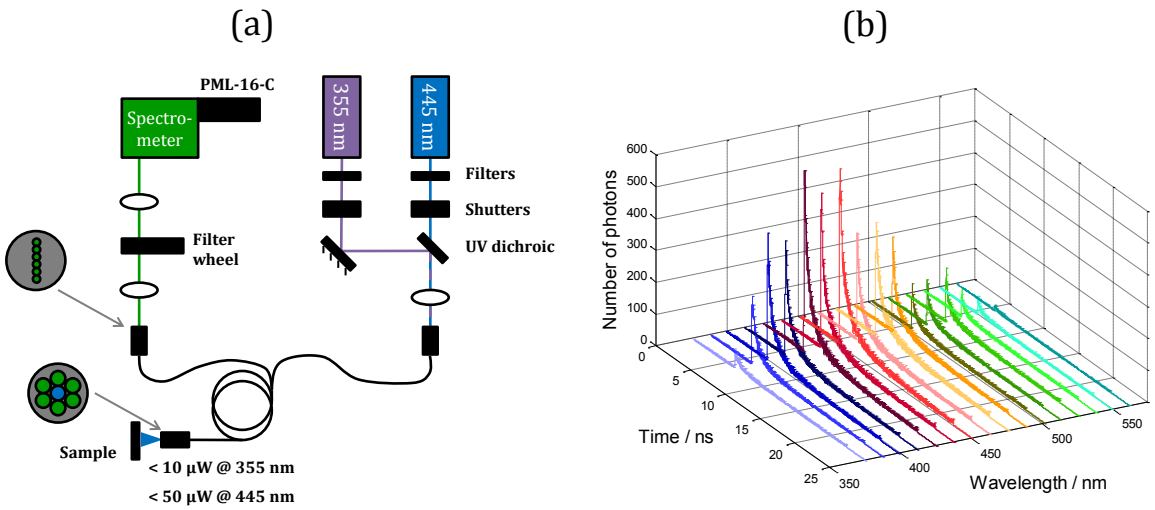


Figure 6-2: (a) Optical layout of the time-resolved fluorescence spectrometer. (b) An example of the raw data acquired with this system. The graph shows 16 spectrally resolved fluorescence decays obtained from human skin *in vivo* using an excitation wavelength of 355 nm. Reproduced with permission from [403].

Excitation was provided by two pulsed laser sources: a frequency tripled ultrafast UV fibre laser (UVPower355, Fianium Ltd., UK), which provided 10 ps pulses at 355 nm with a repetition rate of 37.1 MHz; and a blue diode laser (LDH-P-C-440B, PicoQuant GmbH, Germany), which emitted 50-150 ps pulses at 445 nm with an adjustable repetition rate of up to 40 MHz.

The optical arrangement of the time-resolved spectrometer and the fibre probe are shown in figure 6-3.

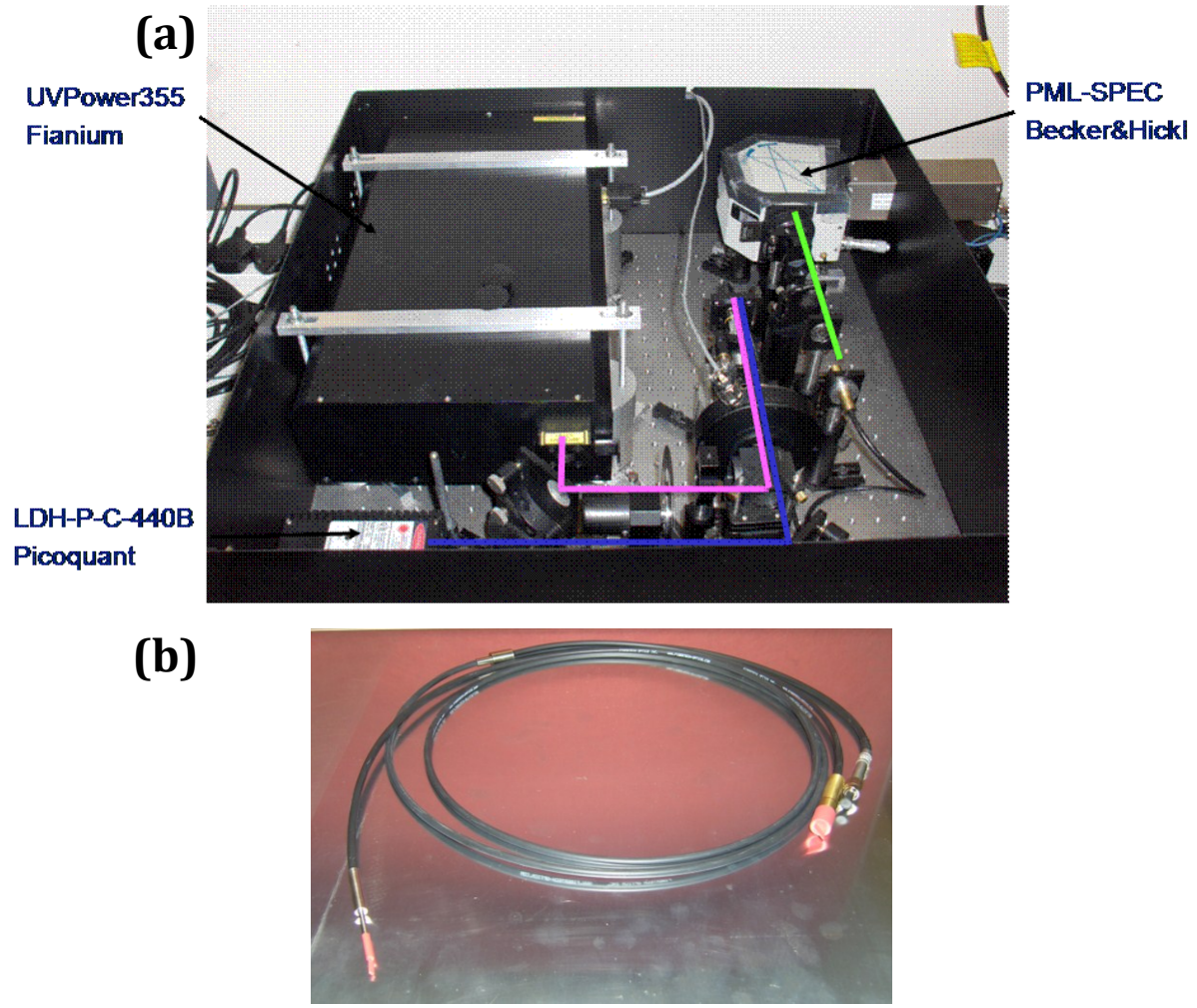


Figure 6-3: (a) Photograph illustrating the optical arrangement of the time-resolved spectrometer with the lid removed. (b) The custom built fibre probe (FiberTech Optica, Canada).

A maximum power of 10 µW for UV irradiation and 50 µW for blue irradiation was set to ensure that no photodamage could be potentially caused as these power levels were below the maximum permissible exposure (MPE) for skin for exposure times as long as 1000 s.

This laser radiation was coupled into the excitation channel of a custom built fibre-optic probe (FiberTech Optica, Canada, figure 6-3(b)) that housed seven optical fibres, each with a diameter of 200 µm and a numerical aperture (NA) of 0.22, six of which served to collect fluorescence and one to deliver the excitation.

At the distal end of the probe, the fibres are arranged with the central excitation fibre surrounded by the six collection fibres (inset at bottom left of figure 6-2(a)). This arrangement was designed to optimise the illumination and collection efficiency while maintaining a relatively small probe size. The distal branch of the probe (common to all optical fibres) was 1 m in length.

Spectral band pass filters were employed to narrow the emission of the laser diode and to reject residual light at other wavelengths emitted by the frequency tripled fibre laser.

Variable neutral density (ND) filters limited the optical power at the sample to 10 μW for UV light and 50 μW for blue light.

Computer controlled mechanical shutters in the two excitation beam paths were used to switch between the two sources. The output from the excitation optical fibre was directed onto the sample over an area of approximately 0.2 mm^2 and the resulting fluorescence was collected by the six multimode collection fibres which surround the central excitation optical fibre in the FiberTech probe.

The output from these collection optical fibres was then imaged onto the input slit of a grating spectrometer (MS125 1/8m, Lot-Oriel, UK) which was attached to a 16 channel multi-anode photomultiplier tube (PMT) detector (PML-16-C, Becker-Hickl GmbH, Germany). The PMT was linked to a computer with a SPC-730 time correlated single photon counting (TCSPC) card running SPCM software (Becker-Hickl GmbH, Germany) so that fluorescence decay profiles could be recorded in 16 spectral channels spanning a wavelength range of 400-600 nm. At the fibre probe output, the 6 collection fibres were aligned vertically in order to maximise the coupling into the input slit of the spectrograph (see inset at top centre of figure 6-2(a)).

A motorised filter wheel was placed in the detection beam path between the fibre probe output and the spectrometer to prevent any stray scattered laser light from reaching the 16 channel detector. The whole system was mounted on a 60 x 60 cm^2 breadboard to facilitate transportation and fully enclosed for safe use in clinical settings.

A single data set acquired using this instrument consisted of two sets of 16 spectrally resolved fluorescence decays, one for 355 nm excitation and one for 445 nm excitation. Typically, for each sample we made three identical measurements with each laser with exposure times of around 5 s per measurement, thus for a total acquisition time is ~30 s. An example of the raw data obtained when exciting human skin with 355 nm excitation is shown in figure 6-2(b).

The raw data is then corrected to account for the instrument response function of the spectrometer and the non-uniform channel sensitivity of the 16 channel PMT as described in [258,328,403]. First, the distal end of the fibre probe was illuminated with white light passed through a calibrated monochromator, which allowed the spectral centre and bandwidth of each detection channel to be determined. Second, the relative sensitivity of each PMT element was found by recording the emission from a calibrated white light source (LS-1-CAL, Ocean Optics, The Netherlands) and this information was then used to correct the fluorescence intensity measured in each spectral channel.

6.2.2 Experimental protocol

Following the clinical consultation, each patient was conducted to the experimental room and prepared for the experiments.

As a prophylactic measure, all patients (and investigators) were asked to wear laser safety goggles for protection against UV and blue wavelengths (figure 6-4) during the procedure.

Prior to the measurements, a plastic spacer was attached and secured to the distal end of the fibre probe. This was used to ensure a consistent fixed distance of 1.5 mm between the tip of the fibre bundle and the skin surface. This resulted in the excitation lasers illuminating an area of skin of approximately 0.2 mm^2.

Before use on each patient, thorough disinfection of the spacer and the distal face of the fibre bundle was performed with high level disinfectant Trigene Advanced wipes (Tristel Solutions Ltd) for non-critical devices. Following this, further disinfection of the spacer was obtained by immersion in a 70% ethanol solution for 15 minutes. Specific advice on this aspect was provided by the host clinical team at Lund University Hospital.

The probe was then placed on a clinical trolley and, when required, passed to the clinical investigator carrying out the measurements.

During the procedure, the probe was held by hand at approximately ~4 cm from the distal end, and placed into contact via the spacer with the area of skin to be studied, exerting constant gentle pressure throughout the measurements.

A circular area of ~2 mm was covered by the probe during the measurements and pictures of the lesion were recorded before and after the measurement. The total time required for each individual measurement was approximately 30 s.



Figure 6-4: Illustration of the experimental measurements. Photograph reproduced with kind permission of patient and investigators.

Using the time-resolved system, and depending on the lesion size, between one and four measurements were taken from the lesion, and two measurements were performed on the perilesional healthy skin surrounding the lesion. Whereas, with the steady state system, only two measurements were taken in each case – one on the lesion and one on the neighbouring normal tissue.

Figure 6-5 shows images of two example lesions with the small solid black circles showing the locations of the time-resolved fluorescence measurements and the large white dotted circles those of the steady state spectrometer. The insets in the figure illustrate how the individual experiments were planned.

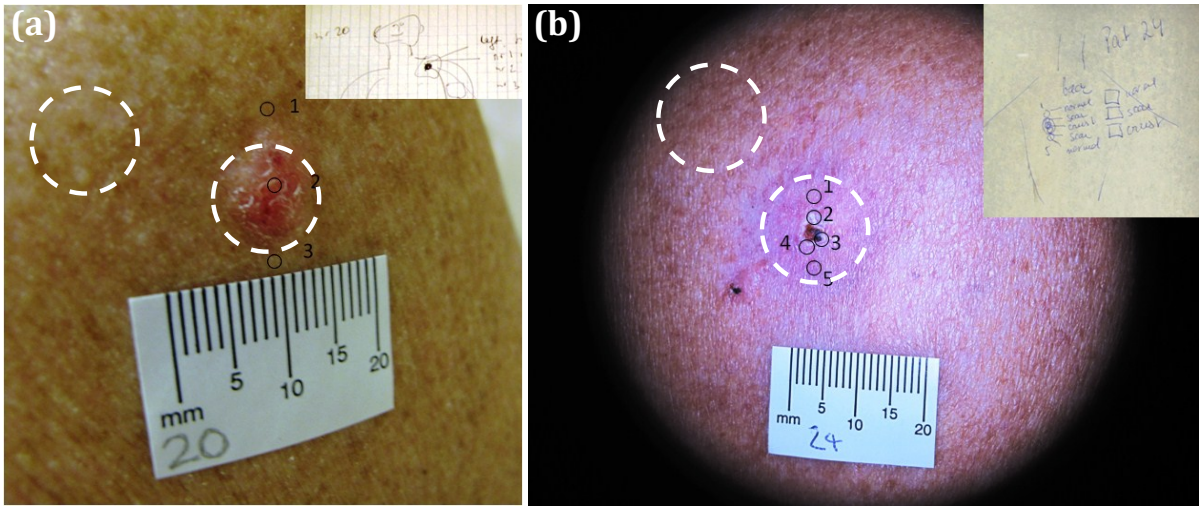


Figure 6-5: **The images show how the fluorescence measurements were planned (in the inset) and performed (main image) prior to the surgical excision. The small black solid circles indicate the sites of the single-point fluorescence lifetime measurements, and the large dotted white circles the sites of the wide-field steady state measurements. (a) Nodular BCC of the left shoulder (lesion 21, patient 20). (b) Actinic keratosis of the back (lesion 25, patient 24).**

During the measurements, the room lights were temporarily switched off to reduce the background on the fluorescence measurements.

Once the measurements had been performed, the entire region irradiated with the time-resolved spectrometer was excised and sent for histopathological assessment.

All used work surfaces were wiped with Trigene Advance wipes after each session.

In table 6-2, a summary of the lesion types and the number of measurements performed is reported.

Lesion type (histopathology)	Number of lesions
BCC	10
SCC	3
Benign naevus	2
Dysplastic naevus	1
Malignant melanoma	3
Actinic keratosis	3
Other	5
Total number of lesions	27
Total number of normal skin sites	27
Total number of measurements	54

Table 6-2: **Summary of the skin lesions studied with the FLS system, reporting the histological diagnoses.**

6.2.3 Fluorescence decay analysis

As discussed in section 3.1.4, autofluorescence from biological tissue displays a multiexponential decay profile due to the vast array of known (and possibly unknown) fluorophores present, and their different chemical states (e.g. oxidised/reduced and free/protein bound).

Two sets of 16 spectrally resolved fluorescence decays were collected and, given the nature of the tissue examined, it is highly probable that each decay reflected the contribution from a number of different fluorophores.

However, as only a limited number of photons were collected in each spectral channel, a double exponential model was considered appropriate and fitted to the fluorescence decay curves. This was performed according to equation 6-1:

$$I(t) = a_1 \exp\left(\frac{-t}{\tau_1}\right) + a_2 \exp\left(\frac{-t}{\tau_2}\right) \qquad \textbf{Equation 6-1}$$

where τ_1 and τ_2 are the two lifetimes, and a_1 and a_2 are the two pre-exponential amplitudes.

The mean fluorescence lifetime in each spectral channel was calculated using in-house software written in Matlab® (MathWorks™).

In order to accurately fit an exponential model to observed fluorescence decay data it is essential to account for the instrument response function (IRF), which essentially describes how the system responds to an infinitely short pulse of light.

In these experiments, the IRF was determined by measuring a solution of the dye DASPI (2-(p-dimethylaminostyryl)-pyridylmethyl iodide, Radiant Dyes Laser Accessories GmbH, Germany) in water. DASPI is a fluorophore that has a fluorescence lifetime of less than 50 ps, which is significantly shorter than the instrument response time and, therefore, provides a good estimate of the IRF. As the emission spectrum of DASPI does not cover the entire collection range of the spectrometer, one representative spectral channel was selected and used for fitting all the spectral channels. This approach was believed to be reasonable as the variation in the shape of the IRF between different spectral channels is low [526].

An adjustable temporal offset was introduced into the exponential fitting model to compensate the variable temporal shift in the IRF across the different spectral channels.

The mean fluorescence lifetime (τ_{mean}) was then calculated in each spectral channel according to equation 6-2.

$$\tau_{mean} = \frac{a_1\tau_1^2 + a_2\tau_2^2}{a_1\tau_1 + a_2\tau_2}$$ **Equation 6-2**

Since the fluorescence lifetime (and the contrast in fluorescence lifetime between healthy and diseased regions of tissue) did not vary significantly with emission wavelength, a spectrally averaged mean fluorescence lifetime was calculated according to equation 6-3 to summarise the fluorescence decay data from each measurement site. This was achieved by averaging the spectrally resolved mean lifetime values and weighting them according to the fluorescence intensity recorded in each channel. Thus, for each measurement site a single intensity-weighted average fluorescence lifetime was obtained.

$$\bar{\tau}_{spectral} = \frac{\sum_{i=1}^{n} I_i\tau_i}{\sum_{i=1}^{n} I_i}$$ **Equation 6-3**

Here, $\tau_{spectral}$ is the spectrally averaged mean lifetime, n is the number of spectral channels included in the average and I_i and τ_i are respectively the intensity and mean lifetime recorded in each of the spectral detection channels.

For each lesion, the difference between these spectrally averaged mean lifetimes was then calculated for the normal and lesional tissue measured on each patient (i.e. $\Delta\tau = \tau_{lesion} - \tau_{normal}$) in order to investigate the diagnostic potential of the fluorescence lifetime data. In this way, the interpatient variation in the fluorescence lifetime measured from normal tissue is compensated for by the paired comparison.

The Wilcoxon signed rank test was performed on the paired differences in the spectrally averaged fluorescence lifetime ($\Delta\tau$) and the mean emission wavelength ($\Delta\lambda$) to determine whether any significant differences existed between the healthy and diseased tissues measured. The null hypothesis was that the mean shift in the mean emission wavelength or spectrally averaged fluorescence lifetime difference was equal to zero.

6.3 Results

6.3.1 Steady state spectral analysis

Figure 6-6 shows the steady state fluorescence spectra acquired from two patients diagnosed with BCC (lesion numbers 11 and 18 respectively). The two graphs show the data from the time-resolved spectrometer for healthy (figure 6-6a) and lesional (figure 6-6b) tissue.

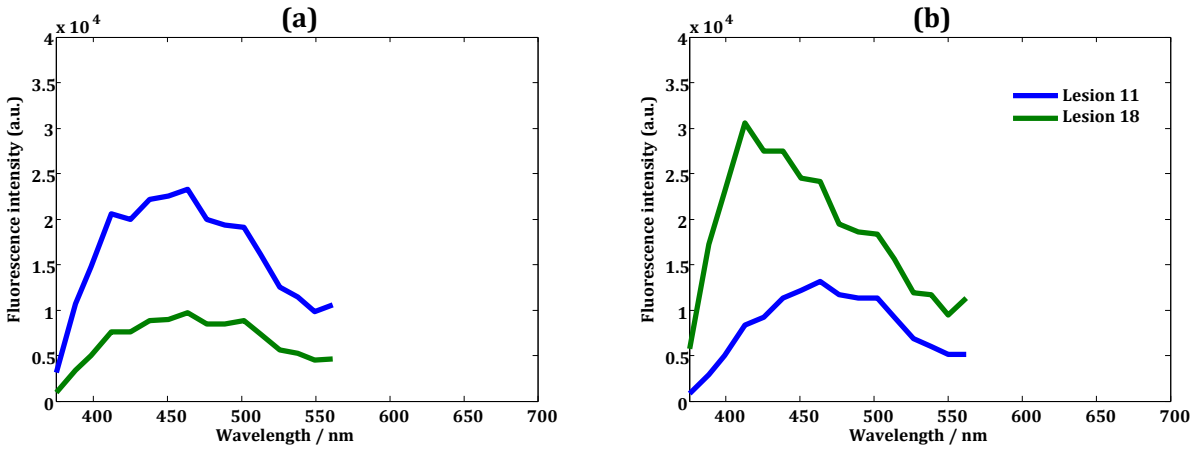


Figure 6-6: Graphs showing the steady state fluorescence emission spectra of healthy tissue (a) adjacent to a lesion, and lesional tissue (b) measurements acquired with the time-resolved spectrometer using 355 nm excitation from lesion numbers 11 and 18.

It is clear from figure 6-6 that there are spectral differences between the 2 BCCs and their adjacent perilesional tissue. However, as expected, there was considerable inter-patient variability in the acquired spectra. For instance, opposite trends can be seen for the two healthy tissues relative to the lesions 11 and 18.

This variation in the measured spectra can be attributed to inter-patient differences in factors such as skin photo-type, level of sun exposure, age and the location of the measurement site on the body [403].

As the analysis of the steady state spectra focussed mainly on the data collected with the spectrometer developed by the Lund investigators, which is, as mentioned above, beyond the scope of this thesis, the interested reader is referred to reference [403]. In summary, the steady state data obtained with the Lund spectrometer showed that the diffuse reflectance and fluorescence intensity excited at 355, 375 and 395 nm were lower in BCCs than on surrounding healthy tissue.

6.3.2 Time-resolved autofluorescence measurements

Figure 6-7 shows the mean fluorescence lifetimes averaged over all BCC patients and recorded in each of spectral channel for healthy and diseased tissue under UV (a) and blue (b) excitation.

The peak fluorescent signal for UV excitation was within the 425-540 nm spectral range, while that for blue excitation was within 475-550 nm.

The fluorescence lifetime and the contrast observed did not vary significantly with emission wavelength over the spectral ranges containing the peak fluorescent signal. Therefore, in order to increase the accuracy of the lifetime information obtained from the data sets, a spectrally integrated, intensity weighted mean fluorescence lifetime was determined for each measurement site for both excitation wavelengths. This enabled the incorporation of a higher number of photons in the decay analysis, while providing a single simple parameter to compare the measurement sites.

It should be noted that, within the spectral range containing the peak fluorescent signal, a slight increase, although not significant, in mean fluorescence lifetime with emission wavelength can be observed for BCCs at 355 nm excitation (figure 6-7(a)), whereas at 445 nm excitation, the mean lifetimes remain nearly constant across the range 477-550 nm (figure 6-7(b)).

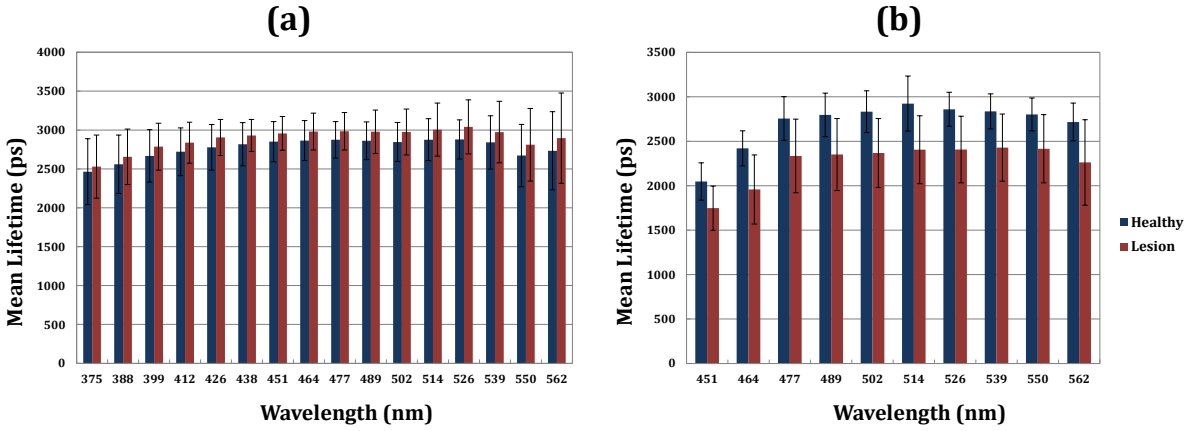


Figure 6-7: Graphs showing the mean fluorescence lifetime in all spectral channels for healthy (blue columns) and lesional tissue (red columns) for (a) 355 nm and (b) 445 nm excitation. The mean values were calculated over all BCC patients and the error bars represent the standard deviation of the measurements.

6.3.3 Paired analysis of normal tissue measurements

Using the spectrally integrated mean lifetime values, the intra-patient variability was first quantified by comparing the lifetimes obtained from the two "normal" perilesional sites measured on each patient.

The mean lifetime shifts in the spectrally averaged mean lifetime (i.e. $\Delta\tau = \tau_{normal1} - \tau_{normal2}$) for each lesion are shown in figure 6-9.

For both 355 nm and 445 nm excitation, the differences are evenly distributed on both sides of the horizontal axis (zero) with mean values of -18 ps and 19 ps respectively.

Lesion 6 shows the highest excursion in mean lifetime difference between the two normal sites for both excitation wavelengths, and this was probably due to the presence of scar tissue near both perilesional measurement sites (figure 6-8, sites No. 1 and 4).



Figure 6-8: Lesion No. 6: Basal cell carcinoma (12 x 10 mm) located on the left shin. A total of 4 measurements (2 on the lesion, 2 on normal surrounding skin) were performed.

As an estimate of the error on the fluorescence lifetime, the mean standard deviations of the normal tissue measurements were also calculated and these were found to be 75 ps with 355 nm excitation and 175 ps with 445 nm excitation.

Significant variations in the measured lifetimes were also observed between patients, and this is evident in figure 6-7, where the error bars indicate a considerable spread in fluorescence lifetime across different patients. Skin photo-type, level of sun exposure, age and body location, may all be responsible of the high inter-patient variability observed.

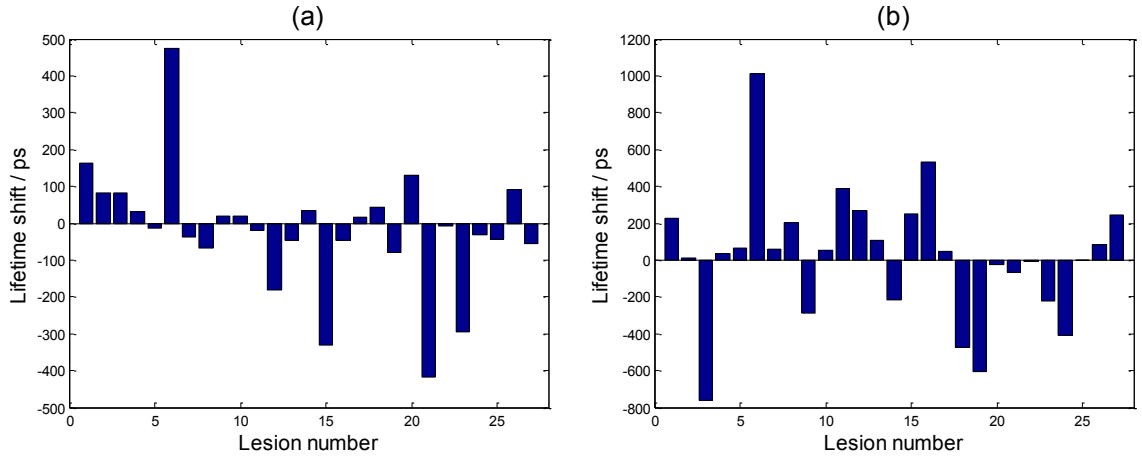


Figure 6-9: Graphs showing the lifetime shifts between the two measurements of the healthy tissue surrounding each lesion (i.e. $\Delta\tau = \tau_{normal}\,1 - \tau_{normal}\,2$) for (a) 355 nm and (b) 445 nm excitation. Figure adapted, with permission, from reference [403].

Ten of 25 patients presented with BCC. Figure 6-9 shows the spectrally resolved fluorescence lifetimes for BCC compared to the normal tissue for each patient after excitation with UV light (355 nm, left panel) and blue light (445 nm, right panel).

The spectrally weighted healthy and lesional lifetimes, averaged across all BCC patients and including all spectral channels, were respectively 2770 ± 250 ps and 2880 ± 409 ps with UV excitation and 3130 ± 413 ps and 2240 ± 480 ps with blue excitation.

Figure 6-10 shows the shift in the spectrally weighted lifetime (i.e. $\Delta\tau = \tau_{lesion} - \tau_{normal}$) observed for all patients with BCC. Again, there is no clear trend in the lifetime shifts of BCCs observed with UV excitation. For blue (445 nm) excitation (Figure 6-10b), on the other hand, the fluorescence lifetimes of BCCs are consistently shorter than those of the surrounding perilesional skin (indicated by negative lifetime shifts for all lesions). The mean lifetime decrease was calculated as 886 ± 655 ps and the lifetime shifts observed in all but one case (lesion 1) were also seen to exceed the estimate of the mean intra-patient variability reported above (175 ps).

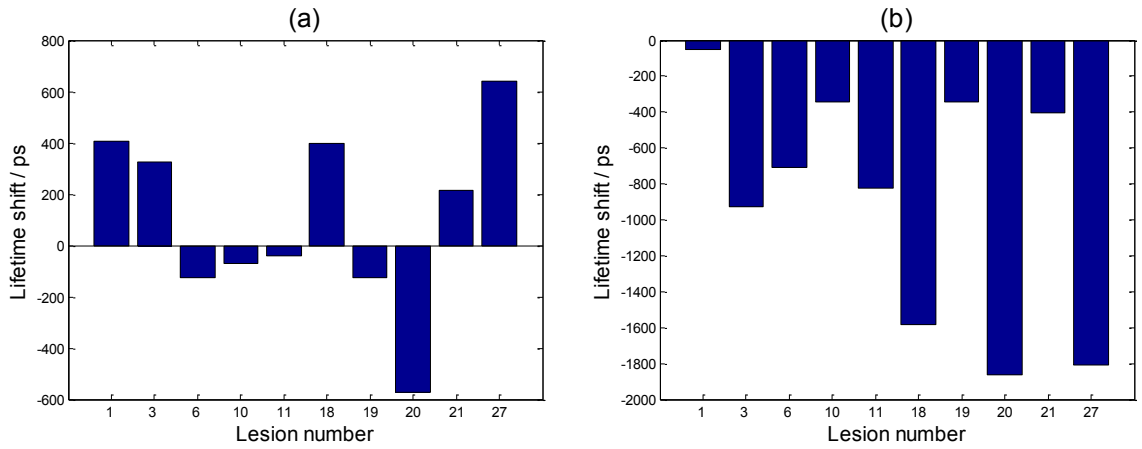


Figure 6-10: Graphs showing the lifetime shifts for all BCC lesions (i.e. $\Delta\tau = \tau_{lesion} - \tau_{normal}$) with (a) UV and (b) blue excitation. Figure adapted and reproduced with permission from [403].

The mean emission wavelength was also calculated for each BCC measurement site and for both excitation wavelengths. However, no significant difference was observed in the mean emission wavelength of healthy skin and BCCs for either excitation wavelength.

In general, the trends observed for BCCs were also seen to hold for all other lesion types. Therefore, in order to test for statistical significance, Wilcoxon signed rank tests were performed on the lifetime shifts for each individual lesion type and for all lesion types combined. The null hypothesis in these significance tests was that, for each lesion type examined, the lifetime shifts had a mean value of zero.

For individual lesion types other than BCCs, there were not enough measurements to reject the null hypothesis and attribute statistical significance to the observed trends. For BCCs alone, however, with 445 nm excitation there was a consistent decrease in fluorescence lifetime (i.e. $\tau_{lesion} < \tau_{normal}$) and this was statistically significant with a *p*-value of 0.002. Furthermore, when investigating all the skin lesions included in this study as an ensemble (i.e. when considering all lesion types together) the same trend was observed, this time with a *p*-value of 5.6×10^{-6}.

In summary, when using 445-nm-excitation, statistically significant differences have been observed between the fluorescence lifetime of healthy tissue and skin cancer. This was shown to be valid for all of the skin neoplasms included in this study all together, and, particularly, when considering only the BCCs.

6.4 Discussion

This chapter has described the application of a fibre-optic coupled time-resolved spectrometer to an *in vivo* investigation of the optical signatures of skin cancer in order to evaluate its potential for use in clinical diagnosis.

The data from the steady state spectrometer developed by the Lund investigators has not been shown in this chapter, but for completeness it should be mentioned that the diffuse reflectance and fluorescence intensity excited at 355 nm, 375 nm and 395 nm were found to be all lower in BCC lesions compared to those of surrounding healthy tissue. These data were in agreement with the observations made by Rajaram [397] and Brancaleon [489].

The data acquired with our instrument (time-resolved spectrometer) show that BCCs exhibit a statistically significant ($p = 0.002$) decrease in their mean fluorescence lifetime relative to neighbouring healthy tissue when excited with 445 nm light (figure 6-10). In addition, the contrast in fluorescence lifetime between healthy and diseased tissue did not vary substantially with emission wavelength (figure 6-7).

The results are also in accordance with previous *ex vivo* measurements made with same system on freshly resected (< 2 hours) NMSC tissue samples [258] and, using the blue excitation source, the absolute values observed *in vivo* are in reasonably good agreement with those seen *ex vivo* for both BCCs and normal skin.

In general, *in vivo* studies of tissue autofluorescence describe reduced fluorescence measured at the tissue surface from cancerous and dysplastic areas compared to normal tissue [275,280,381,397]. Our findings seem in accordance with these studies.

The results are also consistent with prior imaging work using wide field FLIM with 355 nm excitation, where BCCs exhibited shorter mean lifetime values than the surrounding uninvolved skin irrespective of the decay model selected to fit decay data (single vs. stretched exponential) or the long-pass filter used to collect the emitted autofluorescence (375 vs. 455 nm)[270].

Conversely, longer lifetime values for BCC compared to normal skin have been recently reported using TPM at 740 nm excitation *ex vivo* [492]. Additionally, manually segmented BCC cells excited at 760 nm by multispectral multiphoton FLIM tomography were also found to have higher mean fluorescence lifetime values than normal keratinocytes [423].

The main advantage of imaging modalities over point probe spectroscopic measurements is undoubtedly the spatial resolution and the morphological information provided. However, our time-resolved spectrometer has the potential to provide highly accurate combined knowledge of fluorescence emission spectra and fluorescence lifetimes and can provide a convenient and safer route into the clinic for *in vivo* use (a lower total exposure is required compared to equivalent imaging systems).

The time-resolved spectrometer is relatively compact and in the future may be able to be constructed using relatively inexpensive components. The excitation wavelengths used are able to excite a number of tissue fluorophores to generate measurable tissue autofluorescence.

Notably, the instrument described here has been subsequently implemented and adapted for use in hollow organs such as the GI tract and the bladder. The system has been mounted on a small portable optical bench and moved on a compact wheeled trolley. This newly developed version of the spectrometer has been applied to *ex vivo* and *in vivo* fluorescence lifetime measurements of gastrointestinal mucosa during endoscopy. These results will be presented in the next two chapters.

6.5 Conclusions

In summary, the spectrometer described in this study has been shown to provide useful contrast between skin lesions and the neighbouring unaffected tissue, particularly for BCCs.

To the best of our knowledge, this is the first *in vivo* clinical study using a time-resolved fibre-optic spectrofluorometer with dual wavelength laser diode excitation source to investigate the autofluorescence lifetime signatures of skin cancer.

In all the BCCs investigated, with excitation at 445 nm, the fluorescence lifetime was seen to be lower than that of the surrounding healthy tissue and, importantly, in 9 out of 10 cases the decrease in lifetime was greater than the mean intra-patient variation in the measured lifetimes.

Future work in this area should now be driven toward the collection of more *in vivo* data. The collection of more data, and a multicentre extension of this trial, would be desirable to confirm the results obtained on a larger scale, and to investigate more lesion types, such as SCC and melanoma.

Another important aim of the future extension of this study will be to ascertain whether the fluorescence lifetime can be used to differentiate between different lesion types other than between healthy and unhealthy tissue. If the observed trends will be confirmed, the development of wide-field imaging instrumentation could then be guided by the spectroscopic signatures obtained with this instrument.

Chapter 7: Fluorescence lifetime spectroscopy (FLS) of tissue autofluorescence in normal and diseased gastrointestinal tissue measured *ex vivo* using a fibre-optic probe

The work presented in the previous chapter showed that measurements of the fluorescence lifetime emitted from tissue can provide useful information to recognise basal cell carcinomas from normal surrounding skin.

This chapter describes an investigation of temporally and spectrally resolved autofluorescence in 60 GI endoscopic excisional biopsy/resection specimens measured *ex vivo* using a custom built fibre-optic probe. Autofluorescence was quantified immediately following endoscopic biopsy using a fibre-optic-coupled multispectral time-resolved spectrofluorometer with pulsed excitation laser sources operating at two separate excitation wavelengths. The development of the system beyond that used in the previous chapter, the experimental design and protocol, and the procedures adopted to meet safety, disinfection and ethical considerations for use in the hospital setting are also described. The new system was redesigned to make it more compact, portable, and clinically compatible with flexible endoscopes. The software was also simplified to provide easy-to-operate user interface and more intuitive control over all the system.

7.1 Introduction

Neoplasms of the gastrointestinal (GI) tract account for approximately a quarter of worldwide cancer mortality, equivalent to an incidence of about 2 million new cases each year [527,528]. Prevention is based on early detection and excision of premalignant changes (e.g. dysplasia, adenomas) and early stage cancers during endoscopic examination. This significantly increases patient survival while reducing disease progression and direct medical costs [529]. However, early stage lesions are often invisible or difficult to visualise under inspection with white light endoscopy (WLE) alone even for expert endoscopists. In addition, it is often difficult to distinguish between benign and early or pre-malignant lesions, such as between inflammatory disorders and adenomas. Neoplastic polyps are of particular clinical significance because of their established role in the stepwise process that results in colorectal cancer (adenoma-carcinoma sequence) [39]. However, macroscopic discrimination between neoplastic (consisting of adenomas with low grade or high grade dysplasia, and carcinomas) and non-neoplastic (hyperplastic, inflammatory pseudopolyps, hamartomas) polyps during WLE is extremely difficult. Thus, they are all removed when detected. This leads to unnecessary

removal of benign lesions, such as diminutive unimportant polyps, and a considerable number of tissue biopsies, which impose a significant burden on the healthcare system [530] and can be coupled with a low diagnostic yield [243,244]. In addition, removing diminutive polyps is not without some risk, particularly when using polypectomy with cautery, which has repeatedly been shown to be the greatest risk factor for complications such as perforation, bleeding, and post-polypectomy syndrome [531].

Although several adjunct techniques for enhancing contrast have recently become available in the clinical environment, this contrast essentially shows alteration in tissue morphology and architecture, which are unfortunately not always specific and may not reflect (or do so only minimally) the real presence of disease. As a result, despite the use of advanced imaging, in most cases multiple biopsies are still required to confirm or reject the endoscopic diagnosis. In the absence of objective and self-evident findings, the endoscopist has only to rely on his ability, experience, judgement, and a sort of sixth sense.

As discussed in section 2.4, various other optical approaches are being investigated for their potential to provide an *in vivo* label-free "optical biopsy" to aid diagnosis of GI disease, with the ultimate aim of allowing clinicians to avoid multiple unnecessary and/or random biopsies and instead permit targeting of both biopsies and resections. Examples include point probe-based diffuse reflectance spectroscopy [70,71,532], which has been applied to *in vivo* detection of dysplasia in Barrett's oesophagus (BO) [72] and to *ex vivo* surgical specimens of colon cancer [73]. Another example is Raman spectroscopy [203], which has recently been applied in a large study of 305 patients [210]. In this work, it was decided to focus on autofluorescence spectroscopy and lifetime measurements as they can be readily extended from point-based measurements to wide-field imaging once the spectroscopic features presenting the greatest contrast between normal and diseased tissue have been identified.

As discussed in detail in section 3.1.4, tissue autofluorescence arises from intra- and extracellular endogenous fluorophores such as collagen, elastin, pyridine nucleotides and flavins, and the fluorescent signature of these substances – along with their local distributions – have the ability to report on tissue disease state [213]. Further information can be obtained from the fluorescence excitation and emission spectra [213,533] and the fluorescence decay rate (or fluorescence lifetime) [258,265,280,403,534,535].

A number of previous studies have investigated differences in autofluorescence emission spectra between healthy and diseased colonic tissue. Such investigations have demonstrated contrast in a variety of tissue types. For example: between normal tissue and adenomatous (i.e. neoplastic) polyps *ex vivo* [383] [386] [536]; between normal tissue and adenomas *in vivo* [129]; between normal tissue or hyperplastic polyps and adenomas [384]; between

hyperplastic polyps and adenomas [387,388]; and between all three of the above tissue groups [385] [47]. Cancers in the upper GI tract (oesophagus and stomach) have also been investigated [352,371,537].

In addition to measurements of autofluorescence emission spectra, there have also been a number of applications of autofluorescence imaging (AFI) modalities to the study of GI tissue [364,370,390] [356]. AFI has been combined with high-definition video-endoscopy (HDE) [538] and also with NBI in so-called "trimodal imaging", which has been applied to the study of Barrett's neoplasia [357].

Mycek *et al.* [265] performed pioneering work using time-resolved autofluorescence spectroscopy *in vivo* on 24 polyps (13 adenomas, 11 non-adenomas) from 17 patients using an excitation wavelength of 337 nm and detection in the range 530-570 nm. This study demonstrated shorter average lifetimes for pre-neoplastic polyps (adenomas) compared to non-neoplastic polyps (9300 ± 400 ps vs. 10500 ± 700 ps). In work by Li *et al*. in *ex vivo* tissue, longer AF lifetimes were found in cancerous colonic tissues using excitation at 397 nm and detecting at 635 nm compared to normal colon (18,450 vs. 4320 ps). This was attributed to the contribution of protoporphyrin IX (PpIX), which is known to both accumulate in neoplasia and have a long fluorescence lifetime [539]. Pfefer *et al*. [266] used excitation wavelengths of 337 and 400 nm and compared the measurement of fluorescence emission spectra to fluorescence decay profiles acquired at 550 nm *in vivo* in 37 patients undergoing routine endoscopic surveillance for BO. In this study time-resolved fluorescence was unable to achieve sensitivity and specificity values above 60% for discriminating high risk (carcinoma, high grade dysplasia) from low risk (low grade dysplasia, non-dysplastic or indefinite for dysplasia) tissue, whereas moderate overall accuracy was achieved using steady-state fluorescence only.

A small number of studies have applied fluorescence lifetime imaging (FLIM) to the study of GI tissue *ex vivo*. Mizeret *et al*. reported an increased fluorescence lifetime in *ex vivo* human oral carcinoma compared to surrounding uninvolved tissue [65]. This was achieved using a frequency domain technique with 417-nm-excitation and an emission band ranging from 470 nm to 650 nm. Wide-field time-gated FLIM with 355 nm excitation demonstrated a statistically significant increase in the fluorescence lifetime of invasive colonic adenocarcinomas (16 specimens) relative to the surrounding healthy tissue, while a decrease in fluorescence lifetime was observed in two serrated adenomas with focal high grade dysplasia [273].

Despite all of the studies discussed in chapter 3, further research is still required in order to better determine the spectroscopic parameters that will provide the greatest contrast between healthy and diseased GI tissue, in particular for colonic polyps. This is most easily accomplished using point spectroscopy, which discards spatial information and can provide both spectral and

temporal resolution. The resulting data can then be used to guide the development of new autofluorescence based endoscopic devices that aim to rapidly screen large areas of tissue.

The hypothesis was that time-resolved measurements of autofluorescence enable the discrimination of normal and diseased specimens of human GI mucosa.

The aim of this study was to investigate the clinical diagnostic potential of measurements of the fluorescence lifetime and emission spectrum using two separate excitation wavelengths (375 nm and 435 nm) and detection by a time-resolved fluorescence spectrometer in GI tissue that has been freshly biopsied/resected from patients undergoing endoscopy.

7.2 Materials and methods

7.2.1 Patient enrolment

A total of 60 endoscopic samples from different GI sites were collected from 23 patients undergoing GI endoscopy at Charing Cross Hospital, Imperial College Healthcare NHS Trust. Each of these samples was then studied with the point-probe FLS system described below. All samples were submitted for histopathology following the optical measurements. Normal tissue and the following diseases were investigated: colonic polyps, inflammatory bowel disease (IBD), gastric diseases (including cancer, gastritis and polyps) and oesophageal diseases (including reflux oesophagitis and Barrett's oesophagus (BO)).

Patients who participated in the research were recruited by the clinical team and gave their informed consent to participate. The study was carried out with the approval of the National Research Ethics Service (REC reference number 09/H0706/28). In 21 patients who had given their consent to participate in the study, no specimens were taken as there was no indication to biopsy; however, copy of their consent was retained for hospital audit purposes. None of the patients approached for seeking consent refused to participate in the study.

7.2.2 Fluorescence lifetime spectroscopy (FLS) instrumentation

The spectrofluorometer used in this study provided measurements of time-resolved fluorescence spectra (16 spectral detection channels) using two excitation wavelengths. The optical system is similar to that described in section 6.2.1 and references [258,328,403] and is shown in figure 7-1. However, some redesign was needed to make the system more compact and portable, and to ensure full compatibility of the fibre-probe with most endoscopes in terms of length, size, flexibility, and high level disinfectability.

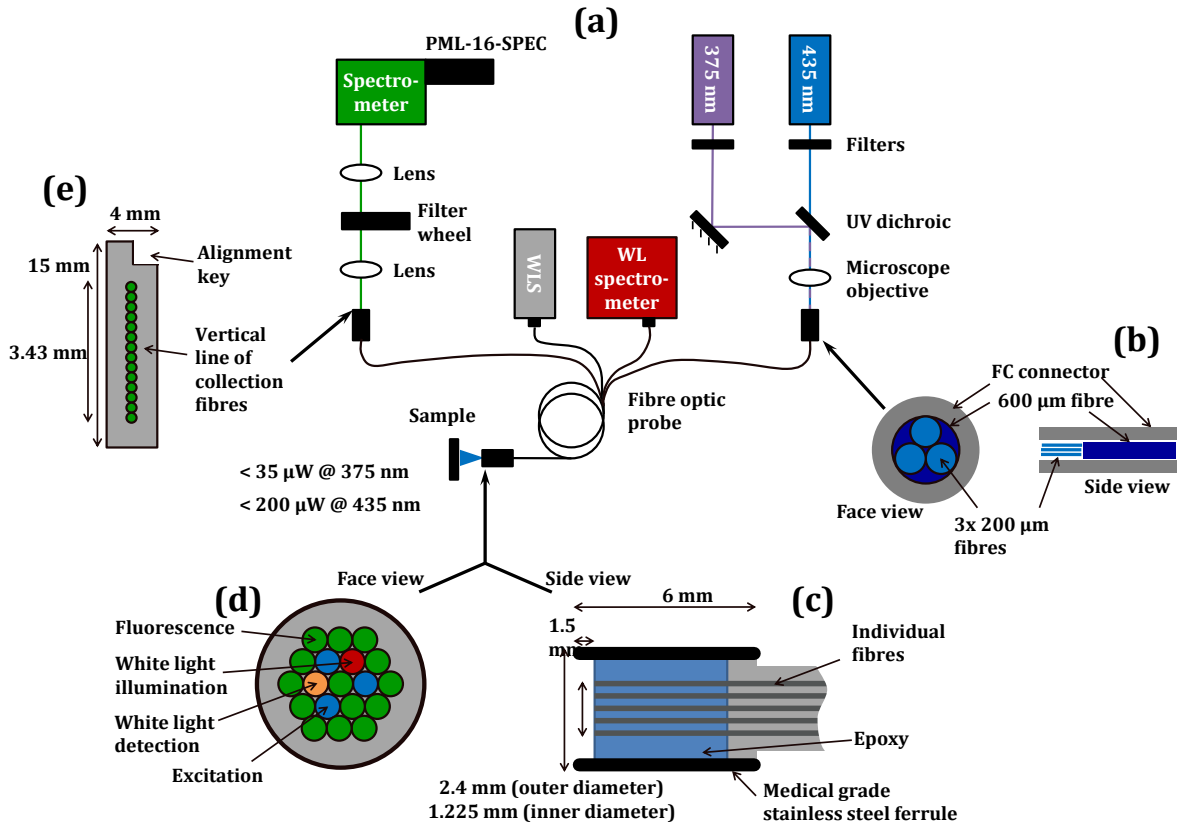


Figure 7-1: (a) Optical configuration of the fibre-optic probe fluorescence lifetime spectroscopy system. Figure (b) shows the proximal end of the excitation branch; figures (c) and (d) respectively show side and face views of the common distal end; and figure (e) shows the proximal end of the fluorescence detection branch. Cores shown in green are fluorescence detection fibres; fibres coloured blue are used to deliver the laser excitation. The red and orange fibres are respectively the delivery and collection cores for the diffuse reflectance measurements; they were unused in this study.

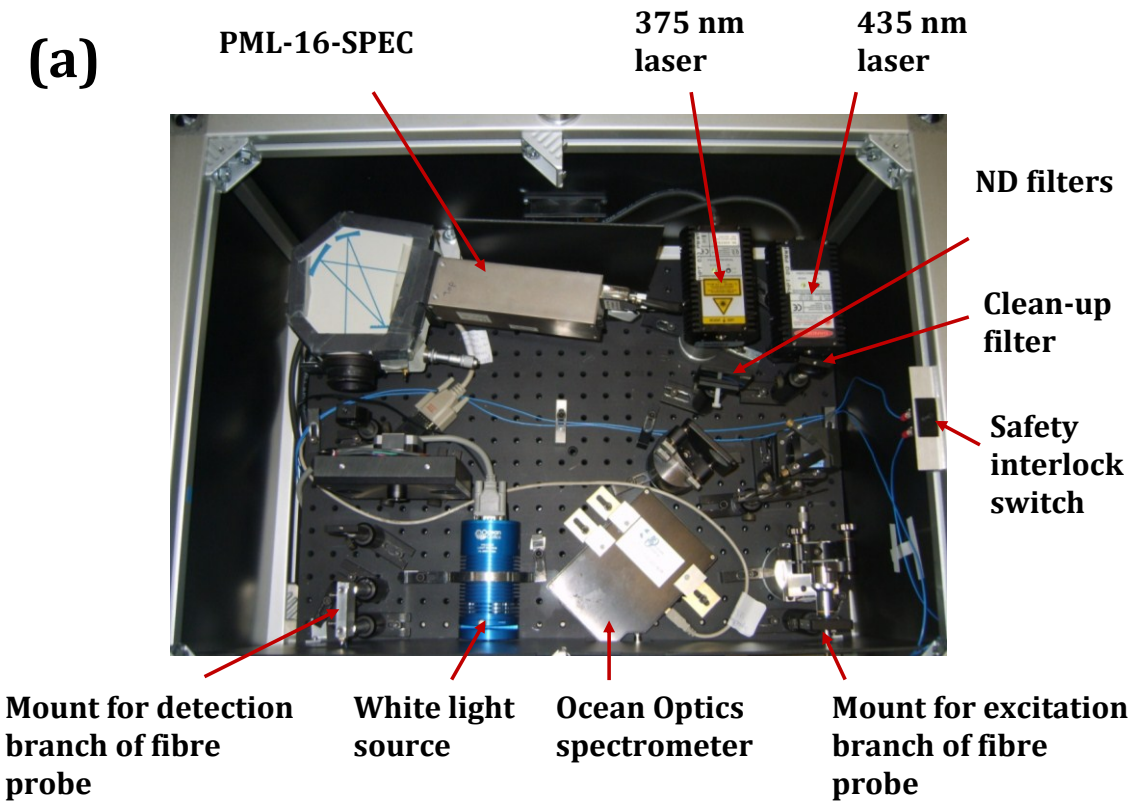
Two pulsed diode lasers were used as excitation sources with central emission wavelengths of 375 nm and 435 nm (LDH-P-C-375B and LDH-P-C-440B respectively, PicoQuant GmbH, Germany). Hereafter, the two laser sources are referred to as the UV and the blue laser.

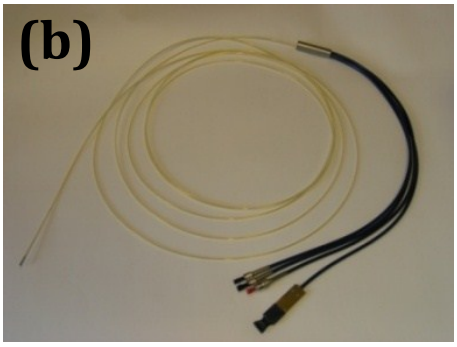
The 375 nm diode laser replaced the previously used frequency tripled Nd fibre laser, which is significantly more compact and stable, making it more suitable for clinical applications. Both lasers emit pulses of 50-150 ps duration and were configured to operate at 20 MHz, The outputs from the two lasers were first combined and are then coupled into the fluorescence excitation channel of a custom-built optical fibre probe (Fibertech GmbH, Germany). This custom fibre probe comprised 19 multimode optical fibres (all of 0.22 NA and 200 µm diameter), of which 3 were used to deliver the laser excitation to the sample and 14 were used to collect the resulting fluorescence. Two fibres in the bundle were reserved for measurements of diffuse reflectance

spectra. However, the sensitivity of the spectrometer was found to be too low to reach the signal available from GI tissue.

The distal branch of the probe (common to all optical fibres) was 3 m in length. The inset (b) in figure 7-1 illustrates the arrangement of the fibres in the excitation branch of the proximal end of the bundle, where the sagittal (side) and the cross sectional (face) view of the probe are shown. At the distal end of the probe the fibres were arranged as shown in the insets (c) and (d) of figure 7-1. The individual fibres are hexagonally packed and secured using epoxy inside a medical grade stainless steel ferrule which is 6 mm long. The ferrule protrudes 1.5 mm beyond the distal face of the fibre bundle and acts as a spacer to ensure that the sample under investigation is always held at a set distance from the output of the fibre probe (figure 7-1 (c)). This results in the excitation lasers illuminating an area of tissue of approximately 0.9 mm^2. In cross section (face view), the fibres are configured as shown in figure 7-1(d) where the excitation fibres are coloured blue, the fluorescence collection fibres are green and the white light illumination and detection fibres are shown in red and orange, respectively. Figure 7-1(e) shows the fluorescence detection branch of the proximal end, where the 14 collection fibres are aligned vertically in order to maximise the coupling into the input slit of the spectrograph.

Figure 7-2 shows a photograph of the optical setup (a) and the fibre-optic probe (b, c).





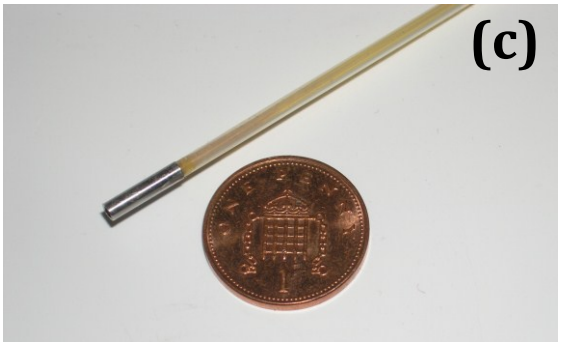


Figure 7-2: **(a) Annotated high angle photograph illustrating the optical arrangement of the time-resolved spectrometer with the lid removed. (b, c) The custom built fibre probe for use in GI endoscopy (Fibertech GmbH, Germany).**

It is worth noting that the fibre probe has been manufactured by Fibertech GmbH (Berlin, Germany), whose main business is the manufacture of clinical fibre optic probes consisting of a single fibre optic cable for laser lithotripsy. Therefore, all of the materials used in the construction of the probe are thoroughly tested for biocompatibility.

A neutral density (ND 0.7) filter was placed in the path of the 375 nm laser in order to limit the average optical power at the sample to 35 µW. A bandpass filter (Z440/20x, Chroma Technology, USA) was used to narrow the spectrum of the 435 nm laser, which provided a maximum average power of 200 µW at the sample.

It should be emphasised that the power was limited in this way to permit *in vivo* use of this system during routine endoscopic examinations - see chapter 8. The use of maximum power levels below those stated above minimises the risk of photodamage as the quoted values are below the maximum permissible exposure (MPE) for skin for exposure times as long as 1000 s (there is no accepted MPE for GI tissue).

The outputs of the two laser sources were controlled via computer and used to illuminate the specimen sequentially. The resulting fluorescence was collected by the 14 fluorescence detection fibres that relayed the collected light to the fluorescence detection arm of the spectrofluorometer (figure 7-1(e)). The output from the collection fibres was imaged onto a 16 channel PMT detector as described in section 6.2.1.

A motorised filter wheel was placed between the fibre probe output and the grating spectrometer. This filter wheel contained two emission filters (E400LPv2 and E475LPv2, Chroma Technology, USA), that were used in combination with the 375 and 435 nm excitation lasers respectively to ensure that no scattered laser radiation reached the PMT detector.

Compared to the study presented in chapter 6, all optical components were mounted on a smaller 30 x 45 cm^2 breadboard, and the breadboard and all electrical components were now housed and enclosed within a compact (182 x 70 x 55 cm^3) wheeled trolley, making clinical measurements within the endoscopy suite possible. The entire system is controlled through software written in LabVIEW 7.1 (National Instruments, USA) meaning that the spectrofluorometer can be used within a clinical environment in a safe and practical manner.

As in the previous study, each measurement consisted of 5 s fluorescence data acquisition with each laser, repeated three times, for a total acquisition time of approximately 30 s. Similarly, two sets of 16 spectrally resolved fluorescence decays (one for each excitation wavelength, with three identical measurements performed in each case) were obtained. In order to analyse the raw fluorescence data it was necessary to determine the wavelength range collected by each PMT element and to determine its relative sensitivity. This was performed in an identical manner to that described in section 6.2.1 and references [258,403].

The computer contains a TCSPC card (SPC-730, Becker-Hickl GmbH, Germany) which is used to control the 16 channel PMT detector and permits the collection of the spectrally-resolved fluorescence decays. The filter wheel is also linked to the computer (using an RS-232 cable) and, thus, the entire system can be controlled through software.

The system (figure 7-3) is fully enclosed using a stainless steel lid and front, back and side panels made from a black, optically absorbent, rigid foam PVC sheet material (Foamalux, Robert Horne Group, UK). It also has a hinged panel (stainless steel) at the front of the optical setup to

allow easy connection and containment of the proximal ends of the fibre probe. This front panel includes a small opening near the centre where the proximal fibres emerge and the fibre probe splitter (the section of the probe in which the individual optical fibres are routed to the appropriate proximal branches) is clamped in place just below this opening. Having the system enclosed in this way means that the optical system is safe for use in a clinic and that the electrical components cannot be accessed. It also permits easy cleaning of the system in the case of any spillage of clinical liquids. The computer also incorporates a medical grade "wipe-clean" keyboard and touchpad, again to allow easy cleaning of all external components.

The panels on the side of the trolley have ventilation holes drilled in to them and two fans are installed on the back. The fans run at all times that the system is turned on and create a constant air flow through the instrument. This air flow acts to cool the interior of the trolley and ensures that no problems arise due to overheating.

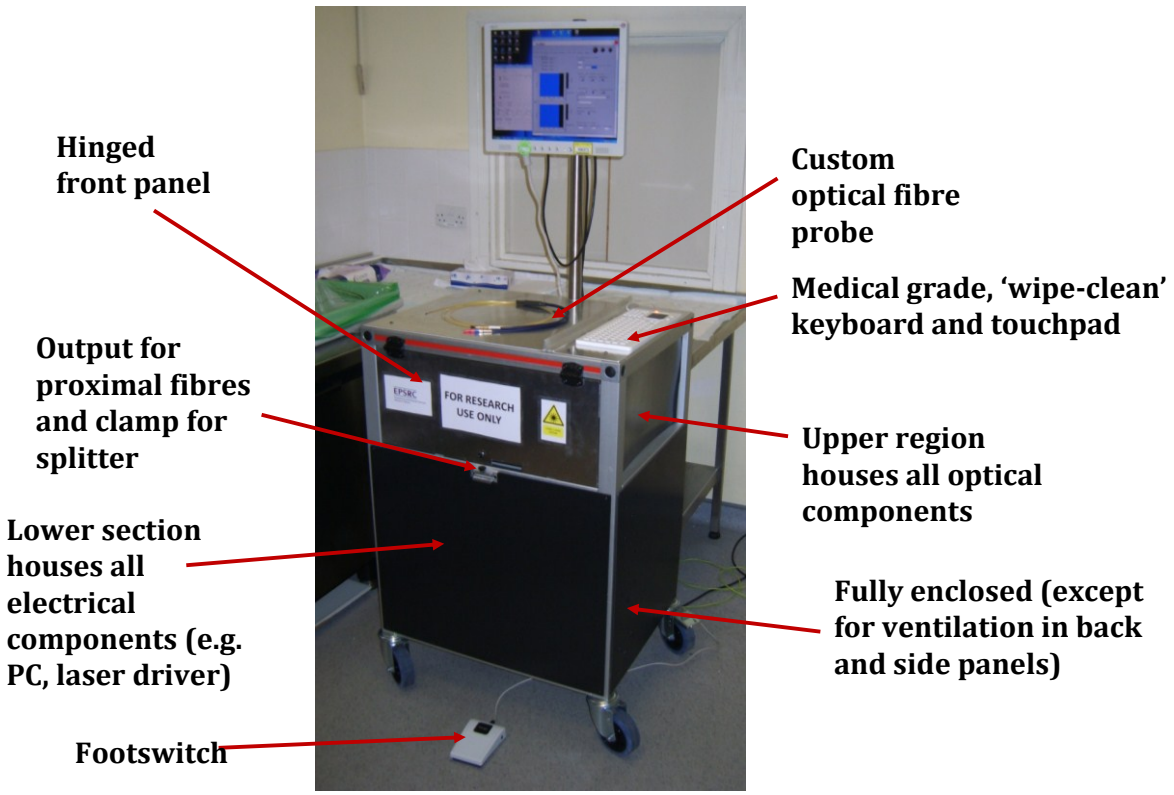


Figure 7-3: Photograph of the transportable trolley which houses the entire spectrometer, showing some important features of the system.

With the optical setup fully enclosed, the only point at which laser radiation is emitted from the system is at the distal end of the fibre probe. As mentioned above, ND filters in the beam paths of the lasers limit the maximum optical power at the distal end of the probe to 35 μW of UV and 200 μW of blue light. Two interlock switches are also located on the trolley to ensure that the lasers cannot be operated when the lid to the optical enclosure is open. Thus, the system as a

whole has been classified as a Class 1 laser product (by Aurora Radiation Protection Services, UK) and, hence, no protective eyewear is required when the system is in normal use.

All electrical elements contained within the trolley are connected to the isolating medical transformer. Hence, the only electrical outlet from the system is the connection of the medical transformer to the mains electricity. This isolating transformer provides an ungrounded "floating" power supply for the system which reduces the leakage current and minimises the risk of electrocution. The medical transformer is connected directly to the mains and, hence, provides power for the entire instrument. There is also an earthing point on the transformer and this is connected to mains earth via an earth bonding cable which provides a low resistance route to ground in the case of any short circuit fault condition. Additionally, a 7 A surge/radio frequency interference (RFI) filter (FA7-RS, RS Components Ltd., UK) is located between the mains power and the medical transformer and this is used to protect all the electrical equipment from the unwanted effects of any power surges.

The computer monitor (also connected to the isolating medical transformer) is mounted on a metal post fixed in place at the back of the trolley. The dimensions of the fully assembled system are as follows: height – 182 cm, width – 70 cm, depth – 55 cm. Thus, the trolley mounted system is relatively compact and can be easily stored, transported and used within a clinical setting.

Control software

The system is controlled exclusively through software. In fact, the powers and repetition rates of the lasers are already set and fixed using the commercial software provided with the laser control unit. Beyond this, the entire system is controlled by software written in-house using LabVIEW 7.1 (National Instruments, USA). This software comprises a single program which regulates the detectors, light sources (using the USB-DAQ device), filter wheel and all acquisition parameters, and a screenshot of the user interface of the software is shown in figure 7-4.

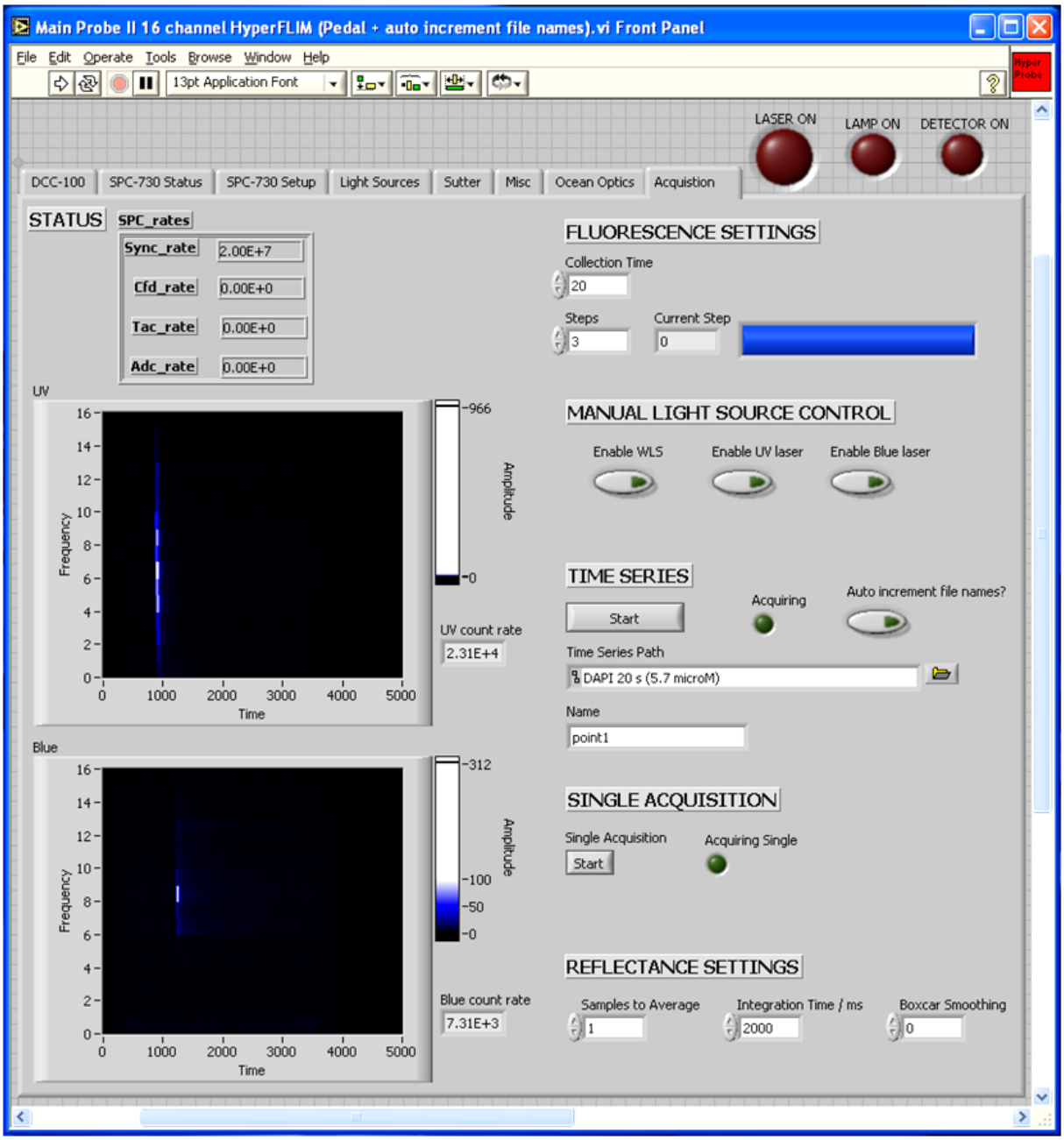


Figure 7-4: Screenshot of the user interface of the LabVIEW software used to control the spectrometer.

The software can be used to control each component in the system individually and also allows the user to automatically acquire data in one of three ways: a single fluorescence acquisition (exciting once with both lasers); a single diffuse reflectance acquisition; or a time series acquisition in which both fluorescence and reflectance data are recorded. In a time series acquisition, time-resolved fluorescence spectra are first recorded using each excitation source in sequence and a chosen number of repeat measurements are made. Secondly, the white light source is used for illumination and a single reflectance spectrum is acquired. In all cases data are recorded as text files showing the fluorescence or reflectance intensity as a function of time and/or wavelength.

A medical grade pedal (Texas Instruments, USA) is connected to the computer (indicated in figure 7-3) and is incorporated into the LabVIEW software. The footswitch is programmed such that depression of the switch creates a new save folder and begins a time series acquisition, saving all data to the newly created folder. This enables a single clinician to operate the system easily while carrying out the endoscopic procedure.

The spectrofluorometer was assembled in the endoscopy unit of Charing Cross Hospital, where it was used to make clinical measurements of human GI tissue *ex vivo* and subsequently *in vivo*. A simple safety instruction document was created for clinical users in order to operate the system safely and effectively. A troubleshooting guide was also prepared to help with software errors or unforeseen technical difficulties.

7.2.3 Experimental procedure

For the *ex vivo* tissue measurements the spectrometer remained in a private lockable room (with black-out curtains) within the endoscopy unit, while endoscopic procedures were carried out in the neighbouring endoscopy suite.

During routine endoscopy, pinch biopsy samples of any suspicious regions of tissue were taken with "jumbo" biopsy forceps (Radial Jaw 3 LC forceps, Boston Scientific, figure 7-5(a)) and any superficial lesions (i.e. polyps) were removed with either a cold or a hot snare (Captivator single-use snares, Boston Scientific, figure 7-5(b)) according to standard patient care. Polyps removed by hot snare polypectomy were sufficiently large that the area measured using the optical system was unaffected by any specimen heating. Samples were 4-15 mm in diameter.

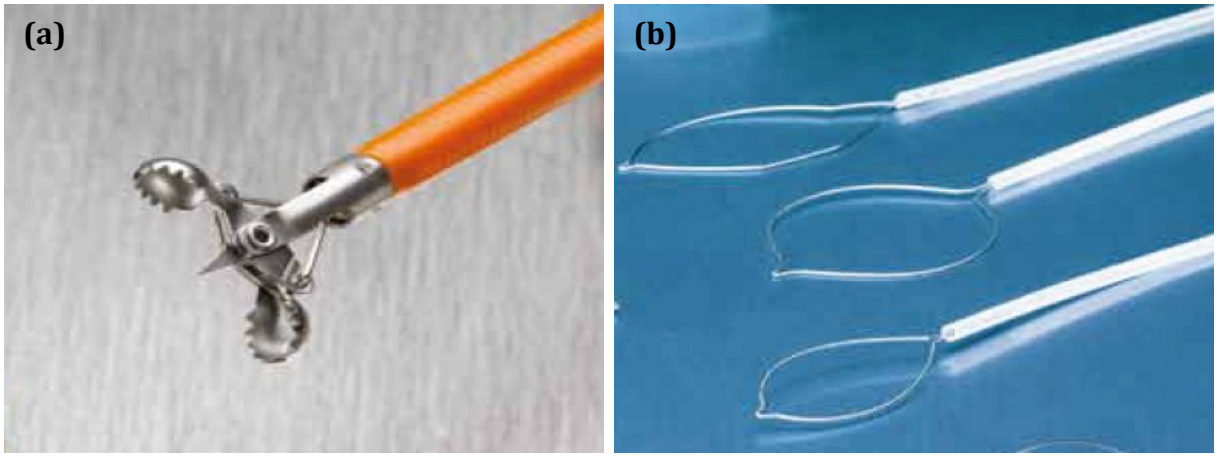


Figure 7-5: (a) Endoscopic biopsy forceps (Radial Jaw 3 LC forceps, Boston Scientific) and (b) polypectomy snares (Captivator single-use snares, Boston Scientific) in use at Charing Cross Hospital. Images adapted and reproduced with permission from [540].

Where clinically possible, at least one biopsy of healthy tissue was also taken from each patient with a suspicious region and the healthy biopsy was taken as close as possible to the suspicious

region. After completion of an endoscopic examination, any tissue samples obtained were immediately delivered to the adjacent spectroscopy room and measured with the FLS system.

All samples were measured within approximately 10 minutes of excision. Once removed, the biopsy samples or excised polyps were carefully teased onto gauze with sterile disposable tweezers, keeping the mucosal surface facing upward.

All samples were washed gently by dripping Hanks' Balanced Salt Solution (HBSS) onto them using a 1 ml syringe (with no needle) and then placed in a plastic culture dish with a glass coverslip base.

The distal tip of the optical fibre probe was then placed *en face* in contact with the sample and data acquisition was performed as described in the previous section. To ensure that the sample was not damaged by mechanical stress and to simulate *in vivo* probing, the distal end of the probe was held by hand, exerting constant gentle pressure throughout the measurements.

To prevent deterioration, samples were kept moist during the measurements and handled minimally. There were no visible changes in the texture or appearance of the samples over the duration of the measurements and the sample thickness always remained consistent (compared to the original condition). Following measurements with the FLS system, all tissue samples were sent for histopathology.

All haematoxylin and eosin (H&E) stained tissue sections were reviewed by an experienced histopathologist (GWS) in order to correlate the histological findings with the fluorescence measurements. Finally, each sample was assigned a unique number for identification purposes and the characteristics of the specimens investigated in this study are summarised in table 4-1.

Tissue type		No. of samples
Endoscopic diagnosis	***Histological diagnosis***	
Colonic polyps	12 tubular adenomas with LGD 2 mixed hyperplastic adenomatous polyp with LGD 2 hyperplastic polyp 1 serrated polyp 3 inflammatory polyp 1 nonspecific reactive changes 1 normal colonic mucosa	22
IBD	1 active chronic inflammation 2 severe chronic ulcerative colitis 2 moderate chronic colitis 1 basal inflammation	6
Gastric disease	1 chronic gastritis *Hp+* 1 chronic gastritis 1 invasive poorly differentiated adenocarcinoma 2 fundic gland polyps	5
Oesophageal disease	1 BO (intestinal metaplasia with no dysplasia) 1 acute reflux oesophagitis	2
Total No. of diseased tissue meas.		35
Normal colon tissue	18 normal colonic mucosa 1 active chronic inflammation	19
Normal stomach tissue	3 normal gastric mucosa 1 invasive poorly differentiated adenocarcinoma	4
Normal oesophageal tissue	2 normal oesophageal mucosa	2
Total No. of normal tissue meas.		25
Total No. of measurements		60

Table 7-1: Summary showing the clinical diagnoses of all the *ex vivo* samples investigated with the endoscopic spectrometer. LGD, low grade dysplasia; IBD, inflammatory bowel disease; *Hp+*, *Helicobacter pylori* positive; BO, Barrett's oesophagus.

7.3 Data analysis

7.3.1 Exponential fitting of fluorescence decays

As discussed in sections 3.1.3 and 6.2.3, a single exponential decay model only provides an accurate description of a fluorescence decay in the case that only a single fluorescent species (with a single radiative decay pathway) is present in the sample being excited. Autofluorescence from biological tissue typically exhibits a complex exponential decay profile as tissue contains several fluorescent species each with a number of possible states (e.g. oxidised/reduced and free/protein bound). Thus, it is appropriate to fit a multi-exponential decay model to the recorded tissue data. As only a limited number of photons are collected in each of the 16 spectral channels, a double exponential model was chosen. Hence, fitting was performed according to equation 6.1.

In order to measure the instrument response function (IRF) in all spectral channels of the 16 channel PMT detector, reflected light IRFs were recorded by placing a diffusely reflecting sample at a short distance (approximately 10 cm) from the distal end of the probe and then adjusting the angle of the grating in the grating spectrometer to direct light onto each PMT element in sequence. This method provides an IRF in all spectral channels, however, it cannot be performed regularly as the calibration of the spectral locations of the 16 PMT elements requires that the grating remains fixed. Thus, this approach relies on the assumption that the IRFs do not vary considerably over time. Additionally, the diffusely reflecting sample was located at a distance from the distal end of the probe and was not in contact with the end of the ferrule as the sample would be in a typical experiment. This introduced a temporal offset between the IRF and the measured data.

To account for the temporal shift of the IRF with respect to the data, the tissue data was therefore fitted with an adjustable temporal offset for each spectral channel.

7.3.2 Fluorescence data analysis

Having fitted the fluorescence decays according to equation 6.1, the mean fluorescence lifetime (τ_{mean}) in each spectral channel was calculated. This was achieved as shown in equation 6.2.

For each tissue type (i.e. different diseases and different regions of healthy tissue), the variation in the mean lifetime was investigated as a function of emission wavelength. In order to summarise the fluorescence lifetime data from each sample in a simple manner, a spectrally averaged fluorescence lifetime was then calculated by averaging the spectrally resolved mean lifetime values and weighting the data according to the fluorescence intensity observed in each channel (see equation 6.3).

For 375 nm excitation, the spectrally averaged mean lifetime was calculated excluding the first and last spectral channels (i.e. over the range 418-582 nm), owing to the weak signal and poor decay fitting in these channels. For 435 nm excitation, the spectrally averaged mean lifetime was calculated over channels 7-15 (481-582 nm) for the same reason. Following the initial analysis, it was observed that the greatest lifetime contrast with 375 nm excitation for IBD was seen in spectral channels 8-13 (494-556 nm) and a 2nd spectrally averaged mean lifetime was therefore calculated over this narrower range.

Finally, for each lesion, the difference between its spectrally averaged mean lifetime and that of a neighbouring healthy tissue sample (excised from the same patient) was calculated (i.e. $\Delta\tau = \tau_{lesion} - \tau_{normal}$) in order to investigate the diagnostic potential of the fluorescence lifetime data. It is noted that this paired analysis of the fluorescence lifetime compensates for inter-patient variation in the fluorescence lifetimes measured for normal tissue.

The spectral properties of the samples were also investigated using fluorescence emission spectra where the area under the fluorescence emission spectrum was normalised to unity. The mean fluorescence emission wavelength was also calculated for each sample and for each excitation wavelength.

Finally, Wilcoxon signed rank tests were performed on all sets of spectrally averaged lifetime or mean emission wavelength shifts in order to investigate whether any statistically significant differences had been observed between healthy and diseased tissue. In all cases, the null hypothesis being tested was simply that the mean shift in the mean emission wavelength or spectrally averaged fluorescence lifetime was equal to zero.

7.4 Results

All analysis was performed based on the histological diagnosis for each sample. Samples were excluded if microscopic analysis revealed normal large bowel mucosa in clinically abnormal samples or histological abnormalities in clinically normal specimens. As only a small number of measurements were made for gastric and oesophageal diseases, the data presented in this section focus solely on the fluorescence measurements performed on normal and diseased colonic specimens, in particular for patients with colonic polyps and IBD.

Normal tissue characterization

In the first part of this study, the measured fluorescence emission spectrum and fluorescence lifetime in histologically normal tissue were investigated, as segmental variations in normal colon morphology from proximal to distal segments – following the sequence caecum, right colon, transverse colon, left colon, rectum (figure 7-6)– are well known [5]. From the caecum to

the rectum there is a gradual significant decrease in the diameter of the crypts, the number of crypts per unit area and the inner intestinal circumference. There is also an increase in thickness of the mucosa from the caecum (0.5 mm) to the rectum (1 mm). Furthermore, crypts are deeper in the rectum and sigmoid colon than they are in the proximal part of the colon. In addition, it must also be considered that patients with IBD have been variably subjected to medical therapy with steroids, immunomodulators, antibiotics and biologics, which might be responsible for further changes in the mucosal layer thickness/permeability across the entire colon compared to that of untreated patients (i.e. those with polyps).

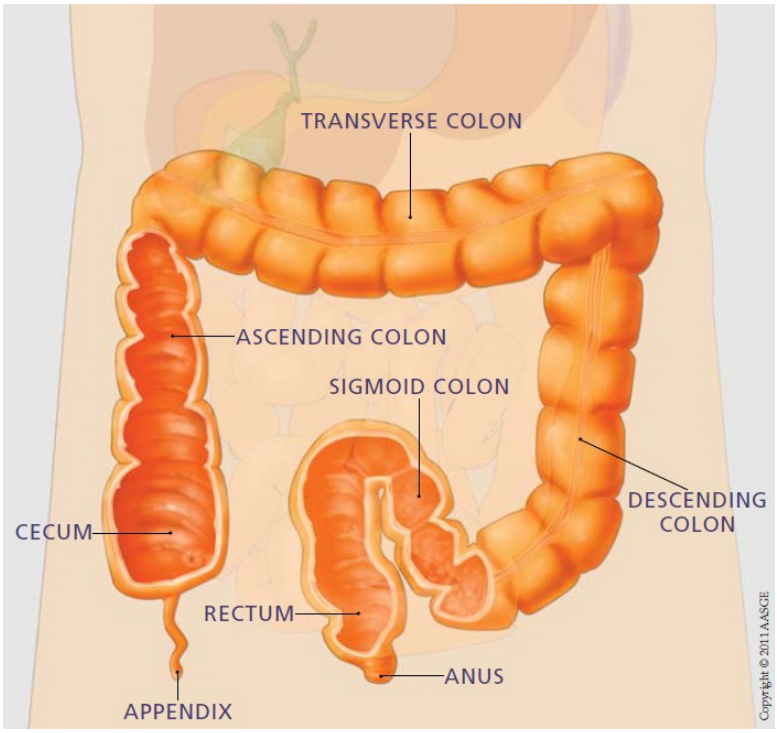


Figure 7-6: Diagram illustrating the different regions of the human colon. Source: American Society for Gastrointestinal Endoscopy (ASGE) Anatomical Images, Colon & Rectum [541].

Figure 7-7(a, b) shows the mean fluorescence emission spectra from histologically normal colon obtained from patients diagnosed with a polyp or IBD. Normal colon from patients with IBD shows a slight shift to shorter emission wavelengths for 375 nm excitation compared to normal colon obtained from patients diagnosed with a polyp. There is also a slight shift to longer emission wavelengths for excitation at 435 nm. However, the change in mean emission wavelength was not found to be statistically significant for either excitation wavelength. The fluorescence lifetime recorded in each spectral channel for normal tissue from patients diagnosed with a polyp and IBD is plotted in figure 7-7(c, d).

For 375 nm excitation, the mean fluorescence lifetime varies slightly with emission wavelength, with a maximum at an emission wavelength of around 500 nm. For 435 nm excitation, the mean fluorescence lifetime is more consistent with emission wavelength.

In order to get a better overview of the fluorescence lifetime, the spectrally averaged fluorescence lifetimes were calculated – see figure 7-7(e) – which shows that there is a higher mean fluorescence lifetime for normal tissue with 435 nm excitation for patients diagnosed with a polyp compared to patients diagnosed with IBD. However, this shift was not found to be statistically significant by two-way ANOVA (normal data was tested according to both diagnosis ($p = 0.11$) and region ($p = 0.30$), null hypothesis that all groups are drawn from populations with the same mean).

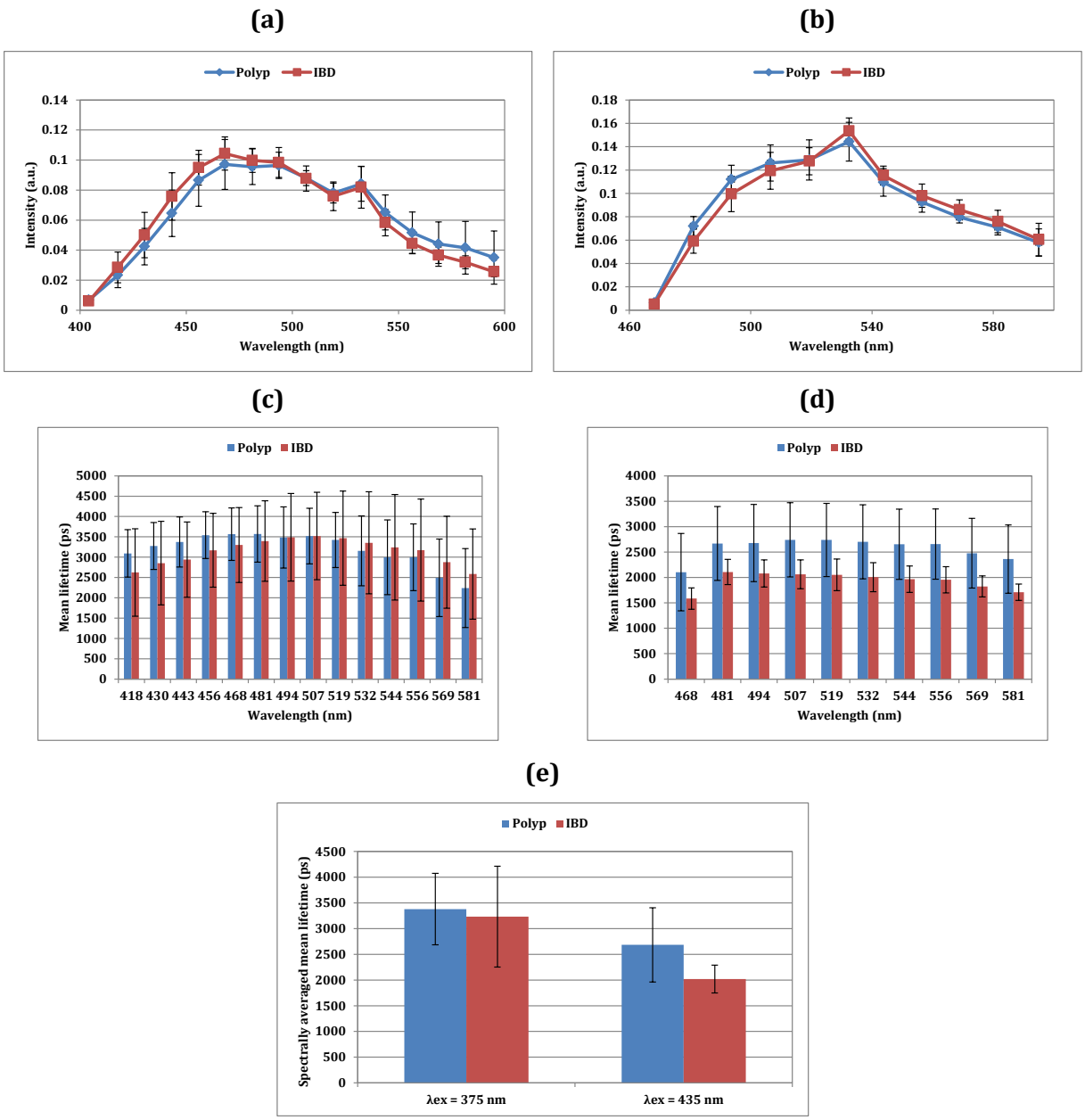


Figure 7-7: Summary of results from normal tissues grouped according to whether the patient was diagnosed with a polyp (*n* = 13) or IBD (*n* = 4). Figures (a) and (b) show the mean fluorescence emission spectra obtained with 375 and 435 nm excitation respectively. Figures (c) and (d) show the spectrally resolved fluorescence lifetimes for 375 and 435 nm excitation respectively. Figure (e) shows the spectrally averaged mean fluorescence lifetimes for both groups and for both excitation wavelengths. The error bars represent ± 1 standard deviation in all panels.

The fluorescence lifetime data from all histologically normal samples were also grouped according to the region of colon from which they were obtained.

Figure 7-8(a, b) shows that there is a slight blue shift in the fluorescence emission spectrum for the two specimens obtained from the rectum for 375 nm excitation, but the shift in mean

emission wavelength was not found to be significant by 2-way ANOVA (grouping data by both diagnosis and region) for either excitation wavelength.

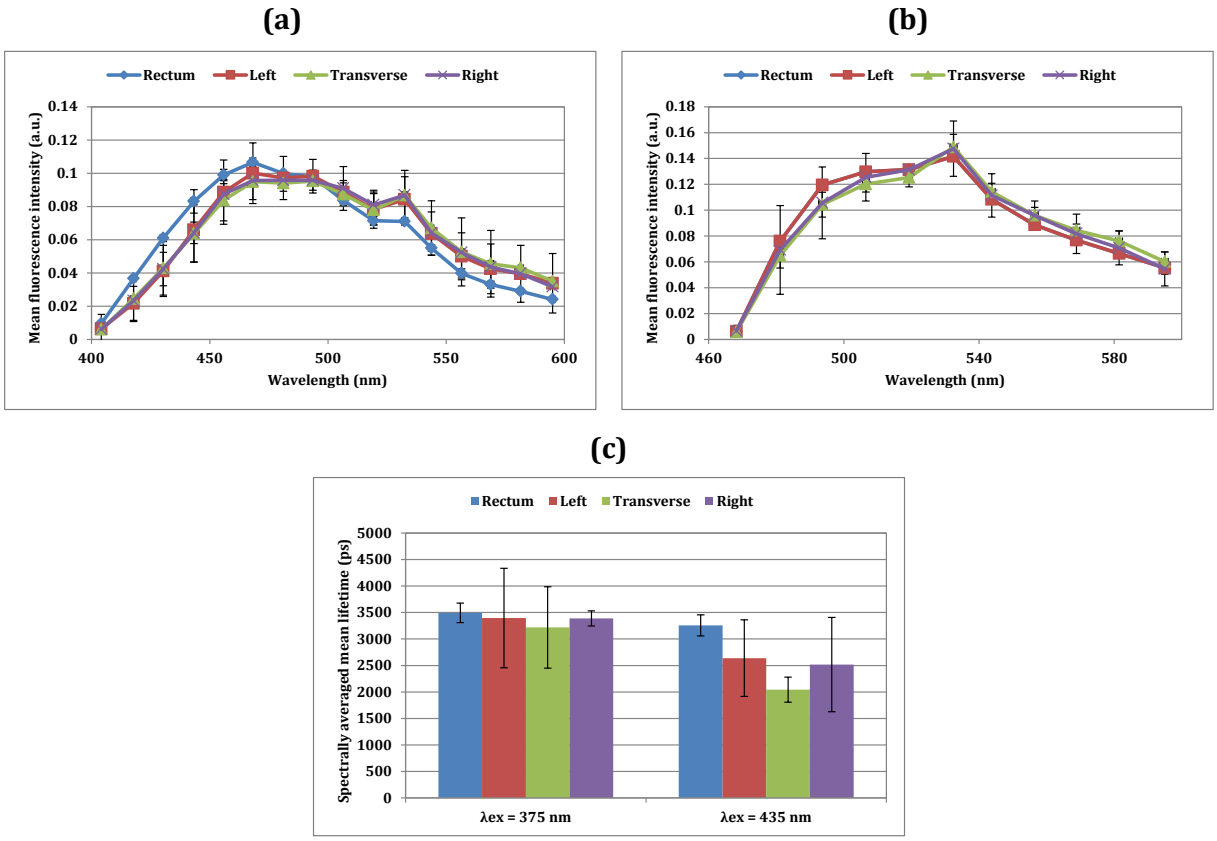
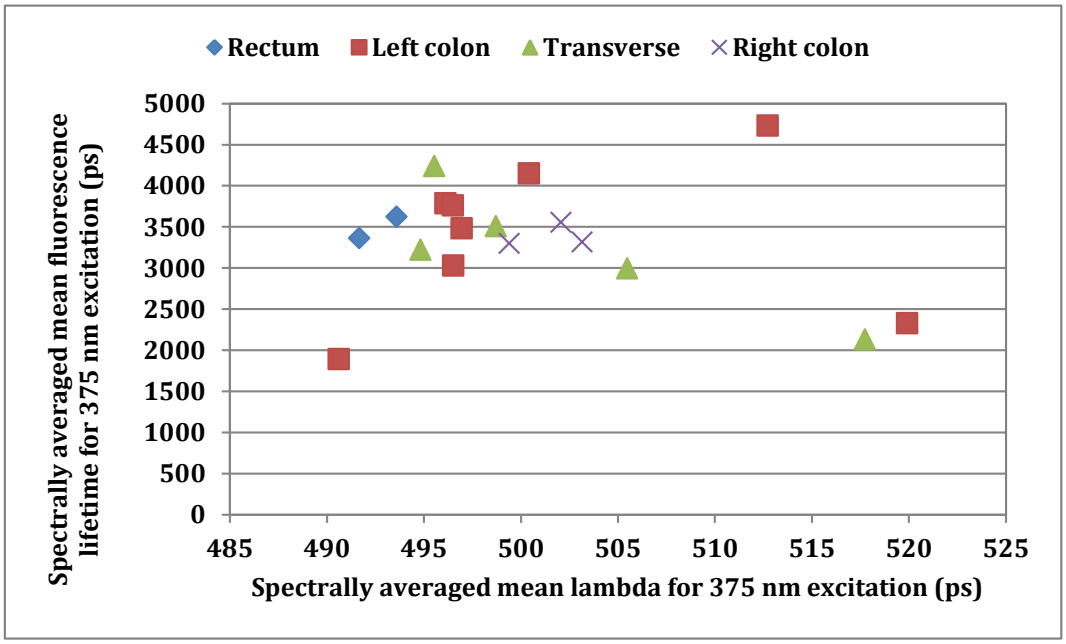


Figure 7-8: Summary of results from normal tissues grouped according to the location that the specimen was taken from. The number of specimens in each group was: rectum (n = 2), left (n = 8), transverse (n = 5), right (n = 3). Figures (a) and (b) show the mean fluorescence emission spectra obtained with 375 and 435 nm excitation respectively. Figure (c) shows the spectrally averaged mean fluorescence lifetimes for all four groups and for both excitation wavelengths. The error bars represent ± 1 standard deviation in all panels.

The mean fluorescence lifetime obtained with 435 nm excitation from the two rectal specimens is longer than that obtained from the other three regions (see figure 7-8(c)). As reported above, a 2-way ANOVA was performed on the spectrally averaged mean fluorescence lifetimes from histologically normal colon grouped according to both diagnosis and region of colon and no statistically significant differences were obtained.

A summary plot of all the normal samples grouped according to their location in the colon for both excitation wavelengths is shown in figure 7-9.

(a)



(b)

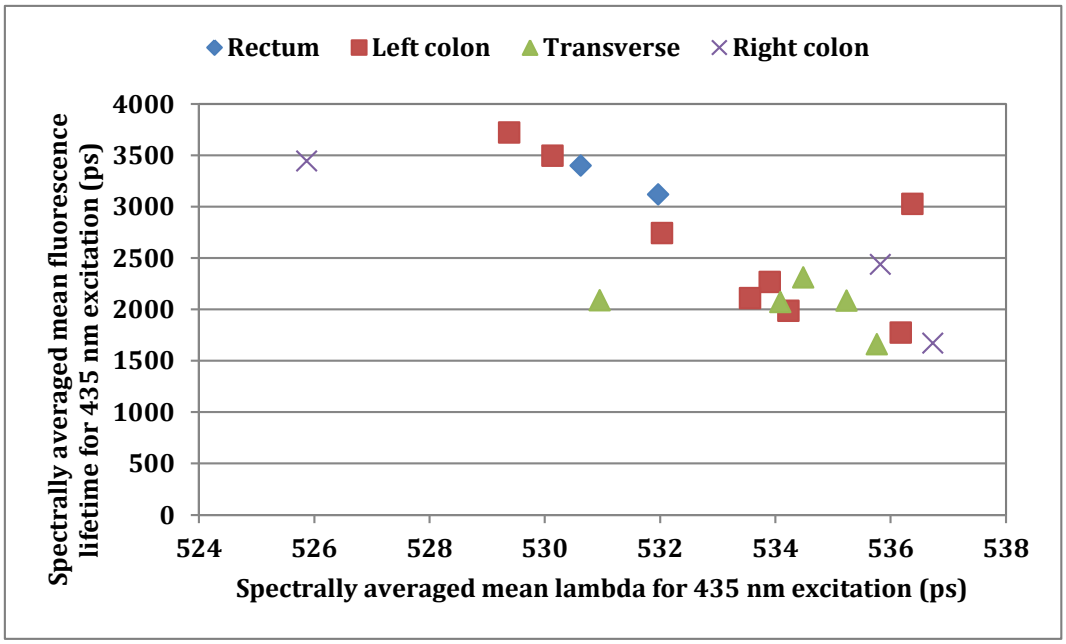


Figure 7-9: Summary of the measured absolute mean fluorescence emission wavelengths and spectrally averaged mean fluorescence lifetimes for all the normal samples divided according to their location in the colon for (a) 375 nm and (b) 435 nm excitation wavelengths.

Diseased vs. normal tissue

Colonic polyps

	Unpaired analysis	Paired analysis
No. of patients	12	11
No. of polyps	21	18
• **Neoplastic**	15	12
• **Non-neoplastic**	6	6
No. of normal specimens	13	12

Table 7-2: Summary of colonic polyps included in study.

Of the 22 clinically identified polyps (see table 4-1), one was excluded as it was found to be normal by histopathology, and the polyp specimens included in the analysis are summarised in table 7-2. Where possible, at least one specimen of normal colon was obtained from all patients.

Figure 7-10(a, b) shows the normalised mean fluorescence spectra observed in normal colon tissue and in neoplastic (tubular adenomas with LGD and mixed hyperplastic adenomatous polyps) and non-neoplastic (hyperplastic and inflammatory) colonic polyps for both excitation wavelengths, and the spectra overlap within the error bars. No statistically significant difference was obtained when comparing the mean fluorescence emission wavelength for either excitation wavelength.

Figure 7-10(c, d) shows the mean fluorescence lifetimes measured in each spectral channel for both 375 and 435 nm excitation. The mean fluorescence lifetimes for neoplastic polyps were shorter than those observed in normal tissue for both excitation wavelengths and this trend was observed in all spectral channels. The spectrally averaged mean fluorescence lifetime (weighted according to the intensity recorded in each spectral channel) for normal tissue, neoplastic and non-neoplastic polyps is shown in figure 7-10(e).

As can be seen from the size of the error bars on fluorescence lifetime measurements in figure 7-10, there is significant inter-patient variability in the measured mean fluorescence lifetime from both normal and diseased specimens. Therefore, in order to overcome this variability a paired analysis was conducted by calculating the difference in spectrally averaged mean fluorescence lifetime between normal and lesional specimens obtained from the same patient. This paired analysis was performed using a total of 30 specimens (see table 7-2). Three polyps obtained from one patient were excluded from the paired analysis as it was not clinically possible to obtain a normal specimen in this patient. In the one patient where two normal

specimens were obtained, the lesional specimens were compared to the anatomically closest normal specimen.

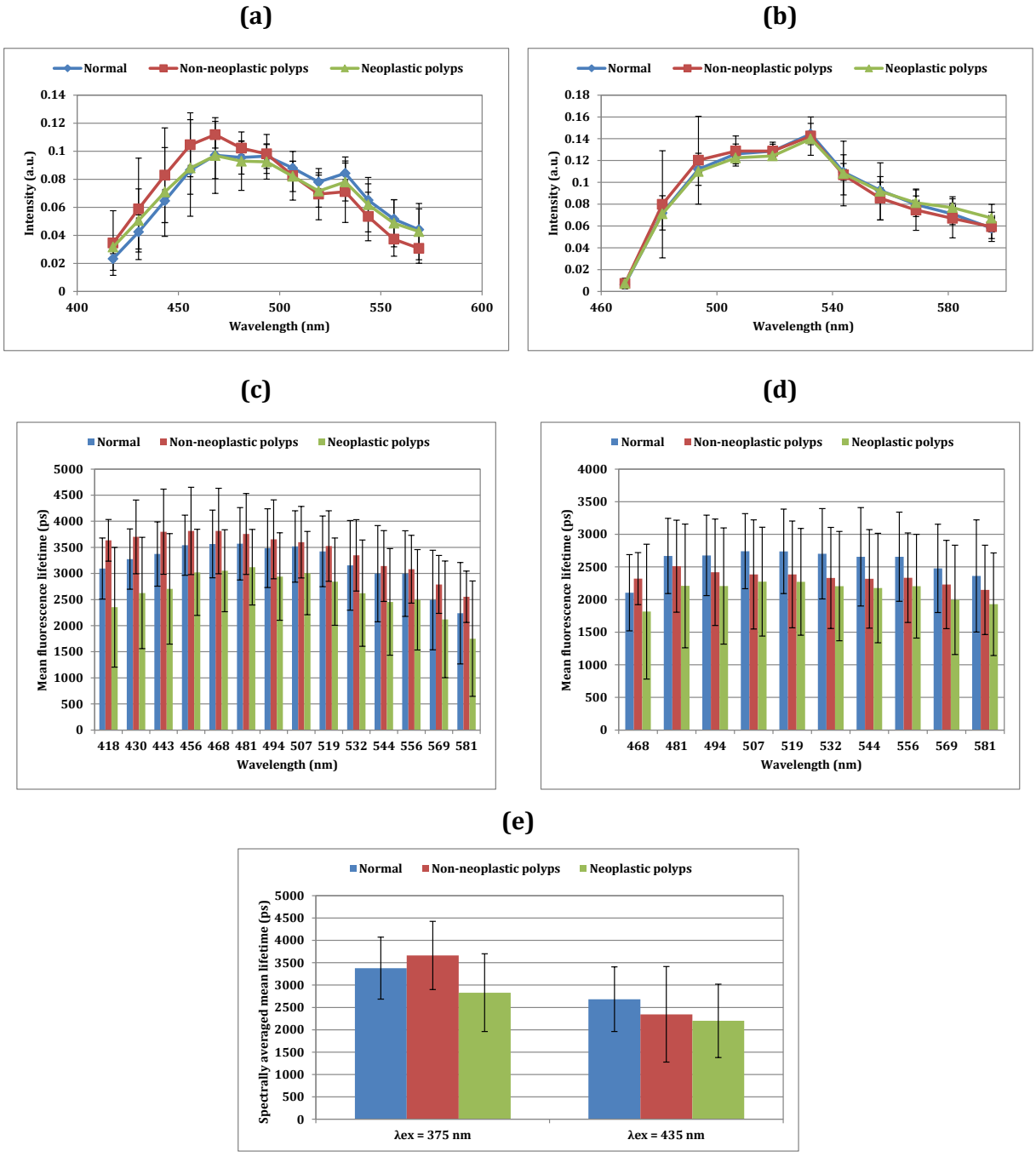


Figure 7-10: Comparison of normal tissue versus neoplastic and non-neoplastic polyp specimens: figures (a) and (b) show the mean fluorescence emission spectra obtained with 375 and 435 nm excitation respectively. Figures (c) and (d) show the spectrally resolved fluorescence lifetimes with 375 and 435 nm excitation respectively. Figure (e) shows the spectrally averaged mean fluorescence lifetimes for all three groups (normal tissues, neoplastic and non-neoplastic polyps) and for both excitation wavelengths. The error bars represent ± 1 standard deviation in all panels.

For each normal-lesion pair, both the shift in mean fluorescence emission wavelength and the shift in spectrally averaged mean fluorescence lifetime were calculated for both excitation wavelengths. The measured shift in mean fluorescence emission wavelength was not found to be statistically significant for either excitation wavelength.

Figure 7-11 shows the shift in the spectrally averaged fluorescence lifetime ($\Delta\tau$) for each normal-lesion pair. The mean values calculated over all pairs for neoplastic and non-neoplastic polyps are summarised in table 7-3.

	Mean shift in spectrally averaged fluorescence lifetime of polyp compared to normal tissue from same or nearest region of colon (ps)	
	UV	Blue
Neoplastic	-230 ± 560	-570 ± 740
Non-neoplastic	25 ± 820	-160 ± 780

Table 7-3: Spectrally averaged fluorescence lifetime shift for neoplastic and non-neoplastic polyps.

A Wilcoxon signed rank test was applied to all sets of paired difference values. The data obtained with 375 nm excitation showed no significant difference while the 435 nm excited data shows a statistically significant decrease in the fluorescence lifetime of neoplastic polyps with respect to healthy tissue (p = 0.021). The difference in spectrally averaged mean lifetime shift between neoplastic and non-neoplastic polyps for 435 nm excitation was not found to be statistically significant (Wilcoxon rank sum test).

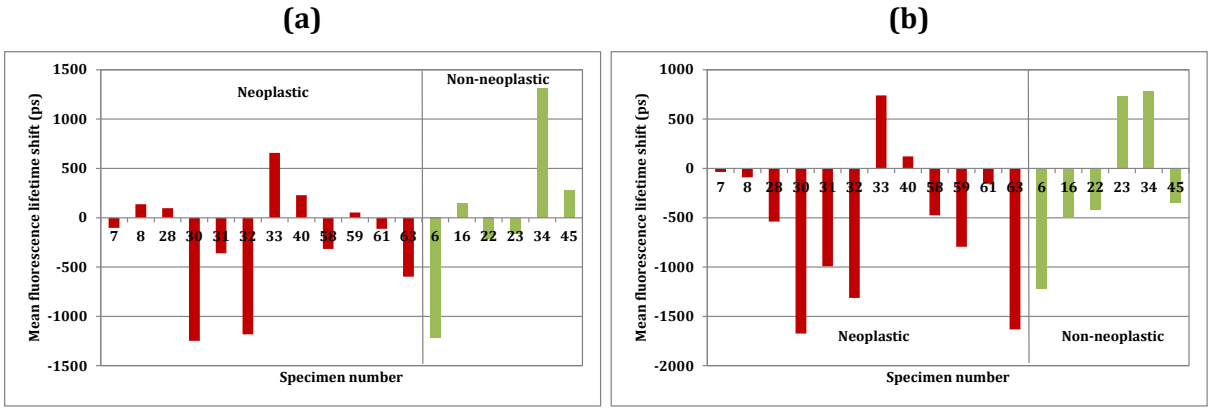


Figure 7-11: Shift in the spectrally averaged mean fluorescence lifetime for (a) 375 nm and (b) 435 nm excitation of neoplastic (red bars) and non-neoplastic (green bars) polyp specimens. Lifetime shifts are calculated using a measurement of normal tissue obtained from the same or nearest region of colon (paired analysis).

Specimen numbers 23, 33 and 34 correspond to patients where the normal sample was not taken from the same region of colon as the polyp. If these specimens are excluded from the analysis then for 435 nm excitation the shift in mean emission wavelength averaged over all specimen pairs becomes 2.6 ± 3.1 nm ($p = 0.019$) and the shift in spectrally averaged mean lifetime averaged over all specimen pairs becomes -690 ± 640 ps ($p = 0.0049$). The increase in mean emission wavelength at this excitation wavelength was found to be correlated with the decrease in fluorescence lifetime ($R^2 = 0.71$), see figure 7-12.

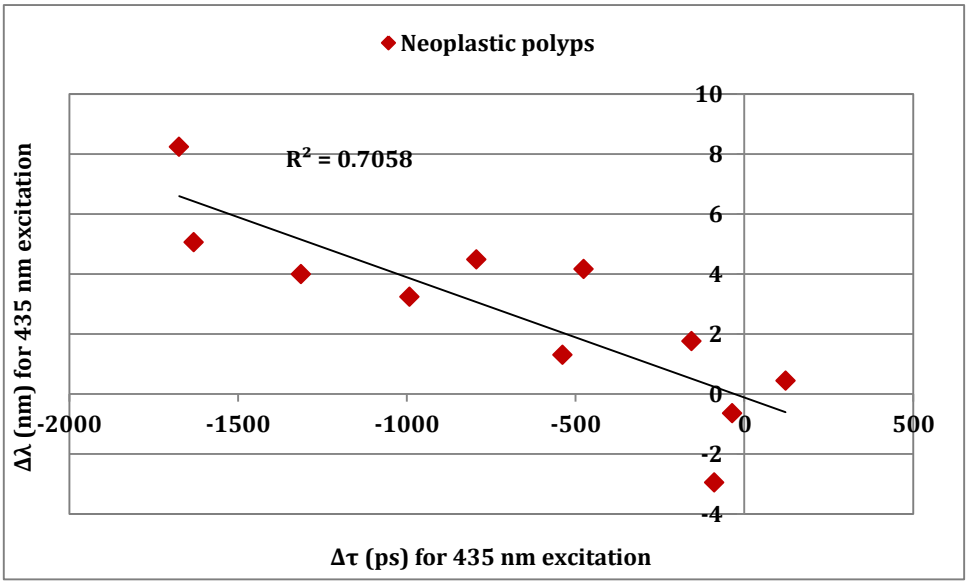


Figure 7-12: Correlation plot of the shift in mean emission wavelength (Δλ) vs. the shift in spectrally averaged mean lifetime averaged over all neoplastic polyp specimen pairs (polyp – normal), where the normal sample was taken from the same region of colon as the polyp, for 435 nm excitation wavelength.

Inflammatory bowel disease

A total of 11 specimens (6 diseased and 5 normal) were measured from 5 patients with IBD. One normal and one IBD specimen (from different patients) were excluded because the histopathological assessment revealed no difference between the normal and the diseased samples. Therefore, the numbers of specimens shown in table 7-4 were analysed.

	Unpaired analysis	Paired analysis
No. of patients	5	3
No. of IBD specimens	5	4
No. of normal specimens	4	3
Total No. of specimens	9	7

Table 7-4: Summary of IBD (inflammatory bowel disease) specimens included in the study, divided by type of analysis performed.

Figure 7-13(a, b) shows the emission spectra obtained for normal and IBD specimens for both excitation wavelengths. For 375 nm excitation, the emission spectrum is shifted to the red for IBD specimens compared to normal, but the shift in mean emission wavelength was not found to be statistically significant ($p = 0.06$). The spectrally resolved mean fluorescence lifetimes are shown in figure 7-13(c, d). With 375 nm excitation the mean fluorescence lifetime observed in IBD was longer than that of normal tissue in all spectral channels and this difference appeared to be greater for longer emission wavelengths. Thus, the spectrally averaged mean fluorescence lifetime was calculated over a reduced spectral emission range of 494-556 nm as this gave the greatest contrast (see figure 7-13(e)).

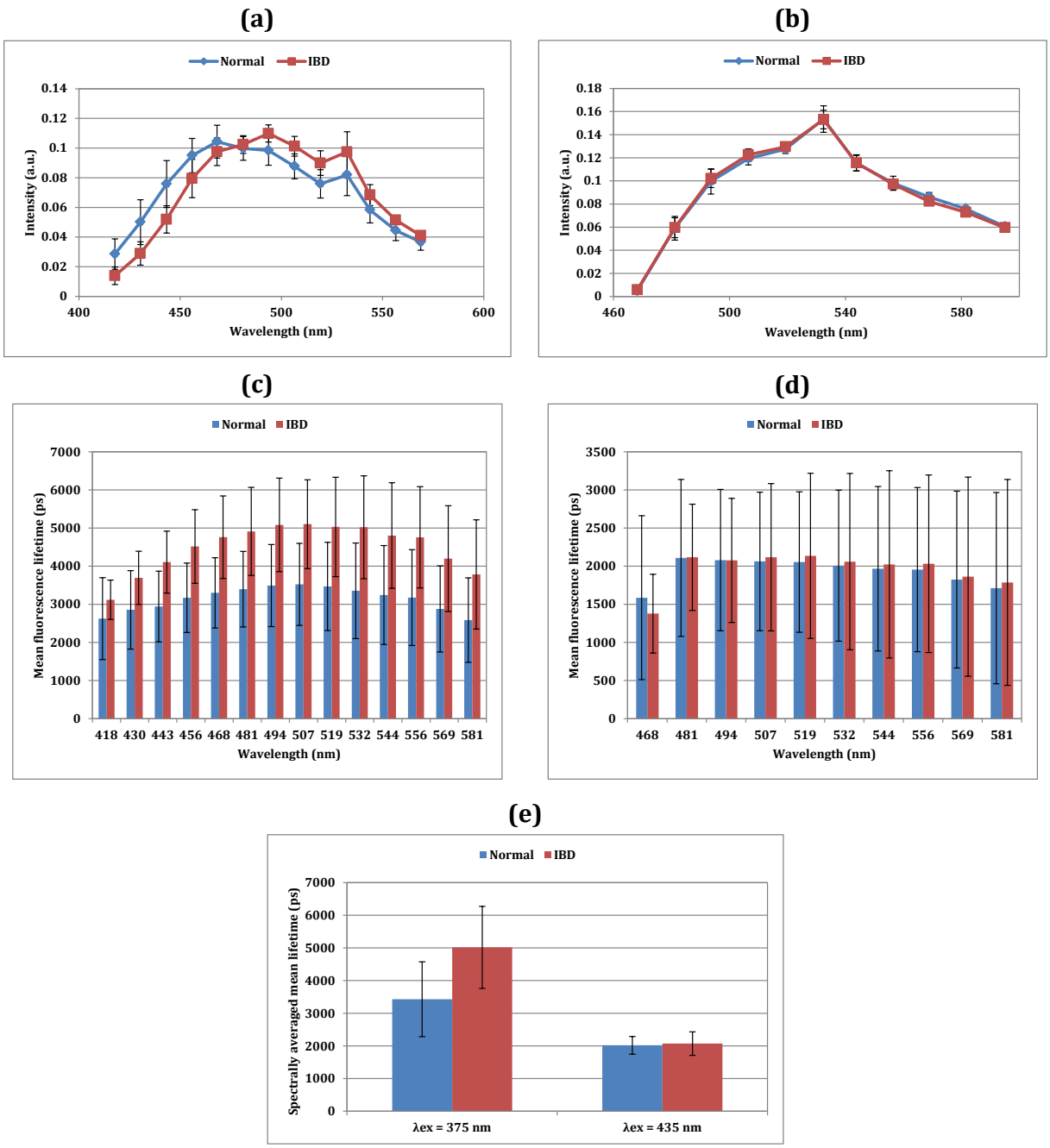


Figure 7-13: Comparison of normal tissue and IBD specimens: figures (a) and (b) show the mean normalised fluorescence emission spectra obtained with 375 nm and 435 nm excitation respectively. Figures (c) and (d) show the spectrally resolved mean fluorescence lifetimes with 375 nm and 435 nm excitation, respectively. Figure (e) shows the mean fluorescence lifetime averaged over the emission spectral range 494-556 nm for both groups and for both excitation wavelengths. The error bars represent ± 1 standard deviation in all panels.

Figure 7-14 shows the shift observed in the spectrally averaged mean fluorescence lifetime for each IBD sample investigated measured with respect to normal tissue obtained from the same patient (paired analysis). With 375 nm excitation, the fluorescence lifetimes of all four IBD samples are longer than those of the nearby normal colon tissue (mean $\Delta\tau = 983 \pm 289$ ps) but

this shift was not found to be statistically significant using the Wilcoxon signed rank test (p = 0.125).

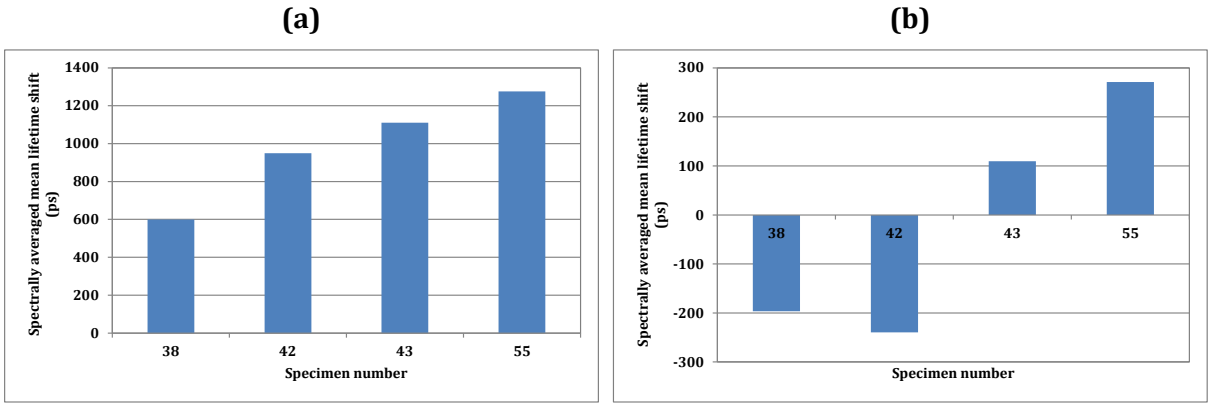


Figure 7-14: Bar graphs showing the shift in the spectrally averaged mean fluorescence lifetime observed in all IBD samples relative to a sample of healthy tissue from the same patient. (a, b) show lifetime shifts obtained with 375 nm and 435 nm excitation respectively. The lifetime shift for 375 nm excitation was obtained using the spectrally averaged mean lifetime calculated over the emission spectral range 494-556 nm.

The paired shift in mean fluorescence emission wavelength between IBD and healthy tissue (mean $\Delta\lambda = 6.9 \pm 6.6$ nm, $p = 0.25$) was investigated, which was also not statistically significant. The lack of statistical significance is due to the relatively large standard deviations on the spectral and lifetime shifts and the small number of measurements made for this disease type. Further measurements would be needed to establish if the trends observed are significant. It is also worth noting that the shifts in the mean fluorescence emission wavelength and the spectrally averaged mean fluorescence lifetime were correlated ($R^2 = 0.90$), see figure 7-15. Additionally, the relative error for the mean shift in spectrally averaged mean lifetime was a factor of 3.4 times smaller than the relative error for the mean shift in mean emission wavelength.

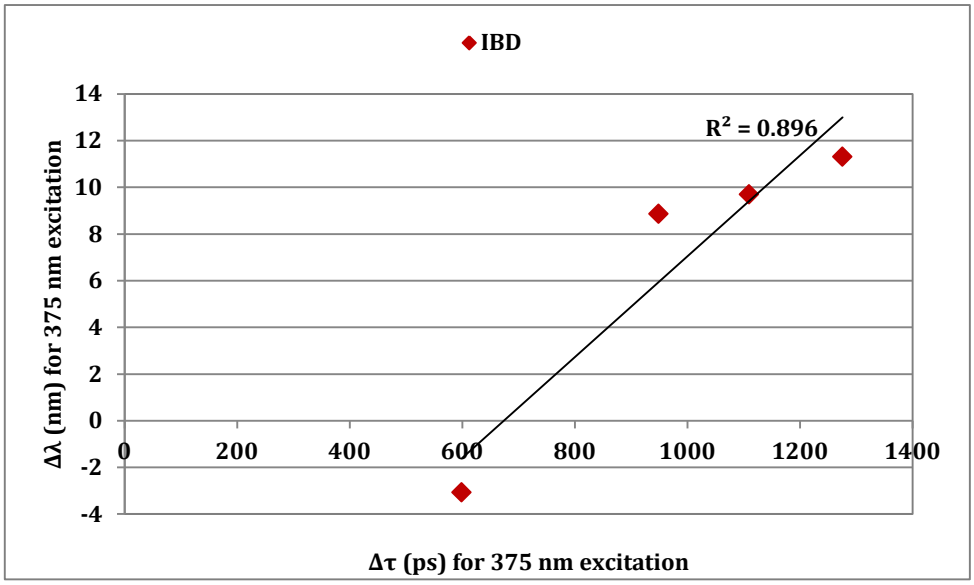
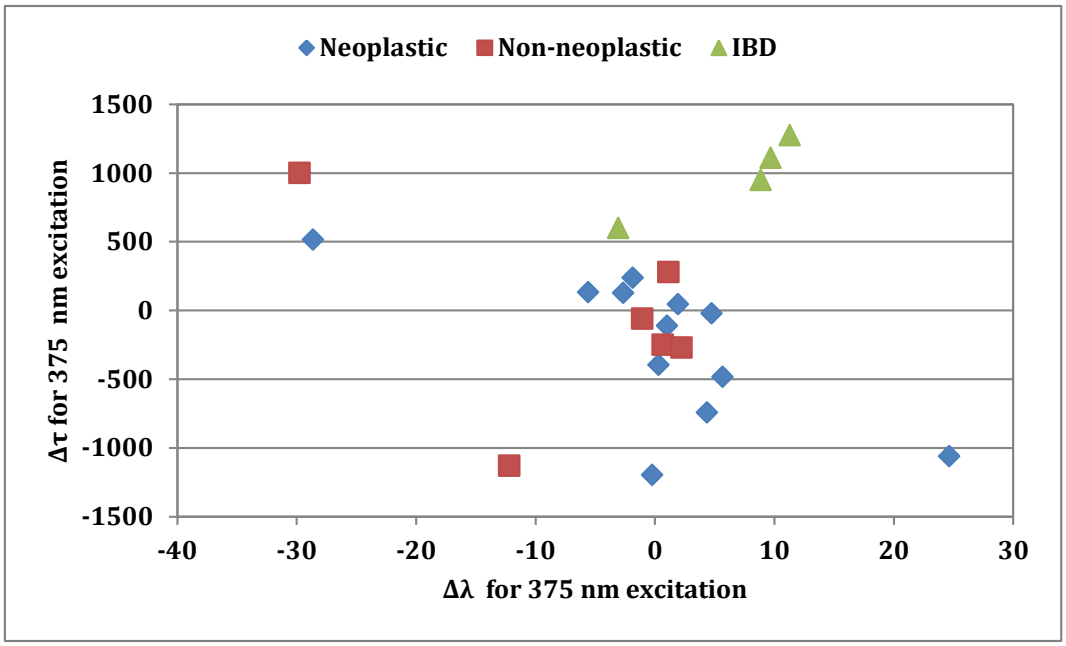


Figure 7-15: Correlation plots of the shift in mean emission wavelength (Δλ) vs. the shift in spectrally averaged mean lifetime averaged over all IBD specimen pairs (IBD – normal) for 375 nm excitation wavelength.

Figure 7-16 shows summary plots of all paired measurements of shift in mean fluorescence lifetime against shift in mean emission wavelength for both excitation wavelengths. Figure 7-16(a) shows a summary plot of all paired measurements of shifts in mean emission wavelength and spectrally averaged mean fluorescence lifetime for 375 nm excitation wavelength. Paired measurements between two regions of normal tissue would be expected to cluster around the origin. However, it was not possible to obtain such specimens in this study and it was therefore not possible to compare the distribution of normal-normal tissue measurements with those obtained from normal-diseased tissue. Figure 7-16(b) shows the equivalent plot for the shift in mean emission wavelength and fluorescence lifetime where the shift in 435 nm excited mean fluorescence emission wavelength is plotted on the horizontal axis and the shift in 435 nm excited spectrally averaged mean fluorescence lifetime is shown on the vertical axis. Polyp specimens tend to show a decrease in the 435 nm excited spectrally averaged fluorescence lifetime and IBD specimens show an increase in the 375 nm excited spectrally averaged fluorescence lifetime as already discussed in the figures above.

(a)



(b)

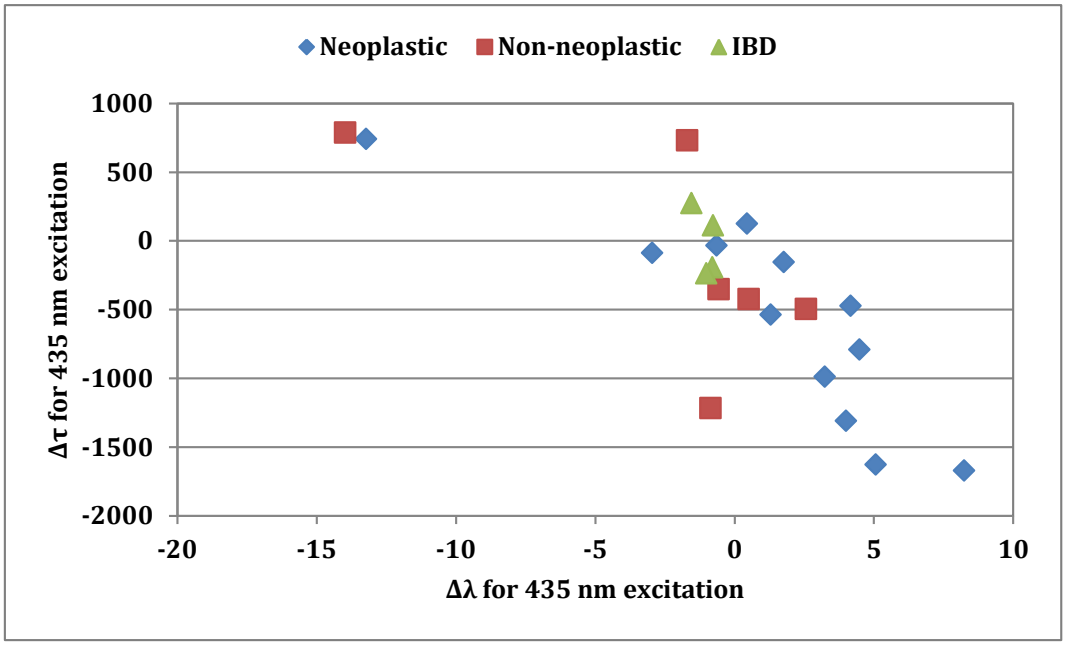


Figure 7-16: **Summary of all measured shifts in mean fluorescence emission wavelength and spectrally averaged mean fluorescence lifetime for (a) 375 nm and (b) 435 nm excitation wavelengths. The lifetime shift for 375 nm excitation was obtained using the spectrally averaged mean lifetime calculated over the emission spectral range 494-556 nm for all points.**

Figure 7-17 shows summary plots of all measured absolute mean emission wavelengths and mean fluorescence lifetimes divided by tissue type (normal colon, neoplastic polyps, non-neoplastic polyps, and IBD) for both excitation wavelengths.

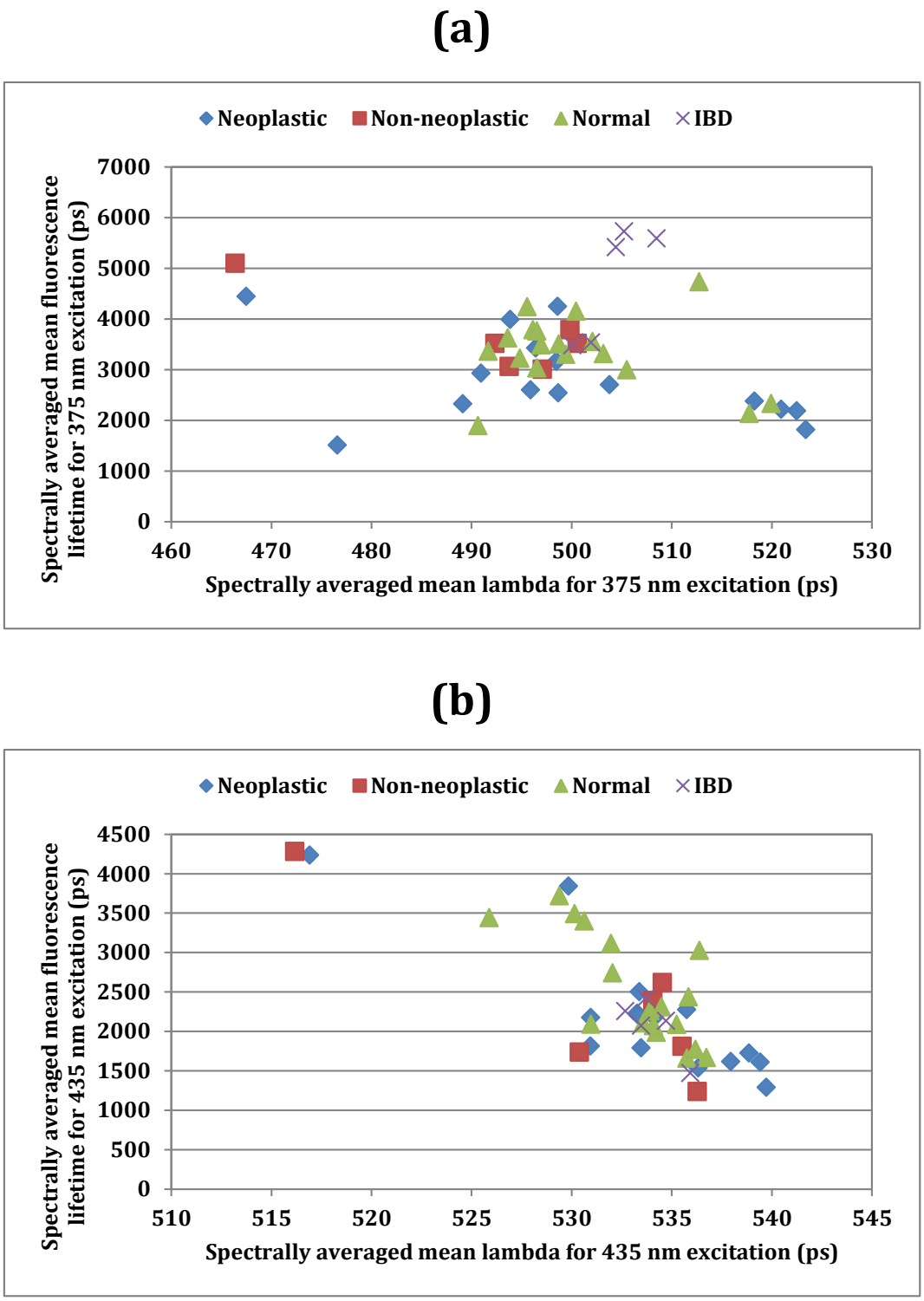


Figure 7-17: Summary of all measured absolute mean fluorescence emission wavelengths and spectrally averaged mean fluorescence lifetimes for (a) 375 nm and (b) 435 nm excitation wavelengths.

7.5 Discussion

In this study, no statistically significant variation was found in mean fluorescence emission wavelength or spectrally averaged mean fluorescence lifetime for normal colon according to type of disease (polyp or IBD) or region of the colon for either of the excitation wavelengths employed. Based on the known variations in these tissues (see text at beginning of results section), significant variation in contrast between regions of colon would have been expected. However, the number of specimens in each group was relatively small and a study on a larger number of specimens would be needed to investigate this further.

For 375 nm excitation the dominant tissue fluorophores within the mucosa are expected to be collagen types I-IV and intracellular NAD(P)H. Collagen type IV is primarily found in the linings surrounding the colonic crypts (basal membranes), whereas collagen types I-III are predominant in the stroma of the lamina propria [7,313]. Collagen fluorescence is particularly complex and a range of values are reported in the literature, e.g. [302,437], and recent measurements of type II collagen obtained with an instrument similar to that used here showed a peak emission wavelength of 390-430 nm and a mean fluorescence lifetime of approximately 10 ns for excitation at 355 nm [329]. NADH has a peak emission wavelength of 460 nm and a mean fluorescence lifetime of 440 ps in its free state [425] and longer decay components typically in the range ~2-2.5 ns when protein bound [542]. These results show a peak fluorescence emission wavelength of 470 nm that is broadly consistent with the fluorescent signal being a combination of collagen and NAD(P)H fluorescence. The fluorescence lifetime measured in this study in the range 3-3.5 ns is also broadly consistent with a combination of the longer decay components found for collagen and those of free and protein-bound NAD(P)H.

In IBD the intestine is chronically infiltrated by inflammatory cells and in the presence of active disease the epithelium can be severely damaged and frayed (goblet cell depletion), leaving large exposed areas of underlying connective tissue. This would be expected to increase the contribution of mucosal collagen fluorescence measured by the fibre-probe for excitation at 375 nm and therefore to produce a corresponding increase in the mean fluorescence lifetime (due to the longer mean fluorescence lifetime of collagen compared to NAD(P)H). An increase in the mean fluorescence lifetime was observed for IBD, see figure 7-13(e), although this was not found to be statistically significant. However, an increase in the contribution of collagen fluorescence to the signal might also be expected to decrease the mean fluorescence emission wavelength but instead an increase was observed (although again not statistically significant).

For 435 nm excitation the dominant fluorescence signal is expected to be due to intracellular flavins within the mucosa with perhaps some additional signal from mucosal collagen, which can be excited at this wavelength [309]. The fluorescence emission spectra peak measured in

this study at ~530 nm is broadly consistent with the emission spectra of flavins [436] and collagen [309]. In a paired analysis of normal and lesional specimens obtained from the same region of colon, it was found that 435-nm-excitation of colonic polyps provides statistically significant differences in both the mean fluorescence emission wavelength (longer) and spectrally averaged mean fluorescence lifetime (shorter) compared to healthy tissue. This shift in mean emission wavelength was found to be correlated ($R^2 = 0.71$) with the shift in mean fluorescence lifetime and the relative error on the mean shift in spectrally averaged mean fluorescence lifetime was lower than that for the shift in mean emission spectrum. The changes in fluorescence emission spectrum and lifetime might be explained by changes in the ratio of free:protein-bound flavin fluorescence [278,295] or by changes in the ratio of intracellular flavin fluorescence to collagen fluorescence.

There are relatively few reports of autofluorescence lifetime (AFL) studies to date. Only one study – by Mycek *et al*. [265] – has investigated single point measurements of AFL on colonic polyps at 337 nm excitation. This was the first study in the human colon that demonstrated differences in fluorescence lifetime decay between normal and dysplastic tissue. However, the study was mainly carried out to assess the ability of time-resolved AF spectroscopy in distinguishing between adenomatous and non-adenomatous polyps and no measurements were obtained from normal tissue. Nevertheless, adenomas showed faster average decays than those of non-adenomas (9300 ± 400 ps vs. 10500 ± 700 ps), where non-adenomas comprised 6 hyperplastic polyps, 3 mucosal prolapses, 1 lymphoid aggregate, and 1 aberrant crypt focus. In the study presented here, no statistically significant differences in the spectrally averaged lifetime between neoplastic and non-neoplastic polyps were found for either excitation wavelength. The shorter excitation wavelength (337 nm) used by Mycek *et al.* may explain differences between their work and that presented here.

7.6 Conclusions

Overall, these results suggest that it may be possible to discriminate polyps from normal tissue and IBD using 435 nm excited fluorescence lifetime measurements and IBD from normal tissue and polyps using the fluorescence lifetime measured with 375 nm excitation but more extensive work is required to confirm the observations made so far and to allow the investigation of additional disease types. While further research is certainly required, these results suggest that the combination of 375 nm and 435 nm excited fluorescence measurements might provide physicians with valuable information on whether the nature of a lesion is proliferative or inflamed during endoscopic procedures. In the future, this work will be extended to *in vivo* measurements and to wide-field FLIM endoscopy.

Chapter 8: Endoscopic fluorescence lifetime spectroscopy (FLS) of gastrointestinal disease: a translational investigation conducted *in vivo* during routine endoscopy

This chapter presents the application of the system described in chapter 7 to an *in vivo* "bench to bedside" translational investigation. A feasibility trial was conducted at Charing Cross Hospital in a cohort of 17 patients clinically referred for endoscopic investigation for a variety of indications. The aim of this study was to investigate the clinical diagnostic potential of measurements of the fluorescence lifetime and emission spectrum in vivo in patients undergoing endoscopy, and to further test the hypothesis that fluorescence lifetime measurements can generate contrast between different tissue types. Indeed, the system was easily operated by the clinical investigators and integrated into the clinical process without interfering with service provision and delivery.

However, *in vivo* measurements of fluorescence lifetime are challenging. A number of changes would be expected to vary between *ex vivo* ad *in vivo* measurements that could alter the tissue AF and fluorescence lifetime detected. These include: a) greater haemoglobin content and higher tissue oxygenation, altering the absorption properties of the tissue; b) changes in the metabolic state of cells (e.g. intracellular NADH and flavin concentrations; c) tissue pH; d) relative motion of the measured tissue with respect to the probe and movement artifacts (e.g. diaphragmatic motion, vascular pulsation, probe slipping, etc.).

The initial data indicates that blue excitation of autofluorescence provides contrast broadly consistent with *ex vivo* measurements, although a study on a greater number of patients is clearly required. This study does demonstrate, however, that such *in vivo* measurements are practical. The experimental design and protocol along with the procedures adopted to meet safety, disinfection and ethical considerations for *in situ* clinical use are described before data are presented.

8.1 Introduction

Over the last ten years, fluorescence lifetime imaging (FLIM) and spectroscopy (FLS) have developed from techniques only available to leading instrumentation research laboratories into techniques that carry the potential to be commonly applied to study biological tissue and cellular interactions. Such a possibility has arisen because of the functional information that

becomes available when detecting the lifetime of fluorophores, partly due to the sensitivity of fluorescence lifetime to the local environment of the fluorescent molecules [543].

As discussed in the previous chapters, FLS has been used to detect changes in tissue state caused by diseases such as cancer [273], atheroma [327,544,545] and osteoarticular arthritis [328,546]. This is due to the fluorescence lifetime signature of endogenous fluorophores such as collagen, elastic, NADH, FAD and porphyrins. It is also possible to use exogenous probes to distinguish disease states, which holds promise for minimally invasive tissue analysis. Whilst there have previously been a few demonstrations of fluorescence lifetime imaging and spectroscopy used in endoscopy, the technique has not been developed into a clinically viable system.

The virtues of a non-invasive method of optical biopsy have been already extolled in section 7.1. However, it is important to reiterate that the inability to distinguish benign or malignant tissue during endoscopic examination inevitably leads to unnecessary biopsies and repeat endoscopies, radiological imaging and treatments. There is an urgent need to improve diagnostic endoscopic imaging capabilities. It is therefore vital to evaluate new approaches to *in situ* optical diagnosis that would allow a legitimate focusing of the increasingly limited resources only on those that require preventative intervention.

Fluorescence lifetime (FL) contrast could be used as a biomarker of tissue abnormalities for *in vivo* endoscopic applications [213,258,265,280,403,534,535] but, to date, we are aware of only a few reports of time-resolved spectroscopy and imaging applied *in vivo* in endoscopy [66,265,266].

Mizeret *et al.* [65] reported the development of instrumentation for time-resolved fluorescence imaging in 1997. Results obtained on a single freshly resected human oral carcinoma were contextually presented to illustrate the potential of the technique. At 417 nm excitation, an area corresponding to CIS exhibited a longer mean fluorescence lifetime than the surrounding uninvolved tissue (3440 ± 700 ns vs. 2500 ± 200 ps). This was achieved using frequency domain FLIM. However, this study was mainly focussed on the instrumentation and, as such, only a single oral mucosa tissue specimen was imaged. In a subsequent report, the feasibility of the imaging instrumentation developed was then demonstrated *in vivo* in the bronchi, displaying a fluorescence lifetime of 2500 ps for healthy bronchial mucosa excited at 514 nm.

Mycek *et al.* [265] performed time-resolved AF spectroscopy *in vivo* on 24 polyps (13 adenomas, 11 non-adenomas) from 17 patients. This was the first study in the colon that demonstrated differences in fluorescence lifetime decay between normal and dysplastic tissue. Adenomas showed faster average decays than those of non-adenomas (9.3 ± 0.4 ns vs. 10.5 ± 0.7 ns).

In a study by Glanzmann *et al.* [255], FLS was applied *in vivo* in one patient with advanced oesophageal cancer with 337 nm excitation and an emission band ranging from 375 nm to 515 nm. Interestingly, the decay profiles between the cancer and the surrounding healthy tissue appeared to change at different wavelength bands, i.e. the fluorescence lifetime for cancer was longer than that of normal mucosa between 375-400 nm (3740 ps vs. 3360 ps, respectively), and shorter between 465-485 nm (3270 ps vs. 3740 ps, respectively). Conversely, the spectra between the two conditions, although different, were not able to differentiate normal from neoplastic tissue. In the same study, they also investigated the use of the photosensitizer mTHPC in three patients with early SCC of the oesophagus undergoing PDT. The oesophagus was excited at 418 nm and fluorescence emission was collected between 580 and 720 nm. However, no significant difference was found between normal and neoplastic mucosa.

Pfefer *et al.* [266] compared temporally- and spectrally-resolved fluorescence spectroscopy at 337, 400 and 550 nm respectively *in vivo* in 37 patients undergoing routine endoscopic surveillance for BO. However, time-resolved fluorescence was unable to achieve sufficient sensitivity and specificity (values above 60%) in discriminating high risk (carcinoma, HGD) from low risk tissue (LGD, non-dysplastic or indefinite for dysplasia BO), whereas moderate overall accuracy was achieved using steady-state fluorescence only.

Recently, Marcu *et al.* [339] demonstrated the feasibility of *in vivo* endoscopic FLIM using a flexible imaging probe at 337 nm excitation on a hamster model of oral carcinoma.

In this chapter, the research question was whether the changes in fluorescence emission spectrum and lifetime observed *ex vivo* could be confirmed *in vivo*. The aim of this study was to investigate the origins of the autofluorescence lifetime contrast observed *in vivo* and to evaluate its potential for *in vivo* diagnosis of GI diseases or precursor conditions.

8.2 Materials and methods

8.2.1 Patient enrolment

In the endoscopy unit of the Charing Cross Hospital, Imperial College Healthcare NHS Trust, the spectrometer was applied *in vivo* in an exploratory feasibility trial from December 2011 to June 2012. A total of 42 measurements of different GI sites were performed in 17 patients undergoing GI endoscopy. Patients who participated in the research were recruited by the clinical investigators (SC, KLR & AVT) of the clinical care team at Charing Cross and the study was carried out with the approval of the National Research Ethics Service Committee London-Stanmore (REC reference number: 11/LO/0728).

As per ethics recommendation, the information sheet about this research was sent to potential participants by post 4 weeks in advance of their appointment, together with the usual documentation about the endoscopy procedures and their risks. This allowed enough time to read and digest the information well in advance of their attendance for their procedures. In 6 patients, who had given their consent to participate in the study, no specimens were taken as there was no indication to biopsy; copy of their consent was however retained for service audit purposes. Only 2 patients refused to participate.

The trial was adopted and registered on the UK Clinical Research Network Study Portfolio (UKCRN ID 12378).

A nonclinical investigator (AJT) of the Photonics Group, licensed with an NHS honorary contract, was present in the endoscopy suite for the majority of the measurements to operate the computer controlling the data acquisition and recording, but did not come into direct contact with the patient, and did not have a clinical role.

8.2.2 Fluorescence lifetime spectroscopy (FLS) instrumentation

The spectrofluorometer used in this study has been described in section 7.2.2. Figure 8-1 shows the experimental set up for *in vivo* measurements using the FLS point probe system in the Endoscopy suite at Charing Cross Hospital.

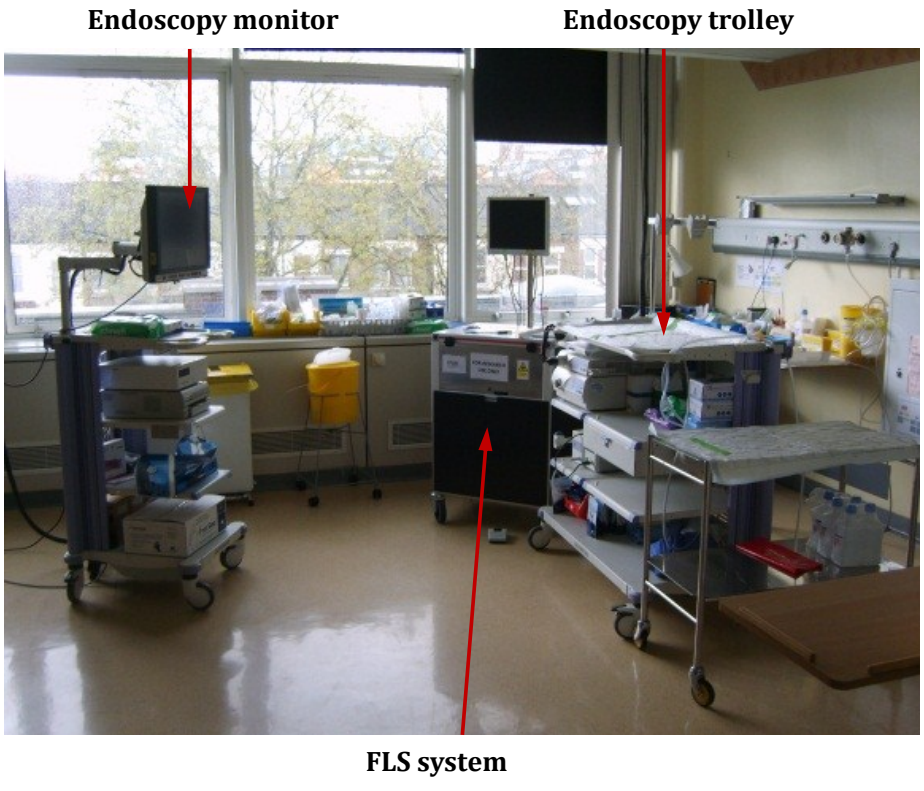


Figure 8-1: Photograph showing the FLS point probe system in the Endoscopy suite at Charing Cross Hospital.

8.2.3 Experimental procedure

For *in vivo* measurements the experimental procedure differed slightly from that used in the *ex vivo* experiments. The spectrometer was moved into the endoscopy suite (Figure 8-1) and placed next to the patient's bed. Then, during the endoscopic examination, measurements were made of any suspicious areas of tissue by inserting the optical fibre probe into the working channel of the endoscope. Figure 8-2 and Figure 8-3 show endoscopic images of the point probe being deployed *in vivo*.

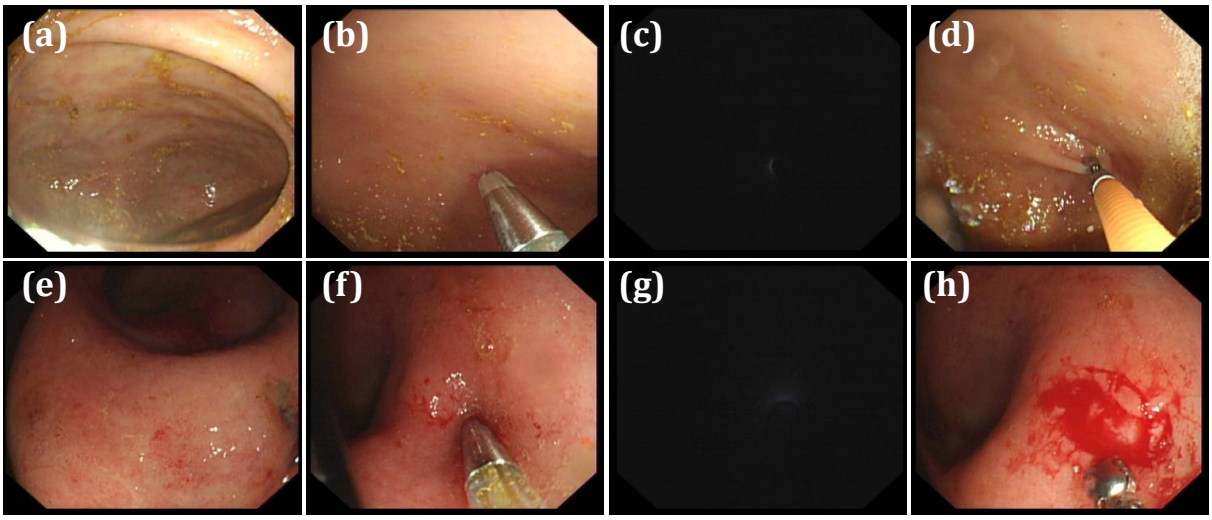


Figure 8-2: Endoscopic images showing the fluorescence lifetime fibre probe spectrometer being deployed *in vivo* to measure normal (a-d) and inflamed (e-h) regions of tissue in the colon. Both measurements were made in the same patient. Each site is illuminated for 10 s with the 375 nm and the 435 nm laser source. During the data acquisition, the endoscope light source is temporarily switched off to avoid damaging to the fibre probe detector, and a semi-circular ring of blue light bleeding through from the outer edge of the fibre probe in contact with the tissue can be seen in figures (c) and (g). Each area of tissue examined with the probe (~0.9 mm^2) was removed by subsequent excisional biopsy (d, h). Source of acquisition: Drs Coda & Thillainayagam, Endoscopy Unit, Charing Cross Hospital, Imperial College Healthcare NHS Trust.

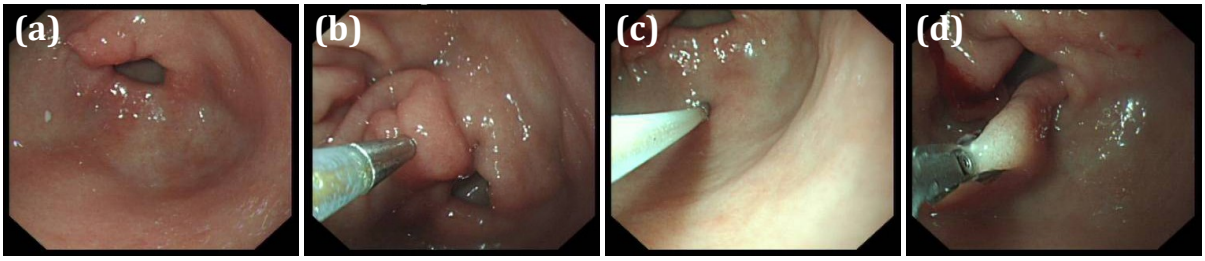


Figure 8-3: Endoscopic images showing the fluorescence lifetime fibre probe spectrometer being deployed *in vivo* to measure abnormal (a, b) and normal (c, d) regions of tissue in the gastric antrum (the distal section of the stomach). Both measurements were made in the same patient. Each areas of tissue examined with the probe (~0.9 mm^2) was removed by subsequent biopsy (d) for histological assessment. Source of acquisition: Drs Coda & Thillainayagam, Endoscopy Unit, Charing Cross Hospital, Imperial College Healthcare NHS Trust.

As for the *ex vivo* experiments, at least one measurement was also made of a complementary region of healthy tissue. After the measurements were complete, all the irradiated regions of tissue were excised (by endoscopic biopsy) and sent for histopathological analysis.

The illumination site was easily identified by a red ring resulting from impression of the ferule on the mucosa and this was shown to be due solely to the pressure exerted by the probe (figure 8-4).

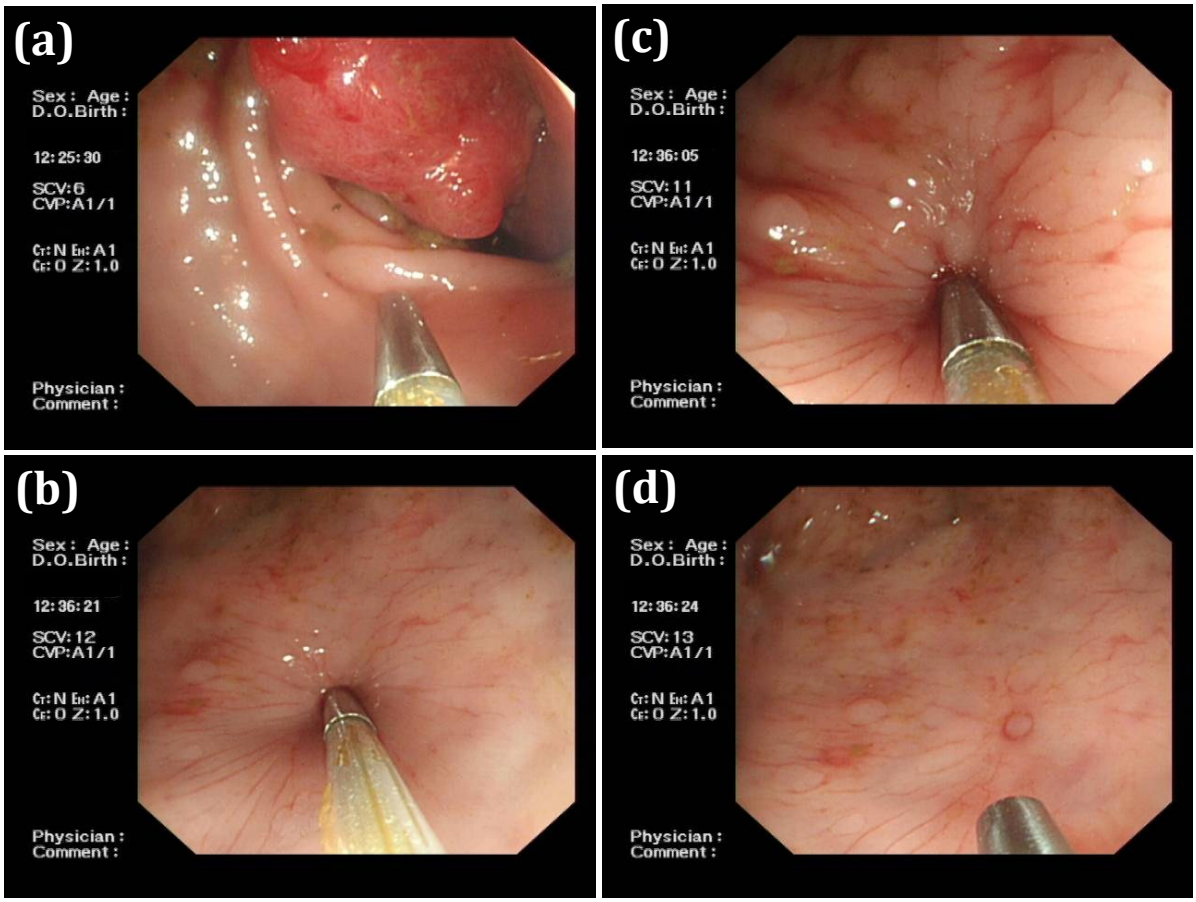


Figure 8-4: (a) Endoscopic image showing the florescence lifetime fibre probe spectrometer being deployed *in vivo* to measure a colon cancer (a) and a neighbouring normal area of mucosa (b, c, d). In (d), a red ring resulting from impression of the ferule on the mucosa is shown (laser switched off). Note that the acquisition time was the same of a normal measurement (~20 s) as shown by the time elapsed on the endoscopy monitor (left). Source of acquisition: Drs Coda & Thillainayagam, Endoscopy Unit, Charing Cross Hospital, Imperial College Healthcare NHS Trust.

Excisional biopsy allowed confirmation of the clinical diagnosis and also ensured that any potentially photodamaged tissue was removed from the patient. It should be noted, however, that the average optical power at the sample was limited to 35 μW of UV and 200 μW of blue light (see section 7.2.2) in order to minimise the risk of tissue damage. The irradiance at these power levels (for both lasers) is lower than the MPE for skin, even for exposures of up to 1000 s in duration, and previous work in the literature indicates that these exposure levels caused no

increase in triphosphate-biotin nick end-labelling (TUNEL) positive cells above baseline compared to controls in porcine oesophagus and colon respectively [547].

For the *in vivo* measurements, the total acquisition time was reduced to approximately 20 s (5 s for each laser but only two repeat measurements were performed), compared to the 30 s acquisition used for *ex vivo* measurements (see section 7.2.2). This was because it is desirable to keep the total acquisition time as short as possible, so to prolong the clinical procedure only marginally, and avoid excessive motion of the measured tissue and probe slipping.

After completion of the experiments, each measured region was assigned a unique number for identification purposes.

The fibre probe was disinfected using the same procedure and disinfection cycle as per standard practice for the standard clinical endoscopes (high grade disinfection). This standard procedure involved a 30 minute cycle in an automated endoscope disinfection machine using Sterilox (PuriCore, UK), within the endoscope re-processing unit (ERU). Once disinfected, the fibre probe was stored within a disposable sterile plastic bag inside an instrument case until the beginning of the procedure and used within 3.5 hours of disinfection. Specific advice on this aspect was provided by the Decontamination Lead at Imperial College Healthcare NHS Trust.

Prior to the procedure, the fibre probe was placed on a sterile tray on an endoscopy trolley and the proximal end was connected to the detection unit. The fibre probe was then passed to the endoscopist by a nurse/assistant when required.

The endoscopist held the distal part of the probe gently (~10 cm from the metallic tip) with one hand, and used the other hand for holding the chassis of the endoscope (as per conventional practice when operating any other accessory device). The endoscopist then inserted and passed the probe through the instrument operating channel until the end of the probe came out from the endoscope working channel and appeared on the screen.

The tip of the probe was then gently advanced until it came into contact with the mucosal surface to be studied. A circular area of ~2 mm was covered by the probe during the measurements and conventional endoscopic images were taken before and after the measurement as record. A minimum of 2 measurements were acquired for each lesion, one performed near the centre of an obvious or suspect lesion, the other on a normal area near to the lesion. During the data acquisition with the fibre probe, the endoscope light source was temporarily switched off to avoid damage to the fibre probe detector.

Table 8-1 shows the clinical and histological diagnoses of all the areas of tissue investigated.

Tissue type	Histological diagnosis	No. of measurements
Colon polyps	6 adenoma with LGD 3 hyperplastic 2 inflammatory 1 quiescent colitis	12
Colon cancer	1 adenocarcinoma	1
IBD	2 UC	2
Oesophageal disease	2 BO (1 with LGD) 1 high grade dysplasia 2 oesophagitis	5
Gastric disease	1 gastritis	1
Duodenal disease	1 duodenitis	1
Normal colon	13 normal colon 1 chronic inflammation	14
Normal oesophagus	4 normal oesophagus	4
Normal stomach	1 normal stomach	1
Normal duodenum	1 normal duodenum	1
Total number of normal tissue measurements		20
Total number of diseased tissue measurements		22
Total number of measurements		42

Table 8-1: Table showing the clinical and histological diagnoses of all the *in vivo* measurement sites investigated with the endoscopic spectrometer.

8.3 Data analysis

Exponential fitting and fluorescence data analysis were performed as described in section 7.3.

8.4 Results

The laser caused no tissue damage that could be detected at the microscopic level using conventional H&E stain. As for the *ex vivo* experiments, all analysis was performed based on the histological diagnosis for each sample. Samples were excluded if histological analysis revealed normal tissue in abnormal samples or histological abnormalities in normal specimens.

The results of this section refer to the analysis performed on colonic polyps, as for other clinical conditions only a small number of measurements were performed.

Normal tissue characterization

As for the *ex vivo* experiments, different regions of endoscopically and histologically normal colon (rectum, left and right colon) were compared with respect to their spectrally averaged normalised emission spectrum and mean fluorescence lifetime.

Figure 8-5(a, b) shows that there is a blue shift in the fluorescence emission spectrum for the measurements obtained from the rectum and the left colon for 375 nm excitation, but the shift in mean emission wavelength was not found to be significant by 1-way ANOVA (grouping data by region) for either excitation wavelength ($p = 0.0569$ and $p = 0.2867$ for 375 nm and 435 nm excitation wavelengths, respectively).

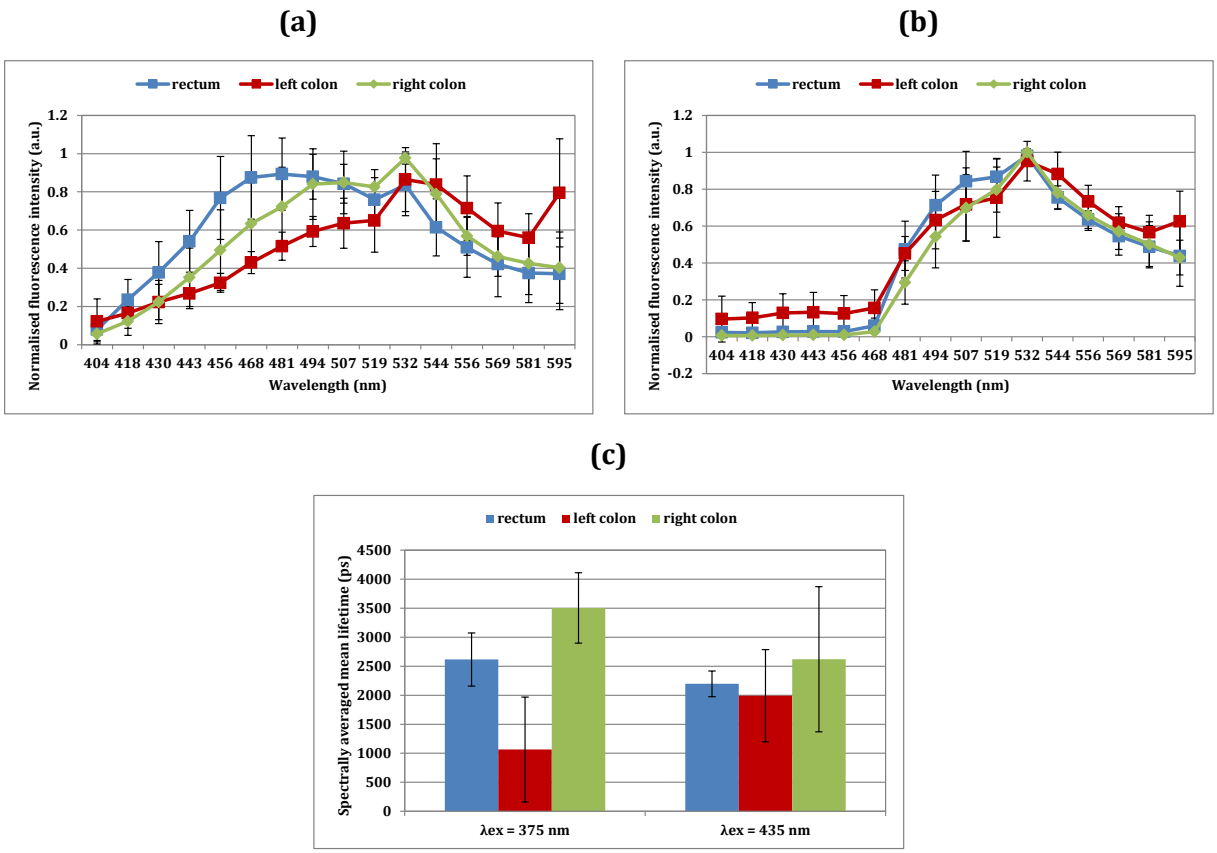


Figure 8-5: Summary of results from normal tissues grouped according to the location that the measurement was performed. The number of specimens in each group was: rectum (*n* = 5), left (*n* = 5), right (*n* = 3). Figures (a) and (b) show the mean fluorescence emission spectra obtained with 375 and 435 nm excitation respectively. Figure (c) shows the spectrally averaged mean fluorescence lifetimes for both groups and for both excitation wavelengths. The error bars represent ± 1 standard deviation in all panels.

The mean fluorescence lifetime obtained with both excitation wavelengths from the right colon is longer than that obtained from the other two regions, particularly between left and right colon with 375 nm - see figure 8-5(c).

As mentioned above, we performed 1-way ANOVA on the spectrally averaged mean fluorescence lifetimes from histologically normal colon grouped according to region of colon and statistically significant differences were obtained for 375 nm excitation ($p = 0.0017$), with the greatest difference observed between right and left colon ($p = 0.001$), while the data obtained with 435 nm excitation showed no significant difference ($p = 0.54$).

There is no similarity between the mean fluorescence emission spectra of normal colon measured *ex vivo* and *in vivo*, with a generally weaker fluorescence intensity observed in the *in vivo* measurements (see section 7.4). Nevertheless, the slight blue shift in the emission spectrum for the rectal specimens seen *ex vivo* at 375 nm excitation is confirmed *in vivo,* although not significant. In contrast, between *ex vivo* and *in vivo* measurements, there is a general agreement of values, within the quoted error bars, in the spectrally averaged mean lifetime between the

measured regions of normal colon (rectum, left colon, and right colon). It is also interesting to note that the rectal specimens, at both excitation wavelengths, maintained a mean fluorescence lifetime longer than that obtained from the left colon both *ex vivo* and *in vivo*.

Diseased vs. normal tissue

Colonic polyp was the disease type for which the greatest number of *in vivo* measurements was made. Of the 12 clinically identified polyps (see table 8-1), one was excluded as it was found to be normal by histopathology, and the polyp specimens included in our analysis are summarised in table 8-2. One measurement of normal colon was obtained from all patients.

	Paired analysis
No. of patients	9
No. of polyps	11
Neoplastic	6
Non-neoplastic	5
No. of normal measurements	9
Total No. of measurements	20

Table 8-2: Summary of colonic polyps included in the *in vivo* study.

Figure 8-6(a, b) shows the normalised mean fluorescence spectra observed in normal colon tissue and in neoplastic (tubular and villous adenomas with LGD) and non-neoplastic (hyperplastic and inflammatory) colonic polyps for both excitation wavelengths, and the spectra overlap within the error bars. No statistically significant difference was obtained when comparing the mean fluorescence emission wavelength for either excitation wavelength.

Figure 8-6(c, d) shows the mean fluorescence lifetimes averaged over all polyp patients and recorded in each spectral channel for healthy colon and for neoplastic and non-neoplastic polyps under UV (c) and blue (d) excitation.

While no obvious trend was seen under 375 nm excitation, the mean fluorescence lifetimes for polyps were shorter than those observed in normal tissue for 435 nm excitation. The spectrally averaged mean fluorescence lifetime (weighted according to the intensity recorded in each spectral channel) is shown in figure 8-6(e).

As can be seen from the size of the error bars on fluorescence lifetime measurements in figure 8-6(e), there is significant inter-patient variability in the measured mean fluorescence lifetime from both normal and polyp specimens.

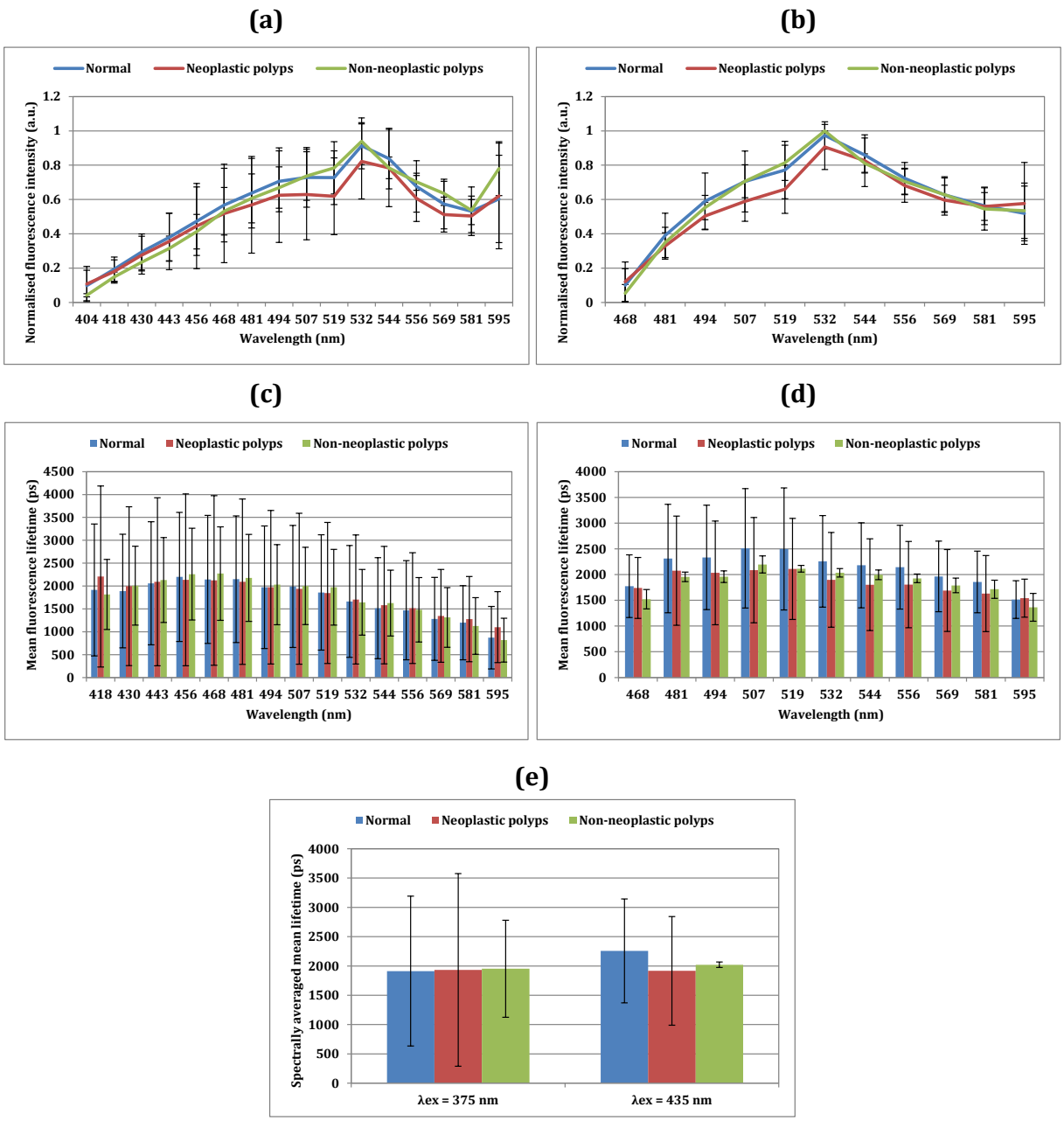


Figure 8-6: Comparison of normal colon versus neoplastic and non-neoplastic polyp measurements: Figures (a) and (b) show the mean fluorescence emission spectra obtained with 375 and 435 nm excitation respectively. Figures (c) and (d) show the spectrally resolved fluorescence lifetimes with 375 and 435 nm excitation respectively. Figure (e) shows the spectrally averaged mean fluorescence lifetimes for the three groups and for both excitation wavelengths. The error bars represent ± 1 standard deviation in all panels.

Figure 8-7 shows the paired analysis calculating the difference in spectrally averaged mean fluorescence lifetime between normal and polyp measurements obtained from the same patient. This paired analysis was performed using a total of 20 specimens (see table 8-2).

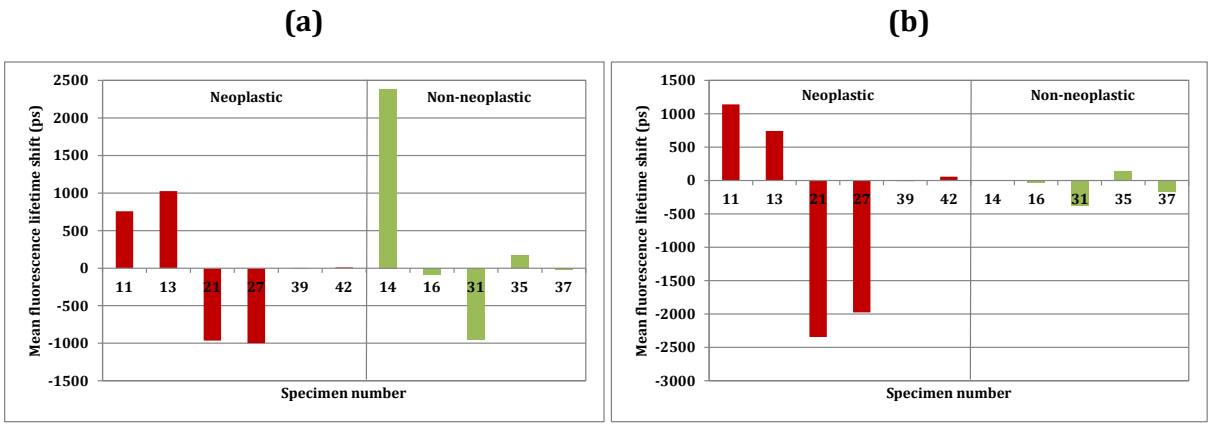


Figure 8-7: Shift in the spectrally averaged mean fluorescence lifetime for (a) 375 nm and (b) 435 nm excitation of neoplastic (red bars) and non-neoplastic (green bars) polyp specimens. Lifetime shifts are calculated using a measurement of normal tissue obtained from the same or nearest region of colon (paired analysis).

For each normal-lesion pair, both the shift in mean fluorescence emission wavelength and the shift in spectrally averaged mean fluorescence lifetime were calculated for both excitation wavelengths. The measured shift in mean fluorescence emission wavelength was not found to be statistically significant for either excitation wavelength. Figure 8-7 shows the shift in the spectrally averaged fluorescence lifetime ($\Delta\tau$) for each normal-lesion pair and the mean values calculated over all pairs were 119 ± 1002 ps and -259 ± 1035 ps for 375 nm and 435 nm excitation respectively. A Wilcoxon signed rank test was applied to all sets of paired difference values. The data obtained with both excitation wavelengths showed no significant difference in the fluorescence lifetime of polyps with respect to healthy tissue ($p = 0.9658$ and $p = 0.6377$ with 375 nm and 435 nm excitation, respectively).

The shift in spectrally averaged mean lifetime for patients with neoplastic polyps (tubular and villous adenomas with LGD) was also compared to those with non-neoplastic polyps (hyperplastic and inflammatory) and the means and standard deviations are presented in table 8-3. No statistically significant differences were found (Wilcoxon rank sum test, $p = 0.9307$ and $p = 0.7922$ with 375 nm and 435 nm excitation, respectively).

	Mean shift in spectrally averaged fluorescence lifetime of polyp compared to normal colon (ps)	
	UV	Blue
Neoplastic (n=6)	-29 ± 842	-399 ± 1435
Non-neoplastic (n=5)	298 ± 1244	-91 ± 199

Table 8-3: Spectrally averaged fluorescence lifetime shift for neoplastic and non-neoplastic polyps.

Comparison of in vivo versus ex vivo data

The data obtained *in vivo* is now compared to the *ex vivo* data reported in chapter 7.

Figure 8-8 shows summary plots of all measured absolute mean emission wavelengths and mean fluorescence lifetimes of normal colon, neoplastic and non-neoplastic polyps *ex vivo* and *in vivo* for both wavelengths. For 375 nm excitation (figure 8-8(a)), there seems to be a shift towards longer mean emission wavelengths and shorter spectrally averaged mean fluorescence lifetimes for the *in vivo* data, whereas for 435 nm excitation (figure 8-8(b)), a clustering of data points can be seen, which suggests a reasonable agreement between *ex vivo* and *in vivo* data.

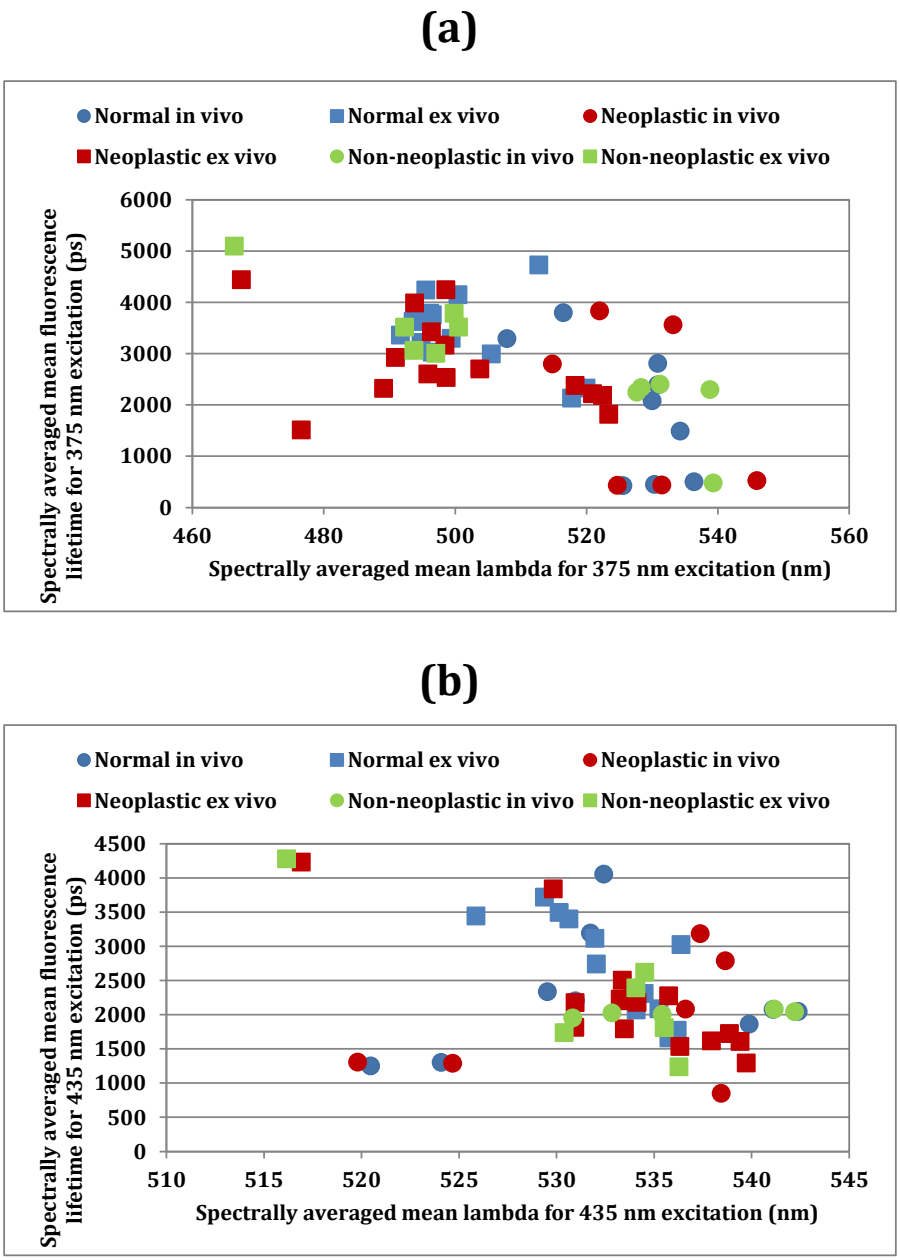


Figure 8-8: Summary of all measured absolute mean fluorescence emission wavelengths and spectrally averaged mean fluorescence lifetimes for (a) 375 nm and (b) 435 nm excitation wavelengths between *ex vivo* (squares) and *in vivo* (circles) normal colon (blue), and neoplastic (red) and non-neoplastic (green) polyps.

8.5 Discussion

This work demonstrated that time-resolved autofluorescence measurements could be readily acquired *in vivo* during routine endoscopy. All technological constraints precluding the transfer from the laboratory to the hospital were successfully overcome.

In this study, however, no significant differences between diseased and normal tissue were found, and this was due to the relatively large standard deviations on the lifetime shifts, the large interpatient variability, and the small number of measurements made for each disease type. Notably, in contrast with the *ex vivo* experiments, statistically significant differences were found for 375 nm excitation in the spectrally averaged mean fluorescence lifetimes from the three regions of normal colon investigated ($p = 0.0017$), with the greatest difference observed between right and left colon. However, significant variation would have been expected for both excitation wavelengths but no significant difference was observed for 435 nm excitation. To the best of our knowledge, this is the first time that autofluorescence variations in normal colonic tissue with region have been investigated. However, the number of specimens in each group was relatively small and a study on a larger number of patients would be needed to investigate this further.

In comparison with the *ex vivo* experiments, we noticed a generally weaker autofluorescence emission *in vivo*, and this may have depended on the relatively shorter total acquisition time for each measurement, the peristaltic motion of the organs during the measurements, as well as on the altered absorption properties of the living tissue caused by greater haemoglobin content and higher oxygenation.

Another limitation is the possible slippage of the probe during the acquisition. The integration of the fibre probe within the flexible shaft of a biopsy forceps would allow the pinching of the tissue in between the cups of the forceps, therefore ensuring a constant contact with the tissue under investigation.

One promising result is the observation that, with 435 nm excitation, the spectrally averaged fluorescence lifetimes measured in both *ex vivo* and *in vivo* diseased and normal tissues agree to within the quoted standard deviation (see ratios ± total relative errors in table 8-4).

The spectrally averaged mean lifetimes for five groups of *ex vivo* measurements (all normal colon specimens, normal colon for polyp specimens, normal colon for IBD specimens, polyps and IBD specimens) were tested for differences with those of the *in vivo* measurements using the Wilcoxon rank sum test (5% significance level) and the *p* values are presented in table 8-4. No statistically significant differences were found in all groups for 435 nm excitation, indicating that data in the *ex vivo* and *in vivo* measurement groups came from continuous distributions

with equal medians. In contrast, for 375 nm excitation, in three groups (all normal colon specimens, normal colon for polyp specimens, and polyps) the *ex vivo* and *in vivo* data were significantly different suggesting that the distributions did not have equal medians.

The fact that the mean lifetime varied under 375-nm-excitation but not with excitation at 435 nm is intriguing and may be partly explained by both the different penetration depths of the two lasers and the different anatomical (structural) and biochemical compositions of the wall of the GI tract through the various regions of colon. The blue light will penetrate further into tissue than the UV radiation, hence, the lifetimes observed with the blue laser are more likely to be sensitive to variations in the thickness of the colonic mucosa. Furthermore, the differences in the fluorescence lifetime detected between *ex vivo* and *in vivo* measurements may also be explained, as discussed above, by changes in haemoglobin content and tissue oxygenation, changes in the metabolic state of cells, tissue pH, and movement artifacts.

While this observation is based on only a small number of *in vivo* measurements, it suggests that the trends documented *ex vivo* in the previous chapter may also be observed *in vivo*.

	Mean lifetime ± SD (ps) *ex vivo*		Mean lifetime ± SD (ps) *in vivo*		Ratio ± TRE *ex vivo*/*in vivo*		*p* values	
Tissue type	**λ_{ex} 375 nm**	**λ_{ex} 435 nm**	**λ_{ex} 375 nm**	**λ_{ex} 435 nm**	**λ_{ex} 375 nm**	**λ_{ex} 435 nm**	**λ_{ex} 375 nm**	**λ_{ex} 435 nm**
Normal colon (all)	3356 ± 718	2552 ± 679	2224 ± 1198	2216 ± 741	1.51 ± 0.58	1.15 ± 0.43	0.01	0.25
Normal colon (polyp)	3378 ± 694	2683 ± 723	1913 ± 1278	2258 ± 886	1.77 ± 0.70	1.19 ± 0.48	0.011	0.23
Normal colon (IBD)	3232 ± 979	2018 ± 269	3212 ± 980	2069 ± 436	1.01 ± 0.43	0.98 ± 0.25	1	0.8
Normal stomach	3020 ± 290	2650 ± 920	3189	2650	0.95	1	-	-
Normal oesophagus	4220	2730	3780 ± 670	3820 ± 730	1.12	0.71	-	-
Polyps	3068 ± 908	2243 ± 872	1941 ± 1274	1964 ± 659	1.58 ± 0.72	1.14 ± 0.51	0.032	0.53
IBD	4748 ± 1138	2071 ± 360	2743 ± 3047	2203 ± 1763	1.73 ± 1.14	0.94 ± 0.82	0.381	1
Colon cancer	-	-	2603	2800	-	-	-	-
Gastric disease	3190 ± 250	2310 ± 910	2864	3238	1.11	0.71	-	-
Oesophageal disease	4380	3090	3740 ± 600	3990 ± 390	1.17	0.77	-	-

Table 8-4: Mean spectrally averaged fluorescence lifetimes observed in all the tissues investigated in this study. Data are presented for both the UV and blue laser and for both *ex vivo* and *in vivo* measurements. Uncertainties denote one standard deviation from the mean. Where no standard deviation is shown, only one measurement was made. SD = standard deviation; TRE = total relative error.

Previous *in vivo* FL studies of colonic polyps have shown 85% sensitivity and 91% specificity in distinguishing colonic adenomatous polyps from non-neoplastic polyps [265]. As in the *ex vivo* measurements, in this study we did not find any statistically significant differences in the spectrally averaged lifetime between neoplastic and non-neoplastic polyps for either excitation wavelength. This discrepancy between our work and that of Mycek *et al*. may again be explained by the different excitation wavelengths used.

However, it is interesting to note that, at 435 nm excitation, polyps exhibited shorter mean FL values than normal tissue, and this, although not statistically significant, was consistent with both our *ex vivo* measurements with the FLS system (chapter 7) and with images acquired with the FLIM confocal microscope (chapter 4).

8.6 Conclusions

In summary, time-resolved fluorescence lifetime spectroscopy using two excitation wavelengths has been applied to the study of tissue abnormalities *in vivo* during routine endoscopy. The mean shift in spectrally averaged fluorescence lifetime of polyps compared to normal colon for 435 nm excitation was found to be negative (-399 ± 1435 ps), in agreement with the *ex vivo* data reported in chapter 7 (-690 ± 640 ps, $p = 0.0049$), however, this was not found to be statistically significant. Spectrally averaged mean fluorescence lifetimes measured *in vivo* were not found to be statistically different from those measured *ex vivo* for 435 nm excitation. However, statistically significant differences were observed between *in vivo* and *ex vivo* measurements for 375 nm excitation. Further improvements will be required to optimise this technique and a larger trial will be needed to rigorously assess its clinical utility.

Current prospective diagnostic accuracy studies with the FLS system are underway to determine if contrast is present in other disease types. If established, it is desirable to progress to the exciting prospect of wide-field FLIM endoscopy imaging, which would be able to screen rapidly a field of view up to many centimetres across. Such a system has the potential to be used as a red-flag screening technique, alerting the clinician to areas requiring more detailed investigation, i.e. by conventional biopsy or a more detailed optical biopsy technique such as the FLS probe.

Chapter 9: Conclusions and outlook

Optically-assisted diagnosis is a thriving field of research that is particularly applicable to the various medical conditions for which biopsies are still required to confirm and characterise the essential nature of diseases. One such example is detection of dysplasia, where an *in situ* "optical biopsy" would be of significant benefit, allowing real-time diagnosis during endoscopy and avoiding multiple and random unnecessary biopsies. Indeed, discrimination between dysplasia and inflammation is still one of the most important dilemmas in GI endoscopy and pathology.

The aim of the work presented in this thesis was to investigate a spectrum of tissue types and states of disease, including premalignant and malignant conditions, by studying tissue autofluorescence and measuring fluorescence lifetime using fluorescence lifetime imaging and spectroscopy. In this thesis, attention was directed towards the differences in autofluorescence, and particularly fluorescence lifetime, found in skin cancer, colonic polyps and inflammatory bowel diseases.

Chapter 2 introduced the clinical context of this research and discussed established and emerging endoscopic techniques, outlining their fundamental principles and *pro et contra*. The clinical and experimental experience was also reviewed and a summary of current unmet clinical needs is provided. In **chapter 3**, the scientific instrumentation context of this thesis was presented, along with a review of the pertinent published literature. A summary of the state-of the-art of fluorescence lifetime endoscopic instrumentation developments at Imperial College London was presented, along with a discussion of limitations in the currently available systems, and future prospects.

Chapters 4 and **5** focussed on *ex vivo* FLIM microscopy-based studies of gastrointestinal disease and bladder cancer, respectively. **Chapter 6** concerned the application of a time-resolved spectrometer to an *in vivo* study of skin cancer. This system was then redesigned to make it more compact and clinically compatible with flexible endoscopes, and applied to both *ex vivo* and *in vivo* investigations of GI disease and the results of these studies were presented in **chapter 7** and **chapter 8**, respectively.

9.1 Summary of results

9.2 Investigation of fluorescence lifetime imaging for label free contrast of gastrointestinal disease

The experimental work discussed in chapter 4 was directed at the autofluorescence signatures of fresh endoscopically resected GI tissue in order to investigate the origins of the contrast generated by FLIM and the relative contributions to tissue autofluorescence from the different areas and structures within the tissue. This was achieved by imaging with a conventional FLIM microscope at 420 nm excitation a total of 71 endoscopic samples from different GI sites collected from 35 patients undergoing either upper or lower GI endoscopy as part of their clinical investigations. This excitation wavelength was used because the ultimate intention was to develop clinical FLIM endoscopes that were expected to utilise excitation in the blue. A total of 481 confocal images were acquired and the FLIM images generated were analysed using manual image processing. Samples were investigated for properties related to emission spectrum, fluorescence decay after pulsed excitation, morphological changes, and correlation with both endoscopic and histological diagnosis.

FLIM was found to allow the visualization of tissue details in some of the most common GI diseases and provide contrast between normal and diseased tissue, particularly for colonic polyps and inflammatory bowel disease, where a statistically significant decrease in fluorescence lifetime relative to biopsy specimens of adjacent normal tissue was observed ($p = 0.024$ and $p = 0.015$ for polyps and IBD, respectively) although the mean fluorescence lifetime shift (i.e. $\tau_{lesion} - \tau_{normal}$) for biopsies of colon cancer and Barrett's oesophagus was not found to be statistically significant for the sample numbers studied. Interestingly, however, the mean fluorescence lifetime of colon cancer biopsies was longer than that of normal adjacent tissue with a mean delta tau shift of 220 ± 187 ps, which is in agreement with a previous *ex vivo* study using wide field FLIM imaging on freshly resected (< 2 hours) surgical samples of colon cancer, although more samples are required to build a statistically significant sample size and this earlier result was obtained using a different excitation wavelength (355 nm) [273].

The autofluorescence signal may be primarily attributed to flavin and collagen fluorescence for the excitation wavelength used (420 nm). Fluorescence lifetime contrast may be due to changes in flavin fluorescence lifetime with disease state or changes in the relative amounts of flavins and collagen with disease, however, further work is needed to clarify this. The possible role of mucins in the fluorescence lifetime changes observed was also raised but further work would be necessary to support this supposition.

This study represents the most comprehensive analysis of confocal FLIM images in normal and diseased human GI mucosal tissues and the only study to use confocal FLIM at 420 nm excitation to image autofluorescence from freshly-resected specimens obtained from patients undergoing endoscopic procedures. Similarly, Professor Hillman's group have presented hyperspectral two-photon microscopy (TPM) paired images and emission spectra from normal and transgenic mouse GI tissue [323]. However, their study involved freshly excised small intestine and colon from 15 (10 normal and 5 transgenic APC *Min/*+) mice, and was mainly carried out to determine the TPM excitation spectral properties of the four layers of the normal GI tract wall. The ability to generate lifetime contrast with blue excitation, as is likely to be used in FLIM endoscopes, supports the potential of FLIM for clinical applications including the *in vivo* detection and characterisation of dysplasia, and the discrimination of inflammatory diseases.

Future work is more likely to involve the collection of a larger, more significant data set to allow confirmation of the observations made and build a bank of *ex vivo* data to permit detailed investigation of the optical signatures of other GI disease types meaning that the worth of confocal FLIM can be assessed over a wider range of GI conditions, including liver, biliary and pancreatic disorders. An increased database of information would also facilitate the development and implementation of FLIM in endoscopic instruments for clinical use, such as the FLIM confocal endomicroscope.

9.3 Investigation of fluorescence lifetime confocal microscopy of bladder cancer as an adjunct to PpIX fluorescence induced PDD

The concept behind a novel approach to PDD of bladder cancer was discussed in chapter 5 and results from a proof-of-principle study based on confocal FLIM microscopy were presented. The aim of this work was to assess whether the fluorescence signature of PpIX, which is known to accumulate preferentially in malignant tissue, could be detected by FLIM, and whether the fluorescence patterns seen could report on the disease state of the tissue. The study employed an imaging protocol that was similar to that described in chapter 4 and involved the comparison of the optical signatures of healthy and neoplastic regions of bladder excised from the same patient undergoing PDD cystoscopy.

Although not significant ($p = 0.06$), an increase of the mean fluorescence lifetime for biopsies of bladder cancer was consistently observed at 405 nm excitation. The longer fluorescence lifetime in neoplastic tissue is consistent with a greater concentration of PpIX compared to normal tissue and with the longer fluorescence lifetime of PpIX compared to baseline tissue autofluorescence. Further work would be useful to characterize bladder biopsies obtained during PDD cystoscopy using FLIM and to correlate the morphological appearance seen in the

confocal FLIM images with the molecular basis of the fluorescence changes observed. A larger data set would also support the development of clinically viable diagnostic equipment such as a wide field FLIM flexible ureteroscope for *in vivo* use in combination with the blue light cystoscopy equipment, as PDD becomes increasingly applied to a great number of endoscopic urological procedures.

9.4 Investigation of time-resolved autofluorescence spectroscopy of skin cancer

Chapter 6 discussed the use of a prototype fluorescence lifetime spectrometer in the first *in vivo* clinical study of the autofluorescence lifetime signatures of skin cancer [403]. This system is a time-resolved fluorescence spectrometer, which records fluorescence decays in 16 spectral channels with two excitation wavelengths (355 nm and 445 nm). The system was transported with a van from London to Lund in Sweden by the Imperial investigators. It was assembled in the dermatology department of Lund University Hospital, and used to interrogate 27 clinically diagnosed skin lesions on a total of 25 patients. For each lesion, a parallel measurement of the neighbouring healthy tissue was also made for comparison.

It was observed that with excitation at 445 nm, basal cell carcinomas (BCCs) – the disease type for which the greatest number of measurements was made – exhibited a statistically significant ($p = 0.002$) decrease in their spectrally averaged mean fluorescence lifetime, relative to the surrounding healthy skin. Importantly, in 9 out of 10 cases this decrease in lifetime was greater in magnitude than the mean intra-patient variation in the measured lifetimes. This indicates the future potential of time-resolved autofluorescence spectroscopy for use in clinical diagnosis.

9.5 Investigation of time-resolved autofluorescence spectroscopy of colonic polyps and inflammatory bowel disease *ex vivo*

Chapter 7 presented an *ex vivo* study of time-resolved autofluorescence spectra of colonic samples collected from patients undergoing endoscopy as part of their clinical investigation. Using a compact fibre-optic coupled fluorescence lifetime spectrometer, the autofluorescence signatures of freshly biopsied/removed colonic tissue were investigated. This instrument provides measurements of time-resolved fluorescence spectra (16 spectral detection channels) with two excitation wavelengths (375 nm and 435 nm) and was designed to be suitable for regular *ex vivo*/*in vivo* research use in the hospital setting, for which clinical input and contributions with regard to specifications and design were provided in order to meet the requirements of safety, capacity to be disinfected and easy portability.

First, the variation in the fluorescence lifetime of normal colon was assessed and it was observed that the lifetime varied based on the region of the colon from which the tissue was excised, with the greatest difference observed between rectum and the rest of the colon with 435 nm excitation, although this shift was not found to be statistically significant for the sample size studied. Subsequently, the analysis of the disease types for which the greatest number of measurements was made (polyps and IBD) was undertaken.

In a paired analysis between normal colon and neoplastic polyps obtained from the same patient, the decrease in 435 nm excited spectrally averaged mean fluorescence lifetime measured over all patients was found to be statistically significant (mean $\Delta\tau$ = -570 $\pm$ 740 ps, n = 12, p = 0.021). If a patient from whom it was not possible to obtain a normal sample from the same region of colon is excluded, then the level of statistical significance increases (mean $\Delta\tau$ = -690 $\pm$ 640 ps, n = 11, p = 0.0049) and the increase in mean emission wavelength also becomes statistically significant (mean $\Delta\lambda$ = 2.6 $\pm$ 3.1 nm, n = 11, p = 0.019). The shift in spectrally averaged mean fluorescence lifetime was found to be correlated with the shift in emission spectrum (R^2 = 0.71) but the shift in the spectrally averaged mean fluorescence lifetime exhibited a less variation between patients than the shift in the mean emission wavelength.

The number of IBD specimens studied was small (n = 4) and relatively large standard deviations on the spectral and lifetime shifts were obtained, so no statistically significant differences were observed. However, with 375 nm excitation, the fluorescence lifetimes of all four IBD samples were longer than those of the nearby normal colon tissue (mean $\Delta\tau$ = 983 $\pm$ 289 ps), and the increase in 375 nm excited fluorescence lifetime was correlated (R^2 = 0.90) with an increase in fluorescence emission wavelength ($\Delta\lambda$ = 6.9 $\pm$ 6.6 nm).

To our knowledge this *ex vivo* study represents the first time that dual-excitation wavelength laser-induced time-resolved fluorescence spectra of normal and diseased GI tissue have been acquired from a significant number of patients and the first time that autofluorescence variations in normal colonic tissue with region or disease have been investigated. While further research is required, our results suggest that the combination of 375 nm and 435 nm excited fluorescence measurements could ultimately help endoscopists decide whether the nature of a lesion is proliferative or inflamed.

9.6 *In vivo* measurements of endoscopic fluorescence lifetime spectroscopy of gastrointestinal disease

Following on from the work presented in chapter 7, the eighth chapter of this thesis outlined the deployment of a clinically viable time-resolved spectrometer *in vivo* during endoscopy. To the

best of our knowledge this was the first *in vivo* study using a clinically compatible endoscopic spectrofluorometer to provide simultaneous measurements of time-resolved fluorescence spectra with two excitation wavelengths (375 nm and 435 nm). This investigation was performed at Charing Cross Hospital and involved the acquisition of 42 measurements from 17 patients undergoing routine endoscopic procedures.

Colonic polyp was the disease type for which the greatest number of measurements was made. Different regions of endoscopically and histologically normal colon (rectum, left and right colon) were first compared with respect to their spectrally averaged normalised emission spectrum and mean fluorescence lifetime. Statistically significant differences were obtained for 375 nm excitation ($p = 0.0017$), with the greatest difference observed between right and left colon ($p = 0.001$), although the data obtained with 435 nm excitation showed no significant difference ($p = 0.54$) for the number of samples studied. Interestingly, the mean fluorescence lifetime obtained with both excitation wavelengths from the right colon was longer than that obtained from the other two regions, particularly between left and right colon with 375 nm excitation.

Subsequent analysis was undertaken to investigate the differences between normal colon and colonic polyps, as only a small number of measurements were performed for other clinical conditions. No statistically significant difference was obtained when comparing the mean fluorescence emission wavelength for either excitation wavelength. A negative shift in the spectrally averaged mean lifetime (i.e. $\tau_{polyp} < \tau_{normal}$) with 435 nm excitation was observed, in agreement with the result seen in the *ex vivo* study, although this was not statistically significant. In contrast, an opposite trend was seen with 375 nm excitation. The lack of statistical significance in the lifetime differences observed was probably due to the relatively large standard deviations on the lifetime shifts, the large inter-patient variability and the small number of measurements made for each disease type.

In comparison with the *ex vivo* experiments, we noticed a generally weaker autofluorescence emission *in vivo* that may have been due to the relatively shorter total acquisition time for each measurement, the peristaltic motion of the organs during the measurements, or on the altered absorption properties of the living tissue caused by greater haemoglobin content and higher oxygenation.

While this experimental work provided a useful step toward the translation of fluorescence lifetime technology to the clinic, a larger data set is required in order to confirm the trends observed and to permit investigation of further disease types. The spectroscopic data obtained could then be used to guide the development of future diagnostic equipment, for example in terms of the optimum excitation and detection wavelengths to be used. Looking ahead, the

integration of this technology in conventional instruments such as biopsy forceps or snares, or in FLIM endoscopes, could be clinically beneficial.

9.7 Challenges and prospects: what went wrong and how could future studies be improved

In this multidisciplinary PhD project, there a number of challenges that arose with respect to the photonics technology, the biomedical analysis and the practical clinical implementation of experimental studies.

From the technological perspective, the clinical approved Cellvizio™ confocal endomicroscope that was developed for real-time FLIM using TCSPC proved unsuitable for imaging tissue autofluorescence at the desired (UV-blue) excitation wavelengths, due to the background fluorescence excited in the imaging fibre bundle. Accordingly, the planned observational work described in chapter 4 was performed using a time-resolved fluorescence lifetime imaging confocal microscope. The Cellvizio™ FLIM instrument was redirected towards tissue imaging with exogenous probes with longer excitation wavelengths.

Throughout the project a range of different excitation wavelengths and optical excitation/detection geometries was employed due to the constraints of the specific components available for particular instruments. This prevented direct comparisons between results from different instruments, leading to non-generalizable results and separate conclusions for each study. The challenges and prospects specific to each of the studies are discussed below:

Chapter 4

The study presented in chapter 4 was primarily set as an exploration of signals and aimed to test the broad hypothesis that fluorescence lifetime measurements can contrast between different tissue types.

The sample size was relatively small for each disease group investigated and more focus could have been placed on a specific condition to measure more samples to achieve a more statistically significant analysis. Reviewing the requests for endoscopy could help identify potential participants in advance and plan dedicated sessions for collecting research specimens without causing disruption to the clinical workflow.

The study would have benefited from a precise histological registration to better establish the biomolecular composition and distribution of fluorophores in the tissues and therefore to identify the potential mechanisms responsible for the altered signals observed in the diseases investigated.

Orientating tissue under the microscope proved to be both difficult and time consuming and alternative approaches should be explored. For instance, the biopsy samples could be manipulated onto a microscope slide (instead of gauze) to keep the mucosal surface facing upward before sandwiching it with a glass coverslip.

A ring of silicone paste could be used to create a sealed compartment for the sample and prevent unwanted movements of the coverslip during imaging. This method was recently described by Pavone *et al.* for imaging fresh endoscopic specimens of human colon using MPM [548].

Fluorescence was detected over a wide detection range (450-680 nm). Dividing the detection bandwidth into two narrower spectral channels (e.g. 430-490 and 500-560 to selectively collect NADH and FAD fluorescence, respectively) would help resolve fluorophores with overlapping fluorescence emission spectra but with different fluorescence decay times (e.g. flavins and lipofuscin).

Each field of view was analysed using histograms of lifetimes across the whole field of view. It could be useful to identify and analyse specific regions of interest within FLIM fields of view, e.g. to calculate the redox ratio (balance between energy production and consumption) for cells in different tissue types, as described by Zhuo and associates [430]. This approach would remove extracellular fluorescence from the lifetime analysis, which could better define the cellular fluorescence.

Manual processing of images was very time consuming. A novel global fitting software package called FLIMfit [549] has now been developed in-house that is able to automatically fit lifetime data in batches and therefore could avoid the manual selection and processing of many acquired images, one by one.

It would be advantageous to move the microscope to the hospital as this would significantly reduce the excision to imaging time interval.

Chapter 5

The detection bandwidth used in this study was too wide to separate the relative contributions of baseline AF and PpIX fluorescence intensity. In future work it is recommended that a narrower spectral band (e.g. 635-710 nm) be employed to select the fluorescence emission of PpIX.

Chapter 6

Of the results presented in this thesis, the *in vivo* experiments undertaken in Lund on skin and basal cell carcinoma indicate the highest diagnostic potential. In 9 out of 10 cases the decrease in lifetime for BCC was greater than the mean intra-patient variation in the measured lifetimes,

suggesting a potential sensitivity of 90%. Future work on BCC could use the results from this study to perform power calculations to design future clinical trials. In future work it would be desirable to study lesions at an earlier stage and establish a better correlation between fluorescence lifetime and diffuse reflectance measurements.

Chapter 7

A limitation of this study is that emitted fluorescence spectra and lifetime were acquired *ex vivo*. All the specimens, although measured within a short time period (< 10 minutes) of excision, are therefore likely to have lower oxyhaemoglobin content compared to in vivo tissue. The resulting change in tissue oxygenation may have altered the absorption properties of the tissue and therefore affected the tissue volume sampled and the fluorescence lifetime detected. However, the measurement time for normal/diseased pairs in this study was reasonably well-matched.

While only a very limited number of IBD specimens have been studied (n=4), a consistent increase in fluorescence lifetime with 375 nm excitation was seen in all specimens, which could be investigated further with a larger number of samples.

In terms of data analysis, statistical testing and performance characterisation, recourse to megavariate analysis would be beneficial.

Directions for future work will involve the generation of a diagnostic model based on both fluorescence emission spectrum and fluorescence lifetime data. However, this would require a greater number of samples than were obtained for this study.

Chapter 8

The main difficulty when using FLS system *in vivo* was to keep the fibre-probe sufficiently still to maintain a constant interface between tissue and tip of the probe. In the future, the integration of the fibre probe within the flexible shaft of biopsy forceps or the addition of a suction port at the tip of the probe would help to ensure a constant contact with the area of mucosa tissue under investigation.

9.8 Final remarks

The work presented in this thesis has used fluorescence lifetime spectroscopy and imaging to investigate tissue autofluorescence and lifetime variations in normal and diseased tissue from a variety of tissue types, including the GI tract, skin, and bladder. Central to the clinical translation of fluorescence lifetime technology for endoscopy is the development of compact instruments that can be deployed in a practical and safe manner by clinical investigators. During this PhD, the clinical application of a novel, compact, fluorescence lifetime spectroscopy (FLS) fibre-optic probe system developed for studying tissue autofluorescence *in vivo* was pioneered. The

usability of this instrument was demonstrated through its application to both *ex vivo* and *in vivo* measurements, making it a practical tool to investigate gastrointestinal disease.

The FLS probe is immediately useable, being fully self-contained and trolley-based such that it can be readily clinically deployed. The fibre-optic probe is thin enough to pass down the working channel of a conventional endoscope to be brought into contact with the epithelium of the patient during endoscopy procedures performed as part of normal clinical care. The potential clinical impact of this new diagnostic approach was recognised by two awards at the major international GI conferences (2012, Cook Medical Marsha Dreyer Award, American Society for Gastrointestinal Endoscopy; 2011, €10,000 prize awarded by the European Federation of the International College of Surgeons).

Further work is required to increase the sample size of the disease groups investigated. Its application could extend to a wide variety of GI diseases, including liver and pancreatic disorders, which was not possible within the time constrains of this project. In the future it is desirable to progress to studies using wide-field endoscopic FLIM, which could potentially enable rapid screening with fields of view extending over several centimetres. Moving to an imaging modality would provide the clinician with an immediate overview on the fluorescence lifetime of normal tissue, thus removing the need for paired measurements of normal and diseased tissue used in this work, and allow areas with differing fluorescence lifetimes to be rapidly located. Ultimately, the development of a rapid optical screening tool, either in the form of a probe or as an integrated endoscope, could permit the identification and treatment of a number of premalignant and malignant conditions at a curable stage, thus enabling to arrest disease progression while preserving organ function and avoiding recourse to aggressive surgery by means of minimally-invasive endoscopic procedures such as radiofrequency ablation (RFA), endoscopic mucosal resection (EMR), and submucosal dissection (ESD), and Natural orifice transluminal endoscopic surgery (NOTES).

References

1. Hellier MD, Williams JG. The burden of gastrointestinal disease: implications for the provision of care in the UK. Gut 2007; 56: 165-166
2. Parliament UK. Written evidence from the British Society of Gastroenterology (CFI 43). In; February 2011
3. http://www.mayoclinic.com/health/medical/IM00374. The gastrointestinal tract. In
4. Gray H, Drake RL, Vogl W et al. Gray's anatomy for students. Philadelphia: Elsevier/Churchill Livingstone; 2010
5. Lumley JSP, Craven JL, Aitken JT. Essential anatomy and some clinical applications. Edinburgh-New York Churchill Livingstone; 1995
6. Gray H, Williams PL, Bannister LH. Gray's anatomy: the anatomical basis of medicine and surgery: Churchill Livingstone; 1995
7. Zhuo S, Yan J, Chen G et al. Label-free imaging of basement membranes differentiates normal, precancerous, and cancerous colonic tissues by second-harmonic generation microscopy. PLoS ONE 2012; 7: e38655
8. Robbins SL, Kumar V, Cotran RS. Robbins and Cotran pathologic basis of disease. Philadelphia, PA: Saunders/Elsevier; 2010
9. Chandrasoma P. Gastrointestinal pathology. Stamford, Conn.: Appleton & Lange; 1999
10. Yamamoto S, Watanabe M, Hasegawa H et al. The risk of lymph node metastasis in T1 colorectal carcinoma. Hepatogastroenterology 2004; 51: 998-1000
11. Gotoda T. A large endoscopic resection by endoscopic submucosal dissection procedure for early gastric cancer. Clin Gastroenterol Hepatol 2005; 3: S71-73
12. Conio M, Ponchon T, Blanchi S et al. Endoscopic mucosal resection. Am J Gastroenterol 2006; 101: 653-663
13. Coda S, Lee SY, Gotoda T. Endoscopic mucosal resection and endoscopic submucosal dissection as treatments for early gastrointestinal cancers in Western countries. Gut Liver 2007; 1: 12-21
14. Coda S, Oda I, Gotoda T et al. EMR and ESD for Early Gastrointestinal Cancers. In: Conio M, Siersema, P.D., Repici, A., Ponchon, T. ed, Endoscopic Mucosal Resection. Oxford: Blackwell Publishing; 2008: 185-196
15. Japanese Gastric Cancer A. Japanese Classification of Gastric Carcinoma - 2nd English Edition. Gastric Cancer 1998; 1: 10-24
16. Participants in the Paris W. The Paris endoscopic classification of superficial neoplastic lesions: esophagus, stomach, and colon: November 30 to December 1, 2002. Gastrointestinal Endoscopy 2003; 58: S3-S43
17. Endoscopic Classification Review G. Update on the Paris Classification of Superficial Neoplastic Lesions in the Digestive Tract. Endoscopy 2005; 37: 570,578
18. Holt BA, Bourke MJ. Wide Field Endoscopic Resection for Advanced Colonic Mucosal Neoplasia: Current Status and Future Directions. Clinical gastroenterology and hepatology 2012; 10: 969-979
19. Axon A. Symptoms and diagnosis of gastric cancer at early curable stage. Best Pract Res Clin Gastroenterol 2006; 20: 697-708
20. Schlemper RJ, Riddell RH, Kato Y et al. The Vienna classification of gastrointestinal epithelial neoplasia. Gut 2000; 47: 251-255
21. Stolte M. The new Vienna classification of epithelial neoplasia of the gastrointestinal tract: advantages and disadvantages. Virchows Arch 2003; 442: 99-106
22. Sugai T, Habano W, Uesugi N et al. Molecular validation of the modified Vienna classification of colorectal tumors. The Journal of molecular diagnostics : JMD 2002; 4: 191-200

23. Watanabe M, Komukai, S., Ajioka, Y., Nisikura, K., Hashidate, H., Kijima, H. Histopathology of m3 and sm1 invasive squamous cell carcinoma of the esophagus with special reference to endoscopic resection. . Stomach and Intestine 1998; 33: 985-992
24. Kashimura H, Ajioka Y, Watanabe H et al. Risk factors for nodal micrometastasis of submucosal gastric carcinoma: assessment of indications for endoscopic treatment. Gastric Cancer 1999; 2: 33-39
25. Yokoyama J, Ajioka, Y., Watanabe, H., et al. Lymh node metastatic and micrometastasis of submucosal invasive colorectal carcinoma: An indicator of the curative potential of endoscopic treatment. Acta Med Biol 2002; 50: 1-8
26. Coda S, Trentino P, Antonellis F et al. A Western single-center experience with endoscopic submucosal dissection for early gastrointestinal cancers. Gastric Cancer 2010; 13: 258-263
27. Coda S, Trentino P. Endoscopic submucosal dissection of a well-differentiated intestinal type intramucosal gastric adenocarcinoma. In: The Dave Project Gastroenterology; 2013
28. Armstrong D, Bennett JR, Blum AL et al. The endoscopic assessment of esophagitis: a progress report on observer agreement. Gastroenterology 1996; 111: 85-92
29. Lundell LR, Dent J, Bennett JR et al. Endoscopic assessment of oesophagitis: clinical and functional correlates and further validation of the Los Angeles classification. Gut 1999; 45: 172-180
30. Moayyedi P, Talley NJ. Gastro-oesophageal reflux disease. Lancet 2006; 367: 2086-2100
31. Coda S, Vergari, M., Verna, F., Falasco, G., Trentino, P. Magnifying Chromoendoscopy for detection and surveillance of Intestinal Metaplasia in Barrett's Esophagus. Gut 2006; 55: A262
32. Tschanz ER. Do 40% of Patients Resected for Barrett Esophagus With High-Grade Dysplasia Have Unsuspected Adenocarcinoma? Archives of Pathology & Laboratory Medicine 2005; 129: 177-180
33. Sharma P, Dent J, Armstrong D et al. The Development and Validation of an Endoscopic Grading System for Barrett's Esophagus: The Prague C & M Criteria. Gastroenterology 2006; 131: 1392-1399
34. Jemal A, Siegel R, Ward E et al. Cancer statistics, 2009. CA Cancer J Clin 2009; 59: 225-249
35. Eaden JA, Abrams KR, Mayberry JF. The risk of colorectal cancer in ulcerative colitis: a meta-analysis. Gut 2001; 48: 526-535
36. Mathy C, Schneider K, Chen YY et al. Gross versus microscopic pancolitis and the occurrence of neoplasia in ulcerative colitis. Inflamm Bowel Dis 2003; 9: 351-355
37. Rutter M, Saunders B, Wilkinson K et al. Severity of inflammation is a risk factor for colorectal neoplasia in ulcerative colitis. Gastroenterology 2004; 126: 451-459
38. Cairns SR, Scholefield JH, Steele RJ et al. Guidelines for colorectal cancer screening and surveillance in moderate and high risk groups (update from 2002). Gut 2010; 59: 666-689
39. Vogelstein B, Fearon ER, Hamilton SR et al. Genetic Alterations during Colorectal-Tumor Development. N Eng J Med 1988; 319: 525-532
40. Morson B. President's address. The polyp-cancer sequence in the large bowel. Proceedings of the Royal Society of Medicine 1974; 67: 451-457
41. Knudson AG. Two genetic hits (more or less) to cancer. Nature reviews Cancer 2001; 1: 157-162
42. http://chmuseum.klchb.gov.tw/know_colon_11.aspx. In
43. Shimoda T, Ikegami M, Fujisaki J et al. Early colorectal carcinoma with special reference to its development de novo. Cancer 1989; 64: 1138-1146
44. Kudo S, Tamura S, Hirota S et al. The problem of de novo colorectal carcinoma. European Journal of Cancer 1995; 31: 1118-1120
45. Hurlstone DP, Cross SS, Adam I et al. A prospective clinicopathological and endoscopic evaluation of flat and depressed colorectal lesions in the United Kingdom. Am J Gastroenterol 2003; 98: 2543-2549

46. Morson BC. Evolution of cancer of the colon and rectum. Cancer 1974; 34: suppl:845-849
47. http://www.epage.ch/EPAGE_ADM/EPAGE1/bonjour.html. European Panel on the Appropriateness of Gastrointestinal Endoscopy. In; 2008
48. Habr-Gama A, Alves PRA, Rex DK. Indications and Contraindications. In, Colonoscopy: Blackwell Publishing Ltd; 2007: 102-110
49. www.olympusamerica.com/msg_section/.../619_b_gifq160.pdf. In
50. Cotton PB, Williams CB. Practical Gastrointestinal Endoscopy. Cambridge: Blackwell Scientific Publications; 1990
51. Anthony J. DiMarino J, Benjamin SB. Gastrointestinal Disease: An Endoscopic Approach: Slack Incorporated; 2002
52. Tytgat G. Gastroenterological Endoscopy: Georg Thieme Verlag; 2010
53. http://emedtravel.files.wordpress.com/2011/04/fiber-optic-endoscope.jpg. In
54. Spach DH, Silverstein FE, Stamm WE. Transmission of Infection by Gastrointestinal Endoscopy and Bronchoscopy. Annals of internal medicine 1993; 118: 117-128
55. www.olympuskeymed.com. In; Issue 1 March 2010
56. Rex DK, Helbig CC. High yields of small and flat adenomas with high-definition colonoscopes using either white light or narrow band imaging. Gastroenterology 2007; 133: 42-47
57. Adler A, Aschenbeck J, Yenerim T et al. Narrow-band versus white-light high definition television endoscopic imaging for screening colonoscopy: a prospective randomized trial. Gastroenterology 2009; 136: 410-416 e411; quiz 715
58. Buchner A. High-Definition Colonoscopy Detects Colorectal Polyps at a Higher Rate Than Standard White-Light Colonoscopy. Clinical gastroenterology and hepatology 2010; 8: 364-370
59. Gono K, Obi T, Yamaguchi M et al. Appearance of enhanced tissue features in narrow-band endoscopic imaging. J Biomed Opt 2004; 9: 568-577
60. Kudo S, Tamura S, Nakajima T et al. Diagnosis of colorectal tumorous lesions by magnifying endoscopy. Gastrointest Endosc 1996; 44: 8-14
61. Nakaniwa N, Namihisa A, Ogihara T et al. Newly developed autofluorescence imaging videoscope system for the detection of colonic neoplasms. Digest Endosc 2005; 17: 235-240
62. Kiesslich R, Burg J, Vieth M et al. Confocal laser endoscopy for diagnosing intraepithelial neoplasias and colorectal cancer in vivo. Gastroenterology 2004; 127: 706-713
63. Wang TD, Friedland S, Sahbaie P et al. Functional Imaging of Colonic Mucosa With a Fibered Confocal Microscope for Real-Time In Vivo Pathology. Clinical Gastroenterology and Hepatology 2007; 5: 1300-1305
64. Meining A, Saur D, Bajbouj M et al. In vivo histopathology for detection of gastrointestinal neoplasia with a portable, confocal miniprobe: an examiner blinded analysis. Clin Gastroenterol Hepatol 2007; 5: 1261-1267
65. Mizeret J, Wagnieres G, Stepinac T et al. Endoscopic tissue characterization by frequency-domain fluorescence lifetime imaging (FD-FLIM). Lasers Med Sci 1997; 12: 209-217
66. Mizeret J, Stepinac T, Hansroul M et al. Instrumentation for real-time fluorescence lifetime imaging in endoscopy. Rev Sci Instrum 1999; 70: 4689-4701
67. Requejo-Isidro J, McGinty J, Munro I et al. High-speed wide-field time-gated endoscopic fluorescence-lifetime imaging. Opt Lett 2004; 29: 2249-2251
68. Munro I, McGinty J, Galletly N et al. Toward the clinical application of time-domain fluorescence lifetime imaging. J Biomed Opt 2005; 10: 051403
69. Krafft C, Ramoji AA, Bielecki C et al. A comparative Raman and CARS imaging study of colon tissue. J Biophotonics 2009; 2: 303-312
70. Georgakoudi I, Jacobson BC, Van Dam J et al. Fluorescence, reflectance, and light-scattering spectroscopy for evaluating dysplasia in patients with Barrett's esophagus. Gastroenterology 2001; 120: 1620-1629

71. Zonios G, Perelman LT, Backman V et al. Diffuse reflectance spectroscopy of human adenomatous colon polyps in vivo. Appl Opt 1999; 38: 6628-6637
72. Lovat LB, Johnson K, Mackenzie GD et al. Elastic scattering spectroscopy accurately detects high grade dysplasia and cancer in Barrett's oesophagus. Gut 2006; 55: 1078-1083
73. Shao X, Zheng W, Huang Z. Polarized near-infrared autofluorescence imaging combined with near-infrared diffuse reflectance imaging for improving colonic cancer detection. Opt Express 2010; 18: 24293-24300
74. Keller R, Winde G, Terpe HJ et al. Fluorescence endoscopy using a fluorescein-labeled monoclonal antibody against carcinoembryonic antigen in patients with colorectal carcinoma and adenoma. Endoscopy 2002; 34: 801-807
75. Mayinger B, Neumann F, Kastner C et al. Early detection of premalignant conditions in the colon by fluorescence endoscopy using local sensitization with hexaminolevulinate. Endoscopy 2008; 40: 106-109
76. Goetz M, Ziebart A, Foersch S et al. In vivo molecular imaging of colorectal cancer with confocal endomicroscopy by targeting epidermal growth factor receptor. Gastroenterology 2010; 138: 435-446
77. Endo T, Awakawa T, Takahashi H et al. Classification of Barrett's epithelium by magnifying endoscopy. Gastrointest Endosc 2002; 55: 641-647
78. Meyer V, Burtin P, Bour B et al. Endoscopic detection of early esophageal cancer in a high-risk population: does Lugol staining improve videoendoscopy? Gastrointest Endosc 1997; 45: 480-484
79. Dawsey SM, Fleischer DE, Wang GQ et al. Mucosal iodine staining improves endoscopic visualization of squamous dysplasia and squamous cell carcinoma of the esophagus in Linxian, China. Cancer 1998; 83: 220-231
80. Inoue H, Rey JF, Lightdale C. Lugol chromoendoscopy for esophageal squamous cell cancer. Endoscopy 2001; 33: 75-79
81. Committee AT, Wong Kee Song LM, Adler DG et al. Chromoendoscopy. Gastrointest Endosc 2007; 66: 639-649
82. Meining A, Rosch T, Kiesslich R et al. Inter- and intra-observer variability of magnification chromoendoscopy for detecting specialized intestinal metaplasia at the gastroesophageal junction. Endoscopy 2004; 36: 160-164
83. Canto MI, Setrakian S, Willis J et al. Methylene blue-directed biopsies improve detection of intestinal metaplasia and dysplasia in Barrett's esophagus. Gastrointest Endosc 2000; 51: 560-568
84. Canto MI, Setrakian S, Willis JE et al. Methylene blue staining of dysplastic and nondysplastic Barrett's esophagus: an in vivo and ex vivo study. Endoscopy 2001; 33: 391-400
85. Ragunath K, Krasner N, Raman VS et al. A randomized, prospective cross-over trial comparing methylene blue-directed biopsy and conventional random biopsy for detecting intestinal metaplasia and dysplasia in Barrett's esophagus. Endoscopy 2003; 35: 998-1003
86. Egger K, Werner M, Meining A et al. Biopsy surveillance is still necessary in patients with Barrett's oesophagus despite new endoscopic imaging techniques. Gut 2003; 52: 18-23
87. Lim CH, Rotimi O, Dexter SP et al. Randomized crossover study that used methylene blue or random 4-quadrant biopsy for the diagnosis of dysplasia in Barrett's esophagus. Gastrointest Endosc 2006; 64: 195-199
88. Sharma P, Weston AP, Topalovski M et al. Magnification chromoendoscopy for the detection of intestinal metaplasia and dysplasia in Barrett's oesophagus. Gut 2003; 52: 24-27
89. Guelrud M, Herrera I, Essenfeld H et al. Enhanced magnification endoscopy: a new technique to identify specialized intestinal metaplasia in Barrett's esophagus. Gastrointest Endosc 2001; 53: 559-565

90. Dinis-Ribeiro M, da Costa-Pereira A, Lopes C et al. Magnification chromoendoscopy for the diagnosis of gastric intestinal metaplasia and dysplasia. Gastrointest Endosc 2003; 57: 498-504
91. Kato S, Fujii T, Koba I et al. Assessment of colorectal lesions using magnifying colonoscopy and mucosal dye spraying: can significant lesions be distinguished? Endoscopy 2001; 33: 306-310
92. Kiesslich R, Jung M. Magnification endoscopy: does it improve mucosal surface analysis for the diagnosis of gastrointestinal neoplasias? Endoscopy 2002; 34: 819-822
93. Le Rhun M, Coron E, Parlier D et al. High resolution colonoscopy with chromoscopy versus standard colonoscopy for the detection of colonic neoplasia: a randomized study. Clin Gastroenterol Hepatol 2006; 4: 349-354
94. Brooker JC, Saunders BP, Shah SG et al. Total colonic dye-spray increases the detection of diminutive adenomas during routine colonoscopy: a randomized controlled trial. Gastrointest Endosc 2002; 56: 333-338
95. Hurlstone DP, Cross SS, Slater R et al. Detecting diminutive colorectal lesions at colonoscopy: a randomised controlled trial of pan-colonic versus targeted chromoscopy. Gut 2004; 53: 376-380
96. Gono K, Yamazaki K, Doguchi N et al. Endoscopic observation of tissue by narrowband illumination. Optical Review 2003; 10: 211-215
97. Kara MA, Peters FP, Rosmolen WD et al. High-resolution endoscopy plus chromoendoscopy or narrow-band imaging in Barrett's esophagus: a prospective randomized crossover study. Endoscopy 2005; 37: 929-936
98. Wolfsen HC, Crook JE, Krishna M et al. Prospective, controlled tandem endoscopy study of narrow band imaging for dysplasia detection in Barrett's Esophagus. Gastroenterology 2008; 135: 24-31
99. Sharma P, Hawes RH, Bansal A et al. Standard endoscopy with random biopsies versus narrow band imaging targeted biopsies in Barrett's oesophagus: a prospective, international, randomised controlled trial. Gut 2013; 62: 15-21
100. East JE, Suzuki N, Saunders BP. Comparison of magnified pit pattern interpretation with narrow band imaging versus chromoendoscopy for diminutive colonic polyps: a pilot study. Gastrointest Endosc 2007; 66: 310-316
101. East JE, Suzuki N, Bassett P et al. Narrow band imaging with magnification for the characterization of small and diminutive colonic polyps: pit pattern and vascular pattern intensity. Endoscopy 2008; 40: 811-817
102. East JE, Suzuki N, Stavrinidis M et al. Narrow band imaging for colonoscopic surveillance in hereditary non-polyposis colorectal cancer. Gut 2008; 57: 65-70
103. East JE, Tan EK, Bergman JJ et al. Meta-analysis: narrow band imaging for lesion characterization in the colon, oesophagus, duodenal ampulla and lung. Aliment Pharmacol Ther 2008; 28: 854-867
104. Adler A, Pohl H, Papanikolaou IS et al. A prospective randomised study on narrow-band imaging versus conventional colonoscopy for adenoma detection: does narrow-band imaging induce a learning effect? Gut 2008; 57: 59-64
105. Adler A, Aschenbeck J, Yenerim T et al. Narrow-Band Versus White-Light High Definition Television Endoscopic Imaging for Screening Colonoscopy: A Prospective Randomized Trial. Gastroenterology 2009; 136: 410-416
106. Dekker E, van den Broek FJ, Reitsma JB et al. Narrow-band imaging compared with conventional colonoscopy for the detection of dysplasia in patients with longstanding ulcerative colitis. Endoscopy 2007; 39: 216-221
107. Miyake Y, Sekiya T, Hara T. A new spectrophotometer for measuring the spectral reflectance of gastric mucous membrane. J Photogr Sci 1989; 0022-3638 37: 134–138
108. Miyake Y, Nakaguchi T, Tsumura N et al. Development of new electronic endoscopes using the spectral images of an internal organ. In, Proceedings of the IS&T/SID's Thirteen Color Imaging Conference; 2005
109. http://www.fujifilm.com/. In

110. Hoffman A, Kagel C, Goetz M et al. Recognition and characterization of small colonic neoplasia with high-definition colonoscopy using i-Scan is as precise as chromoendoscopy. Digestive and liver disease : official journal of the Italian Society of Gastroenterology and the Italian Association for the Study of the Liver 2010; 42: 45-50
111. Pohl J, May A, Rabenstein T et al. Comparison of computed virtual chromoendoscopy and conventional chromoendoscopy with acetic acid for detection of neoplasia in Barrett's esophagus. Endoscopy 2007; 39: 594-598
112. Osawa H, Yamamoto H, Yamada N et al. Diagnosis of endoscopic Barrett's esophagus by transnasal flexible spectral imaging color enhancement. J Gastroenterol 2009; 44: 1125-1132
113. Neumann H, Fry LC, Bellutti M et al. Double-balloon enteroscopy-assisted virtual chromoendoscopy for small-bowel disorders: a case series. Endoscopy 2009; 41: 468-471
114. Hoffman A, Basting N, Goetz M et al. High-definition endoscopy with i-Scan and Lugol's solution for more precise detection of mucosal breaks in patients with reflux symptoms. Endoscopy 2009; 41: 107-112
115. Mlkvy P, Messmann H, Regula J et al. Sensitization and photodynamic therapy (PDT) of gastrointestinal tumors with 5-aminolaevulinic acid (ALA) induced protoporphyrin IX (PPIX). A pilot study. Neoplasma 1995; 42: 109-113
116. Gossner L, Stolte M, Sroka R et al. Photodynamic ablation of high-grade dysplasia and early cancer in Barrett's esophagus by means of 5-aminolevulinic acid. Gastroenterology 1998; 114: 448-455
117. Messmann H, Knuchel R, Baumler W et al. Endoscopic fluorescence detection of dysplasia in patients with Barrett's esophagus, ulcerative colitis, or adenomatous polyps after 5-aminolevulinic acid-induced protoporphyrin IX sensitization. Gastrointest Endosc 1999; 49: 97-101
118. Webber J, Kessel D, Fromm D. Side effects and photosensitization of human tissues after aminolevulinic acid. J Surg Res 1997; 68: 31-37
119. Kriegmair M, Baumgartner R, Knuchel R et al. Detection of early bladder cancer by 5-aminolevulinic acid induced porphyrin fluorescence. J Urol 1996; 155: 105-109; discussion 109-110
120. Leunig A, Rick K, Stepp H et al. Fluorescence imaging and spectroscopy of 5-aminolevulinic acid induced protoporphyrin IX for the detection of neoplastic lesions in the oral cavity. Am J Surg 1996; 172: 674-677
121. af Klinteberg C, Enejder AM, Wang I et al. Kinetic fluorescence studies of 5-aminolaevulinic acid-induced protoporphyrin IX accumulation in basal cell carcinomas. J Photochem Photobiol B 1999; 49: 120-128
122. Endlicher E, Knuchel R, Furst A et al. [Endoscopic fluorescence diagnosis of esophageal carcinoma after sensitization with 5-aminolevulinic acid]. Med Klin (Munich) 2001; 96: 157-160
123. Abdalla SI, Lao-Sirieix P, Novelli MR et al. Gastrin-induced cyclooxygenase-2 expression in Barrett's carcinogenesis. Clinical cancer research : an official journal of the American Association for Cancer Research 2004; 10: 4784-4792
124. von Holstein CS, Nilsson AM, Andersson-Engels S et al. Detection of adenocarcinoma in Barrett's oesophagus by means of laser induced fluorescence. Gut 1996; 39: 711-716
125. Endlicher E, Knuechel R, Hauser T et al. Endoscopic fluorescence detection of low and high grade dysplasia in Barrett's oesophagus using systemic or local 5-aminolaevulinic acid sensitisation. Gut 2001; 48: 314-319
126. Brand S, Wang T, Schomacker K et al. Detection of high-grade dysplasia in Barrett's esophagus by spectroscopy measurement of 5-aminolevulinic acid-induced protoporphyrin IX fluorescence. Gastrointestinal Endoscopy 2002; 56: 479-487
127. Messmann H, Endlicher E, Freunek G et al. Fluorescence endoscopy for the detection of low and high grade dysplasia in ulcerative colitis using systemic or local 5-aminolaevulinic acid sensitisation. Gut 2003; 52: 1003-1007

128. Ochsenkuhn T, Tillack C, Stepp H et al. Low frequency of colorectal dysplasia in patients with long-standing inflammatory bowel disease colitis: detection by fluorescence endoscopy. Endoscopy 2006; 38: 477-482
129. Eker C, Montan S, Jaramillo E et al. Clinical spectral characterisation of colonic mucosal lesions using autofluorescence and delta aminolevulinic acid sensitisation. Gut 1999; 44: 511-518
130. Brand S, Stepp H, Ochsenkuhn T et al. Detection of colonic dysplasia by light-induced fluorescence endoscopy: a pilot study. International journal of colorectal disease 1999; 14: 63-68
131. Izuishi K, Tajiri H, Ryu M et al. Detection of bile duct cancer by autofluorescence cholangioscopy: a pilot study. Hepatogastroenterology 1999; 46: 804-807
132. Endlicher E, Gelbmann CM, Knuchel R et al. Hexaminolevulinate-induced fluorescence endoscopy in patients with rectal adenoma and cancer: a pilot study. Gastrointest Endosc 2004; 60: 449-454
133. Ortner MA, Ebert B, Hein E et al. Time gated fluorescence spectroscopy in Barrett's oesophagus. Gut 2003; 52: 28-33
134. Ortner MA, Fusco V, Ebert B et al. Time-gated fluorescence spectroscopy improves endoscopic detection of low-grade dysplasia in ulcerative colitis. Gastrointest Endosc 2010; 71: 312-318
135. Wong Kee Song L-M, Banerjee S, Desilets D et al. Autofluorescence imaging. Gastrointestinal Endoscopy 2011; 73: 647-650
136. van den Broek FJC, Fockens P, van Eeden S et al. Endoscopic tri-modal imaging for surveillance in ulcerative colitis: randomised comparison of high-resolution endoscopy and autofluorescence imaging for neoplasia detection; and evaluation of narrow-band imaging for classification of lesions. Gut 2008; 57: 1083-1089
137. Falk GW. Autofluorescence endoscopy. Gastrointestinal Endoscopy Clinics of North America 2009; 19: 209-220
138. Minsky M. Microscopy Apparatus. In. U.S.; 1957
139. Minsky M. Memoir on Inventing the Confocal Scanning Microscope. Scanning 1988; 10: 128-138
140. Kumar S. Development of multidimensional fluorescence imaging technology with a view towards the imaging of signalling at the immunological synapse. London Imperial College London; 2010:
141. Committee AT, Kantsevoy SV, Adler DG et al. Confocal laser endomicroscopy. Gastrointest Endosc 2009; 70: 197-200
142. Humphris J, Swartz D, Egan BJ et al. Status of confocal laser endomicroscopy in gastrointestinal disease. Tropical gastroenterology : official journal of the Digestive Diseases Foundation 2012; 33: 9-20
143. Azar FS, Intes X. Translational multimodality optical imaging. Boston: Artech House; 2008
144. Goetz M, Kiesslich R. Advanced imaging of the gastrointestinal tract: research vs. clinical tools? Curr Opin Gastroenterol 2009; 25: 412-421
145. Polglase A, McLaren W, Skinner S et al. A fluorescence confocal endomicroscope for in vivo microscopy of the upper- and the lower-GI tract. Gastrointest Endosc 2005; 62: 686-695
146. Burleson GR, Caulfield MJ, Pollard M. Ozonation of mutagenic and carcinogenic polyaromatic amines and polyaromatic hydrocarbons in water. Cancer Res 1979; 39: 2149-2154
147. Becker V, von Delius S, Bajbouj M et al. Intravenous application of fluorescein for confocal laser scanning microscopy: evaluation of contrast dynamics and image quality with increasing injection-to-imaging time. Gastrointestinal Endoscopy 2008; 68: 319-323
148. Kiesslich R, Neurath MF. Endomicroscopy is born--do we still need the pathologist? Gastrointest Endosc 2007; 66: 150-153

149. Nguyen NQ, Leong RWL. Current application of confocal endomicroscopy in gastrointestinal disorders. Journal of Gastroenterology and Hepatology 2008; 23: 1483-1491
150. De Palma GD. Confocal laser endomicroscopy in the "in vivo" histological diagnosis of the gastrointestinal tract. World J Gastroenterol 2009; 15: 5770-5775
151. Kiesslich R, Gossner L, Goetz M et al. In vivo histology of Barrett's esophagus and associated neoplasia by confocal laser endomicroscopy. Clin Gastroenterol Hepatol 2006; 4: 979-987
152. Kiesslich R, Goetz M, Burg J et al. Diagnosing Helicobacter pylori in vivo by confocal laser endoscopy. Gastroenterology 2005; 128: 2119-2123
153. Neumann H, Vieth M, Raithel M et al. Confocal laser endomicroscopy for the in vivo detection of intraepithelial neoplasia in Peutz-Jeghers polyps. Endoscopy 2010; 42 Suppl 2: E139-140
154. Neufert C, Vieth M, Monkemuller K et al. In vivo diagnosis and characterisation of Whipple's disease. Lancet Infect Dis 2011; 11: 970
155. Sanduleanu S, Driessen A, Gomez-Garcia E et al. In vivo diagnosis and classification of colorectal neoplasia by chromoendoscopy-guided confocal laser endomicroscopy. Clin Gastroenterol Hepatol 2010; 8: 371-378
156. Kang D, Suter MJ, Boudoux C et al. Comprehensive imaging of gastroesophageal biopsy samples by spectrally encoded confocal microscopy. Gastrointestinal Endoscopy 2010; 71: 35-43
157. Yoo H, Kang D, Katz AJ et al. Reflectance confocal microscopy for the diagnosis of eosinophilic esophagitis: a pilot study conducted on biopsy specimens. Gastrointestinal Endoscopy 2011; 74: 992-1000
158. Wallace MB, Sharma P, Lightdale C et al. Preliminary accuracy and interobserver agreement for the detection of intraepithelial neoplasia in Barrett's esophagus with probe-based confocal laser endomicroscopy. Gastrointest Endosc 2010; 72: 19-24
159. Sharma P, Meining AR, Coron E et al. Real-time increased detection of neoplastic tissue in Barrett's esophagus with probe-based confocal laser endomicroscopy: final results of an international multicenter, prospective, randomized, controlled trial. Gastrointest Endosc 2011; 74: 465-472
160. Bajbouj M, Vieth M, Rösch T et al. Probe-based confocal laser endomicroscopy compared with standard four-quadrant biopsy for evaluation of neoplasia in Barrett's esophagus. Endoscopy 2010; 42: 435,440
161. Neumann H, Vieth M, Atreya R et al. First description of eosinophilic esophagitis using confocal laser endomicroscopy (with video). Endoscopy 2011; 43 Suppl 2 UCTN: E66
162. Meining A, Chen YK, Pleskow D et al. Direct visualization of indeterminate pancreaticobiliary strictures with probe-based confocal laser endomicroscopy: a multicenter experience. Gastrointest Endosc 2011; 74: 961-968
163. Loeser CS, Robert ME, Mennone A et al. Confocal Endomicroscopic Examination of Malignant Biliary Strictures and Histologic Correlation With Lymphatics. Journal of Clinical Gastroenterology 2011; 45: 246-252 210.1097/MCG.1090b1013e3181fbdc1038
164. Meining A, Frimberger E, Becker V et al. Detection of Cholangiocarcinoma In Vivo Using Miniprobe-Based Confocal Fluorescence Microscopy. Clinical Gastroenterology and Hepatology 2008; 6: 1057-1060
165. Meining A, Phillip V, Gaa J et al. Pancreaticoscopy with miniprobe-based confocal laser-scanning microscopy of an intraductal papillary mucinous neoplasm (with video). Gastrointestinal Endoscopy 2009; 69: 1178-1180
166. Liu JJ, Wong K, Thiesen AL et al. Increased epithelial gaps in the small intestines of patients with inflammatory bowel disease: density matters. Gastrointestinal Endoscopy 2011; 73: 1174-1180
167. Liu JJ, Madsen KL, Boulanger P et al. Mind The Gaps: Confocal Endomicroscopy Showed Increased Density of Small Bowel Epithelial Gaps in Inflammatory Bowel Disease. Journal of Clinical Gastroenterology 2011; 45: 240-245

168. De Palma GD. *In-vivo* characterization of DALM in ulcerative colitis with high-resolution probe-based confocal laser endomicroscopy. World J Gastroenterol 2011; 17: 677-680
169. van den Broek FJC, van Es JA, van Eeden S et al. Pilot study of probe-based confocal laser endomicroscopy during colonoscopic surveillance of patients with longstanding ulcerative colitis. Endoscopy 2011; 43: 116,122
170. Buchner AM, Wallace MB. Future expectations in digestive endoscopy: competition with other novel imaging techniques. Best Pract Res Clin Gastroenterol 2008; 22: 971-987
171. Buchner AM, Shahid MW, Heckman MG et al. Comparison of Probe-Based Confocal Laser Endomicroscopy With Virtual Chromoendoscopy for Classification of Colon Polyps. Gastroenterology 2010; 138: 834-842
172. Buchner AM, Gomez V, Heckman MG et al. The learning curve of in vivo probe-based confocal laser endomicroscopy for prediction of colorectal neoplasia. Gastrointestinal Endoscopy 2011; 73: 556-560
173. Shahid MW, Buchner AM, Coron E et al. Diagnostic accuracy of probe-based confocal laser endomicroscopy in detecting residual colorectal neoplasia after EMR: a prospective study. Gastrointestinal Endoscopy, DOI: 10.1016/j.gie.2011.08.024:
174. De Palma GD, Staibano S, Siciliano S et al. In vivo characterisation of superficial colorectal neoplastic lesions with high-resolution probe-based confocal laser endomicroscopy in combination with video-mosaicing: A feasibility study to enhance routine endoscopy. Digestive and Liver Disease 2010; 42: 791-797
175. Hsiung P-L, Hardy J, Friedland S et al. Detection of colonic dysplasia in vivo using a targeted heptapeptide and confocal microendoscopy. Nat Med 2008; 14: 454-458
176. Gómez V, Buchner AM, Dekker E et al. Interobserver agreement and accuracy among international experts with probe-based confocal laser endomicroscopy in predicting colorectal neoplasia. Endoscopy 2010; 42: 286,291
177. Inoue H, Sasajima K, Kaga M et al. Endoscopic in vivo evaluation of tissue atypia in the esophagus using a newly designed integrated endocytoscope: a pilot trial. Endoscopy 2006; 38: 891-895
178. Kwon RS, Wong Kee Song LM, Adler DG et al. Endocytoscopy. Gastrointest Endosc 2009; 70: 610-613
179. Sasajima K, Kudo SE, Inoue H et al. Real-time in vivo virtual histology of colorectal lesions when using the endocytoscopy system. Gastrointest Endosc 2006; 63: 1010-1017
180. Cipolletta L, Bianco MA, Rotondano G et al. Endocytoscopy can identify dysplasia in aberrant crypt foci of the colorectum: a prospective in vivo study. Endoscopy 2009; 41: 129-132
181. Neumann H, Vieth M, Neurath MF. Image of the month. Endocytoscopy-based detection of focal high-grade intraepithelial neoplasia in colonic polyps. Clin Gastroenterol Hepatol 2011; 9: e13
182. Kumagai Y, Kawada K, Yamazaki S et al. Endocytoscopic observation for esophageal squamous cell carcinoma: can biopsy histology be omitted? Dis Esophagus 2009; 22: 505-512
183. Pohl H, Rosch T, Tanczos BT et al. Endocytoscopy for the detection of microstructural features in adult patients with celiac sprue: a prospective, blinded endocytoscopy-conventional histology correlation study. Gastrointest Endosc 2009; 70: 933-941
184. Myaing MT, MacDonald DJ, Li X. Fiber-optic scanning two-photon fluorescence endoscope. Optics Letters 2006; 31: 1076-1078
185. Engelbrecht CJ, Johnston RS, Seibel EJ et al. Ultra-compact fiber-optic two-photon microscope for functional fluorescence imaging in vivo. Opt Express 2008; 16: 5556-5564
186. Piyawattanametha W, Cocker ED, Burns LD et al. In vivo brain imaging using a portable 2.9 g two-photon microscope based on a microelectromechanical systems scanning mirror. Opt Lett 2009; 34: 2309-2311

187. Tang S, Jung W, McCormick D et al. Design and implementation of fiber-based multiphoton endoscopy with microelectromechanical systems scanning. J Biomed Opt 2009; 14: 034005
188. Rivera DR, Brown CM, Ouzounov DG et al. Compact and flexible raster scanning multiphoton endoscope capable of imaging unstained tissue. Proc Natl Acad Sci U S A 2011; 108: 17598-17603
189. Campagnola P. Second harmonic generation imaging microscopy: applications to diseases diagnostics. Anal Chem 2011; 83: 3224-3231
190. Sun W, Chang S, Tai DC et al. Nonlinear optical microscopy: use of second harmonic generation and two-photon microscopy for automated quantitative liver fibrosis studies. J Biomed Opt 2008; 13: 064010
191. Tearney GJ, Brezinski ME, Bouma BE et al. In vivo endoscopic optical biopsy with optical coherence tomography. Science 1997; 276: 2037-2039
192. Drexler W, Morgner U, Kartner FX et al. In vivo ultrahigh-resolution optical coherence tomography. Opt Lett 1999; 24: 1221-1223
193. Fockens P. Future developments in endoscopic imaging. Best Pract Res Clin Gastroenterol 2002; 16: 999-1012
194. Tearney GJ, Brezinski ME, Southern JF et al. Optical biopsy in human gastrointestinal tissue using optical coherence tomography. Am J Gastroenterol 1997; 92: 1800-1804
195. Zuccaro G, Gladkova N, Vargo J et al. Optical coherence tomography of the esophagus and proximal stomach in health and disease. Am J Gastroenterol 2001; 96: 2633-2639
196. Das A, Sivak MV, Chak A et al. High-resolution endoscopic imaging of the GI tract: a comparative study of optical coherence tomography versus high-frequency catheter probe EUS. Gastrointestinal Endoscopy 2001; 54: 219-224
197. Zhou C, Adler DC, Becker L et al. Effective treatment of chronic radiation proctitis using radiofrequency ablation. Therapeutic advances in gastroenterology 2009; 2: 149-156
198. Vakoc BJ, Shishko M, Yun SH et al. Comprehensive esophageal microscopy by using optical frequency-domain imaging (with video). Gastrointest Endosc 2007; 65: 898-905
199. Suter MJ, Vakoc BJ, Yachimski PS et al. Comprehensive microscopy of the esophagus in human patients with optical frequency domain imaging. Gastrointest Endosc 2008; 68: 745-753
200. Suter MJ, Nishioka NS, Yoo H et al. S1591: Barrett's Esophagus Screening Using Balloon-Based Optical Frequency Domain Imaging: A Comparison With Endoscopy. Gastrointestinal Endoscopy 2010; 71: AB202
201. Zhou C, Kirtane T, Tsai TH et al. Three-dimensional endoscopic optical coherence tomography imaging of cervical inlet patch. Gastrointest Endosc 2012; 75: 675-677; discussion 677
202. Raman CV, Krishnan KS. A new type of secondary radiation. Nature 1928; 121: 501–502.
203. Shim MG, Song LM, Marcon NE et al. In vivo near-infrared Raman spectroscopy: demonstration of feasibility during clinical gastrointestinal endoscopy. Photochem Photobiol 2000; 72: 146-150
204. Molckovsky A, Song LM, Shim MG et al. Diagnostic potential of near-infrared Raman spectroscopy in the colon: differentiating adenomatous from hyperplastic polyps. Gastrointest Endosc 2003; 57: 396-402
205. Stone N, Kendall C, Shepherd N et al. Near-infrared Raman spectroscopy for the classification of epithelial pre-cancers and cancers. J Raman Spectrosc 2002; 33: 564-573
206. Day JC, Bennett R, Smith B et al. A miniature confocal Raman probe for endoscopic use. Physics in medicine and biology 2009; 54: 7077-7087
207. Kendall C, Day J, Hutchings J et al. Evaluation of Raman probe for oesophageal cancer diagnostics. Analyst 2010; 135: 3038-3041
208. Almond LM, Hutchings J, Kendall C et al. Assessment of a custom-built Raman spectroscopic probe for diagnosis of early oesophageal neoplasia. Journal of Biomedical Optics 2012; 17: 081421-081421

209. Bergholt MS, Zheng W, Lin K et al. In vivo diagnosis of esophageal cancer using image-guided Raman endoscopy and biomolecular modeling. Technol Cancer Res Treat 2011; 10: 103-112
210. Duraipandian S, Bergholt MS, Zheng W et al. Real-time Raman spectroscopy for in vivo, online gastric cancer diagnosis during clinical endoscopic examination. J Biomed Opt 2012; 17: 081418-081418
211. Shao X, Zheng W, Huang Z. Near-infrared autofluorescence spectroscopy for in vivo identification of hyperplastic and adenomatous polyps in the colon. Biosensors and Bioelectronics 2011; 30: 118-122
212. Zhang G, Demos SG, Alfano RR. Far-red and NIR spectral wing emission from tissues under 532 and 632 nm photo-excitation. Lasers in the Life Sciences 1999; 9: 1-16
213. Wagnieres GA, Star WM, Wilson BC. In vivo fluorescence spectroscopy and imaging for oncological applications. Photochem Photobiol 1998; 68: 603-632
214. Wong Kee Song LM, Marcon NE. Fluorescence and Raman spectroscopy. Gastrointest Endosc Clin N Am 2003; 13: 279-296
215. Légaré F, Evans CL, Ganikhanov F et al. Towards CARS Endoscopy. Opt Express 2006; 14: 4427-4432
216. Wang Z, Liu Y, Gao L et al. Use of multimode optical fibers for fiber-based coherent anti-Stokes Raman scattering microendoscopy imaging. Opt Lett 2011; 36: 2967-2969
217. Backman V, Wallace MB, Perelman LT et al. Detection of preinvasive cancer cells. Nature 2000; 406: 35-36
218. Johansson A, Kromer K, Sroka R et al. Clinical optical diagnostics – Status and perspectives. Medical Laser Application 2008; 23: 155-174
219. Marchesini R, Cascinelli N, Brambilla M et al. In vivo spectrophotometric evaluation of neoplastic and non-neoplastic skin pigmented lesions. II: Discriminant analysis between nevus and melanoma. Photochem Photobiol 1992; 55: 515-522
220. Farina B, Bartoli C, Bono A et al. Multispectral imaging approach in the diagnosis of cutaneous melanoma: potentiality and limits. Physics in medicine and biology 2000; 45: 1243-1254
221. Wallace VP, Crawford DC, Mortimer PS et al. Spectrophotometric assessment of pigmented skin lesions: methods and feature selection for evaluation of diagnostic performance. Physics in medicine and biology 2000; 45: 735-751
222. Koenig F, Larne R, Enquist H et al. Spectroscopic measurement of diffuse reflectance for enhanced detection of bladder carcinoma. Urology 1998; 51: 342-345
223. Mourant JR, Bocklage TJ, Powers TM et al. In vivo light scattering measurements for detection of precancerous conditions of the cervix. Gynecol Oncol 2007; 105: 439-445
224. Mourant JR, Bigio IJ, Boyer J et al. Spectroscopic diagnosis of bladder cancer with elastic light scattering. Laser Surg Med 1995; 17: 350-357
225. Bigio IJ, Mourant JR. Ultraviolet and visible spectroscopies for tissue diagnostics: fluorescence spectroscopy and elastic-scattering spectroscopy. Physics in medicine and biology 1997; 42: 803-814
226. Mourant JR, Bigio IJ, Boyer JD et al. Elastic scattering spectroscopy as a diagnostic tool for differentiating pathologies in the gastrointestinal tract: preliminary testing. J Biomed Opt 1996; 1: 192-199
227. Ge Z, Schomacker KT, Nishioka NS. Identification of Colonic Dysplasia and Neoplasia by Diffuse Reflectance Spectroscopy and Pattern Recognition Techniques. Appl Spectrosc 1998; 52: 833-839
228. Dhar A, Johnson KS, Novelli MR et al. Elastic scattering spectroscopy for the diagnosis of colonic lesions: initial results of a novel optical biopsy technique. Gastrointest Endosc 2006; 63: 257-261
229. Roy HK, Gomes A, Turzhitsky V et al. Spectroscopic Microvascular Blood Detection From the Endoscopically Normal Colonic Mucosa: Biomarker for Neoplasia Risk. Gastroenterology 2008; 135: 1069-1078

230. Pyhtila JW, Chalut KJ, Boyer JD et al. In situ detection of nuclear atypia in Barrett's esophagus by using angle-resolved low-coherence interferometry. Gastrointestinal Endoscopy 2007; 65: 487-491
231. Togashi K, Osawa H, Koinuma K et al. A comparison of conventional endoscopy, chromoendoscopy, and the optimal-band imaging system for the differentiation of neoplastic and non-neoplastic colonic polyps. Gastrointestinal Endoscopy 2009; 69: 734-741
232. Rastogi A, Keighley J, Singh V et al. High accuracy of narrow band imaging without magnification for the real-time characterization of polyp histology and its comparison with high-definition white light colonoscopy: a prospective study. Am J Gastroenterol 2009; 104: 2422-2430
233. Kuiper T, van den Broek FJ, Naber AH et al. Endoscopic trimodal imaging detects colonic neoplasia as well as standard video endoscopy. Gastroenterology 2011; 140: 1887-1894
234. Rex DK, Cutler CS, Lemmel GT et al. Colonoscopic miss rates of adenomas determined by back-to-back colonoscopies. Gastroenterology 1997; 112: 24-28
235. van Rijn JC, Reitsma JB, Stoker J et al. Polyp miss rate determined by tandem colonoscopy: a systematic review. Am J Gastroenterol 2006; 101: 343-350
236. Rabeneck L, Paszat LF, Hilsden RJ et al. Bleeding and perforation after outpatient colonoscopy and their risk factors in usual clinical practice. Gastroenterology 2008; 135: 1899-1906, 1906 e1891
237. Thiis-Evensen E, Hoff GS, Sauar J et al. Population-based surveillance by colonoscopy: effect on the incidence of colorectal cancer. Telemark Polyp Study I. Scand J Gastroenterol 1999; 34: 414-420
238. Leung K, Pinsky P, Laiyemo AO et al. Ongoing colorectal cancer risk despite surveillance colonoscopy: the Polyp Prevention Trial Continued Follow-up Study. Gastrointest Endosc 2010; 71: 111-117
239. Pinsky PF, Fleshman J, Mutch M et al. One year recurrence of aberrant crypt foci. Cancer prevention research 2010; 3: 839-843
240. Itzkowitz S, Ullman T. The world isn't flat. Gastrointest Endosc 2004; 60: 426-427
241. Heitmiller RF, Redmond M, Hamilton SR. Barrett's esophagus with high-grade dysplasia. An indication for prophylactic esophagectomy. Ann Surg 1996; 224: 66-71
242. Falk GW, Rice TW, Goldblum JR et al. Jumbo biopsy forceps protocol still misses unsuspected cancer in Barrett's esophagus with high-grade dysplasia. Gastrointest Endosc 1999; 49: 170-176
243. Cross SS, Stone JL. Proactive management of histopathology workloads: analysis of the UK Royal College of Pathologists' recommendations on specimens of limited or no clinical value on the workload of a teaching hospital gastrointestinal pathology service. J Clin Pathol 2002; 55: 850-852
244. Hotouras A, Collins P, Speake W et al. Diagnostic yield and economic implications of endoscopic colonic biopsies in patients with chronic diarrhoea. Colorectal Dis 2012; 14: 985-988
245. Stokes GG. On the Change of Refrangibility of Light. Philosophical Transactions of the Royal Society of London 1852; 142: 463-562
246. Zipfel WR, Williams RM, Webb WW. Nonlinear magic: multiphoton microscopy in the biosciences. Nat Biotechnol 2003; 21: 1369-1377
247. Lakowicz J. Principles of Fluorescence Spectroscopy. 2 ed: KA/PP; 1999
248. Tadrous PJ. Methods for imaging the structure and function of living tissues and cells: 2. Fluorescence lifetime imaging. J Pathol 2000; 191: 229-234
249. Tadrous P. The imaging of benign and malignant breast tissue by fluorescence lifetime imaging and optical coherence tomography [PhD thesis]. London University of London; 2003:
250. Webb SED. Development and Application of Widefield Fluorescence Lifetime Imaging [PhD thesis]. London University of London; 2003:

251. Cubeddu R, Comelli D, D'Andrea C et al. Time-resolved fluorescence imaging in biology and medicine. J Phys D: Appl Phys 2002; 35: R61-R76
252. Lakowicz JR. Principles of Fluorescence Spectroscopy. 3 ed. New York: Springer; 2006
253. Siegel J, Elson DS, Webb SE et al. Studying biological tissue with fluorescence lifetime imaging: microscopy, endoscopy, and complex decay profiles. Appl Opt 2003; 42: 2995-3004
254. Elson DS, Requejo-Isidro J, Munro I et al. Time-domain fluorescence lifetime imaging applied to biological tissue. Photochem Photobiol Sci 2004; 3: 795-801
255. Glanzmann T, Ballini JP, van den Bergh H et al. Time-resolved spectrofluorometer for clinical tissue characterization during endoscopy. Rev Sci Instrum 1999; 70: 4067-4077
256. Pitts JD, Mycek MA. Design and development of a rapid acquisition laser-based fluorometer with simultaneous spectral and temporal resolution. Rev Sci Instrum 2001; 72: 3061-3072
257. Agronskaia AV, Tertoolen L, Gerritsen HC. High frame rate fluorescence lifetime imaging. J Phys D Appl Phys 2003; 36: 1655-1662
258. De Beule PAA, Dunsby C, Galletly NP et al. A hyperspectral fluorescence lifetime probe for skin cancer diagnosis. Rev Sci Instrum 2007; 78: 123101
259. Colyer RA, Lee C, Gratton E. A novel fluorescence lifetime imaging system that optimizes photon efficiency. Microscopy research and technique 2008; 71: 201-213
260. Sanders R, Draaijer A, Gerritsen HC et al. Quantitative pH imaging in cells using confocal fluorescence lifetime imaging microscopy. Analytical biochemistry 1995; 227: 302-308
261. Szmacinski H, Lakowicz JR. Sodium Green as a potential probe for intracellular sodium imaging based on fluorescence lifetime. Analytical biochemistry 1997; 250: 131-138
262. Elson DS, Siegel J, Webb SED et al. Fluorescence lifetime system for microscopy and multiwell plate imaging with a blue picosecond diode laser. Optics Letters 2002; 27: 1409-1411
263. Kamma I, Kommidi P, Reddy BR. Design of a high temperature sensing system using luminescence lifetime measurement. Rev Sci Instrum 2008; 79: 096104
264. Robinson T, Schaerli Y, Wootton R et al. Removal of background signals from fluorescence thermometry measurements in PDMS microchannels using fluorescence lifetime imaging. Lab Chip 2009; 9: 3437-3441
265. Mycek M, Schomacker K, Nishioka N. Colonic polyp differentiation using time-resolved autofluorescence spectroscopy. Gastrointest Endosc 1998; 48: 390-394
266. Pfefer TJ, Paithankar DY, Poneros JM et al. Temporally and spectrally resolved fluorescence spectroscopy for the detection of high grade dysplasia in Barrett's esophagus. Lasers Surg Med 2003; 32: 10-16
267. Butte PV, Pikul BK, Hever A et al. Diagnosis of meningioma by time-resolved fluorescence spectroscopy. Journal of Biomedical Optics 2005; 10:
268. Chen HM, Chiang CP, You C et al. Time-resolved autofluorescence spectroscopy for classifying normal and premalignant oral tissues. Laser Surg Med 2005; 37: 37-45
269. Leppert J, Krajewski J, Kantelhardt SR et al. Multiphoton excitation of autofluorescence for microscopy of glioma tissue. Neurosurgery 2006; 58: 759-767
270. Galletly NP, McGinty J, Dunsby C et al. Fluorescence lifetime imaging distinguishes basal cell carcinoma from surrounding uninvolved skin. Br J Dermatol 2008; 159: 152-161
271. Butte PV, Fang Q, Jo JA et al. Intraoperative delineation of primary brain tumors using time-resolved fluorescence spectroscopy. J Biomed Opt 2010; 15: 027008
272. Cicchi R, Crisci A, Cosci A et al. Time- and Spectral-resolved two-photon imaging of healthy bladder mucosa and carcinoma in situ. Opt Express 2010; 18: 3840-3849
273. McGinty J, Galletly NP, Dunsby C et al. Wide-field fluorescence lifetime imaging of cancer. Biomed Opt Express 2010; 1: 627-640
274. American Cancer Society. Cancer Facts and Figures 2006. In. Atlanta, USA: American Cancer Society; 2006
275. RichardsKortum R, SevickMuraca E. Quantitative optical spectroscopy for tissue diagnosis. Annual Review of Physical Chemistry 1996; 47: 555-606

276. De Veld DCG, Witjes MJH, Sterenborg HJCM et al. The status of in vivo autofluorescence spectroscopy and imaging for oral oncology. Oral Oncol 2005; 41: 117-131
277. Dacosta RS, Wilson BC, Marcon NE. Photodiagnostic techniques for the endoscopic detection of premalignant gastrointestinal lesions. Digestive endoscopy : official journal of the Japan Gastroenterological Endoscopy Society 2003; 15: 153-173
278. Skala MC, Riching KM, Gendron-Fitzpatrick A et al. In vivo multiphoton microscopy of NADH and FAD redox states, fluorescence lifetimes, and cellular morphology in precancerous epithelia. PNAS 2007; 104: 19494-19499
279. Campbell ID, Dwek RA. Biological Spectroscopy. Menlo Park, CA: Benjamin Cummings; 1984
280. Ramanujam N. Fluorescence spectroscopy of neoplastic and non-neoplastic tissues. Neoplasia 2000; 2: 89-117
281. Konig K, Riemann I. High-resolution multiphoton tomography of human skin with subcellular spatial resolution and picosecond time resolution. J Biomed Opt 2003; 8: 432-439
282. Berezin MY, Achilefu S. Fluorescence lifetime measurements and biological imaging. Chem Rev 2010; 110: 2641-2684
283. Ramanujam N. Fluorescence spectroscopy in vivo. In: Meyers RA ed, Encyclopedia of Analytical Chemistry. Chichester: John Wiley & Sons; 2000: 20-56
284. Harden A, Young WJ. The Alcoholic Ferment of Yeast-Juice. In, Proceedings of the Royal Society of London. London; 1906: 369–375
285. Wang HW, Wei YH, Guo HW. Reduced Nicotinamide Adenine Dinucleotide (NADH) Fluorescence for the Detection of Cell Death. Anti-Cancer Agents in Medicinal Chemistry 2009; 9: 1012-1017
286. Kuhn R, Reinemund K, Kaltschmitt H et al. Synthetisches 6.7-Dimethyl-9-d-ribo-flavin. Naturwissenschaften 1935; 23: 260-260
287. Chance B, Schoener B, Oshino R et al. Oxidation-reduction ratio studies of mitochondria in freeze-trapped samples. NADH and flavoprotein fluorescence signals. J Biol Chem 1979; 254: 4764-4771
288. Masters BR, Chance B. Redox confocal imaging: Intrinsic fluorescent probes of cellular metabolism. In: Mason WT ed, Fluorescent and luminescent probes for biological activity: A practical guide to technology for quantitative real-time analysis. London: Academic Press, Inc.; 1993: 44-57
289. Chance B. Pyridine nucleotide as an indicator of the oxygen requirements for energy-linked functions of mitochondria. Circ Res 1976; 38: I31-38
290. Scott TG, Spencer RD, Leonard NJ et al. Emission properties of NADH. Studies of fluorescence lifetimes and quantum efficiencies of NADH, AcPyADH and simplified synthetic models. J Am Chem Soc 1970; 92: 687-695
291. Lakowicz JR, Szmacinski H, Nowaczyk K et al. Fluorescence lifetime imaging of free and protein-bound NADH. Proc Natl Acad Sci U S A 1992; 89: 1271-1275
292. Skala MC, Riching KM, Bird DK et al. In vivo multiphoton fluorescence lifetime imaging of protein-bound and free nicotinamide adenine dinucleotide in normal and precancerous epithelia. J Biomed Opt 2007; 12: 024014-024010
293. Koenig K, Schneckenburger H. Laser-induced autofluorescence for medical diagnosis Journal of fluorescence 1994; 4: 17-40
294. Palero JA, de Bruijn HS, van der Ploeg van den Heuvel A et al. Spectrally resolved multiphoton imaging of in vivo and excised mouse skin tissues. Biophys J 2007; 93: 992-1007
295. Nakashima N, Yoshihara K, Tanaka F et al. Picosecond fluorescence lifetime of the coenzyme of D-amino acid oxidase. J Biol Chem 1980; 255: 5261-5263
296. Yang H, Luo G, Karnchanaphanurach P et al. Protein Conformational Dynamics Probed by Single-Molecule Electron Transfer. Science 2003; 302: 262-266
297. Gelse K, Poschl E, Aigner T. Collagens-structure, function, and biosynthesis. Adv Drug Deliv Rev 2003; 55: 1531-1546

298. Richards-Kortum R, Drezek R, Sokolov K et al. Survey of Endogenous Biological Fluorophores. In: Mycek M-A, Pogue BW eds, Handbook of Biomedical Fluorescence. New York: Marcel Dekker; 2003: 237-264
299. Fujimoto D. Isolation and characterization of a fluorescent material in bovine achilles tendon collagen. Biochem Biophys Res Commun 1977; 76: 1124-1129
300. Eyre DR, Paz MA, Gallop PM. Cross-linking in collagen and elastin. Annu Rev Biochem 1984; 53: 717-748
301. Banerjee B, Miedema BE, Chandrasekhar HR. Role of basement membrane collagen and elastin in the autofluorescence spectra of the colon. J Investig Med 1999; 47: 326-332
302. Maarek JM, Marcu L, Snyder WJ et al. Time-resolved fluorescence spectra of arterial fluorescent compounds: reconstruction with the Laguerre expansion technique. Photochem Photobiol 2000; 71: 178-187
303. Fang Q, Papaioannou T, Jo JA et al. Time-domain laser-induced fluorescence spectroscopy apparatus for clinical diagnostics. Rev Sci Instrum 2004; 75: 151-162
304. Konig K, Flemming G, Hibst R. Laser-induced autofluorescence spectroscopy of dental caries. Cell Mol Biol (Noisy-le-grand) 1998; 44: 1293-1300
305. König K, Schneckenburger H, Rück A et al. In vivo photoproduct formation during PDT with ALA-induced endogenous porphyrins. Journal of Photochemistry and Photobiology B: Biology 1993; 18: 287-290
306. Weedon D. Skin Pathology. Second Edition ed; 2002
307. Byers RJ, Marsh P, Parkinson D et al. Melanosis coli is associated with an increase in colonic epithelial apoptosis and not with laxative use. Histopathology 1997; 30: 160-164
308. Walker NI, Bennett RE, Axelsen RA. Melanosis coli. A consequence of anthraquinone-induced apoptosis of colonic epithelial cells. Am J Pathol 1988; 131: 465-476
309. Schweitzer D, Schenke S, Hammer M et al. Towards metabolic mapping of the human retina. Microsc Res Techniq 2007; 70: 410-419
310. Bottiroli G, Croce AC. Authofluorescence spectroscopy of cells and tissues as a tool for biomedical diagnosis. In: Paulmbo G, Pratesi R eds, Lasers and current optical techniques in biology; 2004: 201
311. Stringari C, Edwards RA, Pate KT et al. Metabolic trajectory of cellular differentiation in small intestine by Phasor Fluorescence Lifetime Microscopy of NADH. Scientific reports 2012; 2: 568
312. Adur J, Pelegati VB, de Thomaz AA et al. Optical Biomarkers of Serous and Mucinous Human Ovarian Tumor Assessed with Nonlinear Optics Microscopies. PLoS One 2012; 7: e47007
313. Hilska M, Collan Y, Peltonen J et al. The distribution of collagen types I, III, and IV in normal and malignant colorectal mucosa. Eur J Surg 1998; 164: 457-464
314. Graham MF, Diegelmann RF, Elson CO et al. Collagen content and types in the intestinal strictures of Crohn's disease. Gastroenterology 1988; 94: 257-265
315. Wintrobe MM, Greer JP. Wintrobe's clinical hematology: Wolters Kluwer Health/Lippincott Williams & Wilkins; 2009
316. Fischbach FT, Dunning MB. A manual of laboratory and diagnostic tests: Wolters Kluwer Health/Lippincott Williams & Wilkins; 2009
317. Kadish KM, Smith KM, Guilard R. The porphyrin handbook: Medical aspects of porphyrins: ACADEMIC PressINC; 2003
318. Piomelli S, Brickman A, Carlos E. Rapid diagnosis of iron deficiency by measurement of free erythrocyte porphyrins and hemoglobin: the FEP/hemoglobin ratio. Pediatrics 1976; 57: 136-141
319. Gao S, Xiufeng L, Ying L et al. Characteristics of blood fluorescence spectra using low-level, 457.9-nm excitation from Ar+ laser. Chin Opt Lett 2004; 2: 160-161
320. Zheng W, Li D, Zeng Y et al. Two-photon excited hemoglobin fluorescence. Biomedical optics express 2010; 2: 71-79
321. Barnes D, Aggarwal S, Thomsen S et al. A characterization of the fluorescent properties of circulating human eosinophils. Photochem Photobiol 1993; 58: 297-303

322. Bottiroli G, Croce AC, Locatelli D et al. Natural fluorescence of normal and neoplastic human colon: a comprehensive "ex vivo" study. Lasers Surg Med 1995; 16: 48-60
323. Grosberg LE, Radosevich AJ, Asfaha S et al. Spectral Characterization and Unmixing of Intrinsic Contrast in Intact Normal and Diseased Gastric Tissues Using Hyperspectral Two-Photon Microscopy. PLoS One 2011; 6: e19925
324. Coyne JD. Melanosis Coli in Hyperplastic Polyps and Adenomata. International Journal of Surgical Pathology 2012, DOI: 10.1177/1066896912468212:
325. Huang Z, Zheng W, Xie S et al. Laser-induced autofluorescence microscopy of normal and tumor human colonic tissue. Int J Oncol 2004; 24: 59-63
326. Suhling K, French PM, Phillips D. Time-resolved fluorescence microscopy. Photochem Photobiol Sci 2005; 4: 13-22
327. Marcu L, Jo JA, Fang Q et al. Detection of rupture-prone atherosclerotic plaques by time-resolved laser-induced fluorescence spectroscopy. Atherosclerosis 2009; 204: 156-164
328. Thompson AJ, Manning HB, Brydegaard M et al. Hyperspectral fluorescence lifetime fibre probe spectroscopy for use in the study and diagnosis of osteoarthritis and skin cancer. In, SPIE Photonics West Biomedical Optics Symposium. San Francisco, CA: SPIE; 2011
329. Manning HB, Nickdel MB, Yamamoto K et al. Detection of cartilage matrix degradation by autofluorescence lifetime. Matrix Biol 2013; 32: 32-38
330. Coda S, Patalay R, Dunsby C et al. In vitro instrumentation. In: Popp J, Tuchin VV, Chiou A, Heinemann S eds, Handbook of Biophotonics. Berlin: Wiley-VCH; 2011
331. O'Connor DV, Phillips D. Time-correlated Single Photon Counting. London: Academic Press; 1984
332. Becker W, Bergmann A, Haustein E et al. Fluorescence lifetime images and correlation spectra obtained by multidimensional time-correlated single photon counting. Microscopy research and technique 2006; 69: 186-195
333. Marcu L, Jo JA, Butte PV et al. Fluorescence lifetime spectroscopy of glioblastoma multiforme. Photochem Photobiol 2004; 80: 98-103
334. Marcu L, Fang Q, Jo JA et al. In vivo detection of macrophages in a rabbit atherosclerotic model by time-resolved laser-induced fluorescence spectroscopy. Atherosclerosis 2005; 181: 295-303
335. Elson DS, Jo JA, Marcu L. Miniaturized side-viewing imaging probe for fluorescence lifetime imaging (FLIM): validation with fluorescence dyes, tissue structural proteins and tissue specimens. New Journal of Physics 2007; 9: 127
336. Kennedy GT, Manning HB, Elson DS et al. A fluorescence lifetime imaging scanning confocal endomicroscope. Journal of Biophotonics 2010; 3: 103-107
337. Fruhwirth GO, Ameer-Beg S, Cook R et al. Fluorescence lifetime endoscopy using TCSPC for the measurement of FRET in live cells. Opt Express 2010; 18: 11148-11158
338. Cheng S, Rico-Jimenez JJ, Jabbour J et al. Flexible endoscope for continuous in vivo multispectral fluorescence lifetime imaging. Opt Lett 2013; 38: 1515-1517
339. Sun Y, Phipps J, Elson DS et al. Fluorescence lifetime imaging microscopy: in vivo application to diagnosis of oral carcinoma. Opt Lett 2009; 34: 2081-2083
340. Sun Y, Hatami N, Yee M et al. Fluorescence lifetime imaging microscopy for brain tumor image-guided surgery. Journal of Biomedical Optics 2010; 15: 056022
341. Laemmel E, Genet M, Le Goualher G et al. Fibered confocal fluorescence microscopy (Cell-viZio) facilitates extended imaging in the field of microcirculation. A comparison with intravital microscopy. J Vasc Res 2004; 41: 400-411
342. Kumar S, Alibhai D, Margineanu A et al. FLIM FRET technology for drug discovery: automated multiwell-plate high-content analysis, multiplexed readouts and application in situ. Chemphyschem 2011; 12: 609-626
343. Lycette RM, Leslie RB. Fluorescence of Malignant Tissue. Lancet 1965; 40: 436
344. Ingrams DR, Dhingra JK, Roy K et al. Autofluorescence characteristics of oral mucosa. Head Neck 1997; 19: 27-32

345. Majumder SK, Gupta PK, Uppal A. Autofluorescence spectroscopy of tissues from human oral cavity for discriminating malignant from normal. Lasers in the Life Sciences 1999; 8: 211-227
346. Wang CY, Chiang HK, Chen CT et al. Diagnosis of oral cancer by light-induced autofluorescence spectroscopy using double excitation wavelengths. Oral Oncol 1999; 35: 144-150
347. Uppal A, Gupta PK. Measurement of NADH concentration in normal and malignant human tissues from breast and oral cavity. Biotechnol Appl Biochem 2003; 37: 45-50
348. Panjehpour M, Overholt BF, Schmidhammer JL et al. Spectroscopic diagnosis of esophageal cancer: new classification model, improved measurement system. Gastrointest Endosc 1995; 41: 577-581
349. Vo-Dinh T, Panjehpour M, Overholt BF et al. In vivo cancer diagnosis of the esophagus using differential normalized fluorescence (DNF) indices. Lasers Surg Med 1995; 16: 41-47
350. Panjehpour M, Overholt BF, Vo-Dinh T et al. Endoscopic fluorescence detection of high-grade dysplasia in Barrett's esophagus. Gastroenterology 1996; 111: 93-101
351. Vo-Dinh T, Panjehpour M, Overholt BF. Laser-induced fluorescence for esophageal cancer and dysplasia diagnosis. Ann N Y Acad Sci 1998; 838: 116-122
352. Mayinger B, Horner P, Jordan M et al. Light-induced autofluorescence spectroscopy for tissue diagnosis of GI lesions. Gastrointest Endosc 2000; 52: 395-400
353. Georgakoudi I, Jacobson BC, Muller MG et al. NAD(P)H and collagen as in vivo quantitative fluorescent biomarkers of epithelial precancerous changes. Cancer Res 2002; 62: 682-687
354. Sud D, Zhong W, Beer DG et al. Time-resolved optical imaging provides a molecular snapshot of altered metabolic function in living human cancer cell models. Opt Express 2006; 14: 4412-4426
355. Niepsuj K, Niepsuj G, Cebula W et al. Autofluorescence endoscopy for detection of high-grade dysplasia in short-segment Barrett's esophagus. Gastrointest Endosc 2003; 58: 715-719
356. Lin B, Urayama S, Saroufeem RM et al. Real-time microscopic imaging of esophageal epithelial disease with autofluorescence under ultraviolet excitation. Opt Express 2009; 17: 12502-12509
357. Curvers WL, Singh R, Song LM et al. Endoscopic tri-modal imaging for detection of early neoplasia in Barrett's oesophagus: a multi-centre feasibility study using high-resolution endoscopy, autofluorescence imaging and narrow band imaging incorporated in one endoscopy system. Gut 2008; 57: 167-172
358. Thomas T, Singh R, Ragunath K. Trimodal imaging-assisted endoscopic mucosal resection of early Barrett's neoplasia. Surg Endosc 2009; 23: 1609-1613
359. Borovicka J, Fischer J, Neuweiler J et al. Autofluorescence endoscopy in surveillance of Barrett's esophagus: a multicenter randomized trial on diagnostic efficacy. Endoscopy 2006; 38: 867,872
360. Fuster MM, Esko JD. The sweet and sour of cancer: glycans as novel therapeutic targets. Nature reviews Cancer 2005; 5: 526-542
361. Laughlin ST, Bertozzi CR. Imaging the glycome. Proc Natl Acad Sci U S A 2009; 106: 12-17
362. Li M, Anastassiades CP, Joshi B et al. Affinity peptide for targeted detection of dysplasia in Barrett's esophagus. Gastroenterology 2010; 139: 1472-1480
363. Bird-Lieberman EL, Neves AA, Lao-Sirieix P et al. Molecular imaging using fluorescent lectins permits rapid endoscopic identification of dysplasia in Barrett's esophagus. Nat Med 2012, DOI: 10.1038/nm.2616:
364. Chwirot BW, Chwirot S, Jedrzejczyk W et al. Ultraviolet laser-induced fluorescence of human stomach tissues: detection of cancer tissues by imaging techniques. Lasers Surg Med 1997; 21: 149-158

365. Abe S, Izuishi K, Tajiri H et al. Correlation of in vitro autofluorescence endoscopy images with histopathologic findings in stomach cancer. Endoscopy 2000; 32: 281-286
366. Silveira L, Jr., Betiol Filho JA, Silveira FL et al. Laser-induced fluorescence at 488 nm excitation for detecting benign and malignant lesions in stomach mucosa. J Fluoresc 2008; 18: 35-40
367. Ohkawa A, Miwa H, Namihisa A et al. Diagnostic performance of light-induced fluorescence endoscopy for gastric neoplasms. Endoscopy 2004; 36: 515-521
368. Ito S, Muguruma N, Kusaka Y et al. Detection of human gastric cancer in resected specimens using a novel infrared fluorescent anti-human carcinoembryonic antigen antibody with an infrared fluorescence endoscope in vitro. Endoscopy 2001; 33: 849-853
369. Xiao SD, Zhong L, Luo HY et al. Autofluorescence imaging analysis of gastric cancer. Chin Dig Dis 2002; 3: 95-98
370. Xiao SD, Ge ZZ, Zhong L et al. Diagnosis of gastric cancer by using autofluorescence spectroscopy. Chin Dig Dis 2002; 3: 99-102
371. Mayinger B, Jordan M, Horbach T et al. Evaluation of in vivo endoscopic autofluorescence spectroscopy in gastric cancer. Gastrointest Endosc 2004; 59: 191-198
372. Lauren P. The Two Histological Main Types of Gastric Carcinoma: Diffuse and So-Called Intestinal-Type Carcinoma. An Attempt at a Histo-Clinical Classification. Acta pathologica et microbiologica Scandinavica 1965; 64: 31-49
373. Kim WJ, Cho, J.Y., Jeong, S.W., Kim, K.M., Choi, I.S., Ham, J.H., Lee, B.Y., Kim, J.O., Lee, J.S., Jin, S.Y. Comparison of Autofluorescence Imaging Endoscopic Findings with Pathologic Findings after Endoscopic Submucosal Dissection of Gastric Neoplasms. Gut Liver 2008; 2: 186-192
374. Chandra M, Scheiman J, Heidt D et al. Probing pancreatic disease using tissue optical spectroscopy. J Biomed Opt 2007; 12: 060501
375. Chandra M, Scheiman J, Simeone D et al. Spectral areas and ratios classifier algorithm for pancreatic tissue classification using optical spectroscopy. J Biomed Opt 2010; 15: 010514
376. Liang Y, Shilagard T, Xiao SY et al. Visualizing hepatitis C virus infections in human liver by two-photon microscopy. Gastroenterology 2009; 137: 1448-1458
377. Romer TJ, Fitzmaurice M, Cothren RM et al. Laser-induced fluorescence microscopy of normal colon and dysplasia in colonic adenomas: implications for spectroscopic diagnosis. Am J Gastroenterol 1995; 90: 81-87
378. Zonios GI, Cothren RM, Arendt JT et al. Morphological model of human colon tissue fluorescence. IEEE transactions on bio-medical engineering 1996; 43: 113-122
379. Wang HW, Willis J, Canto MIF et al. Quantitative laser scanning confocal autofluorescence microscopy of normal, premalignant, and malignant colonic tissues. Ieee Transactions on Biomedical Engineering 1999; 46: 1246-1252
380. Fiarman GS, Nathanson MH, West AB et al. Differences in laser-induced autofluorescence between adenomatous and hyperplastic polyps and normal colonic mucosa by confocal microscopy. Dig Dis Sci 1995; 40: 1261-1268
381. Izuishi K, Tajiri H, Fujii T et al. The histological basis of detection of adenoma and cancer in the colon by autofluorescence endoscopic imaging. Endoscopy 1999; 31: 511-516
382. Manoharan R, Zonios GI, Cothren RMJ et al. Laser-induced fluorescence spectroscopy of colonic dysplasia: prospects for optical histological analysis In: Lakowicz J ed: SPIE; 1995: 417-422
383. Kapadia CR, Cutruzzola FW, O'Brien KM et al. Laser-induced fluorescence spectroscopy of human colonic mucosa. Detection of adenomatous transformation. Gastroenterology 1990; 99: 150-157
384. Cothren R, Richards-Kortum, R., Sivak, M., Fitzmaurice, M., Rava R., Boyce, G., Doxtader, M., Blackman, R., Ivanc, T., Hayes, G. Gastrointestinal tissue diagnosis by laser-induced fluorescence spectroscopy at endoscopy. Gastrointest Endosc 1990; 36: 105-111

385. Cothren R, Sivak M, Van Dam J et al. Detection of dysplasia at colonoscopy using laser-induced fluorescence: a blinded study. Gastrointest Endosc 1996; 44: 168-176
386. Richards-Kortum R, Rava RP, Petras RE et al. Spectroscopic diagnosis of colonic dysplasia. Photochem Photobiol 1991; 53: 777-786
387. Schomacker KT, Frisoli JK, Compton CC et al. Ultraviolet laser-induced fluorescence of colonic polyps. Gastroenterology 1992; 102: 1155-1160
388. Schomacker KT, Frisoli JK, Compton CC et al. Ultraviolet laser-induced fluorescence of colonic tissue: basic biology and diagnostic potential. Lasers Surg Med 1992; 12: 63-78
389. Yang Y TG, Bessler M, Alfano RR. Fluorescence spectroscopy as a photonic pathology method for detecting colon cancer. Lasers Life Sci 1995; 6: 259–276
390. Chwirot BW, Michniewicz Z, Kowalska M et al. Detection of colonic malignant lesions by digital imaging of UV laser-induced autofluorescence. Photochem Photobiol 1999; 69: 336-340
391. van den Broek FJC, Fockens P, van Eeden S et al. Clinical Evaluation of Endoscopic Trimodal Imaging for the Detection and Differentiation of Colonic Polyps. Clinical Gastroenterology and Hepatology 2009; 7: 288-295
392. Boparai KS, van den Broek FJ, van Eeden S et al. Hyperplastic polyposis syndrome: a pilot study for the differentiation of polyps by using high-resolution endoscopy, autofluorescence imaging, and narrow-band imaging. Gastrointest Endosc 2009; 70: 947-955
393. Moriichi K, Fujiya M, Sato R et al. Autofluorescence imaging and the quantitative intensity of fluorescence for evaluating the dysplastic grade of colonic neoplasms. International journal of colorectal disease 2012; 27: 325-330
394. Ueno N, Fujiya M, Moriichi K et al. Endosopic autofluorescence imaging is useful for the differential diagnosis of intestinal lymphomas resembling lymphoid hyperplasia. J Clin Gastroenterol 2011; 45: 507-513
395. Imaizumi K, Harada Y, Wakabayashi N et al. Dual-wavelength excitation of mucosal autofluorescence for precise detection of diminutive colonic adenomas. Gastrointest Endosc 2012; 75: 110-117
396. Pradhan A, Das BB, Yoo KM et al. Time Resolved Fluorescence of Benign and Malignant Breast Tissues. Recent Advances in the Uses of Light in Physics, Chemistry, Engineering, and Medicine 1992; 1599: 81-84
397. Rajaram N, Reichenberg JS, Migden MR et al. Pilot clinical study for quantitative spectral diagnosis of non-melanoma skin cancer. Lasers Surg Med 2010; 42: 716-727
398. Wang TD, Friedland S, Sahbaie P et al. Functional imaging of colonic mucosa with a fibered confocal microscope for real-time in vivo pathology. Clin Gastroenterol Hepatol 2007; 5: 1300-1305
399. Ruhl CE, Sayer B, Byrd-Holt DD et al. Costs of Digestive Diseases. In: Everhart JE ed, The Burden of Digestive Diseases in the United States. Washington, DC: US Government Printing Office; 2008: 137-147
400. Kendall C, Stone N, Shepherd N et al. Raman spectroscopy, a potential tool for the objective identification and classification of neoplasia in Barrett's oesophagus. J Pathol 2003; 200: 602-609
401. Matsuda T, Saito Y, Fu KI et al. Does autofluorescence imaging videoendoscopy system improve the colonoscopic polyp detection rate? A pilot study. American Journal of Gastroenterology 2008; 103: 1926-1932
402. Kara MA, Smits ME, Rosmolen WD et al. A randomized crossover study comparing light-induced fluorescence endoscopy with standard videoendoscopy for the detection of early neoplasia in Barrett's esophagus. Gastrointest Endosc 2005; 61: 671-678
403. Thompson AJ, Coda S, Brydegaard Sørensen M et al. In vivo measurements of diffuse reflectance and time-resolved autofluorescence emission spectra of basal cell carcinomas. J Biophotonics 2012; 5: 240-254

404. Coda S, Kennedy GT, Thompson A et al. Fluorescence Lifetime Imaging For Label-Free Contrast Of Gastrointestinal Diseases. Gastointestinal Endoscopy 2011; April 2011 supplement:
405. Backman V, Roy HK. Light-Scattering Technologies for Field Carcinogenesis Detection: A Modality for Endoscopic Prescreening. Gastroenterology 2011; 140: 35-41.e35
406. Boens N, Qin W, Basaric N et al. Fluorescence lifetime standards for time and frequency domain fluorescence spectroscopy. Anal Chem 2007; 79: 2137-2149
407. http://www.becker-hickl.com/literature.htm. SPCImage 3.1 Data Analysis Software for Fluorescence Lifetime Imaging Microscopy Operating Manual. In
408. Fenoglio-Preiser CM, Amy E. Noffsinger MD, Grant N. Stemmermann MD et al. Gastrointestinal pathology: an atlas and text: Wolters Kluwer Health/Lippincott Williams & Wilkins; 2008
409. Inoue H, Cho JY, Satodate H et al. Development of virtual histology and virtual biopsy using laser-scanning confocal microscopy. Scand J Gastroenterol Suppl 2003, DOI: 37-39
410. Muldoon TJ, Anandasabapathy S, Maru D et al. High-resolution imaging in Barrett's esophagus: a novel, low-cost endoscopic microscope. Gastrointest Endosc 2008; 68: 737-744
411. Goetz M. Confocal Laser Endomicroscopy: Applications in Clinical and Translational Science - A Comprehensive Review. ISRN Pathology 2012; 2012: 13
412. Wallace M, Lauwers GY, Chen Y et al. Miami classification for probe-based confocal laser endomicroscopy. Endoscopy 2011; 43: 882-891
413. http://www.cellvizio.net/self-training. In
414. Manning HB, Kennedy GT, Owen DM et al. A compact, multidimensional spectrofluorometer exploiting supercontinuum generation. J Biophotonics 2008; 1: 494-505
415. Benson RC, Meyer RA, Zaruba ME et al. Cellular autofluorescence--is it due to flavins? J Histochem Cytochem 1979; 27: 44-48
416. Krauss E, Agaimy A, Neumann H et al. Characterization of lymphoid follicles with red ring signs as first manifestation of early Crohn's disease by conventional histopathology and confocal laser endomicroscopy. International journal of clinical and experimental pathology 2012; 5: 411-421
417. Lin B, Urayama S, Saroufeem RMG et al. Characterizing the origin of autofluorescence in human esophageal epithelium under ultraviolet excitation. Opt Express 2010; 18: 21074-21082
418. Dent J, El-Serag HB, Wallander MA et al. Epidemiology of gastro-oesophageal reflux disease: a systematic review. Gut 2005; 54: 710-717
419. Kilgore SP, Ormsby AH, Gramlich TL et al. The gastric cardia: fact or fiction? Am J Gastroenterol 2000; 95: 921-924
420. Cao T, Oliviero M, Rabinovits HS. Squamous cell carcinoma. In: Hofmann-Wellenhof R ed, Reflectance confocal microscopy for skin diseases: Springer; 2012
421. Meinhardt M, Krebs R, Anders A et al. Wavelength-dependent penetration depths of ultraviolet radiation in human skin. J Biomed Opt 2008; 13: 044030
422. Palmer GM, Marshek CL, Vrotsos KM et al. Optimal methods for fluorescence and diffuse reflectance measurements of tissue biopsy samples. Lasers Surg Med 2002; 30: 191-200
423. Patalay R, Talbot C, Alexandrov Y et al. Multiphoton multispectral fluorescence lifetime tomography for the evaluation of basal cell carcinomas. PLoS ONE 2012; 7: e43460
424. Schneckenburger H, Konig K. Fluorescence Decay Kinetics and Imaging of Nad(P)H and Flavins as Metabolic Indicators. Optical Engineering 1992; 31: 1447-1451
425. Vishwasrao HD, Heikal AA, Kasischke KA et al. Conformational dependence of intracellular NADH on metabolic state revealed by associated fluorescence anisotropy. J Biol Chem 2005; 280: 25119-25126
426. Manning H. Development of multi-dimensional fluorescence metrology and application to cartilage degradation in arthritis [PhD Thesis]. London Imperial College London; 2009:

427. Warburg O. On the origin of cancer cells. Science 1956; 123: 309-314
428. Gulledge CJ, Dewhirst MW. Tumor oxygenation: a matter of supply and demand. Anticancer Res 1996; 16: 741-749
429. Zhuo S, Zheng L, Chen J et al. Depth-cumulated epithelial redox ratio and stromal collagen quantity as quantitative intrinsic indicators for differentiating normal, inflammatory, and dysplastic epithelial tissues. Appl Phys Lett 2010; 97: 173701-173703
430. Zhuo S, Yan J, Chen G et al. Label-free monitoring of colonic cancer progression using multiphoton microscopy. Biomed Opt Express 2011; 2: 615-619
431. Skala MC, Squirrell JM, Vrotsos KM et al. Multiphoton microscopy of endogenous fluorescence differentiates normal, precancerous, and cancerous squamous epithelial tissues. Cancer Res 2005; 65: 1180-1186
432. Drezek R, Sokolov K, Utzinger U et al. Understanding the contributions of NADH and collagen to cervical tissue fluorescence spectra: modeling, measurements, and implications. J Biomed Opt 2001; 6: 385-396
433. Rogart JN, Nagata J, Loeser CS et al. Multiphoton imaging can be used for microscopic examination of intact human gastrointestinal mucosa ex vivo. Clin Gastroenterol Hepatol 2008; 6: 95-101
434. Zhuo S, Chen J, Wu G et al. Quantitatively linking collagen alteration and epithelial tumor progression by second harmonic generation microscopy. Appl Phys Lett 2010; 96: 213704
435. Manning HB. Development of multi-dimensional fluorescence metrology and application to cartilage degradation in arthritis [PhD]. London Imperial College; 2010:
436. Huang S, Heikal AA, Webb WW. Two-photon fluorescence spectroscopy and microscopy of NAD(P)H and flavoprotein. Biophys J 2002; 82: 2811-2825
437. Marcu L, Cohen D, Maarek J-MI et al. Characterization of type I, II, III, IV, and V collagens by time-resolved laser-induced fluorescence spectroscopy. In: Alfano RR ed, Optical Biopsy III. San Jose, CA, USA: SPIE; 2000: 93-101
438. Peuchmaur M, Potet F, Goldfain D. Mucin histochemistry of the columnar epithelium of the oesophagus (Barrett's oesophagus): a prospective biopsy study. Journal of Clinical Pathology 1984; 37: 607-610
439. Rothery GA, Patterson JE, Stoddard CJ et al. Histological and histochemical changes in the columnar lined (Barrett's) oesophagus. Gut 1986; 27: 1062-1068
440. Nakao M, Yoshida S, Tanaka S et al. Optical biopsy of early gastroesophageal cancer by catheter-based reflectance-type laser-scanning confocal microscopy. J Biomed Opt 2008; 13: 054043
441. http://www.cancerresearchuk.org/cancer-info/cancerstats/keyfacts/bladder-cancer/uk-bladder-cancer-statistics. In
442. Kumar V, Abbas AK, Aster JC et al. Robbins basic pathology. 9th ed. Philadelphia, PA: Elsevier/Saunders; 2013
443. Colombo R, Naspro R, Bellinzoni P et al. Photodynamic diagnosis for follow-up of carcinoma in situ of the bladder. Therapeutics and clinical risk management 2007; 3: 1003-1007
444. Filbeck T, Pichlmeier U, Knuechel R et al. Do patients profit from 5-aminolevulinic acid-induced fluorescence diagnosis in transurethral resection of bladder carcinoma? Urology 2002; 60: 1025-1028
445. Jocham D, Stepp H, Waidelich R. Photodynamic diagnosis in urology: state-of-the-art. European urology 2008; 53: 1138-1148
446. Jichlinski P, Jacqmin D. Photodynamic Diagnosis in Non-Muscle-Invasive Bladder Cancer. European Urology Supplements 2008; 7: 529-535
447. Kennedy JC, Pottier RH, Pross DC. Photodynamic therapy with endogenous protoporphyrin IX: basic principles and present clinical experience. J Photochem Photobiol B 1990; 6: 143-148

448. Baumgartner R, Kriegmair M, Stepp HG et al. Photodynamic diagnosis following intravesical instillation of aminolevulinic acid (ALA): first clinical experiences in urology. Proc SPIE 1993; 1881: 20-25
449. Jichlinski P, Forrer M, Mizeret J et al. Clinical evaluation of a method for detecting superficial surgical transitional cell carcinoma of the bladder by light-induced fluorescence of protoporphyrin IX following the topical application of 5-aminolevulinic acid: preliminary results. Lasers Surg Med 1997; 20: 402-408
450. Lange N, Jichlinski P, Zellweger M et al. Photodetection of early human bladder cancer based on the fluorescence of 5-aminolaevulinic acid hexylester-induced protoporphyrin IX: a pilot study. British Journal of Cancer 1999; 80: 185-193
451. Baert L, Berg R, Van Damme B et al. Clinical fluorescence diagnosis of human bladder carcinoma following low-dose Photofrin injection. Urology 1993; 41: 322-330
452. Witjes JA, Redorta JP, Jacqmin D et al. Hexaminolevulinate-guided fluorescence cystoscopy in the diagnosis and follow-up of patients with non-muscle-invasive bladder cancer: review of the evidence and recommendations. European urology 2010; 57: 607-614
453. Zaak D, Wieland WF, Stief CG et al. Routine Use of Photodynamic Diagnosis of Bladder Cancer: Practical and Economic Issues. European Urology Supplements 2008; 7: 536 - 541
454. Cauberg EC, de Bruin DM, Faber DJ et al. A new generation of optical diagnostics for bladder cancer: technology, diagnostic accuracy, and future applications. European urology 2009; 56: 287-296
455. Cicchi R, Crisci A, Nesi G et al. Time- and spectral-resolved multiphoton imaging of fresh bladder biopsies. In, Advanced Microscopy Techniques. 1 ed. Munich, Germany: SPIE; 2009: 73670M-73679
456. Wagnières G, Mizeret J, Studzinski A et al. Frequency-Domain Fluorescence Lifetime Imaging for Endoscopic Clinical Cancer Photodetection: Apparatus Design and Preliminary Results. J Fluoresc 1997; 7: 75-83
457. Cubeddu R, Pifferi A, Taroni P et al. Fluorescence lifetime imaging: An application to the detection of skin tumors. Ieee J Sel Top Quant 1999; 5: 923-929
458. Andersson-Engels S, Canti G, Cubeddu R et al. Preliminary evaluation of two fluorescence imaging methods for the detection and the delineation of basal cell carcinomas of the skin. Laser Surg Med 2000; 26: 76-82
459. Kantelhardt SR, Leppert J, Krajewski J et al. Imaging of brain and brain tumor specimens by time-resolved multiphoton excitation microscopy ex vivo. Neuro-Oncology 2007; 9: 103-112
460. Kantelhardt SR, Diddens H, Leppert J et al. Multiphoton excitation fluorescence microscopy of 5-aminolevulinic acid induced fluorescence in experimental gliomas. Lasers Surg Med 2008; 40: 273-281
461. Chang CL, You C, Chen HM et al. Autofluorescence lifetime measurement on oral carcinogenesis. Conf Proc IEEE Eng Med Biol Soc 2004; 4: 2349-2351
462. http://science.tjc.edu/images/kidney/. In
463. Sonn GA, Jones S-NE, Tarin TV et al. Optical Biopsy of Human Bladder Neoplasia With In Vivo Confocal Laser Endomicroscopy. The Journal of urology 2009; 182: 1299-1305
464. Wu K, Liu J-J, Adams W et al. Dynamic Real-time Microscopy of the Urinary Tract Using Confocal Laser Endomicroscopy. Urology 2011; 78: 225-231
465. Govan AD. Pathology Illustrated: Books on Demand; 1991
466. Woolf N. Pathology.: Basic and Systemic: W.B. Saunders Company Limited; 1998
467. Underwood JCE. General and Systematic Pathology: Churchill Livingstone; 2000
468. D'Hallewin M-A, El Khatib S, Leroux A et al. Endoscopic confocal fluorescence microscopy of normal and tumor bearing rat bladder. The Journal of urology 2005; 174: 736-740

469. Bonnal J-L, Rock A, Gagnat A et al. Confocal Laser Endomicroscopy of Bladder Tumors Associated With Photodynamic Diagnosis: An Ex Vivo Pilot Study. Urology 2012; 80: 1162.e1161-1162.e1165
470. Drezek R BC, Pavlova I, et al. Autofluorescence microscopy of fresh cervical-tissue sections reveals alterations in tissue biochemistry with dysplasia. Photochem Photobiol 2001; 73: 636-641
471. Cubeddu R, Canti G, Pifferi A et al. Fluorescence lifetime imaging of experimental tumors in hematoporphyrin derivative-sensitized mice. Photochem Photobiol 1997; 66: 229-236
472. Yeh SC, Diamond KR, Patterson MS et al. Monitoring photosensitizer uptake using two photon fluorescence lifetime imaging microscopy. Theranostics 2012; 2: 817-826
473. König K, Wabnitz H, Dietel W. Variation in the fluorescence decay properties of haematoporphyrin derivative during its conversion to photoproducts. Journal of Photochemistry and Photobiology B: Biology 1990; 8: 103-111
474. Cubeddu R, Canti G, Taroni P et al. Time-gated fluorescence imaging for the diagnosis of tumors in a murine model. Photochem Photobiol 1993; 57: 480-485
475. Schneckenburger H, Konig K, Kunzi-Rapp K et al. Time-resolved in-vivo fluorescence of photosensitizing porphyrins. Journal of Photochemistry and Photobiology B: Biology 1993; 21: 143-147
476. Russell JA, Diamond KR, Collins TJ et al. Characterization of fluorescence lifetime of Photofrin and delta-aminolevulinic acid induced protoporphyrin IX in living cells using single- and two-photon excitation. Ieee J Sel Top Quant 2008; 14: 158-166
477. Kress M, Meier T, Steiner R et al. Time-resolved microspectrofluorometry and fluorescence lifetime imaging of photosensitizers using picosecond pulsed diode lasers in laser scanning microscopes. J Biomed Opt 2003; 8: 26-32
478. Koenig F, McGovern FJ, Althausen AF et al. Laser induced autofluorescence diagnosis of bladder cancer. J Urol 1996, DOI: 1597-1601
479. Anidjar M, Ettori D, Cussenot O et al. Laser induced autofluorescence diagnosis of bladder tumors: dependence on the excitation wavelength. J Urol 1996, DOI: 1590-1596
480. UK CR. http://info.cancerresearchuk.org/cancerstats/types/skin/#incidence. In: Cancer Research UK; 2010
481. [Anonymous]. American Cancer Society. In: American Cancer Society; 2010
482. Diepgen TL, Mahler V. The epidemiology of skin cancer. Br J Dermatol 2002; 146: 1-6
483. Trakatelli M, Ulrich C, del Marmol V et al. Epidemiology of nonmelanoma skin cancer (NMSC) in Europe: accurate and comparable data are needed for effective public health monitoring and interventions. Br J Dermatol 2007; 156: 1-7
484. Mogensen M, Jemec GB. Diagnosis of nonmelanoma skin cancer/keratinocyte carcinoma: a review of diagnostic accuracy of nonmelanoma skin cancer diagnostic tests and technologies. Dermatol Surg 2007; 33: 1158-1174
485. Rajaram N, Aramil TJ, Lee K et al. Design and validation of a clinical instrument for spectral diagnosis of cutaneous malignancy. Appl Opt 2010; 49: 142-152
486. Backman V, Gurjar R, Badizadegan K et al. Polarized light scattering spectroscopy for quantitative measurement of epithelial cellular structures in situ. Ieee J Sel Top Quant 1999; 5: 1019-1026
487. Jacques SL, Roman JR, Lee K. Imaging superficial tissues with polarized light. Lasers Surg Med 2000; 26: 119-129
488. Jacques SL, Ramella-Roman JC, Lee K. Imaging skin pathology with polarized light. J Biomed Opt 2002; 7: 329-340
489. Brancaleon L, Durkin AJ, Tu JH et al. In vivo fluorescence spectroscopy of nonmelanoma skin cancer. Photochemistry and Photobiology 2001; 73: 178-183
490. Masters BR, So PT, Gratton E. Multiphoton excitation microscopy of in vivo human skin. Functional and morphological optical biopsy based on three-dimensional imaging, lifetime measurements and fluorescence spectroscopy. Ann N Y Acad Sci 1998; 838: 58-67

491. Blackwell J, Katika KM, Pilon L et al. In vivo time-resolved autofluorescence measurements to test for glycation of human skin. Journal of Biomedical Optics 2008; 13:
492. De Giorgi V, Massi D, Sestini S et al. Combined non-linear laser imaging (two-photon excitation fluorescence microscopy, fluorescence lifetime imaging microscopy, multispectral multiphoton microscopy) in cutaneous tumours: first experiences. J Eur Acad Dermatol Venereol 2009; 23: 314-316
493. Rajadhyaksha M, Gonzalez S, Zavislan JM et al. In vivo confocal scanning laser microscopy of human skin II: Advances in instrumentation and comparison with histology. Journal of Investigative Dermatology 1999; 113: 293-303
494. Busam KJ, Charles C, Lee G et al. Morphologic features of melanocytes, pigmented keratinocytes, and melanophages by in vivo confocal scanning laser microscopy. Mod Pathol 2001; 14: 862-868
495. Gonzalez S, Tannous Z. Real-time, in vivo confocal reflectance microscopy of basal cell carcinoma. J Am Acad Dermatol 2002; 47: 869-874
496. Huang D, Swanson EA, Lin CP et al. Optical coherence tomography. Science 1991; 254: 1178-1181
497. Boone MA, Norrenberg S, Jemec GB et al. Imaging of basal cell carcinoma by high-definition optical coherence tomography: histomorphological correlation. A pilot study. Br J Dermatol 2012; 167: 856-864
498. Caspers PJ, Lucassen GW, Puppels GJ. Combined in vivo confocal Raman spectroscopy and confocal microscopy of human skin. Biophys J 2003; 85: 572-580
499. Paoli J, Smedh M, Wennberg AM et al. Multiphoton laser scanning microscopy on non-melanoma skin cancer: morphologic features for future non-invasive diagnostics. J Invest Dermatol 2008; 128: 1248-1255
500. Eichhorn R, Wessler G, Scholz M et al. Early diagnosis of melanotic melanoma based on laser-induced melanin fluorescence. J Biomed Opt 2009; 14: 034033
501. Dimitrow E, Ziemer M, Koehler MJ et al. Sensitivity and specificity of multiphoton laser tomography for in vivo and ex vivo diagnosis of malignant melanoma. J Invest Dermatol 2009; 129: 1752-1758
502. Anderson RR, Parrish JA. The optics of human skin. J Invest Dermatol 1981; 77: 13-19
503. Lohmann W, Paul E. In situ detection of melanomas by fluorescence measurements. Naturwissenschaften 1988; 75: 201-202
504. Lohmann W, Nilles M, Bodeker RH. In situ differentiation between nevi and malignant melanomas by fluorescence measurements. Naturwissenschaften 1991; 78: 456-457
505. Sterenborg H, Motamedi M, Wagner RF et al. In-vivo Fluorescence Spectroscopy and Imaging of Human Skin Tumors. Laser Med Sci 1994; 9: 191-201
506. Kollias N, Zonios G, Stamatas GN. Fluorescence spectroscopy of skin. Vibrational Spectroscopy 2002; 28: 17-23
507. Panjehpour M, Julius CE, Phan MN et al. Laser-induced fluorescence spectroscopy for in vivo diagnosis of non-melanoma skin cancers. Lasers Surg Med 2002; 31: 367-373
508. Sun Y, Liu R, Elson DS et al. Simultaneous time- and wavelength-resolved fluorescence spectroscopy for near real-time tissue diagnosis. OPTICS LETTERS 2008; 33: 630-632
509. Konig K. Clinical multiphoton tomography. J Biophotonics 2008; 1: 13-23
510. Koehler MJ, Hahn S, Preller A et al. Morphological skin ageing criteria by multiphoton laser scanning tomography: non-invasive in vivo scoring of the dermal fibre network. Experimental dermatology 2008; 17: 519-523
511. Lee JH, Chen SY, Yu CH et al. Noninvasive in vitro and in vivo assessment of epidermal hyperkeratosis and dermal fibrosis in atopic dermatitis. J Biomed Opt 2009; 14: 014008
512. Chen G, Chen J, Zhuo S et al. Nonlinear spectral imaging of human hypertrophic scar based on two-photon excited fluorescence and second-harmonic generation. Br J Dermatol 2009, DOI:

513. Wetzig T, Kendler M, Maschke J et al. No clinical benefit of preoperative fluorescence diagnosis of basal cell carcinoma localized in the H-zone of the face. Br J Dermatol 2010; 162: 1370-1376
514. Seidenari S, Arginelli F, Dunsby C et al. Multiphoton laser tomography and fluorescence lifetime imaging of basal cell carcinoma: morphologic features for non-invasive diagnostics. Experimental Dermatology 2012; 21: 831-836
515. Ulrich M, Roewert-Huber J, Gonzalez S et al. Peritumoral clefting in basal cell carcinoma: correlation of in vivo reflectance confocal microscopy and routine histology. Journal of cutaneous pathology 2011; 38: 190-195
516. Astner S, Dietterle S, Otberg N et al. Clinical applicability of in vivo fluorescence confocal microscopy for noninvasive diagnosis and therapeutic monitoring of nonmelanoma skin cancer. J Biomed Opt 2008; 13: 014003
517. Guitera P, Menzies SW, Longo C et al. In vivo confocal microscopy for diagnosis of melanoma and basal cell carcinoma using a two-step method: analysis of 710 consecutive clinically equivocal cases. J Invest Dermatol 2012; 132: 2386-2394
518. Nori S, Rius-Diaz F, Cuevas J et al. Sensitivity and specificity of reflectance-mode confocal microscopy for in vivo diagnosis of basal cell carcinoma: a multicenter study. J Am Acad Dermatol 2004; 51: 923-930
519. Paoli J, Smedh M, Ericson MB. Multiphoton laser scanning microscopy--a novel diagnostic method for superficial skin cancers. Seminars in cutaneous medicine and surgery 2009; 28: 190-195
520. Ulrich M, Klemp M, Darvin ME et al. In vivo detection of basal cell carcinoma: comparison of a reflectance confocal microscope and a multiphoton tomograph. J Biomed Opt 2013; 18: 61229
521. Dimitrow E, Riemann I, Ehlers A et al. Spectral fluorescence lifetime detection and selective melanin imaging by multiphoton laser tomography for melanoma diagnosis. Experimental dermatology 2009; 18: 509-515
522. Patalay R. The clinical application of multispectral fluorescence lifetime imaging of human skin using multiphoton microscopy. London Imperial College London; 2013:
523. Sandby-Moller J, Poulsen T, Wulf HC. Influence of epidermal thickness, pigmentation and redness on skin autofluorescence. Photochem Photobiol 2003; 77: 616-620
524. Burns T, Breathnach S, Cox N et al. Rook's Textbook of Dermatology 8th Edition ed: Wiley-Blackwell; 2010
525. Brydegaard M, Lundin P, Guan Z et al. Feasibility study: fluorescence lidar for remote bird classification. Appl Opt 2010; 49: 4531-4544
526. Becker W. User Manual - PML-16-C 16 Channel Detector Head for Time-Correlated Single Photon Counting: Becker & Hickl GmbH; 2006
527. Lambert R, Saito H, Saito Y. High-resolution endoscopy and early gastrointestinal cancer...dawn in the East. Endoscopy 2007; 39: 232-237
528. Boyle P, Levin B. World Cancer Report 2008. In: World Health Organization; 2008
529. Taplin SH, Barlow W, Urban N et al. Stage, age, comorbidity, and direct costs of colon, prostate, and breast cancer care. Journal of the National Cancer Institute 1995; 87: 417-426
530. Rex DK. Risks and potential cost savings of not sending diminutive polyps for histologic examination. Gastroenterol Hepatol 2012; 8: 128-130
531. Singh N, Harrison M, Rex DK. A survey of colonoscopic polypectomy practices among clinical gastroenterologists. Gastrointest Endosc 2004; 60: 414-418
532. Wallace MB, Perelman LT, Backman V et al. Endoscopic detection of dysplasia in patients with Barrett's esophagus using light-scattering spectroscopy. Gastroenterology 2000; 119: 677-682
533. Mycek MA, Pogue BW. Handbook of Biomedical Fluorescence. New York: Taylor & Francis; 2003
534. Marcu L, Butte P, Yong WH et al. Diagnosis of human brain tumor by lifetime fluorescence spectroscopy. In: Applications S ed, 23rd Annual Meeting of the American-

Society-for-Laser-Medicine-and-Surgery. Anaheim, California: Lasers in Surgery and Medicine; 2003: p. 51
535. Marcu L. Fluorescence lifetime techniques in medical applications. Ann Biomed Eng 2012; 40: 304-331
536. Yang Y, Tang GC, Bessler M et al. Fluorescence spectroscopy as a photonic pathology method for detecting colon cancer. Lasers Life Sci 1995; 6: 259-276
537. Mayinger B, Horner P, Jordan M et al. Light-induced autofluorescence spectroscopy for the endoscopic detection of esophageal cancer. Gastrointest Endosc 2001; 54: 195-201
538. Kara MA, Peters FP, Fockens P et al. Endoscopic video-autofluorescence imaging followed by narrow band imaging for detecting early neoplasia in Barrett's esophagus. Gastrointest Endosc 2006; 64: 176-185
539. Li B, Zhang Z, Xie S. Steady state and time-resolved autofluorescence studies of human colonic tissues. Chin Opt Lett 2006; 4: 348-350
540. http://www.bostonscientific.com/global-endoscopy/index.html. In
541. (ASGE) ASfGE. Colon & rectum. ASGE Anatomical Images. In; 2013
542. Chorvat D, Chorvatova A. Multi-wavelength fluorescence lifetime spectroscopy: a new approach to the study of endogenous fluorescence in living cells and tissues. Laser Phys Lett 2009; 6: 175-193
543. Dowling K, Dayel MJ, Lever MJ et al. Fluorescence lifetime imaging with picosecond resolution for biomedical applications. Opt Lett 1998; 23: 810-812
544. Andersson-Engels S, Johansson J, Svanberg K et al. Fluorescence imaging and point measurements of tissue: applications to the demarcation of malignant tumors and atherosclerotic lesions from normal tissue. Photochem Photobiol 1991; 53: 807-814
545. Talbot C, McGinty J, McGhee E et al. Fluorescence Lifetime Imaging and Metrology for Biomedicine. In: Tuchin VV ed, Handbook of Photonics for Biomedical Science. USA: Taylor & Francis Group; 2010
546. Talbot CB, Benninger RKP, de Beule P et al. Application of hyperspectral fluorescence lifetime imaging to tissue autofluorescence: arthritis. 2005, DOI: 10.1117/12.633034: 58620T-58620T
547. Brozyna A, Chwirot BW. Different susceptibility of cells of porcine skin and internal organs to ultraviolet A-induced breaking of nuclear DNA. Photochem Photobiol 2005; 81: 674-681
548. Cicchi R, Sturiale A, Nesi G et al. Multiphoton morpho-functional imaging of healthy colon mucosa, adenomatous polyp and adenocarcinoma. Biomedical optics express 2013; 4: 1204-1213
549. Warren SC, Margineanu A, Alibhai D et al. Rapid global fitting of large fluorescence lifetime imaging microscopy datasets. PLoS One 2013; 8: e70687

Appendix

List of journal publications, book chapters and conference presentations related to the work in the thesis.

Peer Reviewed Articles

- Coda S, Thompson AJ, Kennedy GT, Roche KL, Ayaru L, Bansi DS, Stamp GW, Thillainayagam AV, Dunsby C, and French PMW. **Fluorescence lifetime spectroscopy of tissue autofluorescence in normal and diseased colon measured *ex vivo* using a fibre-optic probe.** In preparation.
- Thompson AJ, Coda S, Sørensen MB, Kennedy GT, Patalay R, Waitong-Brämming U, De Beule PA, Neil MA, Andersson-Engels S, Bendsøe N, French PMW, Svanberg K, and Dunsby, C. ***In vivo*** **measurements of diffuse reflectance and time-resolved autofluorescence emission spectra of basal cell carcinomas.** Journal of Biophotonics 2012. 5:240-254.

Book chapters

- Coda S, Dunsby C. **Chapter 9: Oncology applications Part 4: GI cancer.** In Fluorescence Lifetime Spectroscopy and Imaging - Principles and Applications in Biomedical Diagnostics. Marcu L (ed); French PMW (ed); Elson DS (ed). Taylor & Francis (2013).
- Coda S, Patalay R, Dunsby C, French PMW. ***In vitro*** **Instrumentation.** In Handbook of Biophotonics. Popp J (ed); Tuchin VV (ed); Chiou A (ed); Heinemann S (ed). VCH (2011).

Conference proceedings and published abstracts

- Coda S, Kelly D, Lagarto J, Manning H, Patalay R, Sparks H, Thompson AJ, Warren S, Dudhia J, Gordon Kennedy GT, Nickdel M, Talbot C, Yamamoto K, Neil MA, Itoh Y, McGinty J, Stamp GW, Thillainayagam AV, Dunsby C, and French PMW. **Autofluorescence lifetime imaging and metrology for medical research and clinical diagnosis.** Optical Molecular Probes, Imaging and Drug Delivery (OMP), 14 - 18 April 2013, Waikoloa Beach, Hawaii, USA. Optical Society of America, FLIM of Tissue Autofluorescence MT3C.4.
- Coda S, Thompson A, Lenz MO, Roche KL, Kennedy GT, Talbot CB, Alexandrov Y, Munro I, Neil MA, Stamp GW, Elson DS, Dunsby C, French PMW, and Thillainayagam AV. **Fluorescence lifetime imaging and spectroscopy for label-free contrast of**

gastrointestinal diseases. Gastrointestinal Endoscopy (April 2012 supplement). 2012 ASGE Cook Medical Marsha Dreyer Award.

- Kennedy GT, Coda S, Thompson AJ, Elson DS, Neil MAA, Stamp GW, Thillainayagam A, Viellerobe B, Lacombe F, Dunsby C, and French PMW. **Fluorescence Lifetime Imaging Endoscopy.** Endoscopic Microscopy VI, Proceedings of SPIE Volume: 7893, March 2011. Editor(s): Guillermo J. Tearney; Thomas D. Wang.
- Thompson AJ, Manning H, Brydegaard M, Coda S, Kennedy GT, Patalay R, Waitong-Braemming U, De Beule PA, Neil MA, Andersson-Engels S, Itoh Y, Bendsøe N, Dunsby C, Svanberg K, and French PMW. **Hyperspectral fluorescence lifetime fibre probe spectroscopy for use in the study and diagnosis of osteoarthritis and skin cancer.** Optical Biopsy IX, Proceedings of SPIE Volume: 7895, February 2011. Editor: Robert R. Alfano.
- Coda S, Kennedy GT, Thompson AJ, Talbot CB, Alexandrov Y, Munro I, Neil MA, Stamp GW, Elson DS, Dunsby C, French PMW, and Thillainayagam AV. **Fluorescence Lifetime Imaging of Gastrointestinal Cancers.** Annals of Oncology (May 2011 supplement).
- Coda S, Kennedy GT, Thompson AJ, Talbot CB, Alexandrov Y, Munro I, Neil MA, Stamp GW, Elson DS, Dunsby C, French PMW, and Thillainayagam AV. **Fluorescence Lifetime Imaging For Label-Free Contrast Of Gastrointestinal Diseases.** Gastrointestinal Endoscopy (April 2011 supplement).
- Coda S, Kennedy GT, Thompson AJ, Webster S, Talbot CB, Goldin RD, Neil MA, Stamp GW, Elson DS, Dunsby C, French PMW, and Thillainayagam AV. **Endoscopic Fluorescence Lifetime Imaging for label-free contrast of disease.** Poster presented at the 3rd International Biophotonics & Imaging Graduate Summer School, BIGSS (August 28-September 2, 2010, Ballyvaughan Co. Clare, Ireland. 2nd place prize awarded.

Seminars, invited talks and oral presentations

- Coda S, Thompson AJ, Lenz MO, Roche KL, Kennedy GT, Talbot CB, Alexandrov Y, Munro I, Neil MA, Stamp GW, Elson DS, Dunsby C, French PMW, and Thillainayagam AV. **Fluorescence lifetime imaging and spectroscopy for label-free contrast of gastrointestinal diseases.** Regional Annual British Society of Gastroenterology meeting, 15 March 2013 – The Royal College of Physicians, London
- Coda S. **Endoscopic fluorescence lifetime imaging and spectroscopy for label-free contrast of gastrointestinal diseases.** Photonics Seminar 17 July 2012, Blackett Laboratory 630, Imperial College London.

- Coda S, Thillainayagam, AV. **Enhancing endoscopic diagnosis: Fiat Lux!** Hammersmith Medical Staff Round - 27 June 2012 LT1, Wolfson Education Centre, Hammersmith HospitalChair: Professor Gavin Screaton.
- Thillainayagam AV, Coda S. **Real-time endoscopic fluorescence lifetime imaging and spectroscopy for label-free contrast of gastrointestinal diseases.** Invited talk at the 3rd International Congress of Biophotonics, Jena, Germany, 19-21 June 2012
- Coda S, Kennedy GT, Thompson A, Talbot CB, Alexandrov Y, Munro I, Neil MA, Stamp GW, Elson DS, Dunsby C, French PM, Thillainayagam AV. **Fluorescence Lifetime Imaging For Label-Free Contrast Of Gastrointestinal Diseases.** Oral presentation at the International School of Physics "Enrico Fermi" - Varenna, Lake Como, Italy Course on: Microscopy applied to Biophotonics, 12 - 22 July 2011.
- Coda S, Kennedy GT, Thompson A, Talbot CB, Alexandrov Y, Munro I, Neil MA, Stamp GW, Elson DS, Dunsby C, French PM, Thillainayagam AV. **Fluorescence Lifetime Imaging of Gastrointestinal Diseases.** Oral presentation at the XXVII European Federation Congress of the International College of Surgeons, 10-12 Nov 2011, Rome, Italy. Multi-disciplinary approach to abdominal-pelvic diseases and proper use of new technology. Prize scholarship of € 10,000 from the "Ing. Gennaro De Matteis" Foundation of Rome, XXVII European Federation Congress of the International College of Surgeons, Rome (Italy), November 10, 2011 – Palazzo Marini, Italian Chamber of Deputies.

Honours and awards

- 2012/2013 EPSRC Doctoral Prize Fellowship (£55,460), Engineering and Physical Sciences Research Council, 15 October 2012.
- 2012 ASGE Cook Medical Marsha Dreyer Award, American Society for Gastrointestinal Endoscopy, San Diego, USA, 8 March 2012.
- "Ing. Gennaro De Matteis" Foundation of Rome Research Prize Scholarship (€10,000) awarded by the European Federation of the International College of Surgeons, Palazzo Marini, Italian Chamber of Deputies, Rome, Italy, 10 November 2011.
- 2nd place prize at the 3rd International Biophotonics & Imaging Graduate Summer School (BIGSS), University of Limerick, Ballyvaughan Co. Clare, Ireland, University of Limerick, 2 September 2010.

List of all permission documents and emails seeking permission to republish all the third party copyrighted works in the thesis

Chapter 2

Figure 2-1

Reprint form - MayoClinic.com

Your request has been successfully received! Based on your acceptance of the terms, your request has been approved.

All submissions are monitored. Should Mayo Clinic have any questions or concerns, you may be contacted within three business days of receipt of your form.

Thank you for your interest in Mayo Clinic health information

http://www.mayoclinic.com/health/reprints/MY02145

20/05/2013

Reprint form - MayoClinic.com

Privacy policy (Updated Aug. 10, 2012) Terms and conditions of use policy (Updated Aug. 2, 2011)

LEGAL CONDITIONS AND TERMS OF USE APPLICABLE TO ALL USERS OF THIS SITE. ANY USE OF THIS SITE CONSTITUTES YOUR AGREEMENT TO THESE TERMS AND CONDITIONS OF USE.

© 1998-2013 Mayo Foundation for Medical Education and Research. All rights reserved.

Figure 2-3

Citation: Zhuo S, Yan J, Chen G, Shi H, Zhu X, *et al.* (2012) Label-Free Imaging of Basement Membranes Differentiates Normal, Precancerous, and Cancerous Colonic Tissues by Second-Harmonic Generation Microscopy. PLoS ONE 7(6): e38655. doi:10.1371/journal.pone.0038655

Copyright: © 2012 Zhuo *et al.* This is an open-access article distributed under the terms of the Creative Commons Attribution License, which permits unrestricted use, distribution, and reproduction in any medium, provided the original author and source are credited.

Figure 2-6

Coda, S, Lee SY, and Gotoda T. Endoscopic mucosal resection and endoscopic submucosal dissection as treatments for early gastrointestinal cancers in Western countries. Gut Liver 2007; 1:12-21.

This is an Open Access article distributed under the terms of the Creative Commons Attribution Non-Commercial License (http://creativecommons.org/licenses/by-nc/3.0) which permits unrestricted non-commercial use, distribution, and reproduction in any medium, provided the original work is properly cited.

Figure 2-8 and figure 2-9

SPRINGER LICENSE
TERMS AND CONDITIONS
May 13, 2013

This is a License Agreement between Sergio Coda ("You") and Springer ("Springer") provided by Copyright Clearance Center ("CCC"). The license consists of your order details, the terms and conditions provided by Springer, and the payment terms and conditions.

All payments must be made in full to CCC. For payment instructions, please see information listed at the bottom of this form.

License Number	3146991215844
License date	May 13, 2013
Licensed content publisher	Springer
Licensed content publication	Gastric Cancer
Licensed content title	A Western single-center experience with endoscopic submucosal dissection for early gastrointestinal cancers
Licensed content author	Sergio Coda
Licensed content date	Jan 1, 2010
Volume number	13
Issue number	4
Type of Use	Thesis/Dissertation
Portion	Figures
Author of this Springer article	Yes and you are the sole author of the new work
Order reference number	
Title of your thesis / dissertation	An Investigation of the Diagnostic Potential of Autofluorescence Lifetime Spectroscopy and Imaging for Label-Free Contrast of Disease
Expected completion date	May 2013
Estimated size(pages)	250
Total	0.00 GBP
Terms and Conditions	

Introduction
The publisher for this copyrighted material is Springer Science + Business Media. By clicking "accept" in connection with completing this licensing transaction, you agree that the following terms and conditions apply to this transaction (along with the Billing and Payment terms and conditions established by Copyright Clearance Center, Inc. ("CCC"), at the time that you opened your Rightslink account and that are available at any time at http://myaccount.copyright.com).

Limited License
With reference to your request to reprint in your thesis material on which Springer Science and

Business Media control the copyright, permission is granted, free of charge, for the use indicated in your enquiry.

Licenses are for one-time use only with a maximum distribution equal to the number that you identified in the licensing process.

This License includes use in an electronic form, provided its password protected or on the university's intranet or repository, including UMI (according to the definition at the Sherpa website: http://www.sherpa.ac.uk/romeo/). For any other electronic use, please contact Springer at (permissions.dordrecht@springer.com or permissions.heidelberg@springer.com).

The material can only be used for the purpose of defending your thesis, and with a maximum of 100 extra copies in paper.

Although Springer holds copyright to the material and is entitled to negotiate on rights, this license is only valid, subject to a courtesy information to the author (address is given with the article/chapter) and provided it concerns original material which does not carry references to other sources (if material in question appears with credit to another source, authorization from that source is required as well).

Permission free of charge on this occasion does not prejudice any rights we might have to charge for reproduction of our copyrighted material in the future.

Altering/Modifying Material: Not Permitted
You may not alter or modify the material in any manner. Abbreviations, additions, deletions and/or any other alterations shall be made only with prior written authorization of the author(s) and/or Springer Science + Business Media. (Please contact Springer at (permissions.dordrecht@springer.com or permissions.heidelberg@springer.com)

Reservation of Rights
Springer Science + Business Media reserves all rights not specifically granted in the combination of (i) the license details provided by you and accepted in the course of this licensing transaction, (ii) these terms and conditions and (iii) CCC's Billing and Payment terms and conditions.

Copyright Notice:Disclaimer
You must include the following copyright and permission notice in connection with any reproduction of the licensed material: "Springer and the original publisher /journal title, volume, year of publication, page, chapter/article title, name(s) of author(s), figure number(s), original copyright notice) is given to the publication in which the material was originally published, by adding; with kind permission from Springer Science and Business Media"

Warranties: None

Example 1: Springer Science + Business Media makes no representations or warranties with respect to the licensed material.

Example 2: Springer Science + Business Media makes no representations or warranties with respect to the licensed material and adopts on its own behalf the limitations and disclaimers established by CCC on its behalf in its Billing and Payment terms and conditions for this licensing transaction.

Indemnity
You hereby indemnify and agree to hold harmless Springer Science + Business Media and CCC, and their respective officers, directors, employees and agents, from and against any and all claims arising out of your use of the licensed material other than as specifically authorized pursuant to this license.

No Transfer of License
This license is personal to you and may not be sublicensed, assigned, or transferred by you to any other person without Springer Science + Business Media's written permission.

No Amendment Except in Writing
This license may not be amended except in a writing signed by both parties (or, in the case of Springer

Science + Business Media, by CCC on Springer Science + Business Media's behalf).

Objection to Contrary Terms
Springer Science + Business Media hereby objects to any terms contained in any purchase order, acknowledgment, check endorsement or other writing prepared by you, which terms are inconsistent with these terms and conditions or CCC's Billing and Payment terms and conditions. These terms and conditions, together with CCC's Billing and Payment terms and conditions (which are incorporated herein), comprise the entire agreement between you and Springer Science + Business Media (and CCC) concerning this licensing transaction. In the event of any conflict between your obligations established by these terms and conditions and those established by CCC's Billing and Payment terms and conditions, these terms and conditions shall control.

Jurisdiction
All disputes that may arise in connection with this present License, or the breach thereof, shall be settled exclusively by arbitration, to be held in The Netherlands, in accordance with Dutch law, and to be conducted under the Rules of the 'Netherlands Arbitrage Instituut' (Netherlands Institute of Arbitration).***OR:***

All disputes that may arise in connection with this present License, or the breach thereof, shall be settled exclusively by arbitration, to be held in the Federal Republic of Germany, in accordance with German law.

Other terms and conditions:

v1.3

If you would like to pay for this license now, please remit this license along with your payment made payable to "COPYRIGHT CLEARANCE CENTER" otherwise you will be invoiced within 48 hours of the license date. Payment should be in the form of a check or money order referencing your account number and this invoice number RLNK501019606.
Once you receive your invoice for this order, you may pay your invoice by credit card. Please follow instructions provided at that time.

Make Payment To:
Copyright Clearance Center
Dept 001
P.O. Box 843006
Boston, MA 02284-3006

For suggestions or comments regarding this order, contact RightsLink Customer Support: customercare@copyright.com or +1-877-622-5543 (toll free in the US) or +1-978-646-2777.

Gratis licenses (referencing $0 in the Total field) are free. Please retain this printable license for your reference. No payment is required.

Figure 2-10

BMJ PUBLISHING GROUP LTD. LICENSE
TERMS AND CONDITIONS
May 10, 2013

This is a License Agreement between Sergio Coda ("You") and BMJ Publishing Group Ltd. ("BMJ Publishing Group Ltd.") provided by Copyright Clearance Center ("CCC"). The license consists of your

order details, the terms and conditions provided by BMJ Publishing Group Ltd., and the payment terms and conditions.

All payments must be made in full to CCC. For payment instructions, please see information listed at the bottom of this form.

License Number	3145391249623
License date	May 10, 2013
Licensed content publisher	BMJ Publishing Group Ltd.
Licensed content publication	Gut
Licensed content title	Endoscopic assessment of oesophagitis: clinical and functional correlates and further validation of the Los Angeles classification
Licensed content author	L R Lundell, J Dent, J R Bennett, A L Blum, D Armstrong, J P Galmiche, F Johnson, M Hongo, J E Richter, S J Spechler, G N J Tytgat, L Wallin
Licensed content date	Aug 1, 1999
Volume number	45
Issue number	2
Type of Use	Thesis/Dissertation
Requestor type	Individual
Format	Print and electronic
Portion	Figure/table/extract
Number of figure/table/extracts	1
Will you be translating?	No
Circulation/distribution	10
Title of your thesis / dissertation	An Investigation of the Diagnostic Potential of Autofluorescence Lifetime Spectroscopy and Imaging for Label-Free Contrast of Disease
Expected completion date	May 2013
Estimated size(pages)	250
BMJ VAT number	674738491
Billing Type	Invoice
Billing address	Room 731, Level 7, Blackett Laboratory South Kensington Campus London, other SW7 2AZ United Kingdom
Permissions Cost	0.00 USD
VAT (0.0%)	0.00 USD
Total	0.00 USD
Terms and Conditions	

BMJ Group Terms and Conditions for Permissions

When you submit your order you are subject to the terms and conditions set out below. You will also have agreed to the Copyright Clearance Center's ("CCC") terms and conditions regarding billing and payment https://s100.copyright.com/App/PaymentTermsAndConditions.jsp. CCC are acting as the BMJ Publishing Group Limited's ("BMJ Group's") agent.

Subject to the terms set out herein, the BMJ Group hereby grants to you (the Licensee) a non-exclusive, non-transferable licence to re-use material as detailed in your request for this/those purpose(s) only and in accordance with the following conditions:

1) **Scope of Licence:** Use of the Licensed Material(s) is restricted to the ways specified by you during the order process and any additional use(s) outside of those specified in that request, require a further grant of permission.

2) **Acknowledgement:** In all cases, due acknowledgement to the original publication with permission from the BMJ Group should be stated adjacent to the reproduced Licensed Material. The format of such acknowledgement should read as follows:

"Reproduced from [publication title, author(s), volume number, page numbers, copyright notice year] with permission from BMJ Publishing Group Ltd."

3) **Third Party Material**: BMJ Group acknowledges to the best of its knowledge, it has the rights to licence your reuse of the Licensed Material, subject always to the caveat that images/diagrams, tables and other illustrative material included within, which have a separate copyright notice, are presumed as excluded from the licence. Therefore, you should ensure that the Licensed Material you are requesting is original to BMJ Group and does not carry the copyright of another entity (as credited in the published version). If the credit line on any part of the material you have requested in any way indicates that it was reprinted or adapted by BMJ Group with permission from another source, then you should seek permission from that source directly to re-use the Licensed Material, as this is outside of the licence granted herein.

4) **Altering/Modifying Material:** The text of any material for which a licence is granted may not be altered in any way without the prior express permission of the BMJ Group. Subject to Clause 3 above however, single figure adaptations do not require BMJ Group's approval; however, the adaptation should be credited as follows:

"Adapted by permission from BMJ Publishing Group Limited. [publication title, author, volume number, page numbers, copyright notice year]

5) **Reservation of Rights:** The BMJ Group reserves all rights not specifically granted in the combination of (i) the licence details provided by you and accepted in the course of this licensing transaction, (ii) these terms and conditions and (iii) CCC's Billing and Payment Terms and Conditions.

6) **Timing of Use:** First use of the Licensed Material must take place within 12 months of the grant of permission.

7). **Creation of Contract and Termination:** Once you have submitted an order via Rightslink and this is received by CCC, and subject to you completing accurate details of your proposed use, this is when a binding contract is in effect and our acceptance occurs. As you are ordering rights from a periodical, to the fullest extent permitted by law, you will have no right to cancel the contract from this point other than for BMJ Group's material breach or fraudulent misrepresentation or as otherwise permitted under a statutory right. Payment must be made in accordance with CCC's Billing and Payment Terms and conditions. In the event that you breach any material condition of these terms and condition or any of CCC's Billing and Payment Terms and Conditions, the license is automatically terminated upon written notice from the BMJ Group or CCC or as otherwise provided for in CCC's Billing and Payment Terms and Conditions, where these apply.. Continued use of materials where a licence has been terminated, as well as any use of the Licensed Materials beyond the scope of an unrevoked licence, may constitute intellectual property rights infringement and BMJ Group reserves the right to take any and all action to protect its intellectual property rights in the Licensed Materials.

8. **Warranties:** BMJ Group makes no express or implied representations or warranties with respect to the Licensed Material and to the fullest extent permitted by law this is provided on an "as is" basis. For the avoidance of doubt BMJ Group does not warrant that the Licensed Material is accurate or fit for any particular purpose.

9. **Limitation of Liability:** To the fullest extent permitted by law, the BMJ Group disclaims all liability

for any indirect, consequential or incidental damages (including without limitation, damages for loss of profits, information or interruption) arising out of the use or inability to use the Licensed Material or the inability to obtain additional rights to use the Licensed Material. To the fullest extent permitted by law, the maximum aggregate liability of the BMJ Group for any claims, costs, proceedings and demands for direct losses caused by BMJ Group's breaches of its obligations herein shall be limited to twice the amount paid by you to CCC for the licence granted herein.

10. **Indemnity:** You hereby indemnify and hold harmless the BMJ Group and their respective officers, directors, employees and agents, from and against any and all claims, costs, proceeding or demands arising out of your unauthorised use of the Licensed Material.

11. **No Transfer of License:** This licence is personal to you, and may not be assigned or transferred by you without prior written consent from the BMJ Group or its authorised agent(s). BMJ Group may assign or transfer any of its rights and obligations under this Agreement, upon written notice to you.

12. **No Amendment Except in Writing:** This licence may not be amended except in a writing signed by both parties (or, in the case of BMJ Group, by CCC on the BMJ Group's behalf).

13. **Objection to Contrary terms:** BMJ Group hereby objects to any terms contained in any purchase order, acknowledgment, check endorsement or other writing prepared by you, which terms are inconsistent with these terms and conditions or CCC's Billing and Payment Terms and Conditions. These terms and conditions, together with CCC's Billing and Payment Terms and Conditions (which to the extent they are consistent are incorporated herein), comprise the entire agreement between you and BMJ Group (and CCC) and the Licensee concerning this licensing transaction. In the event of any conflict between your obligations established by these terms and conditions and those established by CCC's Billing and Payment Terms and Conditions, these terms and conditions shall control.

14. **Revocation:** BMJ Group or CCC may, within 30 days of issuance of this licence, deny the permissions described in this licence at their sole discretion, for any reason or no reason, with a full refund payable to you should you have not been able to exercise your rights in full. Notice of such denial will be made using the contact information provided by you. Failure to receive such notice from BMJ Group or CCC will not, to the fullest extent permitted by law alter or invalidate the denial. For the fullest extent permitted by law in no event will BMJ Group or CCC be responsible or liable for any costs, expenses or damage incurred by you as a result of a denial of your permission request, other than a refund of the amount(s) paid by you to BMJ Group and/or CCC for denied permissions.

15. **Restrictions to the license**:

15.1 Promotion: BMJ Group will not give permission to reproduce in full or in part any Licensed Material for use in the promotion of the following:

a) non-medical products that are harmful or potentially harmful to health: alcohol, baby milks and/or, sun beds

b) medical products that do not have a product license granted by the Medicines and Healthcare products Regulatory Agency (MHRA) or its international equivalents. Marketing of the product may start only after data sheets have been released to members of the medical profession and must conform to the marketing authorization contained in the product license.

16. Translation: This permission is granted for non-exclusive world English language rights only unless explicitly stated in your licence. If translation rights are granted, a professional translator should be employed and the content should be reproduced word for word preserving the integrity of the content.

17. **General:** Neither party shall be liable for failure, default or delay in performing its obligations under this Licence, caused by a Force Majeure event which shall include any act of God, war, or threatened war, act or threatened act of terrorism, riot, strike, lockout, individual action, fire, flood, drought, tempest or other event beyond the reasonable control of either party.

17.1 In the event that any provision of this Agreement is held to be invalid, the remainder of the provisions shall continue in full force and effect.

17.2 There shall be no right whatsoever for any third party to enforce the terms and conditions of

this Agreement. The Parties hereby expressly wish to exclude the operation of the Contracts (Rights of Third Parties) Act 1999 and any other legislation which has this effect and is binding on this agreement.

17.3 To the fullest extent permitted by law, this Licence will be governed by the laws of England and shall be governed and construed in accordance with the laws of England. Any action arising out of or relating to this agreement shall be brought in courts situated in England save where it is necessary for BMJ Group for enforcement to bring proceedings to bring an action in an alternative jurisdiction.

If you would like to pay for this license now, please remit this license along with your payment made payable to "COPYRIGHT CLEARANCE CENTER" otherwise you will be invoiced within 48 hours of the license date. Payment should be in the form of a check or money order referencing your account number and this invoice number RLNK501018583.
Once you receive your invoice for this order, you may pay your invoice by credit card. Please follow instructions provided at that time.

Make Payment To:
Copyright Clearance Center
Dept 001
P.O. Box 843006
Boston, MA 02284-3006

For suggestions or comments regarding this order, contact RightsLink Customer Support: customercare@copyright.com or +1-877-622-5543 (toll free in the US) or +1-978-646-2777.

Gratis licenses (referencing $0 in the Total field) are free. Please retain this printable license for your reference. No payment is required.

ELSEVIER LICENSE
TERMS AND CONDITIONS
May 10, 2013

This is a License Agreement between Sergio Coda ("You") and Elsevier ("Elsevier") provided by Copyright Clearance Center ("CCC"). The license consists of your order details, the terms and conditions provided by Elsevier, and the payment terms and conditions.

All payments must be made in full to CCC. For payment instructions, please see information listed at the bottom of this form.

Supplier	Elsevier Limited The Boulevard,Langford Lane Kidlington,Oxford,OX5 1GB,UK
Registered Company Number	1982084
Customer name	Sergio Coda
Customer address	Room 731, Level 7, Blackett Laboratory London, other SW7 2AZ
License number	3145401386752
License date	May 10, 2013

Licensed content publisher	Elsevier
Licensed content publication	The Lancet
Licensed content title	Gastro-oesophageal reflux disease
Licensed content author	Paul Moayyedi,Nicholas J Talley
Licensed content date	24–30 June 2006
Licensed content volume number	367
Licensed content issue number	9528
Number of pages	15
Start Page	2086
End Page	2100
Type of Use	reuse in a thesis/dissertation
Intended publisher of new work	Other
Portion	figures/tables/illustrations
Number of figures/tables/illustrations	1
Format	both print and electronic
Are you the author of this Elsevier article?	No
Will you be translating?	No
Order reference number	
Title of your thesis/dissertation	An Investigation of the Diagnostic Potential of Autofluorescence Lifetime Spectroscopy and Imaging for Label-Free Contrast of Disease
Expected completion date	May 2013
Estimated size (number of pages)	250
Elsevier VAT number	GB 494 6272 12
Permissions price	0.00 GBP
VAT/Local Sales Tax	0.0 USD / 0.0 GBP
Total	0.00 GBP
Terms and Conditions	

INTRODUCTION

1. The publisher for this copyrighted material is Elsevier. By clicking "accept" in connection with completing this licensing transaction, you agree that the following terms and conditions apply to this transaction (along with the Billing and Payment terms and conditions established by Copyright Clearance Center, Inc. ("CCC"), at the time that you opened your Rightslink account and that are available at any time at http://myaccount.copyright.com).

GENERAL TERMS

2. Elsevier hereby grants you permission to reproduce the aforementioned material subject to the terms and conditions indicated.

3. Acknowledgement: If any part of the material to be used (for example, figures) has appeared in our publication with credit or acknowledgement to another source, permission must also be sought from that source. If such permission is not obtained then that material may not be included in your publication/copies. Suitable acknowledgement to the source must be made, either as a footnote or in a reference list at the end of your publication, as follows:

"Reprinted from Publication title, Vol /edition number, Author(s), Title of article / title of chapter, Pages No., Copyright (Year), with permission from Elsevier [OR APPLICABLE SOCIETY COPYRIGHT OWNER]." Also Lancet special credit - "Reprinted from The Lancet, Vol. number, Author(s), Title of article, Pages No., Copyright (Year), with permission from Elsevier."

4. Reproduction of this material is confined to the purpose and/or media for which permission is hereby given.

5. Altering/Modifying Material: Not Permitted. However figures and illustrations may be altered/adapted minimally to serve your work. Any other abbreviations, additions, deletions and/or any other alterations shall be made only with prior written authorization of Elsevier Ltd. (Please contact Elsevier at permissions@elsevier.com)

6. If the permission fee for the requested use of our material is waived in this instance, please be advised that your future requests for Elsevier materials may attract a fee.

7. Reservation of Rights: Publisher reserves all rights not specifically granted in the combination of (i) the license details provided by you and accepted in the course of this licensing transaction, (ii) these terms and conditions and (iii) CCC's Billing and Payment terms and conditions.

8. License Contingent Upon Payment: While you may exercise the rights licensed immediately upon issuance of the license at the end of the licensing process for the transaction, provided that you have disclosed complete and accurate details of your proposed use, no license is finally effective unless and until full payment is received from you (either by publisher or by CCC) as provided in CCC's Billing and Payment terms and conditions. If full payment is not received on a timely basis, then any license preliminarily granted shall be deemed automatically revoked and shall be void as if never granted. Further, in the event that you breach any of these terms and conditions or any of CCC's Billing and Payment terms and conditions, the license is automatically revoked and shall be void as if never granted. Use of materials as described in a revoked license, as well as any use of the materials beyond the scope of an unrevoked license, may constitute copyright infringement and publisher reserves the right to take any and all action to protect its copyright in the materials.

9. Warranties: Publisher makes no representations or warranties with respect to the licensed material.

10. Indemnity: You hereby indemnify and agree to hold harmless publisher and CCC, and their respective officers, directors, employees and agents, from and against any and all claims arising out of your use of the licensed material other than as specifically authorized pursuant to this license.

11. No Transfer of License: This license is personal to you and may not be sublicensed, assigned, or transferred by you to any other person without publisher's written permission.

12. No Amendment Except in Writing: This license may not be amended except in a writing signed by both parties (or, in the case of publisher, by CCC on publisher's behalf).

13. Objection to Contrary Terms: Publisher hereby objects to any terms contained in any purchase order, acknowledgment, check endorsement or other writing prepared by you, which terms are inconsistent with these terms and conditions or CCC's Billing and Payment terms and conditions. These terms and conditions, together with CCC's Billing and Payment terms and conditions (which are incorporated herein), comprise the entire agreement between you and publisher (and CCC) concerning this licensing transaction. In the event of any conflict between your obligations established by these terms and conditions and those established by CCC's Billing and Payment terms and

conditions, these terms and conditions shall control.

14. Revocation: Elsevier or Copyright Clearance Center may deny the permissions described in this License at their sole discretion, for any reason or no reason, with a full refund payable to you. Notice of such denial will be made using the contact information provided by you. Failure to receive such notice will not alter or invalidate the denial. In no event will Elsevier or Copyright Clearance Center be responsible or liable for any costs, expenses or damage incurred by you as a result of a denial of your permission request, other than a refund of the amount(s) paid by you to Elsevier and/or Copyright Clearance Center for denied permissions.

LIMITED LICENSE

The following terms and conditions apply only to specific license types:

15. **Translation**: This permission is granted for non-exclusive world **English** rights only unless your license was granted for translation rights. If you licensed translation rights you may only translate this content into the languages you requested. A professional translator must perform all translations and reproduce the content word for word preserving the integrity of the article. If this license is to re-use 1 or 2 figures then permission is granted for non-exclusive world rights in all languages.

16. **Website**: The following terms and conditions apply to electronic reserve and author websites:
Electronic reserve: If licensed material is to be posted to website, the web site is to be password-protected and made available only to bona fide students registered on a relevant course if:
This license was made in connection with a course,
This permission is granted for 1 year only. You may obtain a license for future website posting,
All content posted to the web site must maintain the copyright information line on the bottom of each image,
A hyper-text must be included to the Homepage of the journal from which you are licensing at http://www.sciencedirect.com/science/journal/xxxxx or the Elsevier homepage for books at http://www.elsevier.com , and
Central Storage: This license does not include permission for a scanned version of the material to be stored in a central repository such as that provided by Heron/XanEdu.

17. **Author website** for journals with the following additional clauses:

All content posted to the web site must maintain the copyright information line on the bottom of each image, and the permission granted is limited to the personal version of your paper. You are not allowed to download and post the published electronic version of your article (whether PDF or HTML, proof or final version), nor may you scan the printed edition to create an electronic version. A hyper-text must be included to the Homepage of the journal from which you are licensing at http://www.sciencedirect.com/science/journal/xxxxx . As part of our normal production process, you will receive an e-mail notice when your article appears on Elsevier's online service ScienceDirect (www.sciencedirect.com). That e-mail will include the article's Digital Object Identifier (DOI). This number provides the electronic link to the published article and should be included in the posting of your personal version. We ask that you wait until you receive this e-mail and have the DOI to do any posting.

Central Storage: This license does not include permission for a scanned version of the material to be stored in a central repository such as that provided by Heron/XanEdu.

18. **Author website** for books with the following additional clauses:
Authors are permitted to place a brief summary of their work online only.
A hyper-text must be included to the Elsevier homepage at http://www.elsevier.com . All content posted to the web site must maintain the copyright information line on the bottom of each image. You are not allowed to download and post the published electronic version of your chapter, nor may you scan the printed edition to create an electronic version.

Central Storage: This license does not include permission for a scanned version of the material to be stored in a central repository such as that provided by Heron/XanEdu.

19. **Website** (regular and for author): A hyper-text must be included to the Homepage of the journal from which you are licensing at http://www.sciencedirect.com/science/journal/xxxxx. or for books to the Elsevier homepage at http://www.elsevier.com

20. **Thesis/Dissertation**: If your license is for use in a thesis/dissertation your thesis may be submitted to your institution in either print or electronic form. Should your thesis be published commercially, please reapply for permission. These requirements include permission for the Library and Archives of Canada to supply single copies, on demand, of the complete thesis and include permission for UMI to supply single copies, on demand, of the complete thesis. Should your thesis be published commercially, please reapply for permission.

21. **Other Conditions**:

v1.6

If you would like to pay for this license now, please remit this license along with your payment made payable to "COPYRIGHT CLEARANCE CENTER" otherwise you will be invoiced within 48 hours of the license date. Payment should be in the form of a check or money order referencing your account number and this invoice number RLNK501018610.
Once you receive your invoice for this order, you may pay your invoice by credit card. Please follow instructions provided at that time.

Make Payment To:
Copyright Clearance Center
Dept 001
P.O. Box 843006
Boston, MA 02284-3006

For suggestions or comments regarding this order, contact RightsLink Customer Support: customercare@copyright.com or +1-877-622-5543 (toll free in the US) or +1-978-646-2777.

Gratis licenses (referencing $0 in the Total field) are free. Please retain this printable license for your reference. No payment is required.

Figure 2-12

College of American Pathologists Copyright Notice

© 2010 College of American Pathologists. Permission to use figures, tables, and *brief* excerpts from this work in scientific and educational works is hereby granted provided that the source is acknowledged. Any use of material in this work that is determined to be "fair use" under Section 107 or that satisfies the conditions specified in Section 108 of the U.S. copyright Law (17 USC, as revised by P.L. 94-553) does not require the society's permission. Republication, systematic reproduction, posting in electronic form on servers, or other uses of this material, except as exempted by the above statements, requires written permission or license from College of American Pathologists.

Figure 2-13

ELSEVIER LICENSE
TERMS AND CONDITIONS
May 11, 2013

This is a License Agreement between Sergio Coda ("You") and Elsevier ("Elsevier") provided by Copyright Clearance Center ("CCC"). The license consists of your order details, the terms and conditions provided by Elsevier, and the payment terms and conditions.

All payments must be made in full to CCC. For payment instructions, please see information listed at the bottom of this form.

Supplier	Elsevier Limited The Boulevard,Langford Lane Kidlington,Oxford,OX5 1GB,UK
Registered Company Number	1982084
Customer name	Sergio Coda
Customer address	Room 731, Level 7, Blackett Laboratory London, other SW7 2AZ
License number	3145811181243
License date	May 11, 2013
Licensed content publisher	Elsevier
Licensed content publication	Gastroenterology
Licensed content title	The Development and Validation of an Endoscopic Grading System for Barrett's Esophagus: The Prague C & M Criteria
Licensed content author	Prateek Sharma,John Dent,David Armstrong,Jacques J.G.H.M. Bergman,Liebwin Gossner,Yoshio Hoshihara,Janusz A. Jankowski,Ola Junghard,Lars Lundell,Guido N.J. Tytgat,Michael Vieth
Licensed content date	November 2006
Licensed content volume number	131
Licensed content issue number	5
Number of pages	8
Start Page	1392
End Page	1399
Type of Use	reuse in a thesis/dissertation
Intended publisher of new work	Other
Portion	figures/tables/illustrations
Number of figures/tables/illustrations	1
Format	both print and electronic
Are you the author of this	No

Elsevier article?	
Will you be translating?	No
Order reference number	
Title of your thesis/dissertation	An Investigation of the Diagnostic Potential of Autofluorescence Lifetime Spectroscopy and Imaging for Label-Free Contrast of Disease
Expected completion date	May 2013
Estimated size (number of pages)	250
Elsevier VAT number	GB 494 6272 12
Permissions price	0.00 GBP
VAT/Local Sales Tax	0.0 USD / 0.0 GBP
Total	0.00 GBP
Terms and Conditions	

INTRODUCTION

1. The publisher for this copyrighted material is Elsevier. By clicking "accept" in connection with completing this licensing transaction, you agree that the following terms and conditions apply to this transaction (along with the Billing and Payment terms and conditions established by Copyright Clearance Center, Inc. ("CCC"), at the time that you opened your Rightslink account and that are available at any time at http://myaccount.copyright.com).

GENERAL TERMS

2. Elsevier hereby grants you permission to reproduce the aforementioned material subject to the terms and conditions indicated.

3. Acknowledgement: If any part of the material to be used (for example, figures) has appeared in our publication with credit or acknowledgement to another source, permission must also be sought from that source. If such permission is not obtained then that material may not be included in your publication/copies. Suitable acknowledgement to the source must be made, either as a footnote or in a reference list at the end of your publication, as follows:

"Reprinted from Publication title, Vol /edition number, Author(s), Title of article / title of chapter, Pages No., Copyright (Year), with permission from Elsevier [OR APPLICABLE SOCIETY COPYRIGHT OWNER]." Also Lancet special credit - "Reprinted from The Lancet, Vol. number, Author(s), Title of article, Pages No., Copyright (Year), with permission from Elsevier."

4. Reproduction of this material is confined to the purpose and/or media for which permission is hereby given.

5. Altering/Modifying Material: Not Permitted. However figures and illustrations may be altered/adapted minimally to serve your work. Any other abbreviations, additions, deletions and/or any other alterations shall be made only with prior written authorization of Elsevier Ltd. (Please contact Elsevier at permissions@elsevier.com)

6. If the permission fee for the requested use of our material is waived in this instance, please be advised that your future requests for Elsevier materials may attract a fee.

7. Reservation of Rights: Publisher reserves all rights not specifically granted in the combination of (i) the license details provided by you and accepted in the course of this licensing transaction, (ii) these terms and conditions and (iii) CCC's Billing and Payment terms and conditions.

8. License Contingent Upon Payment: While you may exercise the rights licensed immediately upon

issuance of the license at the end of the licensing process for the transaction, provided that you have disclosed complete and accurate details of your proposed use, no license is finally effective unless and until full payment is received from you (either by publisher or by CCC) as provided in CCC's Billing and Payment terms and conditions. If full payment is not received on a timely basis, then any license preliminarily granted shall be deemed automatically revoked and shall be void as if never granted. Further, in the event that you breach any of these terms and conditions or any of CCC's Billing and Payment terms and conditions, the license is automatically revoked and shall be void as if never granted. Use of materials as described in a revoked license, as well as any use of the materials beyond the scope of an unrevoked license, may constitute copyright infringement and publisher reserves the right to take any and all action to protect its copyright in the materials.

9. Warranties: Publisher makes no representations or warranties with respect to the licensed material.

10. Indemnity: You hereby indemnify and agree to hold harmless publisher and CCC, and their respective officers, directors, employees and agents, from and against any and all claims arising out of your use of the licensed material other than as specifically authorized pursuant to this license.

11. No Transfer of License: This license is personal to you and may not be sublicensed, assigned, or transferred by you to any other person without publisher's written permission.

12. No Amendment Except in Writing: This license may not be amended except in a writing signed by both parties (or, in the case of publisher, by CCC on publisher's behalf).

13. Objection to Contrary Terms: Publisher hereby objects to any terms contained in any purchase order, acknowledgment, check endorsement or other writing prepared by you, which terms are inconsistent with these terms and conditions or CCC's Billing and Payment terms and conditions. These terms and conditions, together with CCC's Billing and Payment terms and conditions (which are incorporated herein), comprise the entire agreement between you and publisher (and CCC) concerning this licensing transaction. In the event of any conflict between your obligations established by these terms and conditions and those established by CCC's Billing and Payment terms and conditions, these terms and conditions shall control.

14. Revocation: Elsevier or Copyright Clearance Center may deny the permissions described in this License at their sole discretion, for any reason or no reason, with a full refund payable to you. Notice of such denial will be made using the contact information provided by you. Failure to receive such notice will not alter or invalidate the denial. In no event will Elsevier or Copyright Clearance Center be responsible or liable for any costs, expenses or damage incurred by you as a result of a denial of your permission request, other than a refund of the amount(s) paid by you to Elsevier and/or Copyright Clearance Center for denied permissions.

LIMITED LICENSE

The following terms and conditions apply only to specific license types:

15. **Translation**: This permission is granted for non-exclusive world **English** rights only unless your license was granted for translation rights. If you licensed translation rights you may only translate this content into the languages you requested. A professional translator must perform all translations and reproduce the content word for word preserving the integrity of the article. If this license is to re-use 1 or 2 figures then permission is granted for non-exclusive world rights in all languages.

16. **Website**: The following terms and conditions apply to electronic reserve and author websites:
Electronic reserve: If licensed material is to be posted to website, the web site is to be password-protected and made available only to bona fide students registered on a relevant course if:
This license was made in connection with a course,
This permission is granted for 1 year only. You may obtain a license for future website posting,
All content posted to the web site must maintain the copyright information line on the bottom of each image,
A hyper-text must be included to the Homepage of the journal from which you are licensing at http://www.sciencedirect.com/science/journal/xxxxx or the Elsevier homepage for books at http://www.elsevier.com , and

Central Storage: This license does not include permission for a scanned version of the material to be stored in a central repository such as that provided by Heron/XanEdu.

17. **Author website** for journals with the following additional clauses:

All content posted to the web site must maintain the copyright information line on the bottom of each image, and the permission granted is limited to the personal version of your paper. You are not allowed to download and post the published electronic version of your article (whether PDF or HTML, proof or final version), nor may you scan the printed edition to create an electronic version. A hyper-text must be included to the Homepage of the journal from which you are licensing at http://www.sciencedirect.com/science/journal/xxxxx . As part of our normal production process, you will receive an e-mail notice when your article appears on Elsevier's online service ScienceDirect (www.sciencedirect.com). That e-mail will include the article's Digital Object Identifier (DOI). This number provides the electronic link to the published article and should be included in the posting of your personal version. We ask that you wait until you receive this e-mail and have the DOI to do any posting.

Central Storage: This license does not include permission for a scanned version of the material to be stored in a central repository such as that provided by Heron/XanEdu.

18. **Author website** for books with the following additional clauses:
Authors are permitted to place a brief summary of their work online only.
A hyper-text must be included to the Elsevier homepage at http://www.elsevier.com . All content posted to the web site must maintain the copyright information line on the bottom of each image. You are not allowed to download and post the published electronic version of your chapter, nor may you scan the printed edition to create an electronic version.

Central Storage: This license does not include permission for a scanned version of the material to be stored in a central repository such as that provided by Heron/XanEdu.

19. **Website** (regular and for author): A hyper-text must be included to the Homepage of the journal from which you are licensing at http://www.sciencedirect.com/science/journal/xxxxx. or for books to the Elsevier homepage at http://www.elsevier.com

20. **Thesis/Dissertation**: If your license is for use in a thesis/dissertation your thesis may be submitted to your institution in either print or electronic form. Should your thesis be published commercially, please reapply for permission. These requirements include permission for the Library and Archives of Canada to supply single copies, on demand, of the complete thesis and include permission for UMI to supply single copies, on demand, of the complete thesis. Should your thesis be published commercially, please reapply for permission.

21. **Other Conditions**:

v1.6

If you would like to pay for this license now, please remit this license along with your payment made payable to "COPYRIGHT CLEARANCE CENTER" otherwise you will be invoiced within 48 hours of the license date. Payment should be in the form of a check or money order referencing your account number and this invoice number RLNK501018971.
Once you receive your invoice for this order, you may pay your invoice by credit card. Please follow instructions provided at that time.

Make Payment To:
Copyright Clearance Center
Dept 001
P.O. Box 843006
Boston, MA 02284-3006

For suggestions or comments regarding this order, contact RightsLink Customer Support:

customercare@copyright.com **or +1-877-622-5543 (toll free in the US) or +1-978-646-2777.**

Gratis licenses (referencing $0 in the Total field) are free. Please retain this printable license for your reference. No payment is required.

Figures 2-20, 2-22 & 2-25

From: Coda, Sergio

Sent: 23 May 2013 10:48

To: 'info@olympus.co.uk'

Subject: permission to reproduce figures in PhD thesis

Attachments: Olympus GIF Q160.pdf; Olympus EVIS 240 & LUCERA 260 Series GI

Endoscopes endoscope channel guide.pdf

Dear Mr or Madam,

My name is Dr Sergio Coda and I work with Professor Paul French, Dr Christopher Dunsby and Dr Andrew Thillainayagam at Imperial College London in the Optics Department at Imperial College London, and in the Endoscopy Unit at Charing Cross Hospital, Imperial College Healthcare NHS Trust, as a specialist endoscopist doctor. We have been working on a project studying fluorescence lifetime imaging microscopy (FLIM) of human gastrointestinal tissue over the last few years and I would like to request the permission to reproduce the following three figures in my PhD thesis:

Figure 1: EVIS EXERA GASTROINTESTINAL VIDEOSCOPE OLYMPUS GIF TYPE Q160, page 2 of attached brochure.

Figure 2: STANDARD CHANNELS, AIR, WATER & SUCTION, bottom right figure of attached brochure.

Figure 3: Image of an Olympus fibre-optic endoscope that is widely represented on the Internet (see link below):

https://www.google.co.uk/search?q=olympus+brochure+fiberoptic+endoscope&rls=com.microsoft:en-GB:IE-SearchBox&bav=on.2,or.r_cp.r_qf.&bvm=bv.46340616,d.d2k&biw=1680&bih=848&wrapid=tlif136844657199110&um=1&ie=UTF-8&hl=en&tbm=isch&source=og&sa=N&tab=wi&ei=NeCQUZKeIsOfO6CWgPAF#q=olympus+fiberoptic+endoscope&um=1&rls=com.microsoft:en-GB:IE-SearchBox&hl=en&tbm=isch&tbs=simg:CAQSEglaD3SfsoCb3yF1IxvZpPGfPQ&iact=hc&vpx=1009&vpy=513&dur=1150&hovh=162&hovw=312&tx=82&ty=256&ei=ZOCQUZOqI-iJ0AXRuoGgBQ&page=4&tbnh=149&tbnw=287&ved=1t:2220,r:97,s:100&bav=on.2,or.r_cp.r_qf.&bvm=bv.46340616,d.d2k&fp=f6315757a25fed2f&biw=1680&bih=848

The images would be used in the thesis, in an introductory chapter on the established and the newest technological advances in the field of endoscopy.

The PhD thesis would be available in both print form and electronically.

Title of thesis: An Investigation of the Diagnostic Potential of Autofluorescence Lifetime Spectroscopy and Imaging for Label-Free Contrast of Disease.

I would also take this opportunity to express my sincere appreciation for your assistance.

Kind regards,

Dr Sergio Coda

****

Sergio Coda, MD
Clinical Research Fellow
Department of Medicine
Division of Experimental Medicine
Imperial College London

Room 612, Level 6, Blackett Laboratory
South Kensington Campus
Prince Consort Road
London SW7 2AZ
Telephone: 0044 (0) 20 7594 7738
Fax: 0044 (0) 20 7594 7714
E-Mail: s.coda@imperial.ac.uk
URL: http://www1.imperial.ac.uk/medicine/people/s.coda/
****

Figure 2-23

Home Clinical Information Journals & Publications Request Copy Permission

ACP Journals and Books

Your Request Has Been Received

If you have further questions, please direct them to Permissions at 800-730-3610.

Return to Request Copy Permissions

Jobs at ACP Contact Us Privacy Site Map For Advertisers For Media For Governors For Regents

© Copyright 2013 American College of Physicians. All Rights Reserved.

190 North Independence Mall West, Philadelphia, PA 19106-1572

Toll Free: (800) 523.1546 · Local: (215) 351.2400

Inset of figure 2-28

From: prvs=8398c3c88=copyright@osa.org on behalf of pubscopyright

<copyright@osa.org>

Sent: 14 May 2013 17:25

To: Coda, Sergio

Subject: RE: permission to reproduce

Dear Dr. Coda,

Thank you for contacting The Optical Society.

OSA considers your requested use of its copyrighted material to be Fair Use under United States

Copyright Law. It is requested that a complete citation of the original material be included in any publication.

Let me know if you have any questions.

Kind Regards,

Susannah Lehman

Susannah Lehman

May 14, 2013

Authorized Agent, The Optical Society

From: Coda, Sergio [mailto:s.coda@imperial.ac.uk]

Sent: Saturday, May 11, 2013 7:15 AM

To: pubscopyright

Subject: permission to reproduce

Dear Sir or Madam,

I would like to request permission to reproduce the following figure in my PhD thesis:

Re: Zonios, G., L. T. Perelman, V. Backmanet al. 1999. Diffuse reflectance spectroscopy of human

adenomatous colon polyps in vivo. Appl Opt 38:6628-6637.

Figure 1. page 6630.

For PhD thesis/dissertation. Print and electronic copy

Kind regards,

Dr Sergio Coda

****

Sergio Coda, MD
Clinical Research Fellow
Department of Medicine
Division of Experimental Medicine
Imperial College London

Room 612, Level 6, Blackett Laboratory
South Kensington Campus
Prince Consort Road
London SW7 2AZ
Telephone: 0044 (0) 20 7594 7738
Fax: 0044 (0) 20 7594 7714
E-Mail: s.coda@imperial.ac.uk
URL: http://www1.imperial.ac.uk/medicine/people/s.coda/
****

Figure 2-29

From: Coda, Sergio

Sent: 11 May 2013 12:46

To: 'webmaster@fujifilm.co.jp'

Subject: permission to reproduce figure (F.I.C.E. Image Processing Flowchart) in PhD thesis

Attachments: fice[1].pdf

Dear Mr or Madam,

My name is Dr Sergio Coda and I work with Professor Paul French, Dr Christopher Dunsby and Dr Andrew Thillainayagam at Imperial College London in the Optics Department at Imperial College London, and in the Endoscopy Unit at Charing Cross Hospital, Imperial College Healthcare NHS Trust, as a specialist endoscopist doctor. We have been working on a project studying fluorescence lifetime imaging microscopy (FLIM) of human gastrointestinal tissue over the last few years and I would like to request permission to reproduce the following figure from the attached brochure in my PhD thesis: Figure: F.I.C.E. Image Processing Flowchart, Page 4.

The image would be used in the thesis, in an introductory chapter on the newest technological advances in the field of endoscopy.

The PhD thesis would be available in both print form and electronically.

Title of thesis: An Investigation of the Diagnostic Potential of Autofluorescence Lifetime Spectroscopy and Imaging for Label-Free Contrast of Disease.

I would also take this opportunity to express my sincere appreciation for your assistance.

Kind regards,

Dr Sergio Coda

****

Sergio Coda, MD
Clinical Research Fellow
Department of Medicine
Division of Experimental Medicine
Imperial College London

Room 612, Level 6, Blackett Laboratory
South Kensington Campus
Prince Consort Road
London SW7 2AZ
Telephone: 0044 (0) 20 7594 7738
Fax: 0044 (0) 20 7594 7714
E-Mail: s.coda@imperial.ac.uk
URL: http://www1.imperial.ac.uk/medicine/people/s.coda/

****

Figure 2-30

ELSEVIER LICENSE
TERMS AND CONDITIONS
May 13, 2013

This is a License Agreement between Sergio Coda ("You") and Elsevier ("Elsevier") provided by Copyright Clearance Center ("CCC"). The license consists of your order details, the terms and conditions provided by Elsevier, and the payment terms and conditions.

All payments must be made in full to CCC. For payment instructions, please see information listed at the bottom of this form.

Supplier	Elsevier Limited The Boulevard,Langford Lane Kidlington,Oxford,OX5 1GB,UK
Registered Company Number	1982084

Customer name	Sergio Coda
Customer address	Room 731, Level 7, Blackett Laboratory London, other SW7 2AZ
License number	3147080525177
License date	May 13, 2013
Licensed content publisher	Elsevier
Licensed content publication	Digestive and Liver Disease
Licensed content title	Recognition and characterization of small colonic neoplasia with high-definition colonoscopy using i-Scan is as precise as chromoendoscopy
Licensed content author	A. Hoffman,C. Kagel,M. Goetz,A. Tresch,J. Mudter,S. Biesterfeld,P.R. Galle,M.F. Neurath,R. Kiesslich
Licensed content date	January 2010
Licensed content volume number	42
Licensed content issue number	1
Number of pages	6
Start Page	45
End Page	50
Type of Use	reuse in a thesis/dissertation
Portion	figures/tables/illustrations
Number of figures/tables/illustrations	1
Format	both print and electronic
Are you the author of this Elsevier article?	No
Will you be translating?	No
Order reference number	
Title of your thesis/dissertation	An Investigation of the Diagnostic Potential of Autofluorescence Lifetime Spectroscopy and Imaging for Label-Free Contrast of Disease
Expected completion date	May 2013
Estimated size (number of pages)	250
Elsevier VAT number	GB 494 6272 12
Permissions price	0.00 GBP
VAT/Local Sales Tax	0.0 USD / 0.0 GBP
Total	0.00 GBP
Terms and Conditions	

INTRODUCTION

1. The publisher for this copyrighted material is Elsevier. By clicking "accept" in connection with completing this licensing transaction, you agree that the following terms and conditions apply to this transaction (along with the Billing and Payment terms and conditions established by Copyright Clearance Center, Inc. ("CCC"), at the time that you opened your Rightslink account and that are available at any time at http://myaccount.copyright.com).

GENERAL TERMS

2. Elsevier hereby grants you permission to reproduce the aforementioned material subject to the terms and conditions indicated.

3. Acknowledgement: If any part of the material to be used (for example, figures) has appeared in our publication with credit or acknowledgement to another source, permission must also be sought from that source. If such permission is not obtained then that material may not be included in your publication/copies. Suitable acknowledgement to the source must be made, either as a footnote or in a reference list at the end of your publication, as follows:

"Reprinted from Publication title, Vol /edition number, Author(s), Title of article / title of chapter, Pages No., Copyright (Year), with permission from Elsevier [OR APPLICABLE SOCIETY COPYRIGHT OWNER]." Also Lancet special credit - "Reprinted from The Lancet, Vol. number, Author(s), Title of article, Pages No., Copyright (Year), with permission from Elsevier."

4. Reproduction of this material is confined to the purpose and/or media for which permission is hereby given.

5. Altering/Modifying Material: Not Permitted. However figures and illustrations may be altered/adapted minimally to serve your work. Any other abbreviations, additions, deletions and/or any other alterations shall be made only with prior written authorization of Elsevier Ltd. (Please contact Elsevier at permissions@elsevier.com)

6. If the permission fee for the requested use of our material is waived in this instance, please be advised that your future requests for Elsevier materials may attract a fee.

7. Reservation of Rights: Publisher reserves all rights not specifically granted in the combination of (i) the license details provided by you and accepted in the course of this licensing transaction, (ii) these terms and conditions and (iii) CCC's Billing and Payment terms and conditions.

8. License Contingent Upon Payment: While you may exercise the rights licensed immediately upon issuance of the license at the end of the licensing process for the transaction, provided that you have disclosed complete and accurate details of your proposed use, no license is finally effective unless and until full payment is received from you (either by publisher or by CCC) as provided in CCC's Billing and Payment terms and conditions. If full payment is not received on a timely basis, then any license preliminarily granted shall be deemed automatically revoked and shall be void as if never granted. Further, in the event that you breach any of these terms and conditions or any of CCC's Billing and Payment terms and conditions, the license is automatically revoked and shall be void as if never granted. Use of materials as described in a revoked license, as well as any use of the materials beyond the scope of an unrevoked license, may constitute copyright infringement and publisher reserves the right to take any and all action to protect its copyright in the materials.

9. Warranties: Publisher makes no representations or warranties with respect to the licensed material.

10. Indemnity: You hereby indemnify and agree to hold harmless publisher and CCC, and their respective officers, directors, employees and agents, from and against any and all claims arising out of your use of the licensed material other than as specifically authorized pursuant to this license.

11. No Transfer of License: This license is personal to you and may not be sublicensed, assigned, or transferred by you to any other person without publisher's written permission.

12. No Amendment Except in Writing: This license may not be amended except in a writing signed by both parties (or, in the case of publisher, by CCC on publisher's behalf).

13. Objection to Contrary Terms: Publisher hereby objects to any terms contained in any purchase order, acknowledgment, check endorsement or other writing prepared by you, which terms are inconsistent with these terms and conditions or CCC's Billing and Payment terms and conditions. These terms and conditions, together with CCC's Billing and Payment terms and conditions (which are incorporated herein), comprise the entire agreement between you and publisher (and CCC) concerning this licensing transaction. In the event of any conflict between your obligations established by these terms and conditions and those established by CCC's Billing and Payment terms and conditions, these terms and conditions shall control.

14. Revocation: Elsevier or Copyright Clearance Center may deny the permissions described in this License at their sole discretion, for any reason or no reason, with a full refund payable to you. Notice of such denial will be made using the contact information provided by you. Failure to receive such notice will not alter or invalidate the denial. In no event will Elsevier or Copyright Clearance Center be responsible or liable for any costs, expenses or damage incurred by you as a result of a denial of your permission request, other than a refund of the amount(s) paid by you to Elsevier and/or Copyright Clearance Center for denied permissions.

LIMITED LICENSE

The following terms and conditions apply only to specific license types:

15. **Translation**: This permission is granted for non-exclusive world **English** rights only unless your license was granted for translation rights. If you licensed translation rights you may only translate this content into the languages you requested. A professional translator must perform all translations and reproduce the content word for word preserving the integrity of the article. If this license is to re-use 1 or 2 figures then permission is granted for non-exclusive world rights in all languages.

16. **Website**: The following terms and conditions apply to electronic reserve and author websites:
Electronic reserve: If licensed material is to be posted to website, the web site is to be password-protected and made available only to bona fide students registered on a relevant course if:
This license was made in connection with a course,
This permission is granted for 1 year only. You may obtain a license for future website posting,
All content posted to the web site must maintain the copyright information line on the bottom of each image,
A hyper-text must be included to the Homepage of the journal from which you are licensing at http://www.sciencedirect.com/science/journal/xxxxx or the Elsevier homepage for books at http://www.elsevier.com , and
Central Storage: This license does not include permission for a scanned version of the material to be stored in a central repository such as that provided by Heron/XanEdu.

17. **Author website** for journals with the following additional clauses:

All content posted to the web site must maintain the copyright information line on the bottom of each image, and the permission granted is limited to the personal version of your paper. You are not allowed to download and post the published electronic version of your article (whether PDF or HTML, proof or final version), nor may you scan the printed edition to create an electronic version. A hyper-text must be included to the Homepage of the journal from which you are licensing at http://www.sciencedirect.com/science/journal/xxxxx . As part of our normal production process, you will receive an e-mail notice when your article appears on Elsevier's online service ScienceDirect (www.sciencedirect.com). That e-mail will include the article's Digital Object Identifier (DOI). This number provides the electronic link to the published article and should be included in the posting of your personal version. We ask that you wait until you receive this e-mail and have the DOI to do any posting.

Central Storage: This license does not include permission for a scanned version of the material to be stored in a central repository such as that provided by Heron/XanEdu.

18. **Author website** for books with the following additional clauses:
Authors are permitted to place a brief summary of their work online only.
A hyper-text must be included to the Elsevier homepage at http://www.elsevier.com . All content

posted to the web site must maintain the copyright information line on the bottom of each image. You are not allowed to download and post the published electronic version of your chapter, nor may you scan the printed edition to create an electronic version.

Central Storage: This license does not include permission for a scanned version of the material to be stored in a central repository such as that provided by Heron/XanEdu.

19. **Website** (regular and for author): A hyper-text must be included to the Homepage of the journal from which you are licensing at http://www.sciencedirect.com/science/journal/xxxxx. or for books to the Elsevier homepage at http://www.elsevier.com

20. **Thesis/Dissertation**: If your license is for use in a thesis/dissertation your thesis may be submitted to your institution in either print or electronic form. Should your thesis be published commercially, please reapply for permission. These requirements include permission for the Library and Archives of Canada to supply single copies, on demand, of the complete thesis and include permission for UMI to supply single copies, on demand, of the complete thesis. Should your thesis be published commercially, please reapply for permission.

21. **Other Conditions**:

v1.6

If you would like to pay for this license now, please remit this license along with your payment made payable to "COPYRIGHT CLEARANCE CENTER" otherwise you will be invoiced within 48 hours of the license date. Payment should be in the form of a check or money order referencing your account number and this invoice number RLNK501019771.
Once you receive your invoice for this order, you may pay your invoice by credit card. Please follow instructions provided at that time.

Make Payment To:
Copyright Clearance Center
Dept 001
P.O. Box 843006
Boston, MA 02284-3006

For suggestions or comments regarding this order, contact RightsLink Customer Support: customercare@copyright.com or +1-877-622-5543 (toll free in the US) or +1-978-646-2777.

Gratis licenses (referencing $0 in the Total field) are free. Please retain this printable license for your reference. No payment is required.

Figure 2-33

WOLTERS KLUWER HEALTH LICENSE
TERMS AND CONDITIONS
May 13, 2013

This is a License Agreement between Sergio Coda ("You") and Wolters Kluwer Health ("Wolters Kluwer Health") provided by Copyright Clearance Center ("CCC"). The license consists of your order details, the terms and conditions provided by Wolters Kluwer Health, and the payment terms and conditions.

All payments must be made in full to CCC. For payment instructions, please see information listed at the bottom of this form.

License Number	3147080863605
License date	May 13, 2013
Licensed content publisher	Wolters Kluwer Health
Licensed content publication	Current Opinion in Gastroenterology
Licensed content title	Advanced imaging of the gastrointestinal tract: research vs. clinical tools?.
Licensed content author	Goetz, Martin; Kiesslich, Ralf
Licensed content date	Jan 1, 2009
Volume Number	25
Issue Number	5
Type of Use	Dissertation/Thesis
Requestor type	Individual
Author of this Wolters Kluwer article	No
Title of your thesis / dissertation	An Investigation of the Diagnostic Potential of Autofluorescence Lifetime Spectroscopy and Imaging for Label-Free Contrast of Disease
Expected completion date	May 2013
Estimated size(pages)	250
Billing Type	Invoice
Billing address	Room 731, Level 7, Blackett Laboratory South Kensington Campus London, other SW7 2AZ United Kingdom
Total	0.00 GBP
Terms and Conditions	

Terms and Conditions

1. A credit line will be prominently placed and include: for books - the author(s), title of book, editor, copyright holder, year of publication; For journals - the author(s), title of article, title of journal, volume number, issue number and inclusive pages.
2. The requestor warrants that the material shall not be used in any manner which may be considered derogatory to the title, content, or authors of the material, or to Wolters Kluwer.
3. Permission is granted for a one time use only within 12 months from the date of this invoice. Rights herein do not apply to future reproductions, editions, revisions, or other derivative works. Once the 12-month term has expired, permission to renew must be submitted in writing.
4. Permission granted is non-exclusive, and is valid throughout the world in the English language and the languages specified in your original request.
5. Wolters Kluwer cannot supply the requestor with the original artwork or a "clean copy."
6. The requestor agrees to secure written permission from the author (for book material only).
7. Permission is valid if the borrowed material is original to a Wolters Kluwer imprint (Lippincott-Raven Publishers, Williams & Wilkins, Lea & Febiger, Harwal, Igaku-Shoin, Rapid

Science, Little Brown & Company, Harper & Row Medical, American Journal of Nursing Co, and Urban & Schwarzenberg - English Language).

8. If you opt not to use the material requested above, please notify Rightslink within 90 days of the original invoice date.
9. Please note that articles in the ahead-of-print stage of publication can be cited and the content may be re-used by including the date of access and the unique DOI number. Any final changes in manuscripts will be made at the time of print publication and will be reflected in the final electronic version of the issue.
   Disclaimer: Articles appearing in the Published Ahead-of-Print section have been peer-reviewed and accepted for publication in the relevant journal and posted online before print publication. Articles appearing as publish ahead-of-print may contain statements, opinions, and information that have errors in facts, figures, or interpretation. Accordingly, Lippincott Williams & Wilkins, the editors and authors and their respective employees are not responsible or liable for the use of any such inaccurate or misleading data, opinion or information contained in the articles in this section.
10. This permission does not apply to images that are credited to publications other than Wolters Kluwer journals. For images credited to non-Wolters Kluwer journal publications, you will need to obtain permission from the journal referenced in the figure or table legend or credit line before making any use of the image(s) or table(s).
11. The following statement needs to be added when reprinting the material in Open Access publications: 'promotional and commercial use of the material in print, digital or mobile device format is prohibited without the permission from the publisher Lippincott Williams & Wilkins. Please contact journalpermissions@lww.com for further information.
12. In case of **Disease Colon Rectum, Plastic Reconstructive Surgery, The Green Journal, Critical Care Medicine, Pediatric Critical Care Medicine, the American Heart Publications, the American Academy of Neurology** the following guideline applies: no drug brand/trade name or logo can be included in the same page as the material re-used
13. When requesting a permission to translate a full text article, Wolters Kluwer/Lippincott Williams & Wilkins requests to receive the pdf of the translated document
14. Other Terms and Conditions:

v1.6

If you would like to pay for this license now, please remit this license along with your payment made payable to "COPYRIGHT CLEARANCE CENTER" otherwise you will be invoiced within 48 hours of the license date. Payment should be in the form of a check or money order referencing your account number and this invoice number RLNK501019777.
Once you receive your invoice for this order, you may pay your invoice by credit card. Please follow instructions provided at that time.

Make Payment To:
Copyright Clearance Center
Dept 001
P.O. Box 843006
Boston, MA 02284-3006

For suggestions or comments regarding this order, contact RightsLink Customer Support: customercare@copyright.com or +1-877-622-5543 (toll free in the US) or +1-978-646-2777.

Gratis licenses (referencing $0 in the Total field) are free. Please retain this printable license for your reference. No payment is required.

Figure 2-34

ELSEVIER LICENSE
TERMS AND CONDITIONS
May 13, 2013

This is a License Agreement between Sergio Coda ("You") and Elsevier ("Elsevier") provided by Copyright Clearance Center ("CCC"). The license consists of your order details, the terms and conditions provided by Elsevier, and the payment terms and conditions.

All payments must be made in full to CCC. For payment instructions, please see information listed at the bottom of this form.

Supplier	Elsevier Limited The Boulevard,Langford Lane Kidlington,Oxford,OX5 1GB,UK
Registered Company Number	1982084
Customer name	Sergio Coda
Customer address	Room 731, Level 7, Blackett Laboratory London, other SW7 2AZ
License number	3147090567605
License date	May 13, 2013
Licensed content publisher	Elsevier
Licensed content publication	Clinical Gastroenterology and Hepatology
Licensed content title	In Vivo Diagnosis and Classification of Colorectal Neoplasia by Chromoendoscopy-Guided Confocal Laser Endomicroscopy
Licensed content author	Silvia Sanduleanu,Ann Driessen,Encarna Gomez–Garcia,Wim Hameeteman,Adriaan de Bruïne,Ad Masclee
Licensed content date	April 2010
Licensed content volume number	8
Licensed content issue number	4
Number of pages	8
Start Page	371
End Page	378
Type of Use	reuse in a thesis/dissertation
Intended publisher of new work	Other
Portion	figures/tables/illustrations
Number of figures/tables/illustrations	1
Format	both print and electronic
Are you the author of this Elsevier article?	No

Will you be translating?	No
Order reference number	
Title of your thesis/dissertation	An Investigation of the Diagnostic Potential of Autofluorescence Lifetime Spectroscopy and Imaging for Label-Free Contrast of Disease
Expected completion date	May 2013
Estimated size (number of pages)	250
Elsevier VAT number	GB 494 6272 12
Permissions price	0.00 GBP
VAT/Local Sales Tax	0.0 USD / 0.0 GBP
Total	0.00 GBP
Terms and Conditions	

INTRODUCTION

1. The publisher for this copyrighted material is Elsevier. By clicking "accept" in connection with completing this licensing transaction, you agree that the following terms and conditions apply to this transaction (along with the Billing and Payment terms and conditions established by Copyright Clearance Center, Inc. ("CCC"), at the time that you opened your Rightslink account and that are available at any time at http://myaccount.copyright.com).

GENERAL TERMS

2. Elsevier hereby grants you permission to reproduce the aforementioned material subject to the terms and conditions indicated.

3. Acknowledgement: If any part of the material to be used (for example, figures) has appeared in our publication with credit or acknowledgement to another source, permission must also be sought from that source. If such permission is not obtained then that material may not be included in your publication/copies. Suitable acknowledgement to the source must be made, either as a footnote or in a reference list at the end of your publication, as follows:

"Reprinted from Publication title, Vol /edition number, Author(s), Title of article / title of chapter, Pages No., Copyright (Year), with permission from Elsevier [OR APPLICABLE SOCIETY COPYRIGHT OWNER]." Also Lancet special credit - "Reprinted from The Lancet, Vol. number, Author(s), Title of article, Pages No., Copyright (Year), with permission from Elsevier."

4. Reproduction of this material is confined to the purpose and/or media for which permission is hereby given.

5. Altering/Modifying Material: Not Permitted. However figures and illustrations may be altered/adapted minimally to serve your work. Any other abbreviations, additions, deletions and/or any other alterations shall be made only with prior written authorization of Elsevier Ltd. (Please contact Elsevier at permissions@elsevier.com)

6. If the permission fee for the requested use of our material is waived in this instance, please be advised that your future requests for Elsevier materials may attract a fee.

7. Reservation of Rights: Publisher reserves all rights not specifically granted in the combination of (i) the license details provided by you and accepted in the course of this licensing transaction, (ii) these terms and conditions and (iii) CCC's Billing and Payment terms and conditions.

8. License Contingent Upon Payment: While you may exercise the rights licensed immediately upon issuance of the license at the end of the licensing process for the transaction, provided that you have

disclosed complete and accurate details of your proposed use, no license is finally effective unless and until full payment is received from you (either by publisher or by CCC) as provided in CCC's Billing and Payment terms and conditions. If full payment is not received on a timely basis, then any license preliminarily granted shall be deemed automatically revoked and shall be void as if never granted. Further, in the event that you breach any of these terms and conditions or any of CCC's Billing and Payment terms and conditions, the license is automatically revoked and shall be void as if never granted. Use of materials as described in a revoked license, as well as any use of the materials beyond the scope of an unrevoked license, may constitute copyright infringement and publisher reserves the right to take any and all action to protect its copyright in the materials.

9. Warranties: Publisher makes no representations or warranties with respect to the licensed material.

10. Indemnity: You hereby indemnify and agree to hold harmless publisher and CCC, and their respective officers, directors, employees and agents, from and against any and all claims arising out of your use of the licensed material other than as specifically authorized pursuant to this license.

11. No Transfer of License: This license is personal to you and may not be sublicensed, assigned, or transferred by you to any other person without publisher's written permission.

12. No Amendment Except in Writing: This license may not be amended except in a writing signed by both parties (or, in the case of publisher, by CCC on publisher's behalf).

13. Objection to Contrary Terms: Publisher hereby objects to any terms contained in any purchase order, acknowledgment, check endorsement or other writing prepared by you, which terms are inconsistent with these terms and conditions or CCC's Billing and Payment terms and conditions. These terms and conditions, together with CCC's Billing and Payment terms and conditions (which are incorporated herein), comprise the entire agreement between you and publisher (and CCC) concerning this licensing transaction. In the event of any conflict between your obligations established by these terms and conditions and those established by CCC's Billing and Payment terms and conditions, these terms and conditions shall control.

14. Revocation: Elsevier or Copyright Clearance Center may deny the permissions described in this License at their sole discretion, for any reason or no reason, with a full refund payable to you. Notice of such denial will be made using the contact information provided by you. Failure to receive such notice will not alter or invalidate the denial. In no event will Elsevier or Copyright Clearance Center be responsible or liable for any costs, expenses or damage incurred by you as a result of a denial of your permission request, other than a refund of the amount(s) paid by you to Elsevier and/or Copyright Clearance Center for denied permissions.

LIMITED LICENSE

The following terms and conditions apply only to specific license types:

15. **Translation**: This permission is granted for non-exclusive world **English** rights only unless your license was granted for translation rights. If you licensed translation rights you may only translate this content into the languages you requested. A professional translator must perform all translations and reproduce the content word for word preserving the integrity of the article. If this license is to re-use 1 or 2 figures then permission is granted for non-exclusive world rights in all languages.

16. **Website**: The following terms and conditions apply to electronic reserve and author websites:
Electronic reserve: If licensed material is to be posted to website, the web site is to be password-protected and made available only to bona fide students registered on a relevant course if:
This license was made in connection with a course,
This permission is granted for 1 year only. You may obtain a license for future website posting,
All content posted to the web site must maintain the copyright information line on the bottom of each image,
A hyper-text must be included to the Homepage of the journal from which you are licensing at http://www.sciencedirect.com/science/journal/xxxxx or the Elsevier homepage for books at http://www.elsevier.com , and
Central Storage: This license does not include permission for a scanned version of the material to be

stored in a central repository such as that provided by Heron/XanEdu.

17. **Author website** for journals with the following additional clauses:

All content posted to the web site must maintain the copyright information line on the bottom of each image, and the permission granted is limited to the personal version of your paper. You are not allowed to download and post the published electronic version of your article (whether PDF or HTML, proof or final version), nor may you scan the printed edition to create an electronic version. A hyper-text must be included to the Homepage of the journal from which you are licensing at http://www.sciencedirect.com/science/journal/xxxxx . As part of our normal production process, you will receive an e-mail notice when your article appears on Elsevier's online service ScienceDirect (www.sciencedirect.com). That e-mail will include the article's Digital Object Identifier (DOI). This number provides the electronic link to the published article and should be included in the posting of your personal version. We ask that you wait until you receive this e-mail and have the DOI to do any posting.

Central Storage: This license does not include permission for a scanned version of the material to be stored in a central repository such as that provided by Heron/XanEdu.

18. **Author website** for books with the following additional clauses:
Authors are permitted to place a brief summary of their work online only.
A hyper-text must be included to the Elsevier homepage at http://www.elsevier.com . All content posted to the web site must maintain the copyright information line on the bottom of each image. You are not allowed to download and post the published electronic version of your chapter, nor may you scan the printed edition to create an electronic version.

Central Storage: This license does not include permission for a scanned version of the material to be stored in a central repository such as that provided by Heron/XanEdu.

19. **Website** (regular and for author): A hyper-text must be included to the Homepage of the journal from which you are licensing at http://www.sciencedirect.com/science/journal/xxxxx. or for books to the Elsevier homepage at http://www.elsevier.com

20. **Thesis/Dissertation**: If your license is for use in a thesis/dissertation your thesis may be submitted to your institution in either print or electronic form. Should your thesis be published commercially, please reapply for permission. These requirements include permission for the Library and Archives of Canada to supply single copies, on demand, of the complete thesis and include permission for UMI to supply single copies, on demand, of the complete thesis. Should your thesis be published commercially, please reapply for permission.

21. **Other Conditions**:

v1.6

If you would like to pay for this license now, please remit this license along with your payment made payable to "COPYRIGHT CLEARANCE CENTER" otherwise you will be invoiced within 48 hours of the license date. Payment should be in the form of a check or money order referencing your account number and this invoice number RLNK501019796.
Once you receive your invoice for this order, you may pay your invoice by credit card. Please follow instructions provided at that time.

Make Payment To:
Copyright Clearance Center
Dept 001
P.O. Box 843006
Boston, MA 02284-3006

For suggestions or comments regarding this order, contact RightsLink Customer Support: customercare@copyright.com or +1-877-622-5543 (toll free in the US) or +1-978-646-2777.

Gratis licenses (referencing $0 in the Total field) are free. Please retain this printable license for your reference. No payment is required.

Figure 2-35

ELSEVIER LICENSE
TERMS AND CONDITIONS
May 13, 2013

This is a License Agreement between Sergio Coda ("You") and Elsevier ("Elsevier") provided by Copyright Clearance Center ("CCC"). The license consists of your order details, the terms and conditions provided by Elsevier, and the payment terms and conditions.

All payments must be made in full to CCC. For payment instructions, please see information listed at the bottom of this form.

Supplier	Elsevier Limited The Boulevard,Langford Lane Kidlington,Oxford,OX5 1GB,UK
Registered Company Number	1982084
Customer name	Sergio Coda
Customer address	Room 731, Level 7, Blackett Laboratory London, other SW7 2AZ
License number	3147090984363
License date	May 13, 2013
Licensed content publisher	Elsevier
Licensed content publication	Gastrointestinal Endoscopy
Licensed content title	Real-time increased detection of neoplastic tissue in Barrett's esophagus with probe-based confocal laser endomicroscopy: final results of an international multicenter, prospective, randomized, controlled trial
Licensed content author	Prateek Sharma,Alexander R. Meining,Emmanuel Coron,Charles J. Lightdale,Herbert C. Wolfsen,Ajay Bansal,Monther Bajbouj,Jean-Paul Galmiche,Julian A. Abrams,Amit Rastogi,Neil Gupta,Joel E. Michalek,Gregory Y. Lauwers,Michael B. Wallace
Licensed content date	September 2011
Licensed content volume number	74
Licensed content issue number	3
Number of pages	8
Start Page	465

End Page	472
Type of Use	reuse in a thesis/dissertation
Intended publisher of new work	Other
Portion	figures/tables/illustrations
Number of figures/tables/illustrations	1
Format	both print and electronic
Are you the author of this Elsevier article?	Yes
Will you be translating?	No
Order reference number	
Title of your thesis/dissertation	An Investigation of the Diagnostic Potential of Autofluorescence Lifetime Spectroscopy and Imaging for Label-Free Contrast of Disease
Expected completion date	May 2013
Estimated size (number of pages)	250
Elsevier VAT number	GB 494 6272 12
Permissions price	0.00 GBP
VAT/Local Sales Tax	0.0 USD / 0.0 GBP
Total	0.00 GBP
Terms and Conditions	

INTRODUCTION

1. The publisher for this copyrighted material is Elsevier. By clicking "accept" in connection with completing this licensing transaction, you agree that the following terms and conditions apply to this transaction (along with the Billing and Payment terms and conditions established by Copyright Clearance Center, Inc. ("CCC"), at the time that you opened your Rightslink account and that are available at any time at http://myaccount.copyright.com).

GENERAL TERMS

2. Elsevier hereby grants you permission to reproduce the aforementioned material subject to the terms and conditions indicated.

3. Acknowledgement: If any part of the material to be used (for example, figures) has appeared in our publication with credit or acknowledgement to another source, permission must also be sought from that source. If such permission is not obtained then that material may not be included in your publication/copies. Suitable acknowledgement to the source must be made, either as a footnote or in a reference list at the end of your publication, as follows:

"Reprinted from Publication title, Vol /edition number, Author(s), Title of article / title of chapter, Pages No., Copyright (Year), with permission from Elsevier [OR APPLICABLE SOCIETY COPYRIGHT OWNER]." Also Lancet special credit - "Reprinted from The Lancet, Vol. number, Author(s), Title of article, Pages No., Copyright (Year), with permission from Elsevier."

4. Reproduction of this material is confined to the purpose and/or media for which permission is hereby given.

5. Altering/Modifying Material: Not Permitted. However figures and illustrations may be altered/adapted minimally to serve your work. Any other abbreviations, additions, deletions and/or any other alterations shall be made only with prior written authorization of Elsevier Ltd. (Please contact Elsevier at permissions@elsevier.com)

6. If the permission fee for the requested use of our material is waived in this instance, please be advised that your future requests for Elsevier materials may attract a fee.

7. Reservation of Rights: Publisher reserves all rights not specifically granted in the combination of (i) the license details provided by you and accepted in the course of this licensing transaction, (ii) these terms and conditions and (iii) CCC's Billing and Payment terms and conditions.

8. License Contingent Upon Payment: While you may exercise the rights licensed immediately upon issuance of the license at the end of the licensing process for the transaction, provided that you have disclosed complete and accurate details of your proposed use, no license is finally effective unless and until full payment is received from you (either by publisher or by CCC) as provided in CCC's Billing and Payment terms and conditions. If full payment is not received on a timely basis, then any license preliminarily granted shall be deemed automatically revoked and shall be void as if never granted. Further, in the event that you breach any of these terms and conditions or any of CCC's Billing and Payment terms and conditions, the license is automatically revoked and shall be void as if never granted. Use of materials as described in a revoked license, as well as any use of the materials beyond the scope of an unrevoked license, may constitute copyright infringement and publisher reserves the right to take any and all action to protect its copyright in the materials.

9. Warranties: Publisher makes no representations or warranties with respect to the licensed material.

10. Indemnity: You hereby indemnify and agree to hold harmless publisher and CCC, and their respective officers, directors, employees and agents, from and against any and all claims arising out of your use of the licensed material other than as specifically authorized pursuant to this license.

11. No Transfer of License: This license is personal to you and may not be sublicensed, assigned, or transferred by you to any other person without publisher's written permission.

12. No Amendment Except in Writing: This license may not be amended except in a writing signed by both parties (or, in the case of publisher, by CCC on publisher's behalf).

13. Objection to Contrary Terms: Publisher hereby objects to any terms contained in any purchase order, acknowledgment, check endorsement or other writing prepared by you, which terms are inconsistent with these terms and conditions or CCC's Billing and Payment terms and conditions. These terms and conditions, together with CCC's Billing and Payment terms and conditions (which are incorporated herein), comprise the entire agreement between you and publisher (and CCC) concerning this licensing transaction. In the event of any conflict between your obligations established by these terms and conditions and those established by CCC's Billing and Payment terms and conditions, these terms and conditions shall control.

14. Revocation: Elsevier or Copyright Clearance Center may deny the permissions described in this License at their sole discretion, for any reason or no reason, with a full refund payable to you. Notice of such denial will be made using the contact information provided by you. Failure to receive such notice will not alter or invalidate the denial. In no event will Elsevier or Copyright Clearance Center be responsible or liable for any costs, expenses or damage incurred by you as a result of a denial of your permission request, other than a refund of the amount(s) paid by you to Elsevier and/or Copyright Clearance Center for denied permissions.

LIMITED LICENSE

The following terms and conditions apply only to specific license types:

15. **Translation**: This permission is granted for non-exclusive world **English** rights only unless your license was granted for translation rights. If you licensed translation rights you may only translate this content into the languages you requested. A professional translator must perform all translations and

reproduce the content word for word preserving the integrity of the article. If this license is to re-use 1 or 2 figures then permission is granted for non-exclusive world rights in all languages.

16. **Website**: The following terms and conditions apply to electronic reserve and author websites:
Electronic reserve: If licensed material is to be posted to website, the web site is to be password-protected and made available only to bona fide students registered on a relevant course if:
This license was made in connection with a course,
This permission is granted for 1 year only. You may obtain a license for future website posting,
All content posted to the web site must maintain the copyright information line on the bottom of each image,
A hyper-text must be included to the Homepage of the journal from which you are licensing at http://www.sciencedirect.com/science/journal/xxxxx or the Elsevier homepage for books at http://www.elsevier.com , and
Central Storage: This license does not include permission for a scanned version of the material to be stored in a central repository such as that provided by Heron/XanEdu.

17. **Author website** for journals with the following additional clauses:

All content posted to the web site must maintain the copyright information line on the bottom of each image, and the permission granted is limited to the personal version of your paper. You are not allowed to download and post the published electronic version of your article (whether PDF or HTML, proof or final version), nor may you scan the printed edition to create an electronic version. A hyper-text must be included to the Homepage of the journal from which you are licensing at http://www.sciencedirect.com/science/journal/xxxxx . As part of our normal production process, you will receive an e-mail notice when your article appears on Elsevier's online service ScienceDirect (www.sciencedirect.com). That e-mail will include the article's Digital Object Identifier (DOI). This number provides the electronic link to the published article and should be included in the posting of your personal version. We ask that you wait until you receive this e-mail and have the DOI to do any posting.

Central Storage: This license does not include permission for a scanned version of the material to be stored in a central repository such as that provided by Heron/XanEdu.

18. **Author website** for books with the following additional clauses:
Authors are permitted to place a brief summary of their work online only.
A hyper-text must be included to the Elsevier homepage at http://www.elsevier.com . All content posted to the web site must maintain the copyright information line on the bottom of each image. You are not allowed to download and post the published electronic version of your chapter, nor may you scan the printed edition to create an electronic version.

Central Storage: This license does not include permission for a scanned version of the material to be stored in a central repository such as that provided by Heron/XanEdu.

19. **Website** (regular and for author): A hyper-text must be included to the Homepage of the journal from which you are licensing at http://www.sciencedirect.com/science/journal/xxxxx. or for books to the Elsevier homepage at http://www.elsevier.com

20. **Thesis/Dissertation**: If your license is for use in a thesis/dissertation your thesis may be submitted to your institution in either print or electronic form. Should your thesis be published commercially, please reapply for permission. These requirements include permission for the Library and Archives of Canada to supply single copies, on demand, of the complete thesis and include permission for UMI to supply single copies, on demand, of the complete thesis. Should your thesis be published commercially, please reapply for permission.

21. **Other Conditions**:

v1.6

If you would like to pay for this license now, please remit this license along with your payment

made payable to "COPYRIGHT CLEARANCE CENTER" otherwise you will be invoiced within 48 hours of the license date. Payment should be in the form of a check or money order referencing your account number and this invoice number RLNK501019808.
Once you receive your invoice for this order, you may pay your invoice by credit card. Please follow instructions provided at that time.

Make Payment To:
Copyright Clearance Center
Dept 001
P.O. Box 843006
Boston, MA 02284-3006

For suggestions or comments regarding this order, contact RightsLink Customer Support: customercare@copyright.com or +1-877-622-5543 (toll free in the US) or +1-978-646-2777.

Gratis licenses (referencing $0 in the Total field) are free. Please retain this printable license for your reference. No payment is required.

Chapter 3

Figure 3-1

JOHN WILEY AND SONS LICENSE
TERMS AND CONDITIONS
May 13, 2013

This is a License Agreement between Sergio Coda ("You") and John Wiley and Sons ("John Wiley and Sons") provided by Copyright Clearance Center ("CCC"). The license consists of your order details, the terms and conditions provided by John Wiley and Sons, and the payment terms and conditions.

All payments must be made in full to CCC. For payment instructions, please see information listed at the bottom of this form.

License Number	3147111268658
License date	May 13, 2013
Licensed content publisher	John Wiley and Sons
Licensed content publication	Journal of Pathology
Licensed content title	Methods for imaging the structure and function of living tissues and cells: 2. Fluorescence lifetime imaging
Licensed copyright line	Copyright © 2000 John Wiley & Sons, Ltd.
Licensed content author	Paul J. Tadrous
Licensed content date	Jun 27, 2000
Start page	229
End page	234
Type of use	Dissertation/Thesis

Requestor type	University/Academic
Format	Print and electronic
Portion	Figure/table
Number of figures/tables	1
Original Wiley figure/table number(s)	Figure 1
Will you be translating?	No
Total	0.00 USD
Terms and Conditions	

TERMS AND CONDITIONS

This copyrighted material is owned by or exclusively licensed to John Wiley & Sons, Inc. or one of its group companies (each a "Wiley Company") or a society for whom a Wiley Company has exclusive publishing rights in relation to a particular journal (collectively WILEY). By clicking "accept" in connection with completing this licensing transaction, you agree that the following terms and conditions apply to this transaction (along with the billing and payment terms and conditions established by the Copyright Clearance Center Inc., ("CCCs Billing and Payment terms and conditions"), at the time that you opened your RightsLink account (these are available at any time at http://myaccount.copyright.com).

Terms and Conditions

1. The materials you have requested permission to reproduce (the "Materials") are protected by copyright.

2.You are hereby granted a personal, non-exclusive, non-sublicensable, non-transferable, worldwide, limited license to reproduce the Materials for the purpose specified in the licensing process. This license is for a one-time use only with a maximum distribution equal to the number that you identified in the licensing process. Any form of republication granted by this license must be completed within two years of the date of the grant of this license (although copies prepared before may be distributed thereafter). The Materials shall not be used in any other manner or for any other purpose. Permission is granted subject to an appropriate acknowledgement given to the author, title of the material/book/journal and the publisher. You shall also duplicate the copyright notice that appears in the Wiley publication in your use of the Material. Permission is also granted on the understanding that nowhere in the text is a previously published source acknowledged for all or part of this Material. Any third party material is expressly excluded from this permission.

3. With respect to the Materials, all rights are reserved. Except as expressly granted by the terms of the license, no part of the Materials may be copied, modified, adapted (except for minor reformatting required by the new Publication), translated, reproduced, transferred or distributed, in any form or by any means, and no derivative works may be made based on the Materials without the prior permission of the respective copyright owner. You may not alter, remove or suppress in any manner any copyright, trademark or other notices displayed by the Materials. You may not license, rent, sell, loan, lease, pledge, offer as security, transfer or assign the Materials, or any of the rights granted to you hereunder to any other person.

4. The Materials and all of the intellectual property rights therein shall at all times remain the exclusive property of John Wiley & Sons Inc or one of its related companies (WILEY) or their respective licensors, and your interest therein is only that of having possession of and the right to reproduce the Materials pursuant to Section 2 herein during the continuance of this Agreement. You agree that you own no right, title or interest in or to the Materials or any of the intellectual property rights therein. You shall have no rights hereunder other than the license as provided for above in Section 2. No right, license or interest to any trademark, trade name, service mark or other branding ("Marks") of WILEY or its licensors is

granted hereunder, and you agree that you shall not assert any such right, license or interest with respect thereto.

5. NEITHER WILEY NOR ITS LICENSORS MAKES ANY WARRANTY OR REPRESENTATION OF ANY KIND TO YOU OR ANY THIRD PARTY, EXPRESS, IMPLIED OR STATUTORY, WITH RESPECT TO THE MATERIALS OR THE ACCURACY OF ANY INFORMATION CONTAINED IN THE MATERIALS, INCLUDING, WITHOUT LIMITATION, ANY IMPLIED WARRANTY OF MERCHANTABILITY, ACCURACY, SATISFACTORY QUALITY, FITNESS FOR A PARTICULAR PURPOSE, USABILITY, INTEGRATION OR NON-INFRINGEMENT AND ALL SUCH WARRANTIES ARE HEREBY EXCLUDED BY WILEY AND ITS LICENSORS AND WAIVED BY YOU.

6. WILEY shall have the right to terminate this Agreement immediately upon breach of this Agreement by you.

7. You shall indemnify, defend and hold harmless WILEY, its Licensors and their respective directors, officers, agents and employees, from and against any actual or threatened claims, demands, causes of action or proceedings arising from any breach of this Agreement by you.

8. IN NO EVENT SHALL WILEY OR ITS LICENSORS BE LIABLE TO YOU OR ANY OTHER PARTY OR ANY OTHER PERSON OR ENTITY FOR ANY SPECIAL, CONSEQUENTIAL, INCIDENTAL, INDIRECT, EXEMPLARY OR PUNITIVE DAMAGES, HOWEVER CAUSED, ARISING OUT OF OR IN CONNECTION WITH THE DOWNLOADING, PROVISIONING, VIEWING OR USE OF THE MATERIALS REGARDLESS OF THE FORM OF ACTION, WHETHER FOR BREACH OF CONTRACT, BREACH OF WARRANTY, TORT, NEGLIGENCE, INFRINGEMENT OR OTHERWISE (INCLUDING, WITHOUT LIMITATION, DAMAGES BASED ON LOSS OF PROFITS, DATA, FILES, USE, BUSINESS OPPORTUNITY OR CLAIMS OF THIRD PARTIES), AND WHETHER OR NOT THE PARTY HAS BEEN ADVISED OF THE POSSIBILITY OF SUCH DAMAGES. THIS LIMITATION SHALL APPLY NOTWITHSTANDING ANY FAILURE OF ESSENTIAL PURPOSE OF ANY LIMITED REMEDY PROVIDED HEREIN.

9. Should any provision of this Agreement be held by a court of competent jurisdiction to be illegal, invalid, or unenforceable, that provision shall be deemed amended to achieve as nearly as possible the same economic effect as the original provision, and the legality, validity and enforceability of the remaining provisions of this Agreement shall not be affected or impaired thereby.

10. The failure of either party to enforce any term or condition of this Agreement shall not constitute a waiver of either party's right to enforce each and every term and condition of this Agreement. No breach under this agreement shall be deemed waived or excused by either party unless such waiver or consent is in writing signed by the party granting such waiver or consent. The waiver by or consent of a party to a breach of any provision of this Agreement shall not operate or be construed as a waiver of or consent to any other or subsequent breach by such other party.

11. This Agreement may not be assigned (including by operation of law or otherwise) by you without WILEY's prior written consent.

12. Any fee required for this permission shall be non-refundable after thirty (30) days from receipt

13. These terms and conditions together with CCCs Billing and Payment terms and conditions (which are incorporated herein) form the entire agreement between you and WILEY concerning this licensing transaction and (in the absence of fraud) supersedes all prior agreements and representations of the parties, oral or written. This Agreement may not be amended except in writing signed by both parties. This Agreement shall be binding upon and inure to the benefit of the parties' successors, legal representatives, and authorized assigns.

14. In the event of any conflict between your obligations established by these terms and conditions and those established by CCCs Billing and Payment terms and conditions, these terms and conditions shall prevail.

15. WILEY expressly reserves all rights not specifically granted in the combination of (i) the license details provided by you and accepted in the course of this licensing transaction, (ii) these terms and

conditions and (iii) CCCs Billing and Payment terms and conditions.

16. This Agreement will be void if the Type of Use, Format, Circulation, or Requestor Type was misrepresented during the licensing process.

17. This Agreement shall be governed by and construed in accordance with the laws of the State of New York, USA, without regards to such states conflict of law rules. Any legal action, suit or proceeding arising out of or relating to these Terms and Conditions or the breach thereof shall be instituted in a court of competent jurisdiction in New York County in the State of New York in the United States of America and each party hereby consents and submits to the personal jurisdiction of such court, waives any objection to venue in such court and consents to service of process by registered or certified mail, return receipt requested, at the last known address of such party.

Wiley Open Access Terms and Conditions

Wiley publishes Open Access articles in both its Wiley Open Access Journals program [http://www.wileyopenaccess.com/view/index.html] and as Online Open articles in its subscription journals. The majority of Wiley Open Access Journals have adopted the Creative Commons Attribution License (CC BY) which permits the unrestricted use, distribution, reproduction, adaptation and commercial exploitation of the article in any medium. No permission is required to use the article in this way provided that the article is properly cited and other license terms are observed. A small number of Wiley Open Access journals have retained the Creative Commons Attribution Non Commercial License (CC BY-NC), which permits use, distribution and reproduction in any medium, provided the original work is properly cited and is not used for commercial purposes.

Online Open articles Authors selecting Online Open are, unless particular exceptions apply, offered a choice of Creative Commons licenses. They may therefore select from the CC BY, the CC BY-NC and the Attribution-NoDerivatives (CC BY-NC-ND). The CC BY-NC-ND is more restrictive than the CC BY-NC as it does not permit adaptations or modifications without rights holder consent.

Wiley Open Access articles are protected by copyright and are posted to repositories and websites in accordance with the terms of the applicable Creative Commons license referenced on the article. At the time of deposit, Wiley Open Access articles include all changes made during peer review, copyediting, and publishing. Repositories and websites that host the article are responsible for incorporating any publisher-supplied amendments or retractions issued subsequently.
Wiley Open Access articles are also available without charge on Wiley's publishing platform, **Wiley Online Library** or any successor sites.

Conditions applicable to all Wiley Open Access articles:

- The authors' moral rights must not be compromised. These rights include the right of "paternity" (also known as "attribution" - the right for the author to be identified as such) and "integrity" (the right for the author not to have the work altered in such a way that the author's reputation or integrity may be damaged).

- Where content in the article is identified as belonging to a third party, it is the obligation of the user to ensure that any reuse complies with the copyright policies of the owner of that content.

- If article content is copied, downloaded or otherwise reused for research and other purposes as permitted, a link to the appropriate bibliographic citation (authors, journal, article title, volume, issue, page numbers, DOI and the link to the definitive published version on Wiley Online Library) should be maintained. Copyright notices and disclaimers must not be deleted. Creative Commons licenses are copyright licenses and do not confer any other rights, including but not limited to trademark or patent rights.

- Any translations, for which a prior translation agreement with Wiley has not been agreed, must prominently display the statement: "This is an unofficial translation of an article that appeared in a Wiley publication. The publisher has not endorsed this translation."

Conditions applicable to non-commercial licenses (CC BY-NC and CC BY-NC-ND)

For non-commercial and non-promotional purposes individual non-commercial users may access, download, copy, display and redistribute to colleagues Wiley Open Access articles. In addition, articles adopting the CC BY-NC may be adapted, translated, and text- and data-mined subject to the conditions above.

Use by commercial "for-profit" organizations

Use of non-commercial Wiley Open Access articles for commercial, promotional, or marketing purposes requires further explicit permission from Wiley and will be subject to a fee. Commercial purposes include:

- Copying or downloading of articles, or linking to such articles for further redistribution, sale or licensing;
- Copying, downloading or posting by a site or service that incorporates advertising with such content;
- The inclusion or incorporation of article content in other works or services (other than normal quotations with an appropriate citation) that is then available for sale or licensing, for a fee (for example, a compilation produced for marketing purposes, inclusion in a sales pack)
- Use of article content (other than normal quotations with appropriate citation) by for-profit organizations for promotional purposes
- Linking to article content in e-mails redistributed for promotional, marketing or educational purposes;
- Use for the purposes of monetary reward by means of sale, resale, license, loan, transfer or other form of commercial exploitation such as marketing products
- Print reprints of Wiley Open Access articles can be purchased from: corporatesales@wiley.com

  The modification or adaptation for any purpose of an article referencing the CC BY-NC-ND License requires consent which can be requested from RightsLink@wiley.com .

  Other Terms and Conditions:

  BY CLICKING ON THE "I AGREE..." BOX, YOU ACKNOWLEDGE THAT YOU HAVE READ AND FULLY UNDERSTAND EACH OF THE SECTIONS OF AND PROVISIONS SET FORTH IN THIS AGREEMENT AND THAT YOU ARE IN AGREEMENT WITH AND ARE WILLING TO ACCEPT ALL OF YOUR OBLIGATIONS AS SET FORTH IN THIS AGREEMENT.

  v1.8

If you would like to pay for this license now, please remit this license along with your payment made payable to "COPYRIGHT CLEARANCE CENTER" otherwise you will be invoiced within 48 hours of the license date. Payment should be in the form of a check or money order referencing your account number and this invoice number RLNK501019872.
Once you receive your invoice for this order, you may pay your invoice by credit card. Please follow instructions provided at that time.

Make Payment To:
Copyright Clearance Center
Dept 001
P.O. Box 843006
Boston, MA 02284-3006

For suggestions or comments regarding this order, contact RightsLink Customer Support: customercare@copyright.com or +1-877-622-5543 (toll free in the US) or +1-978-646-2777.

Gratis licenses (referencing $0 in the Total field) are free. Please retain this printable license for your reference. No payment is required.

Figure 3-3

JOHN WILEY AND SONS LICENSE
TERMS AND CONDITIONS
May 16, 2013

This is a License Agreement between Sergio Coda ("You") and John Wiley and Sons ("John Wiley and Sons") provided by Copyright Clearance Center ("CCC"). The license consists of your order details, the terms and conditions provided by John Wiley and Sons, and the payment terms and conditions.

All payments must be made in full to CCC. For payment instructions, please see information listed at the bottom of this form.

License Number	3150841013781
License date	May 16, 2013
Licensed content publisher	John Wiley and Sons
Licensed content publication	Digestive Endoscopy
Licensed content title	Photodiagnostic techniques for the endoscopic detection of premalignant gastrointestinal lesions
Licensed copyright line	Copyright © 2003, John Wiley and Sons
Licensed content author	Ralph S. DaCosta,Brian C. Wilson,Norman E. Marcon
Licensed content date	Jul 9, 2003
Start page	153
End page	173
Type of use	Dissertation/Thesis
Requestor type	University/Academic
Format	Print and electronic
Portion	Figure/table
Number of figures/tables	1
Original Wiley figure/table	Figure 1

number(s)

Will you be translating?	No
Total	0.00 USD

Terms and Conditions

TERMS AND CONDITIONS

This copyrighted material is owned by or exclusively licensed to John Wiley & Sons, Inc. or one of its group companies (each a "Wiley Company") or a society for whom a Wiley Company has exclusive publishing rights in relation to a particular journal (collectively WILEY). By clicking "accept" in connection with completing this licensing transaction, you agree that the following terms and conditions apply to this transaction (along with the billing and payment terms and conditions established by the Copyright Clearance Center Inc., ("CCCs Billing and Payment terms and conditions"), at the time that you opened your RightsLink account (these are available at any time at http://myaccount.copyright.com).

Terms and Conditions

1. The materials you have requested permission to reproduce (the "Materials") are protected by copyright.

2.You are hereby granted a personal, non-exclusive, non-sublicensable, non-transferable, worldwide, limited license to reproduce the Materials for the purpose specified in the licensing process. This license is for a one-time use only with a maximum distribution equal to the number that you identified in the licensing process. Any form of republication granted by this license must be completed within two years of the date of the grant of this license (although copies prepared before may be distributed thereafter). The Materials shall not be used in any other manner or for any other purpose. Permission is granted subject to an appropriate acknowledgement given to the author, title of the material/book/journal and the publisher. You shall also duplicate the copyright notice that appears in the Wiley publication in your use of the Material. Permission is also granted on the understanding that nowhere in the text is a previously published source acknowledged for all or part of this Material. Any third party material is expressly excluded from this permission.

3. With respect to the Materials, all rights are reserved. Except as expressly granted by the terms of the license, no part of the Materials may be copied, modified, adapted (except for minor reformatting required by the new Publication), translated, reproduced, transferred or distributed, in any form or by any means, and no derivative works may be made based on the Materials without the prior permission of the respective copyright owner. You may not alter, remove or suppress in any manner any copyright, trademark or other notices displayed by the Materials. You may not license, rent, sell, loan, lease, pledge, offer as security, transfer or assign the Materials, or any of the rights granted to you hereunder to any other person.

4. The Materials and all of the intellectual property rights therein shall at all times remain the exclusive property of John Wiley & Sons Inc or one of its related companies (WILEY) or their respective licensors, and your interest therein is only that of having possession of and the right to reproduce the Materials pursuant to Section 2 herein during the continuance of this Agreement. You agree that you own no right, title or interest in or to the Materials or any of the intellectual property rights therein. You shall have no rights hereunder other than the license as provided for above in Section 2. No right, license or interest to any trademark, trade name, service mark or other branding ("Marks") of WILEY or its licensors is granted hereunder, and you agree that you shall not assert any such right, license or interest with respect thereto.

5. NEITHER WILEY NOR ITS LICENSORS MAKES ANY WARRANTY OR REPRESENTATION OF ANY KIND TO YOU OR ANY THIRD PARTY, EXPRESS, IMPLIED OR STATUTORY, WITH RESPECT TO THE MATERIALS OR THE ACCURACY OF ANY INFORMATION CONTAINED IN THE MATERIALS, INCLUDING, WITHOUT LIMITATION, ANY IMPLIED WARRANTY OF MERCHANTABILITY, ACCURACY, SATISFACTORY QUALITY, FITNESS FOR A PARTICULAR PURPOSE, USABILITY, INTEGRATION OR NON-

INFRINGEMENT AND ALL SUCH WARRANTIES ARE HEREBY EXCLUDED BY WILEY AND ITS LICENSORS AND WAIVED BY YOU.

6. WILEY shall have the right to terminate this Agreement immediately upon breach of this Agreement by you.

7. You shall indemnify, defend and hold harmless WILEY, its Licensors and their respective directors, officers, agents and employees, from and against any actual or threatened claims, demands, causes of action or proceedings arising from any breach of this Agreement by you.

8. IN NO EVENT SHALL WILEY OR ITS LICENSORS BE LIABLE TO YOU OR ANY OTHER PARTY OR ANY OTHER PERSON OR ENTITY FOR ANY SPECIAL, CONSEQUENTIAL, INCIDENTAL, INDIRECT, EXEMPLARY OR PUNITIVE DAMAGES, HOWEVER CAUSED, ARISING OUT OF OR IN CONNECTION WITH THE DOWNLOADING, PROVISIONING, VIEWING OR USE OF THE MATERIALS REGARDLESS OF THE FORM OF ACTION, WHETHER FOR BREACH OF CONTRACT, BREACH OF WARRANTY, TORT, NEGLIGENCE, INFRINGEMENT OR OTHERWISE (INCLUDING, WITHOUT LIMITATION, DAMAGES BASED ON LOSS OF PROFITS, DATA, FILES, USE, BUSINESS OPPORTUNITY OR CLAIMS OF THIRD PARTIES), AND WHETHER OR NOT THE PARTY HAS BEEN ADVISED OF THE POSSIBILITY OF SUCH DAMAGES. THIS LIMITATION SHALL APPLY NOTWITHSTANDING ANY FAILURE OF ESSENTIAL PURPOSE OF ANY LIMITED REMEDY PROVIDED HEREIN.

9. Should any provision of this Agreement be held by a court of competent jurisdiction to be illegal, invalid, or unenforceable, that provision shall be deemed amended to achieve as nearly as possible the same economic effect as the original provision, and the legality, validity and enforceability of the remaining provisions of this Agreement shall not be affected or impaired thereby.

10. The failure of either party to enforce any term or condition of this Agreement shall not constitute a waiver of either party's right to enforce each and every term and condition of this Agreement. No breach under this agreement shall be deemed waived or excused by either party unless such waiver or consent is in writing signed by the party granting such waiver or consent. The waiver by or consent of a party to a breach of any provision of this Agreement shall not operate or be construed as a waiver of or consent to any other or subsequent breach by such other party.

11. This Agreement may not be assigned (including by operation of law or otherwise) by you without WILEY's prior written consent.

12. Any fee required for this permission shall be non-refundable after thirty (30) days from receipt

13. These terms and conditions together with CCCs Billing and Payment terms and conditions (which are incorporated herein) form the entire agreement between you and WILEY concerning this licensing transaction and (in the absence of fraud) supersedes all prior agreements and representations of the parties, oral or written. This Agreement may not be amended except in writing signed by both parties. This Agreement shall be binding upon and inure to the benefit of the parties' successors, legal representatives, and authorized assigns.

14. In the event of any conflict between your obligations established by these terms and conditions and those established by CCCs Billing and Payment terms and conditions, these terms and conditions shall prevail.

15. WILEY expressly reserves all rights not specifically granted in the combination of (i) the license details provided by you and accepted in the course of this licensing transaction, (ii) these terms and conditions and (iii) CCCs Billing and Payment terms and conditions.

16. This Agreement will be void if the Type of Use, Format, Circulation, or Requestor Type was misrepresented during the licensing process.

17. This Agreement shall be governed by and construed in accordance with the laws of the State of New York, USA, without regards to such states conflict of law rules. Any legal action, suit or proceeding arising out of or relating to these Terms and Conditions or the breach thereof shall be instituted in a court of competent jurisdiction in New York County in the State of New York in the United States of

America and each party hereby consents and submits to the personal jurisdiction of such court, waives any objection to venue in such court and consents to service of process by registered or certified mail, return receipt requested, at the last known address of such party.

Wiley Open Access Terms and Conditions

Wiley publishes Open Access articles in both its Wiley Open Access Journals program [http://www.wileyopenaccess.com/view/index.html] and as Online Open articles in its subscription journals. The majority of Wiley Open Access Journals have adopted the Creative Commons Attribution License (CC BY) which permits the unrestricted use, distribution, reproduction, adaptation and commercial exploitation of the article in any medium. No permission is required to use the article in this way provided that the article is properly cited and other license terms are observed. A small number of Wiley Open Access journals have retained the Creative Commons Attribution Non Commercial License (CC BY-NC), which permits use, distribution and reproduction in any medium, provided the original work is properly cited and is not used for commercial purposes.

Online Open articles Authors selecting Online Open are, unless particular exceptions apply, offered a choice of Creative Commons licenses. They may therefore select from the CC BY, the CC BY-NC and the Attribution-NoDerivatives (CC BY-NC-ND). The CC BY-NC-ND is more restrictive than the CC BY-NC as it does not permit adaptations or modifications without rights holder consent.

Wiley Open Access articles are protected by copyright and are posted to repositories and websites in accordance with the terms of the applicable Creative Commons license referenced on the article. At the time of deposit, Wiley Open Access articles include all changes made during peer review, copyediting, and publishing. Repositories and websites that host the article are responsible for incorporating any publisher-supplied amendments or retractions issued subsequently.
Wiley Open Access articles are also available without charge on Wiley's publishing platform, **Wiley Online Library** or any successor sites.

Conditions applicable to all Wiley Open Access articles:

- The authors' moral rights must not be compromised. These rights include the right of "paternity" (also known as "attribution" - the right for the author to be identified as such) and "integrity" (the right for the author not to have the work altered in such a way that the author's reputation or integrity may be damaged).

- Where content in the article is identified as belonging to a third party, it is the obligation of the user to ensure that any reuse complies with the copyright policies of the owner of that content.

- If article content is copied, downloaded or otherwise reused for research and other purposes as permitted, a link to the appropriate bibliographic citation (authors, journal, article title, volume, issue, page numbers, DOI and the link to the definitive published version on Wiley Online Library) should be maintained. Copyright notices and disclaimers must not be deleted. Creative Commons licenses are copyright licenses and do not confer any other rights, including but not limited to trademark or patent rights.

- Any translations, for which a prior translation agreement with Wiley has not been agreed, must prominently display the statement: "This is an unofficial translation of an article that appeared in a Wiley publication. The publisher has not endorsed this translation."

  Conditions applicable to non-commercial licenses (CC BY-NC and CC BY-NC-ND)

  For non-commercial and non-promotional purposes individual non-commercial users may access, download, copy, display and redistribute to colleagues Wiley Open Access articles. In addition, articles adopting the CC BY-NC may be adapted, translated, and text- and data-mined subject to the conditions above.

  Use by commercial "for-profit" organizations

Use of non-commercial Wiley Open Access articles for commercial, promotional, or marketing purposes requires further explicit permission from Wiley and will be subject to a fee. Commercial purposes include:

- Copying or downloading of articles, or linking to such articles for further redistribution, sale or licensing;
- Copying, downloading or posting by a site or service that incorporates advertising with such content;
- The inclusion or incorporation of article content in other works or services (other than normal quotations with an appropriate citation) that is then available for sale or licensing, for a fee (for example, a compilation produced for marketing purposes, inclusion in a sales pack)
- Use of article content (other than normal quotations with appropriate citation) by for-profit organizations for promotional purposes
- Linking to article content in e-mails redistributed for promotional, marketing or educational purposes;
- Use for the purposes of monetary reward by means of sale, resale, license, loan, transfer or other form of commercial exploitation such as marketing products
- Print reprints of Wiley Open Access articles can be purchased from: corporatesales@wiley.com

  The modification or adaptation for any purpose of an article referencing the CC BY-NC-ND License requires consent which can be requested from RightsLink@wiley.com .

  Other Terms and Conditions:

  BY CLICKING ON THE "I AGREE..." BOX, YOU ACKNOWLEDGE THAT YOU HAVE READ AND FULLY UNDERSTAND EACH OF THE SECTIONS OF AND PROVISIONS SET FORTH IN THIS AGREEMENT AND THAT YOU ARE IN AGREEMENT WITH AND ARE WILLING TO ACCEPT ALL OF YOUR OBLIGATIONS AS SET FORTH IN THIS AGREEMENT.

  v1.8

If you would like to pay for this license now, please remit this license along with your payment made payable to "COPYRIGHT CLEARANCE CENTER" otherwise you will be invoiced within 48 hours of the license date. Payment should be in the form of a check or money order referencing your account number and this invoice number RLNK501022678.
Once you receive your invoice for this order, you may pay your invoice by credit card. Please follow instructions provided at that time.

Make Payment To:
Copyright Clearance Center
Dept 001
P.O. Box 843006
Boston, MA 02284-3006

For suggestions or comments regarding this order, contact RightsLink Customer Support: customercare@copyright.com or +1-877-622-5543 (toll free in the US) or +1-978-646-2777.

Gratis licenses (referencing $0 in the Total field) are free. Please retain this printable license for

your reference. No payment is required.

Figure 3-4

JOHN WILEY AND SONS LICENSE
TERMS AND CONDITIONS
May 16, 2013

This is a License Agreement between Sergio Coda ("You") and John Wiley and Sons ("John Wiley and Sons") provided by Copyright Clearance Center ("CCC"). The license consists of your order details, the terms and conditions provided by John Wiley and Sons, and the payment terms and conditions.

All payments must be made in full to CCC. For payment instructions, please see information listed at the bottom of this form.

License Number	3150841356538
License date	May 16, 2013
Licensed content publisher	John Wiley and Sons
Licensed content publication	Photochemistry and Photobiology
Licensed content title	In Vivo Fluorescence Spectroscopy and Imaging for Oncological Applications
Licensed copyright line	Copyright © 2008, John Wiley and Sons
Licensed content author	Georges A. Wagnieres,Willem M. Star,Brian C. Wilson
Licensed content date	Jan 2, 2008
Start page	603
End page	632
Type of use	Dissertation/Thesis
Requestor type	University/Academic
Format	Print and electronic
Portion	Figure/table
Number of figures/tables	1
Original Wiley figure/table number(s)	Figure 1
Will you be translating?	No
Total	0.00 USD
Terms and Conditions	

TERMS AND CONDITIONS

This copyrighted material is owned by or exclusively licensed to John Wiley & Sons, Inc. or one of its group companies (each a "Wiley Company") or a society for whom a Wiley Company has exclusive

publishing rights in relation to a particular journal (collectively WILEY). By clicking "accept" in connection with completing this licensing transaction, you agree that the following terms and conditions apply to this transaction (along with the billing and payment terms and conditions established by the Copyright Clearance Center Inc., ("CCCs Billing and Payment terms and conditions"), at the time that you opened your RightsLink account (these are available at any time at http://myaccount.copyright.com).

Terms and Conditions

1. The materials you have requested permission to reproduce (the "Materials") are protected by copyright.

2.You are hereby granted a personal, non-exclusive, non-sublicensable, non-transferable, worldwide, limited license to reproduce the Materials for the purpose specified in the licensing process. This license is for a one-time use only with a maximum distribution equal to the number that you identified in the licensing process. Any form of republication granted by this license must be completed within two years of the date of the grant of this license (although copies prepared before may be distributed thereafter). The Materials shall not be used in any other manner or for any other purpose. Permission is granted subject to an appropriate acknowledgement given to the author, title of the material/book/journal and the publisher. You shall also duplicate the copyright notice that appears in the Wiley publication in your use of the Material. Permission is also granted on the understanding that nowhere in the text is a previously published source acknowledged for all or part of this Material. Any third party material is expressly excluded from this permission.

3. With respect to the Materials, all rights are reserved. Except as expressly granted by the terms of the license, no part of the Materials may be copied, modified, adapted (except for minor reformatting required by the new Publication), translated, reproduced, transferred or distributed, in any form or by any means, and no derivative works may be made based on the Materials without the prior permission of the respective copyright owner. You may not alter, remove or suppress in any manner any copyright, trademark or other notices displayed by the Materials. You may not license, rent, sell, loan, lease, pledge, offer as security, transfer or assign the Materials, or any of the rights granted to you hereunder to any other person.

4. The Materials and all of the intellectual property rights therein shall at all times remain the exclusive property of John Wiley & Sons Inc or one of its related companies (WILEY) or their respective licensors, and your interest therein is only that of having possession of and the right to reproduce the Materials pursuant to Section 2 herein during the continuance of this Agreement. You agree that you own no right, title or interest in or to the Materials or any of the intellectual property rights therein. You shall have no rights hereunder other than the license as provided for above in Section 2. No right, license or interest to any trademark, trade name, service mark or other branding ("Marks") of WILEY or its licensors is granted hereunder, and you agree that you shall not assert any such right, license or interest with respect thereto.

5. NEITHER WILEY NOR ITS LICENSORS MAKES ANY WARRANTY OR REPRESENTATION OF ANY KIND TO YOU OR ANY THIRD PARTY, EXPRESS, IMPLIED OR STATUTORY, WITH RESPECT TO THE MATERIALS OR THE ACCURACY OF ANY INFORMATION CONTAINED IN THE MATERIALS, INCLUDING, WITHOUT LIMITATION, ANY IMPLIED WARRANTY OF MERCHANTABILITY, ACCURACY, SATISFACTORY QUALITY, FITNESS FOR A PARTICULAR PURPOSE, USABILITY, INTEGRATION OR NON-INFRINGEMENT AND ALL SUCH WARRANTIES ARE HEREBY EXCLUDED BY WILEY AND ITS LICENSORS AND WAIVED BY YOU.

6. WILEY shall have the right to terminate this Agreement immediately upon breach of this Agreement by you.

7. You shall indemnify, defend and hold harmless WILEY, its Licensors and their respective directors, officers, agents and employees, from and against any actual or threatened claims, demands, causes of action or proceedings arising from any breach of this Agreement by you.

8. IN NO EVENT SHALL WILEY OR ITS LICENSORS BE LIABLE TO YOU OR ANY OTHER PARTY OR ANY

OTHER PERSON OR ENTITY FOR ANY SPECIAL, CONSEQUENTIAL, INCIDENTAL, INDIRECT, EXEMPLARY OR PUNITIVE DAMAGES, HOWEVER CAUSED, ARISING OUT OF OR IN CONNECTION WITH THE DOWNLOADING, PROVISIONING, VIEWING OR USE OF THE MATERIALS REGARDLESS OF THE FORM OF ACTION, WHETHER FOR BREACH OF CONTRACT, BREACH OF WARRANTY, TORT, NEGLIGENCE, INFRINGEMENT OR OTHERWISE (INCLUDING, WITHOUT LIMITATION, DAMAGES BASED ON LOSS OF PROFITS, DATA, FILES, USE, BUSINESS OPPORTUNITY OR CLAIMS OF THIRD PARTIES), AND WHETHER OR NOT THE PARTY HAS BEEN ADVISED OF THE POSSIBILITY OF SUCH DAMAGES. THIS LIMITATION SHALL APPLY NOTWITHSTANDING ANY FAILURE OF ESSENTIAL PURPOSE OF ANY LIMITED REMEDY PROVIDED HEREIN.

9. Should any provision of this Agreement be held by a court of competent jurisdiction to be illegal, invalid, or unenforceable, that provision shall be deemed amended to achieve as nearly as possible the same economic effect as the original provision, and the legality, validity and enforceability of the remaining provisions of this Agreement shall not be affected or impaired thereby.

10. The failure of either party to enforce any term or condition of this Agreement shall not constitute a waiver of either party's right to enforce each and every term and condition of this Agreement. No breach under this agreement shall be deemed waived or excused by either party unless such waiver or consent is in writing signed by the party granting such waiver or consent. The waiver by or consent of a party to a breach of any provision of this Agreement shall not operate or be construed as a waiver of or consent to any other or subsequent breach by such other party.

11. This Agreement may not be assigned (including by operation of law or otherwise) by you without WILEY's prior written consent.

12. Any fee required for this permission shall be non-refundable after thirty (30) days from receipt

13. These terms and conditions together with CCCs Billing and Payment terms and conditions (which are incorporated herein) form the entire agreement between you and WILEY concerning this licensing transaction and (in the absence of fraud) supersedes all prior agreements and representations of the parties, oral or written. This Agreement may not be amended except in writing signed by both parties. This Agreement shall be binding upon and inure to the benefit of the parties' successors, legal representatives, and authorized assigns.

14. In the event of any conflict between your obligations established by these terms and conditions and those established by CCCs Billing and Payment terms and conditions, these terms and conditions shall prevail.

15. WILEY expressly reserves all rights not specifically granted in the combination of (i) the license details provided by you and accepted in the course of this licensing transaction, (ii) these terms and conditions and (iii) CCCs Billing and Payment terms and conditions.

16. This Agreement will be void if the Type of Use, Format, Circulation, or Requestor Type was misrepresented during the licensing process.

17. This Agreement shall be governed by and construed in accordance with the laws of the State of New York, USA, without regards to such states conflict of law rules. Any legal action, suit or proceeding arising out of or relating to these Terms and Conditions or the breach thereof shall be instituted in a court of competent jurisdiction in New York County in the State of New York in the United States of America and each party hereby consents and submits to the personal jurisdiction of such court, waives any objection to venue in such court and consents to service of process by registered or certified mail, return receipt requested, at the last known address of such party.

Wiley Open Access Terms and Conditions

Wiley publishes Open Access articles in both its Wiley Open Access Journals program [http://www.wileyopenaccess.com/view/index.html] and as Online Open articles in its subscription journals. The majority of Wiley Open Access Journals have adopted the Creative Commons Attribution License (CC BY) which permits the unrestricted use, distribution, reproduction, adaptation and commercial exploitation of the article in any medium. No permission is required to use the article in this

way provided that the article is properly cited and other license terms are observed. A small number of Wiley Open Access journals have retained the Creative Commons Attribution Non Commercial License (CC BY-NC), which permits use, distribution and reproduction in any medium, provided the original work is properly cited and is not used for commercial purposes.

Online Open articles Authors selecting Online Open are, unless particular exceptions apply, offered a choice of Creative Commons licenses. They may therefore select from the CC BY, the CC BY-NC and the Attribution-NoDerivatives (CC BY-NC-ND). The CC BY-NC-ND is more restrictive than the CC BY-NC as it does not permit adaptations or modifications without rights holder consent.

Wiley Open Access articles are protected by copyright and are posted to repositories and websites in accordance with the terms of the applicable Creative Commons license referenced on the article. At the time of deposit, Wiley Open Access articles include all changes made during peer review, copyediting, and publishing. Repositories and websites that host the article are responsible for incorporating any publisher-supplied amendments or retractions issued subsequently.
Wiley Open Access articles are also available without charge on Wiley's publishing platform, **Wiley Online Library** or any successor sites.

Conditions applicable to all Wiley Open Access articles:

- The authors' moral rights must not be compromised. These rights include the right of "paternity" (also known as "attribution" - the right for the author to be identified as such) and "integrity" (the right for the author not to have the work altered in such a way that the author's reputation or integrity may be damaged).

- Where content in the article is identified as belonging to a third party, it is the obligation of the user to ensure that any reuse complies with the copyright policies of the owner of that content.

- If article content is copied, downloaded or otherwise reused for research and other purposes as permitted, a link to the appropriate bibliographic citation (authors, journal, article title, volume, issue, page numbers, DOI and the link to the definitive published version on Wiley Online Library) should be maintained. Copyright notices and disclaimers must not be deleted. Creative Commons licenses are copyright licenses and do not confer any other rights, including but not limited to trademark or patent rights.

- Any translations, for which a prior translation agreement with Wiley has not been agreed, must prominently display the statement: "This is an unofficial translation of an article that appeared in a Wiley publication. The publisher has not endorsed this translation."

  Conditions applicable to non-commercial licenses (CC BY-NC and CC BY-NC-ND)

  For non-commercial and non-promotional purposes individual non-commercial users may access, download, copy, display and redistribute to colleagues Wiley Open Access articles. In addition, articles adopting the CC BY-NC may be adapted, translated, and text- and data-mined subject to the conditions above.

  Use by commercial "for-profit" organizations

  Use of non-commercial Wiley Open Access articles for commercial, promotional, or marketing purposes requires further explicit permission from Wiley and will be subject to a fee. Commercial purposes include:

  - Copying or downloading of articles, or linking to such articles for further redistribution, sale or licensing;

  - Copying, downloading or posting by a site or service that incorporates advertising with such content;

- The inclusion or incorporation of article content in other works or services (other than normal quotations with an appropriate citation) that is then available for sale or licensing, for a fee (for example, a compilation produced for marketing purposes, inclusion in a sales pack)

- Use of article content (other than normal quotations with appropriate citation) by for-profit organizations for promotional purposes

- Linking to article content in e-mails redistributed for promotional, marketing or educational purposes;

- Use for the purposes of monetary reward by means of sale, resale, license, loan, transfer or other form of commercial exploitation such as marketing products

- Print reprints of Wiley Open Access articles can be purchased from: corporatesales@wiley.com

  The modification or adaptation for any purpose of an article referencing the CC BY-NC-ND License requires consent which can be requested from RightsLink@wiley.com .

  Other Terms and Conditions:

  BY CLICKING ON THE "I AGREE..." BOX, YOU ACKNOWLEDGE THAT YOU HAVE READ AND FULLY UNDERSTAND EACH OF THE SECTIONS OF AND PROVISIONS SET FORTH IN THIS AGREEMENT AND THAT YOU ARE IN AGREEMENT WITH AND ARE WILLING TO ACCEPT ALL OF YOUR OBLIGATIONS AS SET FORTH IN THIS AGREEMENT.

  v1.8

If you would like to pay for this license now, please remit this license along with your payment made payable to "COPYRIGHT CLEARANCE CENTER" otherwise you will be invoiced within 48 hours of the license date. Payment should be in the form of a check or money order referencing your account number and this invoice number RLNK501022684.
Once you receive your invoice for this order, you may pay your invoice by credit card. Please follow instructions provided at that time.

Make Payment To:
Copyright Clearance Center
Dept 001
P.O. Box 843006
Boston, MA 02284-3006

For suggestions or comments regarding this order, contact RightsLink Customer Support: customercare@copyright.com or +1-877-622-5543 (toll free in the US) or +1-978-646-2777.

Gratis licenses (referencing $0 in the Total field) are free. Please retain this printable license for your reference. No payment is required.

Figure 3-9

From: prvs=84665f276=copyright@osa.org on behalf of pubscopyright

<copyright@osa.org>

Sent: 21 May 2013 20:53

To: Coda, Sergio

Subject: RE: permission to reproduce figure in PhD thesis

Dear Dr. Coda,

Thank you for contacting The Optical Society.

OSA considers your requested use of its copyrighted material to be Fair Use under United States

Copyright Law. It is requested that a complete citation of the original material be included in any publication.

Let me know if you have any questions.

Kind Regards,

Susannah Lehman

Susannah Lehman

May 21, 2013

Authorized Agent, The Optical Society

From: Coda, Sergio [mailto:s.coda@imperial.ac.uk]

Sent: Thursday, May 16, 2013 11:59 AM

To: pubscopyright

Subject: permission to reproduce figure in PhD thesis

Dear Sir or Madam,

I would like to request permission to reproduce the following figure in my PhD thesis:

Re: McGinty, J., N. P. Galletly, C. Dunsby et al. 2010. Wide-field fluorescence lifetime imaging of cancer. Biomed. Opt. Express 1:627-640.

Figure 2. page 633.

The PhD thesis would be available in both print form and electronically.

Title of thesis: An Investigation of the Diagnostic Potential of Autofluorescence Lifetime Spectroscopy and Imaging for Label-Free Contrast of Disease.

I would also take this opportunity to express my sincere appreciation for your assistance.

Kind regards,

Dr Sergio Coda

****

Sergio Coda, MD
Clinical Research Fellow

Department of Medicine
Division of Experimental Medicine
Imperial College London

Room 612, Level 6, Blackett Laboratory
South Kensington Campus
Prince Consort Road
London SW7 2AZ
Telephone: 0044 (0) 20 7594 7738
Fax: 0044 (0) 20 7594 7714
E-Mail: s.coda@imperial.ac.uk
URL: http://www1.imperial.ac.uk/medicine/people/s.coda/
****

Figure 3-10

AW: permission to reproduce figure in PhD thesis

Rights DE [RIGHTS-and-LICENCES@wiley-vch.de]

Sent:17 May 2013 18:45

To: Coda, Sergio

Dear Sergio Coda

We hereby grant permission for the requested use expected that due credit is given to the original source.

If material appears within our work with credit to another source, authorisation from that source must be obtained.

Credit must include the following components:

- Books: Author(s)/ Editor(s) Name(s): Title of the Book. Page(s). Publication year. Copyright Wiley-VCH Verlag GmbH & Co. KGaA. Reproduced with permission.
- Journals: Author(s) Name(s): Title of the Article. Name of the Journal. Publication year. Volume. Page(s). Copyright Wiley-VCH Verlag GmbH & Co. KGaA. Reproduced with permission.
- Online Portal: Author(s): Title of the Online portal. Link or DOI. Publication year. Copyright Wiley-VCH Verlag GmbH & Co. KGaA. Reproduced with permission.

With kind regards

Bettina Loycke
Senior Rights Manager
Rights & Licenses

Wiley-VCH Verlag GmbH & Co. KGaA
Boschstraße 12
69469 Weinheim
Germany
www.wiley-vch.de

T +(49) 6201 606-280
F +(49) 6201 606-332
rightsDE@wiley.com

Von: Goldweber, Paulette - Hoboken **Im Auftrag von** Permissions - US
Gesendet: Freitag, 17. Mai 2013 15:44
An: Rights DE
Betreff: FW: permission to reproduce figure in PhD thesis

From: Coda, Sergio [mailto:s.coda@imperial.ac.uk]
Sent: Friday, May 17, 2013 4:59 AM
To: Permissions - US
Subject: permission to reproduce figure in PhD thesis

Dear Sir or Madam,

I would like to request permission to reproduce the following figure in my PhD thesis:

Re: Kennedy, G. T., H. B. Manning, D. S. Elson *et al.* 2010. A fluorescence lifetime imaging scanning confocal endomicroscope. Journal of Biophotonics 3:103-107.
Figure 1. page 104
Permission to reproduce this content could not be granted via the RightsLink® service.
The PhD thesis would be available in both print form and electronically.
Title of thesis: An Investigation of the Diagnostic Potential of Autofluorescence Lifetime Spectroscopy and Imaging for Label-Free Contrast of Disease.
I would also take this opportunity to express my sincere appreciation for your assistance.
Kind regards,
Dr Sergio Coda
****
Sergio Coda, MD
Clinical Research Fellow
Department of Medicine
Division of Experimental Medicine
Imperial College London

Room 612, Level 6, Blackett Laboratory
South Kensington Campus
Prince Consort Road
London SW7 2AZ
Telephone: 0044 (0) 20 7594 7738
Fax: 0044 (0) 20 7594 7714
E-Mail: s.coda@imperial.ac.uk
URL: http://www1.imperial.ac.uk/medicine/people/s.coda/
****

Deutsch:

WILEY-VCH Verlag GmbH & Co. KGaA – A company of John Wiley & Sons, Inc. - Sitz der Gesellschaft:

Weinheim – Amtsgericht Mannheim, HRB 432833 – Vorsitzender des Aufsichtsrates:

Stephen Michael Smith. Persönlich haftender Gesellschafter: John Wiley & Sons GmbH – Sitz der

Gesellschaft: Weinheim – Amtsgericht Mannheim, HRB 432296 – Geschäftsführer:

Bijan Ghawami, Dr. Jon Walmsley

English:

Wiley-VCH Verlag GmbH & Co. KGaA – A company of John Wiley & Sons, Inc. - Location of the Company:

Weinheim - Trade Register: Mannheim, HRB 432833.
Chairman of the Supervisory Board: Stephen Michael Smith. General Partner: John Wiley & Sons GmbH,
Location: Weinheim – Trade Register Mannheim, HRB 432296 –
Managing Directors: Bijan Ghawami, Dr. Jon Walmsley

Figure 3-11

From: prvs=84665f276=copyright@osa.org on behalf of pubscopyright

<copyright@osa.org>

Sent: 21 May 2013 20:53

To: Coda, Sergio

Subject: RE: permission to reproduce figure in PhD thesis

Dear Dr. Coda,

Thank you for contacting The Optical Society.

OSA considers your requested use of its copyrighted material to be Fair Use under United States

Copyright Law. It is requested that a complete citation of the original material be included in any publication.

Let me know if you have any questions.

Kind Regards,

Susannah Lehman

Susannah Lehman

May 21, 2013

Authorized Agent, The Optical Society

From: Coda, Sergio [mailto:s.coda@imperial.ac.uk]

Sent: Friday, May 17, 2013 4:54 AM

To: pubscopyright

Subject: permission to reproduce figure in PhD thesis

Dear Sir or Madam,

I would like to request permission to reproduce the following figure in my PhD thesis:

Re: Requejo-Isidro, J., J. McGinty, I. Munro et al. 2004. High-speed wide-field time-gated endoscopic fluorescence-lifetime imaging. Optics Letters 29:2249-2251.

Figure 1. page 2250

The PhD thesis would be available in both print form and electronically.

Title of thesis: An Investigation of the Diagnostic Potential of Autofluorescence Lifetime Spectroscopy and Imaging for Label-Free Contrast of Disease.

I would also take this opportunity to express my sincere appreciation for your assistance.

Kind regards,

Dr Sergio Coda

****

Sergio Coda, MD
Clinical Research Fellow
Department of Medicine
Division of Experimental Medicine
Imperial College London

Room 612, Level 6, Blackett Laboratory
South Kensington Campus
Prince Consort Road
London SW7 2AZ
Telephone: 0044 (0) 20 7594 7738
Fax: 0044 (0) 20 7594 7714
E-Mail: s.coda@imperial.ac.uk
URL: http://www1.imperial.ac.uk/medicine/people/s.coda/
****

Chapter 4

Figure 4-1c

ELSEVIER LICENSE
TERMS AND CONDITIONS
Jun 07, 2013

This is a License Agreement between Sergio Coda ("You") and Elsevier ("Elsevier") provided by Copyright Clearance Center ("CCC"). The license consists of your order details, the terms and conditions provided by Elsevier, and the payment terms and conditions.

All payments must be made in full to CCC. For payment instructions, please see information listed at the bottom of this form.

Supplier	Elsevier Limited The Boulevard,Langford Lane

	Kidlington,Oxford,OX5 1GB,UK
Registered Company Number	1982084
Customer name	Sergio Coda
Customer address	Room 612, Level 6, Blackett Laboratory
	London, other SW7 2AZ
License number	3163740771844
License date	Jun 07, 2013
Licensed content publisher	Elsevier
Licensed content publication	Gastroenterology
Licensed content title	Light-Scattering Technologies for Field Carcinogenesis Detection: A Modality for Endoscopic Prescreening
Licensed content author	Vadim Backman,Hemant K. Roy
Licensed content date	January 2011
Licensed content volume number	140
Licensed content issue number	1
Number of pages	12
Start Page	35
End Page	41.e5
Type of Use	reuse in a thesis/dissertation
Portion	figures/tables/illustrations
Number of figures/tables/illustrations	1
Format	both print and electronic
Are you the author of this Elsevier article?	No
Will you be translating?	No
Order reference number	
Title of your thesis/dissertation	An Investigation of the Diagnostic Potential of Autofluorescence Lifetime Spectroscopy and Imaging for Label-Free Contrast of Disease
Expected completion date	Jun 2013
Estimated size (number of pages)	250
Elsevier VAT number	GB 494 6272 12
Permissions price	0.00 GBP
VAT/Local Sales Tax	0.0 USD / 0.0 GBP
Total	0.00 GBP
Terms and Conditions	

INTRODUCTION

1. The publisher for this copyrighted material is Elsevier. By clicking "accept" in connection with

completing this licensing transaction, you agree that the following terms and conditions apply to this transaction (along with the Billing and Payment terms and conditions established by Copyright Clearance Center, Inc. ("CCC"), at the time that you opened your Rightslink account and that are available at any time at http://myaccount.copyright.com).

GENERAL TERMS

2. Elsevier hereby grants you permission to reproduce the aforementioned material subject to the terms and conditions indicated.

3. Acknowledgement: If any part of the material to be used (for example, figures) has appeared in our publication with credit or acknowledgement to another source, permission must also be sought from that source. If such permission is not obtained then that material may not be included in your publication/copies. Suitable acknowledgement to the source must be made, either as a footnote or in a reference list at the end of your publication, as follows:

"Reprinted from Publication title, Vol /edition number, Author(s), Title of article / title of chapter, Pages No., Copyright (Year), with permission from Elsevier [OR APPLICABLE SOCIETY COPYRIGHT OWNER]." Also Lancet special credit - "Reprinted from The Lancet, Vol. number, Author(s), Title of article, Pages No., Copyright (Year), with permission from Elsevier."

4. Reproduction of this material is confined to the purpose and/or media for which permission is hereby given.

5. Altering/Modifying Material: Not Permitted. However figures and illustrations may be altered/adapted minimally to serve your work. Any other abbreviations, additions, deletions and/or any other alterations shall be made only with prior written authorization of Elsevier Ltd. (Please contact Elsevier at permissions@elsevier.com)

6. If the permission fee for the requested use of our material is waived in this instance, please be advised that your future requests for Elsevier materials may attract a fee.

7. Reservation of Rights: Publisher reserves all rights not specifically granted in the combination of (i) the license details provided by you and accepted in the course of this licensing transaction, (ii) these terms and conditions and (iii) CCC's Billing and Payment terms and conditions.

8. License Contingent Upon Payment: While you may exercise the rights licensed immediately upon issuance of the license at the end of the licensing process for the transaction, provided that you have disclosed complete and accurate details of your proposed use, no license is finally effective unless and until full payment is received from you (either by publisher or by CCC) as provided in CCC's Billing and Payment terms and conditions. If full payment is not received on a timely basis, then any license preliminarily granted shall be deemed automatically revoked and shall be void as if never granted. Further, in the event that you breach any of these terms and conditions or any of CCC's Billing and Payment terms and conditions, the license is automatically revoked and shall be void as if never granted. Use of materials as described in a revoked license, as well as any use of the materials beyond the scope of an unrevoked license, may constitute copyright infringement and publisher reserves the right to take any and all action to protect its copyright in the materials.

9. Warranties: Publisher makes no representations or warranties with respect to the licensed material.

10. Indemnity: You hereby indemnify and agree to hold harmless publisher and CCC, and their respective officers, directors, employees and agents, from and against any and all claims arising out of your use of the licensed material other than as specifically authorized pursuant to this license.

11. No Transfer of License: This license is personal to you and may not be sublicensed, assigned, or transferred by you to any other person without publisher's written permission.

12. No Amendment Except in Writing: This license may not be amended except in a writing signed by both parties (or, in the case of publisher, by CCC on publisher's behalf).

13. Objection to Contrary Terms: Publisher hereby objects to any terms contained in any purchase

order, acknowledgment, check endorsement or other writing prepared by you, which terms are inconsistent with these terms and conditions or CCC's Billing and Payment terms and conditions. These terms and conditions, together with CCC's Billing and Payment terms and conditions (which are incorporated herein), comprise the entire agreement between you and publisher (and CCC) concerning this licensing transaction. In the event of any conflict between your obligations established by these terms and conditions and those established by CCC's Billing and Payment terms and conditions, these terms and conditions shall control.

14. Revocation: Elsevier or Copyright Clearance Center may deny the permissions described in this License at their sole discretion, for any reason or no reason, with a full refund payable to you. Notice of such denial will be made using the contact information provided by you. Failure to receive such notice will not alter or invalidate the denial. In no event will Elsevier or Copyright Clearance Center be responsible or liable for any costs, expenses or damage incurred by you as a result of a denial of your permission request, other than a refund of the amount(s) paid by you to Elsevier and/or Copyright Clearance Center for denied permissions.

LIMITED LICENSE

The following terms and conditions apply only to specific license types:

15. **Translation**: This permission is granted for non-exclusive world **English** rights only unless your license was granted for translation rights. If you licensed translation rights you may only translate this content into the languages you requested. A professional translator must perform all translations and reproduce the content word for word preserving the integrity of the article. If this license is to re-use 1 or 2 figures then permission is granted for non-exclusive world rights in all languages.

16. **Website**: The following terms and conditions apply to electronic reserve and author websites:
Electronic reserve: If licensed material is to be posted to website, the web site is to be password-protected and made available only to bona fide students registered on a relevant course if:
This license was made in connection with a course,
This permission is granted for 1 year only. You may obtain a license for future website posting,
All content posted to the web site must maintain the copyright information line on the bottom of each image,
A hyper-text must be included to the Homepage of the journal from which you are licensing athttp://www.sciencedirect.com/science/journal/xxxxx or the Elsevier homepage for books athttp://www.elsevier.com , and
Central Storage: This license does not include permission for a scanned version of the material to be stored in a central repository such as that provided by Heron/XanEdu.

17. **Author website** for journals with the following additional clauses:

All content posted to the web site must maintain the copyright information line on the bottom of each image, and the permission granted is limited to the personal version of your paper. You are not allowed to download and post the published electronic version of your article (whether PDF or HTML, proof or final version), nor may you scan the printed edition to create an electronic version. A hyper-text must be included to the Homepage of the journal from which you are licensing athttp://www.sciencedirect.com/science/journal/xxxxx . As part of our normal production process, you will receive an e-mail notice when your article appears on Elsevier's online service ScienceDirect (www.sciencedirect.com). That e-mail will include the article's Digital Object Identifier (DOI). This number provides the electronic link to the published article and should be included in the posting of your personal version. We ask that you wait until you receive this e-mail and have the DOI to do any posting.

Central Storage: This license does not include permission for a scanned version of the material to be stored in a central repository such as that provided by Heron/XanEdu.

18. **Author website** for books with the following additional clauses:
Authors are permitted to place a brief summary of their work online only.
A hyper-text must be included to the Elsevier homepage at http://www.elsevier.com . All content posted to the web site must maintain the copyright information line on the bottom of each image. You

are not allowed to download and post the published electronic version of your chapter, nor may you scan the printed edition to create an electronic version.

Central Storage: This license does not include permission for a scanned version of the material to be stored in a central repository such as that provided by Heron/XanEdu.

19. **Website** (regular and for author): A hyper-text must be included to the Homepage of the journal from which you are licensing at http://www.sciencedirect.com/science/journal/xxxxx. or for books to the Elsevier homepage at http://www.elsevier.com

20. **Thesis/Dissertation**: If your license is for use in a thesis/dissertation your thesis may be submitted to your institution in either print or electronic form. Should your thesis be published commercially, please reapply for permission. These requirements include permission for the Library and Archives of Canada to supply single copies, on demand, of the complete thesis and include permission for UMI to supply single copies, on demand, of the complete thesis. Should your thesis be published commercially, please reapply for permission.

21. **Other Conditions**:

v1.6

If you would like to pay for this license now, please remit this license along with your payment made payable to "COPYRIGHT CLEARANCE CENTER" otherwise you will be invoiced within 48 hours of the license date. Payment should be in the form of a check or money order referencing your account number and this invoice number RLNK501038591.
Once you receive your invoice for this order, you may pay your invoice by credit card. Please follow instructions provided at that time.

Make Payment To:
Copyright Clearance Center
Dept 001
P.O. Box 843006
Boston, MA 02284-3006

For suggestions or comments regarding this order, contact RightsLink Customer Support:customercare@copyright.com or +1-877-622-5543 (toll free in the US) or +1-978-646-2777.

Gratis licenses (referencing $0 in the Total field) are free. Please retain this printable license for your reference. No payment is required.

Figure 4-24

ELSEVIER LICENSE
TERMS AND CONDITIONS
May 17, 2013

This is a License Agreement between Sergio Coda ("You") and Elsevier ("Elsevier") provided by Copyright Clearance Center ("CCC"). The license consists of your order details, the terms and conditions provided by Elsevier, and the payment terms and conditions.

All payments must be made in full to CCC. For payment instructions, please see information

listed at the bottom of this form.

Supplier	Elsevier Limited The Boulevard,Langford Lane Kidlington,Oxford,OX5 1GB,UK
Registered Company Number	1982084
Customer name	Sergio Coda
Customer address	Room 731, Level 7, Blackett Laboratory London, other SW7 2AZ
License number	3151271445255
License date	May 17, 2013
Licensed content publisher	Elsevier
Licensed content publication	Matrix Biology
Licensed content title	Detection of cartilage matrix degradation by autofluorescence lifetime
Licensed content author	Hugh B. Manning,Mohammad B. Nickdel,Kazuhiro Yamamoto,João L. Lagarto,Douglas J. Kelly,Clifford B. Talbot,Gordon Kennedy,Jayesh Dudhia,John Lever,Christopher Dunsby,Paul French,Yoshifumi Itoh
Licensed content date	January 2013
Licensed content volume number	32
Licensed content issue number	1
Number of pages	7
Start Page	32
End Page	38
Type of Use	reuse in a thesis/dissertation
Intended publisher of new work	other
Portion	figures/tables/illustrations
Number of figures/tables/illustrations	1
Format	both print and electronic
Are you the author of this Elsevier article?	No
Will you be translating?	No
Order reference number	
Title of your thesis/dissertation	An Investigation of the Diagnostic Potential of Autofluorescence Lifetime Spectroscopy and Imaging for Label-Free Contrast of Disease
Expected completion date	May 2013
Estimated size (number of pages)	250
Elsevier VAT number	GB 494 6272 12

Permissions price	0.00 GBP
VAT/Local Sales Tax	0.0 USD / 0.0 GBP
Total	0.00 GBP

Terms and Conditions

INTRODUCTION

1. The publisher for this copyrighted material is Elsevier. By clicking "accept" in connection with completing this licensing transaction, you agree that the following terms and conditions apply to this transaction (along with the Billing and Payment terms and conditions established by Copyright Clearance Center, Inc. ("CCC"), at the time that you opened your Rightslink account and that are available at any time at http://myaccount.copyright.com).

GENERAL TERMS

2. Elsevier hereby grants you permission to reproduce the aforementioned material subject to the terms and conditions indicated.

3. Acknowledgement: If any part of the material to be used (for example, figures) has appeared in our publication with credit or acknowledgement to another source, permission must also be sought from that source. If such permission is not obtained then that material may not be included in your publication/copies. Suitable acknowledgement to the source must be made, either as a footnote or in a reference list at the end of your publication, as follows:

"Reprinted from Publication title, Vol /edition number, Author(s), Title of article / title of chapter, Pages No., Copyright (Year), with permission from Elsevier [OR APPLICABLE SOCIETY COPYRIGHT OWNER]." Also Lancet special credit - "Reprinted from The Lancet, Vol. number, Author(s), Title of article, Pages No., Copyright (Year), with permission from Elsevier."

4. Reproduction of this material is confined to the purpose and/or media for which permission is hereby given.

5. Altering/Modifying Material: Not Permitted. However figures and illustrations may be altered/adapted minimally to serve your work. Any other abbreviations, additions, deletions and/or any other alterations shall be made only with prior written authorization of Elsevier Ltd. (Please contact Elsevier at permissions@elsevier.com)

6. If the permission fee for the requested use of our material is waived in this instance, please be advised that your future requests for Elsevier materials may attract a fee.

7. Reservation of Rights: Publisher reserves all rights not specifically granted in the combination of (i) the license details provided by you and accepted in the course of this licensing transaction, (ii) these terms and conditions and (iii) CCC's Billing and Payment terms and conditions.

8. License Contingent Upon Payment: While you may exercise the rights licensed immediately upon issuance of the license at the end of the licensing process for the transaction, provided that you have disclosed complete and accurate details of your proposed use, no license is finally effective unless and until full payment is received from you (either by publisher or by CCC) as provided in CCC's Billing and Payment terms and conditions. If full payment is not received on a timely basis, then any license preliminarily granted shall be deemed automatically revoked and shall be void as if never granted. Further, in the event that you breach any of these terms and conditions or any of CCC's Billing and Payment terms and conditions, the license is automatically revoked and shall be void as if never granted. Use of materials as described in a revoked license, as well as any use of the materials beyond the scope of an unrevoked license, may constitute copyright infringement and publisher reserves the right to take any and all action to protect its copyright in the materials.

9. Warranties: Publisher makes no representations or warranties with respect to the licensed material.

10. Indemnity: You hereby indemnify and agree to hold harmless publisher and CCC, and their respective officers, directors, employees and agents, from and against any and all claims arising out of your use of the licensed material other than as specifically authorized pursuant to this license.

11. No Transfer of License: This license is personal to you and may not be sublicensed, assigned, or transferred by you to any other person without publisher's written permission.

12. No Amendment Except in Writing: This license may not be amended except in a writing signed by both parties (or, in the case of publisher, by CCC on publisher's behalf).

13. Objection to Contrary Terms: Publisher hereby objects to any terms contained in any purchase order, acknowledgment, check endorsement or other writing prepared by you, which terms are inconsistent with these terms and conditions or CCC's Billing and Payment terms and conditions. These terms and conditions, together with CCC's Billing and Payment terms and conditions (which are incorporated herein), comprise the entire agreement between you and publisher (and CCC) concerning this licensing transaction. In the event of any conflict between your obligations established by these terms and conditions and those established by CCC's Billing and Payment terms and conditions, these terms and conditions shall control.

14. Revocation: Elsevier or Copyright Clearance Center may deny the permissions described in this License at their sole discretion, for any reason or no reason, with a full refund payable to you. Notice of such denial will be made using the contact information provided by you. Failure to receive such notice will not alter or invalidate the denial. In no event will Elsevier or Copyright Clearance Center be responsible or liable for any costs, expenses or damage incurred by you as a result of a denial of your permission request, other than a refund of the amount(s) paid by you to Elsevier and/or Copyright Clearance Center for denied permissions.

LIMITED LICENSE

The following terms and conditions apply only to specific license types:

15. **Translation**: This permission is granted for non-exclusive world **English** rights only unless your license was granted for translation rights. If you licensed translation rights you may only translate this content into the languages you requested. A professional translator must perform all translations and reproduce the content word for word preserving the integrity of the article. If this license is to re-use 1 or 2 figures then permission is granted for non-exclusive world rights in all languages.

16. **Website**: The following terms and conditions apply to electronic reserve and author websites:
Electronic reserve: If licensed material is to be posted to website, the web site is to be password-protected and made available only to bona fide students registered on a relevant course if:
This license was made in connection with a course,
This permission is granted for 1 year only. You may obtain a license for future website posting,
All content posted to the web site must maintain the copyright information line on the bottom of each image,
A hyper-text must be included to the Homepage of the journal from which you are licensing at http://www.sciencedirect.com/science/journal/xxxxx or the Elsevier homepage for books at http://www.elsevier.com , and
Central Storage: This license does not include permission for a scanned version of the material to be stored in a central repository such as that provided by Heron/XanEdu.

17. **Author website** for journals with the following additional clauses:

All content posted to the web site must maintain the copyright information line on the bottom of each image, and the permission granted is limited to the personal version of your paper. You are not allowed to download and post the published electronic version of your article (whether PDF or HTML, proof or final version), nor may you scan the printed edition to create an electronic version. A hyper-text must be included to the Homepage of the journal from which you are licensing at http://www.sciencedirect.com/science/journal/xxxxx . As part of our normal production process, you will receive an e-mail notice when your article appears on Elsevier's online service ScienceDirect (www.sciencedirect.com). That e-mail will include the article's Digital Object Identifier (DOI). This

number provides the electronic link to the published article and should be included in the posting of your personal version. We ask that you wait until you receive this e-mail and have the DOI to do any posting.

Central Storage: This license does not include permission for a scanned version of the material to be stored in a central repository such as that provided by Heron/XanEdu.

18. **Author website** for books with the following additional clauses:
Authors are permitted to place a brief summary of their work online only.
A hyper-text must be included to the Elsevier homepage at http://www.elsevier.com . All content posted to the web site must maintain the copyright information line on the bottom of each image. You are not allowed to download and post the published electronic version of your chapter, nor may you scan the printed edition to create an electronic version.

Central Storage: This license does not include permission for a scanned version of the material to be stored in a central repository such as that provided by Heron/XanEdu.

19. **Website** (regular and for author): A hyper-text must be included to the Homepage of the journal from which you are licensing at http://www.sciencedirect.com/science/journal/xxxxx. or for books to the Elsevier homepage at http://www.elsevier.com

20. **Thesis/Dissertation**: If your license is for use in a thesis/dissertation your thesis may be submitted to your institution in either print or electronic form. Should your thesis be published commercially, please reapply for permission. These requirements include permission for the Library and Archives of Canada to supply single copies, on demand, of the complete thesis and include permission for UMI to supply single copies, on demand, of the complete thesis. Should your thesis be published commercially, please reapply for permission.

21. **Other Conditions**:

v1.6

If you would like to pay for this license now, please remit this license along with your payment made payable to "COPYRIGHT CLEARANCE CENTER" otherwise you will be invoiced within 48 hours of the license date. Payment should be in the form of a check or money order referencing your account number and this invoice number RLNK501023213.
Once you receive your invoice for this order, you may pay your invoice by credit card. Please follow instructions provided at that time.

Make Payment To:
Copyright Clearance Center
Dept 001
P.O. Box 843006
Boston, MA 02284-3006

For suggestions or comments regarding this order, contact RightsLink Customer Support: customercare@copyright.com or +1-877-622-5543 (toll free in the US) or +1-978-646-2777.

Gratis licenses (referencing $0 in the Total field) are free. Please retain this printable license for your reference. No payment is required.

Chapter 5

Figure 5-1

Re: permission to reproduce figure in PhD thesis

Betsy Ott [bott@tjc.edu]

Sent:18 May 2013 17:10

To: Coda, Sergio

Permission granted. Citation should include "digital image by Betsy Ott and Pam Gregory, Tyler Junior College, Tyler Texas." Please send the complete reference information when it is published.
Dr. Betsy Ott

Tyler Junior College

Tyler, Texas

On May 18, 2013, at 11:01 AM, "Coda, Sergio" <s.coda@imperial.ac.uk> wrote:

Dear Ms Betsy

I would like to request permission to reproduce the following figure in my PhD thesis:

Re: Bladder wall http://science.tjc.edu/images/kidney/k52k.jpg

The PhD thesis would be available in both print form and electronically.

Title of thesis: An Investigation of the Diagnostic Potential of Autofluorescence Lifetime Spectroscopy and Imaging for Label-Free Contrast of Disease.

I would also take this opportunity to express my sincere appreciation for your assistance.

Kind regards,

Dr Sergio Coda

****

Sergio Coda, MD
Clinical Research Fellow
Department of Medicine
Division of Experimental Medicine
Imperial College London
Room 612, Level 6, Blackett Laboratory
South Kensington Campus
Prince Consort Road
London SW7 2AZ
Telephone: 0044 (0) 20 7594 7738
Fax: 0044 (0) 20 7594 7714
E-Mail: s.coda@imperial.ac.uk
URL: http://www1.imperial.ac.uk/medicine/people/s.coda/
****

Figure 5-2

ELSEVIER LICENSE
TERMS AND CONDITIONS
Jun 03, 2013

This is a License Agreement between Sergio Coda ("You") and Elsevier ("Elsevier") provided by Copyright Clearance Center ("CCC"). The license consists of your order details, the terms and conditions provided by Elsevier, and the payment terms and conditions.

All payments must be made in full to CCC. For payment instructions, please see information listed at the bottom of this form.

Supplier	Elsevier Limited The Boulevard,Langford Lane Kidlington,Oxford,OX5 1GB,UK
Registered Company Number	1982084
Customer name	Sergio Coda
Customer address	Room 612, Level 6, Blackett Laboratory London, other SW7 2AZ
License number	3161270705476
License date	Jun 03, 2013
Licensed content publisher	Elsevier
Licensed content publication	The Journal of Urology
Licensed content title	Optical Biopsy of Human Bladder Neoplasia With In Vivo Confocal Laser Endomicroscopy
Licensed content author	Geoffrey A. Sonn,Sha-Nita E. Jones,Tatum V. Tarin,Christine B. Du,Kathleen E. Mach,Kristin C. Jensen,Joseph C. Liao
Licensed content date	October 2009
Licensed content volume number	182
Licensed content issue number	4
Number of pages	7
Start Page	1299
End Page	1305
Type of Use	reuse in a thesis/dissertation
Intended publisher of new work	other
Portion	figures/tables/illustrations
Number of figures/tables/illustrations	1
Format	both print and electronic
Are you the author of this Elsevier article?	No

Will you be translating?	No
Order reference number	
Title of your thesis/dissertation	An Investigation of the Diagnostic Potential of Autofluorescence Lifetime Spectroscopy and Imaging for Label-Free Contrast of Disease
Expected completion date	May 2013
Estimated size (number of pages)	250
Elsevier VAT number	GB 494 6272 12
Permissions price	0.00 GBP
VAT/Local Sales Tax	0.00 USD / GBP
Total	0.00 GBP
Terms and Conditions	

INTRODUCTION

1. The publisher for this copyrighted material is Elsevier. By clicking "accept" in connection with completing this licensing transaction, you agree that the following terms and conditions apply to this transaction (along with the Billing and Payment terms and conditions established by Copyright Clearance Center, Inc. ("CCC"), at the time that you opened your Rightslink account and that are available at any time at http://myaccount.copyright.com).

GENERAL TERMS

2. Elsevier hereby grants you permission to reproduce the aforementioned material subject to the terms and conditions indicated.

3. Acknowledgement: If any part of the material to be used (for example, figures) has appeared in our publication with credit or acknowledgement to another source, permission must also be sought from that source. If such permission is not obtained then that material may not be included in your publication/copies. Suitable acknowledgement to the source must be made, either as a footnote or in a reference list at the end of your publication, as follows:

"Reprinted from Publication title, Vol /edition number, Author(s), Title of article / title of chapter, Pages No., Copyright (Year), with permission from Elsevier [OR APPLICABLE SOCIETY COPYRIGHT OWNER]." Also Lancet special credit - "Reprinted from The Lancet, Vol. number, Author(s), Title of article, Pages No., Copyright (Year), with permission from Elsevier."

4. Reproduction of this material is confined to the purpose and/or media for which permission is hereby given.

5. Altering/Modifying Material: Not Permitted. However figures and illustrations may be altered/adapted minimally to serve your work. Any other abbreviations, additions, deletions and/or any other alterations shall be made only with prior written authorization of Elsevier Ltd. (Please contact Elsevier at permissions@elsevier.com)

6. If the permission fee for the requested use of our material is waived in this instance, please be advised that your future requests for Elsevier materials may attract a fee.

7. Reservation of Rights: Publisher reserves all rights not specifically granted in the combination of (i) the license details provided by you and accepted in the course of this licensing transaction, (ii) these terms and conditions and (iii) CCC's Billing and Payment terms and conditions.

8. License Contingent Upon Payment: While you may exercise the rights licensed immediately upon issuance of the license at the end of the licensing process for the transaction, provided that you have

disclosed complete and accurate details of your proposed use, no license is finally effective unless and until full payment is received from you (either by publisher or by CCC) as provided in CCC's Billing and Payment terms and conditions. If full payment is not received on a timely basis, then any license preliminarily granted shall be deemed automatically revoked and shall be void as if never granted. Further, in the event that you breach any of these terms and conditions or any of CCC's Billing and Payment terms and conditions, the license is automatically revoked and shall be void as if never granted. Use of materials as described in a revoked license, as well as any use of the materials beyond the scope of an unrevoked license, may constitute copyright infringement and publisher reserves the right to take any and all action to protect its copyright in the materials.

9. Warranties: Publisher makes no representations or warranties with respect to the licensed material.

10. Indemnity: You hereby indemnify and agree to hold harmless publisher and CCC, and their respective officers, directors, employees and agents, from and against any and all claims arising out of your use of the licensed material other than as specifically authorized pursuant to this license.

11. No Transfer of License: This license is personal to you and may not be sublicensed, assigned, or transferred by you to any other person without publisher's written permission.

12. No Amendment Except in Writing: This license may not be amended except in a writing signed by both parties (or, in the case of publisher, by CCC on publisher's behalf).

13. Objection to Contrary Terms: Publisher hereby objects to any terms contained in any purchase order, acknowledgment, check endorsement or other writing prepared by you, which terms are inconsistent with these terms and conditions or CCC's Billing and Payment terms and conditions. These terms and conditions, together with CCC's Billing and Payment terms and conditions (which are incorporated herein), comprise the entire agreement between you and publisher (and CCC) concerning this licensing transaction. In the event of any conflict between your obligations established by these terms and conditions and those established by CCC's Billing and Payment terms and conditions, these terms and conditions shall control.

14. Revocation: Elsevier or Copyright Clearance Center may deny the permissions described in this License at their sole discretion, for any reason or no reason, with a full refund payable to you. Notice of such denial will be made using the contact information provided by you. Failure to receive such notice will not alter or invalidate the denial. In no event will Elsevier or Copyright Clearance Center be responsible or liable for any costs, expenses or damage incurred by you as a result of a denial of your permission request, other than a refund of the amount(s) paid by you to Elsevier and/or Copyright Clearance Center for denied permissions.

LIMITED LICENSE

The following terms and conditions apply only to specific license types:

15. **Translation**: This permission is granted for non-exclusive world **English** rights only unless your license was granted for translation rights. If you licensed translation rights you may only translate this content into the languages you requested. A professional translator must perform all translations and reproduce the content word for word preserving the integrity of the article. If this license is to re-use 1 or 2 figures then permission is granted for non-exclusive world rights in all languages.

16. **Website**: The following terms and conditions apply to electronic reserve and author websites:
Electronic reserve: If licensed material is to be posted to website, the web site is to be password-protected and made available only to bona fide students registered on a relevant course if:
This license was made in connection with a course,
This permission is granted for 1 year only. You may obtain a license for future website posting,
All content posted to the web site must maintain the copyright information line on the bottom of each image,
A hyper-text must be included to the Homepage of the journal from which you are licensing at http://www.sciencedirect.com/science/journal/xxxxx or the Elsevier homepage for books at http://www.elsevier.com , and

Central Storage: This license does not include permission for a scanned version of the material to be stored in a central repository such as that provided by Heron/XanEdu.

17. **Author website** for journals with the following additional clauses:

All content posted to the web site must maintain the copyright information line on the bottom of each image, and the permission granted is limited to the personal version of your paper. You are not allowed to download and post the published electronic version of your article (whether PDF or HTML, proof or final version), nor may you scan the printed edition to create an electronic version. A hyper-text must be included to the Homepage of the journal from which you are licensing athttp://www.sciencedirect.com/science/journal/xxxxx . As part of our normal production process, you will receive an e-mail notice when your article appears on Elsevier's online service ScienceDirect (www.sciencedirect.com). That e-mail will include the article's Digital Object Identifier (DOI). This number provides the electronic link to the published article and should be included in the posting of your personal version. We ask that you wait until you receive this e-mail and have the DOI to do any posting.

Central Storage: This license does not include permission for a scanned version of the material to be stored in a central repository such as that provided by Heron/XanEdu.

18. **Author website** for books with the following additional clauses:
Authors are permitted to place a brief summary of their work online only.
A hyper-text must be included to the Elsevier homepage at http://www.elsevier.com . All content posted to the web site must maintain the copyright information line on the bottom of each image. You are not allowed to download and post the published electronic version of your chapter, nor may you scan the printed edition to create an electronic version.

Central Storage: This license does not include permission for a scanned version of the material to be stored in a central repository such as that provided by Heron/XanEdu.

19. **Website** (regular and for author): A hyper-text must be included to the Homepage of the journal from which you are licensing at http://www.sciencedirect.com/science/journal/xxxxx. or for books to the Elsevier homepage at http://www.elsevier.com

20. **Thesis/Dissertation**: If your license is for use in a thesis/dissertation your thesis may be submitted to your institution in either print or electronic form. Should your thesis be published commercially, please reapply for permission. These requirements include permission for the Library and Archives of Canada to supply single copies, on demand, of the complete thesis and include permission for UMI to supply single copies, on demand, of the complete thesis. Should your thesis be published commercially, please reapply for permission.

21. **Other Conditions**:

v1.6

If you would like to pay for this license now, please remit this license along with your payment made payable to "COPYRIGHT CLEARANCE CENTER" otherwise you will be invoiced within 48 hours of the license date. Payment should be in the form of a check or money order referencing your account number and this invoice number RLNK501034368.
Once you receive your invoice for this order, you may pay your invoice by credit card. Please follow instructions provided at that time.

Make Payment To:
Copyright Clearance Center
Dept 001
P.O. Box 843006
Boston, MA 02284-3006

For suggestions or comments regarding this order, contact RightsLink Customer

Support:customercare@copyright.com or +1-877-622-5543 (toll free in the US) or +1-978-646-2777.

Gratis licenses (referencing $0 in the Total field) are free. Please retain this printable license for your reference. No payment is required.

ELSEVIER ORDER DETAILS	
May 20, 2013	
Order Number	500761762
Order Date	May 20, 2013
Licensed content publisher	Elsevier
Licensed content publication	The Journal of Urology
Licensed content title	Optical Biopsy of Human Bladder Neoplasia With In Vivo Confocal Laser Endomicroscopy
Licensed content author	Geoffrey A. Sonn,Sha-Nita E. Jones,Tatum V. Tarin,Christine B. Du,Kathleen E. Mach,Kristin C. Jensen,Joseph C. Liao
Licensed content date	October 2009
Licensed content volume number	182
Licensed content issue number	4
Number of pages	7
Start Page	1299
End Page	1305
Type of Use	reuse in a thesis/dissertation
Intended publisher of new work	other
Portion	figures/tables/illustrations
Number of figures/tables/illustrations	1
Format	both print and electronic
Are you the author of this Elsevier article?	No
Will you be translating?	No
Order reference number	
Title of your thesis/dissertation	An Investigation of the Diagnostic Potential of Autofluorescence Lifetime Spectroscopy and Imaging for Label-Free Contrast of Disease
Expected completion date	May 2013
Estimated size (number of pages)	250
Elsevier VAT number	GB 494 6272 12
Permissions price	Not Available
VAT/Local Sales Tax	Not Available
Total	Not Available

Figure 5-3

ELSEVIER LICENSE

TERMS AND CONDITIONS

May 20, 2013

This is a License Agreement between Sergio Coda ("You") and Elsevier ("Elsevier") provided by Copyright Clearance Center ("CCC"). The license consists of your order details, the terms and conditions provided by Elsevier, and the payment terms and conditions.

All payments must be made in full to CCC. For payment instructions, please see information listed at the bottom of this form.

Supplier	Elsevier Limited The Boulevard,Langford Lane Kidlington,Oxford,OX5 1GB,UK
Registered Company Number	1982084
Customer name	Sergio Coda
Customer address	Room 731, Level 7, Blackett Laboratory London, other SW7 2AZ
License number	3152990910054
License date	May 20, 2013
Licensed content publisher	Elsevier
Licensed content publication	Urology
Licensed content title	Dynamic Real-time Microscopy of the Urinary Tract Using Confocal Laser Endomicroscopy
Licensed content author	Katherine Wu,Jen-Jane Liu,Winifred Adams,Geoffrey A. Sonn,Kathleen E. Mach,Ying Pan,Andrew H. Beck,Kristin C. Jensen,Joseph C. Liao
Licensed content date	July 2011
Licensed content volume number	78
Licensed content issue number	1
Number of pages	7
Start Page	225
End Page	231
Type of Use	reuse in a thesis/dissertation
Intended publisher of new work	other
Portion	figures/tables/illustrations
Number of figures/tables/illustrations	1
Format	both print and electronic
Are you the author of this Elsevier article?	No
Will you be translating?	No
Order reference number	
Title of your thesis/dissertation	An Investigation of the Diagnostic Potential of Autofluorescence Lifetime Spectroscopy and Imaging for Label-Free Contrast of Disease
Expected completion date	May 2013
Estimated size (number of pages)	250
Elsevier VAT number	GB 494 6272 12

Permissions price	0.00 GBP
VAT/Local Sales Tax	0.0 USD / 0.0 GBP
Total	0.00 GBP

Terms and Conditions

INTRODUCTION

1. The publisher for this copyrighted material is Elsevier. By clicking "accept" in connection with completing this licensing transaction, you agree that the following terms and conditions apply to this transaction (along with the Billing and Payment terms and conditions established by Copyright Clearance Center, Inc. ("CCC"), at the time that you opened your Rightslink account and that are available at any time at http://myaccount.copyright.com).

GENERAL TERMS

2. Elsevier hereby grants you permission to reproduce the aforementioned material subject to the terms and conditions indicated.

3. Acknowledgement: If any part of the material to be used (for example, figures) has appeared in our publication with credit or acknowledgement to another source, permission must also be sought from that source. If such permission is not obtained then that material may not be included in your publication/copies. Suitable acknowledgement to the source must be made, either as a footnote or in a reference list at the end of your publication, as follows:

"Reprinted from Publication title, Vol /edition number, Author(s), Title of article / title of chapter, Pages No., Copyright (Year), with permission from Elsevier [OR APPLICABLE SOCIETY COPYRIGHT OWNER]." Also Lancet special credit - "Reprinted from The Lancet, Vol. number, Author(s), Title of article, Pages No., Copyright (Year), with permission from Elsevier."

4. Reproduction of this material is confined to the purpose and/or media for which permission is hereby given.

5. Altering/Modifying Material: Not Permitted. However figures and illustrations may be altered/adapted minimally to serve your work. Any other abbreviations, additions, deletions and/or any other alterations shall be made only with prior written authorization of Elsevier Ltd. (Please contact Elsevier at permissions@elsevier.com)

6. If the permission fee for the requested use of our material is waived in this instance, please be advised that your future requests for Elsevier materials may attract a fee.

7. Reservation of Rights: Publisher reserves all rights not specifically granted in the combination of (i) the license details provided by you and accepted in the course of this licensing transaction, (ii) these terms and conditions and (iii) CCC's Billing and Payment terms and conditions.

8. License Contingent Upon Payment: While you may exercise the rights licensed immediately upon issuance of the license at the end of the licensing process for the transaction, provided that you have disclosed complete and accurate details of your proposed use, no license is finally effective unless and until full payment is received from you (either by publisher or by CCC) as provided in CCC's Billing and Payment terms and conditions. If full payment is not received on a timely basis, then any license preliminarily granted shall be deemed automatically revoked and shall be void as if never granted. Further, in the event that you breach any of these terms and conditions or any of CCC's Billing and Payment terms and conditions, the license is automatically revoked and shall be void as if never granted. Use of materials as described in a revoked license, as well as any use of the materials beyond the scope of an unrevoked license, may constitute copyright infringement and publisher reserves the right to take any and all action to protect its copyright in the materials.

9. Warranties: Publisher makes no representations or warranties with respect to the licensed material.

10. Indemnity: You hereby indemnify and agree to hold harmless publisher and CCC, and their respective officers, directors, employees and agents, from and against any and all claims arising out of

your use of the licensed material other than as specifically authorized pursuant to this license.

11. No Transfer of License: This license is personal to you and may not be sublicensed, assigned, or transferred by you to any other person without publisher's written permission.

12. No Amendment Except in Writing: This license may not be amended except in a writing signed by both parties (or, in the case of publisher, by CCC on publisher's behalf).

13. Objection to Contrary Terms: Publisher hereby objects to any terms contained in any purchase order, acknowledgment, check endorsement or other writing prepared by you, which terms are inconsistent with these terms and conditions or CCC's Billing and Payment terms and conditions. These terms and conditions, together with CCC's Billing and Payment terms and conditions (which are incorporated herein), comprise the entire agreement between you and publisher (and CCC) concerning this licensing transaction. In the event of any conflict between your obligations established by these terms and conditions and those established by CCC's Billing and Payment terms and conditions, these terms and conditions shall control.

14. Revocation: Elsevier or Copyright Clearance Center may deny the permissions described in this License at their sole discretion, for any reason or no reason, with a full refund payable to you. Notice of such denial will be made using the contact information provided by you. Failure to receive such notice will not alter or invalidate the denial. In no event will Elsevier or Copyright Clearance Center be responsible or liable for any costs, expenses or damage incurred by you as a result of a denial of your permission request, other than a refund of the amount(s) paid by you to Elsevier and/or Copyright Clearance Center for denied permissions.

LIMITED LICENSE

The following terms and conditions apply only to specific license types:

15. **Translation**: This permission is granted for non-exclusive world **English** rights only unless your license was granted for translation rights. If you licensed translation rights you may only translate this content into the languages you requested. A professional translator must perform all translations and reproduce the content word for word preserving the integrity of the article. If this license is to re-use 1 or 2 figures then permission is granted for non-exclusive world rights in all languages.

16. **Website**: The following terms and conditions apply to electronic reserve and author websites:
Electronic reserve: If licensed material is to be posted to website, the web site is to be password-protected and made available only to bona fide students registered on a relevant course if:
This license was made in connection with a course,
This permission is granted for 1 year only. You may obtain a license for future website posting,
All content posted to the web site must maintain the copyright information line on the bottom of each image,
A hyper-text must be included to the Homepage of the journal from which you are licensing at http://www.sciencedirect.com/science/journal/xxxxx or the Elsevier homepage for books at http://www.elsevier.com , and
Central Storage: This license does not include permission for a scanned version of the material to be stored in a central repository such as that provided by Heron/XanEdu.

17. **Author website** for journals with the following additional clauses:

All content posted to the web site must maintain the copyright information line on the bottom of each image, and the permission granted is limited to the personal version of your paper. You are not allowed to download and post the published electronic version of your article (whether PDF or HTML, proof or final version), nor may you scan the printed edition to create an electronic version. A hyper-text must be included to the Homepage of the journal from which you are licensing at http://www.sciencedirect.com/science/journal/xxxxx . As part of our normal production process, you will receive an e-mail notice when your article appears on Elsevier's online service ScienceDirect (www.sciencedirect.com). That e-mail will include the article's Digital Object Identifier (DOI). This number provides the electronic link to the published article and should be included in the posting of your personal version. We ask that you wait until you receive this e-mail and have the DOI to do any

posting.

Central Storage: This license does not include permission for a scanned version of the material to be stored in a central repository such as that provided by Heron/XanEdu.

18. **Author website** for books with the following additional clauses:
Authors are permitted to place a brief summary of their work online only.
A hyper-text must be included to the Elsevier homepage at http://www.elsevier.com . All content posted to the web site must maintain the copyright information line on the bottom of each image. You are not allowed to download and post the published electronic version of your chapter, nor may you scan the printed edition to create an electronic version.

Central Storage: This license does not include permission for a scanned version of the material to be stored in a central repository such as that provided by Heron/XanEdu.

19. **Website** (regular and for author): A hyper-text must be included to the Homepage of the journal from which you are licensing at http://www.sciencedirect.com/science/journal/xxxxx. or for books to the Elsevier homepage at http://www.elsevier.com

20. **Thesis/Dissertation**: If your license is for use in a thesis/dissertation your thesis may be submitted to your institution in either print or electronic form. Should your thesis be published commercially, please reapply for permission. These requirements include permission for the Library and Archives of Canada to supply single copies, on demand, of the complete thesis and include permission for UMI to supply single copies, on demand, of the complete thesis. Should your thesis be published commercially, please reapply for permission.

21. **Other Conditions**:

v1.6

If you would like to pay for this license now, please remit this license along with your payment made payable to "COPYRIGHT CLEARANCE CENTER" otherwise you will be invoiced within 48 hours of the license date. Payment should be in the form of a check or money order referencing your account number and this invoice number RLNK501024540.
Once you receive your invoice for this order, you may pay your invoice by credit card. Please follow instructions provided at that time.

Make Payment To:
Copyright Clearance Center
Dept 001
P.O. Box 843006
Boston, MA 02284-3006

For suggestions or comments regarding this order, contact RightsLink Customer Support: customercare@copyright.com or +1-877-622-5543 (toll free in the US) or +1-978-646-2777.

Gratis licenses (referencing $0 in the Total field) are free. Please retain this printable license for your reference. No payment is required.

Chapter 6

Figures 6-2(a), 6-9, & 6-10

AW: permission to reproduce figures in PhD thesis

Rights DE [RIGHTS-and-LICENCES@wiley-vch.de]

Sent:20 May 2013 15:43

To: Coda, Sergio

Dear Sergio Coda,

We hereby grant permission for the requested use expected that due credit is given to the original source.

If material appears within our work with credit to another source, authorisation from that source must be obtained.

Credit must include the following components:

- Books: Author(s)/ Editor(s) Name(s): Title of the Book. Page(s). Publication year. Copyright Wiley-VCH Verlag GmbH & Co. KGaA. Reproduced with permission.

- Journals: Author(s) Name(s): Title of the Article. Name of the Journal. Publication year. Volume. Page(s). Copyright Wiley-VCH Verlag GmbH & Co. KGaA. Reproduced with permission.

- Online Portal: Author(s): Title of the Online portal. Link or DOI. Publication year. Copyright Wiley-VCH Verlag GmbH & Co. KGaA. Reproduced with permission.

With kind regards

Bettina Loycke
Senior Rights Manager
Rights & Licenses
Wiley-VCH Verlag GmbH & Co. KGaA
Boschstraße 12
69469 Weinheim
Germany

www.wiley-vch.de
T +(49) 6201 606-280
F +(49) 6201 606-332
rightsDE@wiley.com

Von: Coda, Sergio [mailto:s.coda@imperial.ac.uk]
Gesendet: Montag, 20. Mai 2013 12:49
An: Rights DE
Betreff: permission to reproduce figures in PhD thesis

Dear Sir or Madam,

I would like to request permission to reproduce the following figures in my PhD thesis:

Re: Thompson AJ, Coda S, Sørensen MB, ***et al***. In vivo measurements of diffuse reflectance and time-resolved autofluorescence emission spectra of basal cell carcinomas. J. Biophotonics 5, No. 3, 240–254 (2012)

Figure 2, page 243

Figure 7, page 248

Figure 8, page 249

I am co-author of this article.

Permission to reproduce this content could not be granted via the RightsLink® service.

The PhD thesis would be available in both print form and electronically.

Title of thesis: An Investigation of the Diagnostic Potential of Autofluorescence Lifetime Spectroscopy and Imaging for Label-Free Contrast of Disease.

I would also take this opportunity to express my sincere appreciation for your assistance.

Kind regards,

Dr Sergio Coda

****

Sergio Coda, MD
Clinical Research Fellow
Department of Medicine
Division of Experimental Medicine
Imperial College London
Room 612, Level 6, Blackett Laboratory
South Kensington Campus
Prince Consort Road
London SW7 2AZ
Telephone: 0044 (0) 20 7594 7738
Fax: 0044 (0) 20 7594 7714
E-Mail: **s.coda@imperial.ac.uk**
URL: **http://www1.imperial.ac.uk/medicine/people/s.coda/**

****

Chapter 7

Figure 7-5

permission to reproduce figures in PhD thesis

Coda, Sergio

Sent:20 May 2013 12:17

To: Webmaster@bostonscientific.com

Dear Mr or Madam,

My name is Dr Sergio Coda and I work with Professor Paul French, Dr Christopher Dunsby and Dr Andrew Thillainayagam at Imperial College London in the Optics Department at Imperial College London, and in the Endoscopy Unit at Charing Cross Hospital, Imperial College Healthcare NHS Trust, as a specialist

endoscopist doctor. We have been working on a project studying fluorescence lifetime imaging microscopy (FLIM) of human gastrointestinal tissue over the last few years and I would like to request permission to reproduce the following figures from your Website in my PhD thesis:

Figures:

Endoscopic biopsy forceps (Radial Jaw 3 LC forceps, Boston Scientific)

Polypectomy snares (Captivator single-use snares, Boston Scientific)

Images reproduced with permission from:

http://www.bostonscientific.com/global-endoscopy/index.html

The images would be used in the thesis, in a "Materials and methods" section.

The PhD thesis would be available in both print form and electronically.

Title of thesis: An Investigation of the Diagnostic Potential of Autofluorescence Lifetime Spectroscopy and Imaging for Label-Free Contrast of Disease.

I would also take this opportunity to express my sincere appreciation for your assistance.

Kind regards,

Dr Sergio Coda

****

Sergio Coda, MD
Clinical Research Fellow
Department of Medicine
Division of Experimental Medicine
Imperial College London
Room 612, Level 6, Blackett Laboratory
South Kensington Campus
Prince Consort Road
London SW7 2AZ
Telephone: 0044 (0) 20 7594 7738
Fax: 0044 (0) 20 7594 7714
E-Mail: s.coda@imperial.ac.uk
URL: **http://www1.imperial.ac.uk/medicine/people/s.coda/**

****

Figure 7-6

permission to reproduce figure in PhD thesis

Coda, Sergio

Sent:20 May 2013 12:35

To: jmichalek@asge.org

Dear Ms Michalek,

I would like to request permission to reproduce the following figure in my PhD thesis:

Re: Diagram illustrating the different regions of the human colon. Source: American Society for Gastrointestinal Endoscopy (ASGE) Anatomical Images, Colon & Rectum.

http://www.asge.org/uploadedFiles/Members_Only/Colon-Rectum_Anatomical.pdf

I am an ASGE trainee member.

The PhD thesis would be available in both print form and electronically.

Title of thesis: An Investigation of the Diagnostic Potential of Autofluorescence Lifetime Spectroscopy and Imaging for Label-Free Contrast of Disease.

I would also take this opportunity to express my sincere appreciation for your assistance.

Kind regards,

Dr Sergio Coda

****

Sergio Coda, MD
Clinical Research Fellow
Department of Medicine
Division of Experimental Medicine
Imperial College London
Room 612, Level 6, Blackett Laboratory
South Kensington Campus
Prince Consort Road
London SW7 2AZ
Telephone: 0044 (0) 20 7594 7738
Fax: 0044 (0) 20 7594 7714
E-Mail: s.coda@imperial.ac.uk
URL: **http://www1.imperial.ac.uk/medicine/people/s.coda/**

****